LBL-22010
UC-13 c.2

MATERIALS AND MOLECULAR RESEARCH DIVISION

Annual Report 1986

July 1987

TWO-WEEK LOAN COPY
This is a Library Circulating Copy
which may be borrowed for two weeks.

Lawrence Berkeley Laboratory
University of California
Berkeley, California 94720

Prepared for the
U.S. Department of Energy under Contract DE-AC03-76SF00098

LBL-22010
LBL-22010 c.2

LBL-22010

MATERIALS AND MOLECULAR RESEARCH DIVISION

Annual Report 1986

July 1987

Norman E. Phillips, Division Head
Rolf H. Muller, Asst. Division Head for Research
Conway V. Peterson, Asst. Division Head for Administration

Lawrence Berkeley Laboratory
University of California
Berkeley, California 94720

Materials Sciences

Chemical Sciences

Nuclear Sciences

Fossil Energy

Energy Storage Systems

Health and Environmental Sciences

Work for Others

Appendices

Contents

REMARKS BY THE DIVISION HEAD

Norman E. Phillips xi

MATERIALS SCIENCES

Metallurgy and Ceramics

Structure of Materials

Structure and Properties of Transformation Interfaces
Ronald Gronsky, Investigator 1

Microstructure, Properties, and Alloy Design: Inorganic Materials
Gareth Thomas, Investigator 5

Solid-State Phase-Transformation Mechanisms
Kenneth H. Westmacott, Investigator 14

National Center for Electron Microscopy
Gareth Thomas, Ronald Gronsky, and Kenneth H. Westmacott, Investigators 17

In Situ Investigations of Gas-Solid Reactions by Electron Microscopy
J.W. Evans, Investigator 29

Local Atomic Configurations in Solid Solutions
Didier de Fontaine, Investigator 31

Alloy Theory
Didier de Fontaine and Leo M. Falicov, Investigators 34

Mechanical Properties

Environmentally Affected Crack Growth in Engineering Materials
Robert O. Ritchie, Investigator 36

Physical Properties

Interfaces and Ceramic Microstructures
Joseph A. Pask, Investigator 43

High-Temperature Reactions
Alan W. Searcy, Investigator 45

Structure-Property Relationships in Semiconductor Materials
Jack Washburn, Investigator 49

Fundamental Studies of Chemical Properties and Processing of Advanced Structural Ceramics
Lutgard C. De Jonghe, Investigator 54

Structure and Electrical Properties of Composite Materials
Robert H. Bragg, Investigator 58

Ceramic Interfaces
Andreas M. Glaeser, Investigator 61

Solid-State Physics

Experimental Research

Far-Infrared Spectroscopy
Paul L. Richards, Investigator 64

Experimental Solid-State Physics and Quantum Electronics
Y.R. Shen, Investigator 69

Excitations in Solids
Carson D. Jeffries, Investigator 74

Time-Resolved Spectroscopies in Solids
Peter Y. Yu, Investigator 77

Superconductivity, Superconducting Devices, and 1/f Noise
John Clarke, Investigator 79

Theoretical Research

Theoretical Studies of the Electronic Properties of Solid Surfaces
Leo M. Falicov, Investigator 84

Theoretical Solid-State Physics
Marvin L. Cohen, Investigator 87

Surface, Chemisorption, and Theory of Solids
Steven G. Louie, Investigator 92

Materials Chemistry

Chemical Structure

Low-Temperature Properties of Materials
Norman E. Phillips, Investigator 95

Electrochemical Processes
Charles W. Tobias, Investigator 99

High-Temperature and Surface Chemistry

High-Temperature Thermodynamics
Leo Brewer, Investigator 101

Chemistry and Materials Problems in Energy Production Technologies
Donald R. Olander, Investigator 103

Electrochemical Phase Boundaries
Rolf H. Muller, Investigator 106

Solid-State and Surface Reactions
Gabor A. Somorjai, Investigator 109

Nuclear Magnetic Resonance
Alexander Pines, Investigator 119

Synthesis of Novel Solids
Angelica M. Stacy, Investigator 129

Raman Studies of Surface Processes
Gerd M. Rosenblatt, Investigator 131

CHEMICAL SCIENCES

Fundamental Interactions

Photochemical and Radiation Sciences

Photon-Assisted Surface Reactions, Materials, and Mechanisms
Gabor A. Somorjai, Investigator 133

Photochemistry of Materials in the Stratosphere
Harold S. Johnston, Investigator 136

Radiation Chemistry of Aqueous Systems
Michael E. Jayko 138

Chemical Physics

Energy Transfer and Structural Studies of Molecules on Surfaces
Charles B. Harris, Investigator 139

Selective Photochemistry
C. Bradley Moore, Investigator 142

Physical Chemistry with Emphasis on Thermodynamic Properties
Kenneth S. Pitzer, Investigator 144

Molecular Interactions
William A. Lester, Jr., Investigator 147

Spectroscopy and Structures of Reactive Intermediates
Richard J. Saykally, Investigator 151

Theory of Atomic and Molecular Collision Processes
William H. Miller, Investigator 154

Photoelectron Spectroscopy
David A. Shirley, Investigator 158

Crossed Molecular Beams
Yuan T. Lee, Investigator 166

Potential-Energy Surfaces for Chemical Reactions
Henry F. Schaefer III, Investigator 173

Atomic Physics

High-Energy Atomic Physics
Harvey Gould, Investigator 177

Atomic Physics
Michael H. Prior, Investigator 180

Processes and Techniques

Chemical Energy

Formation of Oxyacids of Sulfur from SO_2
Robert E. Connick, Investigator 182

Catalytic Hydrogenation of CO
Gabor A. Somorjai and Alexis T. Bell, Investigators 183

Organometallic Chemistry of Coal Conversion
K. Peter C. Vollhardt, Investigator 187

Synthetic and Physical Chemistry
William L. Jolly, Investigator 189

High-Energy Oxidizers and Delocalized-Electron Solids
Neil Bartlett, Investigator 191

Transition Metal–Catalyzed Conversion of CO, NO, H_2, and Organic Molecules to Fuels and Petrochemicals
Robert G. Bergman, Investigator 196

Chemical Engineering Sciences

High-Pressure Phase Equilibria in Hydrocarbon-Water (Brine) Systems
John M. Prausnitz, Investigator 201

NUCLEAR SCIENCES

Low-Energy Nuclear Sciences

Heavy-Element Chemistry

Actinide Chemistry
Norman M. Edelstein, Richard A. Andersen, Neil Bartlett, John G. Conway, Kenneth N. Raymond, Glenn T. Seaborg, Andrew Streitwieser, Jr., David H. Templeton, and Allan Zalkin, Investigators 205

FOSSIL ENERGY

Electrode Surface Chemistry
P.N. Ross, Investigator 223

Studies of Materials Erosion in Coal Conversion and Utilization Systems
Alan V. Levy, Investigator 225

Catalytic Gasification of Graphite or Carbon
Heinz Heinemann, Investigator, with Gabor A. Somorjai, Investigator, and J. Carrazza 229

ENERGY STORAGE SYSTEMS

Electrochemical Energy Storage
Lutgard C. De Jonghe, James W. Evans, Rolf H. Muller, John Newman, P.N. Ross, and Charles W. Tobias, Investigators 233

Surface Morphology of Metals in Electrodeposition
Charles W. Tobias, Investigator 233

Metal Couples in Non-Aqueous Electrolytes
Charles W. Tobias, Investigator 235

Engineering Analysis of Electrolytic Gas Evolution
Charles W. Tobias, Investigator 237

Surface Layers on Battery Materials
Rolf H. Muller, Investigator 240

Electrode Kinetics and Electrocatalysis
P.N. Ross, Investigator 243

Electrical and Electrochemical Behavior of Particulate Electrodes
J.W. Evans, Investigator 246

Electrochemical Properties of Solid Electrolytes
Lutgard C. De Jonghe, Investigator 248

Analysis and Simulation of Electrochemical Systems
John Newman, Investigator 252

HEALTH AND ENVIRONMENTAL SCIENCES

Semiconductor Materials and Devices
Eugene E. Haller, Investigator 255

WORK FOR OTHERS

Office of Naval Research

Quantum Monte Carlo for Molecular Studies
William A. Lester, Jr., Investigator 261

Properties of Superconducting Thin Films; Electron-Phonon and Non-Phonon Coupling
Vladimir Z. Kresin, Investigator 264

United States Air Force

Quantum Monte Carlo Study of Tetrahydrogen
William A. Lester, Jr., Investigator 266

United States Department of Transportation

Materials for Enhanced Heavy Fuel Capability Marine Diesels
Alan V. Levy, Investigator 267

Electric Power Research Institute

Inhibitive Salts for Reducing High-Temperature Oxidation and Spallation
John Stringer, Acting Investigator 268

Erosion-Corrosion of Materials in Coal-Water Slurries
Alan V. Levy, Investigator 270

Other Private-Sector Contractors

The Norton Company

Sliding Wear of Thermal Spray Chromia Coatings
Alan V. Levy, Investigator 271

Cummins Engine Company

Unlubricated Sliding Wear of Ceramic Materials

Alan V. Levy, Investigator 272

Westinghouse Electric Corporation

Erosion of Hard Material Coating Systems

Alan V. Levy, Investigator 273

APPENDICES

Appendix A. Division Personnel 275

Appendix B. Division Committees 281

Appendix C. List of Divisional Seminars 282

Appendix D. List of Investigators 286

REMARKS BY THE DIVISION HEAD

This past year has been an exciting one for MMRD, with many important research achievements by our investigators, correspondingly important awards (including the Nobel Prize in Chemistry for Yuan Lee), and administrative changes (which had their roots in 1986) that will have a profound effect for the future of the Division. It was also a year of continued constraint in our budget, since the dramatic decline from 1985 to 1986 has not been reversed.

As the end of the year approached, two developments were under way that will have great significance for MMRD in the future. Although they are more appropriately subjects for next year's Annual Report, it seems reasonable to at least mention them here. One is the research on the newly discovered high-critical-current superconducting oxides. These materials were first generally recognized as superconductors at the Materials Research Society meeting in December 1986. Within a matter of days of that news reaching MMRD, Angelica Stacy was making samples of the lanthanum compounds, a broad range of measurements of their physical properties was under way, and MMRD was taking a major role in research on the new materials. In particular, a collaboration between Angie Stacy, Marvin Cohen, and Alex Zettl (who joined the Division at that time) led to an independent discovery of superconductivity in the yttrium compounds shortly before the publication of the original discovery by Paul Chu of the University of Houston. At the time of this writing it is clear that this research and its expansion into areas related to applications in technology will be a major element in our program in the coming years.

The second development of note that can be said to have begun in 1986 is a change in the relation between MMRD and the Center for Advanced Materials (CAM). Toward the end of 1986, LBL Director David A. Shirley had established a task force to recommend on future administrative arrangements for CAM. The recommendations ultimately led to the merger of MMRD and CAM, under the name Materials and Chemical Sciences Division (MCSD). The new arrangement will foster cooperation between the CAM and MMRD programs, but the special nature and identity of the CAM programs will still be emphasized. For example, we will continue to have separate annual reports for CAM and for the rest of MCSD.

The Nobel Prize mentioned above is only the highlight of the usual long list of honors and awards, which include the following:

- Neil Bartlett and Steven G. Louie received Miller Professorships from the University of California Berkeley for 1986–1987.
- Neil Bartlett received the Moissan Medal and was the First Plenary Lecturer of the Moissan Session of the International Symposium on the Centenary of the Discovery of Fluorine.
- Alexis T. Bell was elected to the National Academy of Engineering.
- Robert G. Bergman received the ACS Award in Organometallic Chemistry and the ACS Cope Scholar Award.
- John Clarke was named a Fellow of the Royal Society of London and received the Sustained Outstanding Research award in Solid State Physics in the 1986 Materials Sciences Research Competition.
- James W. Evans was elected Director (Basic Sciences) of The Metallurgical Society.
- Yuan T. Lee received an honorary Doctor of Science Degree from the University of Waterloo, Ontario, and the Peter Debye Award in Physical Chemistry. He also received the National Medal of Science and the Nobel Prize in Chemistry.
- C. Bradley Moore received the 1986 E.O. Lawrence Award and was elected to the National Academy of Sciences.
- M.A. O'Keefe, a staff member at the National Center for Electron Microscopy, was elected a fellow of the Royal Microscopical Society.
- Kenneth S. Pitzer received the Mack Memorial Award from Ohio State University. He was also elected an Honorary Fellow of the Indian Academy of Sciences and was Plenary Lecturer for the Ninth International Conference on

Chemical Thermodynamics and the Second International Symposium on Solubility Phenomena.

- Michael H. Prior and Eugene E. Haller were elected Fellows of the American Physical Society.
- Henry F. Schaefer delivered the J.A. Erskine Lectures, University of Canterbury, Christchurch, New Zealand; and he was the E.C. Franklin Memorial Lecturer, University of Kansas.
- Y. Ron Shen received the Charles H. Townes Award from the Optical Society of America.
- Gabor A. Somorjai received the Engelhard/Henry J. Albert Award from the International Precious Metals Institute. He also received the Palladium Medal from the Precious Metals Institute and was the Musher Lecturer, Hebrew University, Israel.
- David. H. Templeton and Lieselott K. Templeton received the A.L Patterson Award from the American Crystallographic Society.
- Gareth Thomas was elected President of the International Federation of Electron Microscopy Societies.
- K. Peter Vollhardt received the ACS Award in Organometallic Chemistry for 1987. He was also the Syntex Lecturer, University of Colorado; Wilson Baker Lecturer, University of Bristol, England; and Plenary Lecturer, Groupe d'Etudes de Chimie Organometallique, Tolouse, France.
- Kenneth H. Westmacott, with Ulrich Dahmen, Robert Fisher, and Pat Ferguson, received the British Institute of Metals "Elegant Work" Award.

These awards and accomplishments occurred in an atmosphere of budget restriction, as mentioned earlier. Our 1987 DOE budget was increased by only approximately 2% over 1986, which was not sufficient to compensate even for inflation, and the large decrease from 1985 to 1986 remained in effect.

During 1986 MMRD began to implement a long-planned organizational change to Sections based on common scientific interest. In most cases these Sections follow DOE budget categories, but there are some variances. The Sections, with their Section Coordinators, are:

- Chemical Physics (H.S. Johnston)
- Physical Chemistry/Electrochemistry (A.W. Searcy)
- Surface Science/Catalysis (A.T. Bell)
- Synthetic Chemistry/Actinide Chemistry (K.N. Raymond)
- Physical Metallurgy/Ceramics (R.O. Ritchie)
- Solid-State Physics/Novel Materials/ Atomic Physics (S.G. Louie)

Because the scientific interests of so many Investigators cross disciplinary lines, several Investigators are included in more than one Section.

Several new programs have started up or in the process of starting up. One, Alloy Theory, with Didier de Fontaine and Leopoldo Falicov as Investigators, has already begun. In this program, existing electronic-band structure and total-energy computer codes are combined with cluster-variation-method codes to produce phase diagrams from a minimum of empirical information. A second program, Matter at Megabars of Pressure, features Investigators Peter Yu and Marvin Cohen. This program, in which the properties of materials are studied at extremely high pressures, contributed to the discovery of superconductivity in Si at high pressures and confirmed Marvin's predictions of its dependence on pressure and crystal structure.

Projects that are proposed for implementation include Film Formation and Dislocation Substructure in Corrosion-Induced Cracking (with Ron Gronsky, Rob Ritchie, and Thomas Devine as Investigators); and Concepts for the Protection of Metals and Semiconductors (with Phil Ross, Rolf Muller, Charles Tobias, Gerd Rosenblatt, and John Porter as Investigators).

Norman E. Phillips
Division Head
Materials and Molecular Research Division

Materials Sciences

METALLURGY AND CERAMICS

STRUCTURE OF MATERIALS

Structure and Properties of Transformation Interfaces*

Ronald Gronsky, Investigator

INTRODUCTION

The modern science of materials devotes increasing attention to the role of solid-state interfaces; they completely dominate the behavior of electronic devices, and they strongly influence the behavior of ceramic and metallic alloys alike. This program seeks a fundamental understanding of the role of interfaces in materials by applications of high-resolution electron microscopy to determine their local structure and composition, by theoretical modeling to relate these parameters to their actual atomic structure and composition, and by correlations with their properties, including conductivity, diffusivity, ductility, mobility, and reactivity.

1. Interfacial Structure and Composition of Ordered Precipitate Phases in the Al-Ag System (Publications 1, 5, 10, and 17)

J.M. Howe† and R. Gronsky

This work continues to probe the relationship between interfacial structure and growth mechanisms of second-phase particles in aluminum-based alloys. The Al-Ag system has served as a model for the fcc-hcp transformation, and here it is studied with respect to the compositional and structural changes accompanying ordering of the Ag-rich γ' phase. As shown in the high-resolution image of Figure 1-1, there is a light-to-dark contrast change between every other basal plane of the precipitate phase, indicative of a long-range ordering reaction. Quantitative energy-dispersive spectroscopy (see Figure 1-2) confirms that the precipitate phase has composition Ag_2Al, as expected for the fully ordered, congruently melting γ phase. However, convergent-beam electron diffraction (CBED) of a number of different precipitates yields conflicting results; not all of the particles appear to be ordered.

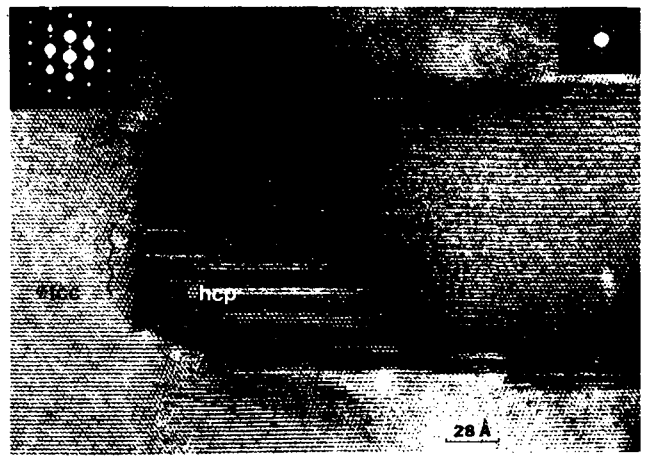

Figure 1-1. High-resolution electron micrograph of the edge of a γ' precipitate in the <110> orientation with corresponding electron diffraction pattern (left) and optical diffractogram (right). Atom positions are shown for the fcc matrix and the hcp precipitate. The staggered appearance of the edge (outlined) is related directly to the atomic mechanism of growth. (XBB 842-1212A)

Further analysis shows that the limiting step in the precipitation reaction is the substitutional diffusion of Ag atoms across kinks in the Shockley partial-dislocation ledges imaged in Figure 1-1. Interestingly, both the structural and chemical changes necessary for growth of the precipitate occur on the same atomic plane, made possible only by the particular interfacial structure observed above. However, the ordering reaction is apparently decoupled from these events. In fact, ordering can follow the attainment of proper structure and composition within the precipitate by a subsequent reaction involving atomic transport along the precipitate basal planes. This explains the apparent anomaly in the CBED results.

*This work was supported by the Director, Office of Energy Research, Office of Basic Energy Sciences, Materials Sciences Division of the U.S. Department of Energy under Contract No. DE-AC03-76SF00098.

†Permanent address: Department of Metallurgical Engineering and Materials Science, Carnegie-Mellon University, Pittsburgh, PA 15213.

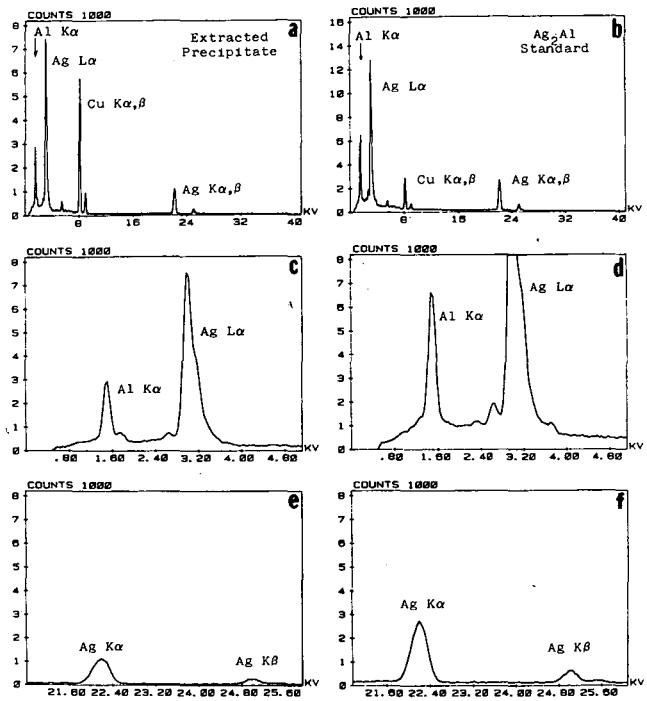

Figure 1-2. Spectra from (a) an extracted precipitate and (b) a standard of Ag_2Al, with enlargements (c-f) comparing the relative sizes of the Al K_α and Ag K_α peaks from the precipitate and standard, respectively. The precipitate is found to have a composition of 66.8 ± 3.8 at% Ag. (XBL 8410-4157)

2. Grain-Boundary Structure and Corrosion in Symmetrical-Tilt Body-Centered Cubic Grain Boundaries (Publications 12 and 22)

E.A. Kamenetzky, X.R. Qian,† Y.T. Chou,† and R. Gronsky

A simple geometrical method has been developed to calculate grain-boundary translations that preserve first and second nearest-neighbor coordination across the boundary plane. These translations form interlocking polyhedral groups of atoms that define a mechanically stable boundary. Further individual atom relaxations can be easily recognized from the geometry of the atom arrangements. The description of boundary structure that results from this model is equivalent to a "soft sphere" analogue, where a range of interatomic distances between the first and second nearest neighbors exists at the grain boundary. To determine the most likely occurring boundary structure, the atomic assembly with the highest coordination and minimum excess volume is iteratively sought.

The expansion data generated by this model correctly predict a critical cusp in the corrosion behavior of symmetrical tilt boundaries of niobium at $\Sigma = 19$ (see Figure 2-1). Significantly, this event was not predicted by earlier energy calculations that used a central-force potential model. It is concluded that the grain-boundary corrosion behavior in niobium is directly related to the grain-boundary free volume. Further correlations are sought with bicrystals of larger misorientation angles.

†Permanent address: Department of Materials Science and Engineering, Lehigh University, Bethlehem, PA 18015.

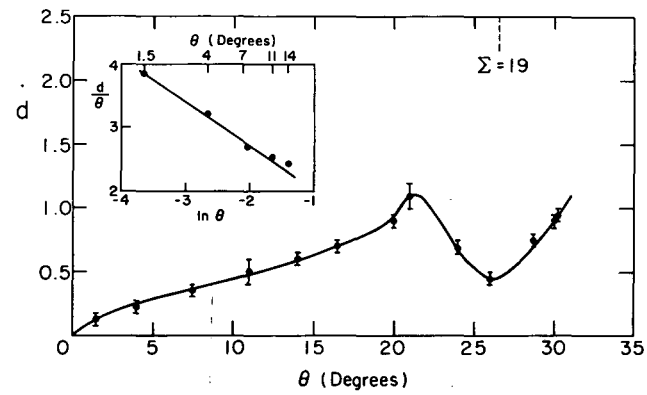

Figure 2-1. Variation of penetration depth d of a nitric/hydrofluoric acid solution into niobium grain boundaries as a function of misorientation angle θ about a [110] tilt axis. The depths of the boundary grooves are expressed in units of $\lambda/2$, where λ is the wavelength of the sodium vapor lamp source used in the multibeam interference microscopy measurements. (XBL 8610-4181)

3. Work in Progress

Also under investigation in this program are the atomic structure of the Al-oxide interface (with J.Y. Lee), the atomic structure and segregation behavior of defects in silicon (with J.H. Rose), grain-boundary structure and segregation in Nb_3Sn superconducting wire (with L. Yamamoto), grain-boundary structure in nanocrystalline ceramics (with R.W. Siegel, Argonne National Laboratory), and continued activity in the analysis of interfaces in electronic materials (with S. Packer, Z. Liliental, and J. Washburn).

1986 PUBLICATIONS AND REPORTS

Refereed Journals

1. J.M. Howe, M. Sarikaya, and R. Gronsky, "Space Group Analyses of Thin Precipitates by Different

Convergent Beam Electron Diffraction Procedures," Acta Crystallogr. **A42**, 368 (1986); LBL-20114.

2. T. Sands, V.G. Keramidas, J. Washburn, and R. Gronsky, "On the Structure and Composition of Ni_xGaAs," Appl. Phys. Lett. **48**, 402 (1986); LBL-20376.
3. T. Sands, V.G. Keramidas, R. Gronsky, and J. Washburn, "Initial Stages of the Pd-GaAs Reaction : Formation and Decomposition of Ternary Phases," Thin Solid Films **136**, 105 (1986); LBL-19133.
4. J.M. Howe, "Metallographic, Diffraction and Scanning Calorimetry Analyses of Precipitates and Recrystallization in an Al-Mn Alloy," Metall. Trans. **17A**, 593 (1986); LBL-19989.
5. J.M. Howe and R. Gronsky, "Quantitative Energy-Dispersive Analyses of γ' Precipitates in an Al-4.2 at% Ag Alloy," Scripta Metall. **20**, 1165 (1986); LBL-18147.
6. Z. Liliental-Weber, R. Gronsky, J. Washburn, N. Newman, W.E. Spicer, and E.R. Weber, "Schottky and Ohmic Au Contacts on GaAs: Microscopic and Electrical Investigation," J. Vac. Sci. Technol. **B4**, 192 (1986); LBL-21010.

Other Publications

7. P.C. Ling and R. Gronsky, "On the Geometrical Relationship between Kikuchi Line Position and Excitation Error in Electron Diffraction," in *Proc. 44th Annual Meeting Elec. Microsc. Soc. Am.*., G.W. Bailey, Ed., San Francisco Press, 1986, p. 870; LBL-21315.
8. Z. Liliental-Weber, C. Nelson, R. Ludeke, R. Gronsky, and J. Washburn, "An Atomic Resolution Microscope Study of Al Contacts on GaAs," in *Proc. 44th Annual Meeting Elec. Microsc. Soc. Am.*, G.W. Bailey, Ed., San Francisco Press, 1986, p. 726; LBL-21282.
9. R. Gronsky, R.L. Hines, and C. Nelson, "Platinum Surface Structures at Atomic Resolution," in *Proc. XIth Int. Cong. on Electron Microscopy, Vol. II*, T. Imura, S. Maruse, and T. Suzuki, eds., Japanese Society of Electron Microscopy, Tokyo, 1986, p. 961.
10. J.M. Howe and R. Gronsky, "Atomic Chemistry by HREM and Image Simulations?" in *Proc. 44th Annual Meeting Elec. Microsc. Soc. Am.*, G.W. Bailey, Ed., San Francisco Press, 1986, p. 828.
11. Y.C. Shih, J. Washburn, E.R. Weber, and R. Gronsky, "The Formation of Amorphous Silicon by Light Ion Damage," in *Proc. Mat. Res. Soc. Symp., San Francisco, CA, April 15–17, 1985, Ion Beam Processes in Advanced Electronic Materials and Device Technology*, F.H. Eisen, T.W. Sigmon, and B.R. Appleton, eds., **45**, 65 (1986); LBL-19466.
12. E.A. Kamenetzky, R. Gronsky, and Y.T. Chou, "Translations and Structure in Symmetrical Tilt Body Centered Cubic Grain Boundaries," in *Proc. 4th Japan Inst. Met. Int. Symp. (JIMIS-4) on Grain Boundary Structure and Related Phenomena*, Minakami Spa, Japan, The Japan Institute of Metals, 1986; LBL-20487.
13. J.M. Howe and R. Gronsky, "Nucleation of γ' Plates from G.P. Zones in an Al-Ag Alloy," in *Proc. 44th Annual Meeting Elec. Microsc. Soc. Am.*, G.W. Bailey, Ed., San Francisco Press, 1986, p. 552.
14. J.H. Rose and R. Gronsky, "The Potential of High Resolution Transmission Electron Microscopy for Imaging Impurities at Dislocations and Grain Boundaries in Silicon," in *Proc. Mat. Res. Soc. Symp., Boston, MA, Dec. 2–7, 1985*, L.W. Hobbs, K.H. Westmacott, and D.B. Williams, eds., **62**, 57 (1986); LBL-20602.
15. T. Sands, V.G. Keramidas, A.J. Yu, K.M. Yu, R. Gronsky, and J. Washburn, "Phase Formation Sequence in the Pd-GaAs System," in *Proc. Mat. Res. Soc. Symp., Boston, MA, Dec. 2–7, 1985, on Thin Films, Interfaces and Phenomena*, R.J. Niemanich, P.S. Ho, and S.S. Lau, eds., **54**, 376 (1986); LBL-20611.
16. Z. Liliental-Weber, N. Neuman, W.E. Spicer, R. Gronsky, J. Washburn, and E.R. Weber, "The Structure and Electrical Properties of Gold Contacts on GaAs," in *Proc. Mat. Res. Soc. Symp., Boston, MA, Dec. 2–7, 1985, on Thin Films, Interfaces and Phenomena*, R.J. Niemanich, P.S. Ho, and S.S. Lau, eds., **54**, 415 (1986); LBL-20618.
17. J.M. Howe and R. Gronsky, "Transmission Electron Microscopy Studies of Precipitate Growth at the Atomic Level," in *Proc. Mat. Res. Soc. Symp., Boston, MA, Dec. 2–7, 1985*, L.W. Hobbs, K.H. Westmacott, and D.B. Williams, eds., **62**, 241 (1986); LBL-20837.
18. T. Sands, "Contributions of Electron Microscopy to the Understanding of Reactions on Compound Semiconductor Surfaces," in *Proc. Mat. Res. Soc. Symp., Boston, MA, Dec. 2–7, 1985*, L.W. Hobbs, K.H. Westmacott, and D.B. Williams, eds., **62**, 25 (1986); LBL-20509.
19. Z. Liliental-Weber, E.R. Weber, N. Newman, W.E. Spicer, R. Gronsky, and J. Washburn, "Observations of Stoichiometry Changes Beneath Metal Contacts on GaAs," in *Defects in Semiconductors, Proc. 14th Int. Conf. on Defects in Semiconductors (1986)*, J. Bourgoin, M. Lannoo, and H.J. von Bardeleben, eds., Trans. Tech Publications, 1986; LBL-22220.

LBL Reports

20. T. Sands, V.G. Keramidas, J. Washburn, and R. Gronsky, "Electron Microscopy of Reactions on Compound Semiconductor Surfaces," J. Elec. Materials (in press); LBL-19764.
21. J.M. Howe, U. Dahmen, and R. Gronsky, "Atomic Mechanisms of Precipitate Plate Growth," submitted to Phil. Mag.; LBL-21705.
22. X.R. Qian, Y.T. Chou, and E.A. Kamenetzky, "The Structure Dependence of Grain Boundary Corrosion in Niobium Bicrystals," J. Less Common Metals (in press); LBL-22496.

23. T. Sands, V.G. Keramidas, A.J. Yu, K.M. Yu, R. Gronsky, and J. Washburn, "Ni, Pd and Pt on GaAs: A Comparative Study of Reacted Film Morphologies," submitted to J. Mat. Res.; LBL-21060.

Invited Talks

24. R. Gronsky, "Experimental Methods for the Study of Interfaces," TMS/AIME Southeast Regional Meeting on "Interface Effects on the Processing and Properties of Materials for High Temperature Service," Oak Ridge, TN, Sept. 25–26, 1986.

25. R. Gronsky, "Atomic Structure of Interfaces in Electronic Materials," Department of Materials Science and Engineering, University of Washington, Seattle, Nov. 10, 1986.

Microstructure, Properties, and Alloy Design: Inorganic Materials*

Gareth Thomas, Investigator

INTRODUCTION

This is a multi-component, interdisciplinary program in advanced inorganic materials involving fundamental quantitative studies of the structure-property relationships in technologically significant materials involved in energy and conservation. All tasks involve characterization of both structure and composition at the highest levels of spatial (transmission electron microscopy) and chemical (spectroscopy) resolutions in order to understand the complexities of structure-chemistry-processing-property relationships, without which alloy design is impossible. Specific tasks include: (a) dual-phase ferrite-martensite steels for rod, bar, and wire; optimization of microstructure and processing; failure analysis of drawn wires; fatigue (with Professor R.O. Ritchie); (b) effect of microalloying on structure properties and processing of dual-phase martensitic-austenite composite steels designed for optimum toughness; and (c) magnetic materials: materials for recording, piezoelectric materials, and rare-earth permanent magnets. The overall objectives are to design new materials or to more efficiently utilize existing materials and processing routes for industrial practice, and to realize materials and energy conservation.

STEELS

1. Design of Dual-Phase Steels for Bars and Rods (Publication 41)

G. Thomas

Low-carbon dual-phase ferrite–lath martensite composite steels for rods and bars have been designed to meet cold-forming requirements. The rounds can be prepared by conventional processing followed by heat treatment or directly on line in rod or bar mills. The products are fine-grained rods or bars that show exceptional promise for applications such as cold drawing to wires without patenting heat treatments, cold heading for fasteners, and as reinforcing bars for the construction industry. These steels also have superior ductility, fatigue, low-temperature toughness, and corrosion resistance compared to conventional mild or high-carbon steels. Specific properties can be tailor made by appropriate design of composition and processing to control the composite microstructure and morphology.

2. Lath Martensite and Bainite in Low Alloy Steels (Publication 42)

M. Sarikaya,† H. Tokushige,‡ and G. Thomas

The morphology and crystallography of lath martensite and bainite have been studied by transmission electron microscopy (TEM), imaging, and diffraction techniques. When quenched from the austenitic phase region, the steels have microduplex structures of packets of dislocated lath martensite with continuous interlath films of retained austenite. Bainites form when interrupted quenching is applied at temperatures around M_s to allow isothermal transformation to take place. The microstructure of lower bainite resembles that of lath martensite, where bainitic dislocated ferrite laths, which now contain unidirectional carbides, are surrounded by thin films of retained austenite. In upper bainite, the boundaries are decorated by interlath carbides, a microstructure observed in martensite tempered at 240–400°C.

Microdiffraction experiments reveal that bainitic ferrite laths are related to adjacent laths as well as the parent austenite through the same orientation relationships found in martensite in the same alloys. This strongly confirms the shear aspect of the bainitic transformation. Bainitic carbides, identified as cementite, are found to have the Isaichev orientation relationship with ferrite, which supports the idea that cementite has transformed directly from austenite. The microstructural and crystallographic characteristics of martensite and bainites in low-carbon steels are very similar, confirming that these microstructures are the products of a continuous range of phase transformations from austenite, where shear is the basis, and the final morphology depends on the time allowed for carbon diffusion and carbide precipitation. Table 2-1 gives a summary of the crystallographic data.

*This work was supported by the Director, Office of Energy Research, Office of Basic Energy Sciences, Materials Sciences Division of the U.S. Department of Energy under Contract No. DE-AC03-76SF00098.

Table 2-1.
Morphology and crystallography of lath martensite and bainite in Fe/Cr/Mn/C steels. (XBL 871-132)

Feature	Martensite	Bainite	
		Lower	Upper
Laths in Packets	high dislocation density laths	dislocated laths	dislocated laths
	dislocation density decreases ---------→		
Common Direction	lath faces $\langle 110 \rangle_M$	lath faces $\langle 110 \rangle_B$	irregular
Interlath Region	continuous retained austenite (quenched) or stringers of M_3C (TME)	non-continuous retained austenite (short isothermal) or carbides (long isothermal)	some retained austenite, but mostly carbides as in TME*
A/F Interface	C enriched	some C enrichement	probably none
Austenite Stability	can be very stable	not very stable	not very stable
Interface plane	$(110)_M // (111)_A$	$(110)_B // (111)_A$	---
A/F orientation relationships	K-S to G-T to N-W	K-S to G-T to N-W	---
Twin Relation of Laths	$(110)_M$ plane	$(112)_F$ plane	not observed
A/F microscopic habit	$(111)_A$	$(111)_A$	inferred
Carbides and Orientation Relationship	Widmanstatten	unidirectional	at boundaries
	Bagaryatskii $(110)_M // (100)_C$ $(111)_M // (010)_C$ $(112)_M // (001)_C$	Isaichev $(111)_B // (010)_C$ $(011)_B // (103)_C$	---
Mechanism of Transformation	shear + interface C diffn and autotempered carbide pptn	shear + C diffusion interlath carbide precipitation	shear + C diffusion interlath carbides

* TME means tempered martensite embrittled condition (27)

†Present address: Materials Science and Engineering, University of Washington, Seattle, WA.

‡Present address: Japan Steel Works, Toyko.

3. Microstructure, Mechanical Properties, and Wear of Fe-3Cr-0.4C Steels (Publication 16)

Y.S. Yoon and G. Thomas

The structure-property relationships of an ultrahigh-strength steel with a chemical composition that is based on Fe-3Cr-0.4C are described. The microstructure, which consists of dislocated lath martensite containing fine carbides and interlath thin films of retained austenite, was found to give combinations of mechanical properties and abrasion resistance that are attractive in comparison to many commercial abrasive alloys. It was also shown that thermo-mechanical treatments can improve both toughness and abrasion resistance by attaining a fine grain size with finely dispersed alloy carbides when microalloying additions (Mo, V) are present.

4. Microstructure of Laser-Hardened Medium Carbon/Chromium Steels (Publication 30)

J. Kusinski† and G. Thomas

Research on the effect of heat treatment on microstructure and mechanical properties of Fe/Cr/C/X steels shows that improvements in toughness, with little or no change in strength, may be realized by proper design of a composite microstructure to achieve fine-grained martensite surrounded by stable austenite films.[1] Laser processing can be expected to modify the mechanical properties of these steels by structure refinement. Samples of Fe-9.85Cr-1Mn-0.5Al-0.20C–(10Cr) and Fe-3.11Cr-

Figure 4-1. Typical compound layer of 3Cr steel after LHT2. SMZ: shallow-melted zone; HAZ: heat-affected zone; TZ: tempered zone. (XBB 862-950)

1.98Mn-0.5Mo-0.26C steels after conventional hardening were laser heat-treated (LHT) by a 1250-kW CO_2 laser, at different velocities (see Figure 4-1). TEM investigations show the structure of the as-melted zones as cellular, consisting of ultrafine, internally twinned martensite surrounded by retained austenite films. The large, primary forming martensite plates were able to cross several cellular crystals (see Figure 4-2 a,b). EDX analysis indicated a higher chromium concentration in such areas compared to the cell centers. Delta-ferrite was present in the 10Cr steel, at the boundary between the melted and heat-affected zones. No significant differences were observed between microstructures of the laser-heated and heat-affected zones of these two steels. The martensitic laths are ultrafine, dislocated with internal microtwinning and surrounded by the retained austenite films (see Figure 4-2 c,d), giving the desired surface structure refinement and consequent improved wear resistance.

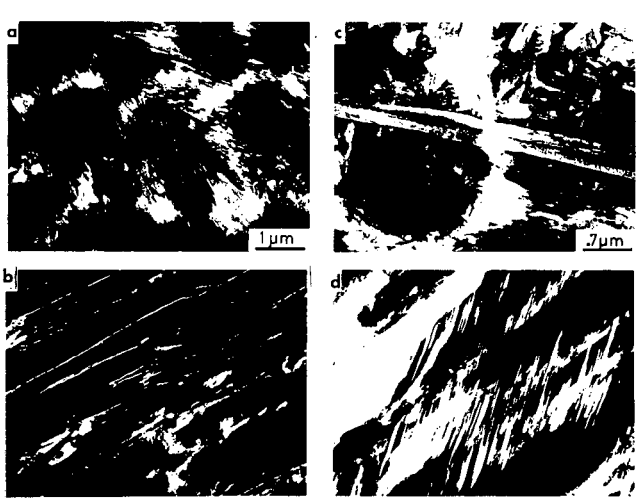

Figure 4-2. TEM microstructures of 3Cr steel after LHT1: (a), (b) microstructure of melted zone; (c) dark-field image of (022) austenite surrounding dislocated lath martensite; (d) dark-field image of $(110)_m$ showing microtwinning in martensite. (XBB 862-957)

†Present address: University of Mining and Metallurgy, Cracow, Poland.

1. G. Thomas, Int. Conf. on Recent Development in Specialty Steels and Hard Materials, Pretoria, South Africa, Nov. 1982, p. 55.

ELECTRONIC MATERIALS

5. The Role of Iron in Mn-Al-C Magnets (Publication 31)

J.S. Gau† and G. Thomas

Extruded Mn-Al-C alloys with the energy product ~(B.H) Max 5–8 MG OE have been developed as low-cost, non-Co-base permanent magnets. In this study, a Matsushita-made 13% Fe-containing Mn-Al-C magnet was examined using microanalysis techniques in both transmission electron microscopy and Mossbauer spectroscopy. This materials consists of a mixture of α-Mn and tetragonal magnetic τ phase containing all the Fe-solute atoms. Mossbauer spectra taken at both room temperature and 4 K reveal a single resonance line, which is, in fact, superimposed by two simple Lorentz-type isomer-shift resonance lines. These results indicate Fe ions to be located at both Mn and Al atomic sites and to carry no magnetic moment.

†Present address: MPI, Minneapolis, MN.

6. Microstructure of Fe-didymium-B Magnets (Publications 1 and 4)

R. Ramesh, J. Chen, K.M. Krishnan, E. Goo, M. Okada, M. Homma, R.K. Mishra, and G. Thomas

A TEM study has been made to characterize the microstructure and composition of the phases in sintered Fe-didymium-B magnets. The main phase is the tetragonal $RE_2Fe_{14}B$ phase. In all samples examined, a triple-junction phase, which frequently extended into two-grain junctions, was observed with a lattice parameter of 5.24 Å and enriched in Ce, Pr, and Nd. The microanalysis of this intergranular phase is shown in Figures 6-1 and 6-2 for two alloys: Fe-32.5wt%[80%Nd-15%Pr-5%Ce]-1wt%B, and Fe-32wt%Nd-1.4wt%B. Microdiffraction proves this phase is fcc and is probably stabilized by oxygen. This phase is probably responsible for magnetic hardening by domain-wall pinning.

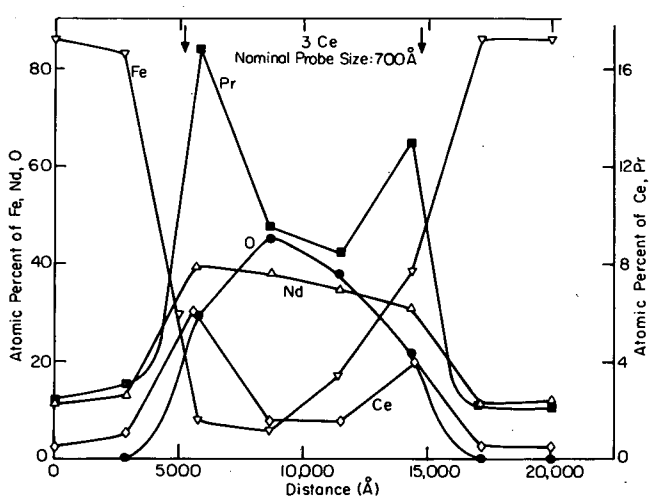

Figure 6-1. Composition profile across the triple grain junction for a [Ce-Pr-Nd]-Ne-B alloy. (XBL 8510-6757)

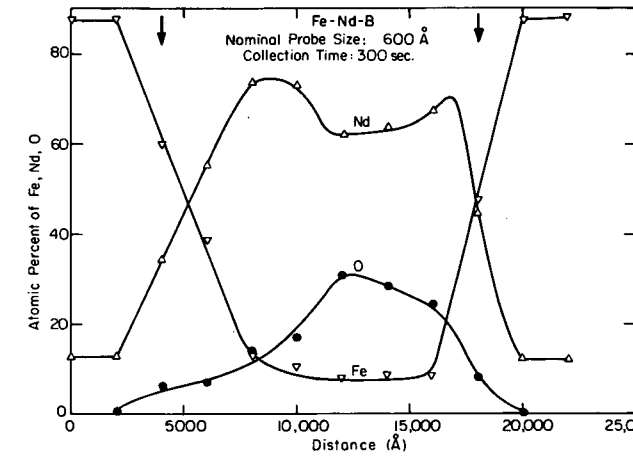

Figure 6-2. Composition profile across the triple grain junction for a ternary Nd-Fe-B alloy. (XBL 8510-6756)

7. Controlled-Atmosphere Annealing of High-Permeability Manganese Zinc Ferrite (Publication 8)

I-N. Lin,[†] R.K. Mishra,[‡] and G. Thomas

The annealing of sintered $(MnZn)Fe_2O_4$ in a controlled atmosphere improves the apparent electrical resistivity through the reduction of the ferrous-ion content. The initial permeability, however, is degraded as a result of annealing. It is suggested that stringent control of the oxygen partial pressure at an earlier stage of processing rather than post-sintering annealing is necessary to raise the intrinsic electrical resistivity of the bulk materials by reducing the ferrous-ion concentration without affecting the magnetic permeability detrimentally.

[†]Present address: Institute of Nuclear Energy Research, Taipei, Republic of China.

[‡]Present address: General Motors Research Laboratory, Warren, MI 48090.

8. Electron Microscopy Characterization of Lead Zirconate Titanate Ceramics at the Morphotropic Phase Boundary Composition (Publication 18)

M.L.A. Dass, U. Dahmen, and G. Thomas

Lead zirconate titanate (PZT) ceramics exhibit excellent dielectric and peizoelectric properties at the morphotropic phase-boundary (MPB) composition, and it is believed that this is due to the coexistence of both tetragonal (T) and rhombohedral (R) phases resulting in easy poling.[1] However, there is no direct evidence to substantiate this belief.

In the present study the structure and chemical composition of PZT ceramics prepared by conventional ceramic processing has been analyzed by electron microscopy. Lattice parameters obtained from x-ray diffraction indicate that the T and R phases are only very slightly distorted from cubic symmetry at the MPB composition. Convergent-beam electron diffraction (CBED) has been used to analyze the structure at the MPB composition using the fact that the symmetry of the CBED pattern is sensitive to the point group of the space lattice rather than the lattice parameters. Examples are given in Figures 8-1 and 8-2.

1. R.E. Newham, in *Phase Diagrams, Materials Science and Technology*, Vol. 5, A.M. Alper, Ed., 1978, p. 45.

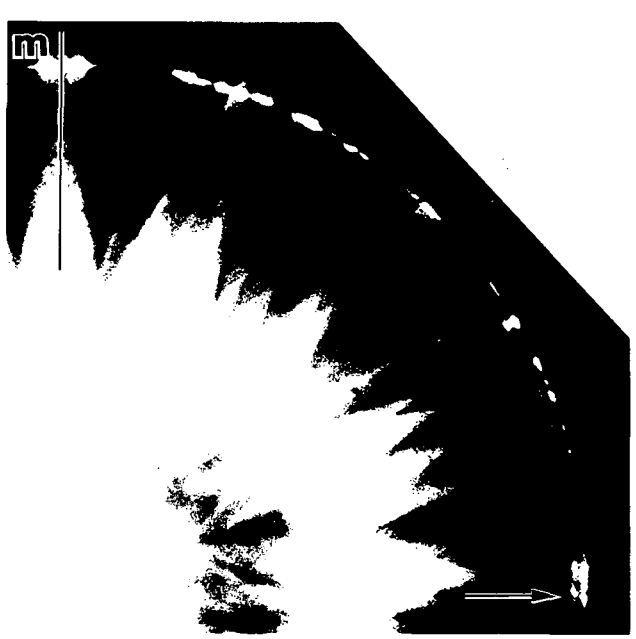

Figure 8-1. Parts of <001> ZAPz obtained from T phase. (XBB 866-4512)

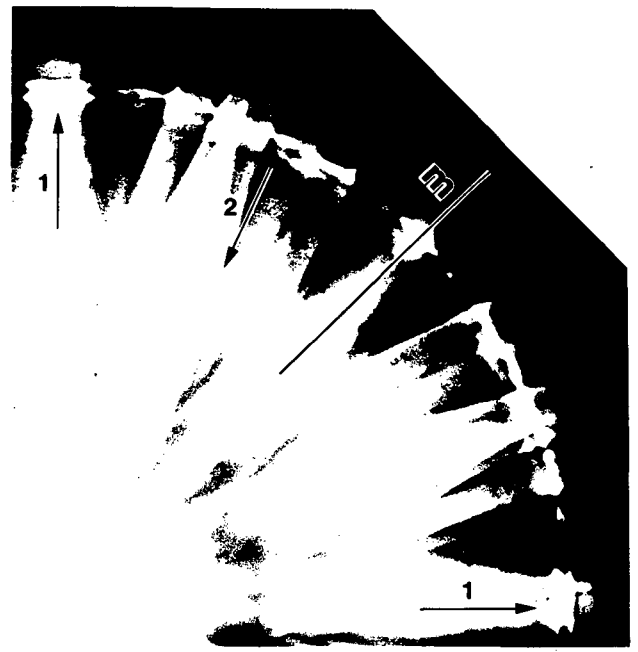

Figure 8-2. R phase of <001> ZAPz showing an inner ring. (XBB 866-4513)

9. Design of Low-Carbon Dual-Phase Steels for High-Strength Wire (Publication 51)

J.H. Ahn and G. Thomas

Dual-phase steels of composition Fe-2%Si-0.1%C have been developed according to design guidelines for optimum cold drawing. This steel can be continuously drawn from rods to strength levels found in commercial high-carbon pearlitic wires without any intermediate patenting treatments during the drawing process. This means potential reduction of production costs and operation complexity.[1] The attractive properties found in the silicon-containing dual-phase steel are attributed to the fine, fibrous, and disconnected lath martensite particles in a fine-grained ferrite matrix.

1. U.S. Patent No. 4,619,714, Oct. 1986, "Controlled Rolling Process for Dual-Phase Steels and Application to Rod, Wire, Sheet and Other Shapes."

10. Work in Progress

Steels

The increasing interest in microalloying promoted a study of the effects small amounts of Nb

(0.03 wt%) on the transformation characteristics, microstructure, and properties of composite martensite-austenite steels at 0.25% C. The CCT diagrams for the steel with and without Nb have been determined, and current research is concerned with the effects of controlled rolling and quenching (J. Kim† and G. Thomas).

The work-hardening characteristics of dual-phase ferrite–lath martensite Fe/Si/C steels with 0.05, 1, and 2 wt% C, respectively, have been determined. The strongest influence on work hardening is the carbon content of martensite. However, if the carbon exceeds 0.4 wt%, formability and toughness decrease due to transformation to twin-plate martensite. These steels have excellent fatigue-crack-growth resistance, and current work is concerned with fatigue behavior after hard drawing to wire (S. Miyasato,‡ R. Ritchie, and G. Thomas).

†Ph. D. Thesis research, sponsored by Pohang Iron and Steel Corp., Republic of Korea.
‡M.S. Thesis research.

Magnetic Materials

An oblique-incidence Co-Ni thin film is considered one of the most appropriate recording media for the next generation of video tape applications. In this study, the evolution of oblique-incidence Co-20%Ni thin films and the effect of deposition parameters on film evolution are being studied by transmission electron stereomicroscopy on thin films prepared with a shallow gradient. Microtome techniques have been developed in order to prepare specimens for electron microscopy (H.M. Ho† and G. Thomas).

Sendust consisting of 84–86 wt% Fe, 9–10 wt% Si, and 5–6 wt% Al exhibits excellent soft magnetic properties such as high magnetic flux density, high permeability, and low coercive force; therefore this alloy has attracted wide attention as recording-head material for high-coercivity recording media. The soft magnetic properties of this alloy, especially the ordering transformation, are known to be very sensitive to heat treatment and composition. The main objective of this research is to correlate the transformation structures with the magnetic properties, using transmission electron microscopy techniques. Materials studied have stoichiometric, iron-rich, and iron-deficient compositions, respectively. These materials are prepared by vacuum induction melting (J.D. Kim† and G. Thomas).

Co-Cr magnetic thin films for perpendicular recording have been investigated extensively for microstructure-magnetic property correlations. However, these correlations are not currently available for the bulk target alloys, and this lack of data serves as the motivation for the current investigation.

Homogenized and water-quenched bulk samples of $Ci_{1-x}Cr_x$ (x = 0.014 to 0.200) reveal a dramatic increase in the stacking-fault density as a function of Cr content, indicating a continuing decrease in stacking-fault energy.

Magnetic measurements on the quenched bulk alloys by vibrating sample magnetometer reveal that the in-plane coercivity is low and independent of fault density and, hence, composition. The role of stacking faults on the coercivity mechanism is still controversial; however, the very low coercivity over the entire composition range under investigation coupled with experimental evidence from Lorentz microscopy shows that stacking faults are not pinning sites for the domain walls but may serve as nucleation sites for reverse domains. Data on saturation magnetization, M_s, are consistent with those in the literature.

The magnetic anistropy field of the alloys decreases with Cr content. However, the bitter colloid technique for domain observation confirms that high anisotropy is present for compositions up to Co–15 at% Cr since such patterns are possible only for materials with anisotropies greater than 10^3erg/cm^3 (L.H. Chan‡).

†Ph.D. Thesis research.
‡M.S. Thesis research.

1986 PUBLICATIONS AND REPORTS

Refereed Journals

1. R. Ramesh, K.M. Krishnan, E. Goo, G.Thomas, M. Okada, and M. Homma, "Microstructure of Fe-Didymium-B Magnets," J. Magn. Mag. Mater. **54–57**, 563 (1986); LBL-19214.
2. G. Thomas, "Modern Electron Microscopy for Materials Characterization," J. Electron Microsc. Techn. **3**, 95 (1986); LBL-19705.†
3. H.M. Ho, E. Goo, and G. Thomas, "Crystal Structure of Acicular γ-Fe_2O_3 Particles Used in Recording Media," J. Appl. Phys. **59**, 1606 (1986); LBL-20040.
4. R.K. Mishra, J.K. Chen, and G.Thomas, "Effect of Annealing on the Microstructure of Sintered Nd-Fe-B Magnets," J. Appl. Phys., **59**, 2244 (1986); LBL-19839.
5. J.M. Rincon, G. Thomas, and J.S. Moya, "Microstructural Study of Sintered Mullite Obtained from Premullite," J. Am. Ceram. Soc. **69**, C-29 (1986).‡

6. K.M. Krishnan, P. Rez, G. Thomas, Y. Yokota, and H. Hashimoto, "The Combined Effect of Acceleration Voltage and Incident Beam Orientation on the Characteristic X-ray Production in Thin Crystals," Philos. Mag. B **53**, 339 (1986); LBL-18934.
7. J. Rincon, G. Thomas, P. Pena, S. De Aza, and J.S. Moya, "Reaction Sintered Zirconia-Mullite Composites with CaO," J. de Physique, Colloque C1 **47**, C1-423 (1986).†
8. I-N. Lin, R.K. Mishra, and G. Thomas, "Controlled Atmosphere Annealing of High-Permeability Manganese Zinc Ferrite," IEEE Trans. Magn., Mag. **22**, 175 (1986); LBL-20140.
9. E. Goo, T. Yamamoto, and K. Okazaki, "Microstructure of Lead-Magnesium Niobate Ceramics," J. Am. Ceram. Soc. **69**, C-188 (1986); LBL-18666.
10. R.H.G. Rau, T.Y. Lin, P.Y. Chow, and G. Thomas, "High Strength, High Ductility Dual Phase Steel Rebars and Prestressing Tendons for Concrete Structures," Our World in Concrete and Structures **V**, 336 (1986); LBL-22336.
11. G. Thomas, "Some Applications of Electron Microscopy in Materials Science," Ultramicrosc. **20**, 239 (1986).
12. J.A. Wazynczuk, R.M. Fisher, and G. Thomas, "Effects of Copper on Proeutectoid Cementite Precipitation," Metall. Trans. A **17A**, 2163 (1986); LBL-21032.

Other Publications

13. G. Thomas, "Characterization of Inorganic Materials," in *Proc. XIth Int. Cong. on Electron Microsc.*, Kyoto, Japan, Sept. 1986, p. 1019; LBL-21332.‡
14. R.S. Rai, T.R. Dinger, and G. Thomas, "High Resolution Electron Microscopy Studies of Y-Si-Al-O-N Glass-Ceramics," ACS Annual Meeting, Chicago, IL, April 27–May 1, 1986; LBL-20607abs.
15. G. Thomas, "Design of Low Carbon Dual Phase Steels for Bars and Wire Rods," in *Mechanical Properties and Phase Transformations in Engineering Materials*, S.D. Antolovich, R.O. Ritchie, and W.W. Gerberich, eds., 1986, p. 147; LBL-20482.
16. Y. Yoon and G. Thomas, "Microstructure, Mechanical Properties and Wear of Fe-3Cr-0.4C Steels," International Symposium on the Plasticity and Resistance to Metal Deformation, Herceg Novi, Yugoslavia, April 1986, p. 64; LBL-18623.
17. T.Y. Lin, P.Y. Chow, G. Thomas, and R.H.G. Rau, "New Developments in High Strength and High Ductility Reinforcing Bars and Prestressing Tendons," Tenth International Congress of the FIP, 1986, p. 24 LBL-22479.
18. M.L.A. Dass, T. Bielicki, G. Thomas, T. Yamamoto, and K. Okazaki, "Microstructural Observations on Lead Zirconate Titanate Ceramics," ACS Annual Meeting, Chicago, IL, April 27–May 1, 1986; LBL-20608abs.
19. K. Srikrishna, G. Thomas, and J.S. Moya, "The Role of Titania in the Microstructural Evolution of Mullite/Zirconia Composites," ACS Annual Meeting, Chicago, IL, April 27–May 1, 1986.†
20. T.A. Bielicki, G. Thomas, and J.S. Moya, "CBED Investigations of Strains in the Microstructure of Mullite/Zirconia Ceramics," ACS Annual Meeting, Chicago, IL, April 27–May 1, 1986.†
21. J. Kusinski and G. Thomas, "Effect of Laser Hardening on Microstructure and Wear Resistance in Medium Carbon/Chromium Steels," in *Laser Processing: Fundamentals, Applications, and Systems Engineering*, SPIE, Bellingham, WA, 1986, p. 150; LBL-21418.
22. T.R. Dinger and G. Thomas, "Crystallization Sequence of an AlN-Y_2O_3-SiO_2 Glass Ceramic," in *Proc. 44th Annual Meeting EMSA*, G.W. Bailey, Ed., San Francisco Press, 1986, p. 446.§
23. R.S. Rai, T.R. Dinger, and G. Thomas, "TEM Studies of Partially Crystallized Y-Si-Al-O-N Glasses," in *Proc. 44th Annual Meeting EMSA*, G.W. Bailey, Ed., San Francisco Press, 1986, p. 444.†
24. H.M. Ho and G. Thomas, "Structure Determination of γ-Fe_2O_3 Particles," in *Proc. 44th Annual Meeting EMSA*, G.W. Bailey, Ed., San Francisco Press, 1986, p. 476; LBL-22285abs.
25. M.L.A. Dass, T.A. Bielicki, G. Thomas, T. Yamamoto, and K. Okazaki, "Convergent Beam Diffraction Studies on Lead Zirconate Titanate Ceramics," in *Proc. 44th Annual Meeting EMSA*, G.W. Bailey, Ed., San Francisco Press, 1986, p. 482; LBL-22475.
26. J. Kusinski, T.A. Bielicki, and G. Thomas, "Structure and Microanalysis of Laser-Melted T1 High-Speed Tool Steel," in *Proc. 44th Annual Meeting EMSA*, G.W. Bailey, Ed., San Francisco Press, 1986, p. 574; LBL-22284.
27. R. Ramesh, T.A. Bielicki, and G. Thomas, "Microanalytical Investigation of Sintered Fe-Nb-B Magnets," in *Proc. 44th Annual Meeting EMSA*, G.W. Bailey, Ed., San Francisco Press, 1986, p. 824; LBL-22286.
28. T.A. Bielicki and G. Thomas, "Microanalytical Investigations of Ordering in Y_2O_3-Doped Tetragonal Zirconia Polycrystals," in *Proc. 44th Annual Meeting EMSA*, G.W. Bailey, Ed., San Francisco Press, 1986, p. 502.†
29. K. Srikrishna, G. Thomas, and J.S. Moya, "AEM Investigation of the Noncrystalline Phase in a Mullite/Zirconia/Titania Composite," in *Proc. 44th Annual Meeting EMSA*, G.W. Bailey, Ed., San Francisco Press, 1986, p. 450.†
30. J. Kusinski and G. Thomas, "Microstructure of Laser Hardened Medium Carbon/Chromium Steels," in *Proc. 44th Annual Meeting EMSA*, G.W. Bailey, Ed., San Francisco Press, 1986, p. 572; LBL-22283.
31. J.S. Gau and G. Thomas, "The Role of Iron in Mn-Al-C Magnets," in *Proc. TMS/AIME Meeting*, Orlando, FL, Oct. 5–9, 1986; LBL-21307abs.
32. K.M. Krishnan and G. Thomas, "Determination of Specific Site Occupation in Crystalline Magnetic Materials by Channeling Enchanced Microanalysis,

A Review," in *Proc. TMS/AIME Meeting*, Orlando, FL, Oct. 5–9, 1986; LBL-21324abs.

33. R.S. Rai, T.R. Dinger, and G. Thomas, "Structural Characterization of Crystalline Phases in Y-Si-Al-O-N Glass Ceramics by High Electron Microscopy," 39th Pacific Coastal Meeting, ACS, Seattle, WA, October 1986.‡
34. K. Srikrishna and G. Thomas, "Microstructural Characterization of Mullite/Zirconia Composites," 39th Pacific Coastal Meeting, ACS, Seattle, WA, October 1986.‡
35. M.L.A. Dass, G. Thomas, T. Yamamoto, and K. Okazaki, "Microstructure and Microanalysis of PZT Ceramics," 39th Pacific Coastal Meeting, ACS, Seattle, WA, October 1986; LBL-21784abs.
36. R.S. Rai, M.A. O'Keefe, and G. Thomas, "Structure Imaging and Defects in Crystallized Oxynitride Glasses," MRS Fall Symposium, Boston, MA, Dec. 1–6, 1986; LBL-21754abs.
37. J.M. Rincon, T. Dinger, J.S. Moya, and T. Osendi, "Microstructure of Mullite/Al_2O_3/ZrO_2 Tough Ceramic Composites," Acta Metall. (in press).†
38. K. Srikrishna, G. Thomas, and J.S. Moya, "Analytical Electron Microscopy of the Glassy Phase in Mullite/Zirconia Composites," in *Ceramic Microstructures '86: Role of Interfaces*, University of California Berkeley, July 28–31, 1986 (in press).†
39. K. Srikrishna, G. Thomas, and J.S. Moya, "Sintering Additives for Mullite/Zirconia Composites," in *Zirconia '86*, Toyko, Japan, Sept. 9–11, 1986 (in press).†

LBL Reports

40. G. Thomas, "Design of Strong, Ductile, HSLA and Dual Phase Steels," in *Proc. First US-Indo Workshop on Iron and Technology*, Ranchi, India, 1986 (in press); LBL-21303.
41. G. Thomas, "Design of Dual Phase Steels for Bars and Rods," in *Int. Symp. on Microalloying and New Processing Approaches for Bar and Forging Steels*, Golden, CO, July 1986 (in press); LBL-21663.
42. M. Sarikaya, H. Tokushige, and G. Thomas, "Lath Martensite and Bainite in Low Alloys Steels," in *ICOMAT'86 Conf.*, Nara, Japan, August 26–30, 1986 (in press); LBL-21794.
43. M.L.A. Dass, U. Dahmen, G. Thomas, T. Yamamoto, and K. Okazaki "Electron Microscopy Characterization of Lead Zirconate Titanate Ceramics at the Morphotropic Phase Boundary Composition," in *Proc. IEEE Int. Symp. on Application of Ferroelectrics*, Lehigh University, PA, June 8–11, 1986 (in press); LBL-20955.
44. R. Ramesh, J.K. Chen, and G. Thomas, "On the Grain Boundary Phase in Iron–Rare Earth–Boron Magnets," J. Appl. Phys. (in press); LBL-20698.
45. G. Thomas, "Grain Boundaries and Interfaces: Some Applications of Electron Microscopy and Microanalysis," in *Ceramic Microstructures '86: Role of Interfaces*, University of California Berkeley, July 28–31, 1986 (in press); LBL-22368.
46. T.A. Bielicki, U. Dahmen, G. Thomas, and K.H. Westmacott, "TEM Investigation of Orthorhombic-Type Phases in Stabilized Zirconcias," in *Zirconia '86*, Tokyo, Japan, Sept. 9–11, 1986 (in press); LBL-22367.
47. R. Ramesh and G. Thomas, "High Voltage Lorentz EM of Fe-Nd-B Magnets," LBL-21746.
48. J. Ulan, E. Kuo, W. Maier, R.S. Rai, and G. Thomas, "The Effect of Lead Acetate in the Preparation of the Lindlar Catalyst," J. Organic Chem. (in press); LBL-21980.
49. B.G. Demczyk and G. Thomas, "Transmission Electron Microscopy Investigation of Ferroelectric Domains in Lanthanum-Modified Lead Titanate Ceramics," submitted to J. Am. Ceram. Soc.; LBL-22298.
50. Y. Yamamoto, K. Okazaki, E. Goo, and G. Thomas, "Microstructure of Lead Titanate Ceramics modified by Alkaline Earth Elements," LBL-21000.
51. J. Ahn (Ph.D. Thesis), "Design of Low-Carbon Dual-Phase Steels for High-Strength Wire," LBL-22591.

Invited Talks

52. G. Thomas, "Microstructure Composite Design for New Steels," First US-India Symposium on Steels, Steel Authority of India, Ltd., Ranchi, India, Jan. 10, 1986.
53. G. Thomas, "Applications of Contemporary Electron Microscopy" and "A Viewpoint of Electron Microscopy in Materials," Stanford University Symposium, Stanford, CA, March 19, 1986.
54. G. Thomas, "Refractories and New Structural Ceramics," Central Institute for Iron and Steel Research, Beijing, Peoples Republic of China, April 1986.
55. G. Thomas, "Alloy Design of Structural Steels," IRSID, Paris, France, May 1986.
56. G. Thomas, "Design of Composite Microstructures for Improved Mechanical Properties of Steels," Boris Kidric Steel, Montenegro Met. Society, Niksic, Yugoslavia, June 1986.
57. G. Thomas, "New Process of Production of Simple Steel for Wire Rods," BSE, Kehl, Federal Republic of Germany, June 1986.
58. G. Thomas, "New Steels for Bars and Long Products," International Conference on Steel, Colorado State University, Golden, CO, July 1986.
59. G. Thomas, "Characterization of Inorganic Materials," North Carolina State University, Raleigh, Oct. 10, 1986.
60. G. Thomas, "The National Center for Electron Microscopy" and "Electronic Microscopy Research on Magnetic Materials," Eastman Kodak Co., San Diego, CA, Oct. 24, 1986.
61. G. Thomas, "Characterization of Interfaces and Grain Boundaries in Ceramics," Ceramic Micro-

structures '86: Role of Interfaces, University of California Berkeley, July 1986.
62. G. Thomas, "Grain Boundaries and Intragranular Phases in Ceramics," Symposium on Ceramics, EMSA, Albuquerque, NM, Aug. 1986.
63. G. Thomas, "High Voltage, High Resolution Electron Microscopy," International Congress on Electron Microscopy, Kyoto, Japan, Sept. 1986.

†Research on zirconia systems sponsored by The National Science Foundation (NSF) under Contract No. DMR 83-1317239.

‡This work supported by NSF under Contract No. DMR 83-1317239.

§Supported by NSF under Contract No. DMR 83-1317239. Supplemental support was provided by the Atlantic Richfield Foundation.

Solid-State Phase-Transformation Mechanisms*

Kenneth H. Westmacott, Investigator

INTRODUCTION

This research is directed towards understanding in detail the structural factors that govern phase changes and phase stability. From such knowledge first-principles alloy design for specific service applications is possible. A variety of electron-optical techniques, especially high-voltage electron microscopy (HVEM) and high-resolution electron microscopy, is used to infer the atomic rearrangements that occur when a product phase precipitates from the parent matrix. Since accommodation of a new phase of disparate size or crystal structure must involve deformation, the role of lattice defects in transformations is a focus of this work. This approach has been successful in identifying the specific defects associated with several classes of transformations characterized by different transformation strains. It has been possible to predict precipitate morphologies (growth directions, habit planes, orientation relationships, etc.) from first principles for several model alloy systems.

Extension of the principles to more complex alloys will contribute both to understanding alloy stability in severe operating conditions and to designing improved materials.

1. A TEM Study of $\alpha''Fe_{16}N_2$ and γ'-Fe_4N Precipitation in Iron-Nitrogen (Publication 10)

U. Dahmen, P. Ferguson,† and K.H. Westmacott

Precipitation of α''-$Fe_{16}N_2$ and γ'-Fe_4N in thin foil and bulk-aged nitrogen-ferrite was studied by *in situ* HVEM and conventional TEM techniques. Detailed analyses of the precipitate morphology, symmetry, and internal fine structure have led to an improved understanding of the factors controlling the growth habits. The observed habit planes and orientation relationships for both types of precipitate are in good agreement with theoretical predictions.

Evidence for various modes of strain accommodation was found, including formation of polytypes in the γ' phase (see Figure 1-1) and formation of groups of self-accommodating variants of both α'' and γ' particles.

*This work was supported by the Director, Office of Energy Research, Office of Basic Energy Sciences, Materials Sciences Division of the U.S. Department of Energy under Contract No. DE-AC03-76SF00098.

†Present address: Cookson Group, Wallsend, United Kingdom.

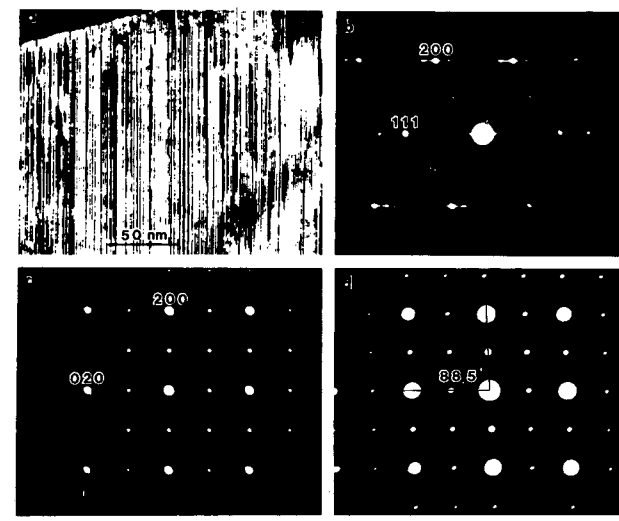

Figure 1-1. (a) Dark-field image of periodically faulted extracted γ' plate and (b) corresponding [011] pattern. Extra spots at 1/6 111 positions and the splitting of the 100 superlattice spot (see arrows) indicate formation of 18H polytype related to cubic γ' by a shear of 0.12 (see lines). (c) [001] pattern from an unfaulted and (d) from a periodically faulted γ' plate. The distortion due to polytype formation is apparent in (d). (XBB 864-3432)

2. High-Resolution Observations of Pentagonally Twinned Precipitate Needles in Aluminum (Publication 2)

U. Dahmen and K.H. Westmacott

Unusual pentagonally twinned precipitates were observed in a high-resolution transmission electron microscopy study of needle-shaped germanium particles in aluminum. In the example shown in Figure 2-1 (taken on the NCEM Atomic Resolution Microscope), the electron beam has been aligned along the needle axis. It is seen that the <100> axis of the aluminum matrix is exactly parallel to a <110> axis of the germanium precipitate. The precipitate mirror plane and 2-fold axis are indicated,

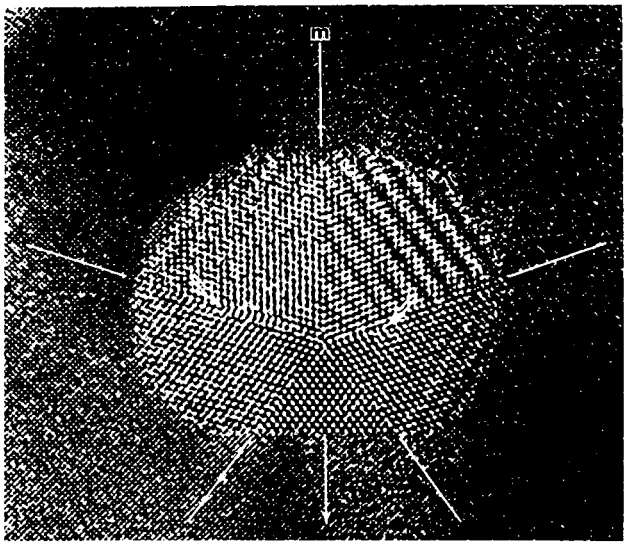

Figure 2-1. High-resolution micrograph of pentagonally twinned Ge precipitate in Al matrix. Specimen water-quenched from 540°C and aged one hour at 240°C. (XBB 864-2117)

and the extra planes required to fill the close failure of a 5-fold twin in the diamond-cubic structure are arrowed.

3. Microstructural Changes in (Mg) PSZ During Aging at 1000°C (Publication 13)

K.H. Westmacott, A. Thorel,† D. Broussaud,† and J.Y. Laval†

A (Mg) partially stabilized zirconia (PSZ) aged for various times at 1000°C has been characterized by transmission electron microscopy and correlated with earlier fracture-property measurements. The most important microstructural features in terms of explaining an observed deterioration in both rupture strength and fracture toughness are a grain boundary phase (0) rich in Mg and Si with orthorhombic crystal structure (probably an olivine) and a glassy phase that progressively precipitates preferentially at interphase interfaces. A loss in rupture strength is attributed to formation of a glassy film on the boundaries between the (0) phase and the ZrO_2 matrix (see Figure 3-1). Similarly, the development of a continuous glassy film at the interfaces between

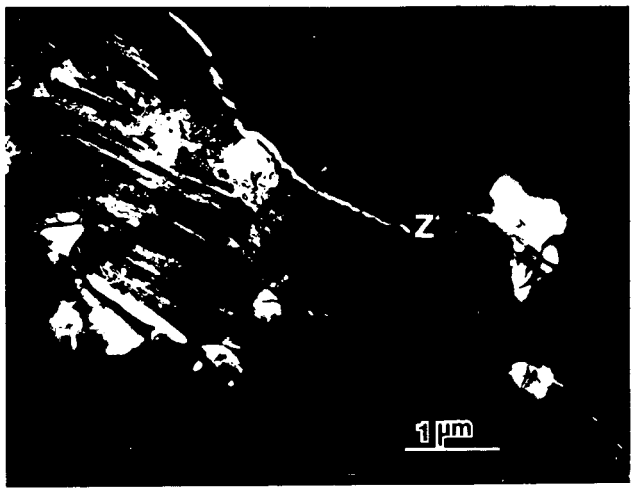

Figure 3-1. A propagating crack, Z, in a (Mg) PSZ specimen aged at 1000°C for 100 hours is observed to follow a path that links up the (0) grains (light phase). (XBB 864-3481)

monoclinic particles and the matrix can account for the decrease in fracture toughness. Results obtained by conventional imaging, high-resolution, and analytical electron microscopy support these conclusions.

---

†Permanent address: Laboratoire d'Étude et de Synthèse des Microstructures CNRS-ESPCI, 10, rue Vauquelin, 75231 Paris, France.

1986 PUBLICATIONS AND REPORTS

Refereed Journals

1. U. Dahmen and K.H. Westmacott, "A Simple Model for the Prediction of Coherent and Semicoherent Plate Precipitate Habit Planes," Acta Metall. **34**, 475 (1986); LBL-19442.
2. U. Dahmen and K.H. Westmacott, "Observations of Pentagonally-Twinned Precipitate Needles of Germanium in Aluminum," Science **233**, 875 (1986); LBL-21344.
3. J.B. Posthill, P. Hogwood, and D.V. Edmonds, "Precipitation at the Tungsten-Tungsten Interface in Tungsten-Nickel-Iron Heavy Alloys," Powder Metallurgy **29**, 45 (1986); LBL-19120.
4. P. Veyssiere and K.H. Westmacott, "*In-Situ* Observations of Partial Dislocation Climb in Ni_3Al," Philos. Mag. A **53**, 563 (1986); LBL-19464.

5. K.H. Westmacott, U. Dahmen, and M.J. Witcomb, "An HVEM Study of an Unusual Ordering Reaction in Platinum-Carbon," Metall. Trans. A **17A**, 807 (1986); LBL-19636.

Other Publications

6. U. Dahmen, C. Nelson, and K.H. Westmacott, "An Atomic Resolution Study of Precipitates in an Al-Ge Alloy," in *Proc. 44th Ann. Meeting EMSA*, 1986, p. 538; LBL-21287.

LBL Reports

7. K.H. Westmacott, U. Dahmen, A. Thorel, and J.Y. Laval, "Precipitation in a (Mg) Partially-Stabilized Zirconia During Aging at 1000°C," in *Ceramic Microstructures* '86: *Role of Interfaces*, University of California Berkeley, July 28–31, 1986 (in press); LBL-22140.
8. T.A. Bielicki, U. Dahmen, G. Thomas, and K.H. Westmacott, "TEM Investigation of Orthorhombic-Type Phases in Stabilized Zirconias," in *Proc. Zirconia '86*, Tokyo, Japan, September 9–11, 1986 (in press); LBL-22367.
9. U. Dahmen, "Phase Transformations, Crystallographic Aspects," in *Encyclopedia of Physical Science and Technology*, R.A. Meyers, Ed., Academic Press (in press); LBL-21423.
10. U. Dahmen, P. Ferguson, and K.H. Westmacott, "A TEM Study of $\alpha''Fe_{16}N_2$ and $\gamma'Fe_4N$ Precipitation in Iron-Nitrogen," Acta Metall. (in press); LBL-21441.
11. J. Howe, U. Dahmen, and R. Gronsky, "Atomic Mechanisms of Precipitate Plate Growth," submitted to Philos. Mag. A; LBL-21705.
12. K.H. Westmacott and U. Dahmen, "Recent TEM Studies of Precipitate Growth Mechanisms," Revue de Physique Appliquee (in press); LBL-21504.
13. K.H. Westmacott, A. Thorel, D. Broussaud, and J.Y. Laval, "Microstructural Changes in (Mg) PSZ During Aging at 1000°C," Ultramicrosc. (in press); LBL-21335.

Invited Talks

14. K.H. Westmacott, "Microstructural Changes in Partially-Stabilized Zirconia During 1000°C Aging," Frontiers in Electron Microscopy, Argonne National Laboratory, Batavia, IL, April 20–23, 1986.
15. K.H. Westmacott, *et al.*, "Mechanical Properties and Microstructural Characterization of Partially-Stabilized Zirconia," U.C. Berkeley/Grande Ecoles Conference, Berkeley, CA, May 21–23, 1986.
16. U. Dahmen *et al.*, "Precipitation in a (Mg) Partially-Stabilized Zirconia," International Symposium on Ceramic Microstructures '86, Berkeley, CA, July 1986.
17. P. Veyssiere and K.H. Westmacott, "*In situ* HVEM Studies of Climb-Dissociation of Dislocations in Ni_3Al," Micro '86, Cambridge, United Kingdom, July 5–8, 1986.
18. U. Dahmen *et al.*, "An Atomic Resolution Study of Precipitates in an Al-Ge Alloy," EMSA Meeting, Albuquerque, NM, 1986.
19. U. Dahmen, "TEM Studies of Carbide and Nitride Precipitation in Alloys," Sandia National Laboratory, Livermore, CA, Nov. 18, 1986.

National Center for Electron Microscopy*

Gareth Thomas, Ronald Gronsky, and Kenneth H. Westmacott, Investigators

INTRODUCTION

The National Center for Electron Microscopy (NCEM) provides state-of-the-art facilities for electron-optical characterization of materials. Its resident staff operate, maintain, design, and develop equipment and software, making it available to all Center users, and in addition conduct their own forefront research on problems in the materials sciences.

Central to NCEM are two unique high-voltage electron microscopes, a 1.5-MeV machine (the High-Voltage Electron Microscope, or HVEM), which is the most powerful in the U.S., and a 1-MeV machine (the Atomic Resolution Microscope, or ARM), which offers the best resolution in the world (better than 1.6 Å). These instruments are supported on special vibration-proof structures and are backed by a host of "feeder" microscopes (for specimen-screening, preliminary experiments, and complementary microanalysis), by specimen-preparation facilities, and by image processing and analysis facilities, all housed within the same building and completely dedicated to electron microscopy. This integrated approach to materials characterization makes NCEM popular with scientists from around the world.

Guidance is provided by a steering committee, chaired by J.J. Hren (North Carolina State University), and staffed by C.W. Allen (Argonne National Laboratory), J.M. Gibson (A.T.T.), D.G. Howitt (University of California, Davis), F. Ponce (Xerox Palo Alto Research Center), J. Barry (Arizona State University), L.E. Thomas (Westinghouse), T. Hayes (LBL), and the investigators on this project. Meetings are held twice per year.

Research on the HVEM covers a wide spectrum of projects, including phase-transformation studies in metals, ceramics, and minerals; semiconductor-device and amorphous-metal investigations; and biological and medical-science applications.

Full use of the microscopes continued during 1986. The average weekly usage was maintained at ~85%, with three 4-hour shifts per day. As in earlier years, about 25% of the outside users of the facilities were from industry, and 25% were from other universities and government laboratories. 20% of the HVEM users were from the biological sciences. At present, there are approximately 50 active projects under way.

During the year the performance and capabilities of the HVEM continued to be upgraded. A modification of the electronic circuits to the tilt coils has been made to allow users the option of employing hollow-cone illumination for imaging. A modified top entry stage with Z-height control is now available for Lorentz microscopy. An emergency air supply system, which will protect the microscope from mechanical damage in the event of loss of compressed air during a severe earthquake, is now installed.

The ARM remains the highest-performance instrument of its kind. Users are carefully screened to show need for its superior capabilities, and they now conduct research on a wide variety of materials problems by direct imaging of atomic structure. During 1986 the usage record was maintained at better than 80%. The remaining time was devoted to regular servicing essential for maintaining peak performance at the 0.16-nm, level. Very little time was lost for unscheduled repairs, and the reliability of the instrument is now well established. A number of achievements in ultrahigh-resolution imaging were made, and these are detailed later in this report.

The analytical microscope is fully utilized in support of Center research. Current projects on the instrument include standard analyses as well as the development and refinement of new techniques and software for quantification.

The NCEM computer system is designed to assist interpretation of electron microscope images in three ways: (1) real-time enhancement of live video-rate TV images from the electron microscopes under control of the microscope operator; (2) interactive *a posteriori* processing of stored experimental images at a work station hosted by the computer; and (3) matching experimental images to ones simulated from a proposed model structure at a work station controlled by the host computer, in order to confirm (or reject) the suitability of the model.

While the hardware for operation (1) is not yet installed, both operations (2) and (3) are now running and available for use by outside users at a two-station Gould IP8500 image processor controlled by the microVAX. For implementation of operation (3), a second microVAX is available to control sets of DataCube modules that will digitize a video image in real time, store it in memory, and average it over

*This work was supported by the Director, Office of Energy Research, Office of Basic Energy Sciences, Materials Sciences Division of the U.S. Department of Energy under Contract No. DE-AC03-76SF00098.

a (selected) time interval to improve the signal-to-noise ratio and display the enhanced image on the microscope operator's monitor. A small array processor (MCS ZIP3232) will provide background correction and the capability to present the operator with the diffractogram of the image.

1. Recent Transmission Electron Microscopy Applications (Publication 1)

D. Ackland, U. Dahmen, C.J. Echer, R. Kilaas, K.M. Krishnan, C. Nelson, M.A.O'Keefe, W. Smith, and J. Turner

This paper describes the conceptual basis for the systems design and new equipment integration at NCEM. Computer-aided image processing helps scientists develop better structural models that, in turn, help define new directions for improved image processing. Several examples are cited to demonstrate how improvements in experimental techniques, high voltage, high resolution, and microanalytical capabilities, combined with computer processing, impact on materials characterization.

A double-tilt, ambient-temperature straining stage with combined mechanical and piezoelectric drive is now available. It enables direct observation of slip propagation as the minitensile sample is strained at a controlled rate. Events can be recorded on video tape for detailed frame-by-frame analysis. An example of a straining sequence in a polycrystalline stainless steel sample from the work of Ohio State University researcher W.A.T. Clark is shown in Figure 1-1. In the first two frames (Figures 1-1 a and b), dislocation slip bands are seen to approach the boundary, causing an increasing stress concentration, which is made visible through strain-lobe contrast at two different pile-ups in Figure 1-1c. From observations such as these it is possible to deduce micromechanisms of slip propagation. When used in conjunction with a detailed contrast analysis it will be possible to determine the boundary orientation, dislocation Burgers vectors, line directions, and positions. These experimental parameters can be used to calculate the local stress field and to identify the fundamental mechanisms of slip propagation across grain boundaries.

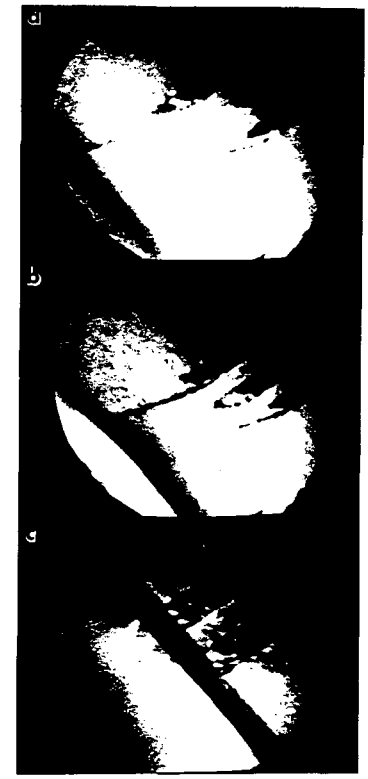

Figure 1-1. Sequence of micrographs showing pile-up of dislocations at a grain boundary in stainless steel. (XBB 8610-8556)

2. Channelling Enhanced Microanalysis: New Developments (Publications 7, 55, and 56)

K.M. Krishnan

A novel crystallographic technique to determine specific site occupations of elemental additions in crystalline materials has been formulated over the past few years. This technique, called channelling enhanced microanalysis, is based on the dependence of electron-induced characteristic x-ray emissions on the orientation of the incident electron beam. It involves no adjustable parameters, is applicable to trace-element concentrations (0.2–0.3 wt%, or 10^{20} atoms/cm^3), can distinguish neighbors in the periodic table, involves no external standards, and can be routinely performed at high spatial resolutions (~10–40 nm).

Recently, a systematic experimental study has been carried out to determine the effect of the

acceleration voltage as an independent parameter on the orientation dependence of characteristic x-ray production. An "inversion" voltage has been experimentally observed to occur at 270 kV for $MgAl_2O_4$, in agreement with earlier predictions. Further, this "inversion" voltage has been shown to be different from the conventional critical-voltage effect.

The role of the tangential component of parallelism of an electron beam in a conventional transmission electron microscope, where the specimen is immersed in a magnetic field, in performing such channelling experiments has also been investigated. The best results are not always obtained for the case of a probe convergent on the specimen surface, even when the convergence angle is less than the operating Bragg diffraction angle. A simple experiment to determine when this tangential component would be critical has been designed, and the results are shown in Figure 2-1.

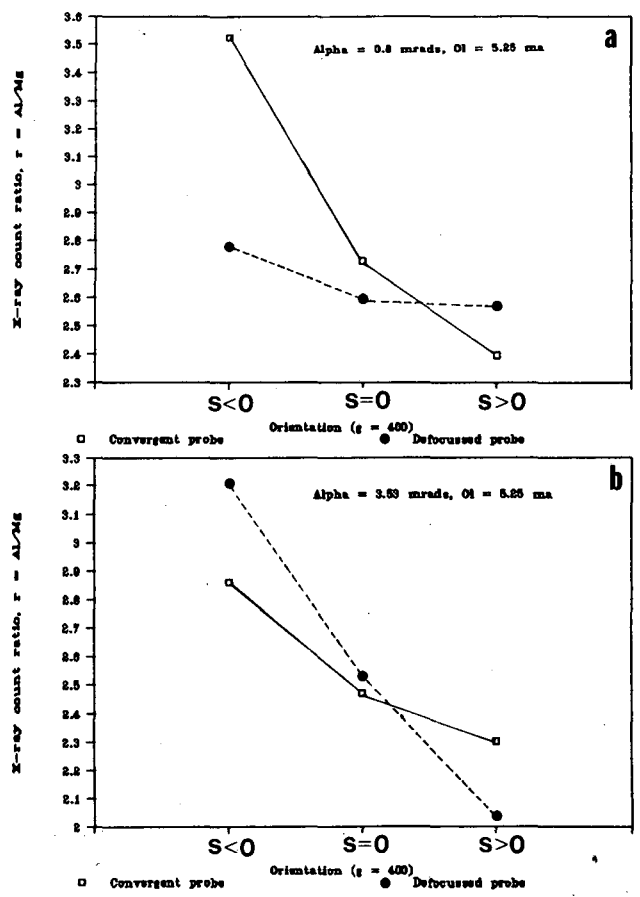

Figure 2-1. Effect of illumination (incident-probe conditions) on the orientation dependence of characteristic x-ray production: (a) small convergence angle (α = 0.8 mrad), which gives better results for the incident probe convergent (520 nm diameter) on the specimen surface; (b) larger convergence angle (α = 3.5 mrad), which gives better orientation dependence for a defocused probe (1300 nm diameter), giving rise to sharp diffraction spots in the back focal plane of the objective postfield. (XBL 8612-4827)

3. Microanalytical Electron Microscopy: Applications in Materials Research (Publications 5, 11, 39, and 44)

C. Echer and K.M. Krishnan

The incorporation of a fine-probe forming system in an electron microscope and the development of related spectroscopic and diffraction techniques has made it possible to obtain structural and chemical information from materials at high spatial resolutions. Two specific examples are given here of the applications of these microanalytical techniques, which include convergent-beam electron diffraction (CBED), energy-dispersive x-ray spectroscopy (EDXS), and electron-energy-loss spectroscopy (EELS), to materials research.

(1) The composition of the icosahedral phase in rapidly solidified alloys of Al-Mn has been determined at high spatial resolutions by EDXS using convergent probes of 200 nm diameter. For an alloy of starting composition 74.7 wt% Al–25.3 wt% Mn, the icosahedral phase was found to have a composition of 20.3 ± 2.0 at% Mn, balance Al, while the metastable matrix phase was found to contain 4.5 ± 0.4 at% Mn. However, more recent work shows that the morphology of the alloy as well as the composition of the icosahedral phase varies with the concentration of the molten alloy and the rate of solidification. Efforts to determine the metastable phase diagram for this and the Al-Ru systems are now in progress.

(2) The design of stable Ohmic and Schottky contacts to compound semiconductors is determined largely by the ability to predict the phase-formation sequence of a metal-semiconductor reaction at the contact interface. For the Ni-InP system three previously unreported ternary phases have been observed to be the primary products of the reaction. The first phase, amorphous Ni_xInP (x = 2.7), forms at the Ni/InP interface by a solid-state vitrification process at low temperatures (T<200°C). Amorphous Ni_xInP crystallizes at 300°C to form a hexagonal Ni_xInP phase (a_0 = 0.412 nm, c_0 = 0.483 nm) and at 500°C forms a monoclinic phase (a_0 = 0.681 nm, b_0 = 0.529 nm, c_0 = 1.28 nm, and β = 95°) with nominal composition Ni_2InP.

4. New Image-Simulation Software Development at the NCEM (Publication 51)

R. Kilaas

A new highly interactive and user-friendly software package for simulation and processing of high-resolution transmission electron micrographs has been developed at NCEM. Designed to be used by scientific visitors to the center, the software is completely menu-driven from a graphics terminal with a mouse and requires little or no computer knowledge for proper usage. Although the software is written to ensure maximum performance using hardware available to NCEM, the hardware-dependent code is kept in separate modules that are easily modified. The new software package combines an unparalleled ease of use with the latest theory in the field of simulation of high-resolution transmission electron micrographs.

5. An Improved Photographic Process for CBED Applications (Publication 62)

J.H. Turner and K.M. Krishnan

It is well recognized that the use of the conventional D-19 process to develop photographic negatives used in transmission electron microscopy for CBED applications suffers from two inherent limitations: the wide intensity range in the actual electron exposure and the narrow latitude of film development. Further, the exposure meters in commercial microscopes are unreliable for these applications.

The use of a surface developer, pyrocatechol, to process transmission electron microscope negatives has been shown to have significant advantages. The process that we have developed is tolerant of a large margin of error in the electron exposure, produces a negative that not only retains details both in the highlight as well as the faint regions but also preserves local contrast, is relatively easy to print, has a large development-time latitude, and can be developed under safe-light conditions. Improved acuteness and an enhanced signal-to-noise ratio due to prolonged exposures associated with this process have also been observed. Typical results using this process are shown in Figure 5-1.

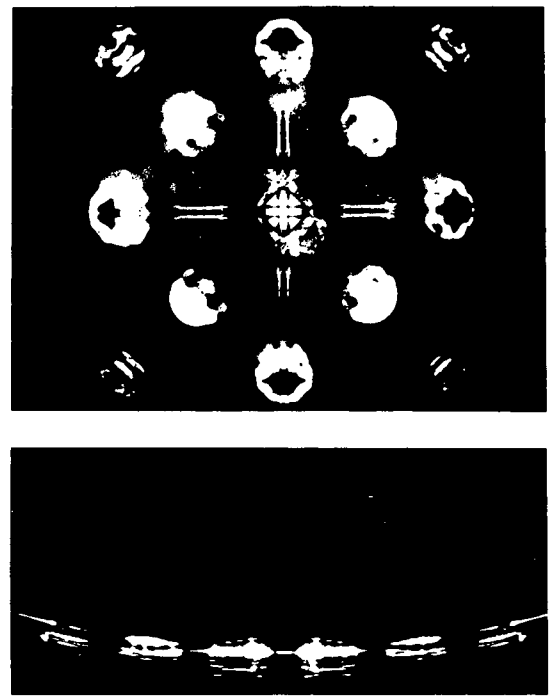

Figure 5-1. A [100] zone-axis pattern of $MgAl_2O_4$ obtained using the pyrocatechol developer. Details of the zero-order Laue zone and a segment of the first-order Laue zone, including the (1,21,1) and (1,21,1) reflections, are shown. Both these regions were printed from the same negative. (XBB 864-2943)

6. Precipitation in a (Mg) Partially Stabilized Zirconia (PSZ) During Aging at 1000°C (Publication 43)

K.H. Westmacott, U. Dahmen, A. Thorel,[†] and J.Y. Laval[‡]

A variety of grain-boundary phases found in a commercially supplied (Mg) PSZ were identified by microanalysis and CBED. The phases identified included Forsterite (Mg_2SiO_4), magnesium aluminate ($MgAl_2O_4$), and magnesia (MgO). Forsterite was also found in a purer research-grade material but in smaller volume fractions. A high-resolution study of interfaces in material aged to 1000°C showed the presence of thin glassy films. In the example shown in Figure 6-1, lattice fringes are clearly resolved in the two phases, but at the interface between them a thin layer of noncrystalline material is observed.

Figure 6-1. ARM image of a partially stabilized zirconia alloy aged at 1000°C. Note the thin film of a noncrystalline phase along the interphase interface. (XBB 8612-10255)

This supports an earlier suggestion that these films are responsible for a deterioration in fracture properties observed in aged material.

---

†Permanent address: Centre des Materiaux de l'Ecole Nationale et Superieure des Mines de Paris, BP 87, 91003 Evry Cedex, France.

‡Permanent address: Laboratoire d'Etude et de Synthese des Microstructures, CNRS-E.S.P.C.I., 75231, Paris Cedex 05, France.

7. Some HVEM Applications at the NCEM (Publication 61)

G. Thomas

The utilization of HVEM instruments for materials-research problems is now well established, especially for *in situ* dynamic experiments at high resolution to the atomic level. The facilities at NCEM are now being used for a wide range of projects by scientists from the USA and abroad. In this brief review mention is made of some examples of in-house research works, including studies of semiconductor interfaces, icosohedral phases, ceramics, and ferrous alloys. One of the main points to be emphasized is that HVEM should not be regarded as a "separate" field of electron microscopy but as complementary instrumentation to conventional and analytical instruments. Clearly the availability of an integrated laboratory allows the same specimens to be examined in different microscopes so that the particular advantages of each microscope can be used to obtain as complete a characterization of the material as is possible. However, more attention should be paid to equipping commercial HVEM instruments with analytical capabilities.

8. Structural Transformations in the Decomposition of $Mg(OH)_2$ and $MgCO_3$ (Publication 48)

M.G. Kim, U. Dahmen, and A.W. Searcy

A transmission electron microscopy study has been carried out to understand the structural transformation mechanism of decomposition of $Mg(OH)_2$ and $MgCO_3$ in vacuum. Both $Mg(OH)_2$ and $MgCO_3$ decompose topotactically to yield porous pseudomorphic MgO of normal structure with definite orientation relationships. The decomposition of $Mg(OH)_2$ yields MgO with a single orientation relationship, but that of $MgCO_3$ leads to one major and two minor orientation relationships with two, six, and three variants, respectively. The major orientation relationships in the formation of 2–3 nm cubic MgO particles are discussed in terms of a correlation between oxygen octahedra in the reactant solids. The small cubic MgO particles may aggregate spontaneously to reduce the excess surface energy and result in minute cracks. The decomposition of $Mg(OH)_2$ forms a continuous network of cracks of about 2 μm mesh size (see Figure 8-1a), while the decomposition of $MgCO_3$ shows the cracks to radiate from isolated centers (see Figure 8-1b).

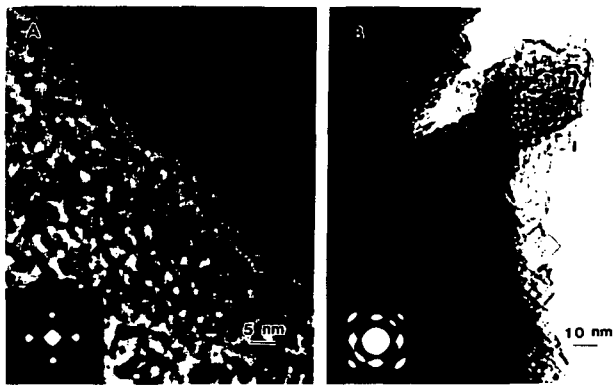

Figure 8-1. TEM micrographs of MgO produced from $Mg(OH)_2$ (A) and $MgCO_3$ (B). (XBB 867-5723)

9. The Surface Structure of Pt Crystallites Supported on Carbon Black (Publication 12)

M.L. Sattler and P.N. Ross

Using the high-resolution transmission electron microscopy techniques of weak-multibeam dark-field and direct-lattice imaging, platinum particles ranging in size from 0.8 to 50 nm were imaged and their surface structure characterized. Figure 9-1 gives an example of a high-resolution image of a 20-nm particle oriented toward [100] to show dominant (110) surface planes. The platinum crystallites were evaluated for specific catalytic activity with respect to crystallite size. It was found that the rate of electrochemical oxygen reduction decreased for catalysts having a particle size of less than 3.5 nm. We suggest that the dominating (111) surfaces and rough (110) regions on these small particles are less active than (100) and (100) vicinal planes.

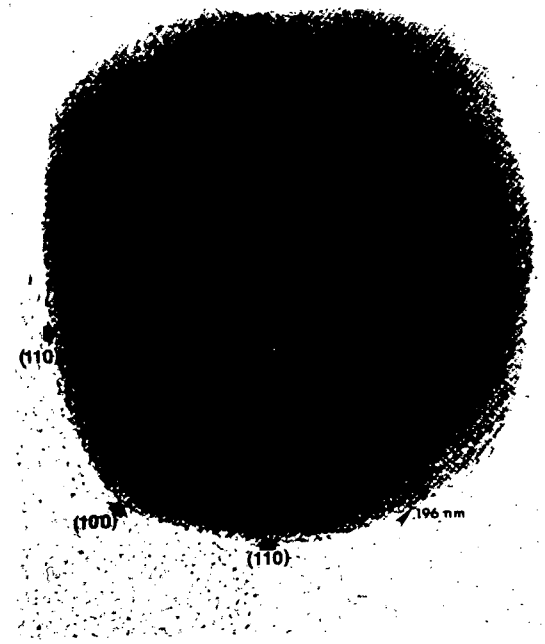

Figure 9-1. High-resolution image of a Pt particle oriented toward the (400) zone, showing a 1.96-Å separation between (100) planes. The particle is typical of catalyst particles of this type having rough (110) surfaces. (XBB 871-118)

10. Identification of Phases and Surfaces in Small TiO_2 Catalyst Particles using High-Resolution Electron Microscopy/Spectroscopy Techniques (Publication 59)

M.L. Sattler, M.G. Reichmann, and A.T. Bell

Crystalline TiO_2 particles on amorphous SiO_2 support were prepared under strict conditions so that they contained specific phases of anatase, rutile,

and/or TiO_2(B). The sizes of these particles were determined by electron-microscopy measurements to be between 2 and 10 nm in diameter, while the thickness of the support was estimated to be 50 nm. The different phases of TiO_2 particles were identified from lattice images obtained of the catalyst materials by high-resolution electron microscopy. From these images individual TiO_2 particles were isolated; optical-diffraction patterns were thus obtained from a statistically significant number of particles and were carefully measured to determine the d-spacings of the lattice fringes. Using this information, surface habit planes were identified from their relationship with the resolved lattice planes. Typically, the anatase particles tended to orient themselves so that the [111] zone was imaged and relatively large (101) and (004) planes dominated the surfaces. The particles having phases of TiO_2(B) and rutile were not so numerous or predictable. Corroboration of this technique for phase/surface plane identification was produced by computer image processing of the digitized high-resolution images (see Figure 10-1). Furthermore, comparisons of the results of this electron-microscopy procedure were made against the results taken from x-ray diffraction and Raman spectroscopy measurements.

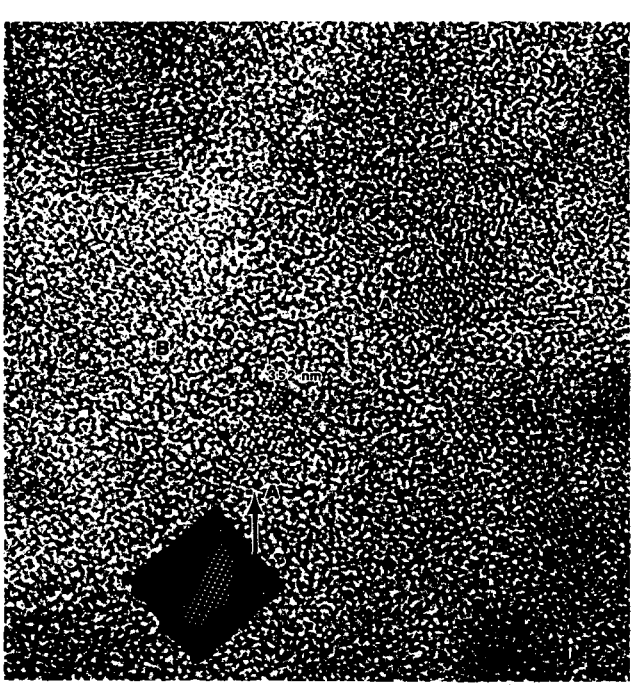

Figure 10-1. High-resolution image of 80-Å TiO_2 particles on a thick amorphous SiO_2 support. Phases of anatase (A) and TiO_2(B) (B) are identified in the micrograph. Additionally, one anatase particle is shown after image processing, where large (101) surfaces are distinguished. (XBB 871-119)

CRITICAL VOLTAGE STUDIES OF METALS AND ALLOYS

NCEM has unique capabilities for experimental measurements and theoretical interpretation of a "critical voltage" phenomenon that is observed in high-voltage electron microscopy and diffraction. The technique can be used to determine basic parameters such as atomic scattering amplitudes (needed to simulate high-resolution images) and Debye temperatures, as well as structure-sensitive factors in alloys such as ordering or bonding changes, as illustrated in the following abstracts of recent work.

11. Structure Factors and Debye Temperatures of Al-Li Solid-Solution Alloys (Publication 27)

A.G. Fox and R.M. Fisher

By combining the accurate low-angle x-ray structure factors of Al-Li solid-solution alloys (containing 5.25 and 8.06 at% Li) determined by the critical-voltage technique in high-energy electron diffraction (HEED) with higher-angle values obtained by interpolation between best pure-element form factors, a complete set of accurate x-ray structure factors for these alloys has been produced.

From these results it was found that the Debye temperatures of Al-Li solid-solution alloys are higher than those of pure aluminum, a result obviously consistent with an increase in Young's modulus; i.e., the stiffness of the alloy is greater than that of pure aluminum. This increase appears to arise predominantly from an increase in the force constant between nearest-neighbor (n-n) lithium atoms in the alloy as compared with the value for pure lithium. This occurs because the n-n lithium atoms are closer together in Al-Li solid-solution alloys than they are in pure lithium.

Because the lithium atoms are closer together in the alloys, the electron charge density ρ associated with the valence electrons in the alloys is likely to be higher than if ρ is considered unchanged by alloying. This suggested increase in the charge density of the alloy valence electrons was confirmed, as the experimental 111 low-angle structure factors of the alloys were found to be significantly higher than the equivalent values obtained by interpolation between the best pure-element form factors. Such electronic changes are to be expected for Al-Li alloys, as aluminum and lithium have a valency difference of two.

12. Low-Angle Atomic-Scattering Factors and the Charge Density of Beryllium (Publication 26)

A.G. Fox and R.M. Fisher

The x-ray structure factors for the 27 lowest-angle Bragg reflections of beryllium measured by Brown[1] have been placed on an absolute scale using the very accurate 1011 and 0002 low-angle structure factors that have been determined by HEED. A set of atomic-scattering (form) factors were calculated from these results; these form factors appear to be much more accurate than those deduced from the x-ray measurements. At higher angles ($\sin \theta/\lambda > 0.7$ $Å^{-1}$) these form factors agree quite closely with the best theoretical free-atom values, suggesting that the core (1s) electrons adopt the same configuration in both atomic and solid Be. The low-angle form factors deviate considerably from the best free-atom values, and these deviations can be explained as corresponding to $(sp^2)^a$ $(sp)^b$ hybridization of the Be atoms, with $b > a$. This is consistent with a bonding charge density between Be atoms along the c axis through the tetrahedral vacancy, which is in agreement with previous work.

1. P.J. Brown, Philos. Mag. **26**, 1377 (1972).

13. The Effect of Lead Acetate in the Preparation of the Lindlar Catalyst (Publication 63)

J.G. Ulan, E. Kuo, W.F. Maier, R.S. Rai, and G. Thomas

The effect of the Lindlar treatment for the preparation of Pd catalysts for the *cis*-selective hydrogenation of alkynes is investigated with hydrogenation studies on 2-hexyne as a model compound. The study emphasizes the effect of lead on the hydrogenation selectivity of Pd catalysts. The role of the additives in the catalysts is examined by high-resolution transmission electron microscopy. The effect of lead deposition on the catalytic activity and selectivity of Pd surfaces is studied with lead-coated Pd foils. No selectivity-enhancing effects are attributed to the deposition of lead on the Pd particles. The only important effect of the Lindlar procedure is the catalyst pretreatment itself, which causes morphological changes of the Pd particles responsible for the observed increase in selectivity.

14. Computer-Simulated Images of Platinum Clusters in the Channels of Y Zeolites. I. Zone-Axis Results (Publication 49)

I.Y. Chan,† R. Csencsits, M.A. O'Keefe, and R. Gronsky

Computer image simulation has been used to investigate the visibility of a 13-atom platinum cluster within Y zeolite channels in high-resolution electron microscopy images, examining the effects of specimen thickness, objective lens defocus, and the location of the Pt cluster within the host zeolite matrix. Simulations were carried out using the 81D version of the SHRLI computer programs running on a VAX 8600. The dynamical electron-scattering calculation used the multislice method, with a slice thickness of 4.988 Å and a unit-cell thickness of 35 Å along the [110] zeolite direction. The calculation carried 3017 diffracted beams through the crystal, requiring 12,097 phase-grating coefficients out to 4.22 $Å^{-1}$ in the [110] zone (i.e., h,k = ±104), for a JEM 200CX electron microscope.

Figure 14-1 shows the results for a 70-Å thick crystal; it is clear that, although the presence of the Pt cluster does affect the image, its presence may be ambiguous. Exact orientation, minimum thickness, and proper focus series are essential for detection, which becomes impossible as the host crystal exceeds 500 Å in thickness and its contribution to the image overwhelms that of the cluster. The ease of detection increases dramatically, however, with increasing cluster size.

†Present address: Chevron Research Co., Richmond, CA 94082-0627.

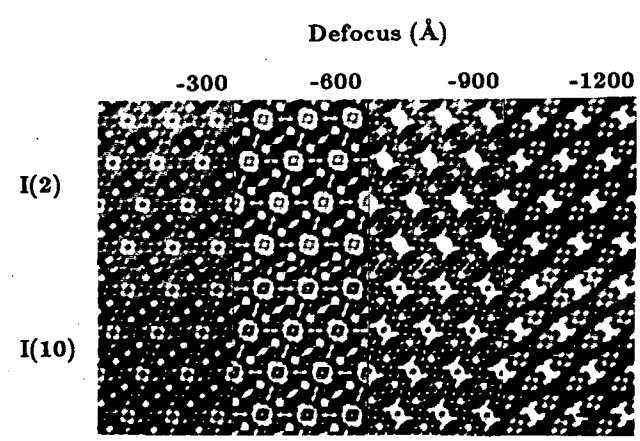

Figure 14-1. Computed Y zeolite images. Specimen thickness = 70 Å. |I(2): without Pt cluster; |I(10): with Pt cluster. Bar (I) alongside number indicates 14.3 Å. (XBB 862-769)

15. Atomic Mechanisms of Precipitate Plate Growth (Publication 50)

J. Howe,[†] U. Dahmen, and R. Gronsky

In this investigation the techniques of high-resolution transmission electron microscopy, image simulations, EDXS, and CBED are used to characterize the atomic structure, chemistry and growth mechanisms of γ plate-shaped precipitates in an Al-4.2 at% Ag alloy aged for 30 min at 350°C. The results of these studies show that γ precipitates have the composition Ag_2Al and are ordered during the early stages of growth, where the A-planes in the hcp precipitates contain nearly pure Ag and B-planes have the composition Al_2Ag. In addition, the precipitate/matrix interphase boundary is largely coherent and faceted along low-energy precipitate/matrix directions, and both the lengthening and thickening of γ plates occur by a terrace-ledge-kink mechanism, where the limiting step in the growth process appears to be the substitutional diffusion of Ag atoms across kinks in the Shockley partial dislocation ledges (see Figure 15-1) that terminate in the Ag-rich A-planes. The complementary information obtained from each of these techniques allows the mechanisms of precipitate growth to be understood at the atomic level.

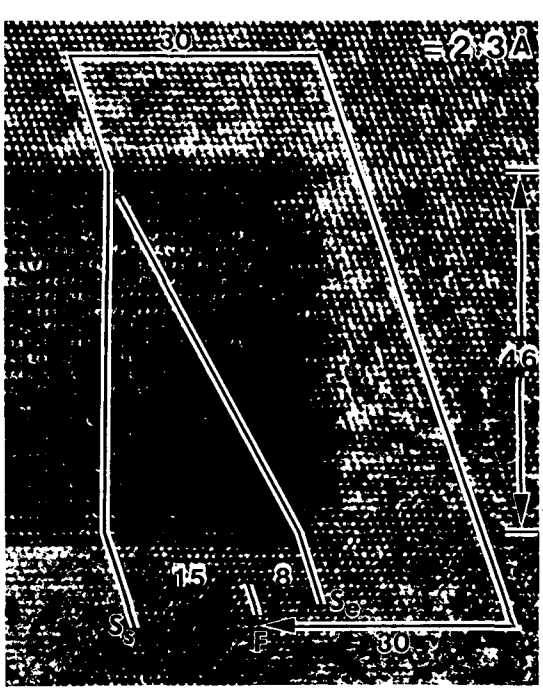

Figure 15-1. High-resolution image of a γ precipitate edge, 46 Å thick, in a <110>//<1120> orientation at −1690 Å defocus. A 2:1 ratio of 30° to 90° Shockley partial dislocations at the edge is revealed by the two Burgers circuits shown. The start of the 90° edge and 30° screw Burgers circuits are indicated by S_e and S_s, respectively, while F indicates the finish of the circuits. (XBB 840-9360)

[†]Permanent address: Department of Metallurgical Engineering and Materials Science, Carnegie Mellon University, Pittsburgh, PA 15213.

16. Work in Progress

Research programs at NCEM's computing facility include the following:

1. Integration of purchased and in-house software for the processing (SEMPER programs) and simulation (CEMPAS programs) of high-resolution TEM images, and strain-contrast images (Head-Humble programs) on the NCEM computer system.
2. Setting up of purchased hardware and development of software to enable the real-time video-rate capture and enhancement of images from the ARM and HVEM video cameras.
3. Image interpretation and structure determination using image simulation and comparison for various materials, including: (a) a metastable orthorhombic phase of zirconia, (b) phases of yttrium disilicate, (c) GaAs/GaAlAs quantum-well structures, (d) mullite, (e) SiAlON, (f) silicon nitride, (g) anatase/rutile, and (h) detection of Pt clusters in Y-zeolite.

1986 PUBLICATIONS AND REPORTS

Refereed Journals

1. D. Ackland, C. Echer, R. Kilaas, K. Krishnan, C. Nelson, M.A. O'Keefe, W. Smith, and J. Turner, "Recent TEM Applications," J. Metals **38**, 19 (1986); LBL-22332.
2. U. Dahmen and K.H. Westmacott, "High-Resolution Observations of Pentagonally-Twinned Precipitate Needles in Aluminium," Science **233**, 875 (1986); LBL-21344.
3. A.G. Fox and R.M. Fisher, "Accurate Structure Factor Determination and Electron Charge Distributions of Binary Cubic Solid Solutions," Philos. Mag. **53**, 815 (1986).
4. R. Kilaas, "On the Improved Phase-Grating Method," Ultramicrosc. **19**, 23 (1986); LBL-19799.
5. K.M. Krishnan, R. Gronsky, and L.E. Tanner, "Determination of the Composition of the Icosahedral Phase in Rapidly Solidified Al-Mn Quasicrystals at High Spatial Resolution," Scripta Metall. **20**, 239 (1986); LBL-20369.

6. K.M. Krishnan, R.S. Rai, G. Thomas, N.D. Corbin, and J.W. McCauley, "Characterization of Long Period Polytypoid Structures in the Al_2O_3-AlN System," Mat. Res. Soc. Proc. **60**, 211 (1986); LBL-20644.
7. K.M. Krishnan, P. Rez, G. Thomas, Y. Yokota, and H. Hashimoto, "The Combined Effect of Acceleration Voltage and Incident Beam Orientation on the Characteristic X-Ray Production in Thin Crystals," Philos. Mag. B **53**, 339 (1986); LBL-18934.
8. M.A. Meyers and H.-R. Pak, "Observation of an Adiabatic Shear Band in Titanium by High-Voltage Transmission Electron Microscopy," Acta Metall., July 1986.
9. R.E. Packard, J.P. Pekola, P.B. Price, R.N.R. Spohr, K.H. Westmacott, and Z. Yu-Qun, "Manufacture, Observation, and Test of Membranes with Locatable Single Pores," Rev. Sci. Instrum. **57**, 1654 (1986).
10. H.R. Pak and L.-M. Hsiung, "Cyclic Deformation Behaviour of Ni_3Ge Single Crystals at Room Temperature," Philos. Mag. A **53**, 887 (1986).
11. R. Ramesh, K.M. Krishnan, E. Goo, G. Thomas, M. Okada, and M. Homma, "Microstructure of Fe-Didymium-B Magnets," J. Magn. Magn. Mater. **54**, 563 (1986); LBL-19214.
12. M.L. Sattler and P.N. Ross, "The Surface Structure of Pt Crystallites Supported on Carbon Black," Ultramicrosc. **20**, 21 (1986); LBL-20873.
13. G. Thomas, "Modern Electron Microscopy for Materials Characterization," J. Elec. Microsc. Tech. **3**, 95 (1986); LBL-20224.
14. P. Veyssiere and K.H. Westmacott, "In-situ Observations of Partial Dislocation Climb in Ni_3Al," Philos. Mag. A **53**, 563 (1986); LBL-19464.
15. H.-R. Wenk, H.J. Bunge, E. Jansen, and J. Pannetier, "Preferred Orientation of Plagioclase-Neutron Diffraction and U-Stage Data," Tectonophys. **126**, 271 (1986).
16. K.H. Westmacott and U. Dahmen, "Recent TEM Studies of Precipitate Growth Mechanisms," Revue de Phys. Appliq. **21**, 757 (1986); LBL-21504.
17. K.H. Westmacott, U. Dahmen, and M. Witcomb, "An HVEM Study of an Unusual Ordering Reaction in Platinum-Carbon," Metall. Trans. A **17A**, 807 (1986); LBL-19636.

Other Publications

18. J. Bastacky, "High-Voltage Electron Microscopy of Unsectioned Human Lung Alveolar Walls," in *Proc. 44th Annual Meeting EMSA*, G.W. Bailey, Ed., San Francisco Press, 1986, p. 224; LBL-21374.
19. H.J. Brion and P. Haasen, "Screw Dislocation Networks Generated by Stage IV Compression of Ge and Si," May 1986.
20. I.Y. Chan, R. Csencsits, M.A. O'Keefe, and R. Gronsky, "Computer Simulated Images of Platinum Clusters in the Channels of Y Zeolites. I. Zone-Axis Results," J. Catal. (1986); in *Proc. 44th Annual Meeting EMSA*, G.W. Bailey, Ed., San Francisco Press, 1986, p. 776; LBL-20599.
21. S. Christy, H.R. Pak, and M.A. Meyers, "Effect of Metallurgical Parameters on Dynamic Fracture by Spalling of Copper," in *Metallurgical Applications of Shock-Wave and High Strain-Rate Phenomena,* L.E. Murr, K.P. Staudhammer, and M.A. Meyers, eds., Marcel Dekker, 1986, p. 835.
22. U. Dahmen, C. Nelson, and K.H. Westmacott, "An Atomic Resolution Study of Precipitates in an Al-Ge Alloy," in *Proc. 44th Annual Meeting EMSA*, G.W. Bailey, Ed., San Francisco Press, 1986, p. 538; LBL-21287.
23. M.L.A. Dass, U. Dahmen, G. Thomas, Y. Yamamoto, and K. Okazaki, "Electron Microscopy Characterization of Lead Zirconate Titanate Ceramics at the Morphotropic Phase Boundary Composition," in *Proc. IEEE Int. Symp. on Application of Ferroelectrics*, June 8–11, 1986, Lehigh University, Bethlehem, PA, p. 146; LBL-20955.
24. D.C. Dufner and L. Eyring, "High-Resolution Transmission Electron Microscopy and X-ray Microanalysis of Chemical Reactions in the Gold-Tin Thin Film System," J. Solid State Chem. (in press).
25. D.C. Dufner and L. Eyring, "High-Resolution Transmission Electron Microscopic Observations of Beta-Tin Thin Films," submitted to Thin Solid Films.
26. A.G. Fox and R.M. Fisher, "Low-Angle Atomic Scattering Factors and the Charge Density of Beryllium," submitted to Philos. Mag.
27. A.G. Fox and R.M. Fisher, "Structure Factors and Debye Temperatures of Al-Li Solid Solution Alloys," submitted to Acta Crystallogr.
28. R. Hull and S.J. Rosner, "Atomic Structure of the GaAs/Si Interface," submitted to Appl. Phys. Lett.
29. S.P. Kirkwood, E.A. Munn, and G.A. Brooks, "Mitochondrial Reticulum in Limb Skeletal Muscle," Am. Physiolog. Soc. C395 (1986).
30. K.M. Krishnan and G. Thomas, "Determination of Specific Site Occupation in Crystalline Magnetic Materials by Channelling Enhanced Microanalysis: a Review," TMS/AIME Fall Meeting, Orlando, FL, Oct. 5–9, 1986; LBL-21324abs.
31. S.M. Koch, S.J. Rosner, R. Hull, G.W. Yoffe, and J.S. Harris, Jr., "The Growth of GaAs on Si by MBE," in *Proc. Int. Conf. on Molecular Beam Epitaxy,* York, United Kingdom, Sept. 1986, to be published in J. Crystal Growth.
32. J.W. McCauley, K.M. Krishnan, R.S. Rai, G. Thomas, A. Zangvill, R.W. Doser, and N.D. Corbin, "Anion Controlled Microstructures in the AlN-Al_2O_3 Systems," in *Ceramic Microstructures '86: Role of Interfaces,* J.A. Pask and A.G. Evans, eds., Plenum Press, New York (in press).
33. H.R. Pak, C.L. Wittman, and M.A. Meyers, "High Voltage Transmission Electron Microscopy of Shear Bands in Titanium and AISI 4340 Steel," in *Metallurgical Applications of Shock-Wave and High-Strain-Rate Phenomena,* L.E. Murr, K.P. Staudhammer, and M.A. Meyers, eds., Marcel Dekker, 1986, p. 749;

34. M.A. Parker and R. Sinclair, "*In-situ* HREM and HVEM Studies of Silicon Epitaxial Regrowth," in *Proc. XIth Int. Cong. on Electron Microscopy*, Kyoto, Japan, Sept. 1986, p. 991.
35. R.S. Rai, M.A. O'Keefe, and G. Thomas, "Structure Imaging and Defects in Crystallized Oxynitride Glasses," in *Proc. MRS Fall Symposium*, Boston, MA, Dec. 1–4, 1986; LBL-21754.
36. R.S. Rai, T.R. Dinger, and G. Thomas, "TEM Studies of Partially Crystallized Y-Si-Al-O-N Glasses," in *Proc. 44th Annual Meeting EMSA*, G.W. Bailey, Ed., San Francisco Press, 1986, p. 444.
37. D.K. Sadana, M.H. Norcott, R.G. Wilson, and U. Dahmen, "Transmission Electron Microscopy of Aluminum-Implanted and Annealed (100) Si: Direct Evidence of Aluminum Precipitate Formation," submitted to Mat. Sci. Lett.
38. T. Sands, C.C. Change, V.G. Keramidas, K.M. Krishnan, and J. Washburn, "Formation of Amorphous and Crystalline Ternary Phases During the Ni-InP Reaction," submitted to Appl. Phys. Lett.
39. E. Schweda, Z.-C Kang, and L. Eyring, "*In-situ* Oxidation and Reduction of the Oxides of Cerium, Praseodymium and Ytterbium by High Voltage Electron Microscopy," submitted to Acta Metall.
40. S. Takeda, J. Kulik, D. de Fontaine, and L.E. Tanner, "Antiphase Boundaries in Cu-Pd Observed by High Resolution and High Voltage Electron Microscopy," in *Proc. XIth Int. Cong. on Electron Microscopy*, Kyoto, Japan, Sept. 1986, p. 957.
41. S. Takeda, J. Kulik, and D. de Fontaine, "Spinodal Ordering Beyond the Lifshitz Point in Cu-Pd Observed in the High Voltage Electron Microscope," in *Proc. XIth Int. Cong. on Electron Microscopy*, Kyoto, Japan, 1986, p. 1001.
42. G. Thomas "Characterisation of Inorganic Materials," in *Proc. XIth Int. Cong. on Electron Microscopy*, Kyoto, Japan, Sept., 1986, p. 1019; LBL-21332.
43. K.H. Westmacott and U. Dahmen, "Topics in Precipitation and Ordering Reaction and Their Related Phenomena," in *Proc. Int. Symp. Behavior of Lattice Imperfections in Materials,* Osaka, Japan, Nov. 18–20, 1985; LBL-20460.

LBL Reports

44. N. Bartlett, J. Kouvetakis, R. Kaner, and K.M. Krishnan, "Novel Metallic and Semiconductive Graphites," Science (in press); LBL-22543.
45. K.H. Westmacott, U. Dahmen, A. Thorel, and J.Y. Laval, "Precipitation in a (Mg) Partially Stabilized Zirconia During Aging at 1000°C," in *Ceramic Microstructures '86: Role of Interfaces*, J.A. Pask and A.G. Evans, eds., Plenum Press, New York (in press); LBL-22140.
46. T.A. Bielicki, U. Dahmen, G. Thomas, and K.H. Westmacott, "TEM Investigation of Orthorhombic-Type Phases in Stabilized Zirconias," in *Proc. Zirconia '86*, Tokyo, Japan, Sept. 9–11, 1986 (in press); LBL-22367.
47. U. Dahmen, P. Ferguson, and K.H. Westmacott, "A TEM Study of α''-$Fe_{16}N_2$ and γ'-Fe_4N Precipitation in Iron-Nitrogen," submitted to Acta Metall.; LBL-21441.
48. M.G. Kim, U. Dahmen, and A.W. Searcy, "Origin of Cracking Phenomena Observed in Decomposition Reactions," in *Ceramic Interfaces '86: Role of Interfaces,* J.A. Pask and A.G. Evans, eds., Plenum Press, New York (in press); LBL-22160.
49. I.Y. Chan, R. Csencsits, M.A. O'Keefe, and R. Gronsky, "Computer Simulated Images of Platinum Clusters in Channels of Y-zeolites I. Zone Axis Results," J. Catal. (in press); LBL-21430.
50. J. Howe, U. Dahmen, and R. Gronsky, "Atomic Mechanisms of Precipitate Plate Growth," submitted to Philos. Mag. A.; LBL-21705.
51. R. Kilaas, "New Image Simulation Software Development at the National Center for Electron Microscopy," submitted to Ultramicrosc.; LBL-22783.
52. R. Kilaas, M.A. O'Keefe, and K.M. Krishnan, "On the Inclusion of Upper Laue Layers in Computational Methods in High Resolution Transmission Electron Microscopy," Ultramicrosc. (in press); LBL-20836.
53. M.G. Kim, U. Dahmen, and A.W. Searcy, "Shape and Size of Crystalline MgO Particles Formed by the Decomposition of $Mg(OH)_2$," submitted to J. Am. Ceram. Soc.; LBL-22159.
54. M.G. Kim, U. Dahmen, and A.W. Searcy, "Structural Transformations in the Decomposition of $Mg(OH)_2$ and $MgCO_3$," J. Am. Ceram. Soc. (in press); LBL-21587.
55. K.M. Krishnan, "When is 'Parallel' Illumination Best Parallel for ALCHEMI.," Ultramicrosc. (in press); LBL-22618.
56. K.M. Krishnan, "Atomic Site and Species Determinations Using Channelling and Related Effects in Analytical Electron Microscopy," submitted to Ultramicrosc.; LBL-22305.
57. J. Kulik, S. Takeda, and D. de Fontaine, "Long Period Superstructures in Ag_3Mg," LBL-21610.
58. W.F. Maier, S.J. Chettle, and R.S. Rai, "The Metamorphosis of Palladium and its Relation to Selectivity in the Rosenmund Reaction," J. Am. Chem. Soc. (in press); LBL-20037.
59. M.L. Sattler, M.G. Reichmann, and A.T. Bell, "Identification of Phases and Surfaces in Small TiO_2 Catalyst Particles Using High Resolution Electron Microscopy/Spectroscopy Techniques, Part I," submitted to Ultramicrosc.; LBL-22765.
60. S. Takeda, J. Kulik, and D. de Fontaine, "Spinodal Ordering Beyond the Lifshitz Point in Cu_3Pd Observed by High-Voltage Electron Microscopy," submitted to Acta Metall.; LBL-22035.
61. G. Thomas, "Some HVEM Applications at the NCEM, University of California," Special Symposium on High Voltage Electron Microscopy, Osaka, Japan, Nov. 1985; LBL-19971.

62. J. Turner and K.M. Krishnan, "An Improved Photographic Process for Convergent Beam Electron Diffraction Applications," J. Elec. Microsc. Techniques (in press); LBL-21581.
63. J.G. Ulan, E. Kuo, W.F. Maier, R.S. Rai, and G. Thomas, "The Effect of Lead Acetate in the Preparation of the Lindlar Catalyst," J. Organic Chem. (in press); LBL-21980.

Invited Talks

64. M.A. O'Keefe, "Image Formation in the Electron Microscope," Xerox Palo Alto Research Center, Palo Alto, CA, Sept. 5, 1986.
65. M.A. O'Keefe, "Image Simulation for High Resolution Electron Microscopy," Shell Meeting on Electron Microscopy, Shell Development Corp., Houston, TX, Nov. 3, 1986; Department of Materials Engineering, North Carolina State University, Raleigh, Nov. 7, 1986.
66. K. Krishnan, "Microanalytical Electron Microscopy: Some Developments and Applications in Materials Research," California Institute of Technology, Pasadena, April 15, 1986.
67. K.H. Westmacott, "Microstructural Changes in Partially-Stabilized Zirconia During 1000°C Aging," Frontiers in Electron Microscopy, Argonne National Laboratory, Batavia, IL, April 20–23, 1986.
68. U. Dahmen, "Precipitation in a (Mg) Partially Stabilized Zirconia," Ceramic Microstructures '86, Berkeley, CA, July 1986.
69. U. Dahmen, "An Atomic Resolution Study of Precipitates in an Al-Ge Alloy," 44th Annual EMSA Meeting, Albuquerque, NM, Aug. 1986.
70. R. Gronsky, "High Resolution Electron Microscopy, Instrumentation and Practice," Arizona State University Winter School on Imaging and Microanalysis with High Spatial Resolution, Tempe, AZ, Jan. 7–11, 1986.
71. R. Gronsky, "The Microstructure of the Pretransformation State," TMS/AIME Annual Meeting, New Orleans, LA, March 2–6, 1986.
72. R. Gronsky, "Structural Analysis: What Can be Done with Atomic Resolution Microscopy," TMS/AIME Annual Meeting, New Orleans, LA, March 2–6, 1986.
73. R. Gronsky, "High Resolution Electron Microscopy," Analytical Electron Microscopy Short Course, The Major Analytical Instrumentation Center, University of Florida, Gainesville, March 24–27, 1986.
74. R. Gronsky, "High Voltage Electron Microscopy," Conference on Frontiers of Electron Microscopy in Materials Science, Argonne National Laboratory, Argonne, IL, April 20–23, 1986.
75. R. Gronsky, "Real-Time TEM," Symposium on Materials Characterization, MRS Spring Meeting, Palo Alto, CA, April 15–18, 1986.
76. R. Gronsky, "Theory and Applications of Atomic Resolution Electron Microscopy," Symposium on Frontiers of Atomic Resolution Electron Microscopy, Xerox Palo Alto Research Center, Palo Alto, CA, May 23, 1986.
77. R. Gronsky, "Electron Microscopy at Atomic Resolution," Whitney Symposia on Science and Technology VII: Imaging Technology and Applications, General Electric Corporate Research and Development, Schenectady, NY, June 10–13, 1986.
78. R. Gronsky, "Transmission Electron Methods," Scanning Electron Microscopy Short Course, University of California, Davis, Sept. 7–12, 1986.
79. M.L. Sattler, "The Surface Structure of Pt Crystallites Supported on Carbon Black," Workshop on Atomic Structure and Properties of Small Particles, Wickenburg, AZ, Jan. 7–11, 1986.
80. G. Thomas, "Microstructure Composite Design for New Steels," First US-India Symposium on Steel, Steel Authority of India, Ltd., Ranchi, India, Jan. 10, 1986.
81. G. Thomas, "Applications of Contemporary Electron Microscopy" and "A Viewpoint of Electron Microscopy in Materials," Stanford Symposium, March 19, 1986.
82. G. Thomas, "Refractories and New Structural Ceramics," Central Institute for Iron and Steel Research, Beijing, Peoples Republic of China, April 1986.
83. G. Thomas, "Alloy Design of Structural Steels," IRSID, Paris, France, May 1986.
84. G. Thomas, "Design of Composite Microstructures for Improved Mechanical Properties of Steels," Boris Kidric Steel, Montenegro Metallurgical Society, Niksic, Yugoslavia, June 1986.
85. G. Thomas, "New Process of Production of Simple Steel for Wire Rods," BSE, Kehl, Federal Republic of Germany, June 1986.
86. G. Thomas, "New Steels for Bars and Long Products," International Conference on Steel, Colorado State University, Golden, July 1986.
87. G. Thomas, "Characterization of Inorganic Materials," North Carolina State University, Raleigh, Oct. 10, 1986.
88. G. Thomas, "The National Center for Electron Microscopy" and "Electron Microscopy Research on Magnetic Materials," Eastman Kodak Co., San Diego, CA, Oct. 24, 1986.
89. G. Thomas, "Characterization of Interfaces and Grain Boundaries in Ceramics," Ceramic Microstructures '86, University of California Berkeley, July 1986.
90. G. Thomas, "Grain Boundaries and Integranular Phases in Ceramics," Symposium on Ceramics, 44th Annual Meeting EMSA, Albuquerque, NM, Aug. 1986.
91. G. Thomas, "High Voltage, High Resolution Electron Microscopy," International Congress on Electron Microscopy, Kyoto, Japan, Sept. 1986.

In Situ Investigations of Gas-Solid Reactions by Electron Microscopy*

J.W. Evans, Investigator

INTRODUCTION

This work is concerned with the microstructural changes resulting from gas-solid reactions. Of particular interest is the nucleation and growth of the solid products from the parent phase. The experimental tools used in this investigation are the environmental cells that are placed in the two high-voltage transmission electron microscopes at LBL. This cell enables a solid to be contacted with a gas at elevated temperatures without adversely effecting the vacuum in the microscope column. The evolution of the microstructure as the reaction proceeds can then be observed at high magnification. Conventional transmission electron microscopy of cross-sectioned reacted samples is used to better describe the phases occurring at the reaction front. Secondary-ion mass spectroscopy (SIMS) is used to obtain in-depth composition profiles of the relevant elements in the solid product and reactant.

This year an investigation of the thermal oxidation of gallium arsenide by dry oxygen in the temperature range of 300°C to 600°C was advanced. Poor kinetics hinder practical use of the amorphous oxide layer produced at lower temperatures. An evolution of the morphology of the Ga_2O_3 product at temperatures above 400°C was observed before the equilibrium β-Ga_2O_3 was obtained. The fate of arsenic was also studied, and SIMS results showed that it builds up at the oxide-GaAs interface. Work continues on the oxidation of other compound semiconductor materials. A few preliminary results on the thermal oxidation of InP indicated a transition of the product from amorphous to polycrystalline In_2O_3 at about 450°C.

*This work was supported by the Director, Office of Energy Research, Office of Basic Energy Sciences, Materials Sciences Division of the U.S. Department of Energy under Contract No. DE-AC03-76SF00098.

1. Effect of Dopants on Thermal Oxidation of Gallium Arsenide (Publication 1)

O.R. Monteiro and J.W. Evans

The environmental cells within the Hitachi HU-650 and the Kratos EM 1500 transmission microscopes have been used to study the oxidation of doped and undoped gallium arsenide by dry oxygen. At temperatures below 400°C, amorphous reaction products were observed. Their growth kinetics were, however, exceedingly slow for use in semiconductor processing. At temperatures around 500°C and above, polycrystalline β-Ga_2O_3 was formed after epitaxially grown γ-Ga_2O_3. A unique orientation relationship between the γ-Ga_2O_3 and the parent GaAs was found (Figure 1-1). Doping elements have a remarkable effect on the oxidation kinetics. Arsenous oxide and elemental arsenic were only detected in the Cr-doped gallium arsenide. When Te- or Si-doped and undoped gallium arsenide were oxidized, the only As oxide detected was As_2O_5. This fact has not been reported hitherto. SIMS was then used to access in-depth concentration profiles of the relevant elements. The Cr-doped samples produced the thinnest oxide layers when compared to the Sr- and Te-doped samples. In all three cases the dopant builds up in the oxide, reaching concentrations of more than an order of magnitude higher than the one in the bulk semiconductor.

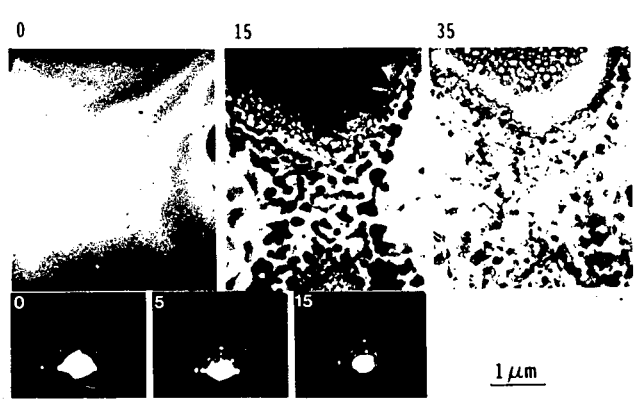

Figure 1-1. A sequence of electron images showing morphological changes accompanying the oxidation of GaAs at 600°C and 20 Torr oxygen pressure. The diffraction patterns show a unique orientation relationship between the GaAs and γ-Ga_2O_3:

$$\langle 001 \rangle_{GaAs} \;//\; \langle 001 \rangle_{\gamma-Ga_2O_3}$$
$$\{110\}_{GaAs} \;//\; \{GaAs\}_{\gamma-Ga_2O_3}$$

The oxidation times are indicated at the top left hand side of each bright-field image and diffraction pattern. (XBB 869-7878)

2. Work in Progress

Thermal oxidation of GaAs using an O_2-NH_3 mixture is under way. This mixture seems to yield oxides with better properties than the ones obtained with pure oxygen. Oxidation studies of undoped InP are also being carried out. Initial *in situ* experiments established that at temperatures below 450°C an amorphous oxide forms upon oxidation. Such an oxide cannot be clearly characterized, and it appears to be a mixture of indium and phosphorous oxides. At higher temperatures polycrystalline In_2O_3 forms. Further work is required to determine the behavior of phosphorous. Another set of gas-solid reactions that are suitable for study by dynamic TEM (e-cell) are those occurring during chemical vapor deposition. They have enormous importance in microfabrication processes and a very strong dependence on substrate characteristics. Studies are currently being undertaken to evaluate the feasibility of studying the deposition of tungsten on silicon from WF_6 within the e-cell.

1986 PUBLICATIONS AND REPORTS

LBL Reports

1. O.R. Monteiro and J.W. Evans, "*In-Situ* Observations of the Effect of the Dopants on the Thermal Oxidation of Gallium Arsenide," LBL-22504.

Invited Talks

2. J.W. Evans and O.R. Monteiro, "Dynamic Observations on the Thermal Oxidation of Gallium Arsenide," Fall Meeting of the Electrochemical Society, SOTAPOCS V, San Diego, CA, Oct. 24–26, 1986; LBL-22509.

Local Atomic Configurations in Solid Solutions*

Didier de Fontaine, Investigator

INTRODUCTION

This investigation is concerned with ordering phenomena in alloys, more particularly long-period ordered superstructures in binary fcc alloys. Two systems have been selected for experimental study: Ag_3Mg and Cu_3Pd; the former exhibits sharp antiphase boundary structures allowing comparison to be made between observed and theoretically predicted structures. Detailed structural observation is carried out by high-resolution transmission electron microscopy (TEM), and the theoretical model used is that of the Axial Next-Nearest-Neighbor Ising (ANNNI) model. A systematic investigation of long- and short-range order in Cu-Pd is undertaken by *in situ* variation of temperature and electron irradiation dose rate in the high-voltage electron microscope at the National Center for Electron Microscopy at LBL. Samples of different compositions, heat treatments, and pressure histories are examined. Results are compared to predictions obtained from electronic-structure calculations.

1. Applications of the ANNNI Model to Long-Period Superstructures in Some Noble Metal Alloys (Publication 4)

D. de Fontaine, A. Finel,† S. Takeda,‡ and J. Kulik

The phenomenon of long-period superstructures in ordered alloys is analyzed in terms of the ANNNI model. New ground-state results are presented and applied to the case of one-dimensional periodic antiphase structures in Cu_3Pd. The difference between systems with diffuse antiphase domain boundaries (as in Cu_3Pd) and sharp boundaries (as in Ag_3Mg) is discussed and is argued to be due to the influence of the strength of the effective transverse-pair interactions compared to that of the axial interactions along the long-period direction. Atomic-resolution transmission electron micrographs are presented for Cu_3Pd and Ag_3Mg, which clearly illustrate the distinction (see Figure 1-1).

*This work was supported by the Director, Office of Energy Research, Office of Basic Energy Sciences, Materials Sciences Division of the U.S. Department of Energy under Contract No. DE-AC03-76SF00098.

†Present address: ONERA, BP 72, 92322 Chatillon Cedex, France.

‡Permanent address: Dept. of Physics, College of General Education, Osaka University, Toyonaka, Osaka 560, Japan.

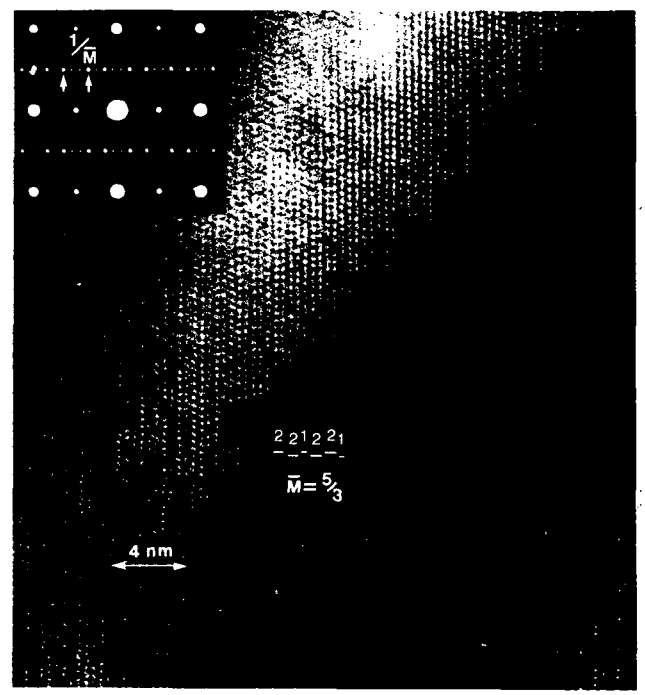

Figure 1-1. High-resolution bright-field image of a <221> polytype from a Ag–26 at% Mg specimen annealed at 382°C. (XBB 862-889)

2. Long-Period Superstructures in Ag_3Mg (Publication 15)

J. Kulik, S. Takeda,† and D. de Fontaine

One-dimensional long-period superstructures in Ag_3Mg have been studied by high-resolution electron microscopy and electron diffraction. Several new polytypes have been found (see Figure 1-1). A free-energy model involving competing-pair interactions is discussed as a possible candidate for describing the configurational statistics of this alloy system.

†Permanent address: Dept. of Physics, College of General Education, Osaka University, Toyonaka, Osaka 560, Japan.

3. Simple Models for the Omega Phase Transformation (Publication 16)

D. de Fontaine

In the late sixties, it was recognized that the omega phase transformation occurring in bcc Ti, Zn, and Hf alloys was a displacive transition that could be described, at least qualitatively, by simple models. Since the displacive wave responsible for the transition to perfect omega was a Brillouin zone-boundary wave, displacements and volume changes were rather small, in contrast to the classical martensite case. The nonideal, or modulated, omega phase requires further consideration and calls for soliton models, for example. Recent first-principles electronic-structure calculations, briefly reported upon here, have also shed light on the athermal omega transformation.

4. Spinodal Ordering Beyond the Lifshitz Point in Cu_3Pd Observed by High-Voltage Electron Microscopy (Publication 17)

S. Takeda,† J. Kulik, and D. de Fontaine

Cu-Pd samples of compositions varying from 16 to 26 at% Pd were irradiated *in situ* in the 1.5-MeV electron microscope at various temperatures. Low-temperature (−180°C) irradiation produced completely disordered solid solutions, room-temperature irradiation produced steady-state short-range order (SRO), and high-temperature irradiation tended to produce the expected equilibrium long-range order. In particular, the 18 and 20% samples irradiated at room temperature exhibited steady-state modulated SRO, although only the simple $L1_2$ ordered structure was expected at equilibrium. It is suggested that spinodal ordering is responsible for these effects. An fcc-based Cu-Pd phase diagram is proposed, the phase diagram incorporates ordering stability loci and a metastable Lifshitz point.

†Permanent address: Dept. of Physics, College of General Education, Osaka University, Toyonaka, Osaka 560, Japan.

5. Work in Progress

A more detailed kinetic theory of "Spinodal Ordering Beyond the Lifshitz Point" is being developed based on the Lyapunov function concept introduced by G. Martin. Good qualitative agreement with experiment has been obtained. Phase diagrams for long-period superstructures in fcc ordered alloys are being calculated in the mean-field approximation. The first-order nature of the transitions has been correctly predicted.

1986 PUBLICATIONS AND REPORTS

Refereed Journals

1. A. Finel and D. de Fontaine, "The Uniaxial Brickwork Model, Exact Results and CVM Approximation," J. Stat. Phys. **43**, 663 (1986); LBL-19284.
2. A. Finel and D. de Fontaine, "The Two-Dimensional ANNNI Model in the CVM Approximation," J. Stat. Phys. **43**, 645 (1986); LBL-19393.
3. D. de Fontaine, A. Finel, and T. Mohri, "Comparison of Short-Range Order Intensity Obtained by Monte Carlo Simulation and by the Cluster Variation Method," Scripta Metall. **20**, 1045 (1986); LBL-21358.

Other Publications

4. D. de Fontaine, A. Finel, S. Takeda, and J. Kulik, "Applications of the ANNNI Model to Long-Period Superstructures in Some Noble Metal Alloys," in *Noble Metals Alloys: Phase Diagrams, Alloy Phase Stability, Thermodynamic Aspects, Properties and Special Features*, T.B. Massalski, W.B. Pearson, L.H. Bennett, and Y.A. Chang, eds., The Metallurgical Soc., 1986, p. 49; LBL-20044.
5. H. Yamauchi and D. de Fontaine, "Cu-Ag-Au Plausible Phase Diagrams," in *Computer Modeling of Phase Diagrams*, L.H. Burnett, Ed., The Metallurgical Society, 1986.
6. S. Takeda, J. Kulik, D. de Fontaine, and L.E. Tanner, "Antiphase Boundaries in Cu-Pd Observed By High Resolution and High Voltage Electron Microscopy," in *Proc. XIth Int. Cong. on Electron Microscopy*, Kyoto, 1986, p. 957.
7. S. Takeda, J. Kulik, and D. de Fontaine, "Spinodal Ordering Beyond the Lifshitz Point in Cu-Pd Observed in the High Voltage Electron Microscope," in *Proc. XIth Int. Cong. on Electron Microscopy*, Kyoto, 1986, p. 1001.
8. D. de Fontaine, "Atomic Resolution Microscopy Study of Ordered Ag_3Mg," abstract presented at the TMS-AIME Annual Meeting, New Orleans, LA, March 5, 1986.
9. P. Turchi,† M. Sluiter,‡ D. de Fontaine, and A. Finel, "Prototype Binary Alloy Phase Diagrams from Tight-Binding Electronic Structure Calculations," abstract presented at the TMS-AIME Annual Meeting, New Orleans, LA, March 3, 1986.
10. S. Takeda, J. Kulik, and D. de Fontaine, "One-Dimensional Long-Period Superstructures in $Cu_{3+x}Pd_{1-x}$ Observed by High Resolution Electron

Microscopy" abstract presented at the TMS-AIME Annual Meeting, New Orleans, LA, March 5, 1986.

11. S. Takeda, J. Kulik, S. Lacey, and D. de Fontaine, "Spinodal Ordering Beyond the Lifshitz Point in Cu-Pd Observed Under High Voltage Electron Microscopy," abstract presented at the TMS-AIME Annual Meeting, New Orleans, LA, March 5, 1986.
12. J. Kulik, S. Takeda, and D. de Fontaine, "Long-Period Superstructures in Cu_3Pd and Ag_3Mg Alloys," abstract presented at the American Physical Society Meeting, Las Vegas, NV, April 1–4, 1986.
13. P. Turchi,† D. de Fontaine, G.M. Stocks, W.H. Butler, A. Gonis, and A.J. Freeman, "Effective Interactions in Substitutionally Disordered Alloys: Tight-Binding Approximation," abstract presented at the American Physical Society Meeting, Las Vegas, NV, April 1–4, 1986.
14. A. Gonis, A.J. Freeman, G.M. Stocks, W.H. Butler, P. Turchi,† and D. de Fontaine, "Effective Interactions in Substitutionally Disordered Alloys: First-Principles Calculations," abstract presented at the American Physical Society Meeting, Las Vegas, NV, April 1–4, 1986.

LBL Reports

15. J. Kulik, S. Takeda, and D. de Fontaine, "Long Period Superstructures in Ag_3Mg," Acta Metall. (in press); LBL-21610.
16. D. de Fontaine, "Simple Models for the Omega Phase Transformation," TMS-AIME Symposium, March 3, 1986, accepted by Metall. Trans.; LBL-21555.
17. S. Takeda, J. Kulik, and D. de Fontaine, "Spinodal Ordering Beyond the Lifshitz Point in Cu_3Pd Observed by High-Voltage Electron Microscopy," accepted by Acta Metall.; LBL-22035.

Invited Talks

18. D. de Fontaine, "Long-Period Superstructures and Spinodal Ordering in Electron Irradiated Cu_3Pd and Ag_3Mg," MMRD Annual Review Symposium, Feb. 27, 1986.
19. P. Turchi, "From Electronic Band Structure to Phase Diagrams," Nuclear Chemistry Division, Lawrence Livermore National Laboratory, Livermore, CA, March 18, 1986.†
20. D. de Fontaine, "Spinodal Ordering Beyond the Lifshitz Point," National Bureau of Standards, Washington, D.C., March 24, 1986.
21. D. de Fontaine, "High Resolution and High Voltage TEM Studies of Long-Period Superstructures in Ordered Alloys," Lawrence Berkeley Laboratory Materials Science Review, DOE, Washington, D.C., March 25, 1986.
22. D. de Fontaine, "Alloy Phase Diagrams from First Principles," Materials Science Dept. Seminar, U.C. Berkeley, April 10, 1986.
23. D. de Fontaine, "Spinodal Ordering Beyond the Lifshitz Point," Physical Metallurgy Gordon Research Conference, Andover, NH, July 20–25, 1986.
24. D. de Fontaine, three lectures on "Alloy Phase Stability," International School on Electronic Band Structure and its Applications, IIT, Bombay, India, Oct. 31, Nov. 3, and Nov. 4, 1986.
25. D. de Fontaine, "Long-Period Superstructures in Ag_3Mg and Cu_3, Pd Studied by High-Resolution and High-Voltage TEM," Metallurgy Dept., IIT, Kanpur, India, Nov. 6, 1986.
26. D. de Fontaine, "Alloy Phase Stability," Physics Department, University of Madras, Madras, India, Nov. 10, 1986.
27. D. de Fontaine, "Long-Period Superstructures in Ordered Alloys," Physics Division, Indira Ghandi Center for Atomic Research, Kalpakkam, India, Nov. 12, 1986.

---

†Postdoctoral support funded by Lawrence Livermore National Laboratory, Livermore, CA, under Contract No. LLNL 6870305.

‡Graduate student support funded by National Science Foundation Grant No. DMR 8311013.

Alloy Theory*

Didier de Fontaine and Leo M. Falicov, Investigators

INTRODUCTION

Temperature-composition phase diagrams are of great practical interest since they constitute "road maps," as it were, of thermodynamic systems such as binary, ternary, ..., alloys. Phase diagrams are generally determined experimentally, but the exciting possibility now exists of deriving certain classes of diagrams virtually from first principles. What is needed is to combine accurate electronic band structure and statistical mechanical calculations. Reliable theoretical models are available and computer codes have been developed. For instance, the electronic structure of disordered alloys can be calculated from existing coherent potential approximation (CPA) codes, and, on the statistical thermodynamic side, the cluster variation method (CVM) recently has yielded realistic phase diagrams, thermodynamic functions, long- and short-range order information, and so on. The purpose of this project is to combine existing electronic-band structure and total-energy computer codes with CVM codes to produce phase diagrams from a minimum of empirical information, to compare various approximate computational methods, and to compare results with available experimental data.

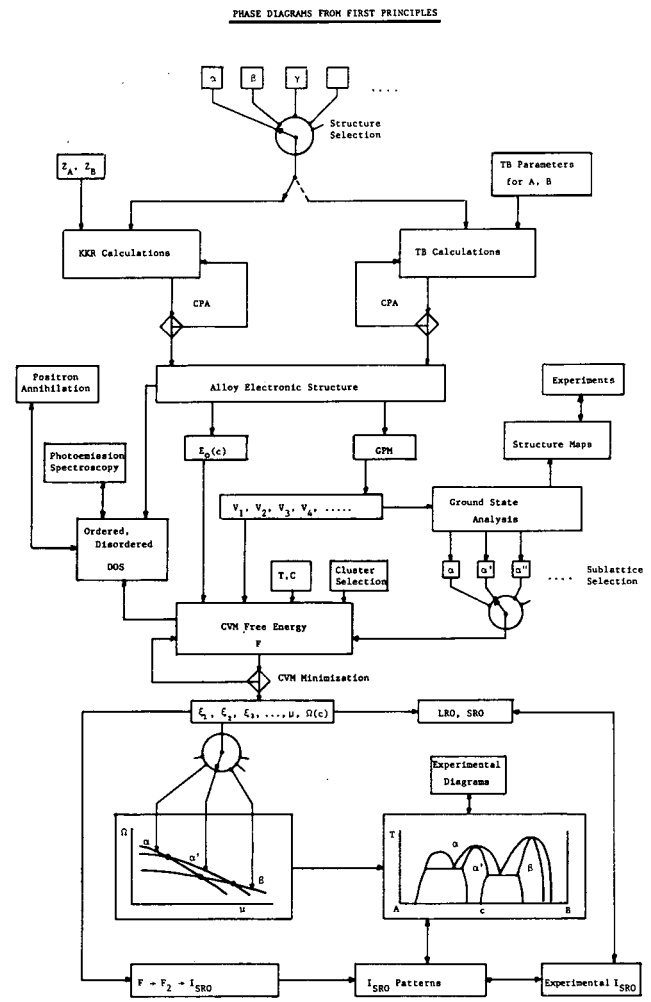

Figure 1-1. Flow chart of quantum-mechanical and statistical thermodynamical calculations required to obtain alloy phase diagrams. Possible experimental verifications are also indicated. (XBL 873-1121)

1. Alloy Phase Stability (Publication 1)

D. de Fontaine

Certain classes of temperature-composition alloy phase diagrams may now be calculated virtually from first principles. The procedure envisaged is the following: a crystal lattice fcc(α), bcc(β),..., is selected, and the energy (E_0) of the completely disordered state at zero Kelvin is calculated by CPA. Either the KKR or tight-binding (TB) formalisms may be used (see Figure 1-1). Then effective-pair (and multiplet) interactions (V_n) are calculated by the generalized perturbation method (GPM). These concentration-dependent interactions allow the ordered ground states to be determined, hence the sublattice structures α', α'' for α; β', β'' for β, etc. Interactions and sublattices are inserted into the CVM formalism, and the resulting free energy is minimized. The same procedure is repeated for each lattice. Free-energy curves are plotted, common tangents are constructed, and the phase diagram is obtained. This general procedure has been followed for paramagnetic transition-metal alloys in a simple TB approximation, for fcc prototype systems, and the results are encouraging.

2. Work in Progress

Calculations of transition-metal alloy equilibria are being extended to the combined fcc and bcc

*This work was supported by the Director, Office of Energy Research, Office of Basic Energy Sciences, Materials Sciences Division of the U.S. Department of Energy under Contract No. DE-AC03-76SF00098.

cases. Also, s and p orbitals are being added to the d-orbital codes to treat nontransition metals and alloys. Binary and ternary noble metal alloys are also being investigated in an exact s-band treatment of small tetrahedral clusters.

1986 PUBLICATIONS AND REPORTS

Other Publications

1. D. de Fontaine, "Alloy Phase Stability," to be published in "Lecture Note on International School on Electronic Band Structure and its Applications," held at IIT Kanpur, India, Oct. 1986, M. Yussouff, Ed., Springer-Verlag, 1987; LBL-22608.
2. M. Sluiter,† P. Turchi,‡ and D. de Fontaine, "Prediction of Ordering in Binary Transition Metal Alloys," submitted to J. Phys. F.
3. P. Turchi,‡ M. Sluiter,† and D. de Fontaine, "Prototype FCC Based Binary Alloy Phase Diagrams from Tight Binding Electronic Structure Calculations," submitted to Phys. Rev. B.

Invited Talks

4. D. de Fontaine, "Alloy Phase Stability," Physics Department, University of Madras, Madras, India, Nov. 10, 1986.
5. D. de Fontaine, "Alloy Phase Diagrams from First Principles: A Possibility?" Indira Gandhi Center for Atomic Research, Physics Division, Kalpakkam, India, Nov. 11, 1986.

---

†Graduate student salary supported by National Science Foundation Grant No. DMR 8311013 and the Department of Materials Science and Mineral Engineering, University of California Berkeley.

‡Postdoctoral salary supported by Lawrence Livermore National Laboratory, Livermore, CA, under Contract No. LLNL 6870305.

MECHANICAL PROPERTIES

Environmentally Affected Crack Growth in Engineering Materials*

Robert O. Ritchie, Investigator

INTRODUCTION

The objective of this program is to examine, from both macroscopic and microscopic perspectives, the mechanics and micromechanisms of the subcritical growth of cracks in engineering materials. Primary studies are currently devoted to (i) brittle fracture in low-strength steels by transgranular cleavage, where statistical models have been developed to predict lower shelf fracture toughness, (ii) ductile fracture in low-alloy steels, where models for crack growth toughness have been investigated by defining the microstructural factors governing the behavior of stationary and growing cracks, (iii) fatigue crack initiation and growth in duplex microstructures, where utilization of the concepts of crack tip shielding through crack deflection and the premature closing of cracks (crack closure) has led to the development of dual-phase steels with remarkable resistance to fatigue, and (iv) variable-amplitude fatigue crack propagation in titanium alloys, where studies have been focused on defining the primary mechanisms for crack growth retardation following tensile overloads. The highlight of the past year has been the adaptation of our statistical model for transgranular cleavage fracture to predict the role of microstructure in influencing the lower-temperature fracture toughness of metals containing a known distribution of particles.

*This work was supported by the Director, Office of Energy Research, Office of Basic Energy Sciences, Materials Sciences Division of the U.S. Department of Energy under Contract No. DE-AC03-76SF00098.

1. Statistical Analysis of Cleavage Fracture Ahead of Sharp Cracks and Rounded Notches (Publications 1 and 2)

T. Lin, A.G. Evans, and R.O. Ritchie

Mechanisms of initiation and unstable propagation of transgranular cleavage cracks have been compared for brittle fracture ahead of sharp cracks and rounded notches, e.g., for fatigue precracks and Charpy V-notches, respectively, in standard toughness specimens. The comparison is made over a range of temperatures, from the lower shelf into the ductile/brittle transition region, for a single-phase material containing a known distribution of particles where weakest-link statistics can be used to model the onset of catastrophic failure. Using linear and nonlinear elastic solutions for the stress distribution ahead of a sharp crack, and slip-line field solutions modified for a power hardening material, for the rounded notch, statistical modeling is employed to define the critical dimensions ahead of the crack or notch tip where initial cracking events are most probable. The analysis provides an interpretation of the role of stress gradient in governing microscopic fracture behavior. Predictions are evaluated by comparison with experimental results on the low-temperature flow, Charpy V-notch, and plane-strain fracture toughness behavior of a low-carbon mild steel with simple ferrite/grain boundary carbide microstructures (see Figure 1-1).

2. Stochastic Modeling of the Independent Roles of Particle Size and Grain Size in Transgranular Cleavage Fracture (Publication 16)

T. Lin, A.G. Evans, and R.O. Ritchie

The independent roles of grain size and particle size on fracture toughness have been investigated over a range of temperatures from the lower shelf into the early ductile/brittle transition region (see Figure 2-1). The results are interpreted in terms of a

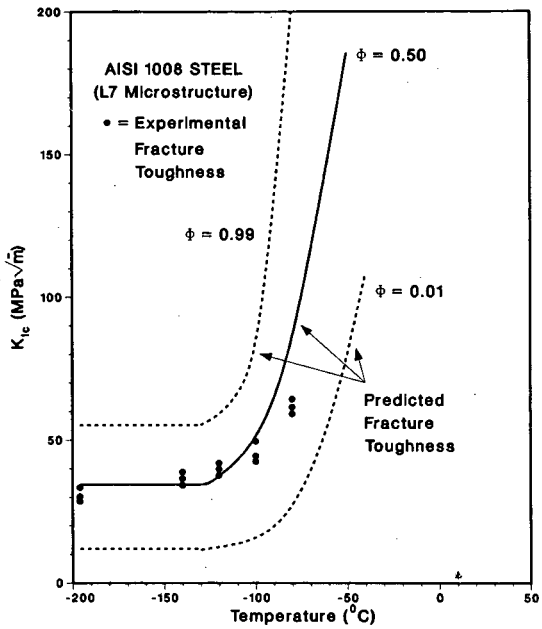

Figure 1-1. Experimental measurements of the temperature dependence of plane strain fracture toughness K_{IC} in AISI 1008 steel (L7 microstructure) based on precracked four-point bend tests. Results above −100°C were computed from nonlinear elastic J_{IC} measurements. Also shown are the model predictions of K_{IC}, indicating median values (Φ = 0.50) and the anticipated statistical variation (Φ = 0.01 and 0.99). (XBL 861-141)

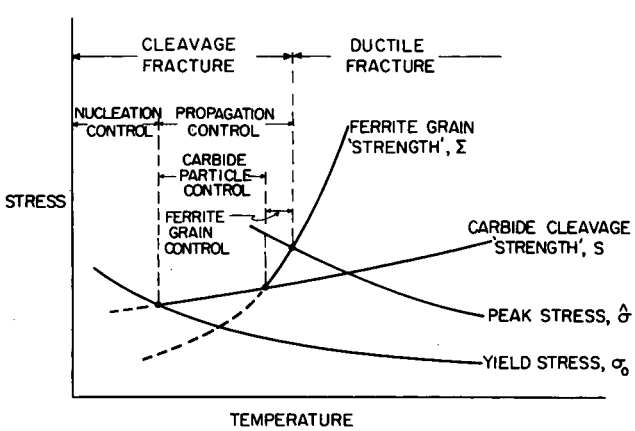

Figure 2-1. Schematic representation of the variation with temperature of the cleavage fracture "strength," resulting from either particle microcracks or grain-size microcracks, indicating the regions of nucleation and propagation control for the ductile-brittle transition. (XBL 865-7675)

weakest-link statistical model of cleavage fracture wherein the onset of failure coincides with the critical propagation of a particle microcrack into the matrix (see Figure 2-2). It is shown that, for a fixed particle-size distribution, both sharp-crack and rounded-notch toughness decrease with increasing

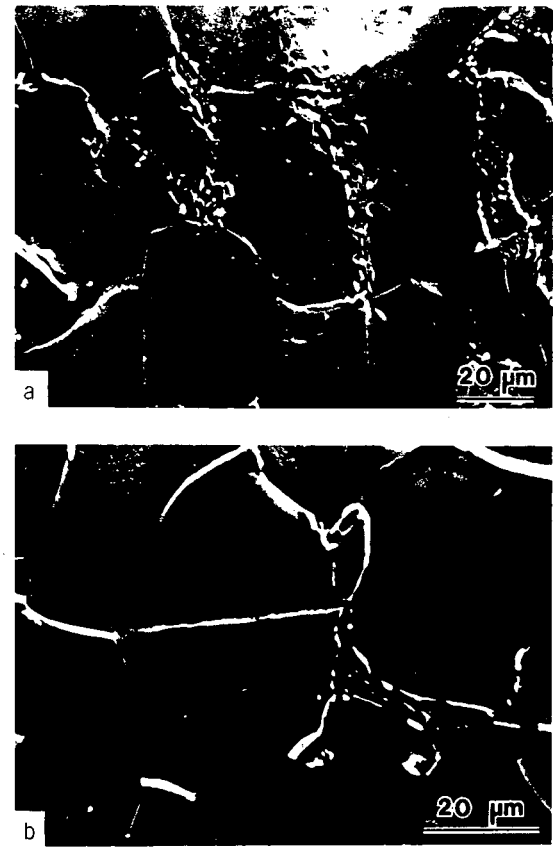

Figure 2-2. Micrograph showing (a) the existence of microvoids formed in the immediate vicinity of the tip of the precrack, and (b) grain-size microcracks arrested at ferritic grain boundaries, several grains ahead of the tip. Both phenomena are characteristic of cleavage fracture at temperatures in the early ductile/brittle transition range. (XBB 857-5775)

grain size. However, at fixed grain size, the sharp-crack toughness increases, while the rounded-notch toughness decreases with increasing particle size. Such effects result primarily from the difference in the number of activated particles in the plastic zone.

3. Crack Initiation and Crack Growth Toughness (Publication 23)

T.S. Oh and R.O. Ritchie

The role of microstructure in influencing crack initiation and crack growth toughness and the morphology of the crack path was examined for three steels of different strength levels (σ_0) with the objectives of (i) verifying fundamental relationships between crack initiation toughness, J_{IC}, and crack growth toughness, the tearing modulus T_R; (ii)

assessing the influence of the microstructure on J_{IC} and T_R; and (iii) estimating J_{IC} using simple micromechanical modeling procedures. HP 9-4-20, ASTM A710, and 9Ni steels were heat treated to systematically control the microstructure and particle spacings. Fracture-surface microroughness was measured stereographically and correlated to the local effective fracture strain $\bar{\epsilon}_f^*$ and fracture toughness J_{IC}. The effective fracture strain and J_{IC} were found to be proportional to the local fracture microroughness, and J_{IC} could be estimated at least qualitatively using a microroughness parameter and the characteristic distance l_o^*. In these steels, microstructural changes that increase fracture strain and decrease yield strain improve both J_{IC} and T_R but have a larger effect on T_R (see Figure 3-1), the latter being confirmed to increase monotonically with the nondimensional crack initiation toughness, $J_{IC}(E/l_o^*\sigma_o^2)$. Observation of crack profiles revealed a

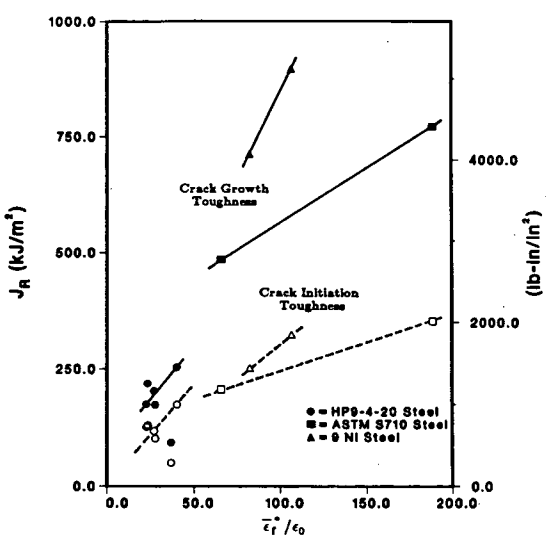

Figure 3-1. Variation in crack initiation and crack growth toughness with microstructure, as defined by the ratio of fracture strain to yield strain. (XBL 871-83)

zigzag fracture that propagated along either the spiral slip lines emanating from the blunted crack tip (for ASTM A710 steel and 9Ni steel), or the straight slip lines characteristic of a nonblunted notch (for HP 9-4-20 steel). The process of the crack initiation and growth in ASTM A710 steel shows that ductile microcracks are formed at large inclusions ahead of the crack tip, and the crack propagates by joining these tearing microcracks to the main crack tip by shear localization (see Figure 3-2). Fracture toughness J_{IC} and T_R values of HP 9-4-20 steel increased as the austenitizing temperature was raised from

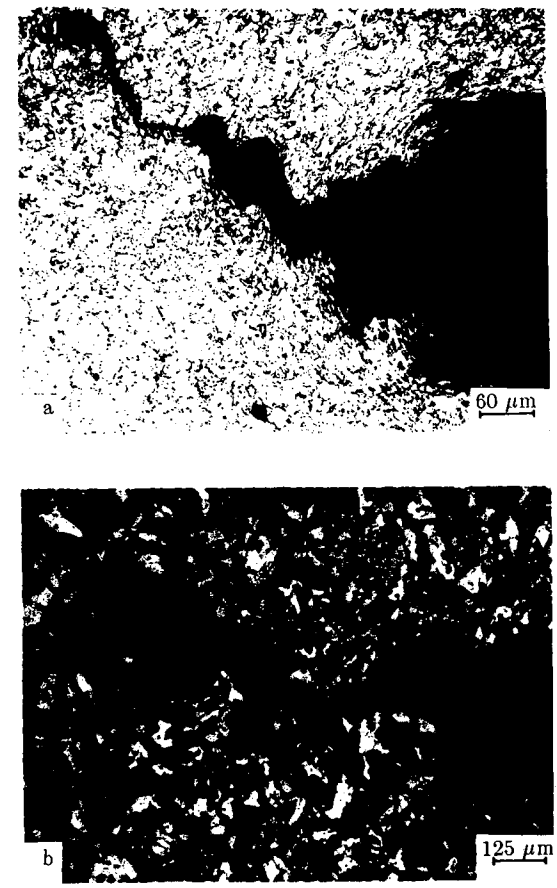

Figure 3-2. Stable ductile crack propagation via shear instability between neighboring voids and the main crack tip for an ASTM A710-4 steel. (Optical micrograph, etched in 2% nital.) (XBB 8610-8634A)

1050°C to 1200°C. However, the fracture toughness decreased with increase in austenitizing time from 1 hour to 10 or 100 hours at an austenitizing temperature of 1200°C, an observation attributed to overheating, arising from an intergranular cavitation-type failure.

4. Fundamentals of Fracture and Fatigue: A Basis for Alloy Design (Publication 7)

R.O. Ritchie, W.W. Gerberich, and S.D. Antolovich

Micromechanics and mechanisms describing fundamental aspects of failure by fatigue and fracture have been examined from the perspective of alloy design of superior engineering metals and alloys. The physical basis for intrinsic fracture toughness in materials was derived through several micromechan-

ical models for both brittle and ductile fracture, specifically for cleavage, microvoid coalescence, and transitional fracture modes. Second, factors governing the rate of growth of fatigue cracks were modeled with emphasis on the role of crack tip shielding mechanisms such as crack closure (see Figure 4-1). Examples of the design of microstructures giving optimum resistance to fatigue crack propagation have been developed, with emphasis on high-temperature behavior.

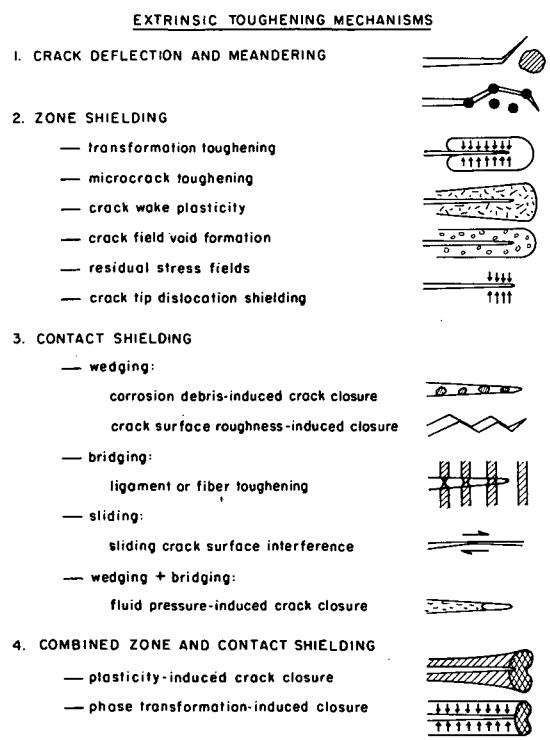

Figure 4-1. Schematic representation of the classes and mechanisms of crack tip shielding. (XBL 861-7432)

5. Development of Unusually High Fatigue Resistance in Dual-Phase Steels (Publications 18 and 22)

J. Shang, J.-L. Tzou, and R.O. Ritchie

The role of crack tip shielding in retarding the initiation and growth of fatigue cracks has been examined in duplex microstructures, with the objective of achieving maximum resistance to fatigue. Specifically, duplex ferritic-martensitic structures have been developed in common engineering AISI 1008 and 1015 mild steels through intercritical annealing to promote shielding without loss in strength. The shielding is developed primarily from crack deflection and resultant crack closure (see Figure 5-1), such that unusually high long-crack propagation resistance is obtained. With such techniques,

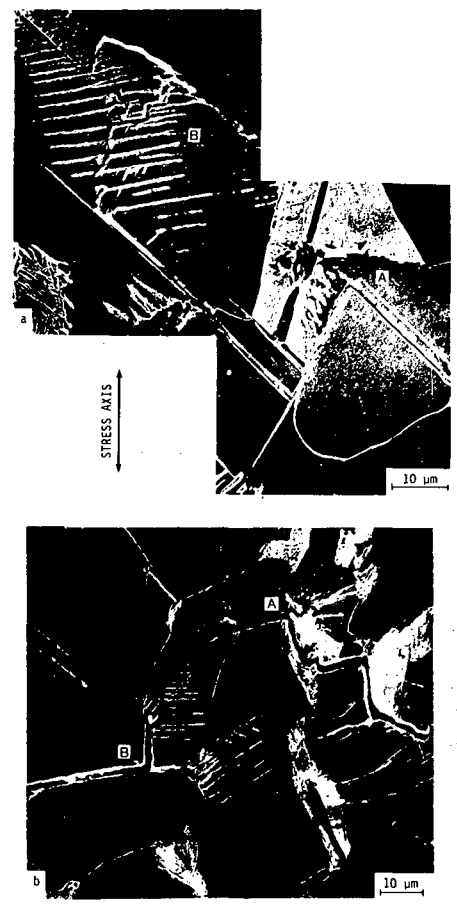

Figure 5-1. Small fatigue crack growth in (a) duplex 26% martensite and (b) 46% martensite microstructures in AISI 1008 steel, showing preferential growth in the ferrite, abrupt crack deflection at the martensite phase (regions A), and slip-band activity, blunting, and deflection at ferrite grain boundaries (regions B). Arrow indicates direction of applied tensile stress. (Etched in 2% nital.) (XBB 8610-7958)

it is found that the fatigue threshold ΔK_{TH} in AISI 1008 can be increased by more than 100% to over 20 MPa$\sqrt{m}$, without sacrifice in strength, representing the highest ambient temperature threshold reported for a metallic alloy to date. Similar but smaller increases are found in AISI 1015. The effect of the dual-phase microstructures on crack initiation and small-crack (10–1000 μm) growth, however, is markedly different, characteristic of behavior influenced by the mutual competition of intrinsic and extrinsic (shielding) "toughening" mechanisms (see Figure 5-2). Accordingly, the duplex micro-

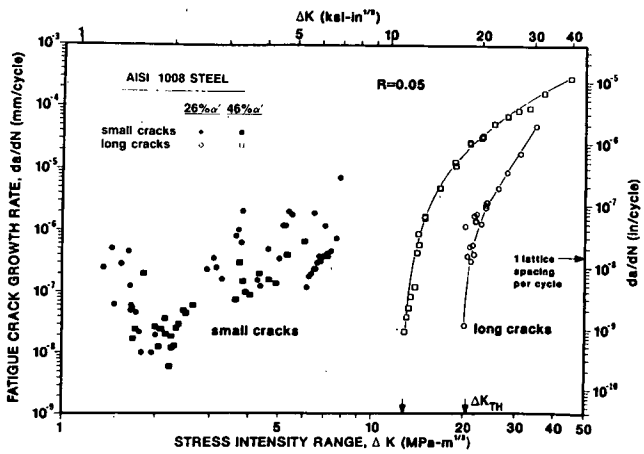

Figure 5-2. Comparison of the fatigue crack growth rates of long ($\gtrsim$ 20 mm) and naturally occurring small (10–1000 μm) cracks in duplex 26% and 46% martensite microstructures in AISI 1008 steel. Note how long crack growth rates (at fixed ΔK) are significantly slower in the 26% martensite structure, whereas small crack growth rates are marginally slower in the 46% martensite structure. (XBL 869-11702)

structures, which appear to show the highest resistance to the growth of long cracks, show the lowest resistance to crack initiation and small-crack growth. In general, dual-phase steels are found to display remarkable fatigue properties, with fatigue limits as high as 58% of the tensile strengths and fatigue thresholds in the range of 13–20 MPa$\sqrt{m}$.

6. Mechanisms of Variable Amplitude Fatigue Crack Propagation in Structural Titanium Alloys (Publication 17)

C.M. Ward-Close† and R.O. Ritchie

A comparative study has been made of the transient fatigue crack growth rate behavior following tensile overloads at low (near-threshold) and high stress-intensity ranges in an α/β-type titanium alloy IMI 550, with specific emphasis of the role of crack closure mechanisms. After tensile overloads, fatigue cracks in both coarse-grained α and fine-grained α/β microstructures were observed initially to accelerate, followed by significant retardation, before growth rates returned to their baseline levels (see Figure 6-1). The initial acceleration was attributed to an immediate reduction in near-tip closure, as indicated by metallographic sectioning, and a slight decrease in far-field closure, as measured by back-face compliance methods (see Figure 6-2). Subsequent retardation was not associated with marked changes in far-

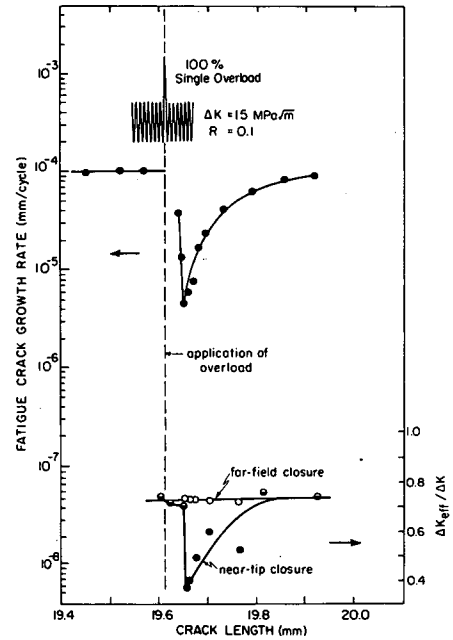

Figure 6-1. Variation in fatigue crack growth and corresponding variation in far-field and near-tip crack closure following 100% single tensile overloads at a constant baseline ΔK of 15 MPa$\sqrt{m}$ in α/β-annealed titanium alloy microstructure. Note how variation in local "driving force," ΔK_{eff}, corrected for near-tip closure, corresponds with the variation in post-overload growth rates. (XBL 863-7552)

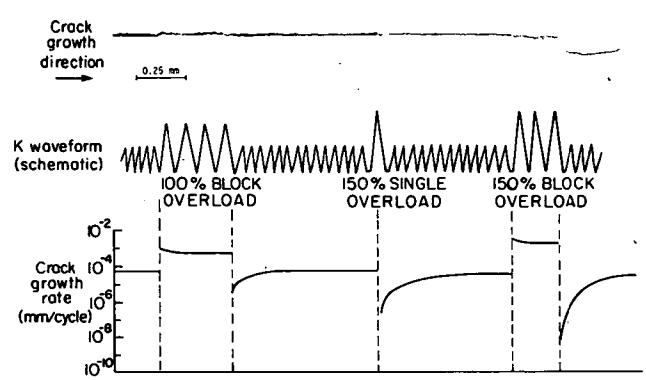

Figure 6-2. Metallographic section through a fatigue crack in α/β-annealed titanium alloy microstructure subjected to 100% block overload, 150% single overload, and 150% block overload at a constant baseline ΔK of 15 MPa$\sqrt{m}$, showing corresponding variation in growth rates. Note that after the single overload, crack blunting and opening occurs behind the tip, whereas the crack is closed directly ahead. Also significant crack deflection is only observed after the 150% high-low block loading sequence. (XBL 863-7551)

field closure, although there were indications on compliance curves of a second "closure point" at a higher load, suggesting an approximate 50% increase in near-tip closure. Load-interaction effects were

found to be most severe where specific mechanisms of crack closure were prominent. Thus, the maximum post-overload retardations were seen in the coarse-grained α microstructure, and when baseline stress-intensity ranges were close to the threshold ΔK_{TH}, or when the maximum overload stress intensities approached the fracture toughness.

---

†On leave from the Royal Aircraft Establishment, Farnborough, U.K.

1986 PUBLICATIONS AND REPORTS

Refereed Journals

1. T. Lin, A.G. Evans, and R.O. Ritchie, "A Statistical Model of Brittle Fracture by Transgranular Cleavage," J. Mechanics Phys. Solids **34**, 477 (1986); LBL-19673.
2. T. Lin, A.G. Evans, and R.O. Ritchie, "Statistical Analysis of Cleavage Fracture ahead of Sharp Cracks and Rounded Notches," Acta Metall. **34**, 2205 (1986); LBL-19928.
3. J. Glazer, S.L. Verzasconi, E.N.C. Dalder, W. Yu, R.A. Emich, R.O. Ritchie, and J.W. Morris, Jr., "Cryogenic Mechanical Properties of Al-Cu-Li-Zr Alloy 2090," Adv. Cryogenic Eng. **32**, 397 (1986); LBL-19232.
4. K.T. Venkateswara Rao, W. Yu, and R.O. Ritchie, "On the Growth of Small Fatigue Cracks in Aluminum-Lithium Alloy 2090," Scripta Metall. **20**, 1459 (1986); LBL-21883.
5. R.O. Ritchie and J. Lankford, "Small Fatigue Cracks: A Statement of the Problem and Potential Solutions," Mat. Sci. Eng. **84**, 11 (1986).†
6. R.O. Ritchie and P. Lubock, "Fatigue Life Estimation Procedures for the Endurance of a Cardiac Valve Prosthesis: Stress/Life and Damage-Tolerant Analyses," J. Biomech. Eng., Trans. ASME **108**, 153 (1986).

Other Publications

7. R.O. Ritchie, W.W. Gerberich, and S.D. Antolovich, "Fundamentals of Fracture and Fatigue: A Basis for Alloy Design," in *Mechanical Properties and Phase Transformations in Engineering Materials*, S.D. Antolovich, R.O. Ritchie, and W.W. Gerberich, Eds., TMS-AIME, Warrendale, PA, 1986, p. 99; LBL-20125.
8. R.O. Ritchie and W.Yu, "Short Crack Effects in Fatigue: A Consequence of Crack Tip Shielding," in *Small Fatigue Cracks*, R.O. Ritchie and J. Lankford, Eds., TMS-AIME, Warrendale, PA, 1986, p. 167.†
9. R.D. Pendse and R.O. Ritchie, "Influence of High Pressure Hydrogen Pre-Exposure on Crack Growth under Monotonic and Cyclic Loading," in *Modeling Environmental Effects on Crack Growth Processes*, R.H. Jones and W.W. Gerberich, Eds., TMS-AIME, Warrendale, PA, 1986, p. 321.‡
10. R.H. Dauskardt and R.O. Ritchie, "Fatigue Crack Propagation Behavior in Pressure Vessel Steels for High Pressure Hydrogen Service," in *High Strength Steels for Pressure Containment*, E. Nisbett, Ed., ASME PVP Vol. 114/MPC Vol. 27, American Society for Mechanical Engineers, New York, 1986, p. 17.‡
11. R.O. Ritchie, E. Zaiken, and A.F. Blom, "Is the Concept of a Fatigue Threshold Meaningful in the Presence of Compression Cycles?" in *Basic Questions in Fatigue*, Vol. I, ASTM STP 924, J.T. Fong and R.J. Fields, Eds., American Society for Testing and Materials, Philadelphia, PA (in press).†
12. R.O. Ritchie, W. Yu, A.F. Blom, and D.K. Holm, "Development of Fatigue Crack Closure with the Extension of Long and Short Flaws in Aluminum Alloy 2124: A Comparison of Experimental and Numerical Results," in *Fatigue Crack Closure*, ASTM STP, J.C. Newman, Jr., and W. Elber, Eds., American Society for Testing and Materials, Philadelphia, PA (in press).†
13. W. Yu and R.O. Ritchie, "Fatigue Crack Propagation in 2090 Aluminum-Lithium Alloy: Effect of Compression Overload Cycles," J. Eng. Mater. Tech., Trans. ASME, Series H **109** (in press).†
14. R.H. Dauskardt, R.D. Pendse, and R.O. Ritchie, "Effects of Pre-Existing Grain Boundary Microvoid Distributions on Fracture Toughness and Fatigue Crack Growth in Steel," accepted by Acta Metall.‡

LBL Reports

15. R.O. Ritchie, "A Comparison of Fatigue Crack Propagation in Modes I and III," in *Fracture Mechanics 18th Symposium*, ASTM STP, R.P. Reed and D.T. Read, Eds., American Society for Testing and Materials, Philadelphia, PA (in press); LBL-19828.
16. T. Lin, A.G. Evans, and R.O. Ritchie, "Stochastic Modeling of the Independent Roles of Particle Size and Grain Size in Transgranular Cleavage Fracture," Metall. Trans. A (in press); LBL-21393.
17. C.M. Ward-Close and R.O. Ritchie, "On the Role of Crack Closure Mechanisms in Influencing Fatigue Crack Growth Following Tensile Overloads in Titanium Alloys: Near-Threshold vs. Higher ΔK Behavior," in *Fatigue Crack Closure*, ASTM STP, J.C. Newman, Jr., and W. Elber, Eds., American Society for Testing and Materials, Philadelphia, PA (in press); LBL-21485.
18. J.K. Shang, J.-L. Tzou, and R.O. Ritchie, "Role of Crack Tip Shielding in the Initiation and Growth of Long and Small Fatigue Cracks in Duplex Microstructures," submitted to Metall. Trans. A; LBL-21895.
19. T. Lin (Ph.D. thesis), with R.O. Ritchie, "Stochastic Modeling of Cleavage Fracture Ahead of Rounded Notches and Sharp Cracks," LBL-21928.

20. K.T. Venkateswara Rao, W. Yu, and R.O. Ritchie, "Fatigue Crack Propagation in Aluminum-Lithium Alloy 2090: Part I. Long Crack Behavior," submitted to Metall. Trans. A; LBL-22178.
21. K.T. Venkateswara Rao, W. Yu, and R.O. Ritchie, "Fatigue Crack Propagation in Aluminum-Lithium Alloy 2090: Part II. Small Crack Behavior," submitted to Metall. Trans. A; LBL-22179.
22. J.K. Shang and R.O. Ritchie, "On the Development of Unusually High Fatigue Crack Propagation Resistance in Steels: Crack Tip Shielding in Duplex Microstructures," in *Mechanical Behaviour of Materials V*, Proc. Fifth Int. Conf. (ICM-5), Beijing, China, Pergamon Press, Oxford, U.K. (in press); LBL-22350.
23. T.S. Oh (M.S. thesis), with R.O. Ritchie, "A Study of Ductile Fracture for Stationary and Growing Cracks," LBL-22486.

Invited Talks

24. R.O. Ritchie and W. Yu, "Comparison of Long and Short Fatigue Crack Growth Behavior in the Near-Threshold Regime," Second International Engineering Foundation Conference on "Small Cracks," Santa Barbara, CA, Jan. 8, 1986.†
25. R.O. Ritchie and R. Gronsky, "Materials," College of Engineering Retreat, Napa, CA, Feb. 1986.
26. R.O. Ritchie, "Recent Advances in the Modeling of Fracture and Fatigue," Department of Mechanical Engineering, University of Houston, TX, Feb. 1986.
27. R.O. Ritchie, "Crack Tip Shielding in Fatigue," MMRD Annual Review, LBL, Feb. 1986.
28. R.O. Ritchie, W.W. Gerberich, and S.D. Antolovich, "Fundamentals of Alloy Design for Crack Initiation and Growth," Earl R. Parker Symposium on Structure/Property Relationships, 115th AIME Annual Meeting, New Orleans, LA, March 2–6, 1986.
29. R.O. Ritchie, T. Lin, and A.G. Evans, "Stochastic Approach to the Modeling of Cleavage Fracture," Symposium on Stochastic Approaches to Fracture, 115th AIME Annual Meeting, New Orleans, LA, March 2–6, 1986.
30. R.O. Ritchie and R.D. Pendse, "Influence of High Pressure Hydrogen on Fatigue Crack Growth in Pressure Vessel Steels," WESTEC Meeting, Los Angeles, CA, March 18, 1986.‡
31. R.O. Ritchie, "Statistics of Fracture Processes," Robert J. Cloud & Associates, Berkeley, CA, March 1986.
32. R.O. Ritchie, "Fatigue Crack Propagation: Shielding Mechanisms," Garrett Turbine, Phoenix, AZ, April 11, 1986.
33. R.O. Ritchie, "Aluminum-Lithium Alloys," Boeing Commercial Co., Seattle, WA, April 1986.
34. R.O. Ritchie, "Micromechanics of Small Crack Growth," AFWAL/MLLN, Materials Laboratory, Materials Behavior Branch, Wright-Patterson Air Force Base, Dayton, OH, April 17, 1986.
35. R.O. Ritchie, "Study of Damage Mechanisms Affecting Fatigue and Creep Rupture in Cr-Mo Steels," DOE AR&TD Fossil Energy Materials Review, Germantown, MD, May 6, 1986.‡
36. R.O. Ritchie, "Statistical Modeling of Cleavage Fracture," Mechanics Colloquia Series, the Technological Institute, Northwestern University, Evanston, IL, May 16, 1986.
37. R.O. Ritchie, "Small Crack Behavior: A Consequence of Crack Tip Shielding," NSF Workshop on Microcracking in Rocks, Park City, UT, May 29–30, 1986.†
38. R.O. Ritchie, "Statistical Modeling of the Transition from Microcracks to Macrocracks," NSF Workshop in Microcracking in Rocks, Park City, UT, May 29–30, 1986.
39. R.O. Ritchie, "Fatigue," University Extension Course on Fatigue and Fracture, University of California Berkeley, June 1986.
40. R.O. Ritchie, "Physical Basis of Fracture Toughness in Metals and Ceramics," University Extension Course on Fatigue and Fracture, University of California Berkeley, June 1986.
41. R.O. Ritchie, "Fatigue of Aluminum-Lithium Alloys," Center for Advanced Materials Light Alloys Review, LBL, June 1986.
42. R.O. Ritchie, "Sub-Critical Crack Growth in Metal-Ceramic Composites," Center for Advanced Materials Interface Program Review, LBL, Aug. 1986.
43. R.O. Ritchie, "Fatigue Crack Growth in Aluminum-Lithium Alloys," Northrop Corporation, Hawthorne, CA, Aug. 1986.
44. R.O. Ritchie, "Crack Tip Shielding: A Metallurgist's Perspective," Gordon Research Conference on Ceramics, Meriden, NH, Aug. 14, 1986.
45. R.O. Ritchie, "Intrinsic vs. Extrinsic Toughening of Metals, Ceramics and Composites," Alcoa Technical Center, Pittsburgh, PA, Aug. 29, 1986.
46. R.O. Ritchie, "Statistical Modeling of Fracture," Department of Materials Science and Mineral Engineering Seminar, University of California Berkeley, Sept. 25, 1986.
47. R.O. Ritchie, "Fatigue of Aluminum-Lithium Alloys: Long vs. Small Crack Behavior," Lockheed Palo Alto Research Labs, Palo Alto, CA, Oct. 29, 1986.
48. R.O. Ritchie, "Fatigue Crack Growth Properties of Aluminum-Lithium Alloys," Materials Engineering Department, San Jose State University, San Jose, CA, Nov. 13, 1986.

†Supported by the Air Force Office of Scientific Research under Grant No. AFOSR-82-0181.

‡Supported by the Advanced Research and Development, Fossil Energy Materials Program, U.S. Department of Energy, through Subcontract 19X-27429C with Oak Ridge National Laboratory under Martin-Marietta Contract No. DE-AC05-84OR21400.

PHYSICAL PROPERTIES

Interfaces and Ceramic Microstructures*

Joseph A. Pask, Investigator

INTRODUCTION

The purpose of this work is to advance the basic understanding of the nature of interfaces (primarily those between dissimilar materials, such as metals and ceramics), particularly in terms of bonding and the factors that control the development of adherence. This understanding is critical to the development of composites, protective coatings, and glass- and ceramic-to-metal seals, and to the reduction of corrosion at interfaces. The work involves studies of thermodynamics and kinetics of reactions at interfaces, and wetting and spreading of liquids.

Another objective of this work is to advance the understanding of the factors that play roles in the development of desired microstructures in ceramic materials, with and without a liquid phase. This understanding depends on a knowledge of the stable and metastable phase equilibrium of interfacial phenomena from a thermodynamics point of view and of mass-transport mechanisms during sintering.

1. Chemical Reactions and Adherence at Glass/Metal Interfaces: An Analysis (Publication 1)†

A.P. Tomsia and J.A. Pask

A review of wetting, spreading, and reactions of sodium disilicate glass on metals was prepared. The selected metals represented a wide range of activity. Most of them were either principal constituents of dental alloys or were present as alloying additions. Conditions for the occurrence of the different types of redox reactions at glass/metal interfaces were analyzed. All of the reactions have an effect in some way, both chemically and physically, on the bonding of glass to metal.

†Support was received from the National Institute of Dental Research of the National Institutes of Health under Grant No. DE-05460.

2. Bonding of Dental Glass to Nickel-Chromium Alloys (Publication 2)†

A.P. Tomsia and J.A. Pask

Two 80Ni-20Cr-type alloys, one 99.99% pure and one with 98% purity (the major impurity being Si), on atmospheric oxidation formed a multilayer oxide scale with an outer layer of NiO and a single-layer scale with an outer portion rich in Cr_2O_3, respectively. An applied K-aluminosilicate glass at 1020°C penetrated the latter oxide scale. Adherence was present at all interfaces due to the existence of chemical equilibrium. However, only the latter produced a satisfactory assembly because fractures occurred in the multilayer oxide scale and in the glass close to the oxide/glass interface, respectively.

†Support was received from the National Institute of Dental Research of the National Institutes of Health under Grant No. DE-05460.

3. Work in Progress

Studies of reactions between metals/alloys and glass are continuing. The redox reactions that occur at interfaces between these materials are important, because the glass in the interfacial zone becomes saturated with oxides of the substrate metal, leading to thermodynamic equilibrium and chemical bond-

*This work was supported by the Director, Office of Energy Research, Office of Basic Energy Sciences, Materials Sciences Division of the U.S. Department of Energy under Contract No. DE AC03-76SF00098.

ing at the interface. Particular attention is being addressed to systems of NiCr-based alloys and glass; of interest is the effect of various additives to the alloy on its oxidation characteristics. This study is supported by the National Institute of Dental Research of the National Institutes of Health.

Interpretation of published data and supporting additional experimental studies on phase relationship in the SiO_2-Al_2O_3 system are also continuing. Mullite ($3Al_2O_3 \cdot 2SiO_2$) powders are being prepared by colloidal and polymeric sol-gel techniques and sintered. The resulting microstructures are being characterized.

1986 PUBLICATIONS AND REPORTS

Refereed Journals

1. A.P. Tomsia and J.A. Pask, "Chemical Reactions and Adherence at Glass/Metal Interfaces: An Analysis," Dent. Mater. **2**, 10 (1986).†
2. A.P. Tomsia and J.A. Pask, "Bonding of Dental Glass to Nickel-Chromium Alloys," J. Am. Ceram. Soc. **69**, C-239 (1986).†

†Support was received from the National Institute Dental Research of the National Institutes of Health under Grant No. DE-05460.

High-Temperature Reactions*

Alan W. Searcy, Investigator

INTRODUCTION

The central purposes of this program are to develop improved thermodynamic and kinetic models of important processes in materials science and to subject the models to critical experimental tests. A theoretical breakthrough has been the reconciliation of the kinetics to the thermodynamics of equilibria among edge, surface, and bulk molecules in crystalline particles. The new understanding of the thermodynamics of equilibrium that was thus obtained has been applied to derive the conditions for particle-vapor equilibrium and the driving forces for sintering of anisotropic particles and for exaggerated grain growth. The expressions for sintering and grain growth are consistent with experimental observations that had not been explained by classical surface thermodynamic theory. A new theory for sintering in temperature gradients has been obtained as a consequence of extending the new thermodynamic approach to nonisothermal systems. Complementary experimental studies of sintering, adsorption, and surface diffusion are being conducted. Transmission electron microscopy (TEM) is being used to study sintering and the reaction of $BaCO_3$ with TiO_2. Tests of the predicted influence of temperature gradients on sintering are being evaluated in collaboration with Dario Beruto of the University of Genoa.

1. Theory for Sintering in Temperature Gradients: The Role of Long-Range Mass Transport (Publications 3 and 8)

A.W. Searcy

Essentially all evaluations of sintering data assume the major driving force to be the potential reductions in surface energies that can be produced by particle and aggregate shape changes. Furthermore, when vapor transport is negligible, mass transport during sintering is usually assumed to occur only over distances of the order of the dimensions of the individual particles of an aggregate. An extension of the model developed by the investigator to predict equilibrium vacancy distributions between sites of different bonding energies[1] shows that these two assumptions are probably both wrong under some conditions of practical importance. The new analysis indicates that, on a one-component, one-phase system, temperature gradients produce a driving force for diffusional mass transport by any path that can be expressed as the gradient in vapor pressure with temperature. Figure 1-1 shows that for

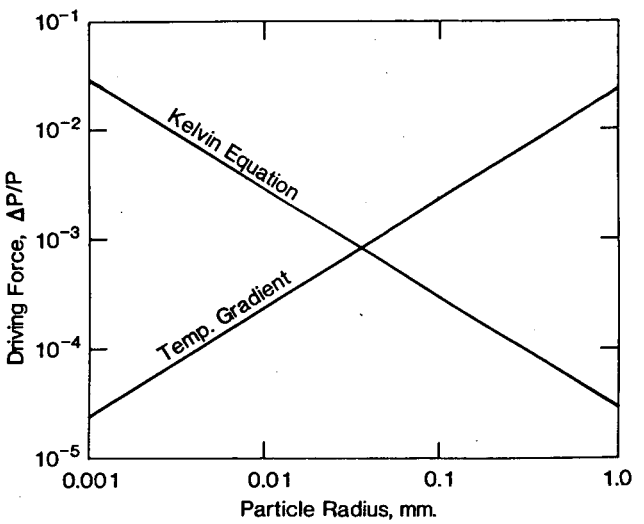

Figure 1-1. Comparison of pressure gradients calculated as pressure differences ΔP divided by the standard vapor pressure P for silver spheres from the Kelvin equation and from a 1°C/mm temperature gradient. (Neck radii are assumed to be 1/10 the particle radii.) (XBL 8611-4339)

silver at 1175 K, a temperature gradient of only 1°C/mm imposes a larger pressure gradient across any particle of more than 30 μm in radius than does differences in particle curvature. Furthermore, because ledge growth by statistical fluctuation rather than diffusion is often rate limiting for crystalline particles,[2] diffusion distances may be much greater than the radius of individual particles. It is suggested that in appropriate temperature gradients densification can be produced by surface diffusion from the hottest region of a body to cooler regions. The driving force for such transport is, as illustrated by Figure 1-2 for silver and MgO, potentially several orders of magnitude higher than that from surface-energy differences. Experimental tests of the theory are suggested.

*This work was supported by the Director, Office of Energy Research, Office of Basic Energy Sciences, Materials Sciences Division of the U.S. Department of Energy under Contract No. DE-AC03-76SF00098.

1. A.W. Searcy, J. Chem. Phys. **81**, 2489 (1984); **83**, 3095 (1985).
2. A.W. Searcy, J. Am. Ceram. Soc. **68**, C 267 (1985).

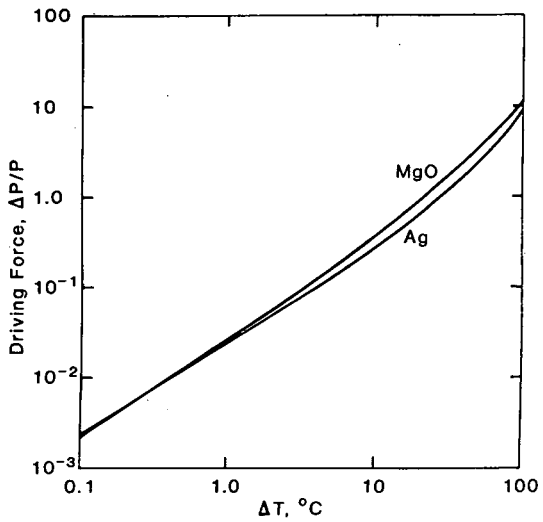

Figure 1-2. Driving force for a slow surface step as a function of temperature difference. Data for silver near 1175 K and for MgO vaporized as Mg and 1/2 O_2 near 1500 K. (XBL 8611-4338)

2. Shape and Size of Crystalline MgO Particles Formed by the Decomposition of $Mg(OH)_2$ (Publication 5)

M.G. Kim, U. Dahmen, and A.W. Searcy

From x-ray diffraction (XRD) line-broadening measurements, the crystals of MgO formed by decomposition of $Mg(OH)_2$ have been reported to be probably octahedral, and to be ~5 nm or more in cross section. TEM measurements by us show that MgO forms from $Mg(OH)_2$ decomposition in vacuum as cubes with 2 ± 0.2 nm edge lengths. The discrepancy in MgO particle sizes measured by TEM and XRD is suggested to arise because the MgO cubes are almost perfectly aligned within aggregates of 0.1 μm or greater cross section. This hypothesis will be tested by TEM and XRD measurements with MgO prepared by decomposition of $MgCO_3$. This MgO is formed as cubes of about 3 nm edge length, but in aggregates of less perfect alignment.

3. Origin of Cracking Phenomena Observed in Decomposition Reactions (Publication 6)

M.G. Kim, U. Dahmen, and A.W. Searcy

The development of cracks in the decomposition of $Mg(OH)_2$ and $MgCO_3$ was observed directly by TEM and scanning electron microscopy. Clear differences in the crack morphologies were found for the two solids. Decomposing $Mg(OH)_2$ formed a continuous network of cracks of about 2 μm mesh size, while decomposing $MgCO_3$ showed cracks that radiated from isolated centers (Figure 3-1).

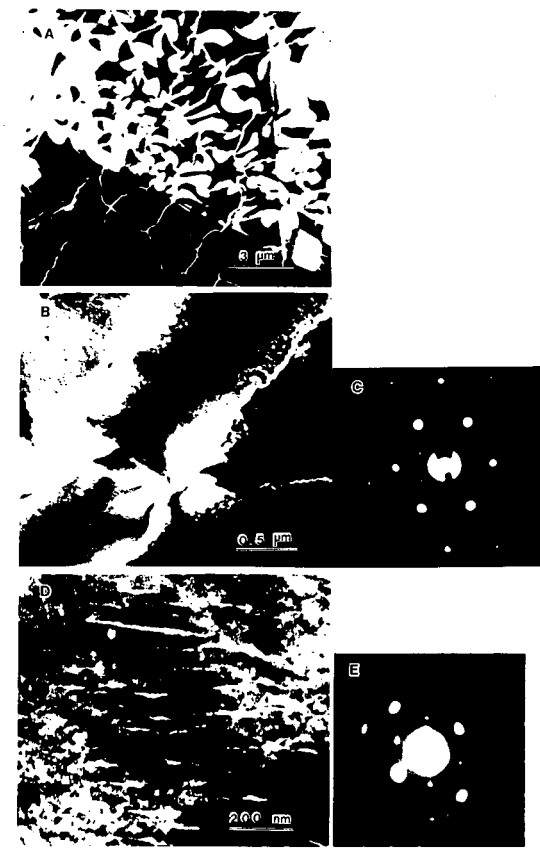

Figure 3-1. TEM micrographs of partly decomposed $Mg(OH)_2$: (A) and (B) [0001] $Mg(OH)_2$ and their corresponding diffraction pattern (C); (D) [1120] $Mg(OH)_2$ and its corresponding diffraction pattern (E). (XBB 854-3157)

As reported by earlier investigations, cracks formed in only partially decomposed $Mg(OH)_2$ propagate even through the undecomposed $Mg(OH)_2$. This fact was apparent from observation of both $Mg(OH)_2$ and MgO spots in electron-diffraction patterns taken just after cracking. Previous investigators proposed that the cracking occurred to relieve a critical strain that arose from the coherent nucleation of MgO in the $Mg(OH)_2$ matrix. However, this model is inconsistent with present experimental observations.

The only identifiable driving force for the cracking is the high excess surface energy of the product solid MgO particles of ~2 nm cross section. The

cracks may form as a consequence of aggregation of these particles to reduce the surface energy. The isolated crack centers observed in partially decomposed $MgCO_3$ do not extend into the reactant solid but are confined to the porous product solid MgO. The observed orientation relationship between $MgCO_3$ and MgO suggests that no plausible semicoherent reaction interfaces exist for the decomposition of $MgCO_3$. This fact implies that the cracking is not a consequence of an elastic strain but of the aggregation of MgO particles that are initially evenly spaced (Figure 3-2) in both decomposition reactions.

Detailed characteristics of the cracking observed in the decomposition of $Mg(OH)_2$ and $MgCO_3$ are presented and discussed.

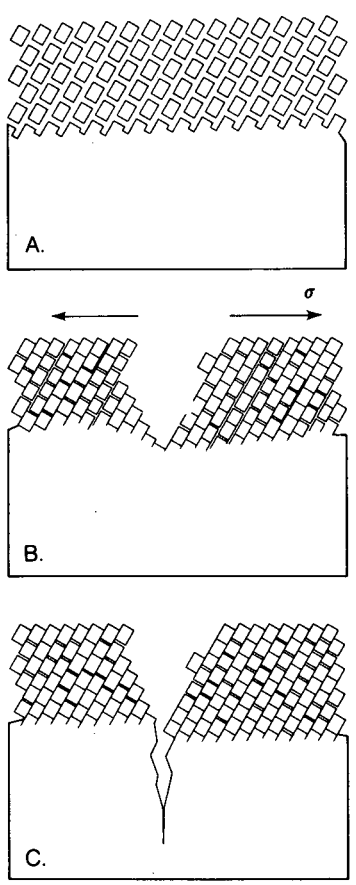

Figure 3-2. Schematic drawing of MgO partial aggregation, which is suggested to explain the cracking in Figure 3-1. (XBL 854-2137)

4. Thermodynamics of Two Two-Dimensional Phases Formed by CO_2 Chemisorption on MgO (Publication 7)

D. Beruto,† R. Botter,† and A.W. Searcy

Variations in concentrations of CO_2 adsorbed on MgO with temperature at constant pressure and with pressure at constant temperature at 880 K to 950 K indicate a miscibility gap in surface coverage. In the low-coverage region the enthalpy of chemisorption is -183 ± 10 J/(mole-deg.). The molar enthalpy and entropy of transition from the low- to the high-coverage phase are -9 ± 5 kJ and -13 ± 10 J/deg. The enthalpies and entropies of adsorption show that the CO_2 is much more strongly held as CO_3^{-2} ions on the MgO surface than in $MgCO_3$.

To account for the strong chemisorption, the number of Mg^{+2} ions bound to each surface CO_3^{-2} ion on MgO at 600 K to 1000 K must be higher than reported from infrared measurements of CO_2 adsorbed as CO_3^{-2} on MgO near room temperature. Hysteresis in the isothermal adsorption and desorption plots in the vicinity of the steep variation in equilibrium coverage with pressure (Figure 4-1) suggests that transformation between the two coverage regimes may require a reordering of CO_3^{-2} on surface sites.

†Present address: Universita di Genova, Italy

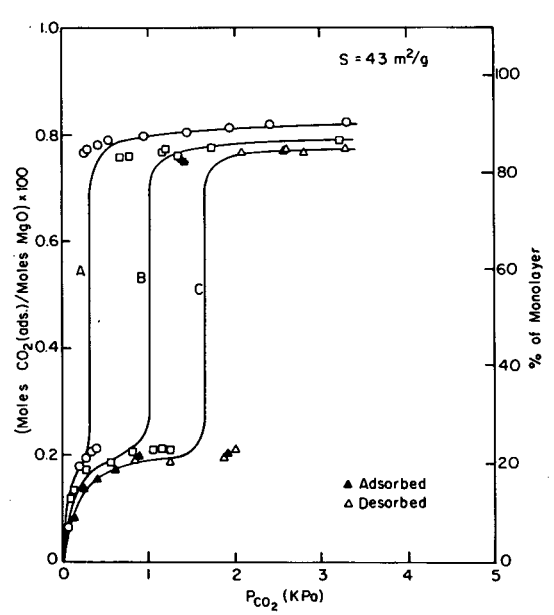

Figure 4-1. Isotherms for CO_2 adsorption. (A) at 893 K; (B) at 933 K; (C) at 953 K. (XBL 859-6602)

1986 PUBLICATIONS AND REPORTS

Refereed Journals

1. A.W. Searcy, "Origins of Planar, Concave, and Convex Boundaries during Exaggerated Grain Growth," J. Am. Ceram. Soc. **69**, C-91-2 (1986); LBL-20524.

Other Publications

2. A.W. Searcy, "The Kinetics of Particle-Vapor Equilibrium," in *High Temperature Materials Chemistry-III*, Z.A. Munir and D. Cubicciotti, eds., The Electrochemical Society, Pennington, N.J., 1986, p. 14; LBL-20408.

LBL Reports

3. A.W. Searcy, "Theory for Sintering in Temperature Gradients: The Role of Long Range Mass Transport," J. Am. Ceram. Soc. (in press); LBL-21776.
4. M.G. Kim, U. Dahmen, and A.W. Searcy, "Structural Transformations in the Decomposition of $Mg(OH)_2$ and $MgCO_3$," J. Am. Ceram. Soc. (in press); LBL-21587.
5. M.G Kim, U. Dahmen, and A.W. Searcy, "Shape and Size of Crystalline MgO Particles Formed by the Decomposition of $Mg(OH)_2$," LBL-22159.
6. M.G. Kim, U. Dahmen, and A.W. Searcy, "Origin of Cracking Phenomena Observed in Decomposition Reactions," Ceramic Microstructures '86 (in press); LBL-22160.
7. D. Beruto, R. Botter, and A.W. Searcy, "Thermodynamics of Two, Two-Dimensional Phases Formed by CO_2 Chemisorption on MgO," LBL-22161.
8. A.W. Searcy, "Sintering Theory for Crystalline Solids," Ceramic Microstructures '86 (in press); LBL-22162.

Invited Talks

9. M.G. Kim, U. Dahmen, and A.W. Searcy, "TEM Study of Sintering of 2 nm MgO Cubes," 88th Annual Meeting, American Ceramic Society, Chicago, IL, April 29, 1986.
10. A.W. Searcy, "Theory for Sintering in Temperature Gradients: The Role of Long Range Mass Transport," 88th Annual Meeting, American Ceramic Society, Chicago, IL, April 29, 1986.
11. A.W. Searcy, "Sintering Theory for Crystalline Solids," Ceramic Microstructures '86, Berkeley, CA, July 29, 1986.
12. M.G. Kim, U. Dahmen, and A.W. Searcy, "Origin of Cracking Phenomena Observed in Decomposition Reactions," Ceramic Microstructures '86, Poster Session, Berkeley, CA, July 30, 1986.
13. M.G. Kim, M. Cima, and A.W. Searcy, "Comparison of Sizes Measured for Very Small MgO Crystals by TEM and XRD Methods," 39th Pacific Coast Regional Meeting, American Ceramic Society, Seattle, WA, Oct. 30, 1986.
14. A.W. Searcy, "The 10^{18} Particle Problem in Sintering," Basic Science Division Meeting, American Ceramic Society, New Orleans, LA, Nov. 5, 1986.

Structure-Property Relationships in Semiconductor Materials*

Jack Washburn, Investigator

INTRODUCTION

The purpose of this program is to advance the understanding of the effects of structural defects, including the structure of interfaces, on the electrical or optical properties of semiconductor materials. Systems chosen for study are those that have interfaces and defects that are formed during the processing steps used for state-of-the-art solid-state device manufacture, such as ion implantation, oxidation, and contact formation.

The approach leads naturally to areas of basic research interest: for example, an improved understanding of (1) orientation relationships and mechanisms of accommodation of misfit at epitaxial interfaces, (2) the factors that determine electrical behavior of contacts between different classes of metals and 3–5 semiconductors, and (3) the origin of defects and amorphous zones caused by electron and ion damage in compound semiconductors.

High-resolution transmission electron microscopy (TEM), particularly on cross-section samples and, when possible, with computer simulation of images, has proved to be a powerful tool for revealing and identifying fine-scale defects and interface structure. The TEM information is also frequently combined with supplementary structural observations on the same specimens from electron paramagnetic resonance (EPR), Rutherford backscattering (RBS), secondary-ion mass spectroscopy (SIMS), x-ray diffraction, or microanalytical electron microscopy.

1. Observation of Stoichiometry Deviations Beneath Metal Contacts on GaAs (Publication 13)

Z. Liliental-Weber, E.R. Weber, N. Newman, W.E. Spicer, R. Gronsky, and J. Washburn

The structure of metal-semiconductor Schottky contacts (Au-GaAs, Al-GaAs, and $TiSi_2$-GaAs) were investigated by high-resolution and analytical electron microscopy. Figure 1-1 shows a high-resolution image of a Au-GaAs interface. Distortion of the GaAs lattice is indicated within a few interatomic distances from the abrupt interface; the arrows show irregularities. EDX spectra showed an increase of As in the GaAs layers immediately adjacent to the Au.

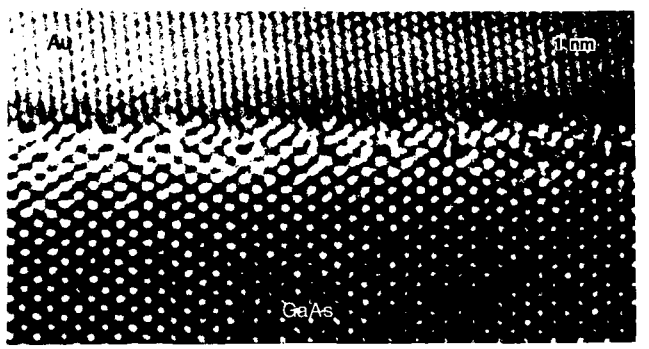

Figure 1-1. High-resolution image of the Au/GaAs (110) interface annealed at 405°C for 10 min in N_2 atmosphere. Note the twisting of the $(111)_{Au}$ planes toward the $(200)_{GaAs}$ planes and the distortion of the GaAs within a few interatomic distances of the interface. (XBB 872-992)

Figure 1-2 shows an interface between Al and GaAs. Using a beam diameter of 0.1 nm, an increase in the As/Ga ratio was again observed for this interface for the near-interface layers. Similar results were obtained for the $TiSi_2$ contact.

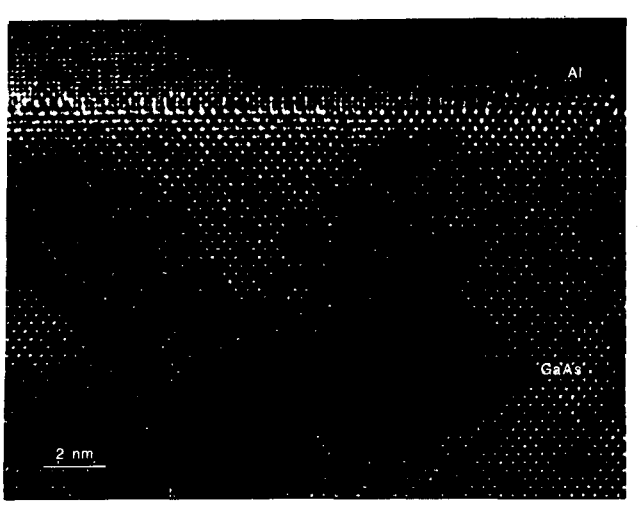

Figure 1-2. High-resolution image at the Al/GaAs (100) interface grown in a MBE chamber with 25°C substrate temperature. Note that (200) atomic layers in Al (2-Å spacing) are clearly resolved by the Atomic Resolution Microscope. (XBB 868-6011)

This work was supported by the Director, Office of Energy research, Office of Basic Energy Sciences, Materials Sciences Division of the U.S. Department of Energy under Contract No. DE-AC03-76SF00098.

This investigation of three different Schottky contacts on GaAs has shown structural distortion and deviation from stoichiometry in the anion-rich direction within the first few atomic layers of the semiconductor adjacent to the metal.

These results are consistent with defect models that relate the Fermi-level pinning to anion-rich lattice defects such as As_{Ga} antisite defects or larger As-rich clusters

2. Phase-Formation Sequence and Reacted Film Morphologies for Ni, Pd, and Pt on GaAs (Publications 9, 10, 14, and 17)

T. Sands, V.G. Keramidas, J. Washburn, R. Gronsky, K.M. Yu, A.J. Yu, and S.K. Cheung

Advanced compound semiconductor devices require increasingly stable, shallow, and uniform metallized layers for ohmic and Schottky contacts. However, the design of new multielemental contact metallization systems is limited by the paucity of information regarding the structure, composition, and stability of phases resulting from the interaction of single metal layers with compound semiconductors.

The reactions between (100) GaAs and the near-noble metals Ni, Pd, and Pt have been investigated by high-resolution TEM, energy-dispersive analysis of x-rays in scanning TEM, and RBS. Emphasis is placed on the evolution of the phase distributions and interface morphologies during annealing at temperatures up to 480°C.

For Ni the first reaction product is shown to have the composition Ni_3GaAs. Based on this composition and lattice-parameter measurements, it is proposed that the structure of Ni_3GaAs is closely related to that of γ-Ni_3Ga_2, a derivative of the hexagonal B8 structure type.

For Pd, annealing of a 15-nm film on {100} GaAs at 150°C yields a planar monocrystalline film of the first ternary phase ($\sim Pd_{3.9}Ga_{1.1}As_{0.9}$), which is a rectifying contact to n-GaAs with a barrier height of ~0.76 eV. A subsequent annealing treatment at 350°C converts the film to a second ternary phase ($\sim Pd_{3.3}Ga_{1.2}As_{0.8}$) that exhibits a rough interface with GaAs, severely degraded electrical properties, and a lower barrier height. The reduction in the measured barrier height is attributed to thermionic-field emission at sharp corners and protrusions in the Pd_xGaAs/GaAs interface. The implications of these results for the use of Pd in multielemental contacts to GaAs are also discussed.

Of the near-noble metals, only Pt shows no evidence of reaction with GaAs during deposition and specimen preparation. Even after annealing at 220°C for 10 min, only a slight reaction is indicated by image contrast below the native oxide–hydrocarbon layer. Annealing at ~315°C for 10 min, however, results in an extensive reaction. A reacted layer forms below the native oxide–hydrocarbon layer. Plan-view diffraction patterns and RBS results suggest that the reaction is incomplete and that the probable layer sequence is $Pt/Pt_3Ga/PtAs_2/GaAs$.

After annealing at 410 and 480°C for 10 min, the reaction is nearly complete, with only PtGa and $PtAs_2$ detected by diffraction and RBS. The behavior of a thin (1–2 nm) native oxide–hydrocarbon layer during the Ni/GaAs, Pd/GaAs, and Pt/GaAs reactions is also investigated. Only the Ni/GaAs reaction is noticeably impeded by this intervening layer. In contrast, the Pd/GaAs and Pt/GaAs reactions tend to mechanically disperse the native oxide layers.

3. Reactions at the Indium-GaAs Interface (Publications 8 and 16)

J. Ding, J. Washburn, T. Sands, and V.G. Keramidas

Graded $In_{1-x}Ga_xAs$ layers on GaAs grown by molecular-beam epitaxy (MBE) have been shown to make low-resistance ohmic contacts to n-GaAs. The grading is thought to be necessary to smooth out the conduction-band discontinuity so that ohmic conduction can occur. To better understand the interface region between GaAs and In, the reactions that occur in evaporated indium films on GaAs after heating (up to 650°C) have been studied by high-resolution TEM and electron and x-ray diffraction.

The effects of a thin (~1.3-nm) intervening native GaAs oxide interface layer on the In/GaAs reaction have also been investigated by comparing the reactions of In on GaAs substrates with the native oxide either present or desorbed. TEM of cross-section samples reveals that the thin native oxide layer, when present, disrupts the In/GaAs orientation relationship in as-deposited samples and prevents an extensive reaction between In and GaAs at 305°C. These data also show that the In/GaAs reaction at 350°C proceeds by dissolution of the GaAs substrate into the molten In followed by the subsequent nucleation and growth of epitaxial $In_{1-x}Ga_xAs$ particles, with $x \leqslant 0.2$ or $x \geqslant 0.8$ only, indicating immiscibility. The $In_{1-x}Ga_xAs$/GaAs interfaces are found to be structurally and composi-

tionally abrupt to within ~3 nm (see Figure 3-1). Histograms of the compositions of the $In_{1-x}Ga_xAs$ precipitates formed during annealing confirm the existence of a miscibility gap in the InAs-GaAs pseudo-binary system. It follows that the formation of graded $In_{1-x}Ga_xAs$ ($0 < x < 1$) layers by thermal reaction of In on GaAs is not possible under furnace-annealing conditions (slow heating and cooling) unless the annealing temperature is above the critical temperature, estimated in this study to be between 575°C and 605°C. If a graded layer is indeed necessary to form a low-resistance In-base ohmic contact to n-GaAs (i.e., to smooth out the InAs-GaAs conduction-band discontinuity), our results suggest that fabrication of graded $In_{1-x}Ga_xAs$/GaAs ohmic contacts by thermal reaction must involve annealing at temperatures above the critical temperature.

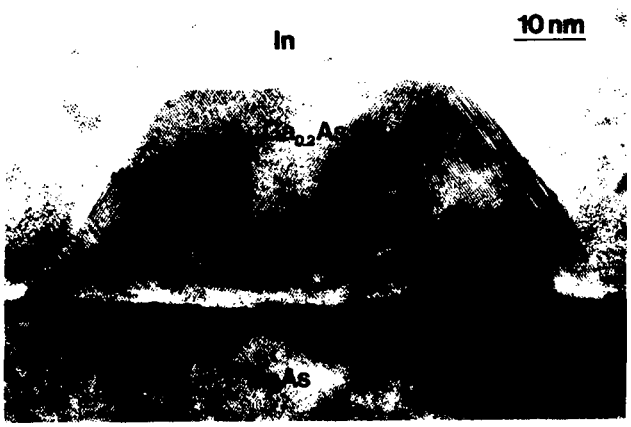

Figure 3-1. Lattice image of $In_{0.8}Ga_{0.2}As$ phase layer on GaAs. The interface between the two layers is structurally abrupt to within ~3 nm. (XBB 862-932)

4. The Structure and Electrical Properties of Au Contacts to GaAs (Publications 2, 4, 12, and 15)

Z. Liliental, W.E. Spicer, E.R. Weber, J. Washburn, N. Newman, D. Coulman, and G. Reid

The structure and electrical properties of Au contacts to GaAs have been studied by analytical and high-resolution TEM combined with electrical characterization and photoemission spectroscopy (PES). The contacts were prepared by *in situ* deposition of Au onto ultrahigh-vacuum cleaved n-GaAs (110) surfaces. The effects of annealing on the electrical, morphological, and chemical properties of the Au:GaAs contacts were studied. It was shown that the formation of Schottky contacts is correlated with the change in stoichiometry of the GaAs substrate near the Au/GaAs interface. The change to ohmic behavior for the samples annealed above the Au-Ga eutectic was explained by leakage currents at the periphery of the devices.

The change to "ohmic" behavior has been correlated with the formation of very thin, predominantly Au, crystallites on the surface of the GaAs at the periphery of the contact. These crystallites were typically 5–10 μm long and 500–2000 Å wide and are crystallographically oriented along the GaAs <110> direction. TEM and AES sputter profiles have shown that these fingers are ~100–150 Å thick. Either glancing-incidence sputtering using 1-keV Ar ions with sample rotation, or a wet chemical mesa etch (H_2SO_4:H_2O_2:H_2O), was used to selectively remove the crystallites from around the periphery. AES, SEM, and TEM results confirmed the removal of the crystallites. Electrical measurements after this treatment then showed a return to rectifying behavior for the diodes. These results demonstrate that the presence of the thin Au crystallites was correlated with the "Ohmic" behavior in this system.

The morphology of the overlayer was found to depend strongly on annealing and surface treatment. TEM results indicated that the interface is flat and abrupt for all unannealed diodes, as well as for annealed diodes formed on atomically clean surfaces. For annealed diodes formed on the air-exposed surfaces, the metal-semiconductor interface contains large metallic protrusions extending up to several hundred Angstroms into the semiconductor. For comparison to practical structures, the morphology of annealed diodes formed using typical commercial processing technology [i.e., formed on chemically prepared (100) surfaces annealed in forming gas] was also investigated using TEM. The interface for these structures is more complex than interfaces formed on the atomically clean and air-exposed cleaved (100) surfaces. Evidence that Au diffuses through the interfacial native oxide layer and forms islands in intimate contact with the semiconductor was found. The results of this study show that, upon annealing, the interfacial chemistry and morphology depend strongly on the surface preparation of GaAs before gold deposition.

5. A Model of Amorphous Silicon Layer Regrowth (Publication 11)

P. Ling and J. Washburn

Ion implantation into silicon usually results in formation of an amorphous silicon layer that recrystallizes during subsequent annealing. A new model is presented that combines heterogenous nucleation and growth to explain the mechanism of the crystal regrowth of amorphous silicon, in contact with a Si single-crystal substrate. This model explains the effects of substrate orientation and impurity concentration on the kinetics of crystal regrowth.

The model is based on nucleation and migration of growth steps at the crystal-amorphous interface. It is assumed that (1) the nuclei are disc shaped and one or two atomic layers thick at the amorphous-crystalline interface; (2) new nuclei can form on the top of expanding nuclei. This is equivalent to saying that the total nucleation rate is constant during the time of the regrowth process, since the total interface area for nucleation is constant; (3) the impurity concentration does not change during regrowth, and the migration rate of the growth steps (the growth rate of the nuclei) is constant; (4) the number of atoms per unit volume in the crystalline phase is equal to that in the amorphous phase; and (5) the regrowth rate R is defined as $R = a/t^*$, where a is the disc thickness and t^* is the time at which the area swept by growth steps is equal to the substrate area.

Based on these assumptions, the regrowth occurs as follows: after nucleation, disc-shaped growth steps at the amorphous-crystalline interface migrate in a direction parallel to the faces of the disc (expansion). When they grow large enough, these growth steps meet each other and form a complete (crystalline) layer of atoms over the entire interface. The amorphous-crystalline interface has advanced into the amorphous region by a distance equal to the height of the growth steps, and the regrowth rate is a/t^*.

6. Determination of As and Ga Planes by Convergent-Beam Electron Diffraction (Publication 7)

Z. Liliental-Weber and L. Parechanian-Allen

Convergent-beam electron diffraction using either the (200) systematic row or the (011) zone axis was successfully applied to determine the crystal polarity in (011) GaAs samples. This method makes it possible to distinguish the stacking sequence of the As and Ga planes. The information existing in the 200 disk of the diffraction pattern is different, depending on whether a particular disk refers to the As or the Ga plane. Therefore, this method can be generally applied in TEM for *in situ* samples and without any chemical etching.

1986 PUBLICATIONS AND REPORTS

Refereed Journals

1. Z. Liliental, R.W. Carpenter, and J.C. Kelly, "The Structure of Rapid Thermally Annealed Nitrogen-Implanted Silicon," Thin Solid Films **138**, 141 (1986); LBL-19717.
2. Z. Liliental-Weber, N. Newman, W.E. Spicer, R. Gronsky, J. Washburn, and E.R. Weber, "The Structure and Electrical Properties of Gold Contacts on GaAs," Mat. Res. Soc. Proc. **54**, 415 (1986); LBL-20618.
3. Z. Liliental-Weber, R.W. Carpenter, and J.C. Kelly, "The Structure of Oxygen Implanted Silicon Before and After Heat Pulse Annealing," Mat. Res. Soc. Proc. "Rapid Thermal Processing" **52**, 139 (1986); LBL-20631.
4. Z. Liliental-Weber, R. Gronsky, J. Washburn, N. Newman, W.E. Spicer, and E.R. Weber, "Schottky and Ohmic Au Contacts on GaAs; Microscopical and Electrical Investigation," J. Vac. Sci. Technol. **B4**, 912 (1986); LBL-21010.
5. Z. Liliental-Weber, C. Nelson, R. Ludeke, R. Gronsky, and J. Washburn, "An Atomic-Resolution Microscope Study of Al Contacts on GaAs," Proc. 44th Ann. Meet. EMSA, Albuquerque, 1986, J.W. Bailey, Ed., San Francisco Press, 1986, p. 726; LBL-21282.
6. Z. Liliental-Weber, "Structure and Properties of Metal-GaAs Interfaces," in *Advanced Processing and Characterization of Semiconductors III*, D.K. Sadana and M.I. Current, eds., Proc. SPIE **623**, 237 (1986); LBL-20957.
7. Z. Liliental-Weber and L. Parechanian-Allen, "Determination of As and Ga Planes by Convergent Beam Electron Diffraction," Appl. Phys. Lett. **49**, 1190 (1986); LBL-21873.
8. J. Ding, J. Washburn, T. Sands, and V.G. Keramidas, "In/GaAs Reaction; Effect of an Intervening Oxide Layer," Appl. Phys. Lett. **49**, 818 (1986); LBL-21568.
9. T. Sands, V.G. Keramidas, J. Washburn, and R. Gronsky, "Structure and Composition of Ni_xGaAs," Appl. Phys. Lett. **48**, 402 (1986); LBL-20376.
10. T. Sands, V.G. Keramidas, A.J. Yu, K.M. Yu,† R. Gronsky, and J. Washburn, "Phase Formation Sequence in the Pd-GaAs System," Mat. Res. Soc. Symp. Proc. **54**, 367 (1986); LBL-20611.

11. P. Ling and J. Washburn, "A Model of Amorphous Silicon Layer Regrowth," Mat. Res. Soc. Symp. Proc. **45**, 47 (1985).
12. Z. Liliental-Weber, J. Washburn, N. Newman, W.E. Spicer, and E.R. Weber, "Morphology of Au/GaAs Interfaces," Appl. Phys. Lett. **49**, 1514 (1986); LBL-20956.

Other Publications

13. Z. Liliental-Weber, E.R. Weber, N. Newman, W.E. Spicer, R. Gronsky, and J. Washburn, "Observation of Stoichiometry Changes Beneath Metal Contacts on GaAs," in *Defects in Semiconductors*, Materials Science Forum, Vol. 10–12, H.J. von Bardeleben, Trans Tech Publications Ltd., 1986, p. 1223; LBL-22220.
14. T. Sands, K.M. Yu,† S.K. Cheung, and V.G. Keramidas, "$Pd_xGaAs/GaAs$: Correlation between Interface Structure, Morphology and Electrical Properties," Proc. 1986 Northeast Regional Meeting on Semiconductor-Based Heterostructures: *Interfacial Structure and Stability*, M. Green, Ed., AIME, Pittsburgh, 1986 (in press).

LBL Reports

15. D. Coulman, N. Newman, G. Reid, Z. Liliental-Weber, E.R. Weber, and W.E. Spicer, "A Chemical and Structural Investigation of Schottky and Ohmic Au/GaAs Contacts," in *Proc. 10th Int. Vacuum Congress*, Baltimore, 1986; J. Vac. Sci. Tech. (in press); LBL-22262.
16. J. Ding, J. Washburn, T. Sands, and V.G. Keramidas, "Influence of the InAs-Gas Miscibility Gap on the In/GaAs Reaction," 13th International Symposium on Gallium Arsenide and Related Compounds, Las Vegas, NV, Sept. 28–Oct. 1, 1986; LBL-22081.
17. T. Sands, V.G. Keramidas, A.J. Yu, K.M. Yu,† R. Gronsky, and J. Washburn, "Ni, Pd and Pt on GaAs: A. Comparative Study of Reacted Film Morphologies," LBL-21060.
18. Z. Liliental, R. Gronsky, J. Washburn, N. Newman, W.E. Spicer, and E.R. Weber, "Schottky and Ohmic Au Contacts on GaAs," LBL-20734.

Invited Talks

19. J. Washburn, "Electron Microscopy of Reactions on Compound Semiconductor Surfaces," Solid State Sciences Seminar, Sandia National Laboratories, Albuquerque, NM, May 21, 1986.
20. Z. Liliental-Weber, "Structural Characterization of III-V Semiconductors," Seminar on III-V Semiconductor Materials and Devices, Palo Alto, CA, May 1985.
21. Z. Liliental-Weber, "The Structure of Metal/GaAs Interfaces and Correlation With Their Electrical Properties," SPIE, January 1986.
22. T. Sands, "Compound Formation at Metal GaAs Interfaces," Dept. of Materials Science and Engineering, Cornell University, Ithaca, NY, Oct. 3, 1985.
23. T. Sands, "Electron Microscopy of Interfaces in Reacted Metal/GaAs Contacts," Fall Meeting, Northern California Society for Electron Microscopy, University of California, Davis, Oct. 9, 1985.
24. T. Sands, "Electron Microscopy of Reaction Products at Metal/Gallium Arsenide Interfaces," 1986 Spring Meeting, TMS/ AIME, New Orleans, LA, March 1986; Department of Metallurgical Engineering, Ohio State University, Columbus, OH, April 1986.

†Supported by the Center for Advanced Materials.

Fundamental Studies of Chemical Properties and Processing of Advanced Structural Ceramics*

Lutgard C. De Jonghe, Investigator

INTRODUCTION

Fabrication of reliable ceramics, either for structural, electronic, or other applications, requires complete control of the powder structure, the powder compaction, and the densification process. Control of these parameters is aimed at improving the microstructural and microchemical uniformity of the ceramics at a finer and finer scale. Achieving uniformity is even more critical in the fabrication of multiphase ceramics, such as particulate composites. This work examines and broadens the fundamental understanding of the processes involved in particle consolidation and subsequent densification. Applications of the perspectives that are developed focus on structural ceramics and on some electronic ceramics. The ceramics studied in this program include silicon carbide, silicon nitride, magnesium oxide, zinc oxide, and barium titanate. Advanced characterization tools, including x-ray photoelectron spectroscopy (XPS), angle-resolved photoelectron spectroscopy, Auger analysis, and high-resolution and microanalytical transmission electron microscopy, are used in the analysis of surface chemistry of as-fabricated and of chemically treated powders and their sintered compacts. The key technique in the analysis of the relationship between the structure of the compacted powder and its evolution during densification is loading dilatometry. This technique was first developed in this laboratory and combines the simultaneous measurement of creep and densification of powder compacts. It allows the definition of fundamental parameters describing quantitatively the densification of single-phase and multi-phase ceramics.

*This work was supported by the Director, Office of Energy Research, Office of Basic Energy Sciences, Materials Sciences Division of the U.S. Department of Energy under Contract No. DE-AC03-76SF00098.

1. Fundamental Studies of Ceramic Fabrication (Publications 1, 2, 8, 9, 10, 12, and 13)

L.C. De Jonghe, M.N. Rahaman, M. Lin, M. Weiser, S. Varanasi, G. Hseuh, and R. Brook[†]

Creep-sintering experiments, in which the uniaxial low-load creep response of a sintering compact is measured during its densification, has been used to clarify a number of fundamental aspects of the densification process. It has permitted the examination of the simultaneous action of applied stress and sintering stress, thus allowing predictions for any densifying system in which stresses arise. Such systems are the ones in which heterogeneities are present, either by design, as in particular composites, or by accident.

The systems examined so far include powder compacts of ZnO, CdO, MgO, and glass, as well as particular composites of ZnO with a dispersed SiC phase, and glass powder with dispersed SiC particles.

The loading-dilatometry data have shown that it is possible to separate kinetic, microstructural, and driving-force parameters for densification in a relatively straightforward manner, without the necessity of making structural assumptions about the system. The driving force for sintering can be expressed as a measurable equivalent applied hydrostatic stress. Stresses arising from densification incompatibilities can then be estimated with continuum calculations. This procedure allows for the hydrostatic back stresses—arising in densification of particular composites—to be determined quantitatively. For ceramic-matrix composites these stresses can approach the sintering stress, thus arresting densification. The parameter of importance for the system is $4G\tau/\eta$, where G is the shear modulus of the porous matrix, τ is the relaxation time of the process that stores strain, and η is the quasi-steady-state creep viscosity. For ceramic-matrix composites this parameter is easily about 100, leading to a dependence of the grain-size-compensated matrix-densification rate, $\dot{\epsilon}_\rho$, of a particular composite of the type $\dot{\epsilon}_\rho G^n \approx A(1-f)/f$, where f = volume fraction of the second phase, G = grain size, and A and n are mechanism-dependent constants (see Figure 1-1). For glass, the ratio $4G\tau/\eta$ is much lower, leading to a densification rate of the matrix that is independent of the amount of the second phase.

[†]Permanent address: University of Leeds, United Kingdom.

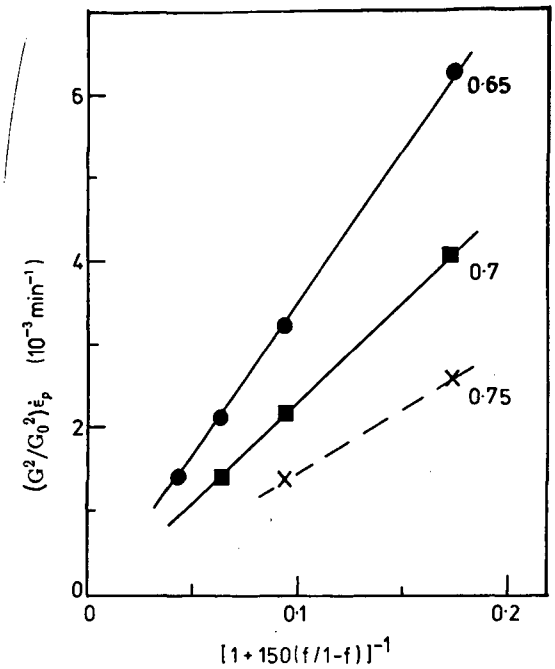

Figure 1-1. Grain-size-compensated densification rate of ZnO containing a dispersion of silicon carbide particles, at constant densities of 0.65, 0.7, and 0.75 of the theoretical density, versus the volume fraction function f. The linear dependence indicates agreement with the theory. (XBL 8611-4716)

2. Surface Chemistry of Silicon-Based Ceramic Powders (Publications 5 and 11)

L.C. De Jonghe, M.N. Rahaman, and Y. Boiteux

Surface chemistry is an important factor in the behavior of powders during densification and in the development of the properties of the final product. Therefore, surface characterization of some silicon carbides and silicon nitrides has been carried out by Auger analysis and by XPS. For the silicon nitride powder it was found that the particles are covered with a layer of an oxynitride glass that is nitrogen-rich near the oxide/nitride interface (see Figures 2-1 and 2-2). Nearly all oxygen could be accounted for by the glassy surface layer. For silicon carbide a discrete, stoichiometric silica layer was present, covered by a complex hydrocarbon contamination layer. The results for the silicon carbide were confirmed by an angle-resolved XPS analysis of oxidized, flat, dense silicon carbide surfaces (see Figure 2-3).

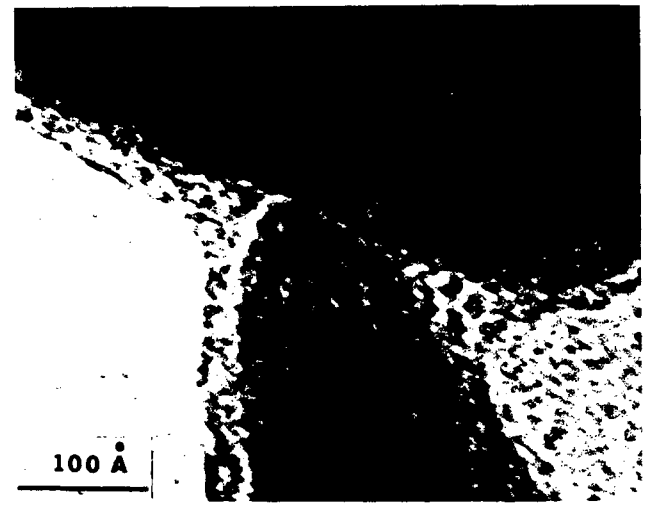

Figure 2-1. High-resolution transmission electron micrograph of Starck silicon nitride, showing an amorphous, fairly uniform surface layer of a silicon oxynitride glass of about 3 to 5 nm thick. (XBB 850-8115)

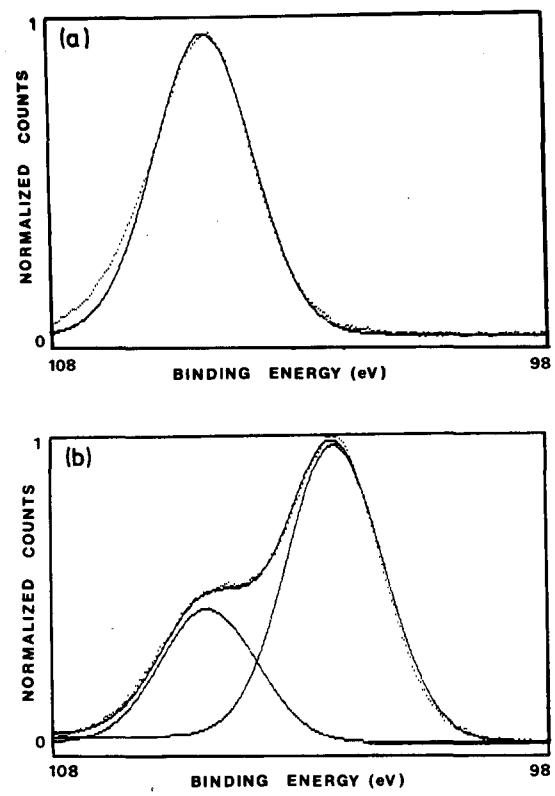

Figure 2-2. The silicon 2p line spectra in (a) GTE silicon nitride and (b) Norton silicon carbide. (XBL 859-4106)

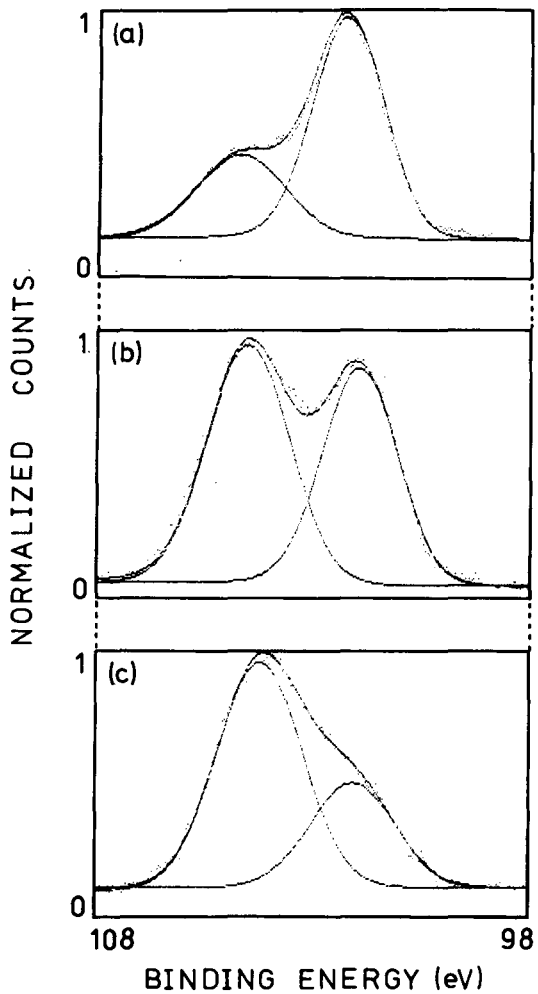

Figure 2-3. Silicon 2p line spectra for a flat, room-temperature oxidized SiC surface as a function of take-off angle: (a) 0°, (b) 40°, and (c) 70°. (XBL 865-1725)

3. Ceramic/Metal Interfaces (Publications 4, 6, 7, and 14)

L. De Jonghe, S. Shinde, I. Reimanis, D. Olson, and R.A. Miler[†]

Changes occurring at the interface between nickel metal and porous zirconia were examined for specimens subjected to oxidation at 900°C in air. A nickel oxide layer that can interact with the stabilizers used in the zirconia develops at the interfaces. The interactions can be understood simply in terms of the phase diagrams of the nickel oxide and the stabilizing oxide. The most severe interfacial degradation occurs for stabilizer/NiO systems that form extensive solid solutions, such as MgO and CaO. Degradation in actual thermal-barrier coatings was also examined. Bond-coat oxidation was found to be the major source of loss of mechanical integrity. The phases appearing as a result of the oxidation included NiO as well as Al_2O_3. The ceramic barrier layer shows a gradual increase in the monoclinic phase with heat treatment at 900°C in air. The bond-coat layer shows aluminum depletion. The formation of the oxidation products and their chemical interaction with the barrier coating, including extraction of the stabilizing oxide from the zirconia, leads to interface fracture (see Figure 3-1) and may constitute the first phase of coating degradation during prolonged exposure at elevated temperatures.

[†]Permanent address: NASA-Lewis, Cleveland, OH.

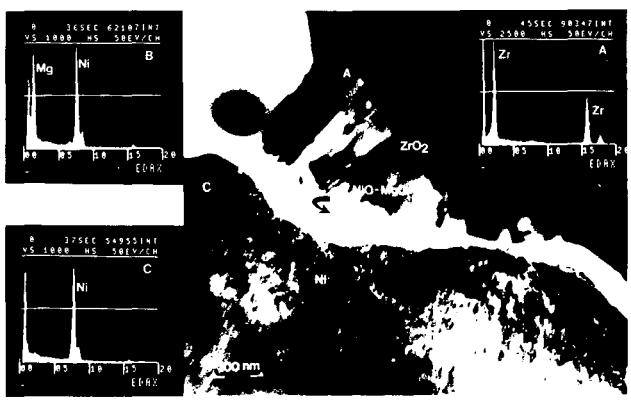

Figure 3-1. Interfacial reaction at NiO-ZrO_2 (calcia-stabilized) interface. A thin band of zirconia has transformed to monoclinic zirconia (inset microdiffraction pattern, top left). The superimposed EDX spectrum (bottom left) shows Ca depletion from the twinned region. (XBB 858-6912).

1986 PUBLICATIONS AND REPORTS

Refereed Journals

1. M.N. Rahaman, L.C. De Jonghe, and R. Brook, "The Effect of Shear Stress on Sintering," J. Am. Ceram. Soc. **69**, 53 (1986); LBL-18706.
2. L.C. De Jonghe, M.N. Rahaman, and G.C-H. Hsueh, "Transient Stresses In Bimodal Compacts During Sintering," Acta Metall. **34**, 1467 (1986); LBL-19224.
3. M.N. Rahaman, L.C. De Jonghe, and G.C-H. Hsueh, "Creep During Sintering of Porous Compacts," J. Am. Ceram. Soc. **69**, 58 (1986); LBL-19360.
4. S. Shinde and L.C. De Jonghe, "Cross-Sectional TEM Specimens from Metal-Ceramic Composites," J. Electron Microsc. Tech. **3**, 361 (1986); LBL-20074.
5. M.N. Rahaman, Y. Boiteux, and L.C. De Jonghe, "Surface Characterization of Silicon Nitride and Silicon Carbide Powders," Amer. Ceram. Soc. Bull. **65**, 1171 (1986); LBL-20389.

6. S.L. Shinde, I.E. Reimanis, and L.C. De Jonghe, "Evolution of the Nickel/Zirconia Interface," Ceram. Eng. Sci. Proc. 7, 1027 (1986); LBL-21044.
7. S.L. Shinde, I.E. Reimanis, and L.C. De Jonghe, "Degradation Mechanisms in Thermal Barrier Coatings," Ceram. Eng. Sci. Proc. 7, 1032 (1986); LBL-21043.

LBL Reports

8. M.W. Weiser and L.C. De Jonghe, "Rearrangement During Sintering in Two-Dimensional Arrays," accepted by J. Am. Ceram. Soc.; LBL-20633.
9. M.N. Rahaman and L.C. De Jonghe, "Creep and Densification of Glass Powder Compacts: I Effect of Applied Stress and Temperature," LBL-20713.
10. M.N. Rahaman, L.C. De Jonghe, and R.J. Brook, "Creep and Densification of Glass Powder Compacts: II Effect of Particle Size," LBL-20714.
11. M.N. Rahaman and L.C. De Jonghe, "Angle-Resolved XPS Analysis of Oxidized Polycrystalline SiC Surfaces," LBL-21460.
12. L.C. De Jonghe, M.N. Rahaman, and M. Lin, "The Role of Powder Packing in Sintering," LBL-21507.
13. M. Lin, M.N. Rahaman, and L.C. De Jonghe, "Creep-Densification and Microstructural Evolution in Heterogeneous MgO Powder Compacts," LBL-21508.
14. S. Shinde, I. Reimanis, and L.C. De Jonghe, "Degradation in a Thermal Barrier Coating," LBL-21045.

Invited Talks

15. L.C. De Jonghe, "Fundamental Aspects of Ceramic Fabrication," Sandia National Laboratory, Albuquerque, NM, Oct. 1985.
16. L.C. De Jonghe, "Sintering Forces in Two Dimensions," American Ceramic Society, Baltimore, MD, Nov. 1985.
17. L.C. De Jonghe, "Fundamental Aspects of Ceramic Fabrication," Kyocera, Kagoshima, Japan, Jan. 1986.
18. L.C. De Jonghe, "Fundamental Studies in Ceramic Processing," Rutgers University, Piscataway, NJ, Feb. 1986.
19. L.C. De Jonghe, "Perspectives in Sintering," University of California Berkeley, April 1986.
20. L.C. De Jonghe, "Role of Stresses in the Sintering of Heterogeneous Powder Compacts," Max Planck Institut für Metallforschung, Stuttgart, Federal Republic of Germany, June 1986.
21. L.C. De Jonghe, "Perfect Ceramics?" MPI, Stuttgart, Federal Republic of Germany, June 1986.
22. L.C. De Jonghe, "Nouveaux Developments du Procede Sol-Gel pour Elaboration des Poudres destinees au Frittage," EPFL, Lausanne, Switzerland, Sept. 1986.

Structure and Electrical Properties of Composite Materials*

Robert H. Bragg, Investigator

INTRODUCTION

The goal of this work is to understand how the structure-sensitive properties of carbon materials, such as mechanical strength, tensile creep, magnetic susceptibility, and the Hall coefficient, are related to their microstructure. The microstructure and concomitant changes in these properties undergo several disorder-order transformations when soft carbons are annealed in inert atmospheres above 2000°C. This graphitization is thus energy intensive and the critical process in the manufacture of carbon products, or in the prediction of property changes at high temperatures, high pressures, or other extreme environments. The process appears to be governed by the annihilation of a hierarchy of carbon interstitials that anneal with activation energies of 238, 269, and 330 kcal/mole as the carbon interlayer spacing decreases during annealing stepwise from 3.440 Å to 3.40 Å, 340 Å to 3.375 Å, and 3.375 Å to 3.354 Å, respectively. The graphitization-induced changes are characterized using wide-range x-ray diffraction, small-angle x-ray scattering at room temperature, and measurements of electrical conductivity, Hall coefficient, and magnetoresistance at temperatures down to 2 K and in magnetic fields to 5 T. In collaboration with Y. Kaburagi, Y. Hishiyama, and D.F. Baker, some studies of thermoelectric power in hard carbons are made in the range of 1.4 to 300 K.

1. Interstitials in Graphite and Disordered Carbon (Publication 3)

J. Lachter and R.H. Bragg

A montage of the changes in mean interlayer spacing induced in graphite by fast neutron irradiation or mechanical grinding is shown in Figure 1-1. The arrests that are clearly evident at spacings of 3.44 Å, 3.40 Å, and 3.375 Å are thus independent of the mode of disordering of the graphite structure. Conversely, these same arrests are observed when highly unordered carbons are graphitized. Thus it appears that graphitization of unordered carbons is the reverse process of disordering of graphite. Since the disordering processes leading to Figure 1-1 involve only carbon, the increases in the interlayer spacing must be attributed to single carbon interstitials or interstitial clusters of increasing complexity. There is considerable experimental and theoretical justification for a C_I interstitial.[1,2] It is not shared between layers; i.e., it does not sit in tetrahedral or octahedral sites as in the usual ceramic or metallic structures, but instead it is grafted onto one layer (either side) in a position about 1.2 Å above the center of a six-membered ring, with a binding energy well above 200 kcal/mole. Figure 1-1 suggests that, over the range of layer spacings encountered in graphitization—3.44 Å down to 3.354 Å—there are three distinct interstitial carbon configurations, but their structures are not known.

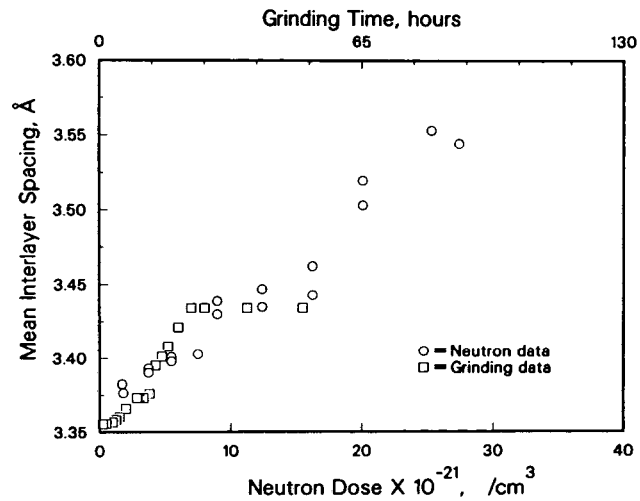

Figure 1-1. Changes in the interlayer spacing of graphite during ○ neutron irradiation and □ mechanical grinding. (XBL 876-2815)

1. J. Maire and J. Mering, J. Chem. Phys. **57**, 803 (1966).
2. J. Abrahamsen and R.G.A.R. Maclagan, Carbon **22**, 291 (1984).

2. Nonkinetic Changes in Heat-Treated Glass-Like Carbons: Part I: Pore Size and Bulk Dimensions (Publication 12)

J. Lachter, B.N. Mehrotra,† L.G. Henry,‡ and R.H. Bragg

Small-angle x-ray scattering measurements were used to characterize the radius of gyration R_g of the

*This work was supported by the Director, Office of Energy Research, Office of Basic Energy Sciences, Materials Sciences Division of the U.S. Department of Energy under Contract No. DE-AC03-76SF00098.

pores in a glass-like carbon heat-treated between 1000°C and 2800°C for periods up to 150 hr. Measurements were also made of the irreversible bulk dimensional changes Δl, and both dimensional parameters were found to undergo a nonkinetic increase when the annealing temperature was increased stepwise above 1000°C. Figure 2-1 shows that the relative changes $\Delta R_g/R_g$ and $\Delta l/l$ fall into three distinct regions of annealing temperature. There is first an initial increase in these ratios as the annealing temperature increases up to 1600°C, followed by a plateau from 1600°C up to about 2200°C, above which the ratios increase even more steeply than in the first region. However, the maximum dilatation $\Delta l/l$ is scarcely 3%, whereas $\Delta R_g/R_g$ increases more than twofold. The increase in the first region is attributed to the release of residual pyrolysis gases and hydrogen in the pores. The sharper increase in the highest-temperature region results from the anisotropy mismatch of the thermal-expansion coefficients. This effect is very large because the expansion perpendicular to the layers increases as T^2 and is about 30 times that parallel to the layers, which only increases linearly with T. The intermediate region is attributed to a combination of the two mechanisms. These data illustrate the extreme sensitivity of the internal pore structure to processing conditions, and explain why, for example, glass-like carbon can be prepared to function as a molecular sieve.

†Present address: Advanced Microdevices, Sunnyvale, CA.

‡Present address: National Semiconductor, Mountain View, CA.

1. S. Bose and R.H. Bragg, Carbon **19**, 289 (1981).

2. B.J. Kelly and R. Taylor, in *Chemistry and Physics of Carbon*, P.L. Walker, Jr., Ed., Marcel Dekker, New York, Vol. 10, p. 26 (1973).

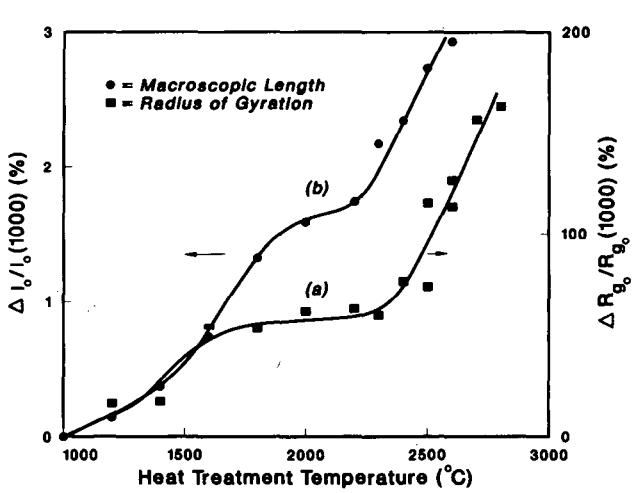

Figure 2-1. Comparison of dilation of pores ■ and bulk volume ● as a function of heat-treatment temperature. (XBL 876-2816)

3. Work in Progress

Work on the elucidation of the mechanism of graphitization is proceeding in four primary directions, all based on the model shown in Figure 3-1, which shows a scheme of discrete interlayer spacings derived from Figure 1-1 and other sources. Figure 3-1 also indicates that the energy input required to produce more disorder (characterized by higher interlayer spacings) decreases the greater the amount of preexisting disorder. Thus, when the process is reversed, annealing should become more difficult as the disorder is removed. On the interstitial model this is interpreted to indicate that the dissociation of interstitials and their removal should become progressively more difficult as the annealing proceeds. This prediction has been borne out by a preliminary analysis of data obtained during the graphitization of a pyrocarbon. In one of the thrusts a detailed analysis is being made of the kinetics of graphitization of pyrocarbon and the characteristic activation energies in the regions shown. This involves extensive use of the computer in fitting the data to analytical models of the kinetics of interstitial annihilation.

In a second thrust, annealing experiments are in progress to determine the kinetics of graphitization of graphite that has been disordered by grinding. The objective here is to demonstrate that the mechanism of graphitization is essentially the annealing of carbon interstitials, irrespective of how they are created. The third thrust involves correlation of the interlayer spacings with electronic properties of the interstitials, in particular the Hall coefficient and the magnetic susceptibility. The fourth

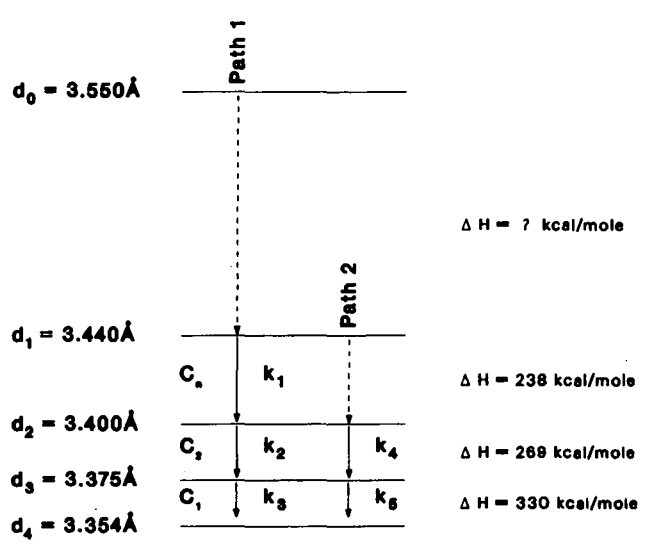

Figure 3-1. Schematic of the interstitial configurations and bonding energies in graphite. (XBL 876-2817)

thrust addresses the problem of determining the structure of the interstitials themselves, and for this it is planned to make direct determinations using C^{13} nuclear magnetic resonance.

1986 PUBLICATIONS AND REPORTS

Refereed Journals

1. K. Kawamura and R.H. Bragg, "Carbonization and Graphitization of Coal Tar Pitch Mixed with Trinitrophenol," Carbon **24**, 227 (1986); LBL-18783.
2. K. Kawamura and R.H. Bragg, "Graphitization of Pitch Coke: Kinetics of Changes in Mean Interlayer Spacing, Strain and Weight," Carbon **24**, 301 (1986); LBL-19301.
3. J. Lachter and R.H. Bragg, "Interstitials in Graphite and Disordered Carbon," Phys. Rev. B, Rapid Communications **33**, 8093 (1986); LBL-20995.
4. M. Tidjani, J. Lachter, T.S. Kabre, and R.H. Bragg, "Structural Disorder Induced in Graphite by Grinding," Carbon **24**, 447 (1986); LBL-20908.
5. J. Lachter, R.H. Bragg, and E. Close, "Graphical Analysis of Processes with Multiple Activation Energies," J. Appl. Phys. **60**, 1841 (1986); LBL-21096.
6. Y. Kaburagi, Y. Hishiyama, D.F. Baker, and R.H. Bragg, "Thermoelectric Power of Glassy Carbon," Philos. Mag. B **54**, 381 (1986).

Other Publications

7. R.H. Bragg, J. Lachter, and L.G. Henry, "Pore Growth in Annealed Glass-Like Carbon," Carbon '86, Extended Abstracts, Baden-Baden, 1986.
8. J. Lachter and R.H. Bragg, "Stepwise Processes in the Ordering and Disordering of Carbon," Carbon '86, Extended Abstracts, Baden-Baden, 1986.

LBL Reports

9. J. Lachter, L.G. Henry, R.H. Bragg, and S. Spooner, "Pore Growth Kinetics in Heat Treated Glass-Like Carbon," J. Mat. Res. (in press); LBL-21328.
10. K. Kawamura, R.H. Bragg, and J. Lachter, "Graphitization of Pyrocarbon: Kinetics of Changes in Mean Interlayer Spacing, Bulk Dimensions, Crystallite Size and Strain," submitted to Carbon; LBL-17982.
11. J. Lachter, D.F. Baker, and R.H. Bragg, "Effect of Grinding on the Structure of Glass-Like Carbon," submitted to J. Am. Ceram. Soc.; LBL-22552.
12. L. Henry, J. Lachter, and R.H. Bragg, "Non-Kinetic Changes in Heat Treated Glass-Like Carbons," Carbon (in press); LBL-22358.
13. L. Henry, J. Lachter, R.H. Bragg, and S. Spooner, "Characterization of Pore Size and Shape in Glass Like Carbons Using Small Angle X-Ray Scattering," submitted to J. Appl. Cryst.; LBL-20996.
14. J. Lachter, L. Henry, and R.H. Bragg, "Determination of the Shape and Size of Voids in Glass-Like Carbons," submitted to J. Appl. Cryst.; LBL-21329.
15. L. Henry, J. Lachter, and R.H. Bragg, "Conversion of a Diffractometer to Small Angle X-Ray Measurements," submitted to Rev. Sci. Instrum.; LBL-21448.
16. J. Lachter and R.H. Bragg, "Surface Area Kinetics in Glass-Like Carbons Revisited," submitted to J. Mat. Res.; LBL-22603.
17. L. Henry, J. Lachter, and R.H. Bragg, "An Indirect Determination of the Compton Scattering in Amorphous Carbons," submitted to J. Appl. Cryst.; LBL-15611.

Invited Talks

18. R.H. Bragg, "The Mechanism of Graphitization," Centre de Recherche sur les Solides a Organization Cristalline Imparfaite, University of Orleans, France.
19. R.H. Bragg, "The Mechanism of Graphitization," Centre National Recherche Scientifique, University of Bordeaux, France.

Ceramic Interfaces*

Andreas M. Glaeser, Investigator

INTRODUCTION

Numerous properties of ceramics depend strongly on microstructure, necessitating control of microstructural characteristics developed during processing. This research program focuses on improving our understanding of several processes that dictate the microstructural changes occurring during both materials fabrication and utilization. Current efforts are directed at: examination of the effects of crystallization, polymorphic phase transformations, and particle substructure on microstructure evolution in model powder compacts of chemically synthesized, amorphous, "monodispersed" TiO_2; the development of techniques for generating controlled pore structures at bicrystal and single-crystal-polycrystal interfaces; development of thermodynamic and kinetic descriptions of the stability of continuous intergranular phases (e.g., fibers in polycrystalline matrix composites); theoretical assessment of the effects of anisotropic surface and grain boundary energies on microstructural evolution during sintering and grain growth; and modeling the effects of concurrent grain-boundary migration and grain boundary tracer self-diffusion on calculated apparent grain-boundary diffusivities.

1. The Morphological Stability of Continuous Phases (Publications 5, 6, 8, and 10)

W.C. Carter and A.M. Glaeser

A thermodynamic analysis of the morphological stability of continuous intergranular phases, incorporating the number of bounding grains **n** and dihedral angle ψ as variables, has been presented. For each **n**, the minimum thermodynamically unstable wavelength of an infinitesimal amplitude perturbation coincides with the Rayleigh result ($2\pi R_c$) for $\psi = 180°$. For $\mathbf{n} = 2$, the ratio $\lambda_{min}/2\pi R_c$ decreases with ψ, approaching a limit of $(0.7)^{1/2}$ as $\psi \rightarrow 0°$. For $\mathbf{n} \geqslant 3$, $\lambda_{min}/2\pi R_c$ increases with decreasing ψ and tends to infinity as $\psi \rightarrow \pi - (2\pi/n)$, or equivalently as the interface curvature vanishes. For fixed ψ, the stability increases with **n**. The results have applicability to a wide range of phenomena, e.g., gas flow through densifying powder compacts, swelling of nuclear fuel elements, stability of fibers in composites, etc. In addition, a thermodynamic treatment of the effect of finite amplitude perturbations on the stability of continuous phases has been developed. For infinitesimal perturbations, the analysis yields a minimum wavelength of $2\pi R$ (= λ_{min}), the Rayleigh result. As perturbation amplitude increases, the critical wavelength λ_{crit} at which further increase in amplitude is energetically favorable decreases. For sufficiently large amplitude perturbations, λ_{crit} approaches values as low as $\simeq 0.533 \cdot (\lambda_{min})$.

2. The Role of Particle Substructure in the Sintering of Monosized Titania (Publication 11)

L.H. Edelson and A.M. Glaeser

Chemically synthesized, monodispersed titania particles ($\simeq$0.35 μm diameter) were found to be porous agglomerates of $\simeq$60 Å primary particles. The total volume shrinkage during sintering was 84%. Five contributions to the total shrinkage (water loss, crystallization, interagglomerate densification, anatase-rutile conversion, and interagglomerate densification), as well as the temperature ranges for the associated processes, were identified. Approximately half the total compact shrinkage is the result of particle substructure. The results indicate the importance of controlling interagglomerate structure and are believed to have important implications for the processing of other chemically synthesized, monosized powders.

3. Production of Controlled Morphology Intergranular Pore Structures (Publication 9)

J. Rödel and A.M. Glaeser

A new technique for producing intergranular pore structures with controlled pore size, spacing, and number has been developed. The technique combines a photolithographic process, ion beam etching, and hot pressing of an etched single crystal to either a second single crystal or to polycrystalline material. To date the technique has been applied to alumina. New experimental opportunities emerge

*This work was supported by the Director, Office of Energy Research, Office of Basic Energy Sciences, Materials Sciences Division of the U.S. Department of Energy under Contract No. DE-AC03-76SF00098.

for fundamental studies of grain growth under the influence of pore drag, pore morphology evolution, surface energy anisotropy and interfacial energetics, and Ostwald ripening of pores.

4. Work In Progress

Packing geometry (pore/grain coordination number) and interfacial energies (dihedral angle) mutually determine the thermodynamic stability of pores/grains in polycrystals. While effects of spatial variations in packing geometry have been considered, those of dihedral angle variations have not. Effects of dihedral angle distribution shape on pore stability and grain growth behavior are being evaluated.

Grain boundary migration affects tracer penetration during a grain boundary diffusion experiment. Previous work has treated the case where lattice diffusion perpendicular to the boundary contributes negligibly to the total tracer penetration. Current work seeks to evaluate the effect of the boundary displacement to lattice diffusion distance ratio on tracer concentration depth profiles, and thus, calculated boundary diffusivities.

Controlled morphology intergranular pore arrays have been developed. During annealing, facetting of initially round pores has been observed. In addition, pores with varying aspect ratio have been generated; we anticipate that these will allow study of the Rayleigh instability of intergranular phases. Complementary theoretical work on this topic is in progress. Finally, work seeking to evaluate pore–grain boundary interactions during abnormal grain growth has been initiated.

The effects of monovalent and divalent impurities on the propensity for abnormal grain growth in high-density, high-purity, fine grain size sodium chloride compacts is being examined. Correlations between dopant type, dopant concentration, and grain boundary mobilities are being sought.

1986 PUBLICATIONS AND REPORTS

Refereed Journals

1. A.M. Glaeser and J.W. Evans, "The Effect of Grain Boundary Migration on Apparent Boundary Diffusion Coefficients," Acta Metall. **34**, 1545 (1986); LBL-19831.
2. A.M. Glaeser, H.K. Bowen, and R.M. Cannon, "Grain Boundary Migration in LiF: I. Mobility Measurements," J. Am. Ceram. Soc. **69**, 119 (1986); LBL-19158.†
3. A.M. Glaeser, H.K. Bowen, and R.M. Cannon, "Grain Boundary Migration in LiF: II. Microstructural Characteristics," J. Am. Ceram. Soc. **69**, 299 (1986); LBL-19159.†
4. A.M. Glaeser, H.K. Bowen, and R.M. Cannon, "Background Impurity Effects on Grain Boundary Migration in LiF," Mater. Sci. Eng., **79**, 111 (1986); LBL-19846.†

Other Publications

5. W.C. Carter and A.M. Glaeser, "The Morphological Stability of Continuous Intergranular Phases," in *Tailoring of Multiphase and Composite Ceramics*, R.E. Tressler, Ed., Plenum Press, New York, 1986 p. 15; LBL-19161.

LBL Reports

6. W.C. Carter and A.M. Glaeser, "The Morphological Stability of Continuous Intergranular Phases: Thermodynamic Considerations," Acta Metall. (in press); LBL-20673.
7. L.H. Edelson and A.M. Glaeser, "Method of Removing Surface Porosity on Glassy Carbon Tiles," Carbon (in press); LBL-20130.
8. W.C. Carter and A.M. Glaeser, "The Effect of Finite Amplitude Perturbations on the Stability of Continuous Phases," LBL-21197.
9. J. Rödel and A.M. Glaeser, "Production of Controlled Morphology Pore Arrays: Implications and Opportunities," LBL-22717.
10. W.C. Carter (M.S. Thesis), "The Morphological Stability of Continuous Intergranular Phases: Thermodynamic Considerations," LBL-22754.
11. L.H. Edelson (M.S. Thesis), "The Role of Particle Substructure in the Sintering of Monosized Titania," LBL-22753.

Invited Talks

12. W.C. Carter, "Geometrical Aspects of Sintering," 38th Pacific Coast Regional Meeting, Irvine, CA, Oct. 28, 1985.
13. A.M. Glaeser, "Effects of Grain Boundary Migration on Apparent Grain Boundary Diffusion Coefficients," 38th Pacific Coast Regional Meeting, Irvine, CA, Oct. 29, 1985.
14. A.M. Glaeser, "Microstructural Development During Firing," International Society for Hybrid Electronics, International Microelectronics Symposium, Anaheim, CA, Nov. 12, 1985.
15. A.M. Glaeser, "Microstructure Development and Grain Growth in Alumina," Lawrence Livermore National Laboratory, Livermore, CA, Nov. 14, 1985.
16. L.H. Edelson, "Atmospheric Effects during Sintering of Monosized TiO_2," 88th Annual Meeting of the American Ceramic Society, Chicago, IL, April 29, 1986.

17. W.C. Carter, "Metastable Pores Revisited," 88th Annual Meeting of the American Ceramic Society Chicago, IL, April 30, 1986.
18. A.M. Glaeser, "Asepcts of Ceramic Fabrication: Prediction, Processing, Performance," Materials Science and Engineering Seminar, University of California, Berkeley, Sept. 11, 1986.

†Research sponsored by the National Science Foundation, Division of Materials Research, Contract No. 77-11685 DMR.

SOLID-STATE PHYSICS

EXPERIMENTAL RESEARCH

Far-Infrared Spectroscopy*

Paul L. Richards, Investigator

INTRODUCTION

Improvements in infrared technology are making possible increases in the sensitivity of many types of infrared measurements. In this project, improved types of infrared sources, spectrometers, and detectors are being developed. Improved infrared techniques are being used to do experiments in areas of fundamental and applied infrared physics where their impact is expected to be large.

Progress in infrared technology includes: (a) development of a new source for broadly tuned far-infrared spectroscopy based on harmonic generation from microwave oscillators; (b) development of a variable-temperature apparatus for accurate measurements of polarized far-infrared reflectivity and transmissivity of solid samples over the temperature range from 5 to 300 K; (c) evaluation of new concepts for ultrasensitive photoconductive detectors for the 50–1000 μm range. In addition, (d) the bolometric detector previously developed for far-infrared spectroscopy is being reconfigured as a microcalorimeter to measure the heat capacity of monolayers deposited on metal surfaces.

Infrared experiments in progress include: (a) an experimental test with unprecedented accuracy of the Planck theory for the shape of the spectral emissivity curve of a blackbody; (b) measurements of the infrared emission spectra of molecules chemically adsorbed on metal surfaces; (c) measurements of the infrared spectra of one-dimensional conductors; and (d) measurements of the heat capacity of monolayer films on metal surfaces.

*This work was supported by the Director, Office of Energy Research, Office of Basic Energy Sciences, Materials Sciences Division of the U.S. Department of Energy under Contract No. DE-AC03-76SF00098.

1. Vibrational Linewidths of Adsorbed Molecules: Experimental Considerations and Results (Publication 22)

R.G. Tobin

In recent years, the study of the vibrational linewidths of chemisorbed molecules has been an area of intense experimental and theoretical interest. Much of the research into these linewidths is motivated by the possibility that they are determined by the finite lifetime of the vibrationally excited state. Since the vibrational lifetime is a measure of the rate of energy transfer between the adsorbed molecule and the substrate, it is central to the understanding of such surface phenomena as sticking, desorption, diffusion, and surface chemical reactions. However, it is clear that many experimentally observed linewidths are determined by effects other than lifetime broadening. Thus, the identification of the dominant line-broadening mechanism is of fundamental importance.

This review focuses on the experimental progress that has been made using high-resolution infrared spectroscopy to identify the line-broadening mechanisms on clean, well-characterized surfaces. Theoretical calculations of various line-broadening mechanisms are first reviewed (see Figure 1-1). Both lifetime broadening processes (e.g., energy relaxation into substrate phonons or electron-hole pairs) and other processes (e.g., dephasing and inhomogeneous broadening) are described. Theoretical work on inhomogeneous broadening is particularly limited, despite the fact that it is an important mechanism for many experimental systems. Infrared experimental techniques and data are then reviewed critically. The utility of line-shape and linewidth measurements, isotope effects, temperature dependences, and

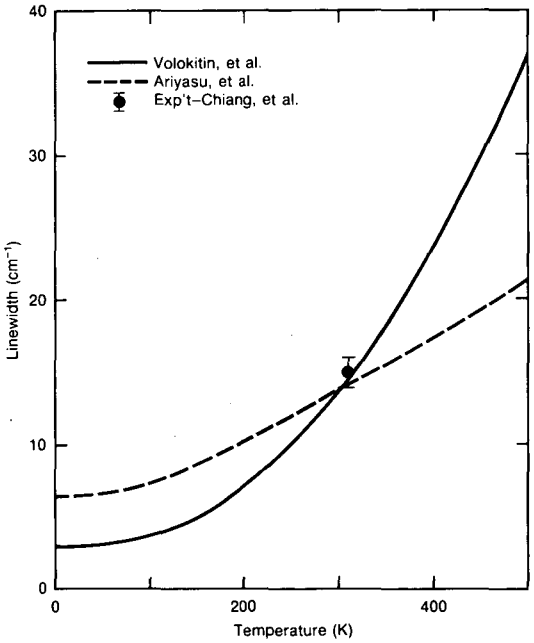

Figure 1-1. Two alternative theoretical predictions for the temperature dependence of the linewidth contribution due to vibrational decay into substrate phonons of the molecule-substrate mode of CO on Ni(100). The dotted line represents the prediction of Ariyasu *et al.* for a two-phonon process. The solid line is the prediction of Volokitin *et al.* for phonon processes of all orders, and it is dominated by the three-phonon contribution. Our experimental result, reported by Chiang *et al.*, is also shown. More data are clearly needed; experiments are in progress. (XBL 869-8970A)

other methods is assessed. A detailed analysis is then presented of those cases in which identification of the line-broadening mechanism has been made.

2. An Infrared-Emission Study of the C=O Stretch Vibration of Bridge-Bonded CO on Pt(111) (Publications 21 and 25)

R.G. Tobin, R.B. Phelps, and P.L. Richards

We have studied the C=O stretch vibration of bridge-bonded CO on Pt(100) in the temperature range from 225 K to 300 K. Our spectra are qualitatively different from those previously reported by Hayden and Bradshaw in that we do not observe the line near 1810 cm^{-1} that they attributed to threefold bonded CO. We observe only a single line at 1849 cm^{-1} (see Figure 2-1). As the coverage is increased beyond 0.5 monolayer, the linewidth decreases, reaching its minimum value near $\theta = 0.54$. Little change in the frequency or integrated intensity of the

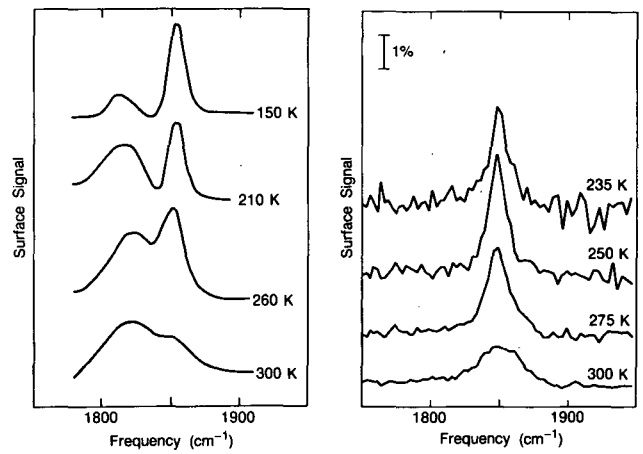

Figure 2-1. IR spectra of CO on Pt(111) at various temperatures, in the region of the C = O stretch vibration of bridge-bonded CO. On the left as measured by Hayden and Bradshaw. The line near 1810 cm^{-1} was attributed to CO bonded in threefold sites. On the right as measured in the present work. No line near 1810 cm^{-1} is observed. The discrepancy illustrates some of the dangers of surface vibrational spectroscopy. We attempted to reproduce the spectra of Hayden and Bradshaw by varying the surface conditions but were not able to do so. (XBL 864-7628A)

line is seen. These observations tend to support "fault line" models for the high-coverage structure of CO on Pt(111). The minimum linewidth of the line is 11.5 ± 0.6 cm^{-1} for temperatures below 275 K, rising rapidly to ~34 cm^{-1} at 300 K (see Figure 2-2). This temperature dependence cannot be

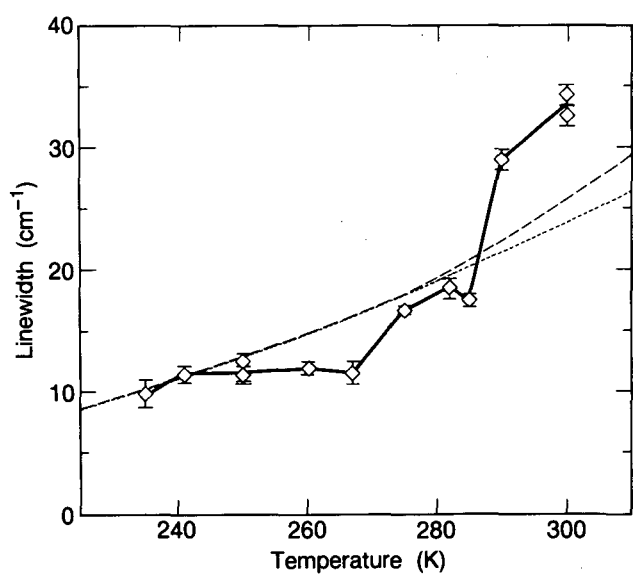

Figure 2-2. Linewidth of the bridge-bonded CO vibration as a function of temperature. The dotted line represents the best fit to a model of dephasing by interaction with other vibrational modes. The dashed line represents the best fit to a model of dephasing by interaction with electron-hole pairs. Neither model adequately fits the data. We conclude that the observed linewidth is due to inhomogeneous broadening associated with an order-disorder transition in the overlayer. (XBL 868-8920)

explained by current models of homogeneous broadening. We attribute it to inhomogeneous broadening associated with an order-disorder transition in the overlayer.

3. Optical Efficiency of Far-Infrared Photoconductors (Publication 6)†

J-Q. Wang, P.L. Richards, J.W. Beeman, N.M. Haegel, and E.E. Haller

We report an experimental and theoretical study to optimize the geometry of far-infrared photoconductive detectors with diffraction-limited throughput. Factors considered in this optimization include internal optical path relative to measured absorption length (as shown in Figure 3-1), photoconductive gain, uniformity of illumination, cosmic-ray cross section, and compatibility of the design with the requirements of one- and two-dimensional arrays. A rod-shaped detector geometry with square cross section, electrodes on the lateral faces, and a beveled backface to trap the radiation by total internal reflection was found to have responsivity nearly equal to the best detectors in integrating cavities, and to be superior in all other respects. Detailed design information for this detector is presented.

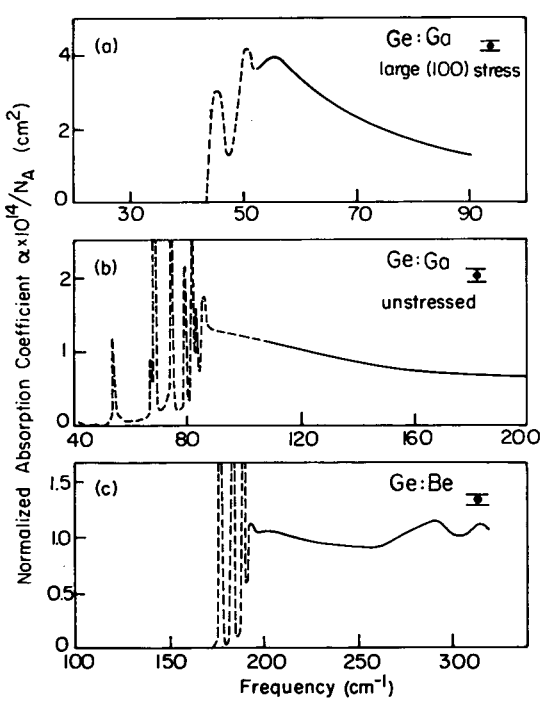

Figure 3-1. Ratio of frequency-dependent absorption coefficients $\alpha(\nu)$ to acceptor concentration N_A for (a) Ge:Ga with infrared propagating perpendicular to a large (100) uniaxial stress, (b) for Ge:Ga with no stress, and (c) for Ge:Be. Typical estimated errors are shown. In the region covered by dashed lines, the absorption is due primarily to transitions to bound states. The solid lines show absorption due primarily to the generation of free carriers. The application of a large stress in the (100) direction increases the peak value of by α factor of 3. These data are used to determine the optimum dimensions of photoconductive detectors. (XBL 866-7698)

†Samples for this study were provided by the group led by Prof. E.E. Haller. Prof. Haller's work is supported by the Engineering Division of LBL.

4. Far-Infrared Response of $(TaSe_4)_2I$: Observation of the Charge-Density-Wave Optical Phason (Publication 23)†

M.S. Sherwin, A. Zettl, and P.L. Richards

Over 30 years ago, Fröhlich proposed a novel mechanism for charge transport in a coupled electron-phonon system having undergone a Peierls transition: a displacement of the phase of the charge density wave (CDW). The field of CDW dynamics has been an area of vigorous research since 1976, when nonlinear dc conductivity was first observed in $NbSe_3$ and attributed to a sliding CDW Fröhlich mode. More recent microwave studies of the CDW materials $NbSe_3$, TaS_3, and $(TaSe_4)_2I$ have found a resonance in the ac conductivity, and this resonance has been attributed to the excitation of the pinned $q = 0$ acoustic phason, first predicted by Lee, Rice, and Anderson (LRA). In the past it has been assumed that, at frequencies above this resonance, the response spectrum would be rather featureless (with the exception of low-lying phonon modes) until normal carriers are excited across the Peierls gap at $h\nu = 2\Delta$.

We report measurements of the far-infrared (FIR) conductivity of $(TaSe_4)_2I$ parallel to the crystal-chain direction (c axis), in the frequency range 8 to 350 cm^{-1}. We find a giant peak in the conductivity at 38 cm^{-1} (see Figure 4-1), which is roughly 40 times larger than the frequency of the microwave resonance and 50 times smaller than the frequency of the Peierls gap associated with $(TaSe_4)_2I$. The FIR peak has approximately 80 times the oscillator strength of the microwave peak associated with the pinned-phason mode. The temperature dependence of the FIR peak indicates that it is associated with the condensation of the CDW. We argue that the phason branch of the CDW dispersion must in fact be split into an acoustic and an optical branch, and we interpret the FIR peak as arising from the excitation of the $q = 0$ optical phason. Based on the phason dispersion relation derived by

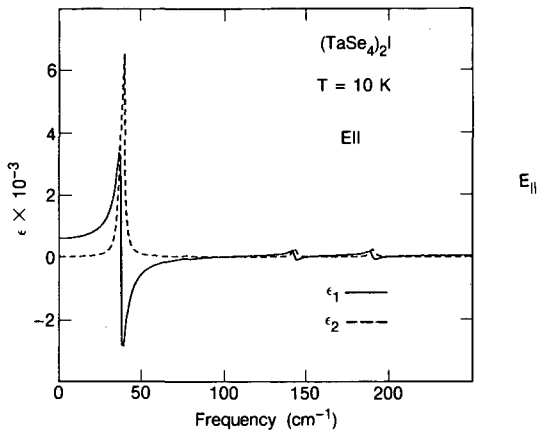

Figure 4-1. Complex dielectric function $\epsilon = \epsilon_1 + i\epsilon_2$ for $(TaSe_4)_2I$ at 10 K, as determined by an oscillator fit to the far-infrared reflectivity. The giant peak in ϵ_2 arises from the optical branch of the phason first identified by this work. (XBL 871-7515)

LRA, we estimate that this optical phason should be observed near 39 cm^{-1}, in excellent agreement with our experimental results. The dramatic optical-phason mode first identified by this work is a generally occurring effect. It may already have been observed, but not correctly interpreted, in the other CDW compounds $NbSe_3$ and $K_{0.3}MoO_3$.

†This is a collaborative project with Prof. A. Zettl. Prof. Zettl's research is supported in part by the National Science Foundation.

5. Work in Progress

Measurements of the temperature dependence of the linewidth of the molecule-substrate mode of CO on Ni(100) are being made to distinguish between different theoretical predictions for the effects of multiple phonon relaxation.

Our new technique for measuring the heat capacity of monolayer overlayers on solid surfaces is being used to measure the melting transition of monolayers of ^4He on metal films.

Measurements of the spectral shape of the emission from a blackbody as a function of temperature and far-infrared frequency are in progress.

Construction has begun on a new source for broadly tuned far-infrared spectroscopy based on harmonic generation from microwave oscillators.

1968 PUBLICATIONS AND REPORTS

Refereed Journals

1. A.V. Räisänen, W.R. McGrath, P.L. Richards, and F.L. Lloyd, "Broad-Band RF Match to mm-Wave SIS Quasiparticle Mixer," IEEE Trans. Microwave Theory Tech. **MTT-33**, 1495 (1985).†
2. A.V. Räisänen, W.R. McGrath, D.G. Crété, and P.L. Richards, "Scaled Model Measurements of Embedding Impedances for SIS Waveguide Mixers," Int. J. IR and MM Waves **6**, 1169 (1985).†
3. D.W. Face, D.E. Prober, W.R. McGrath, and P.L. Richards, "High Quality Tantalum Superconducting Tunnel Junctions for Microwave Mixing in the Quantum Limit," Appl. Phys. Lett. **48**, 1098 (1986).†
4. W.R. McGrath, A.V. Räisänen, and P.L. Richards, "Variable-Temperature Loads for Use in Accurate Noise Measurements of Cryogenically-Cooled Microwave Amplifiers and Mixers," Int. J. IR and MM Waves **7**, 543 (1986).†
5. A.V. Räisänen, D.G. Crété, P.L. Richards, and F.L. Lloyd, "Wide-Band, Low Noise MM-Wave SIS Mixers with a Single Tuning Element," Int. J. IR and MM Waves **7**, 1835 (1986).‡
6. J-Q. Wang, P.L. Richards, J.W. Beeman, N.M. Haegel, and E.E. Haller, "Optical Efficiency of Far-Infrared Photoconductors," Appl. Opt. **25**, 4127 (1986); LBL-21958.§

Other Publications

7. J.B. Peterson, P.L. Richards, J.L. Bonomo, and T. Timusk, "New Measurements of the Spectrum of the Cosmic Microwave Background," in *Inner Space/Outer Space*, E.W. Kolb *et al.*, eds., Univ. of Chicago Press, Chicago/London, 1986, p. 119; LBL-18073.‖
8. P.L. Richards, "Analog Superconducting Electronics," Physics Today, March 1986, p. 54.†
9. R.G. Tobin and P.L. Richards, "The Line Shapes of the Molecule-Substrate and C = O Stretch Modes of CO on Pt(111) Studied by Infrared Emission Spectroscopy," Program and Abstracts of the 46th Annual Conference on Physical Electronics, 1986, p. C8; LBL-21510abs.
10. A.V. Räisänen, W.R. McGrath, D.G. Crété, and P.L. Richards, "Embedding Impedance Measurements for mm-Wave SIS Mixers," 15th European Conf. Proc., 1985, p. 285.†
11. D.G. Crété, W.R. McGrath, P.L. Richards, and F.L. Lloyd, "Performance of Heterodyne Mixers Using Arrays of SIS Junctions," 10th Infrared and mm-Wave Conf., Digest of Technical Papers (1985), p. 129.†

12. R.G. Tobin and P.L. Richards, "The Adsorbate-Substrate Mode of CO on Pt(111) Studied by Infrared Emission Spectroscopy," Bull. Am. Phys. Soc. **31**, 535 (1986); LBL-20694abs.
13. T.W. Kenny and P.L. Richards, "Heat Capacity Measurements of Monolayers of ^{4}He Adsorbed on Evaporated Metal Films," Bull. Am. Phys. Soc. **31**, 280 (1986); LBL-20695abs.
14. P.L. Richards, "Superconducting Receiver for Molecular Line Astronomy," Bull. Am. Phys. Soc. **31**, 308 (1986).†‡
15. D.G. Crété, A.V. Räisänen, W.R. McGrath, P.L. Richards, and F.L. Lloyd, "Low-Noise 80–115 GHz SIS Mixers with a Single Tuning Element," 11th Int. Conf. on Infrared and mm-Waves, conference summary abstract.‡
16. G.H. Rieke, C. Lada, M. Lebofsky, F. Low, P. Strittmatter, E. Young, J. Arens, E. Haller, P. Richards, C. Beichman, T.N. Gautier, J. Mould, G. Neugebuer, S. Gaalema, and M. Werner, "MIPS: The Multiband Imaging Photometer for SIRTF," Conf. Proc. SPIE **589**, 242 (1985).**
17. A.V. Räisänen, D.G. Crété, P.L. Richards, and F.L. Lloyd, "Low Noise SIS Mixer with Gain for 80–115 GHz," European Space Agency Workshop Proc. ESA **SP-260**, 255 (1986).‡
18. A.V. Räisänen, D.G. Crété, P.L. Richards, and F.L. Lloyd, "Wide-Band, Ultra Low Noise MM-Wave Mixers with a Single Tuning Element," 16th European Microwave Conf. Proc., p. 252 (1986).‡

LBL Reports

19. R.G. Tobin and P.L. Richards, "An Infrared Emission Study of the Molecule-Substrate Mode of CO on Pt(111)," Surf. Sci. (in press); LBL-21506.
20. R.G. Tobin and P.L. Richards, "The Vibrational Line Shapes of CO on Pt(111) Studied by Infrared Emission Spectroscopy," J. Vac. Sci. Technol. (in press); LBL-21505.
21. R.G. Tobin, R.B. Phelps, and P.L. Richards, "An Infrared Emission Study of the C = O Stretch Vibration of Bridge-Bonded CO on Pt(111)," Surf. Sci. (in press); LBL-22229.
22. R.G. Tobin, "Vibrational Linewidths of Adsorbed Molecules: Experimental Considerations and Results," Surf. Sci. (in press); LBL-21912.
23. M.S. Sherwin, A. Zettl, and P.L. Richards, "Far Infrared Response of $(TaSe_4)_2I$: Observation of the Charge Density Wave Optical Phason," LBL-22624.††
24. T.W. Kenny and P.L. Richards, "Heat Capacity Measurements of Multilayers Adsorbed on Evaporated Metal Films," Bull. Am. Phys. Soc. (in press); LBL-22625abs.
25. R.B. Phelps, R.G. Tobin, and P.L. Richards, "The C = O Stretch Mode of Bridge-Bonded CO on Pt(111) Studied by Infrared Emission Spectroscopy," Bull. Am. Phys. Soc. (in press); LBL-22626abs.

Invited Talks

26. P.L. Richards, "Superconducting Receivers for Molecular Line Astronomy," March Meeting of the American Physical Society, Las Vegas, NV, March 31–April 4, 1986, Bull. Am. Phys. Soc. **31**, 308 (1986).
27. P.L. Richards, "Infrared Spectroscopy of Molecules Adsorbed on Metal Surfaces," Physics Department Colloquium, U.C. Santa Barbara, Jan. 28, 1986.
28. P.L. Richards, "Superconducting Quasiparticle Tunnel Junctions as Quantum Limited Detectors and Mixers for Microwave Radiation," Seminar, Department of Electrical Engineering and Computer Science, U.C. Berkeley, Feb. 26, 1986.
29. P.L. Richards, "SIS Mixers," West Coast Superconductive Electronics Meeting, Berkeley, CA, March 7, 1986.
30. P.L. Richards, "Spectrum of the Cosmic Microwave Background Revisited," Physics Department Colloquium, U.C. San Diego, April 10, 1986.
31. P.L. Richards, "Superconducting Microwave Heterodyne Receivers Approaching the Quantum Limit," Physics Department Colloquium, Stanford University, Palo Alto, CA, May 20, 1986.
32. P.L. Richards, "Progress in the Development of SIS Quasiparticle Mixers," Applied Superconductivity Conference, Baltimore, MD, Sept. 28–Oct. 3, 1986.
33. P.L. Richards, "Superconductive Mixers," Air Force Applications of Cryoelectronics, Dayton, OH, Oct. 30, 1986.
34. P.L. Richards, "SIS Quasiparticle Mixers," Joint Services Electronics Programs Review, Berkeley, CA, Nov. 5, 1986.
35. R.G. Tobin. "Infrared Vibrational Spectroscopy of Molecules Adsorbed on Metal Surfaces," Xerox Palo Alto Research Center, Palo Alto, CA, Feb. 14, 1986; National Bureau of Standards, Gaithersburg, MD, March 17, 1986; University of Maryland, College Park, March 18, 1986; AT&T Bell Laboratories, Murray Hill, NJ, March 20, 1986; IBM Thomas J. Watson Research Center, Yorktown Heights, NY, March 25, 1986; IBM Almaden Research Center, San Jose, CA, May 21, 1986.
36. A.E. Lange, "Absolute Radiometry of the Diffuse Submillimeter Background," Workshop on Far Infrared Astronomy, Max-Planck-Institut, Bonn, Federal Republic of Germany, Dec. 12, 1985; NASA Ames Research Center, Moffet Field, CA, Feb. 25, 1986; Space Sciences Laboratory, Berkeley, CA, Oct. 13, 1986; Space Sciences Colloquium, University of Chicago, Chicago, IL, Oct. 22, 1986.

---

†Supported by ONR.

‡Supported by AFOSR.

§Collaboration with Prof. E.E. Haller, whose research is supported by the Engineering Division of LBL.

‖Supported in part by NASA.

**Supported by SIRTF.

††Collaboration with Prof. Zettl, whose research is supported by NSF.

Experimental Solid-State Physics and Quantum Electronics*

Y.R. Shen, Investigator

INTRODUCTION

The main object of this program is to further basic understanding of laser interaction with matter. The emphasis is on the development of linear and nonlinear optical techniques for material studies and actual applications of these techniques to material studies. Both theoretical and experimental research on various aspects of interaction of light with matter are being carried out in this program. Newly developed techniques are being used to study problems of current interest: surface physics, phase transitions, laser chemistry, spectroscopy of excited species, and so on. Nonlinear optical effects in matter not yet well understood are also being investigated.

Current research is largely concentrated on optical studies of surfaces and interfaces. (1) Nonlinear optical techniques are developed as new tools for surface studies. (2) Basic understanding of surface nonlinear optical properties and processes is searched for. (3) The techniques are applied to the studies of surfaces or adsorbates at surfaces under various circumstances. Some effort is devoted to collaboration with Y.T. Lee's group on laser molecular spectroscopy in a molecular beam, and with theorists on calculations of quantum optics problems.

1. Optical Second-Harmonic Generation as a Surface Microprobe (Publication 3)

G.T. Boyd, Y.R. Shen, and T.W. Hansch

Optical second-harmonic generation (SHG) with a tightly focused laser beam can provide a sensitive surface microprobe that lends itself readily to a new type of scanning microscope. It has a resolution limited in principle only by the optical wavelength, and has the unique capability of probing the morphology of the surface molecular layers.

To demonstrate such surface microscopy, we have used SHG to map out a laser-ablated hole in a monolayer of dye molecules. The layer was deposited by spin-coating a dilute solution of rhodamine 6G onto a clean fused-silica substrate. Absorption measurements confirmed that an average of one dye monolayer was adsorbed on the surface. A hole was then ablated in the dye layer. The ablated hole was scanned by the probe laser in a zigzag pattern. The resulting SHG image is shown in Figure 1-1.

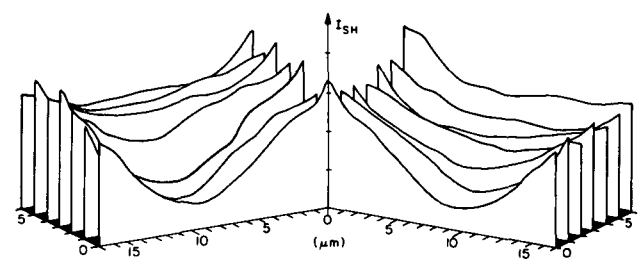

Figure 1-1. SH image of an ablated hole in a rhodamine 6G monolayer. (XBL 8512-6878)

The SH signal depends on the fourth power of the local field at the pump frequency. Therefore SH surface microscopy should be particularly sensitive to microscopic surface defects. For both metals and semiconductors, surface protrusions and edges should yield a much stronger signal than surrounding flatter regions.

The above demonstrations also suggest that it should be possible to design a monolayer optical memory device that could be read out by SHG. One could even imagine a three-dimensional storage medium of high density by spacing monolayers with 10–100 μm of transparent centrosymmetric material. We speculate that read and write capability may be realized by using photosensitive materials that can be altered by optical excitation and perhaps healed by heating.

2. Studies of Alkali Adsorption on Rh(111) using Optical Second-Harmonic Generation (Publication 2)

H.W.K. Tom, C.M. Mate, X.D. Zhu, J.E. Crowell, Y.R. Shen, and G.A. Somorjai

Optical SHG has been demonstrated to have enough sensitivity to detect a submonolayer of

*This work was supported by the Director, Office of Energy Research, Office of Basic Energy Sciences, Materials Sciences Division of the U.S. Department of Energy under Contract No. DE-AC03-76SF00098.

adsorbate on a substrate. In a recent experiment, the technique was used to study submonolayers of atomic and diatomic adsorbates on a Rh(111) surface in ultrahigh vacuum.[1] It was found that upon adsorption of CO and O, the SH signal from the Rh(111) surface decreased. The result can be explained in a simple physical way: CO and O are electron acceptors; upon adsorption, they partially localize the nearly free electrons on the metal surface. Since the optical nonlinearity of a metal surface can be largely accounted for by the nearly free electrons, it is expected to be reduced by the localization of such electrons. This being the case, one should find an increase in surface nonlinearity if electron donors are adsorbed on a metal surface.

We report here that when alkali atoms are adsorbed on Rh(111), the SH signal from Rh(111) indeed increases drastically, as shown in Figure 2-1. Our results indicate, however, that the very large increase in surface nonlinearity due to adsorption of alkali atoms cannot be explained simply by the increase in the number of nearly free electrons in metal, but is most likely the consequence of a significant modification of the optical transitions between alkali-derived states resulting from a relative shift of the Fermi level. The absorption of alkali atoms on transition metals is of great importance. The alkalis are known to be promoters for certain catalytic processes, e.g., the dissociation of CO and N_2 for hydrocarbon and ammonia synthesis, respectively.

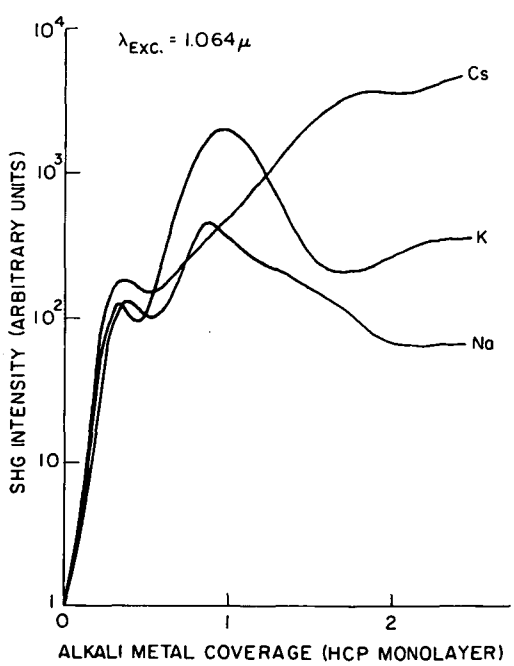

Figure 2-1. Second-harmonic output as a function of alkali metal coverage for Na, K, and Cs on Rh(111) with a 1.06-μm laser excitation. (XBL 843-6722)

1. H.W.K. Tom, C.M. Mate, C.D. Zhu, J.E. Crowell, T.F. Heinz, G.A. Somorjai, and Y.R. Shen, Phys. Rev. Lett. **52**, 348 (1984).

3. General Considerations on Optical Second-Harmonic Generation from Surfaces and Interfaces (Publication 7)

P. Guyot-Sionnest, W. Chen, and Y.R. Shen

Second-harmonic generation from an interface, in relation to the second-order nonlinearities of the interface layer and the adjacent bulk, is considered. We show by a formal derivation that both structural asymmetry and field discontinuity at an interface contribute to the second-order optical nonlinearity of the interface. If the refractive indices of the bonded media are not matched, the optical-field component along the surface normal varies rapidly across the interface layer. Consequently, the optical response of the interface layer is nonlocal. It involves not only the electric-dipole contribution, but also all the multipole contributions. As far as SHG from an interface is concerned, however, one can show that the nonlinear response of the interface layer can be described effectively by a local surface nonlinear polarization. The interface nonlinearity is then represented by a local (or electric-dipole-allowed) surface nonlinear susceptibility tensor.

Measurement of SHG from the interface allows us to deduce the surface nonlinear susceptibility. The bulk nonlinearity may complicate the measurement. It is, however, much weaker, especially in media with a large dielectric constant. Surface modification can be monitored by observing the induced change in the surface nonlinear susceptibility. A monolayer of atoms or molecules chemically adsorbed on centrosymmetric metals or semiconductors should be readily detectable. On insulator surfaces, on the other hand, easy detection of molecular adsorbates would require molecules with sufficiently large intrinsic nonlinearity unless chemical adsorption of the molecules results in the establishment of highly nonlinear bonds between the molecules and the surface.

4. Photoinduced Luminescence from the Noble Metals and its Enhancement on Roughened Surfaces (Publication 8)

G.T. Boyd, Z.H. Yu, and Y.R. Shen

Photoluminescence has been used extensively in the study of semiconductors. Its use in characterizing carrier relaxation and band structures of metals is, however, rare. The only relatively careful study was on single-photon luminescence from copper and gold by Mooradian in 1969.[1]

Single-photon- and multiphoton-induced luminescence spectra were obtained from clean samples of silver, copper, and gold with both smooth and rough surfaces. The spectra reveal new features that are correlated with interband transitions at selected symmetry points in the Brillouin zone. Calculating luminescence spectra based on simplified models of the band structures of the noble metals and taking into account the Fresnel local-field corrections, we find qualitative agreement with the observed spectra from smooth samples. The agreement between theory and experiment is less satisfactory for rough samples. The influence of surface roughness on the luminescence is largely attributable to local-field enhancement in the rough surface protrusions. This is consistent with the observation of surface-enhanced Raman scattering on such metals, i.e., the primary role of the surface roughness is to enhance the local optical fields and thus improve the efficiency of light absorption and emission.

1. A. Mooradian, Phys. Rev. Lett. **22**, 185 (1969).

5. Rydberg Spectroscopy of H_2 via Stepwise Resonant Two-Photon Ion-Pair ($H^+ + H^-$) Production (Publication 4)

A.H. Kung. R.H. Page, R.J. Larkin, Y.R. Shen, and Y.T. Lee

Recently, extensive spectroscopic work on H_2, especially in the range of photon energy below 17 eV, has led to a good understanding of the autoionization process through Rydberg transitions that converge to $H_2^+(X^2\Sigma_g^+)$ and up to $\nu^+ = 7$. Extension of the same level of understanding to series that converge to higher vibrational states ($\nu^+ > 7$) and to other important processes such as ion-pair formation and dissociation ionization is, however, inhibited by the limited amount of data available above 17 eV. Spectroscopic study of these highly excited states is made difficult by weak transition probability and the lack of intense light sources at these frequencies. With the recent advances in the development of tunable coherent extreme-uv sources, it is now possible to apply nonlinear optical spectroscopy to the investigation of these highly excited states. By use of resonant two-photon excitation, the weak transition probabilities due to small Franck-Condon factors for single-photon excitation can be greatly improved. New excited states whose transitions cannot be reached from the ground state can be studied. The spectrum can also be simplified by selective labeling of the rotational states. We report the first application of two-step doubly resonant excitation followed by negative (H^-) ion detection to study the Rydberg states of H_2 above 17 eV. High-resolution spectra of new Rydberg states with high convergence limits (to $H_2^+X^2\Sigma_g$, $\nu^+ = 9$, $N^+ = 1,3$) were obtained and analyzed. Part of the results are shown in Figure 5-1. The Fano-line profiles were resolved and reversal of the profile index along the series was observed, the latter for the first time in H_2. Dynamical information, such as lifetimes and relative transition strengths from low electronic states to Rydberg states and ion-pair dissociation continuum, was deduced. Use of H^- detection was essential in this study, because the alternative method of probing these Rydberg states via autoionization and H_2^+ detection results in two orders of magnitude larger ion signal but yields a very poor spectrum dominated by an intense ionization continuum.

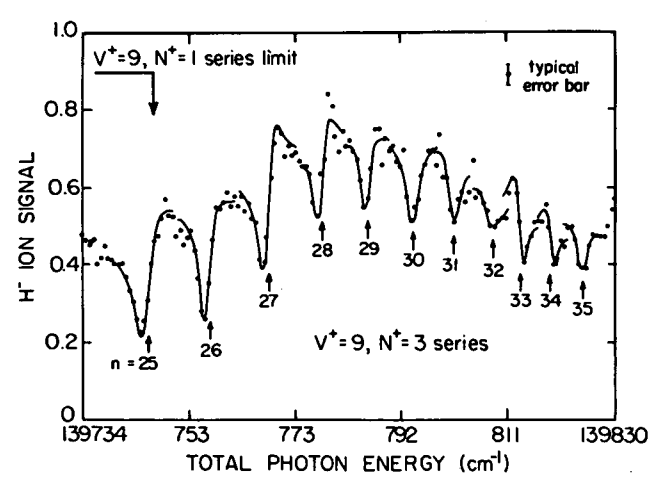

Figure 5-1. Expanded ion-pair production spectrum of H_2 between the $N^+ = 1$ and $N^+ = 3$ series limits showing the fitted Fano-line profiles: solid curves, calculated profile; circles, experimental points; and arrows, fitted line-center positions. (XBL 8510-6631)

6. Population Redistribution Induced by Multiphoton Processes (Publication 6)

C.Y. Fong and Y.R. Shen

Strong interaction of light with matter is a subarea of special interest in nonlinear optics. It refers to cases in which light and matter are so strongly coupled that the usual pictures derived from perturbation approaches are no longer valid.

We consider the problem of multiphoton pumping of a multilevel system. We are interested in the population redistribution possibly induced by strong laser excitations. Such a problem has long been a subject of extensive theoretical investigation. The possibility that significant fractions of the population can be selectively pumped into certain excited states by stepwise multiphoton excitations also makes the problem relevant for spectroscopic studies of highly excited systems, for example, studies of the physics and chemistry of excited-state atoms and molecules, multiphoton ionization, and isotope separation.

We have studied theoretically the effects of relaxation rates, dipole-matrix elements, level degeneracies, and detunings on the population redistribution induced by multiphoton processes in three- and four-level systems. It is shown that population inversion can always be established if the pumps have sufficiently high intensity. Longitudinal relaxations and detunings appear to play more important roles in controlling the population distribution. The qualitative understanding achieved here can be extended to n levels with n-photon pumping.

7. Work in Progress

Surface optical second-harmonic generation is being used to study surface nonlinear optical properties of metals. The results will be compared with theoretical calculations, yielding information about the electronic properties of the metal surfaces. The effects of adsorbates on the results will also be studied.

An experiment is being carried out to demonstrate that both structural and field discontinuities at an interface contribute to the nonlinearity of the interface. The relative importance of the two depends on the excitation frequency.

A new surface analytical tool based on optical sum-frequency generation is being developed. It is an extension of the optical second-harmonic generation technique, but is much more powerful than the latter since surface vibrational spectroscopy with a submonolayer sensitivity can now be studied using this technique.

In continuous collaboration with Y.T. Lee, overtone spectroscopy (v = 2 and 3) of the C-H stretch mode of benzene is being carried out using the saturation spectroscopic technique in a cooled molecular beam. Very narrow lines, much narrower than previously reported, have been observed. The local-mode character begins to show up at v = 3.

1986 PUBLICATIONS AND REPORTS

Refereed Journals

1. H.W.K. Tom, X.D. Zhu, G.A. Somorjai, and Y.R. Shen, "Investigation of the Si(111)-(7 × 7) Surface by Second-Harmonic Generation: Oxidation of the Effects of Surface Phosphorus," Surf. Sci. **167**, 167 (1986); LBL-19661.
2. H.W.K. Tom, C.M. Mate, X.D. Zhu, J.E. Crowell, G.A. Somorjai, and Y.R. Shen, "Studies of Alkali Adsorption on Rh(111) Using Optical Second-Harmonic Generation," Surf. Sci. **172**, 466 (1986); LBL-20066.
3. G.T. Boyd, Y.R. Shen, and T.W. Hansch, "Continuous-Wave Second-Harmonic Generation as a Surface Microprobe," Opt. Lett. **11**, 97 (1986); LBL-20287.
4. A.H. Kung, R.H. Page, R.J. Larkin, Y.T. Lee, and Y.R. Shen, "Rydberg Spectroscopy of H_2 via Stepwise Resonant Two-Photon Ion-Pair ($H^+ + H^-$) Production," Phys. Rev. Lett. **56**, 328 (1986); LBL-20378.
5. Y.R. Shen, "Surface Second Harmonic Generation: A New Technique for Surface Studies," Ann. Rev. Mater. Sci. **16**, 69 (1986); LBL-20384.
6. C.Y. Fong and Y.R. Shen, "Population Redistribution Induced by Multiphoton Processes," J. Opt. Soc. Am. **B3**, 649 (1986); LBL-20442.
7. P. Guyot-Sionnest, W. Chen, and Y.R. Shen, "General Considerations on Optical Second-Harmonic Generation from Surfaces and Interfaces," Phys. Rev. B **33**, 8254 (1986); LBL-20801.
8. G.T. Boyd, Z.H. Yu, and Y.R. Shen, "Photoinduced Luminescence from the Noble Metals and its Enhancement on Roughened Surfaces," Phys. Rev. B **33**, 7923 (1986); LBL-20802.
9. Y.R. Shen, "Basic Considerations of Four-Wave Mixing and Dynamic Gratings," IEEE J. Quant. Electron. **QE-22**, 1196 (1986); LBL-21081.

Other Publications

10. A.S. Sudbø, P.A. Schulz, Y.R. Shen, and Y.T. Lee, "Molecular-Beam Studies of Laser-Induced Multiphoton Dissociation," in *Multiple-Photon Excitation*

and Dissociation of Polyatomic Molecules, C.D. Cantrell, Ed., Springer-Verlag, Berlin, 1986, p. 95; LBL-8993.

11. Y.R. Shen, "Applications of Optical Second-Harmonic Generation to Surface Science," in *New Laser and Optical Technologies of Chemistry and Structure at Interfaces*, R.B. Hall and A.B. Ellis, eds., Verlag Chemie, Berlin, 1986, p. 151; LBL-18463.
12. Y.R. Shen, "Nonlinear Optics and Surface Science," in *Beam-Solid Interactions and Phase Transitions*, H. Kurz, G.L. Olson, and J.M. Poate, eds., Materials Research Society, Pittsburgh, 1986, p. 39; LBL-20064.
13. P. Guyot-Sionnest, W. Chen, and Y.R. Shen, "Basic Considerations on Surface Optical Nonlinearities," in *Proc. Int. Conf. on Lasers '85*, Las Vegas, NV, December 2–6, 1985, p. 12; LBL-20065.
14. Y.R. Shen, "Second Harmonic Generation at Liquid/Solid Interfaces," Bull. Am. Phys. Soc. **31**, 360 (1986); LBL-20723abs.
15. G.T. Boyd, Z.H. Yu, and Y.R. Shen, "Photo-Induced Luminescence from the Noble Metals and its Enhancement on Roughened Surfaces," Bull. Am. Phys. Soc. **31**, 690 (1986); LBL-20725abs.
16. Y.R. Shen, A Few Recent Experiments on Surface Studies by Second-Harmonic Generation," in *Methods of Laser Spectroscopy,* Y. Prior, A. Ben-Reuven, and M. Rosenbluh, eds., Plenum, New York, 1985, p. 259; LBL-20727.
17. A.H. Kung, R.H. Page, R.J. Larkin, Y.R. Shen, and Y.T. Lee, "XUV Spectroscopy of H_2," J. Opt. Soc. Am. **B3**, 254 (1986); LBL-21076abs.
18. R.H. Page, Y.T. Lee, and Y.R. Shen, "Important Developments in Overtone Spectroscopy," J. Opt. Soc. Am. **B3**, 254 (1986); LBL-21634abs.
19. X.D. Zhu, H. Suhr, and Y.R. Shen, "Surface Vibrational Spectroscopy by Infrared-Visible Sum-Frequency Generation (SFG)," J. Opt. Soc. Am. **B3**, 252 (1986); LBL-21635abs.

LBL Reports

20. X.D. Zhu, H. Suhr, and Y.R. Shen, "Surface Vibrational Spectroscopy by Infrared-Visible Sum-Frequency Generation," Rapid Commun., Phys. Rev. B (in press); LBL-21636.
21. P. Guyot-Sionnest, Y.R. Shen, and T.F. Heinz, "Comments on 'Determination of the Nonlinear Optical Susceptibility $\chi^{(2)}$ of Surface Layers' by B. Dick *et al.*," submitted to Appl. Phys.; LBL-21637.
22. P. Guyot-Sionnest and Y.R. Shen, "Local and Nonlocal Surface Nonlinearities for Surface Optical Second Harmonic Generation," submitted to Phys. Rev. B; LBL-22490.

Invited Talks

23. Y.R. Shen, "Second Harmonic Generation at Liquid/Solid Interfaces," March APS Meeting, Las Vegas, NV, March 31–April 4, 1986.
24. G.T. Boyd, "Photo-Induced Luminescence from the Noble Metals and Its Enhancement on Roughened Surfaces," March APS Meeting, Las Vegas, NV, March 31–April 4, 1986.
25. G.T. Boyd, "CW Surface Second Harmonic Generation as a Surface Micro-Probe," Conference on Lasers and Electro-optics, San Francisco, CA, June 9–13, 1986.
26. A.H. Kung, "XUV Spectroscopy of H_2," International Quantum Electronics Conference, San Francisco, CA, June 9–13, 1986.
27. R.H. Page, "Important Developments in Overtone Spectroscopy," International Quantum Electronics Conference, San Francisco, CA, June 9–13, 1986.
28. Y.R. Shen, "Recent Advances in Surface Studies by Optical SHG," DuPont Central Research Lab., Experimental Station, Wilmington, DE, July 10, 1986.
29. X.D. Zhu, "Surface Vibrational Spectroscopy by Infrared-Visible Sum-Frequency Generation (SFG)," International Quantum Electronics Conference, San Francisco, CA, June 9–13; 1986; Gordon Research Conference on Vibrational Spectroscopy, Wolfeboro, NH, Aug. 11–15, 1986.
30. Y.R. Shen, "Surface Studies by SHG," 3M Central Research Labs., St. Paul, MN, Aug. 20, 1986.
31. Y.T. Lee, "New Horizons in the Overtone Spectroscopy of Benzene," Symposium on State-to-State Chemistry, Anaheim, CA, Sept. 7–12, 1986.

Excitations in Solids*

Carson D. Jeffries, Investigator

INTRODUCTION

The central objectives of this program are: (i) to experimentally study nonlinear dynamical instabilities in solids; (ii) to develop theoretical models from first principles that can interpret observed behavior, within the context of nonlinear dynamical systems theory. These solid-state systems are being studied: spin waves in magnetic spheres and films; plasmas in semiconductors; domain-wall motion in magnetic and ferroelectric materials; and acoustic waves. The observed behavior is complex and usually includes periodic motion, intermittency, and chaotic behavior; there is a correspondence with onset of turbulence in hydrodynamic systems. Experimental procedures are used to produce bifurcation diagrams, phase portraits, Poincaré sections, power spectra, and fractal dimensions of the attractor. These same quantities are computed from theory and compared to data. In a sense, the dynamics observed, and the understanding, appear to be universal. The results have a bearing on a very general class of nonlinear dissipative systems of practical importance and on devices of technological interest.

1. Quasiperiodic Transitions to Chaos of Instabilities in an Electron-Hole Plasma Excited by ac Perturbations at One and at Two Frequencies (Publications 1 and 6)

G.A. Held and C.D. Jeffries

Many physical systems are known to follow a quasiperiodic route to chaos. As some control parameter is increased, the system undergoes a transition from periodicity to quasiperiodicity (i.e., simultaneous oscillations at two or more incommensurate frequencies) to low-dimensional chaos. Recent theoretical advances have resulted in universal and quantitative predictions concerning the transitions between two-frequency quasiperiodicity, mode-locked states, and chaos. Transitions between three-frequency quasiperiodicity and chaos are less well understood; theoretically it is uncertain whether stable three-frequency quasiperiodic states should even exist.

Spontaneous current oscillations at $f_o \approx 10^5$ Hz in an electron-hole plasma in a Ge crystal in parallel electric and magnetic dc fields are known to be a result of unstable traveling helical plasma waves; under increased dc drive the oscillations exhibit a period-doubling route to chaos. To test predictions of a universal two-frequency quasiperiodic transition we additionally drive the crystal with an external oscillator of voltage V_1 and frequency f_1. With the frequency ratio held at the golden mean, $f_o/f_1 = \sigma_g = (\sqrt{5-1})/2$, the observed power spectra and Poincaré sections are shown in Figure 1-1 for several values of V_1. Chaos sets in, Figure 1-1(b), where the section of the torus begins to wrinkle. These data are replotted, as in Figure 1-2, to enable comparison with theory. The first-generation peaks, labeled 1, are as predicted. However, the higher-generation peaks 2, 3, 4, ..., are not found to clearly form a self-similar pattern; the reasons for this are under further study.

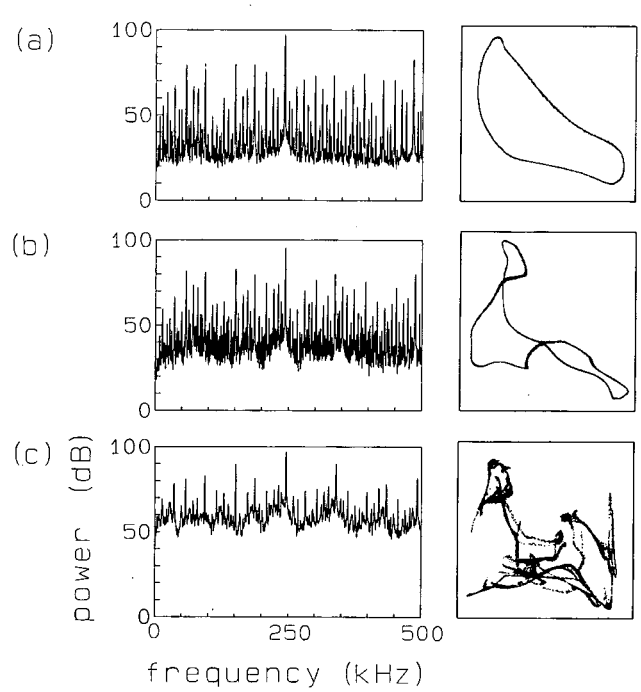

Figure 1-1. Power spectra of plasma current I(t) and Poincaré sections, I(t) vs. $I(t+1/f_1)$ at golden-mean winding number for various values V_1: (a) V_1 = 195 mV; (b) V_1 = 274 mV, onset of chaos; (c) 374 mV, more chaotic. (XBL 8512-5072)

In the same system data were taken with an additional driving oscillator at f_2. Stable three-frequency (f_o, f_1, f_2) quasiperiodic states were

*This work was supported by the Director, Office of Energy Research, Office of Basic Energy Sciences, Materials Sciences Division of the U.S. Department of Energy under Contract No. DE-AC03-76SF00098.

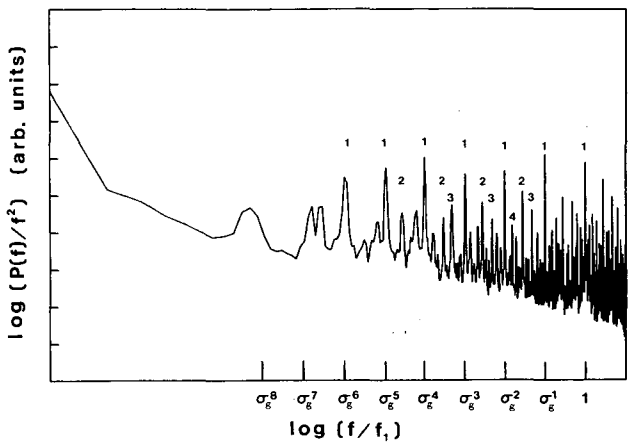

Figure–1-2. Power spectra of plasma current at onset of chaos, Figure 1-1(b); $\log[P(f)/f^2]$ on vertical axis, $\log(f/f_1)$ on horizontal axis. The plot roughly agrees with theoretical predictions for the quasiperiodic route at the golden-mean winding number. (XBL 8510-4243A)

observed. With increased drive V_1, two routes to chaos were observed: (i) first, mode locking to two frequencies; (ii) a direct and abrupt three-frequency transition to chaos.

2. Suppression of Period-Doubling and Nonlinear Parametric Effects in Periodically Perturbed Systems (Publications 2 and 4)†

P. Bryant and K. Wiesenfeld

We consider the effect on a generic period-doubling bifurcation of a periodic perturbation, whose frequency ω_1 is near the period-doubled frequency $\omega_0/2$. The perturbation is shown to always suppress the bifurcation, shifting the bifurcation point and stabilizing the behavior at the original bifurcation point. We derive an equation characterizing the response of the system to the perturbation, analysis of which reveals many interesting features of the perturbed bifurcation, including (1) the scaling law relating the shift of the bifurcation point and the amplitude of the perturbation, (2) the characteristics of the system's response as a function of bifurcation parameter, (3) parametric amplification of the perturbation signal, including nonlinear effects such as gain saturation and a discontinuity in the response at a critical perturbation amplitude, (4) the effect of the detuning $(\omega_1-\omega_0/2)$ on the bifurcation, and (5) the emergence of a closely spaced set of peaks in the response spectrum. An important application is the use of period-doubling systems as small-signal amplifiers, e.g., the superconducting Josephson parametric amplifier.

†Research in collaboration with K. Wiesenfeld, whose work was supported by DOE Contract No. DE-AC02-76CH00016 and NSF Grant No. PHY-81-15541.

3. The Dynamics of Phase Locking and Points of Resonance in a Forced Magnetic Oscillator (Publication 7)

P. Bryant and C. Jeffries

We report data on an experimental system: a forced symmetric oscillator containing a saturable inductor with magnetic hysteresis. It displays a Hopf bifurcation to quasiperiodicity, entrainment horns, and chaos. We study in detail the bifurcations and hysteresis occurring near points of resonance (particularly "strong resonance") and show how the observed behavior can be understood using Arnold's theory. Much of the behavior relating to the entrainment horns is explored: period doubling and symmetry-breaking bifurcations; homoclinic bifurcations; and crises and other bifurcations taking place at the horn boundaries. Important features of the behavior related to symmetry properties of the oscillator are studied and explained through the concept of a half-cycle map. The system is shown to exhibit a Hopf bifurcation from a phase-locked state to periodic "islands," similar to those found in Hamiltonian systems. An initialization technique is used to observe the manifolds of saddle orbits and other hidden structures. An unusual differential equation model is developed that is irreversible and generates a noninvertible Poincaré map of the plane. Noninvertibility of this planar map has important effects on the behavior observed. The Poincaré map may also be approximated through experimental measurements, resulting in a planar map with parameter dependence. This model gives good correspondence with the system in a region of the parameter space.

4. Work in Progress

Detailed experiments are in progress to study the interactions between spin-wave modes excited in spheres of yttrium iron garnet by pumping the Suhl instability subsidiary absorption at 9.2 GHz. The dynamical behavior of the magnetization is observed under high resolution by varying two parameters: dc

field and microwave pump power. Quite varied behavior is found: (i) onset of instability by excitation of a single spin-wave mode; (ii) excitation of two or more modes leading to auto-oscillations and a period-doubling transition to chaos; (iii) three or more mode excitations leading to a quasiperiodic route to chaos; (iv) abrupt transitions to chaos with hysteresis. A first-principles theoretical model is being numerically evaluated; it predicts much of the above behavior.

Studies of plasma instabilities in Ge rods are being extended to test recent predictions of nonlinear-dynamics theory: a section of a trajectory in phase space is usually observed to be a fractal object, but with some regions visited more frequently than others. To describe this a scaling index α is introduced with a distribution of values, $f(\alpha)$; this function has been computed for the period doubling and the quasiperiodic transitions to chaos. Measurements here aim at an experimental measurement of these distributions.

The experimental work is being extended to domain-wall motion in magnetic materials and spin waves in thin ferromagnetic films.

1986 PUBLICATIONS AND REPORTS

Refereed Journals

1. G.A. Held and C.D. Jeffries, "Quasiperiodic Transitions to Chaos of Instabilities in an Electron-Hole Plasma Excited by ac Perturbations at One and at Two Frequencies," Phys. Rev. Lett. **56**, 1183 (1986); LBL-20862.
2. P. Bryant and K. Wiesenfeld,† "Suppression of Period-Doubling and Nonlinear Parametric Effects in Periodically Perturbed Systems," Phys. Rev. A **33**, 2525 (1986); LBL-20284.

Other Publications

3. C.D. Jeffries, "Nonlinear Dynamics in Solid State Systems," in *Perspectives in Nonlinear Dynamics*, R. Cawley, A. Saenz, M. Schlesinger, and W. Zachary, eds., World Scientific Publishers, Singapore, 1986, p. 124.
4. P. Bryant and K. Wiesenfeld,† "Suppression of Period Doubling and Nonlinear Parametric Effects in Periodically Perturbed Systems," Bull. Am. Phys. Soc. **31**, 419 (1986); LBL-20755abs.
5. K. Wiesenfeld† and P. Bryant, "What Nonlinear Dynamics Has to Say About the Noise Rise in Josephson Junction Parametric Amplifiers," Bull. Am. Phys. Soc. **31**, 419 (1986).
6. G.A. Held and C. Jeffries, "Universal Transitions to Chaos of Instabilities in an Electron-Hole Plasma Excited by One and Two Frequency ac Perturbations," Bull. Am. Phys. Soc. **31**, 363 (1986); LBL-20754abs.

LBL Reports

7. P. Bryant and C. Jeffries, "The Dynamics of Phase Locking and Points of Resonance in a Forced Magnetic Oscillator," Physica (in press); LBL-21133.
8. P. Bryant, K. Wiesenfeld,† and B. McNamara,‡ "Noise Rise in Parametric Amplifiers," LBL-22128.

Invited Talks

9. C.D. Jeffries, "Nonlinear Dynamics of Some Solid State Systems: an Overview," Research Group in Nonlinear Systems and Dynamics, University of California, Berkeley, Sept. 10, 1986.
10. C.D. Jeffries, "Experiments on Nonlinear Spin Wave Dynamics," Nonlinear Dynamics Seminar, University of California, Santa Barbara, Oct. 24, 1986.
11. C.D. Jeffries, "Nonlinear Dynamics in Solids," Physics Department Colloquium, University of Maryland, College Park, Nov. 4, 1986.
12. C.D. Jeffries, "Spin Wave Instabilities in Garnets," U.S. Naval Research Laboratory, Washington, DC, Nov. 5, 1986.
13. C.D. Jeffries, "Helical Plasma Wave Instabilities in Ge Rods," U.S. Naval Research Laboratory, Washington, DC, Nov. 6, 1986.
14. C.D. Jeffries, "Nonlinear Dynamics of Spin Waves and Plasma Waves," Physics Department Colloquium, University of California, Santa Cruz, Nov. 20, 1986.

†Supported by U.S. Department of Energy under Contract No. DE-AC02-76CH00016.

‡Supported by U.S. Office of Naval Research.

Time-Resolved Spectroscopies in Solids*

Peter Y. Yu, Investigator

INTRODUCTION

The purpose of this project is to use picosecond and subpicosecond laser pulses generated by modelocked dye lasers to study ultrafast interactions between elementary excitations in solids. Using the short laser pulses, nonequilibrium phonons and carriers are excited in semiconductors, such as GaAs, and their dynamics are probed by Raman scattering. From analysis of the light-scattering spectra by the photoexcited electron-hole plasmas, the scattering time and the temperature of the plasmas are determined. The influence of defects and external perturbations such as hydrostatic pressure is also investigated.

The effect of pressure on the electrical and optical properties of semiconductors with diamond and zincblende-type crystal structures is investigated. By measuring the resistance of samples as a function of pressure, the semiconductor-to-metal transition pressure can be determined. The electron-phonon interaction in the metallic phase is studied by measuring the temperature dependence of the resistance. Many of the metallic high-pressure phases of semiconductors are found to be superconducting. Whenever the high-pressure phase is superconducting, the pressure dependence on the transition temperature is measured. The possible relationship between the transition temperature and soft phonon modes associated with structural phase transitions is also under investigation.

1. Picosecond Time-Resolved Raman Scattering from Photoexcited Electron-Hole Plasmas in GaAs (Publication 3)

Y. Huang and P.Y. Yu

Dense hot electron-hole plasmas have been excited in GaAs by picosecond dye laser pulses. The dynamics of the plasmas can be studied as a function of time by Raman scattering of a suitably delayed probe pulse following the excitation pulse. From analysis of the scattering spectra due to single-particle excitations, the relaxation times of hot electrons in GaAs are determined.

2. Superconductivity and Phase Transitions in High-Pressure Metallic Phases of Si and Related Semiconductors (Publications 1, 2, 4, and 5)

D. Erskine, P.Y. Yu, K.J. Chang, and M.L. Cohen

A technique has been developed for performing electrical measurements on samples under high pressure and at low temperatures using diamond anvil cells. Using this technique the pressure dependence of the superconducting transition temperatures in Si, GaAs, and GaP has been measured to pressures exceeding 45 GPa. In hexagonal Si, which exists at pressures between 16 and 40 GPa, the superconducting transition temperature shows a very unusual dependence on pressure. It first decreases with pressure, reaches a minimum of about 3 K at 38 GPa, and then increases sharply to 4.9 K before the transition to the hexagonal close-packed phase (see Figure 2-1). These experimental results are in good qualita-

*This work was supported by the Director, Office of Energy Research, Office of Basic Energy Sciences, Materials Sciences Division of the U.S. Department of Energy under Contract No. DE-AC03-76SF00098.

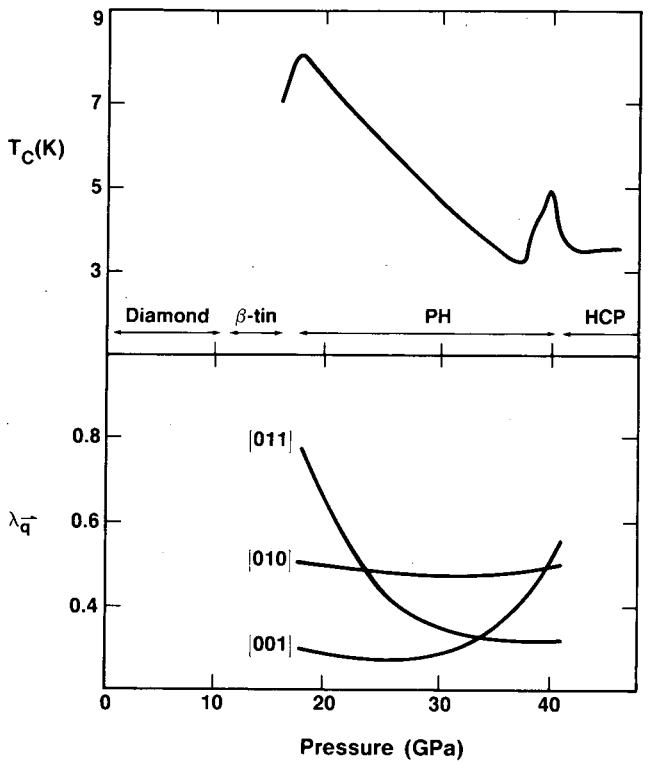

Figure 2-1. Top: measured superconducting transition temperature T_c for silicon versus pressure. Bottom: calculated pressure-dependent electron-phonon λ interaction strength for three phonon wave vectors. (XBL 871-351)

tive agreement with theoretical predictions by the group of M.L. Cohen based on *ab initio* pseudopotential calculations. The theoretical results suggested that the superconducting transition temperatures in hexagonal Si should increase at 16 and 40 GPa because of strong coupling between the electrons and soft phonon modes associated with the structural phase transitions at those two pressures.

3. Work in Progress

A colliding-pulse modelocked dye laser is under construction. This dye laser will produce pulses about 100 femtoseconds in duration and at repetition rates of about 100 MHz. With these shorter pulses it will be possible to study the properties of the photoexcited electron-hole plasmas before the plasmas thermalize with the longitudinal optical phonons in GaAs.

Construction is also under way for new diamond anvil cells that will allow pressure above 100 GPa to be achieved at low temperatures. In collaboration with materials scientists at the Center for Advanced Materials at LBL, work has been initiated in capacitance measurements under pressure using the diamond anvil cell. These measurements will allow properties of deep levels to be investigated as a function of pressure.

1986 PUBLICATIONS AND REPORTS

Refereed Journals

1. D. Erskine and P.Y. Yu, "Dependence of Superconducting Transition Temperature on Pressure in Primitive Hexagonal Si," Phys. Rev. Lett. **56**, 2270 (1986); LBL-21047.
2. D. Erskine, P.Y. Yu, K.J. Chang, and M.L. Cohen, "Superconductivity and Phase Transitions in Compressed Si to 45 GPa," Phys. Rev. Lett. **57**, 2741 (1986); LBL-21496.

LBL Reports

3. Y. Huang and P.Y. Yu, "Picosecond Time-Resolved Raman Scattering from Photoexcited Electron-Hole Plasma in GaAs," LBL-21989.
4. D. Erskine, P.Y. Yu, K.J. Chang, and M.L. Cohen, "Stability of the Si Lattice: Electron-Phonon Interactions and Superconductivity in Hexagonal Si," LBL-21990.
5. D. Erskine and P.Y. Yu, "A New Technique for Making Electrical Measurements in a Diamond Anvil Cell at Cryogenic Temperatures," Rev. Sci. Instrum. (in press); LBL-22485.

Invited Talks

6. P.Y. Yu, "Femtosecond Relaxation Times of Hot Electrons in GaAs from Picosecond Raman Scattering," Physics Department, Simon Fraser University, Burnaby, B.C., June 15, 1986.
7. Y. Huang, "Time-Resolved Raman Study of Photoexcited Electron-Hole Plasma in GaAs," Tenth International Conference on Raman Spectroscopy, Eugene, OR, Sept. 2, 1986.
8. P.Y. Yu, "Physics under High Pressure at Low Temperatures: Superconductivity in Si," Condensed Matter Physics seminar, Department of Physics, University of California, Irvine, Nov. 11, 1986.
9. P.Y. Yu, "Spectroscopic Studies of Relaxation Processes of Hot Carriers in GaAs," Quantum Electronic, High Speed Electronic, and Compound Semiconductor Devices Seminar, Department of Electrical Engineering and Computer Sciences, University of California, Berkeley, Nov. 19, 1986.

Superconductivity, Superconducting Devices, and 1/f Noise*

John Clarke, Investigator

INTRODUCTION

Dc Superconducting QUantum Interference Devices (SQUIDs) are being used in a wide variety of applications, including geophysical measurements, noise thermometry, and nuclear and quadrupole magnetic resonance in the frequency range from a few kHz to 100 MHz. SQUIDs are being operated at temperatures down to 20 mK to study their ultimate noise limitations for such applications as transducers for gravity-wave antennas. The dependence of the low-frequency flicker (1/f) noise on the materials from which the SQUIDs are fabricated is being investigated. The stability and noise properties of all-Nb Josephson junctions are being studied. The lifetime of current-biased Josephson tunnel junctions against macroscopic quantum tunneling is being measured, with particular emphasis on the effects of dissipation. The parameters of these junctions are determined in the classical limit, in part by the effect of microwave irradiation on the lifetime. A detailed study is being made of the excess low-frequency noise induced in metal films by electron and ion bombardment in an electron microscope. In addition to yielding information on the origin of the noise, these measurements may provide a new technique for investigating mobile defects in metals.

1. Nuclear Electric Quadrupole Induction of Atomic Polarization (Publication 4)

T. Sleator,† E.L. Hahn,† M.B. Heaney, C. Hilbert, and J. Clarke

We have observed a new effect in a magnetic-resonance experiment in which processing nuclear-quadrupole moments induce electric-dipole moments in neighboring atoms. A single crystal of $NaClO_3$ is placed between the plates of a capacitor and the ^{35}Cl nuclei are excited into coherent precession by the standard pulsed method for nuclear-quadrupole resonance (NQR). After the pulse, the coherent precession of the nuclear-quadrupole moments is measured as a voltage across the capacitor resulting from the quadrupole-induced electric polarization. A net electric-dipole moment is induced in the neighboring environment of the nucleus provided the crystal is noncentrosymmetric. The capacitor is part of a high-Q RLC circuit at 4.2 K tuned to the ^{35}Cl nuclear-precession frequency of $\omega_0/2\pi$ = 30.7 MHz. The circuit is inductively coupled to a rf amplifier based on a dc SQUID that allows very sensitive detection of the induced voltage. An array of Josephson junctions in series with the resonant circuit acts as a Q-spoiler to shorten the recovery time after the rf pulse.

Figures 1-1(a) and (b) show the results obtained with the [100] and [111] axes perpendicular to the capacitor plates. The thin lines show the predictions of the theory, which has been developed to account for the experimental observations: the agreement is very good. This technique provides new information on the structure of noncentrosymmetric crystals, since the measurement voltage depends on the arrangement and polarizability of atoms in the immediate neighborhood of nuclear-quadrupole

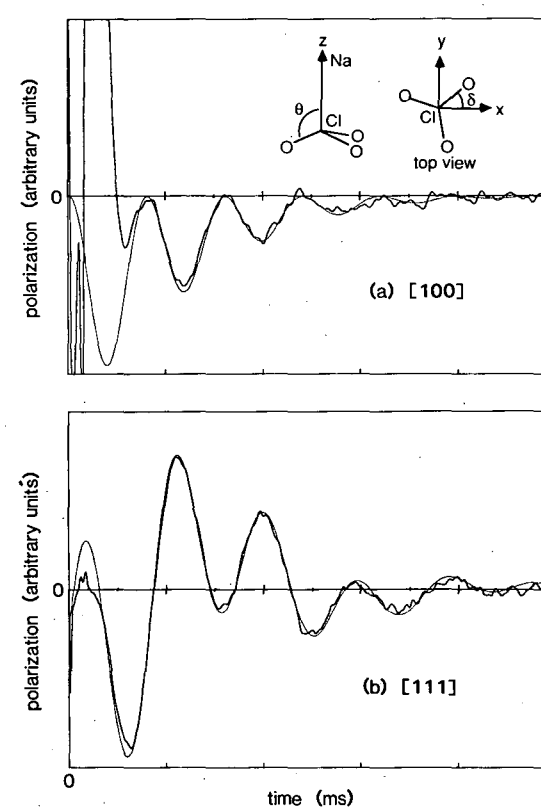

Figure 1-1. Measured electric polarization envelopes (heavy curves) for the crystal directions [100] (a) and [111] (b) perpendicular to the capacitor plates. Thin lines are fits to theory. Inset in (a) shows configuration of $NaClO_3$ molecules. (XBL 867-2795)

*This work was supported by the Director, Office of Energy Research, Office of Basic Energy Sciences, Materials Sciences Division of the U.S. Department of Energy under Contract No. DE-AC03-76SF00098.

moments. The signal is particularly sensitive to bond angles, for example, the angle indicated in the inset of Figure 1-1(a).

†Supported by National Science Foundation.

2. One-Third (Period Three) Harmonic Generation in Microwave-Driven Josephson Tunnel Junctions (Publication 6)

J.B. Hansen,† J. Clarke, J. Mygind,†
G.A. Ovsyannikov, and H. Svensmark†

There has been considerable recent interest in the subharmonic and chaotic behavior of driven, dissipative nonlinear systems. One example is the current-biased Josephson tunnel junction in the presence of microwave radiation, which has been the subject of extensive digital and analog computer simulations. One prediction for the junction in the zero-voltage state is the existence of narrow bands of even and odd subharmonic solutions in the microwave amplitude-frequency plane, often separated by regions of chaos.

We have made the first experimental confirmation of these effects by observing one-third harmonic (period 3) generation at zero dc bias in the pump frequency range 8 to 20 GHz. The observed signal was as much as 50 dB or more above the noise background with a linewidth of less than 100 Hz (determined by the spectrum analyzer). We made extensive measurements of the harmonic signal as a function of the pump amplitude ρ_m normalized to the junction critical current (I_o) and the microwave frequency Ω normalized to the junction plasma frequency (ω_{po}). To make quantitative comparisons between experiment and simulations, we made detailed *in situ* measurements of I_o, ω_{po}, and the damping of the junction. We also determined the microwave current by measuring the suppression of I_o at each microwave frequency.

From these experiments, we produced state diagrams for the one-third harmonic generation: an example is shown in Figure 2-1. The data map out a single, broad band in the ρ_m-Ω plane. The figure also contains the results of digital simulations that we carried out with a Runge-Kutta technique using the measured experimental parameters. These points again map out a broad region in which the one-third harmonic exists. We note that the experimental and simulated data lie in the same frequency range, and that the ranges in microwave amplitude differ by at most a factor of 2. Given the uncertainties in the experimental parameters and the omission of noise in the simulation, the agreement between experiment and simulation is quite satisfactory.

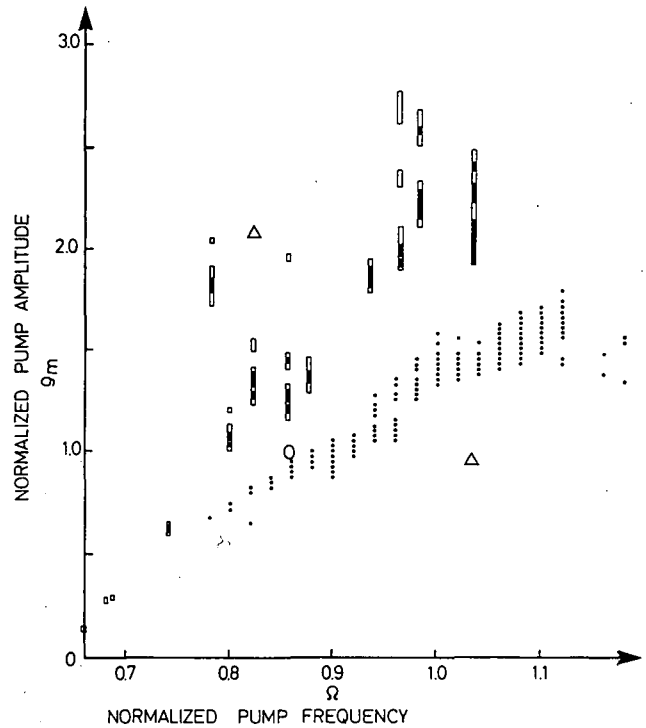

Figure 2-1. Normalized microwave pump amplitude ρ_m vs. normalized pump frequency showing regions for which one-third (and one-half) harmonic signal occurs. *Experiment*: ■ narrow-band one-third harmonic at V = 0; □ broad-band noisy or intermittent one-third harmonic at V = 0; Δ one-third and 0 one-half harmonic at V = $\hbar\omega_m/6e$ and $\hbar\omega_m/4e$, respectively. Experimental parameters are I_o = 163 μA, $\omega_{po}/2\pi$ = 14.45 GHz, α = 0.05, and T_{bath} = 4.2 K. *Simulations*: ● narrow-band one-third harmonic at V = 0 (α = 0.05). (XBL 873-1120)

†Supported by the Danish Natural Science Research Council.

3. Current Noise in the dc SQUID (Publication 5)

J.M. Martinis and J. Clarke

The dc SQUID, consisting of two resistively shunted tunnel junctions incorporated into a superconducting loop, is the basis of a class of amplifiers with exceedingly high sensitivity. The SQUID is characterized by four transfer functions that relate the voltage V across the SQUID and bias current I to the flux Φ threading the loop and current J circulating around the SQUID loop. The noise of the

device is characterized by the spectral sensitivities $S_V(f)$ and $S_J(f)$ of the noises in V and J, and $S_{VJ}(f)$, the cross-spectral noise in V and J (f is the frequency). Proper amplifier design requires a knowledge of all 7 quantities. However, until the present work there has been no experimental determination of S_J and S_{VJ}.

We performed experiments on a planar, thin-film SQUID with a spiral input coil. The shunt resistances of the two junctions were deliberately made very small to enhance the magnitude of the current noise. The coil was coupled to the input coil of a second SQUID (B), which thus detected the current noise in the first SQUID (A). A cooled, resonant tank circuit connected across SQUID A enabled us to measure the voltage noise. The two noises and their cross-correlation were measured with a spectrum analyzer.

The values of S_V, S_J, and S_{VJ} as functions of Φ exhibited the same qualitative features that we observed in analog computer simulations, while the magnitudes agreed to better than a factor of 2. Given the general uncertainties in the values of the parameters and in the possible effects of parasitic capacitances, which we have neglected, the overall level of agreement is quite acceptable. Thus, we now have a knowledge of all the parameters required to design SQUID amplifiers with gain and noise temperature that come close to the predicted values.

4. Excess Noise in dc SQUIDS from 4.2 to 0.22 K (Publication 14)

F.C. Wellstood, C. Urbina, and J. Clarke

The white noise of a dc SQUID operated in the liquid ^{4}He temperature range arises from Nyquist noise in the resistive shunts and has been well understood for a number of years. At low frequencies, SQUIDs exhibit "1/f noise," that is, noise with a spectral density scaling as $1/f^m$, where m is close to unity. This noise may arise from either fluctuations in the critical current of the Josephson junctions or from "flux noise" of unknown origin. However, until now there have no measurements of the noise in SQUIDs at temperatures below 1 K. Such experiments are not only of fundamental interest for the light they may shed on the noise-generation process but also of considerable importance in SQUIDs used as transducers for gravity-wave antennas.

We have measured the noise properties of thin-film dc SQUIDs at temperatures down to 22 mK. We voltage-biased each SQUID by connecting its terminals across a small resistor, with an appropriate current bias, and the input coil of a second, flux-locked dc SQUID. Thus, the output of the second SQUID was proportional to the current fluctuations in the first. Both SQUIDs were heavily shielded and attached to the mixing chamber of a dilution refrigerator.

Figure 4-1 shows the rms excess flux noise at 1 Hz, $S_\Phi^{1/2}$(1 Hz), vs temperature for 12 representative devices. While the noise above 1 K varies widely, that at or below 0.1 K is relatively consistent. For example, for SQUID A1 the excess noise drops rapidly as the temperature is lowered below 4.2 K, reaches a minimum at about 1 K, and increases to a plateau below about 0.5 K. In C2, on the other hand, the noise increases monotonically as the temperature is lowered below 4.2 K. We have shown that this low-temperature noise is a "flux noise," rather than a critical-current noise. Although a large number of possible sources of this noise have been eliminated, the origin has not yet been identified. Work is continuing in an attempt to track down and eliminate the source of the excess noise.

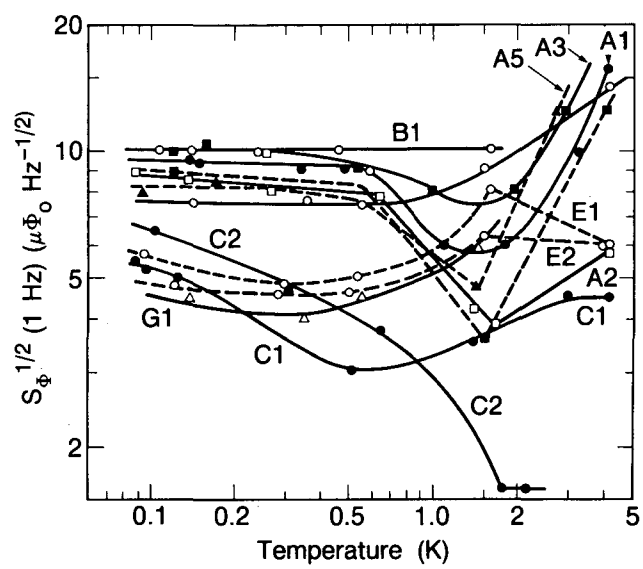

Figure 4-1. Excess equivalent flux noise $S_\Phi^{1/2}$(Hz) vs temperature for 12 SQUIDs at $\Phi = \Phi_0/4$. (XBL 869-8945)

5. Low-Frequency Noise in Nb-Al_2O_3-Nb Josephson Tunnel Junctions (Publication 16)

B. Savo, F.C. Wellstood, and J. Clarke

A number of authors have demonstrated that Nb-Al_2O_3-Nb Josephson tunnel junctions combine

high-quality electrical characteristics with excellent long-term durability. For such junctions to be suitable for dc SQUIDs, however, it is necessary that the low-frequency noise in the critical current be very low to avoid degrading the performance of the SQUID.

We have measured the 1/f noise of a series of these junctions in the liquid ^{4}He temperature range using a dc SQUID as an amplifier. Each junction was resistively shunted to eliminate hysteresis. Typical power spectra $S_{I_o}(f)$ are shown in Figure 5-1. In Figure 5-1(a), for a junction at 4.2 K we see a Lorentzian-shaped feature in the frequency range 1 to 10 Hz. This feature arises from the trapping and untrapping of a *single* electron in the barrier, a process that produces a random telegraph signal. The pulse in critical current corresponding to this process is shown in the inset. When the junction is cooled to 1.4 K, the Lorentzian disappears [Figure 5-1(b)], leaving a very low residual level of 1/f noise. Figure 5-1(c) shows the noise from a second junction at 1.4 K.

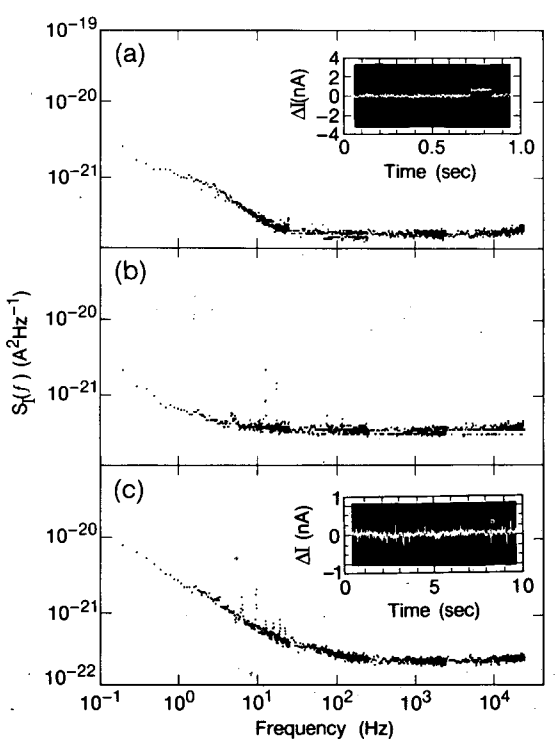

Figure 5-1. (a) Power spectrum of current noise in 3 × 3 μm^2 junction at 4.2 K; inset shows corresponding switching of a single trap as a function of time. (b) Power spectrum of same junction at 1.4 K. (c) Power spectrum of 11 × 11 μm^2 junction at 1.4 K; inset shows several switching events involving at least two traps. (XBL 871-7540)

The magnitude of the noise for 4 junctions is characterized by

$$S_{I_o}^{1/2}(1\ \mathrm{Hz})A^{1/2}/I_o = (14 \pm 6)\mathrm{pA}\mu\mathrm{m}/\mu\mathrm{AHz}^{-1/2},$$

where A is the junction area and I_o is the critical current. This noise level is generally lower than that in our Nb-NbOx-PbIn junctions. Given the high degree of reliability and the low noise level of the all-Nb junctions, we plan to fabricate all future SQUIDs using this technology. It appears likely that companies manufacturing SQUIDs will adopt this process.

6. Work in Progress

In collaboration with Professor A. Pines, we have constructed a dc SQUID amplifier for the detection of zero-field nuclear magnetic resonance (NMR) in the frequency range up to 100 kHz. Work on NQR and NMR in the radiofrequency range is continuing, in collaboration with Professor E.L. Hahn. The emphasis is on the detection of NMR in an external magnetic field in samples with low densities of resonant nuclei, for example, doped semiconductors. In collaboration with Dr. W. King of Argonne National Laboratory, we are measuring the low-frequency noise in copper films induced by electron and Ar^+ irradiation at temperatures down to 4 K. By studying the effects of impurities such as Be on the noise, we hope to be able to identify the precise mechanism of the noise generation.

1986 PUBLICATIONS AND REPORTS

Refereed Journals

1. J. Clarke, "SQUIDs, Brains, and Gravity Waves," Phys. Today **39**, 36 (1986); LBL-21082.
2. M. Devoret, D. Esteve, J.M. Martinis, and J. Clarke, "De nouveaux effects quantiques mis en evidence dans une junction Josephson," La Recherche **16**, 1528 (1986).
3. G. Schön and J. Clarke, "Macroscopic Quantum Phenomena in Josephson Elements," Europhys. News **17**, 94 (1986).
4. T. Sleator, E.L. Hahn, M.B. Heaney, C. Hilbert, and J. Clarke, "Nuclear Electric Quadrupole Induction of Atomic Polarization," Phys. Rev. Lett. **57**, 2756 (1986); LBL-21994.
5. J.M. Martinis and J. Clarke, "Current Noise Measured in the DC SQUID," J. Low Temp. Phys. **65**, 459 (1986); LBL-21757.

6. J.B. Hansen, J. Clarke, J. Mygind, G.A. Ovsyannikov, and H. Svensmark, "One-Third (Period Three) Harmonic Generation in Microwave-Driven Josephson Tunnel Junctions," Appl. Phys. Lett. **49**, 1744 (1986); LBL-22241.

Other Publications

7. J. Pelz and J. Clarke, "The Effects of 500 keV Electron Irradiation and Subsequent Annealing on 1/f Noise in Copper Films," in *Noise in Physical Systems and 1/f Noise-1985*, A. D'Amico and P. Mazzetti, eds., Elsevier Science Publishers, 1986, p. 415; LBL-20385.
8. J. Pelz and J. Clarke, "Temperature Dependence of 500 keV Electron Irradiation-Induced 1/f Noise in Copper Films," Bull. Am. Phys. Soc. **31**, 527 (1986); LBL-20728abs.
9. F.C. Wellstood, C. Urbina, and J. Clarke, "Noise in dc SQUIDs below 1 K," Bull. Am. Phys. Soc. **31**, 386 (1986); LBL-20729abs.
10. T. Sleator, "Observation of Spontaneous Emission from Nuclear Spins," Bull. Am. Phys. Soc. **31**, 360 (1986); LBL-20730abs.
11. C. Hilbert, J.M. Martinis, and J. Clarke, "Radiofrequency Amplifier Based on a DC Superconducting Quantum Interference Device," U.S. Patent DOE S-60, 394 (1986).

LBL Reports

12. J.M. Martinis, M.H. Devoret, and J. Clarke, "Experimental Tests for the Quantum Behavior of a Macroscopic Degree of Freedom: The Phase Difference Across a Josephson Junction," LBL-21936.
13. J. Pelz and J. Clarke, "Comment on 'Sensitivity of the Conductance of a Disordered Metal to the Motion of a Single Atom: Implications for 1/f Noise,' " LBL-21937.
14. F.C. Wellstood, C. Urbina, and J. Clarke, "Excess Noise in dc SQUIDs from 4.2 K to 0.022 K," LBL-22328.
15. J. Mygind, J.B. Hansen, J. Clarke, G.A. Ovsyannikov, and H. Svensmark, "Period Three Generation on Microwave-Induced Constant-Voltage Steps of Josephson Tunnel Junctions," LBL-22431.
16. B. Savo, F.C. Wellstood, and J. Clarke, "Low Frequency Excess Noise in Nb-Al_2O_3-Nb Josephson Tunnel Junctions," LBL-22744.

Invited Talks

17. F. Wellstood, "Dc SQUIDs with Low 1/f Noise," West Coast Superconductive Electronic Meeting, Berkeley, CA, March 7, 1986.
18. J. Clarke, "SQUIDs, Brains, and Gravity Waves," Seminar, CEN Saclay, France, March 12, 1986; Seminar, École Normale Superiéure, Paris, France, April 11, 1986; Colloquium, C.N.R.S., Grenoble, France, May 14, 1986; Colloquium, Univ. de Paris-Sud, Lab. de Phys. des Solids, Orsay, France, May 15, 1986.
19. J. Clarke, "Macroscopic Quantum Effects in a Josephson Junction," 6th General Conference of the Condensed Matter Division of the European Physics Society, Stockholm, Sweden, March 24, 1986; Annual Condensed Matter Meeting of the German Physics Society, Freudenstadt, Federal Republic of Germany, April 8, 1986; Cavendish Lab., Cambridge, England, April 30, 1986; Joint Colloq. at the ETH and Univ. of Zurich, Switzerland, May 7, 1986.
20. J. Pelz, "Temperature Dependence of 500 keV Electron Irradiation-Induced 1/f Noise in Copper Films," March Meeting, American Physical Society, Las Vegas, NV, March 31–April 4, 1986.
21. F.C. Wellstood, "Noise in DC SQUIDs below 1K," March Meeting American Physical Society, Las Vegas, NV, March 31–April 4, 1986.
22. T. Sleator, "Observation of Spontaneous Emission from Nuclear Spins," March Meeting, American Physical Society, Las Vegas, NV, March 31–April 4, 1986.
23. J. Clarke, "Quantum Noise in Josephson Junctions and dc SQUIDs," CEN Saclay, France, April 16, 1986.
24. J. Clarke, "Magnetic Resonance with SQUIDs," CEN Saclay, France, April 17, 1986.
25. R. Miracky, "Deterministic Hopping in a Josephson Circuit Described by a One-Dimensional Map, Qualitative Methods for the Analysis of Nonlinear Dynamics," New England College, Herinke, NJ, June 10, 1986.
26. J. Clarke, "One-Third Harmonic Radiation Emitted from Microwave-Driven Josephson Junction," Applied Superconductivity Conference, Baltimore, MD, Sept. 28–Oct. 3, 1986.
27. F. Wellstood, "Excess Noise in dc SQUIDs from 4.2 K to 90 mK," Applied Superconductivity Conference, Baltimore, MD, Sept. 28–Oct. 3, 1986.
28. J. Clarke, "Macroscopic Quantum Tunneling and Quantized Energy Levels in a Josephson Junction," University of British Columbia, Vancouver, B.C., Oct. 23, 1986; National Bureau of Standards, Washington, D.C., Nov. 21, 1986; Physics Department, Harvard University, Cambridge, MA, Nov. 24, 1986; Institute for Theoretical Physics, University of Calif., Santa Barbara, Dec. 3, 1986.
29. J. Clarke, "The Experimental Status of Macroscopic Quantum Tunneling," MQT86, Institute for Physics, Imperial College of Science and Technology, London, England, Dec. 15, 1986.

THEORETICAL RESEARCH

Theoretical Studies of the Electronic Properties of Solid Surfaces*

L.M. Falicov, Investigator

INTRODUCTION

The purpose of this research is to further basic understanding of the physical properties of materials and materials systems such as surfaces and interfaces. The emphasis is on carrying out quantum-mechanical calculations on realistic systems so that a microscopic understanding may be obtained from first principles. Studies include bulk materials, surfaces and chemisorbed systems, interfaces, defects in solids, and clusters. Comparisons with experiment show that the calculations are accurate and of predictive power. Bulk materials research is focused on electronic, magnetic, structural, and vibrational properties; crystal-structure determination; solid-solid phase transformations at high pressure; and defect properties. Surface and interface research is focused on atomic, electronic, and magnetic structures.

1. Calculation of Fluctuations and Photoemission Properties in a Tetrahedral-Cluster Model for an Intermediate-Valence System (Publication 6)

A. Reich and L.M. Falicov

An exact solution of a four-site tetrahedral crystal model, the smallest face-centered cubic crystal, was obtained in the case of an intermediate-valence system. The model consisted of: (a) one extended orbital and one localized orbital per atom; (b) an interatomic transfer term between extended orbitals; (c) an interatomic hybridization between the localized and extended orbitals; (d) strong intra-atomic Coulomb repulsion between opposite-spin localized states; and (e) intermediate-strength intra-atomic Coulomb repulsion between the localized and extended states. These competing effects were examined as they manifested themselves in the intermediate-valence, photoemission, inverse photoemission, and thermodynamic properties.

2. Photoemission, Inverse Photoemission, and Fluctuations in an Exactly Soluble Many-Body Cluster Model of bcc Iron (Publication 19)

E.C. Sowa and L.M. Falicov

An exact solution for a two-site crystal model, the smallest body-centered cubic crystal, was obtained for iron. The model consisted of five d-like orbitals per site per spin, with interatomic hopping terms and an on-site Coulomb interaction of the fullest generality allowed by atomic symmetry. The ground state, depending on the choice of one-electron parameters, was found in one case to be a fully saturated ferromagnet, and in another to be an unsaturated ferromagnet with strong antiferromagnetic fluctuations. The many-body energy-level spectrum, intracluster charge and spin fluctuations, and photoemission and inverse photoemission densities of states for both cases were calculated and compared with experiment.

3. Central-Cell and Screening Effects on the Binding Energies of Neutral Chalcogen Impurities in Silicon (Publication 2)

L.E. Oliveira† and L.M. Falicov

The binding energies of D^0 states in S-, Se-, and Te-doped silicon crystals were calculated within a variational scheme in the effective-mass approximation and with a Chandrasekhar-type variational function for the two-electron envelopes. Central cells were modeled with a constant core potential within the impurity sphere. Screening effects for the poten-

*This work was supported by the Director, Office of Energy Research, Office of Basic Energy Sciences, Materials Sciences Division of the U.S. Department of Energy under Contract No. DE-AC03-76SF00098.

tial and the electron-electron interaction were taken into account by means of a position-dependent dielectric function. Results were compared with recent theoretical and experimental work. It was found that central-cell effects and position-dependent screening are essential to account for the experimental data.

†Present address: Instituto de Física, Universidade Estadual de Campinas, Campinas 13100, São Paulo, Brazil.

4. Energy Spectra of Donors and Acceptors in Quantum-Well Structures: Effect of Spatially Dependent Screening (Publication 7)

L.E. Oliveira† and L.M. Falicov

The energy spectra of shallow donors and acceptors in GaAs-$Ga_{1-x}Al_xAs$ quantum-well structures were calculated. The binding energies of the impurities were obtained within a variational calculation in the effective-mass approximation. Calculations were performed for simple neutral and double singly ionized impurities as functions of the position of the impurity in a GaAs quantum well of infinite depth and for various slab thicknesses. The effect of the spatially dependent screening was modeled with a dielectric response of the form $\epsilon^{-1}(r) = \epsilon_0^{-1} + (1 = \epsilon_0^{-1})\, e^{-r/a}$, with a screening parameter a = 1.1 a.u. characteristic of bulk GaAs. Results were compared with Bastard's theory, which is based on a constant e_0 screening, and it was found that spatially dependent screening effects were small for donors down to very thin slab thicknesses, but could be quite important for all acceptors in GaAs quantum wells over a large range of slab thicknesses. Calculated results with improved statistics were in quantitative agreement with experimental data on neutral donors and acceptors.

†Present address: Instituto de Física, Universidade Estadual de Campinas, Campinas 13100, São Paulo, Brazil.

1986 PUBLICATIONS AND REPORTS

Refereed Journals

1. L.E. Oliveira and L.M. Falicov, "Effect of Compressive Uniaxial Stress on the Binding Energies of D^- Centers in Si:P and Si:As," Phys. Rev. B **33**, 6990 (1986); LBL-20489.†
2. L.E. Oliveira and L.M. Falicov, "Central-Cell and Screening Effects on the Binding Energies of Neutral Chalcogen Impurities in Silicon," Phys. Rev. B **33**, 8765 (1986); LBL-20987.†
3. J.C. Parlebas, R.H. Victora, and L.M. Falicov, "Exact Solution of a Four-Site Crystal Model for an Intermediate-Valence System," J. Phys. (Paris) **47**, 1029 (1986).‡ § ‖
4. C.A. Balseiro and L.M. Falicov, "Effect of High Magnetic Fields on the Electronic Structure of Density-Wave Systems," Phys. Rev. B. **34**, 863 (1986).‡ **
5. J.M. Kahn, L.M. Falicov and E.E. Haller, "Isotope-Induced Symmetry Change in Dynamic Semiconductor Defects," Phys. Rev. Lett. **57**, 2077 (1986); LBL-21885.
6. A. Reich and L.M. Falicov, "Calculation of Fluctuations and Photoemission Properties in a Tetrahedral-Cluster Model for an Intermediate-Valence System," Phys. Rev. B. **34**, 6752 (1986); LBL-21792.
7. L.E. Oliveira and L.M. Falicov, "Energy Spectra of Donors and Acceptors in Quantum-Well Structures: Effect of Spatially-Dependent Screening," Phys. Rev. B. **34**, 8676 (1986); LBL-21600.†

Other Publications

8. L.M. Falicov, "Electronic and Magnetic Properties of Noble-Metal and Transition-Metal Alloys, Interfaces and Overlayers," in *Noble Metal Alloys*, T.B. Massalski, W.B. Pearson, L.H. Bennett, and Y.A. Chang, eds., The Metallurgical Society of AIME, Warrendale, PA, 1986, p. 17; LBL-19695.
9. J.C. Parlebas, R.H. Victora, and L.M. Falicov, "Four-Site Crystal Model for an Intermediate-Valence System," J. Magn. Magn. Mater. **54–57**, 405 (1986).‡ § ‖
10. F. Aguilera-Granja, J.L. Moran-Lopez, and L.M. Falicov, "Magnetism and Spatial Order Transformation of Systems Chemisorbed on Ferromagnetic Substrates," J. Magn. Magn. Mater. **54–57**, 817 1986).‡ ** ††
11. C.A. Balseiro and L.M. Falicov, "Quasi-One-Dimensional Density-Wave Systems in High Magnetic Fields," Springer Proc. Phys. **14**, 146 (1986).‡ **
12. R.H. Victora, "Magnetic and Electronic Properties of Transition-Metal Surfaces and Overlayers," Springer Proc. Phys. **14**, 25 (1986); LBL-22239.§
13. L.M. Falicov and J.L. Moran-Lopez, ed., *Magnetic Properties of Low-Dimensional Systems*, Springer Proc. Phys. **14**.‡‡
14. L.M. Falicov and C.A. Balseiro, "The Effect of Magnetic Fields on the Electronic Structure of Density-Wave Systems," Physica **143** B, 167 (1986); LBL-21604.**

LBL Reports

15. J.M. Kahn, E.E. Haller, and L.M. Falicov, "Copper-Dihydrogen Complex Shallow Acceptors in High-Purity Germanium," LBL-20687abs.
16. J.M. Kahn, E.E. Haller, and L.M. Falicov, "Copper-Dihydrogen Acceptors in High-Purity Germanium," LBL-21183.
17. J.M. Kahn, E.E. Haller, and L.M. Falicov, "Copper-Dihydrogen Acceptors in High-Purity Germanium," LBL-21424.
18. D.D. Nolte, E.E. Haller, L.M. Falicov, and P. Omling, "The Effect of Uniaxial Stress on Iron-Boron and Iron-Aluminum Defects in Silicon," LBL-22110.[§§]
19. E.C. Sowa and L.M. Falicov, "Photoemission, Inverse Photoemission, and Fluctuations in an Exactly Soluble Many-Body Cluster Model of bcc Iron," LBL-22297.[¶¶]
20. J.M. Kahn, R.E. McMurray, Jr., E.E. Haller, and L.M. Falicov, "Trigonal Hydrogen-Related Acceptor Complexes in Germanium," LBL-22609abs.

Invited Talks

21. L.M. Falicov, "Summary and Conclusions," plenary talk at the International Workshop on the Magnetic Properties of Low-Dimensional Systems, Taxco, Mexico, January 9, 1986.
22. L.M. Falicov, "Effect of High Magnetic Fields on the Electronic Structure of Density-Wave Systems," Exxon Corporate Research Laboratories, Annandale, NJ, February 27, 1986; NORDITA Symposium on Frontiers in Condensed Matter Physics, Copenhagen, Denmark, March 20, 1986; XV Yamada Conference on the Physics and Chemistry of Quasi-One-Dimensional Conductors, Lake Kawaguchi, Japan, May 28, 1986; Institute for Theoretical Physics, Chinese Academy of Sciences, Beijing, Peoples Republic of China, June 6, 1986; Tsing-hua University of Science and Technology, Beijing, Peoples Republic of China, June 9, 1986; Instituto de Fisica "Gleb Wataghin," UNICAMP, Campinas, Brazil, August 12, 1986; Departamento de Fisica, PUC, Rio de Janeiro, Brazil, August 19, 1986.
23. L. M. Falicov, "1986: Open Problems in Condensed Matter Physics," Plenary lecture, Sixth General Conference, Condensed Matter Division, European Physical Society, Stockholm, Sweden, March 25, 1986; Instituto de Fisica "J.A. Balseiro," Centro Atomico Bariloche, S.C. de Bariloche, Argentina, December 15, 1986.
24. L.M. Falicov, "Theory of Edge and Kink Sites in Catalytic Chemistry," Symposium on Surface Science and Catalysis: Chemistry and Physics of Clusters, Annual Meeting, American Chemical Society, New York, NY, April 15, 1986.
25. L.M. Falicov, "Condensed Matter: Order, Disorder and Something in Between," Center for Pure and Applied Mathematics, University of California, Berkeley, April 24, 1986; Department of Physics, Peking University, Beijing, Peoples Republic of China, June 10, 1986.
26. L.M. Falicov, "Magnetism and Correlations in Transition Metals," Department of Physics, Peking University, Beijing, Peoples Republic of China, June 5, 1986.
27. L.M. Falicov, "Fluctuations and Photoemission Properties of Strongly Correlated Metals," Department of Physics, Peking University, Beijing, Peoples Republic of China, June 6, 1986; Instituto de Fisica, Universidade Federal Fluminense, Niteroi, Brazil, August 20, 1986; Centro Brasileiro de Pesquisas Fisicas, Rio de Janeiro, Brazil August 20, 1986; Department of Physics, University of California, Berkeley, October 1, 1986; Department of Physics, University of South Carolina, Columbia, SC, October 30, 1986; Instituto de Fisica "J.A. Balseiro," Centro Atomico Bariloche, S.C. de Bariloche, Argentina, December 16, 1986.
28. L.E. Oliveira, "Energy Spectra of Donors and Acceptors in Quantum-Well Structures: Effect of Spatially-Dependent Screening," Instituto de Fisica, Universidade Federal Fluminense, Niteroi, Brazil, August 26, 1986.
29. L.M. Falicov, "Dynamic Impurities in Ultrapure Semiconductors," SEMICON 86, International School on the Physics, Chemistry and Engineering of Semiconductors, Buenos Aires, Argentina, December 10 and 12, 1986.
30. L.M. Falicov, "Summary and Conclusions," SEMICON 86, International School on the Physics, Chemistry and Engineering of Semiconductors, Buenos Aires, Argentina, December 12, 1986.

[†]Collaboration with Brazilian researchers was supported in part by the National Science Foundation through Grant No. INT-83-12951.

[‡]Secretarial assistance and publication costs were supported in part by the National Science Foundation through Grant No. DMR-81-06494.

[§]Student stipend supported by a fellowship from the A.T. & T. Bell Laboratories.

[¶]Postdoctoral fellowship supported by NATO and by the Conservatoire National des Arts et Metiers (France).

[**]Postdoctoral fellowship supported by the J.S. Guggenheim Foundation.

[††]Collaboration with Mexican researchers was supported in part by the National Science Foundation through Grant No. INT-80-18688.

[‡‡]The Taxco, Mexico, Conference on Magnetic Properties of Low-Dimensional Systems (January 6–9, 1986) was supported in part by the National Science Foundation through Grant No. INT-85-18609.

[§§]Collaboration with researchers at LBL funded through the Center for Advanced Materials, supported by the Director, Office of Energy Research, Office of Basic Energy Sciences, Materials Sciences Division of the U.S. Department of Energy under Contract No. DE-AC03-76SF00098.

[¶¶]Student stipend supported by a fellowship from the Shell Corporation.

Theoretical Solid-State Physics*

Marvin L. Cohen, Investigator

INTRODUCTION

It is now possible to start with a simple model of a solid composed of atomic cores and itinerant valence electrons and compute the total energy for a given structural arrangement of atoms with enough precision to predict the existence of new solids and their properties. The application of the model based on the pseudopotential method can be used to compute properties of solids. With only information about the constituent atoms, the electronic, structural, vibrational, and even superconducting properties of solids are calculated from first principles.

SUPERCONDUCTIVITY AND ELECTRON-PHONON INTERACTIONS

1. Electron-Phonon Interactions and Superconductivity in Si, Ge, and Sn (Publication 20)

K.J. Chang and M.L. Cohen

The pseudopotential–total-energy method is used to calculate the phonon frequency, the electron density of states at the Fermi level, and the electron-phonon coupling constant for the group-IV elements in the metallic β-Sn structure. For these elements, the normal-state behavior is similar to that found in other simple and transition metals; the phonon frequencies, force constants, and electron-phonon matrix elements increase with increasing average electron density. With use of a semiempirical treatment of the electron-phonon coupling calculated for one phonon wave vector, the superconducting transition temperatures at normal and high pressures are examined. The superconducting transition temperature decreases while the magnitude of its pressure coefficient increases in going to heavier elements. This behavior is in good agreement with experiment. For Si and Ge, the superconducting behavior is similar to that of white tin. Because of competition and compensation between the cutoff in the phonon spectrum and the electron-phonon matrix element, the electron-phonon coupling λ's are similar for the three elements. Hence, the Debye temperature, which is the prefactor of the McMillan equation, dominates in determining the superconducting critical temperatures.

2. Calculation of the Pressure Dependence of the Superconducting Transition Temperature of Aluminum (Publication 21)

M.M. Dacorogna, M.L. Cohen, and P.K. Lam

The pressure dependence of the superconducting transition temperature of aluminum is studied by self-consistently calculating the phonon frequencies and the electron-phonon coupling as functions of volume. The rapid change in T_c with pressure in aluminum is reproduced well by the calculation.

HIGH-PRESSURE AND STRUCTURAL PROPERTIES OF SOLIDS

3. *Ab initio* Study of the Structural Properties of Magnesium (Publication 7)

M.Y. Chou and M.L. Cohen

Structural properties of magnesium in the hcp structure are calculated using the *ab initio* pseudopotential method within the local-density-functional formalism. The calculated lattice constants, cohesive energy, bulk modulus, and Poisson's ratio are in good agreement with experimental values. A comparison with the results of beryllium is also discussed.

4. Rhombohedral Phase Stability of the Group-VA Elements (Publication 12)

K.J. Chang and M.L. Cohen

The structural stability of the rhombohedral and simple-cubic phases is studied for the group-VA elements. Using an *ab initio* pseudopotential total-energy method, the calculated phonon frequencies

*This work was supported jointly by the Director, Office of Energy Research, Office of Basic Energy Sciences, Materials Science Division of the U.S. Department of Energy under Contract No. DE-AC03-76SF00098, and by the National Science Foundation under Grant No. DMR8319024.

for the longitudinal acoustic mode at the corner of the simple cubic Brillouin zone are found to soften. This suggests that all group-V elements are likely to form in the rhombohedral structure with respect to the simple cubic phase. At high pressures, the rhombohedral stability is diminished, causing a transition to the simple cubic structure.

5. Structural Properties of NaCl and KCl under Pressure (Publication 13)

S. Froyen and M.L. Cohen

The pseudopotential method within the local-density approximation is used to investigate the static and structural properties of NaCl and KCl. Calculated values for the lattice constants and bulk moduli are in good agreement with experiment. The pressure phase transformation to the CsCl structure is studied, and the role of the C_{44} shear instability as a transformation path is investigated and dismissed. The tetragonal distortion of the CsCl phase, which has been found in other alkali halides at high pressures, appears not to exist in KCl. Finally, we have calculated the electronic energy levels at symmetry points in the Brillouin zone as a function of volume.

6. Electronic and Structural Properties of BN and BP (Publication 17)

R.M. Wentzcovitch, K.J. Chang, and M.L. Cohen

We present a pseudopotential study within the local-density formalism of the structural and electronic properties of zincblende BN and BP. The ground-state properties of these systems, such as bulk moduli, lattice constants, cohesive energies, and frequencies of the TO phonon mode, are in good agreement with experimental results. The valence charge density of BP shows two local maxima along the bond, which is similar to the case of diamond. In contrast, the charge density of BN is similar to that of a typical III-V compound semiconductor. The resulting band structures have some important features that are in disagreement with previously published work. Like most III-V compound semiconductors, the fundamental gap in BP decreases with decreasing volume. The corresponding gap in BN, however, increases with decreasing volume, as was also found in diamond.

7. First-Principles Study of the Structural Properties of Alkali Metals (Publication 23)

M.M. Dacorogna and M.L. Cohen

The structural properties of lithium, sodium, and potassium are studied with use of an *ab initio* pseudopotential method to calculate the total energies of these systems as a function of volume. The results show very small energy differences between the bcc, fcc, and hcp phases in these materials, in good agreement with the measured crystal structures for all three metals. The lattice constants are computed to within 2% of experiment except for sodium, where the calculation gives a lattice constant 3% smaller than experiment.

CLUSTERS

8. Electronic Shell Structure in Simple Metal Clusters (Publication 4)

M.Y. Chou and M.L. Cohen

The total energies of simple metal clusters (sodium, magnesium, and aluminum) containing up to 100 valence electrons are calculated in the spherical jellium approximation using the local-density-functional scheme. Because of the existence of electronic shell structure, there are abrupt changes in the total energy at certain cluster sizes. This behavior accounts for the peaks or steps found in the mass spectrum of sodium clusters. Predictions for the sizes of magnesium and aluminum clusters, which should be abundant in the mass spectra, are also discussed.

9. Elastic Jellium Sphere in a Static Electric Field (Publication 15)

P. Sheng, M.Y. Chou, and M.L. Cohen

The electronic and ionic response of a small metal particle in a static electric field is studied within the jellium model in which the ionic jellium background is assumed to be elastically deformable. Results of the calculation indicate that while the polarizability of the particle remains remarkably constant as the jellium stiffness is relaxed from perfect rigidity, there are nevertheless significant departures

from the rigid jellium model in both the ionic and/or electronic makeup of the polarizability and the associated charge-density modulations. In particular, for Na clusters of up to 92 atoms, the ionic component is shown to account for ~10–15% of the total polarizability. Numerically evaluated charge-modulation profiles, together with the variation of ionic polarizability with elastic stiffness, are presented and discussed.

STACKING FAULTS IN SILICON

10. Theoretical Study of Stacking Faults in Silicon (Publication 1)

M.Y. Chou, M.L. Cohen, and S.G. Louie

The intrinsic and extrinsic stacking faults along the [111] direction in silicon are studied within the local-density-functional approach with *ab initio* pseudopotentials using a plane-wave basis set. The stacking-fault energy is obtained from first principles and is found to be in reasonably good agreement with experimental values. Electronic defect states are found within the energy gap. The defect state with energy 0.1 eV above the valence-band maximum is consistent with photoluminescence data. The electron density near the fault is found to deviate only slightly from the perfect crystal. The Hellmann-Feynman force theorem is used to study the forces on atoms near the fault and to determine the resulting structural relaxations. It is found that the interplanar separations increase by about 1% to achieve vanishing forces. This relaxation does not appreciably affect the stacking-fault energy, the eigenvalues, and other electronic properties.

1986 PUBLICATIONS AND REPORTS

Refereed Journals

1. M.Y. Chou, M.L. Cohen, and S.G. Louie, "Theoretical Study of Stacking Faults in Silicon," Phys. Rev. B **32**, 7979 (1985); LBL-20798.
2. M.L. Cohen, "Calculation of Bulk Moduli of Diamond and Zinc-blende Solids," Phys. Rev. B **32**, 7988 (1985).†
3. M.L. Cohen, K.J. Chang, and M.M. Dacorogna, "Theoretical Study of Superconductivity in Highly Condensed Si," Physica **135B**, 129 (1985).
4. M.Y. Chou and M.L. Cohen, "Electronic Shell Structure in Simple Metal Clusters," Phys. Lett. **113A**, 420 (1986).
5. S.L. Richardson, M.L. Cohen, S.G. Louie, and J.R. Chelikowsky, "Electron Charge Densities at Conduction-Band Edges of Semiconductors," Phys. Rev. B **33**, 1177 (1986); LBL-20796.‡
6. R.M. Wentzcovitch, S.L. Richardson, and M.L.Cohen, "Electronic Charge Densities at Valence and Conduction Band Edges of ZnSe and CdTe," Phys. Lett. **114A**, 203 (1986).‡
7. M.Y. Chou and M.L. Cohen, "*Ab initio* Study of the Structural Properties of Magnesium," Solid State Commun. **57**, 785 (1986).
8. Y.K. Vohra, K.E. Brister, S. Desgreniers, A.L. Ruoff, K.J. Chang, and M.L. Cohen, "Phase-Transition Studies of Germanium to 1.25 Mbar," Phys. Rev. Lett. **56**, 1944 (1986).
9. M.L. Cohen, "Prediction of New Materials and Properties of Solids," Int. J. Quantum Chem. **XXIX**, 843 (1986).
10. K.J. Chang and M.L. Cohen, "Structural Stability of Phases of Black Phosphorus," Phys. Rev. B **33**, 6177 (1986).
11. M.Y. Chou, M.L. Cohen, and S.G. Louie, "Theoretical Compton Profiles of Graphite and LiC_6," Phys. Rev. B **33**, 6619 (1986).
12. K.J. Chang and M.L. Cohen, "Rhombohedral Phase Stability of the Group-VA Elements," Phys. Rev. B **33**, 7371 (1986).
13. S. Froyen and M.L. Cohen, "Structural Properties of NaCl and KCl under Pressure," J. Phys. C **19**, 2623 (1986).
14. D. Vanderbilt, S.G. Louie, and M.L. Cohen, "Calculation of Anharmonic Phonon Couplings in C, Si, and Ge," Phys. Rev. B **33**, 8740 (1986); LBL-20805.
15. P. Sheng, M.Y. Chou, and M.L. Cohen, "Elastic Jellium Sphere in a Static Electric Field," Phys. Rev. B **34**, 732 (1986).
16. S.B. Zhang, M.L. Cohen, and S.G. Louie, "Structural and Electronic Properties of the Al-GaAs(110) Interface," Phys. Rev. B **34**, 768 (1986).
17. R.M. Wentzcovitch, K.J. Chang, and M.L. Cohen, "Electronic and Structural Properties of BN and BP," Phys. Rev. B **34**, 1071 (1986).
18. S. Fahy, S.G. Louie, and M.L. Cohen, "Pseudopotential Total-Energy Study of the Transition from Rhombohedral Graphite to Diamond," Phys. Rev. B **34**, 1191 (1986); LBL-21151.
19. S.B. Zhang and M.L. Cohen, "Surface States on GaAs(110)," Surf. Sci. **172**, 754 (1986).†
20. K.J. Chang and M.L. Cohen, "Electron-Phonon Interactions and Superconductivity in Si, Ge, and Sn," Phys. Rev. B **34**, 4552 (1986).
21. M.M. Dacorogna, M.L. Cohen, and P.K. Lam, "Calculation of the Pressure Dependence of the Superconducting Transition Temperature of Aluminum," Phys. Rev. B **34**, 4865 (1986).

22. M.L. Cohen, "Predicting New Solids and Superconductors," Science **234**, 549 (1986).
23. M.M. Dacorogna and M.L. Cohen, "First Principles Study of the Structural Properties of Alkali Metals," Phys. Rev. B **34**, 4996 (1986).
24. P.K. Lam, M.M. Dacorogna, and M.L. Cohen, "Self-Consistent Calculation of Electron-Phonon Couplings," Phys. Rev. B **34**, 5065 (1986).
25. D. Erskine, P.Y. Yu, K.J. Chang, and M.L. Cohen, "Superconductivity and Phase Transitions in Compressed Si to 45 GPa," Phys. Rev. Lett. **57**, 2741 (1986).
26. R.M. Wentzcovitch and M.L. Cohen, "Theory of Structural and Electronic Properties of BAs," J. Phys. C **34**, 6791 (1986).
27. K.J. Chang and M.L. Cohen, "First Principles Study of the Structural Properties of Ge," Phys. Rev. B **34**, 8581 (1986).

Other Publications

28. M.L. Cohen, "*Ab initio* Calculations of Structural Properties of Solids," in *Proc. Second Int. Conf. on Science of Hard Materials*, E.A. Almond, C.A. Brookes, and R. Warren, eds., Rhodes, Greece, September 23–28, 1984, Institute of Physics, Bristol, England, 1986, p. 1.
29. M.L. Cohen, "Pseudopotential Calculations of Structural Properties of Solids," in *1985 Proc. MRS*, Mat. Res. Soc. Symp. Proc. **63**, 107 (1986).
30. M. Hanfland, K. Syassen, S. Fahy, S.G. Louie, and M.L. Cohen, "The First-Order Raman Mode of Diamond Under Pressure," Physica **139** and **140B**, 516 (1986).†
31. M.L. Cohen, "Properties of Materials: Calculations," in *The Encyclopedia of Materials Science and Engineering*, M.B. Bever, Ed., Pergamon, Oxford, 1986, p. 3974.
32. M.L. Cohen, "Theoretical Model for Predicting Superconductors and New Solid Structures," J. Metals **38**, 55 (1986).
33. M.L. Cohen, "Tribute to Minko Balkanski," Solid State Commun. **60**, xii (1986).
34. S.B. Zhang, M.L. Cohen, and S.G. Louie, "Reconstruction and Electronic Properties of the AlGaAs(110) Interface," Bull. Am. Phys. Soc. **31**, 247 (1986).
35. R.M. Wentzcovitch, K.J. Chang, and M.L. Cohen, "Electronic and Structural Properties of BN and BP," Bull. Am. Phys. Soc. **31**, 301 (1986).
36. K.J. Chang and M.L. Cohen, "Structural Stability of Black Phosphorus," Bull. Am. Phys. Soc. **31**, 301 (1986).
37. S. Fahy, S.G. Louie, and M.L. Cohen, "Theoretical Study of the Graphite-Diamond Transition," Bull. Am. Phys. Soc. **31**, 301 (1986).
38. K.J. Chang and M.L. Cohen, "High-Pressure Hexagonal Phases of Germanium," Bull. Am. Phys. Soc. **31**, 203 (1986).
39. P. Sheng, M.Y. Chou, and M.L. Cohen, "Elastic Jellium Sphere in a Static Electric Field," Bull. Am. Phys. Soc. **31**, 636 (1986).
40. M.Y. Chou, M.L. Cohen, and S.G. Louie, "Theoretical Study of Compton Profiles of Graphite and LiC_6," Bull. Am. Phys. Soc. **31**, 643 (1986).
41. S.G. Louie and M.L. Cohen, "Quantum Mechanical Calculations of Structural Properties of Materials," in *Proc. 14th General Meeting Int. Mineralog. Assn.*, 1986, p. 159.

Invited Talks

42. M.L. Cohen, "Predicting High-Pressure Structures and Superconductivity of Solids," Departments of Chemistry, Physics, and Geophysics, University of Hawaii, Honolulu, Jan. 6, 1986.
43. M.L. Cohen, "Predicting New Solids and Superconductors," Department of Chemistry, University of California, Berkeley, Feb. 11, 1986.
44. M.L. Cohen, "Predicting New Solids and Superconductors," Department of Physics, University of California, Santa Barbara, March 11, 1986.
45. M.L. Cohen, "Care and Nurturing of the Science and Engineering Talent Pool," Engineering Deans' Institute, Long Beach, CA, March 12, 1986.
46. M.L. Cohen, "Predicting New Solids and Superconductors," National Bureau of Standards, Gaithersburg, MD, April 25, 1986.
47. M.L. Cohen, "High Pressure Physics: A New 'Old Field,' " Department of Physics, University of California, Berkeley, May 7, 1986.
48. M.L. Cohen, "Predicting Properties of Solids," Texas Instruments, Dallas, TX, May 8, 1986.
49. M.L. Cohen, "Interventions for Nurturing the Science and Engineering Talent Pool," Government-University-Industry Research Roundtable, Washington, DC, May 20, 1986.
50. M.L. Cohen, "Predicting High Pressure Structures and Superconductivity of Solids," Gordon Conference on Research at High Pressures, Kimball Union Academy, Meriden, NJ, June 23, 1986.
51. M.L. Cohen, "Pseudopotential and Local Density Methods for Solids and Clusters," Aspen Center for Physics, Aspen, CO, July 8, 1986.
52. M.L. Cohen, "Interventions in Science and Engineering Education" (panel participant), Franklin Institute, Philadelphia, PA, September 29, 1986.
53. M.L. Cohen, "Predicting New Solids and Superconductors," IBM Research Laboratories, Yorktown Heights, NY, Sept. 30, 1986.
54. M.L. Cohen, "Predicting New Solids and Superconductors," Department of Physics, University of Tokyo, Japan, Oct. 17, 1986.
55. M.L. Cohen, "Shell Structure in Clusters," NEC Symposium on Microclusters, Hakone, Japan, Oct. 20, 1986.
56. M.L. Cohen, "Predicting the Properties of Semiconductors," NEC Research Laboratories, Tokyo, Japan, Oct. 24, 1986.

57. M.L. Cohen, "Research Opportunities and Industry-University Co-operation," Workshop on Science and Technology with Soft X Rays, Xerox Palo Alto Research Center, Palo Alto, CA, Nov. 6, 1986.
58. M.L. Cohen, "Honoring Minko Balkanski, the 1986 MRS von Hippel Award Winner," Materials Research Society Fall Meeting, Boston, MA, Dec. 3, 1986.
59. M.L. Cohen, "Theory and New Directions in Materials Science," University of Hawaii, Honolulu, December 11, 1986.

†Supported by NSF Grant DMR8319024.

‡Supported through the Center for Advanced Materials Division by the Director, Office of Energy Research, Office of Basic Energy Sciences, Materials Sciences Division of the U.S. Department of Energy under Contract No. DE-AC03-76SF00098.

Surface, Chemisorption, and Theory of Solids*

Steven G. Louie, Investigator

INTRODUCTION

The purpose of this work is to further basic understanding of the electronic and structural properties of materials and materials systems such as surfaces and interfaces. Quantum-mechanical calculations are carried out on realistic systems so that a microscopic understanding of material properties may be obtained from first principles. The research effort encompasses the study of bulk materials, surfaces and chemisorption systems and defects, and the formulation and development of new theoretical techniques for calculating ground-state and excited-state properties. Current projects include work on surface atomic and electronic structures, structural and vibrational properties of solids, phonon-phonon interactions, and solid-solid phase transformations.

1. *Ab Initio* Study of Electronic and Structural Properties of Transition Metals (Publications 7, 13, and 17)

C.T. Chan, S.G. Louie, D. Vanderbilt, and J.R. Chelikowsky

The electronic, cohesive, and structural properties of Mo, W, Ru, and Pd in the bcc, fcc, and hcp structures were calculated from first principles using a local orbital–total energy method. The determined properties are in excellent agreement (generally at a few percent level) with experiment. The work gives a detailed account of the structural-energy differences between the hcp and the cubic phases of these materials. Their structural properties at high pressures are predicted.

*This work was supported by the Director, Office of Energy Research, Office of Basic Energy Sciences, Materials Sciences Division of the U.S. Department of Energy under Contract No. DE-AC03-76SF00098.

2. General Self-Consistent Scheme for Bulk and Surface Electronic Structure Calculation in the Local-Orbital Formalism (Publications 3 and 4)†

C.T. Chan, D. Vanderbilt, and S.G. Louie

A general self-consistency procedure for electronic-structure calculation formulated in momentum space is developed. The present formulation has the merit of bringing the self-consistency problem for different basis sets to the same footing. The method is made efficient by exploiting the translational and space-group symmetries of the system under consideration. Application has been made to compute the structural and vibrational properties of bulk semiconductors, transition metals, and those of the W(001) surface.

†Supported in part (postdoctoral salary) by NSF Grant No. DMR8319024.

3. Pseudopotential Total-Energy Study of the Transition from Rhombohedral Graphite to Diamond (Publication 10)†

S. Fahy, S.G. Louie, and M.L. Cohen

The path maintaining rhombohedral symmetry in the transition from graphite to diamond that minimizes the energy at each value of the bond length between layers is determined. The energy barrier for this path is found to be 0.33 eV. The total energy of the solid is calculated using local-density-functional theory with *ab initio* pseudopotentials. In contrast to recent extended-Huckel-theory results, throughout most of the transition the structure is found to remain semimetallic or semiconducting. A final rapid opening of the gap to the insulating diamond phase develops as the interlayer carbon-carbon bonds form. The behavior of rhombohedral graphite under conditions of isotropic pressure is also examined. We predict that rhombohedral graphite will transform to diamond, without thermal or catalytic activation, at an isotropic pressure of 80 GPa if it maintains its rhombohedral symmetry. Our analysis, moreover, suggests that in general cross linking of hexagonal-ring carbon compounds leading to local tetrahedral coordination should be favored when the interlayer distance between hexagonal rings is between 2.1 and 2.3 Å.

†Supported in part (graduate student salary) by NSF Grant No. DMR8319024.

4. Calculation of Anharmonic Phonon Couplings in C, Si, and Ge (Publication 6)†

D. Vanderbilt, S.G. Louie, and M.L. Cohen

Frozen-phonon total-energy calculations are used to extract anharmonic phonon couplings for the tetrahedral elements C, Si, and Ge. The local-density approximation is employed, with a localized-orbital basis used for C and a plane-wave expansion used for Si and Ge. The bare interactions between optical phonons are completely determined through fourth order at the Brillouin-zone center. These are used to compute renormalized couplings in which a vertex is screened by virtual phonons. The renormalized couplings are found to have the wrong sign to allow formation of a proposed two-phonon bound state in diamond.

†Supported in part (postdoctoral salary) by NSF Grant No. DMR8319024.

5. Theoretical Compton Profiles of Graphite and LiC_6 (Publications 5 and 18)†

M.Y. Chou, M.L. Cohen, and S.G. Louie

Within the impulse approximation, Compton profiles of graphite and LiC_6 for several symmetry directions are calculated using the wave functions obtained from pseudopotential local-density-functional calculations. Excellent agreement is found when the calculated profiles are compared with the experimental results. The intercalation effects were analyzed in the difference profile between these two materials.

†Supported in part (graduate student salary) by NSF Grant No. DMR8319024.

6. Spin-Orbit Splitting in Semiconductors and Insulators from the *Ab Initio* Pseudopotential (Publication 11)†

M.S. Hybertsen and S.G. Louie

The expressions required for using the vector (spin-orbit) part of the *ab initio* pseudopotential in a crystalline calculation are derived. Inclusion of the spin-orbit interaction using the vector part of the pseudopotential in first order reproduces the measured spin-orbit splittings in Ge as well as the rare-gas solids and agrees with all-electron calculations.

†Supported in part (graduate student salary) by NSF Grant No. DMR8319024.

1986 PUBLICATIONS AND REPORTS

Refereed Journals

1. M.Y. Chou, M.L. Cohen, and S.G. Louie, "Theoretical Study of Stacking Faults in Silicon," Phys. Rev. B **32**, 7979 (1985); LBL-20798.†
2. S.L. Richardson, M.L. Cohen, S.G. Louie, and J.R. Chelikowsky, "Electron Charge Densities at Conduction-Band Edges of Semiconductors," Phys. Rev. B **33**, 1177 (1986); LBL-20796.†
3. C.T. Chan, D. Vanderbilt, and S.G. Louie, "Application of a General Self-Consistent Scheme in the Linear Combination of Atomic Orbitals Formalism to the Electronic and Structural Properties of Si and W," Phys. Rev. B **33**, 2455 (1986); LBL-20797.†
4. C.T. Chan and S.G. Louie, "Theoretical Study of the Surface Energy and Surface Relaxation of W(001) Surface," Phys. Rev. B **33**, 2861 (1986); LBL-20799.
5. M.Y. Chou, M.L. Cohen, and S.G. Louie, "Theoretical Compton Profiles of Graphite and LiC_6," Phys. Rev. B **33**, 6619 (1986).†
6. D. Vanderbilt, S.G. Louie, and M.L. Cohen, "Calculation of Anharmonic Phonon Couplings in C, Si, and Ge," Phys. Rev. B **33**, 8740 (1986); LBL-20805.†
7. C.T. Chan, D. Vanderbilt, S.G. Louie, and J.R. Chelikowsky, "Theoretical Study of the Cohesive and Structural Properties of Mo and W in bcc, fcc, and hcp Structures," Phys. Rev. B **33**, 7941 (1986); LBL-20804.
8. M. Hanfland, K. Syassen, S. Fahy, S.G. Louie, and M.L. Cohen, "The First-Order Raman Mode of Diamond under Pressure," Physica **139** and **140** B, 516 (1986).§
9. S.B. Zhang, M.L. Cohen, and S.G. Louie, "Structural and Electronic Properties of the Al-GaAs(110) Interface," Phys. Rev. B **34**, 768 (1986).§
10. S. Fahy, S.G. Louie, and M.L. Cohen, "Pseudopotential Total Energy Study of the Transition from Rhombohedral Graphite to Diamond," Phys. Rev. B **34**, 1191 (1986); LBL-21151.†
11. M.S. Hybertsen and S.G. Louie, "Spin-Orbit Splitting in Semiconductors and Insulators from the *ab initio* Pseudopotential," Phys. Rev. B **34**, 2920 (1986); LBL-21471.†
12. M.S. Hybertsen and S.G. Louie, "Electron Correlation in Semiconductors and Insulators: Band Gaps and Quasiparticle Energies," Phys. Rev. B **34**, 5390 (1986).§

13. J.R. Chelikowsky, C.T. Chan, and S.G. Louie, "Theoretical Study of the Electronic, Structural, and Cohesive Properties of Ruthenium," Phys. Rev. B **34**, 6656 (1986); LBL-21699.
14. D. Tomanek, C.T. Chan, and S.G. Louie, "*Ab Initio* Calculation of Coverage-Dependent Adsorption Properties of H on Pd(001)," Phys. Rev. Lett. **57**, 2594 (1986); LBL-21777.‡

Other Publications

15. S.B. Zhang, M.L. Cohen, and S.G. Louie, "Reconstruction and Electronic Properties of the AlGaAs(110) Interface," Bull. A.P.S. **31**, 247 (1986).§
16. S. Fahy, S.G. Louie, and M.L. Cohen, "Theoretical Study of the Graphite-Diamond Transition," Bull. A.P.S. **31**, 301 (1986).†
17. C.T. Chan, S.G. Louie, D. Vanderbilt, and J.R. Chelikowsky, "Application of a Fully Self-Consistent Pseudopotential LCAO Method to the Bulk and Surface Structural Properties of Transition Metals," Bull. A.P.S. **31**, 481 (1986).
18. M.Y. Chou, M.L. Cohen, and S.G. Louie, "Theoretical Study of Compton Profiles of Graphite and LiC_6," Bull. A.P.S. **31**, 643 (1986).†
19. M.S. Hybertsen and S.G. Louie, "Quasiparticle Energies and Band Gaps in Semiconductors and Insulators," Bull. A.P.S. **31**, 665 (1986).§
20. S.G. Louie and M.L. Cohen, "Quantum Mechanical Calculations of Structural Properties of Materials," in *Extended Abstracts of the 14th General Meeting of the International Minerological Association*, 1986, p. 159.†

LBL Reports

21. S.G. Louie, "Calculating and Predicting the Properties of Materials," in *Proc. Workshop on Scientific Applications and Algorithm Design for High Speed Computing*, Urbana, IL, 1986 (in press); LBL-21470.†
22. C.T. Chan, S.G. Louie, and J.C. Phillips, "Potential Fluctuations and Density of Gap States in Amorphous Semiconductors," Phys. Rev. B (in press); LBL-21868.†
23. D. Tomanek, S.G. Louie, H.J. Mamin, D.W. Abraham, R.E. Thomson, E. Ganz, and J. Clarke, "Theory and Observation of Highly Asymmetric Atomic Structure in Scanning Tunneling Microscopy Images of Graphite," submitted to Phys. Rev. Lett.; LBL-22338.‡
24. S. Fahy, K.J. Chang, S.G. Louie, and M.L. Cohen, "Pressure Coefficients of Band Gaps of Diamond," submitted to Phys. Rev.; LBL-22307.†

Invited Talks

25. S.G. Louie, "Calculating and Predicting the Properties of Materials," Workshop on Scientific Applications and Algorithm Design for High Speed Computing, University of Illinois at Urbana-Champaign, April 8, 1986.
26. S.G. Louie (with M.L. Cohen), "Quantum Mechanical Calculations of Structural Properties of Materials," 14th General Meeting of the International Minerological Association, Stanford, CA, July 18, 1986.
27. S.G. Louie, "Quasiparticle Energies in Semiconductors and Insulators," 18th International Conference on the Physics of Semiconductors, Stockholm, Sweden, Aug. 12, 1986.
28. D. Tomanek, "*Ab Initio* Calculation for Chemisorption Systems," Surface Science and Catalysis Seminar, LBL, Berkeley, CA, Sept. 25, 1986.
29. S.G. Louie, panelist, "Beyond Density Functional Theory," International School on Electronic Band Structure Calculations and Its Applications, Indian Institute of Technology, Kanpur, India, Oct. 24, 1986.
30. S.G. Louie, "Theory of Quasiparticle Energies and Excitation Spectra of Semiconductors and Insulators," International School on Electronic Band Structure Calculations and Its Applications, Indian Institute of Technology, Kanpur, India, Oct. 27–29, 1986.
31. S.G. Louie, "Optical Properties, Band Gaps, and Quasiparticle Energies in Solids," Atoms, Molecules, and Condensed Matter Seminar, Harvard University, Cambridge, MA, Nov. 21, 1986.

---

†Supported in part by NSF Grant No. DMR8319024.

‡Supported through the Center for Advanced Materials Division by the Director, Office of Energy Research, Office of Basic Energy Sciences, Materials Sciences Division of the U.S.Department of Energy under Contract No. DE-AC03-76SF00098.

§Supported by the National Science Foundation.

MATERIALS CHEMISTRY

CHEMICAL STRUCTURE

Low-Temperature Properties of Materials*

Norman E. Phillips, Investigator

INTRODUCTION

The major objective of this program is to obtain information that contributes to an understanding of the behavior of materials by the measurement of their low-temperature properties, particularly specific heats, C. There are numerous special cases in which specific-heat data provide either a test of theoretical models or values of important parameters that could not otherwise be obtained. Much of the work is in the region below 1 K, where the temperature scale is not well established. Because accurate temperature determinations are important for specific-heat measurements, research is also conducted on methods of temperature measurement. In the year covered by this report, most of the effort continued to be concentrated on heavy-fermion compounds, but in the last few weeks of the year measurements were undertaken on the newly discovered high-critical-temperature superconducting oxides. Measurements on several samples of UBe_{13} have shown that the linear term in the superconducting-state specific heat, C_s, is not an intrinsic property of the material and is probably associated with parts of the sample that are not superconducting; and a small, previously unrecognized feature in C_s that may be related to the "second transition" in $(U,Th)Be_{13}$ has been observed. The pressure and field dependences of C have been shown to be strikingly similar for $CeCu_6$, suggesting similar effects on the interactions. The interplay between heavy-fermion behavior, antiferromagnetism, and spin-glass ordering in $(Ce,Gd)Al_3$ has been mapped out.

*This work was supported by the Director, Office of Energy Research, Office of Basic Energy Sciences, Materials Sciences Division of the U.S. Department of Energy under Contract No. DE-AC03-76SF00098.

1. Low-Temperature Specific Heat of UBe_{13} (Publication 12)

R.A. Fisher, S.E. Lacy, C. Marcenat, J.A. Olsen, N.E. Phillips, Z. Fisk,† A.L. Giorgi,† J.L. Smith,† and G.R. Stewart† ‡

Measurements of C_s of UBe_{13} have been extended to near 0.1 K for four samples of different quality (as determined by the sharpness of the superconducting transition) (see Figure 1-1). Linear terms in C_s occur only for the poorest samples, clearly suggesting that they are not intrinsic properties of UBe_{13} but are associated with parts of the sample that do not become superconducting. This has important implications for C_s of heavy-fermion superconductors more generally because linear terms in C_s for UPt_3 and $CeCu_2Si_2$ have been interpreted as fundamental properties characteristic of the superconducting state. For UBe_{13}, the major contribution to C_s is a T^3 term, as has been reported previously, but in the best samples there is a small but significant additional feature near 0.5 K that must reflect some previously unrecognized feature of the superconducting

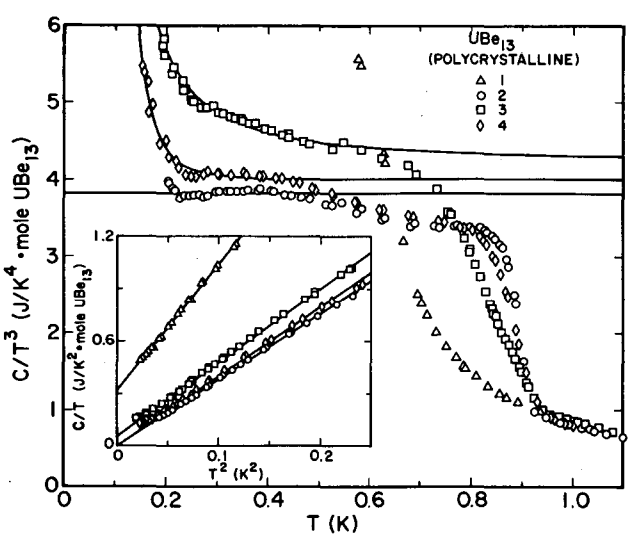

Figure 1-1. Low-temperature behavior of C for UBe_{13}. The linear terms (the intercepts on the C/T axis of the inset) are greater for samples with broader transitions (the drop in C/T^3 near 0.9 K). (XBL 8611-4564)

state, possibly related to the second transition that has been observed in $(U,Th)Be_{13}$ and that may be an indication of triplet spin-pairing superconductivity.

†Los Alamos National Laboratory, Los Alamos, NM 87545.

‡Present address: Department of Physics, University of Florida, Gainesville, FL 32611.

2. Thermodynamic and Transport Properties, and Pressure Dependence of the Specific Heat of Heavy-Fermion Compounds (Publications 9 and 11)

A. Amato,† D. Jaccard,† J. Flouquet,‡ F. Lapierre,‡ J.L. Tholence,‡ N.E. Phillips, R.A. Fisher, S.E. Lacy, C. Marcenat, J.A. Olsen, Z. Fisk,§ A.L. Giorgi,§ J.L. Smith,§ and G.R. Stewart§‖

$CeCu_6$ is in many ways similar to $CeAl_3$ but was shown earlier not to display the maximum in C/T that has been associated with the development of coherence in a Kondo lattice. The measurements have now been extended to nonzero pressures and magnetic fields (see Figures 2-1 and 2-2). In both cases, the effects are dramatic and similar to those in $CeAl_3$, suggesting that the interplay between intersite

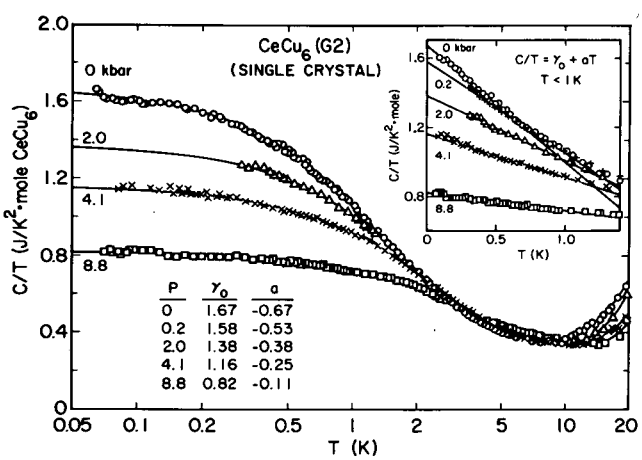

Figure 2-1. Pressure dependence of C/T for $CeCu_6$. (XBL 8612-4876)

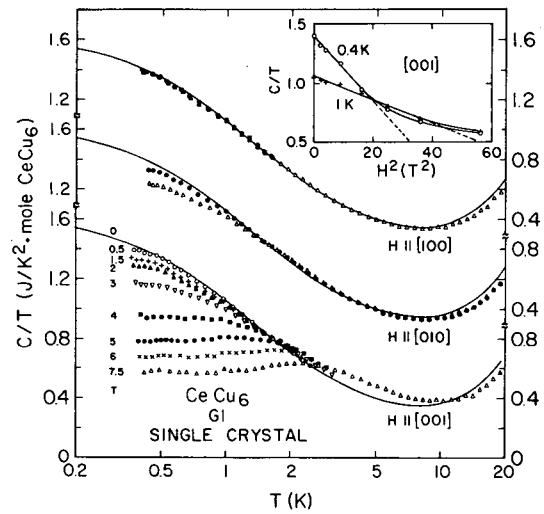

Figure 2-2. Magnetic-field dependence of C/T for single-crystal $CeCu_6$. (XBL 868-3094)

and intrasite interactions is similar in the two materials in spite of the difference with respect to a maximum in C/T.

†Physics Department, University of Geneva, Switzerland.

‡CRTBT-CNRS, Grenoble, France.

§Los Alamos National Laboratory, Los Alamos, NM 87545.

‖Present address: Department of Physics, University of Florida, Gainesville, FL 32611.

3. Anomalous Percolation-Threshold Behavior in the Spin-Glass-Like, Heavy-Fermion System $(Ce,Gd)Al_3$ (Publication 10)

A.S. Edelstein,† R.L. Holtz,† D.J. Gillespie,† M. Rubinstein,† J. Tyson,† R.A. Fisher, and N.E. Phillips

Measurements have now been extended to six samples of $(Ce,Gd)Al_3$ covering the full range of compositions from $CeAl_3$ to $GdAl_3$. At low Gd concentrations, the system retains its heavy-fermion properties, with spin-glass ordering occurring at remark-

ably high temperatures—well above those of the magnetic ordering in any of the pure rare-earth trialuminides that have localized magnetic moments (see Figure 3-1). This enhancement of the interaction that leads to magnetic ordering is a new feature of the heavy-fermion state. There is also an interesting and novel interplay between antiferromagnetism and spin-glass behavior.

†Naval Research Laboratory, Washington, D.C. 20375.

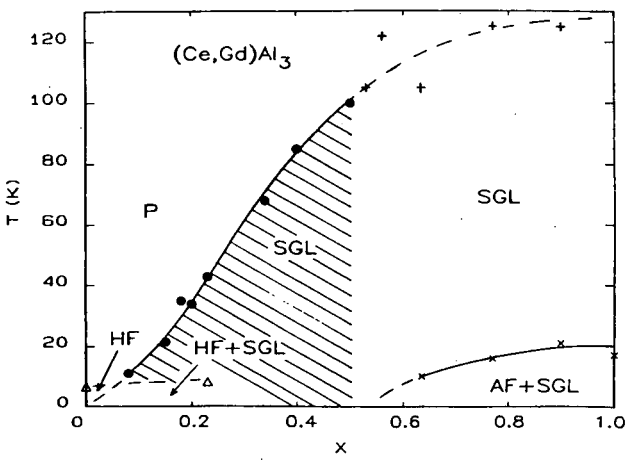

Figure 3-1. Tentative phase diagram for $(Ce,Gd)Al_3$. The symbols AF, HF, P, and SGL represent the antiferromagnetic, heavy-fermion, paramagnetic, and spin-glass-like phases, respectively. (XBL 877-3202)

4. Work in Progress

$(U,Th)Be_{13}$ is unique among known heavy-fermion superconductors in showing a second transition, which has been compared with the second transition in ^3He and possible consequences of triplet spin pairing. Preliminary measurements have shown that both transitions are suppressed (above 0.1 K) at a pressure of 8 kbar.

The heavy-fermion compound $U_{1-x}Th_xBe_{13}$ has attracted a great deal of attention because, for $0 < x < 4$, there is a complicated dependence of T_c on x, and a region of x in which there are two successive transitions that occur with decreasing temperature, as might be expected for a triplet-pairing superconductor (and as observed in ^3He). However, the real nature of the second transition is still an open question. Preliminary specific-heat measurements, on a sample with relatively broad transitions and a linear term in C_s have shown that both transitions are sharply depressed by an applied pressure of 8 kbar. The measurements will be extended to intermediate pressures to follow the course of the transitions as a function of pressure, and, later, to new samples with sharper transitions that are currently being prepared at Los Alamos National Laboratory (LANL). The results will give insight into the nature of the second transition that cannot be obtained by other measurements.

A new sample of UBe_{13} with a relatively sharp transition temperature has been prepared at LANL. Measurements of C_s and the normal-state specific heat C_n have already been made at zero pressure. The measurements will be extended to high pressure to investigate the pressure dependence of the interesting structure in the temperature dependences of C_n and C_s at zero pressure (a continued increase in C_n/T with decreasing temperature, and a change in the coefficient of the T^3 term in C_s). The results will give information about the interactions between the heavy fermions in the normal state and, possibly, about the nature of the superconducting state.

The previously published data on C(P) of $CeAl_3$ left questions about its behavior at very low but nonzero pressures that could not be addressed with the apparatus in use at the time. A new pressure cell that uses He as a pressure-transmitting medium is nearly complete and will be used to measure C(P) at $P < 0.5$. The extreme pressure dependence that must occur in this pressure region in the vicinity of the maximum in C/T will be of considerable interest in connection with the nature of the interactions between the heavy fermions (coherence) that are believed to dominate the low-temperature specific heat of this material.

BaLaCuO has recently been reported as exhibiting superconductivity at a record-high temperature — depending somewhat on the sample, but in the vicinity of 30 K. If this is a bulk transition, it constitutes a dramatic breakthrough in the quest for higher T_c. In a collaboration with A.M. Stacy, C will be measured to answer definitively the question of whether it is a bulk transition, and to measure the normal-state parameters that are fundamental in determining T_c.

Interesting magnetic properties in several rare-earth phosphides have been discovered by A.M. Stacy and colleagues. Some of them may also be heavy-fermion compounds or at least intermediate-valence compounds. Measurements of C will be made on some of these materials to increase our understanding of them, in particular to determine the density of electronic states and (from the hyperfine field) the valence.

1986 PUBLICATIONS AND REPORTS

Refereed Journals

1. G.E. Brodale, R.A. Fisher, N.E. Phillips, C.M. Lisse, and A.S. Edelstein, "Specific Heat of $CeAl_3$ Below 20 K in Fields to 8 T: Effect of $CeAl_2$ and/or Ce_3Al_{11} Phases," J. Magn. Magn. Mater. **54–57**, 416 (1986); LBL-20218.
2. G.E. Brodale, R.A. Fisher, N.E. Phillips, J. Flouquet, and C. Marcenat, "Pressure Dependence of the Specific Heat of $CeAl_3$," J. Magn. Magn. Mater. **54–57**, 416 (1986); LBL-20019.
3. G.E. Brodale, R.A. Fisher, N.E. Phillips, and K. Matho, "Approach to Magnetic Saturation in *Cu*Mn and *Ag*Mn," J. Magn. Magn. Mater. **54–57**, 194 (1986); LBL-20220.
4. G.E. Brodale, R.A. Fisher, N.E. Phillips, G.R. Stewart, and A.L. Giorgi, "Pressure Dependence of Spin-Fluctuation Effects in the Specific Heat of Heavy-Fermion Superconductor UPt_3," Phys. Rev. Lett. **57**, 234 (1986); LBL-21787.
5. J.A. Olsen, R.A. Fisher, N.E. Phillips, G.R. Stewart, and A.L. Giorgi, "Specific Heat of Heavy Fermion Superconductors Under Pressure," Second Workshop on Actinides Under Pressure, Karlsruhe, Federal Republic of Germany, June 2–3, 1986; Physica **144B**, 54 (1986); LBL-21788
6. A.S. Edelstein, R.L. Holtz, D.J. Gillespie, R.A. Fisher, and N.E. Phillips, "Heavy-Fermion, Kondo, Spin Glass-Like and Antiferromagnetic Behavior in $(Ce,Gd)Al_3$," International Conference on Anomalous Rare Earths and Actinides, Grenoble, France, July 7–11, 1986; J. Magn. Magn. Mater. **63–64**, 335 (1987); LBL-21789.
7. N.E. Phillips, R.A. Fisher, J. Flouquet, A.L. Giorgi, J.A. Olsen, and G.R. Stewart, "Pressure Dependences of the Specific Heats of UPt_3, UBe_{13}, and $CeAl_3$," International Conference on Anomalous Rare Earths and Actinides, Grenoble, France, July 7–11, 1986; J. Magn. Magn. Mater. **63–64**, 332 (1987); LBL-21790.

LBL Reports

8. A.S. Edelstein, R.A. Fisher, and N.E. Phillips, "The Temperature Dependence of the Specific Heat and Entropy of $CeAl_3$," Conference on Magnetism and Magnetic Materials, Baltimore, MD, Nov. 17–20, 1986; J. Appl. Phys. (in press); LBL-22444.
9. A. Amato, D. Jaccard, J. Flouquet, L. Lapierre, J.L. Tholence, R.A. Fisher, S.E. Lacy, J.A. Olsen, and N.E. Phillips, "Thermodynamic and Transport Properties of $CeCu_6$," submitted to J. Low Temp. Phys.; LBL-22942.
10. A.S. Edelstein, R.L. Holtz, D.J. Gillespie, M. Rubinstein, J. Tyson, R.A. Fisher, and N.E. Phillips, "Anomalous Percolation-Threshold Behavior in the Spin-Glass-Like, Heavy-Fermion System $(Ce,Gd)Al_3$," submitted to Phys. Rev. Lett.; LBL-23101.
11. N.E. Phillips, R.A. Fisher, S.E. Lacy, C. Marcenat, J.A. Olsen, J. Flouquet, A. Amato, D. Jaccard, Z. Fisk, A.L. Giorgi, J.L. Smith, and G.R. Stewart, "Pressure Dependence of the Specific Heat of Heavy-Fermion Compounds," 5th Int. Conf. on Valence Fluctuations, Bangalore, India, Jan. 5–9, 1987, to be published in the Proceedings; LBL-22813.
12. R.A. Fisher, S.E. Lacy, C. Marcenat, J.A. Olsen, Z. Fisk, N.E. Phillips, A.L. Giorgi, J.L. Smith, and G.R. Stewart, "Low-Temperature Specific Heat of UBe_{13}," 5th Int. Conf. on Valence Fluctuations, Bangalore, India, Jan. 5–9, 1987, to be published in the Proceedings; LBL-22814.

Electrochemical Processes*

Charles W. Tobias, Investigator

INTRODUCTION

This program is designed to advance the scientific foundations of electrochemical engineering and to broaden the range of useful applications of electrochemical transformations. Electrolysis processes have inherent advantages over thermochemical methods with respect to material yield and energy efficiency. However, in spite of their long history of economically significant applications, cell processes have not achieved their potential with respect to performance and range of applications in chemical synthesis, nor in energy conversion or storage. A major reason for this condition is the complex nature of transport phenomena in ionic media, as they are coupled to charge-transfer processes at the electrode surface.

- A model is established for the precise control of composition in the electrodeposition, under pulsed-current conditions, of binary and ternary allows.
- In projects jointly directed with Dr. R.H. Muller, novel methods are explored for the reduction of mass-transfer resistance in high-rate applications, including in electroforming of metals, and in electroorganic synthesis. The effects of suspended inert solid particles in flowing electrolytes, on transport rates, and on current distribution are measured and correlated.

Applied research on the "Surface Morphology of Metals in Electrodeposition," on "Engineering Analysis of Electrolytic Gas Evolution," and on "Metal Couples in Non-Aqueous Electrolytes" is supported by the Assistant Secretary of Conservation and Renewable Energy, Office of Energy Storage and Distribution of the U.S. Department of Energy under Contract No. DE-AC03-76SF00098.

*This work was supported by the Director, Office of Energy Research, Office of Basic Energy Sciences, Materials Sciences Division of the U.S. Department of Energy under Contract No. DE-AC03-76SF00098.

1. The Periodic, Electrochemical Codeposition of Cadmium and Tellurium (Publication 4)

M.W. Verbrugge and C.W. Tobias

A mathematical model is presented for the codeposition of cadmium and tellurium onto a rotating-disk electrode. The treatment incorporates the equation of convective diffusion for liquid-phase mass transport, Butler-Volmer expressions for charge-transfer reactions, and a thermodynamic model for individual component activities in the solid state. Because of the formation of CdTe, a compound that has a large negative free energy of formation, the cadmium-deposition reaction occurs at potentials substantially positive to its standard electrode potential ($V^o = -0.40$ V). This reaction, along with the deposition of tellurium ($V^o = +0.55$ V), produces an electrodeposit that contains cadmium, tellurium, and cadmium telluride. The model can be used to calculate transient current-potential relationships, ionic concentration profiles, and deposit compositions. Transport and kinetic parameters for cadmium and tellurium deposition are reported; a multidimensional optimization routine is used to evaluate physicochemical parameters from experimental data for the codeposition process. The model shows reasonable agreement with results obtained from the periodic co-electrodeposition of Cd and Te onto a rotating-disk electrode. A more sophisticated model would incorporate double-layer adsorption, the capacitance of the double layer (for processes in which the pulse-current frequency is comparable to, or larger than, the inverse of the characteristic time for the double-layer charging processes), and a more general treatment of the electrodeposit, including solid-state kinetic processes.

2. The Transient and Periodic Illumination of a Semiconductor-Electrolyte Interface (Publications 2 and 6)

M.W. Verbrugge and C.W. Tobias

The analysis of the response of a photoelectrochemical system to a variable light source offers a convenient means for the characterization of a semiconductor-electrolyte interface. Analytic solutions have been obtained for the minority-carrier concentration at a semiconductor surface during pulse, step, sinusoidal, and periodic square-pulse illumination of a semiconductor-electrolyte interface.

In addition, the analytic solutions can be used to describe accurately the low-level-injection behavior of wide-band-gap semiconductors commonly used in photoelectrolysis cells and other photoelectrochemical systems. For these systems, since the periodic illumination of a photoelectrochemical cell results in a periodic photoresponse, the analytic solutions are useful for the evaluation of system physicochemical parameters. The periodic-illumination technique is analogous to the traditional cyclic chronopotentiometry and chronoamperometry electrochemical techniques. In particular, the cycle period of the varying light source can be adjusted to match the time constants of the photoelectrochemical cell processes, which makes this technique a valuable analytical tool for the investigation of semiconductor-electrolyte interfaces.

Steady-state and variable-frequency illumination is employed to examine the photovoltaic properties of electrodepositing Cd-Te thin films. The effect of illumination on the composition of Cd-Te deposits formed with a triangular-wave current source is demonstrated. It is shown by means of optical and electron microscopy that a rectangular-pulse current source significantly influences the surface morphology of Cd and Cd-Te electrodeposits. The photoactivity of Cd-Te deposits is found to depend on the pulse-current frequency.

3. Work in Progress

Mass-transfer enhancement by concentrated suspensions of inert solids is investigated at a rotating-disk electrode. The effects of particle size and shape, concentration, and rate of rotation are evaluated experimentally, and a theoretical model is advanced to explain the mechanism by which unexpectedly high boundary-layer thinning is achieved.

The feasibility of electroforming at high rates (> 5 A/cm^2) is evaluated for the deposition of copper on a cylindrical electrode, rotating in the center of a baffled cylindrical cell. A theoretical model is advanced to explain the mechanism underlying the development of roughness in electroforming without inhibitors.

1986 PUBLICATIONS AND REPORTS

Refereed Journals

1. C.A. Coughenowr, B.A. Dissaux, R.H. Muller, and C.W. Tobias, "Electrochemical Machining of Refractory Material," J. Appl. Electrochem. **16**, 345 (1986); LBL-18365 Rev.

Other Publications

2. M.W. Verbrugge and C.W. Tobias, "The Transient and Periodic Illumination of a Semiconductor-Electrolyte Interface," LBL-21795 (also, Extended Abstracts of the Electrochemical Society, Vol. 86-2, no. 128, Oct. 1986). Full paper published in *Proc. Symp. Electrochemical and Thermal Modeling of Battery Fuel Cell and Photoenergy Conversion Systems*, Vol. 86-12, Oct. 1986.
3. D.S. Fischl, R.H. Muller, and C.W. Tobias, "The Effect of Flow Obstacles on Mass Transfer to Planar Electrodes," in *Proc. Symp. Engineering of Industrial Electrolytic Processes*, U. Landau, R. White, and R Varjian, eds., Vol. 86-8, The Electrochemical Society, 1986; LBL-16422.

LBL Reports

4. M.W. Verbrugge and C.W. Tobias, "The Periodic, Electrochemical Codeposition of Cadmium and Tellurium," accepted by AIChE J.; LBL-21013.
5. R.A. Atanasoski, H.H. Law, R.E. McIntosh, and C.W. Tobias, "Electrochemical Analysis of Trace Amounts of Water in Propylene Carbonate Electrolytes," accepted by Electrochimica Acta; LBL-22467.
6. M.W. Verbrugge and C.W. Tobias, "Some Experimental Aspects of the Codeposition of Cadmium and Tellurium," submitted to J. Electrochem Soc.; LBL-22519.

HIGH-TEMPERATURE AND SURFACE CHEMISTRY

High-Temperature Thermodynamics*

Leo Brewer, Investigator

INTRODUCTION

The understanding of high-temperature chemistry is not only important for processes carried out at high temperatures, such as those of fusion and fission reactors and fossil-fuel power generators, but it is also important for the preparation and fabrication of ceramics, metals, semiconductors, and many other materials. The understanding of high-temperature behavior is complicated by the occurrence of unusual species and phases that are often unstable at conventional temperatures. It is difficult to carry out measurements to obtain the data needed for the design of high-temperature systems. Thus it is most important to develop broad predictive models that provide reliable predictions of high-temperature behavior. The experiments that we have been carrying out are aimed at the testing or development of such predictive models. Previous research in this program has led to the development of a variety of successful models of predictive capability for the behavior of gases, refractory containment materials, and many metallic systems. As an example it has been possible to calculate binary molybdenum phase diagrams with practical engineering accuracy even for systems for which no measurements have ever been reported. At the present time the main thrust of our research is aimed at providing quantitative predictive models for the strongly interacting transition-metal alloys exhibiting generalized Lewis Acid-Base behavior. A variety of experimental methods are being used to characterize the thermodynamics of these systems.

*This work was supported by the Director, Office of Energy Research, Office of Basic Energy Sciences, Materials Sciences Division of the U.S. Department of Energy under Contract No. DE-AC03-76SF00098.

1. The Unusual Bonding of Actinide Systems (Publication 4)

L. Brewer

The actinide elements have unusual bonding capabilities because of the availability of 5*f*, 5*d*, 7*p*, and 7*s* orbitals. Spectroscopic data along with predictive models are complete enough to assign promotion energies for the various electronic configurations and the bonding contribution of the various types of electrons. The availability of a number of electronic configurations of comparable stability makes it possible for actinide metals to form complex crystal structures in which atoms in different lattice positions have different electronic configurations and different sizes. Bonding models provide predictions of thermodynamic properties that can be used to calculate phase diagrams of many systems with reasonable accuracy. The major challenge is provided by mixtures of actinide metals with platinum-group metals because of very strong generalized Lewis Acid-Base interactions that are difficult to characterize with sufficient accuracy. The behavior of a wide range of actinide systems to being reviewed.

2. The Thermodynamic Behavior of the Nb-Pd and Nb-Rh Systems (Publication 5)

L. Brewer and M.J. Cima

Phase equilibrium studies with pairs of oxides NbO, NbO_2, $NbO_{2.42}$, $NbO_{2.47}$, and Nb_2O_5 with Nb-Pd alloys and Nb-Rh alloys have allowed us to characterize the niobium activity for several compositions of the Nb-Pd and Nb-Rh systems. The new results are in good agreement with previously determined carbide and nitride equilibrium measurements. Additional determinations of the niobium activity in Nb-Pd alloys have been carried out using high-temperature solid-electrolyte cells. Excellent agreement has been found by the various methods, which indicates that all substantial systematic errors have been controlled. The cell data provide a titra-

tion curve of niobium activity as a function of palladium composition that indicates that the strong generalized Lewis Acid-Base interaction between Nb and Pd is due primarily to one of the nonbonding pairs of palladium and that the second nonbonding pair is in an orbital that is so contracted that there is only a small amount of overlap with the vacant Nb orbital. For rhodium with a smaller nuclear charge, the *d* orbitals are not as contracted, and the nonbonding electron pair of rhodium bonds better than the most contracted pair of palladium but does not bond as well as the better bonding pair of palladium. These data will allow the development of a crystal field model to allow prediction of the bonding capabilities of the various electron pairs that are nonbonding in the pure platinum-group metals.

3. Work in Progress

The titration data obtained for the Nb-Pd system offers the exciting possibility of developing a bonding model that would provide quantitative characterization of the bonding capability of different *d* orbitals. This would allow quantitative predictions of the degree of interaction for different combinations of transition metals from the left half of the Periodic Table and lanthanides and actinides with platinum-group metals. The test of this model will require additional measurements for mixtures of metals with different combinations of 3*d*, 4*d*, and 5*d* orbitals. Particular emphasis will be placed on alloys of Ti, V, and Nb because of the variety of oxide pairs that can be used to fix the metal activity. The use of cell measurements will allow measurements of several combinations of the elements Ti, Zr, Hf, V, Nb, and Ta with Ru, Rh, Pd, Os, Ir, and Pt. Also vapor-pressure measurements using the King furnace as well as additional ternary diagram evaluations will be useful. The strong interactions of platinum-group metals with transition metals of the third to fifth groups have not been widely recognized. This lack of recognition has caused difficulties in the use of the platinum-group metals. The ability to quantitatively predict the degree of interaction should greatly improve the utilization of these metals.

1986 PUBLICATIONS AND REPORTS

Refereed Journals

1. T.B. Massalski, H. Okamoto, and L. Brewer, "The Au-Mo (Gold-Molybdenum) System," Bull. Alloy Phase Diagrams 7, 449 (1986); LBL-22482.

Other Publications

2. L. Brewer, "Gases (A) Spectroscopy of Interest to High-Temperature Chemistry, and (B) Reactions Between Gases and Condensed Phases," in *Bibliography on the High-Temperature Chemistry and Physics of Materials,* Vol. 30, Part 2, M.B. Hocking and V. Vasantasree, eds., IUPAC Commission on High Temperatures and Refractory Materials, London, 1986; LBL-22493.
3. L. Brewer and R.H. Lamoreaux, in *Binary Alloy Phase Diagrams,* T.B. Massalski, Ed., American Society for Metals, Metals Park, OH, 1986.

LBL Reports

4. L. Brewer, "The Unusual Bonding of Actinide Systems," J. Less-Common Metals (in press); LBL-22481.
5. M.J. Cima (Ph.D. Thesis), "Thermochemical Properties of Group IVB and VB Transition Metal Alloys with Platinum Group Metals: Acid-Base Stabilization," LBL-21951.

Invited Talks

6. L. Brewer, "The Generalized Lewis-Acid-Base Theory: Surprising Recent Developments," Louis Jacob Bircher Lecture in Chemistry, Vanderbilt University, Nashville, TN, Feb. 28, 1986.
7. L. Brewer, "The Problems of Attaining Equilibrium with Refractory Materials," Metallurgical Society, New Orleans, LA, March 4, 1986.
8. L. Brewer and M. Cima, "Generalized Lewis Acid-Base Titration of Niobium Metal by Palladium Metal," San Francisco Bay Area High Temperature Symposium, Palo Alto, CA, April 17, 1986.
9. L. Brewer, "Lewis Acid-Base Interaction of Actinides with Platinum Group Metals," R.D. Baker Memorial Symposium, Los Alamos National Laboratory, Los Alamos, NM, May 12, 1986.
10. L. Brewer, "Generalized G.N. Lewis Acid-Base Interactions," Polaroid Corporation, Cambridge, MA, July 25, 1986.
11. L. Brewer, "Theory of Alloying," General Electric Corporation, Schenectady, NY, Aug. 18, 1986.
12. L. Brewer, "The Critical Dependence of High Temperature Chemistry upon Calorimetry," plenary lecture, Calorimetry Conference, Somerset, NJ. Aug. 20, 1986.
13. L. Brewer, "The Unusual Bonding of Actinide Systems," American Chemical Society, Anaheim, CA, Sept. 10, 1986.

Chemistry and Materials Problems in Energy Production Technologies*

Donald R. Olander, Investigator

INTRODUCTION

This experimental research program has two principal objectives. The first is concerned with the chemical and physical behavior of materials of nuclear reactor systems, both fission and fusion. The experiments are designed to explore the fundamental processes that underlie the performance of these materials in their service environments, which are characterized by combinations of high temperature, intense radiation fields, and reactive gases or liquids.

The second direction of the project is the study of gas-solid chemical reactions such as corrosion or etching by the method of molecular beams coupled with mass spectrometry. The objective of these studies is to understand the kinetics and mechanisms of such reactions in clean, well-characterized systems.

1. Numerical Modeling of Heat and Mass Transport During Rapid Heating and Vaporization of Binary Solids by Absorbing Radiation—Application to UO_2 (Publication 1)

C.H. Tsai and D.R. Olander

Pulsed surface irradiation of an absorbing material induces a temperature transient that leads to melting and vaporization. If the target is a two-component solid that evaporates incongruently, the near-surface composition is also perturbed. A mathematical model and numerical-solution scheme have been developed to simulate the heat and mass transport processes that result from rapid energy deposition on the surface of a binary solid. The response surface method was used to determine the loss of precision in such a computation due to uncertainties in the materials properties at high temperatures.

Application of the method to incongruently vaporizing UO_2 irradiated by a pulsed laser demonstrated the extent of oxygen depletion of the surface and revealed the sensitivity of the computed temperatures and vaporization rates arising from lack of knowledge of the diffusivity of oxygen in liquid UO_2.

2. Reactions of Chlorine with Liquid Metals. 3. Bismuth (Publication 2)

M. Balooch, D.R. Olander, and W.J. Siekhaus

The reaction of molecular chlorine with solid and liquid bismuth was studied by modulated-molecular-beam–mass-spectrometric methods over the temperature range 400–800 K and equivalent chlorine pressures of 5×10^{-6} to 2×10^{-4} Torr. The sole reaction product with solid Bi(0001) was $BiCl_3$. This species disappeared at the melting point. The molecular-beam data collected on the trichloride product exhibited nonlinearity and evidence of both branched and series processes in the mechanism. These results, in conjunction with data obtained in a prior investigation of the system by thermal-desorption spectroscopy, permitted development of a model of the reaction on the surface of the solid. With liquid bismuth, only BiCl was detected as reaction product. Its reaction probability increased with temperature, most likely because of a corresponding increase in the chlorine-sticking probability. The 45° phase lag exhibited by this species indicated that the kinetics were dominated by solution and diffusion of chlorine in the bulk liquid bismuth.

3. Oxidation of UO_2 by High-Pressure Steam (Publication 3)

D.R. Olander

Thermodynamically, the oxygen potential of pure steam increases as the pressure increases. As a result, high-pressure steam can produce more highly oxidized urania than can steam at atmospheric pressure. Oxygen-to-uranium ratios as high as 2.60 can theoretically be attained in steam at 150 atm and temperatures near 1600 K. Oxidation to this extent can render the fuel nearly as important a source of hydrogen as the cladding in severe fuel-damage accidents. Fuel oxidation by steam, however, is endothermic and provides a heat sink rather than a heat source.

*This work was supported by the Director, Office of Energy Research, Office of Basic Energy Sciences, Materials Sciences Division of the U.S. Department of Energy under Contract No. DE-AC03-76SF00098.

4. Oxygen Mass-Transport Effects During Hydrogen Reduction of UO_2 (Publication 4)

D.R. Olander and D.F. Dooley

Reduction of UO_{2+x} was studied in a molecular-beam system, in which a collisionless flux of atomic hydrogen strikes a portion of the surface of the solid and the reaction-product water is detected by an *in situ* mass spectrometer. The experiment revealed kinetic limitations due to both surface chemical reaction and to transport processes, the latter including surface diffusion of oxygen as well as bulk diffusion. A quantitative model of the reduction process showed that the surface reaction rate was linear in the H-atom beam intensity and in the excess O/U ratio above a minimum value for detectable reaction. The bulk diffusion coefficient of oxygen determined from the data at 585°C agreed well with the measurement of Lay.[1] The surface diffusion coefficient at the same temperature was found to be $\sim 1\ cm^2/s$, suggesting ideal two-dimensional gas behavior of oxygen on the urania surface.

1. K.W. Lay, J. Am. Chem. Soc. **53**, 369 (1970).

5. Reactions of Chlorine with Liquid Metals. 4. Tin (Publication 5)

M. Balooch, D.R. Olander, and W.J. Siekhaus

The reaction of molecular chlorine with solid and liquid tin was studied by modulated-molecular-beam mass spectrometry and Auger electron spectrometry. The temperature range was 350–700 K, and equivalent chlorine pressures between 2×10^{-5} and 5×10^{-4} Torr were used. At constant pressure, the production rate of the sole reaction product ($SnCl_2$) increased with temperature with no sign of a discontinuity at the melting point. The reaction was nonlinear with respect to chlorine equivalent pressure. The model developed for the lead-chlorine system was applicable to the tin-chlorine system. However, solution diffusion of chlorine in the liquid metal did not appear to be significant for the tin reaction.

6. Combined Grain-Boundary and Lattice Diffusion in Fine-Grained Ceramics (Publication 6)

D.R. Olander

A mathematical model of species transport in a fine-grained polycrystalline body is developed and applied to postirradiation anneal experiments of volatile fission-product release from UO_2 and to oxygen self-diffusion in the same material. The model treats the simultaneous transport paths of (1) direct volume diffusion (the only mechanism available in single crystals) and (2) lattice diffusion from the grain interior to the grain boundaries, followed by migration in the latter. The two physical properties controlling the release process are (1) the diffusion coefficient in the lattice and (2) the product of the grain-boundary diffusivity and the solute segregation coefficient between the lattice and the grain boundaries. To determine these properties, either two independent-release tests with specimens of different grain size or a measurement of the concentration distribution of the diffusing species in the specimen after the anneal is needed.

7. Work in Progress

The high-temperature oxidation of Zircaloy by steam-hydrogen mixtures is being investigated by electrobalance methods. Oxygen self-diffusion in the tetragonal modification of zirconia is to be measured.

High-intensity millisecond laser pulses are being used to investigate the rapid high-temperature vaporization of ceramic oxides.

The reactions of atomic hydrogen with UO_2 and with silicon are being investigated in the modulated molecular-beam apparatus.

1986 PUBLICATIONS AND REPORTS

Refereed Journals

1. C.H. Tsai and D.R. Olander, "Numerical Modeling of Heat and Mass Transport During Rapid Heating

and Vaporization of Binary Solids by Absorbing Radiation—Application to UO_2," J. Nucl. Mater. **137**, 279 (1986); LBL-15124.

2. M. Balooch, D.R. Olander, and W.J. Siekhaus, "Reactions of Chlorine with Liquid Metals. 3. Bismuth," J. Phys. Chem. **90**, 1671 (1986); LBL-20029.
3. D.R. Olander, "Oxidation of UO_2 by High Pressure Steam," Nucl. Technol. **74**, 215 (1986); LBL-20531.
4. D.R. Olander and D.F. Dooley, "Oxygen Mass Transport Effects During Hydrogen Reduction of UO_{2+x}," J. Nucl. Mater. **139**, 237 (1986); LBL-20652.
5. M. Balooch, D.R. Olander, and W.J. Siekhaus, "Reactions of Chlorine with Liquid Metals. 4. Tin," J. Phys. Chem. **90**, 4397 (1986); LBL-20849.
6. D.R. Olander, "Combined Grain Boundary and Lattice Diffusion in Fine-Grain Ceramics," Adv. Ceram. **17**, 271 (1986); LBL-19535.

LBL Reports

7. D.R. Olander, "Lattice and Grain Boundary Diffusion in Thorium-Uranium Oxides," LBL-20880.
8. H. Ohashi, D.R. Olander, and S. Yagnik, "The Collimator Efficiency in Laser Vaporization Studies Using Mass Spectrometric Detection," LBL-21513.
9. D.R. Olander, "Ceramics in Fission and Fusion Technology," LBL-21481.
10. C.H. Tsai and D.R. Olander, "The Transition from Free Molecule to Collisional Flow During Vaporization Into Vacuum by the Test-Particle Method," LBL-21404.
11. M. Balooch, D.R. Olander, and W.J. Siekhaus, "Reaction of Water and Oxygen with Liquid Uranium," LBL-22468.

Invited Talks

12. D.R. Olander, "Laser Pulse Vaporization of Refractory Materials," American Institute of Mining Engineers, New Orleans, March 3, 1986.
13. D.R. Olander, "Oxidation of UO_2 in High Pressure Steam," Bay Area Conference on High Temperature Science Technology, Menlo Park, CA, April 17, 1986.
14. D.R. Olander, "The Reaction of Silicon with Atomic Hydrogen by Modulated Molecular Beam Mass Spectrometry," Forty-Sixth Annual Conference on Physical Electronics, Austin, TX, June 16, 1986.
15. D.R. Olander, "Research in Support of the AVLIS Process—The Uranium Water Reaction," Physical Chemistry Department, Centre d'Etudes Nucléaires, Saclay, France, June 19, 1986.
16. D.R. Olander, "Ceramics in Fission and Fusion Technology," World Congress on High-Tech Ceramics, Milan, Italy, June 25, 1986.
17. D.R. Olander, "Molecular Beam Studies of Etching and Decomposition Reactions," Gordon Research Conference on Electronic Materials, Concord, NH, Aug. 1986.
18. D.R. Olander, "Laser Vaporization of Refractory Materials," Bay Area High Temperature Conference, Livermore, CA, Nov. 1986.

Electrochemical Phase Boundaries*

Rolf H. Muller, Investigator

INTRODUCTION

This work concerns the mechanisms of nucleation and growth in the electrocrystallization of metals from aqueous solutions. Factors that affect the micromorphology and microtopography of the resulting metal are investigated. These factors include the action of molecules adsorbed on the metal and the effect of ionic mass transfer and electric field in the solution. Another research direction concerns the study of thin electrolyte films on metal surfaces where surface forces responsible for film formation are investigated.

Research on electrochemical mass-transfer and high-rate electrodeposition and dissolution, conducted jointly with C.W. Tobias, is described under "Electrochemical Processes," C.W. Tobias, Investigator. Another project, concerned with applications in battery technology, "Surface Layers on Battery Materials," supported by the Assistant Secretary for Conservation and Renewable Energy, Office of Energy Storage and Distribution of the U.S. Department of Energy, is reported under "Electrochemical Energy Storage."

1. Electrochemical Machining of Refractory Materials (Publication 1)

C.A. Coughanowr,† B.A. Dissaux, R.H. Muller, and C.W. Tobias

The feasibility of the electrochemical machining (ECM) of pure TiC, ZrC, TiB_2, and ZrB_2 has been established. In addition, the ECM behavior of a cemented TiC/10% Ni composite has been investigated and compared to that of its components, TiC and nickel. ECM was carried out in 2M KNO_3 and in 3M NaCl at applied voltages of 10–31 V and current densities of 15–115 A cm^{-2}. Post-ECM surface studies on the TiC/Ni composite showed preferential dissolution of the TiC phase during machining.

†Present address: University of Florida, Gainsville, FL 32611.

*This work was supported by the Director, Office of Energy Research, Office of Basic Energy Sciences, Materials Sciences Division of the U.S. Department of Energy under Contract No. DE-AC03-76SF00098.

2. Limiting Currents of High-Rate Metal Deposition on a Rotating Cylinder (Publication 4)

D.P. Barkey, R.H. Muller, and C.W. Tobias

Measurement of steady-state limiting currents of metal deposition at high rates has been achieved through the use of fast current sweeps. Current densities of copper deposition of up to 5.0 A/cm^2 were obtained at a rotating-cylinder electrode in a cell with radial baffles. The baffles were introduced to suppress entrainment of air, but they also produced some mass-transfer enhancement. Limiting current densities to smooth cylinders were in agreement with the Reynolds and Schmidt number exponents of the correlation of Eisenberg, Tobias, and Wilke.[1] The Re and Sc numbers were varied from 10^4 to 2×10^5 and from 8×10^2 to 8×10^3, respectively. Limiting current densities to rough surfaces were also measured and correlated. The large number of possible baffle configurations makes the limiting currents measured specific to this system. However, the results provide information on the magnitude and functional dependence of transport enhancement to rotating cylinders in baffled cells.

1. M. Eisenberg, C.W. Tobias, and C.R. Wilke, J. Electrochem. Soc. **101**, 306 (1954).

3. The Long-Term Stability of Aqueous KOH Films on Platinum (Publication 2)

J.R. Gyory and R.H. Muller

Time-invariant liquid films of 0.01 to 1M KOH and $NaClO_4$ have been observed on vertically oriented platinum and gold surfaces 4 cm wide and 10 cm high in a closed isothermal system that prevented the existence of surface-tension gradients caused by local temperature or concentration differences. The instantaneous film thickness at any point on the surface was measured by thin-film interference colors. These films initially thin as would be expected when only viscous and gravitational forces are considered. However, after about 20 hours the thinning slows and eventually stops, and a time-invariant electrolyte film remains on the surface. This time-invariant film has been observed for up to 60 days, when the experiment was terminated. The time-invariant film profile is predicted by a model based on dispersion theory. Long-range van der

Waals interactions between the solid substrate, thin electrolyte film, and saturated vapor phase stabilize the film against further thinning caused by gravity. The magnitude of this interaction is characterized by the Hamaker constant, which can be calculated independently using Lifshitz' general theory of van der Waals interactions. The order of magnitude and sign of the Hamaker constant derived from film-profile measurements for the gold/1M KOH/air system agrees with that calculated from Lifshitz' theory for the gold/water/air system.

4. Structural Changes of Thin Lead Films During Low-Energy Ion Bombardment (Publication 3)

M.T. Armstrong and R.H. Muller

In order to determine composition profiles of an electrodeposited metal layer, the ion-bombardment damage in thin (<100 nm) lead films on copper substrates has been investigated. The results have shown that the assumption of uniform film removal, on which the determination of composition profiles by ion bombardment and Auger spectroscopy is based, did not apply to these films, whether they were produced by vapor or electrochemical deposition. Spectroscopic ellipsometer measurements were interpreted for the early stages of ion bombardment by the removal of a very thin (3 nm) lead oxide layer from the (porous) lead film and for the later stages by the formation of a pitted lead film with exposed copper substrate (see Figure 4-1). The re-interpretation of Auger spectra in terms of a pitted surface agrees quantitatively with the data derived from the ellipsometer measurements and confirms the validity of the optical island-film model used.[1] The formation of pits has also been observed by SEM at a late stage in their growth.

1. R.H. Muller and J.C. Farmer, Surf. Sci. **135**, 521 (1983).

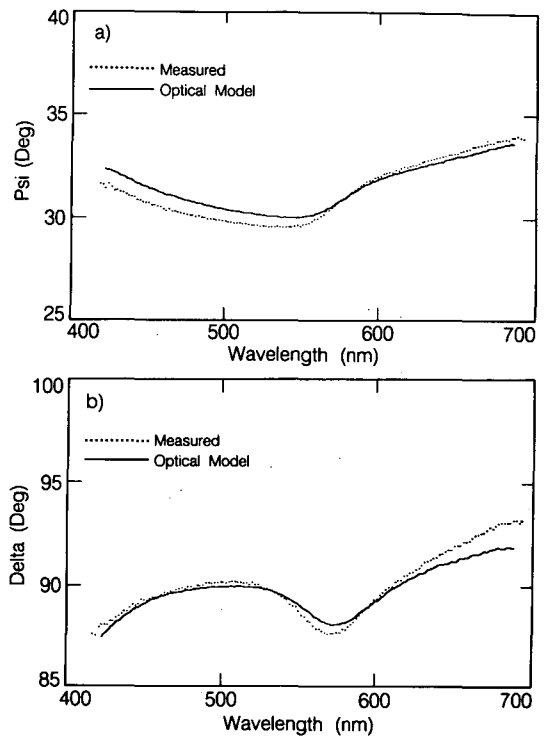

Figure 4-1. Comparison of the measured ellipsometer parameters delta and psi to those calculated for the pitted-film optical model. 0.039 C/cm^2 (369-Å compact) lead deposit after 35 min of ion bombardment. The optical model consists of a 0.74 coverage of lead islands with an underlying 30-Å lead film. Both the islands and continuous film have a porosity of 0.2. The substrate is bulk copper. (a) delta; (b) psi. (XBL 848-8659)

5. The Effect of Flow Obstacles on Mass Transfer to Planar Electrodes (Publication 5)

D.S. Fischl, R.H. Muller, and C.W. Tobias

The effectiveness of mass-transfer enhancement by small obstacles attached to the cathode in an electrochemical flow cell 50.8 cm long and 0.5 cm square in cross section has been investigated. Pressure drop and limiting current for the reduction of ferricyanide were measured in the range of $80 \leqslant \mathrm{Re} \leqslant 3200$. Using obstacles of rectangular cross-section extending 0.0254 to 0.160 cm from the surface, the spacing-to-height ratio ranged from 9 to 170. Flow patterns around obstacles were visualized using suspensions of inert materials and recorded by dark field photography.

Depending on the flow rate, addition of the obstacles can increase mass-transfer rates by as much as five times over those in the unobstructed system. The degree of enhancement increases with decreasing obstacles spacing up to an optimal spacing that is approximately 15 times the obstacle size and corresponds to the largest elongation of the recirculation zone observed downstream from an obstacle.

At $\mathrm{Re} \simeq 100$, the mass-transfer rate is approximately doubled upon addition of the optimal number of obstacles without appreciably affecting the pressure drop. The largest enhancement (5-fold) occurs at the upper laminar flow regime with a 2.7-fold increase in the pressure drop. These comparisons are made at the same flow rate.

In the unobstructed system, improved mass-transfer rates (limiting currents) are achieved by increasing the flow rate to produce turbulent flow. This approach involves large pressure drops and consequently large pumping power requirements. An increase in the limiting current by the addition of obstacles, on the other hand, requires only a very small fraction (2–5%) of the pumping power required to obtain the same limiting current achieved by increasing the flow rate in the unobstructed system. Obstacles therefore produce efficient mixing near the electrode surface and correspondingly high mass-transfer rates without causing large energy dissipation in the bulk fluid.

6. Work in Progress

Copper deposition in the presence of thiourea has been found to result in increasingly bright surfaces as thiourea concentration is increased, indicating the importance of mass transfer for the replacement of reacted adsorbate to the most accessible parts of the surface. The existence of a barrier film for the diffusion of inhibitor is now being investigated. Such a film had been proposed as a leveling mechanism according to which the decrease in the supply of inhibitor to recessed portions of the surface is accentuated. Molecules of inhibitors and their decomposition products at the surface will be identified by Raman spectroscopy to determine residence times and flux densities for use in models of convective diffusion.

Studies of liquid films on metal surfaces are being concluded by a computation of the effect of solute concentration on the Hamaker constant and, thus, the predicted time-independent film profile. Also, a theory of film drainage in which van der Waals interactions are included in the hydrodynamic equations is being developed. As a further test of theory, predicted film profiles will be compared to measurements for materials with dielectric functions widely different from those of the media used so far.

The microtopography of copper surfaces obtained by high-rate electrodeposition on rotating-cylinder electrodes without inhibitor has been found to depend primarily on the ratio of the applied current density to the limiting current density under the same conditions of concentration, rotation rate, and temperature. Closer to the limiting current, a rougher deposit is obtained. To a smaller degree roughness also depends on the absolute current density and the deposit thickness. An automated Fourier analysis of surface profiles has been implemented in order to determine the limit of stability for random surface imperfections and the relation of the critical size of imperfections to predictions based on boundary-layer dimensions (directed jointly with C.W. Tobias).

The use of suspended particles to increase the rate of mass transfer to electrodes is being investigated with a rotating disk. With high particle concentrations (above 30 vol%) limiting currents are increased several-fold by the presence of the particles at high rotation rates. Theoretical models for the enhancement of transport, which take the interaction between particles into account, are being developed (directed jointly with C.W. Tobias).

1986 PUBLICATIONS AND REPORTS

Refereed Journals

1. C.A. Coughanowr, B.A. Dissaux, R.H. Muller, and C.W. Tobias, "Electrochemical Machining of Refractory Materials," J. Appl. Electrochem. **16**, 345 (1986).

LBL Reports

2. J.R. Gyory and R.H. Muller, "The Long-Term Stability of Aqueous KOH Films on Platinum," LBL-22523.
3. M.T. Armstrong and R.H. Muller, "Structural Changes of Thin Lead Films during Low-Energy Ion Bombardment," LBL-22522.
4. D.B. Barkey, R.H. Muller, and C.W. Tobias, "Limiting Currents of High-Rate Metal Deposition on a Rotating Cylinder," LBL-22540.
5. D.S. Fischl, R.H. Muller, and C.W. Tobias, "The Effect of Flow Obstacles on Mass Transfer to Planar Electrodes," in *Proc. Symp. Engineering of Industrial Electrolytic Processes*, U. Landau, R. White, and R. Varjian, eds., Vol. 86-8, The Electrochemical Society, 1986; LBL-16422.

Solid-State and Surface Reactions*

Gabor A. Somorjai, Investigator

INTRODUCTION

This research program is centered on studies of the atomic structure of solid surfaces and adsorbed monolayers and on investigations of the surface science of catalyzed reactions, friction, and wear. Well-characterized crystal surfaces are used at low and high pressures. The macroscopic catalytic and mechanical properties are correlated with the atomic structure, chemical bonding, and composition at the surface and in the near-surface region.

The materials that are the focus of our studies are transition metals and their oxides or sulfides. These include iron, molybdenum, rhenium, vanadium, rhodium, and platinum. The adsorbates are mostly hydrocarbons, oxygen, nitrogen, hydrogen, and water.

The investigations are directed toward atomic-scale understanding of the friction, wear, and catalytic behavior of solid surfaces.

1. Coadsorption Structures of Benzene and Carbon Monoxide on Rh(111) and Pt(111) by HREELS and LEED (Publication 1)

C.M. Mate and G.A. Somorjai

High-resolution electron-energy-loss spectroscopy (HREELS) and low-energy electron diffraction (LEED) have been used to investigate several overlayer structures of benzene and carbon monoxide coadsorbed on Rh(111) and Pt(111). Three structures were analyzed with dynamical LEED intensity calculations to yield detailed bond-length information. They may be labeled:

I. Rh(111)–c($2\sqrt{3} \times 4$) rect–C_6H_6 + CO,
II. Rh(111)–(3×3)–C_6H_6 + 2CO, and
III. Pt(111)–($2\sqrt{3} \times 4$) rect–$2C_6H_6$ + 4CO.

Our HREELS studies imply that the benzene molecules are intact and lie parallel to the surface. HREELS also established that the observed LEED patterns mentioned above are due to coadsorbed CO. The C-O stretch frequencies are such that, on Rh, the CO molecules appear to occupy hollow sites of the substrate, while on Pt they probably are located on bridge sites. There is no sign of CO tilting from the surface normal.

2. Studies of Alkali Adsorption on Rh(111) Using Optical Second-Harmonic Generation (Publication 7)

H.W.K. Tom, C.M. Mate, X.D. Zhu, J.E. Crowell, T.F. Heinz, Y.R. Shen, and G.A. Somorjai

Dramatic changes were observed in the optical second-harmonic generation from the Rh(111) crystal surface as the surface was covered with alkali atoms. For low alkali coverage, these changes are explained qualitatively in terms of optical transitions between alkali atomic-derived electronic states and, for high coverage, in terms of the plasmon resonance of the alkali layer. The results establish the surface specificity of second-harmonic generation to the topmost 1 or 2 atomic layers of alkali metals.

3. Investigation of the Si(111)–(7×7) Surface by Second-Harmonic Generation: Oxidation and the Effects of Surface Phosphorus (Publication 6)

H.W.K. Tom, X.D. Zhu, Y.R. Shen, and G.A. Somorjai

We have studied the initial stages of oxidation, the temperature dependence of the surface electronic structure, and the effect of phosphorus on oxidation of the Si(111)–(7×7) surface using optical second-harmonic generation. We have also observed a ($\sqrt{3} \times \sqrt{3}$)R30° LEED pattern due to surface reconstruction induced by 0.5% P on Si(111).

4. The Delocalized Quantum Nature of Hydrogen Adsorbed on the Rh(111) Crystal Surface (Publication 34)

C.M. Mate and G.A. Somorjai

We observe, by electron energy loss spectroscopy (EELS), excitations between the ground-state band and all low-lying energy bands for the motion of hydrogen and deuterium atoms on the Rh(111) crys-

*This work was supported by the Director, Office of Energy Research, Office of Basic Energy Sciences, Materials Sciences Division of the U.S. Department of Energy under Contract No. DE-AC03-76SF00098.

tal surface. The absence of a deuterium isotope shift for the lowest energy excitation, the observation of broad energy bands, and good agreement with theoretical calculations for hydrogen on Ni(111) all provide strong experimental evidence for delocalized, quantum behavior of adsorbed hydrogen atoms on the Rh(111) surface.

5. Bonding and Thermal Decomposition of Propylene, Propadiene, and Methylacetylene on the Rh(111) Single-Crystal Surface (Publication 32)

B.E. Bent, C.M. Mate, J.E. Crowell, B.E. Koel, and G.A. Somorjai

We have studied the reactions of propylene, propadiene, and methylacetylene with Rh(111) crystal faces in ultrahigh vacuum (UHV) from 80 to 800 K using LEED, HREELS, and thermal-desorption spectroscopy (TDS). All three hydrocarbons adsorb intact at 80 K, bonding with the surfaces through their unsaturated carbon-carbon bonds. At this temperature, methylacetylene forms a p(2 × 2) LEED pattern, while propylene and propadiene adsorb as disordered monolayers. Above 200 K the first CH bonds are broken and all the C_3 hydrocarbons form p(2 × 2) LEED patterns, which are stable up to 270 K. The propylene fragment in this temperature range is propylidyne ($\equiv CCH_2CH_3$), while propadiene isomerizes to methylacetylene. By room temperature all the C_3 hydrocarbons have decomposed to ethylidyne ($\equiv CCH_3$) and polymerized C_xH fragments. Surface hydrogen is instrumental in the C-C bond breaking, and partial deuteration studies were performed to determine which C-C bonds break first. The ethylidyne species are stable up to 400 K, above which they decompose to C_xH fragments. The bonding and the thermal-decomposition pathways for these molecule on Rh(111) are discussed; in addition, a comparison is made to Pt(111) surface chemistry.

6. The Adsorption and Reactions of Hydrocarbons on Molybdenum Single-Crystal Surfaces, when Clean and in the Presence of Co-Adsorbed Sulfur or Carbon (Publication 31)

D.G. Kelly, M. Salmeron, and G.A. Somorjai

The chemisorption and reactions of thiophene, 1,3-butadiene. butenes, and n-butane on clean Mo(100), and with sulfur or carbon overlayers, have been investigated using TDS. The predominant reaction at low additive coverage (0–0.2 monolayer of S or C), and at low ambient pressure (10^{-10} Torr) for unsaturated hydrocarbons is decomposition. Butane is the least reactive of the hydrocarbons, and a large fraction (95%) desorbs molecularly at all additive coverages. As additive (S or C) coverage increases, the amount of decomposition decreases, enabling other reaction pathways to become more probable. Hydrogenation, partial dehydrogenation, and isomerization reactions are detected. Molecular binding on the additive overlayers was also found to be very different. On sulfur overlayers the binding of the hydrocarbons was weak (physisorption), usually on the order of the heat of sublimation (9–10 kcal/mol). However, molecular binding on carbon overlayers was stronger: the heat of desorption was 17–23 kcal/mol for thiophene and butadiene, 12–15 kcal/mol for the butenes, and 11 kcal/mol for butane. In addition, isomerization of 1-butene to 2-butene occurred on the carbon overlayer. It is suggested that the metal sites control the reaction observed (except for isomerization). This accounts for the similarity in surface reaction product distributions, and explains why the difference in molecular hydrocarbon bindings between the sulfur-covered and carbon-covered surfaces plays a minor role in these reactions.

7. LEED Theory for Incommensurate Overlayers: Application to Graphite on Pt(111) (Publication 30)

Z.P. Hu, D.F. Ogletree, M.A. Van Hove, and G.A. Somorjai

A dynamical LEED analysis is applied to study the structure of incommensurate overlayers. The previously described beam-set-neglect method is extended to the incommensurate case, providing an efficient theoretical scheme for calculating the required LEED beam intensities.

This method is used to investigate the structure of an incommensurate graphite overlayer on the Pt(111) surface by analyzing the specular diffraction beam intensities at various angles. The measured LEED intensities are well represented by a surface model consisting of a graphite layer 3.70 ± 0.05 Å above the Pt(111) surface, supported by at least a partial layer of "intercalated" carbidic carbon atoms chemisorbed in threefold hollow sites 1.25 ± 0.10 Å above the Pt(111) surface. A "data-subdivision"

method is applied in the R-factor analysis to distinguish between the different R-factor minima.

8. Direct Determination of Blocking of Surface Defects by Carbonaceous Deposits during Hydrocarbon Reaction on Platinum Single Crystals (Publication 25)

F. Zaera and G.A. Somorjai

A CO titration technique has been developed to quantitatively determine the presence of different kinds of catalytic sites on single-crystal surfaces. A direct correlation was found between platinum catalytic activity for conversion of hydrocarbons and the existence of bare defects on the metal surface. Isomerization and hydrogenolysis of either isopentane or butane is enhanced by the presence of steps or kinks on the catalyst surface. The same effect is not observed for methylcyclopentane of n-hexane conversion, where carbonaceous deposits cover the surface defects within a few minutes of starting the reactions.

9. Thermal Decomposition of Benzene on the Rh(111) Crystal Surface (Publication 8)

B.E. Koel, J.E. Crowell, B.E. Bent, C.M. Mate, and G.A. Somorjai

Benzene decomposition on the Rh(111) crystal surface has been studied over the temperature range of 300–800 K using HREELS, TPD, and LEED. Our results show that benzene decomposition begins at 400 K, forming a mixture of CH and C_2H species. The relative amounts of these two species varies with temperature; at 470 K, the concentration ratio of CH to C_2H is 0.4. Above 500 K, these fragments dehydrogenate and condense to form C_nH polymers. By 800 K, the adsorbed monolayer is completely dehydrogenated, forming a polymeric carbon monolayer with a vibrational spectrum similar to that of an ordered graphite monolayer. We propose that benzene decomposition on Rh(111) proceeds by decyclotrimerization to form three acetylenes that immediately decompose to CH and C_2H species.

10. The Structure of the $(\sqrt{3} \times \sqrt{3})R30°$ Superlattice Phase on (111) α-Cu-16 at.% Al: a LEED Intensity Analysis (Publication 2)

R.J. Baird, D.F. Ogletree, M.A. Van Hove, and G.A. Somorjai

A dynamical LEED analysis is presented of the $(\sqrt{3} \times \sqrt{3})R30°$ superlattice on the (111) surface of an α-Cu-Al alloy single crystal with a bulk Al concentration of 16%. This surface ordering contrasts with the lack of long-range order in the bulk. In the ordered surface the Al atoms are found to be substitutionally arranged within the topmost layer with $(\sqrt{3} \times \sqrt{3})R30°$ symmetry. No evidence for the ordering of Al in deeper layers is detected by this analysis. the fcc-(111) stacking sequence is maintained at the surface, and the surface atoms occupy positions within ± 0.05 Å of bulk Cu lattice positions; i.e., no appreciable top-layer spacing change and no mixed-layer buckling are detected.

11. Surface-Science Studies of Catalysis: the Classification of Reactions (Publication 12)

F. Zaera, A. Gellman, and G.A. Somorjai

We have reviewed the results of selected surface-science studies of catalytic processes. Our conclusions, drawn from many such studies, are that reactions that occur over metal-based catalysts can be divided into three classes: (1) those occurring on the bare metal surface, (2) those occurring on active overlayers bound to the metal, and (3) those occurring on coadsorbate modified metal surfaces. Case histories are given describing catalytic processes fitting each category.

12. The Structure of a (2×2) Sulfur Overlayer on the Ir(110)–(1×2) Reconstructed Surface (Publication 43)

C.M. Chan and M.A. Van Hove

A (2×2) sulfur overlayer structure formed on the reconstructed Ir(110)–(1×2) surface has been

analyzed by LEED. The missing-row reconstruction of the substrate is found to be maintained, with a reduction of the clean-surface relaxations back toward bulk-like interatomic distances: the first two interlayer spacings are changed by Δd_{12}= −3.3% and Δd_{23}= 1.3% relative to the bulk. Each sulfur atom is found to reside on a (111) facet over a hollow site formed by two first-layer substrate atoms and one second-layer substrate atom, close to a "bulk site" of the substrate lattice (asymetrically off center towards the trough). The Ir-S bond length is 2.26 Å for the second-layer Ir atoms and 2.39 Å for the first-layer Ir atoms.

13. Ethylene on Rh(111) Single-Crystal Surfaces: Molecular Adsorption and Conversion to Ethylidyne—an HREELS, LEED, and TDS Study (Publication 33)

B.E. Bent, C.M. Mate, and G.A. Somorjai

Ethylene adsorption on Rh(111) between 90 and 300 K was studied by TDS, LEED, and HREELS. Between 90 and 200 K ethylene is molecularly adsorbed; ordered (2 × 2) and ($\sqrt{3} \times \sqrt{3}$)R30° structures can be formed. The HREELS vibrational spectra of these monolayers are interpreted using the Dewar-Chatt-Duncanson model for ethylene coordination with gas-phase ethylene and 1,2-dibromoethane as model compounds for the surface-bonding extremes. It is shown that the traditional CH_2 functional group modes are coupled in adsorbed ethylene so that they do not adequately describe the normal modes of vibration. However, by considering the couplings of these functional-group modes, we show that the C-C stretch force constant in adsorbed ethylene can be predicted from the deuterated ethylene vibrational frequencies. For ethylene on Rh(111) the C-C force constant is about 7.7 mdyne/Å, which by empirical correlations corresponds to a C-C bond length of 1.4 Å and a C-C bond order of 1.5. Bond orders and bond lengths for molecularly adsorbed ethylene on other transition-metal surfaces are also predicted and discussed. The conversion of ethylene to ethylidyne above 200 K on Rh(111) is discussed in light of published molecular-orbital calculations and TDS studies of the hydrogenation of ethylene to ethane at low temperature. A new mechanism for ethylidyne formation involving partial hydrogenation of C_2H_4 to C_2H_5 is proposed.

14. Ammonia Synthesis over Rhenium Single-Crystal Catalysts: Structure Sensitivity, Kinetics, and the Effects of K and O (Publication 10)

M. Asscher, J. Carrazza, M. Khan, K. Lewis, and G.A. Somorjai

Ammonia synthesis was investigated over model single-crystal and polycrystalline foil rhenium catalysts at 20-atm reactant pressure and in the temperature range of 720–900 K. The structure sensitivity of this reaction on four rhenium single crystals was studied. A remarkable sensitivity to the catalysts' surface structure was observed, with reactivity ratios of 1:94:920:2820 for the Re(0001), Re(10$\bar{1}$0), Re(11$\bar{2}$0), and Re(11$\bar{2}$1) crystal faces, respectively. The importance of high-coordination metal atom sites in both the first and second layers is clearly indicated by these results. An apparent activation energy for the reaction of 20.4 ± 1.1 kcal/mole was observed, regardless of the catalysts' surface structure. Kinetic data, pressure dependence analysis, and isotope effects indicate that, as with the iron catalyst, the rate-limiting step for the reaction is the dissociative chemisorption of the nitrogen molecule. Potassium atoms on the clean rhenium catalysts were found neither to promote nor to poison the reaction. The coadsorption of potassium with oxygen does not suppress the reactivity of the catalyst, and stabilization of the potassium atoms on the surface occurs. The presence of oxygen alone appears to increase the reaction rate.

15. Ammonia Synthesis over Iron Single-Crystal Catalysts: the Effects of Alumina and Potassium Promotion (Publication 26)

S.R. Bare, D.R. Strongin, and G.A. Somorjai

The effects of potassium and aluminum oxide in increasing the rate of ammonia synthesis from nitrogen and hydrogen have been investigated over model iron single-crystal catalysts at 20 atm reactant pressure. Elemental potassium does not remain on the iron surface under reaction conditions, but a small amount of potassium can be stabilized at higher temperatures by coadsorption with aluminum oxide. The cooperative interaction between the potassium and oxidized aluminum may be due to compound

formation. A massive restructuring of a Fe(110) surface, induced by the presence of aluminum oxide and 5 atm nitrogen at 450°C, was observed. This restructured surface exhibits substantial ammonia-synthesis activity, which may be due to the formation of crystallites of (111) planes during the restructuring. There is no increase in ammonia-synthesis activity (promotion) for a Fe(110) surface following nitrogen treatment alone, nor any promotional effect for an iron single-crystal surface with submonolayer amounts of oxidized aluminum and potassium adsorbed without nitrogen treatment.

16. The Effects of Aluminum Oxide in Restructuring Iron Single-Crystal Surfaces for Ammonia Synthesis (Publication 39)

D.R. Strongin, S.R. Bare, and G.A. Somorjai

The effect of aluminum oxide and potassium on ammonia synthesis over the (111), (100), and (110) faces of iron has been investigated. A restructuring of the Fe(110) and Fe(100) surfaces, induced by the presence of aluminum oxide and 20 Torr of water vapor, takes place, making the restructured surfaces almost as active as the clean Fe(111) plane in the ammonia synthesis reaction (20 atm reactant pressure of hydrogen and nitrogen). The high activity of the restructured surfaces is maintained for over four hours of ammonia synthesis. Without the presence of aluminum oxide, treatment of the Fe(110) and Fe(100) surfaces with 20 Torr of water vapor again produces restructured surfaces that are almost as active as the Fe(111) plane for a short period. However, in this case deactivation of the restructured surfaces into the respective clean, unrestructured surfaces occurs within one hour of ammonia synthesis. Restructuring of the Fe(111) surface with 20 Torr of water vapor produces only a slight decrease in ammonia-synthesis activity. The enhancement in rate of the restructured Fe(110) and Fe(100) surfaces, with or without aluminum oxide, might be explained by the formation of active surface orientations for ammonia synthesis [i.e., Fe(111) and Fe(211)], which contain C_7 sites (iron atoms with seven nearest neighbors), during the water-vapor treatments. These restructured surfaces are only stable in ammonia synthesis conditions when aluminum oxide is present.

Potassium adsorbed alone or with coadsorbed aluminum oxide exhibits no promotional effects under the water-vapor pretreatment conditions used in this study.

17. Hydrogenation of Chemisorbed Ethylene on Clean, Hydrogen-Covered, and Ethylidyne-Covered Platinum (111) Crystal Surfaces (Publication 14)

D. Godbey, F. Zaera, R. Yeates, and G.A. Somorjai

The hydrogenation of chemisorbed ethylene was examined on platinum (111) single crystals under ultrahigh vacuum using TPD. Ethane was formed in a self-hydrogenation process with an activation energy of 18 kcal/mole, while in the presence of preadsorbed hydrogen, ethane was formed with an activation energy of 6 kcal/mole. A mechanism, which is supported by a computer simulation, is proposed for the low-pressure hydrogenation.

At temperatures below 320 K, an ethylidyne-saturated Pt(111) surface requires hydrogen pressures greater than 10^{-5} Torr for coadsorption. Ethylene binds to this surface very weakly or not at all, and consequently no ethane was observed to desorb from this surface during TPD.

The results obtained support the model of direct participation of a carbonaceous layer during the steady-state catalytic hydrogenation of ethylene on Pt(111) at atmospheric pressures and room temperature, as previously reported.

18. A New System for LEED Intensity Measurements using a Real-Time Digital Video Processor (Publication 18)

D.F. Ogletree, J.E. Katz, and G.A. Somorjai

A new system for LEED intensity measurements has been developed, using a video camera and digital processing of the video signal. Complete two-dimensional LEED patterns are digitized in real time with high resolution using a commercial digital video processor. Intensity-voltage (I-V) data on all beams are collected simultaneously. A microcomputer analysis program automatically tracks the diffraction beams as a function of energy, and calculates beam position, size, and integrated intensity, including a local background correction. Using a video tape recorder for intermediate data storage, a complete set

of I-V curves can be collected in less than 100 seconds.

19. Methylcyclopentane Conversion over Platinum Single-Crystal Surfaces: Evidence for the Cyclic Mechanism of n-Hexane Isomerization (Publication 15)

F. Zaera, D. Godbey, and G.A. Somorjai

The surface structure and temperature dependence of methylcyclopentane conversion was investigated near atmospheric pressure at 540–650 K over four platinum single-crystal surfaces with flat (100) and (111), and stepped (332) and (557) orientations. The atomic structure and surface composition of the active catalysts were determined before and after reactions using LEED and Auger electron spectroscopy.

Selective ring opening to produce 2- and 3-methylpentanes readily occurred on both flat surfaces studied, the (111) and the (100). The rate of formation of methylpentanes was found to be nearly 3.5 times faster on the (100) surface than on the (111) surface. The presence of steps on the platinum surface had no significant effect on the rates of ring opening or aromatization, since these line defects were quickly covered with carbonaceous deposits, as shown by carbon monoxide titration of the active sites.

Methylcyclopentane and n-hexane yield the same distribution of isomers (2- and 3-methylpentanes), and the activation energy for the formation of these products from both n-hexane and methylcyclopentane are identical within experimental error. These results indicate that the formation of methylcyclopentane on the platinum surface is an intermediate step for the isomerization of n-hexane.

20. The Importance of C_7 Sites and Surface Roughness in Ammonia Synthesis over Iron (Publication 27)

D.R. Strongin, J. Carrazza, S.R. Bare, and G.A. Somorjai

We have obtained data that further support the contention that C_7 sites (Fe atoms with seven nearest neighbors) are those most active in iron ammonia-synthesis catalysts.

21. The Tilting of CO Molecules Chemisorbed on a Pt(110) Surface: a Molecular-Orbital Study (Publication 35)

M.I. Ban, M.A. Van Hove, and G.A. Somorjai

The tilting of carbon monoxide molecules adsorbed on a Pt(110) surface has been modeled by using the extended Huckel molecular-orbital (EHMO) method. Electronic properties, including total energies, were obtained for various adsorbate-substrate cluster systems. The tilting away from the surface normal is due to excessive close-packing of CO molecules along the atomic ridges of the Pt(110) surface. It is found energetically favorable for the tilting to alternate on either side of each ridge in a zigzag fashion, as indicated by glide-plane symmetry in observed LEED patterns.

22. An Ultrahigh-Vacuum Sample Manipulator for Angle-Resolved Electron Spectroscopy (Publication 37)

D.G. Ogletree, K. Frank, and G.A. Somorjai

A new and simple design for a precision sample manipulator suitable for LEED and for angle-resolved electron spectroscopies is described. The sample holder is supported in an off-axis position on a conventional rotary feedthrough mounted on an XYZ translation stage. The sample may be tilted and independently rotated around its azimuth while being cooled below 150 K or heated above 2000 K. The manipulator construction is nonmagnetic and ultrahigh-vacuum compatible.

23. A Radiotracer (^{14}C) and Catalytic Study of Thiophene Hydrodesulfurization on the Clean and Carbided Mo(100) Single-Crystal Surface (Publication 38)

M.E. Bussell and G.A. Somorjai

The role of adsorbed carbon overlayers and possible product poisoning (H_2S and cis-2-butene) in the thiophene hydrodesulfurization (HDS) reaction over Mo(200) single-crystal surfaces was investigated. Using the beta-emitting ^{14}C isotope, it was shown that adsorbed carbon remains on the Mo(100) sur-

face after many thiophene turnovers (TN $\sim 10^3$). HDS activities measured for carbided surfaces were found to be identical to that of initially clean Mo(100) single crystals, suggesting that the active catalyst surface is carbon-covered. Deactivation of the single-crystal catalysts was caused by adsorption of H_2S onto the active HDS sites. Removal of the H_2S by evacuation of the reaction mixture readily regenerated the catalyst's activity towards a fresh mixture of thiophene and hydrogen. The product cis-2-butene had no effect on the activity of the catalysts.

24. Catalytic Hydrodesulfurization over the Mo(100) Single-Crystal Surface I: Kinetics and Overall Mechanism (Publication 40)

A.J. Gellman, D. Neiman, and G.A. Somorjai

The hydrodesulfurization of thiophene is catalyzed by the Mo(100) crystal surface at high pressures. The product distribution is similar to that detected over a high-surface-area powdered MoS_2 catalyst. Detailed kinetic studies have been performed in the 1-atm pressure regime and in the temperature range of 250–425°C. The initial reaction steps involve the desulfurization of thiophene to produce butadiene with an activation energy of 14.4 kcal/mole. Butenes and butane are produced via the subsequent hydrogenation of butadiene. The catalytic surface is predominantly covered with the partially hydrogenated hydrocarbon intermediates in the hydrogenation pathway. The hydrogen coverage, on the other hand, is very low and varies in proportion to $P^{1/2}(H_2)$.

25. Catalytic Hydrodesulfurization over the Mo(100) Single-Crystal Surface II: The Role of Adsorbed Sulfur and Mechanism of the Desulfurization Step (Publication 41)

A.J. Gellman, M.E. Bussell, and G.A. Somorjai

The study of thiophene hydrodesulfurization over initially clean Mo(100) surfaces has been extended to include sulfided surfaces. Low sulfur coverages ($0 \leqslant \theta_s < 0.67$) inhibit HDS activity. Increasing the sulfur coverage in the range $0.67 \leqslant \theta_s \leqslant 1.0$ produces a surface with an HDS activity of about half that of the clean Mo(100) surface. Excessive exposure of the surface to a sulfur-containing environment results in the formation of a MoS_2 layer that is, at least in part, responsible for complete catalytic deactivation. Radiotracer (^{35}S) labeling techniques have been used to measure rates of hydrogenation of sulfur adsorbed on the Mo(100) surface. In ambient atmospheres of both hydrogen (1 atm) and the thiophene HDS reaction mixture [$P(H_2)$ = 1 atm, P(Th) = 2.5 Torr], the rate of hydrogenation of adsorbed sulfur is two orders of magnitude less than the HDS rate. This rules out the formation of a Mo-S species as a possible step in the thiophene desulfurization reaction.

26. Work in Progress

Studies of organic monolayers, their structure, and decomposition, are being extended to iron and molybdenum crystal surfaces. Digital high-sensitivity low-energy electron diffraction is being used to study the surface structures of disordered monolayers on metal surfaces.

The platinum-rhenium and cobalt-molybdenum alloy systems are being studied using single crystals to elucidate the catalytic behavior of alloys for hydrocarbon-conversion reactions.

Potassium and alumina additives to iron greatly accelerate the rate of ammonia synthesis. Their role is being verified by combined surface science and catalytic studies. Their possible role in ammonia synthesis over rhenium surfaces is being explored.

1986 PUBLICATIONS AND REPORTS

Refereed Journals

1. C.M. Mate and G.A. Somorjai, "CO-Induced Ordering of Benzene in Rh(111) and Pt(111) Crystal Surfaces," Surf. Sci. **160**, 542 (1985); LBL-18502.
2. R.J. Baird, D.F. Ogletree, M.A. Van Hove, and G.A. Somorjai, "The Structure of the ($\sqrt{3} \times \sqrt{3}$) R30° Superlattice Phase on (111) α-Cu-16 at.% Al; a LEED Intensity Analysis," Surf. Sci. **165**, 345 (1986); LBL-19632.
3. C.M. Mate, B.E. Bent, and G.A. Somorjai, "Carbon Monoxide Induced Ordering of Adsorbates on the Rh(111) Crystal Surface," J. Electron Spectrosc. **39**, 205 (1986); LBL-20360.
4. M.A. Van Hove, R.F. Lin, and G.A. Somorjai, "The Surface Structure of Coadsorbed Benzene and Carbon Monoxide on the Rhodium (111) Single Crystal Determined from Low-Energy Electron Diffraction Intensities," J. Am. Chem. Soc. **108**, 2532 (1986); LBL-20137.

5. C.-M. Chan and M.A. Van Hove, "Confirmation of the Missing-Row Model with Three-Layer Relaxations for the Reconstructed Ir(110)-(1×2) Surface," Surf. Sci. **171**, 226 (1986).
6. H.W.K. Tom, X.D. Zhu, Y.R. Shen, and G.A. Somorjai, "Investigation of the Si(111)-(7×7) Surface by Second-Harmonic Generation: Oxidation and the Effects of Surface Phosphorus," Surf. Sci. **167**, 107 (1986); LBL-19661.
7. H.W.K. Tom, C.M. Mate, X.D. Zhu, J.E. Crowell, T.F. Heinz, Y.R. Shen, and G.A. Somorjai, "Studies of Alkali Adsorption on Rh(111) Using Optical Second-Harmonic Generation," Surf. Sci. **172**, 466 (1986); LBL-19634.
8. B.E. Koel, J.E. Crowell, B.E. Bent, C.M. Mate, and G.A. Somorjai, "Thermal Decomposition of Benzene on the Rh(111) Crystal Surface," J. Phys. Chem. **90**, 2949 (1986); LBL-20362.
9. M. Asscher and G.A. Somorjai, "Reactive Scattering," Chapter 21 in *Molecular Beam Surface Science Scattering*, published in Surf. Sci. **173**, 351 (1986); LBL-19921.
10. M. Asscher, J. Carrazza, M. Khan, K. Lewis, and G.A. Somorjai, "The Ammonia Synthesis Over Rhenium Catalysts. Structure Sensitivity, Kinetics and the Effects of K and O," J. Catal. **98**, 277 (1986); LBL-18200.
11. M.M. Khan and G.A. Somorjai, "A Kinetic Study of Partial Oxidation of Methane with Nitrous Oxide on a Molybdena-Silica Catalyst," J. Catal. **91**, 263 (1985); LBL-17408.
12. F. Zaera, A. Gellman, and G.A. Somorjai, "Surface Science Studies of Catalysis: Classification of Reactions," Acct. Chem. Res. **19**, 24 (1986); LBL-19118.
13. J. Carrazza and G.A. Somorjai, "Structure Sensitivity and Catalytic Reactions," Indust. Eng. Fund. **25**, 63 (1986); LBL-19628.
14. D. Godbey, F. Zaera, R. Yeates, and G.A. Somorjai, "Hydrogenation of Chemisorbed Ethylene on Clean, Hydrogen, and Ethylidyne Covered Platinum(111) Crystal Surface," Surf. Sci. **167**, 150 (1986); LBL-19911.
15. F. Zaera, D. Godbey, and G.A. Somorjai, "Methylcyclopentane Conversion Over Platinum Single Crystal Surfaces: Evidence for the Cyclic Mechanism of n-Hexane Isomerization," J. Catal. **101**, 73 (1986); LBL-19080.
16. R. Yeates and G.A. Somorjai, "Surface Structure Sensitivity of Alloy Catalysis of Hydrocarbon Reactions. N-hexane Conversion on the Pt(100) and Pt(111)-Au Crystal Surfaces," J. Catal. **102**, 6964 (1986); LBL-19332.
17. F. Zaera, A. Gellman, and G.A. Somorjai, "Surface Science Studies of Catalysis: Classification of Reactions," Acct. Chem. Res. **19**, 24 (1986); LBL-19118.
18. D.F. Ogletree, J.E. Katz, and G.A. Somorjai, "A New System for LEED Intensity Measurements Using a Real-Time Digital Video Processor," Rev. Sci. Instrum. **57**, 3012 (1986); LBL-21743.
19. D.F. Ogletree, M.A. Van Hove, and G.A. Somorjai, "LEED Intensity Analysis of the Structures of Clean Pt(111) and CO Adsorbed on Pt(111) in the c(4×2) Arrangement," Surf. Sci. **173**, 351 (1986); LBL-19920.
20. Y.C. Xie, B.M. Naasz, and G.A. Somorjai, "Alcohol Synthesis from CO and H_2 over Molybdenum Sulfide. The Effect of Pressure and Promotion by Potassium Carbonate," J. Appl. Catal. **27**, 233 (1986); LBL-20359.
21. F. Zaera and G.A. Somorjai, "The Direct Determination of Blocking of Surface Defects by Carbonaceous Deposits During Hydrocarbon Reactions on Platinum Single Crystals," Langmuir **2**, 686 (1986); LBL-20639.

LBL Reports

22. M. Kudo, R.C. Yeates, and G.A. Somorjai, "Photoemission Studies on Gold-Covered Pt(111) and Pt(100) Surfaces," LBL-18035.
23. A.J. Gellman, W.T. Tysoe, and G.A. Somorjai, "The Binding of Sulfur to the Mo(100) Surface: An XPS/UPS Study," LBL-20357.
24. C.M. Mate, B.E. Bent, and G.A. Somorjai, "Vibrational Spectroscopy of Hydrogen Adsorbed on Metal Surfaces," in *Hydrogen in Catalysis*, Z. Paal, Ed. (in press); LBL-20361.
25. F. Zaera and G.A. Somorjai, "The Role of Hydrogen in Low and High Pressure Hydrocarbon Reactions over Metal Single Crystal Surfaces," in *Hydrogen in Catalysis*, Z. Paal, Ed. (in press); LBL-19932.
26. S.R. Bare, D.R. Strongin, and G.A. Somorjai, "The Ammonia Synthesis over Iron Single Crystal Catalysts: The Effects of Alumina and Potassium Promotion," accepted by J. Phys. Chem.; LBL-20818.
27. D.R. Strongin, J. Carrazza, S.R. Bare, and G.A. Somorjai, "The Importance of C_7 Sites and Surface Roughness in the Ammonia Synthesis RXN over Iron," accepted by J. Catal.; LBL-21500.
28. M.A. Van Hove, R.F. Lin, G.S. Blackman, and G.A. Somorjai, "LEED Intensity Analysis of the Structure of Coadsorbed Benzene and CO on Rh(111)," submitted to Acta Crystallogr.; LBL-21501.
29. D.F. Ogletree, M.A. Van Hove, and G.A. Somorjai, "Benzene and Carbon Monoxide Adsorbed on Pt(111), A LEED Intensity Analysis," submitted to Surf. Sci.; LBL-21502.
30. Z. Hu, D.F. Ogletree, M.A. Van Hove, and G.A. Somorjai, "LEED Theory for Incommensurate Overlayers: Application to Graphite on Pt(111)," Surf. Sci. (in press); LBL-21511.
31. D.F. Kelly, M. Salmeron, and G.A. Somorjai, "The Adsorption and Reactions of Hydrocarbons on Molybdenum Single Crystal Surfaces: When Clean and in the presence of CO-adsorbed Sulfur and Carbon," Surf. Sci. (in press); LBL-21251.

32. B.E. Bent, C.M. Mate, J.E. Crowell, B.E. Koel, and G.A. Somorjai, "Bonding and Thermal Decomposition of Propylene, Propadiene and Methylacetylene on the Rh(111) Single Crystal Surface," submitted to J. Phys. Chem.; LBL-21540.
33. B.E. Bent, C.M. Mate, and G.A. Somorjai, "Ethylene on Rh(111) Single Crystal Surfaces: Molecular Adsorption and Conversion to Ethylidyne—An HREELS, LEED and TDS Study of Crystal Surfaces," submitted to Surf. Sci.; LBL-21539.
34. C.M. Mate and G.A. Somorjai, "The Delocalized Quantum Nature of Hydrogen Adsorbed on the R(111) Crystal Surface," submitted to Solid State Commun.; LBL-21545.
35. M.I. Ban, M.A. Van Hove, and G.A. Somorjai, "The Tilting of CO Molecules on a Pt(110) Surface—A Molecular Orbital Study," submitted to Surf. Sci.; LBL-21554.
36. S. Bare and G.A. Somorjai, "Surface Chemistry," to be published in *Encyclopedia of Physical Science and Technology*; LBL-20904.
37. D.F. Ogletree, K. Frank, and G.A. Somorjai, "An Ultra-High Vacuum Sample Manipulator for Angle-Resolved Electron Spectroscopy," submitted to J. Vac. Sci. Technol.; LBL-21694.
38. M.E. Bussell and G.A. Somorjai, "A Radiotracer(^{14}C) and Catalytic Study of Thiophene Hydrodesulfurization on the Clean and Carbided Mo(100) Single Crystal Surface," submitted to J. Catal.; LBL-22141.
39. D.R. Strongin, S.R. Bare, and G.A. Somorjai, "The Effects of Aluminum Oxide in Restructuring Iron Single Crystal Surfaces for Ammonia Synthesis," accepted by J. Catal.; LBL-21836.
40. A.J. Gellman, D. Neiman, and G.A. Somorjai, "Catalytic Hydrodesulfurization over the Mo(100) Single Crystal Surface I: Kinetics and Overall Mechanism," accepted by J. Catal.; LBL-20356.
41. A.J. Gellman, M.E. Bussell, and G.A. Somorjai, "Catalytic Hydrodesulfurization over the Mo(100) Single Crystal Surface II: Kinetics and Overall Mechanism," accepted by J. Catal.; LBL-21891.
42. M.A. Van Hove, R.F. Lin, D.F. Ogletree, G.S. Blackman, C.M. Mate, and G.A. Somorjai, "Coadsorption Structures of Benzene and Carbon Monoxide on Rh(111) And Pt(111) by HREELS and LEED," J. Vac. Sci. Technol. (in press); LBL-22079.
43. C.-M. Chan and M.A. Van Hove, "The Structure of a (2×2) Sulfur Overlayer on the Ir(110)-(1×2) Reconstructed Surface," submitted to Surf. Sci.; LBL-21908.

Invited Talks

44. G.A. Somorjai, "The Structure and Bonding of Organic Molecules on Metal Surfaces," Dreyfus Symposium on the Chemistry and Physics of Surfaces and Clusters, University of Illinois, Champaign-Urbana, Oct. 11, 1985.
45. G.A. Somorjai, "Molecular Ingredients of Heterogeneous Catalysis—New Horizons of High Technology," Staff Technical Conference, Amoco Corporation Research Department, Naperville, IL, Oct. 17, 1985.
46. G.A. Somorjai, S. Bare, and D. Strongin, "Ammonia Synthesis Over Iron Single Crystal Catalysts: The Effects of Alumina and Potassium Promotion," California Catalysis Society 1985 Fall Meeting, Newport Beach, CA, Oct. 18, 1985.
47. G.A. Somorjai, "Catalytic Applications of Surface Science," Colloquia — Fall 1985, Department of Chemistry, Rutgers University, New Brunswick, NJ, Nov. 5, 1985.
48. G.A. Somorjai and D. Godbey, "The Chemistry and Structure of Rhenium Modified Platinum (111) Single Crystal Surfaces," Seventh Surface/Interface Research Meeting of the NCCAVS, Berkeley, CA, Dec. 11, 1985.
49. G.A. Somorjai, "Surface Chemistry and Catalytic Chemistry of Platinum Correlations with Palladium and Rhodium," The Noyes Lecture, Department of Chemistry, University of Texas, Austin, Jan. 30, 1986.
50. G.A. Somorjai, "Surface Acidity in Metal Catalysis," Superacid Meeting, Hydrocarbon Research Institute, University of Southern California, Los Angeles, CA, Feb. 1, 1986.
51. M.A. Van Hove and G.A. Somorjai, "Large Ring Distortions Observed in Benzene Chemisorbed on Single-Crystal Metal Surfaces," 11th Austin Symposium on Molecular Structure, Austin, TX, March 3, 1986.
52. G.A. Somorjai, "The Surface Chemical Bond," Brookhaven National Laboratory, Upton, NY, March 7, 1986.
53. G.A. Somorjai, "The Structure and Bonding of Organic Monolayers on Metal Surfaces," Georgetown University, Washington, D.C., March 12, 1986.
54. G.A. Somorjai, "The Molecular View of Heterogeneous Metal Catalysis," International Conference on the Mechanisms of Heterogeneous Catalysis, Lyon, France, April 1, 1986.
55. G.A. Somorjai, "The Structure and Bonding of Organic Molecules on Metal Surfaces," Musher Lecture, Hebrew University, Jerusalem, Israel, April 7, 1986.
56. G.A. Somorjai, "The Structure and Bonding of Organic Molecules on Metal Surfaces," Technion, Haifa, Israel, April 8, 1986.
57. G.A. Somorjai, "The Surface Science of Metal Catalysis," Hebrew University, Jerusalem, Israel, April 11, 1986.
58. G.A. Somorjai, "Correlation between the Chemical Bonding of Small Molecules in Clusters and on Metal Surfaces," American Chemical Society National Meeting, New York, April 16, 1986.
59. G.A. Somorjai, "Iron and Its Oxides, Their Characterization, Surface, and Catalytic Chemistry," 20th

Great Lakes Regional Meeting, American Chemical Society, Milwaukee, WI, June 2, 1986.

60. G.A. Somorjai, "The Surface Science and Catalytic Studies of PtAu, PtCu and PtRe Alloy Single Crystal Surfaces," Rocky Mountain Regional Meeting, American Chemical Society, Denver, CO, June 11, 1986.
61. G.A. Somorjai, "The Applications of Precious Metals in Surface Science and Catalysis," International Precious Metals Institute Conference and Exhibition, Lake Tahoe, NV, June 12, 1986.
62. G.A. Somorjai, Gordon Research Conferences—Catalysis, Colby-Sawyer College, New London, NH, June 23–27, 1986.
63. G.A. Somorjai, "Thermal Decomposition of Acetylene and Ethylene Coadsorbed with Carbon Monoxide on the Rh(100) Single Crystal Surface: the Formation of Ethylidyne (CCH_3)," American Chemical Society 192nd National Meeting, Anaheim, CA, Sept. 8, 1986.
64. M.A. Van Hove, "Techniques of Surface Crystallography," National Tsing Hua University, Hsinchu, Taiwan, Dec. 23, 1985.
65. M.A. Van Hove, "Surface Structure Determination by Low-Energy Electron Diffraction," National Taiwan University, Taipei, Taiwan, Dec. 24, 1985.
66. M.A. Van Hove, "Electron Scattering Techniques of Surface Crystallography," University of Wisconsin, Milwaukee, Jan. 23, 1986.
67. M.A. Van Hove, "Overview of Surface Structures," University of Wisconsin, Milwaukee, Jan. 30, 1986.
68. M.A. Van Hove, "Recent Structure Determinations by LEED," University of Wisconsin, Madison, Feb. 17, 1986,
69. M.A. Van Hove, "Theory of Diffuse LEED," University of Wisconsin, Milwaukee, Feb. 20, 1986.
70. M.A. Van Hove, "Structures of Adsorbed Hydrocarbons on Metal Surfaces by LEED Theoretical Techniques," University of California, La Jolla, March 31, 1986.
71. M.A. Van Hove, "Adsorption Structure of Organic Molecules on Metal Surfaces," University of British Columbia, Vancouver, June 17, 1986.
72. M.A. Van Hove, "Progress in the Structure Determination of Benzene and CO Structures on Metal Surfaces," University of Milan, Italy, July 7, 1986.
73. M.A. Van Hove, "Structure Determination of Molecular Adsorbates on Metal Surfaces," University of Florence, Italy, July 9, 1986.

Nuclear Magnetic Resonance*

Alexander Pines, Investigator

INTRODUCTION

The nuclear magnetic resonance (NMR) program has two complementary directions. The first is the development of new concepts and techniques in NMR in order to extend the applicability of the spectroscopy to a wider range of problems and materials. Such a program demands a study of the interaction of nuclear spins with each other, with other degrees of freedom such as molecular rotations, and with external excitations such as radiofrequency pulses and light. It also requires the development of new theoretical tools and the design and implementation of novel experimental methods. Such methods entail a substantial effort in the design and fabrication of next-generation NMR equipment. Some developments currently under way in this direction are multiple-quantum NMR and clustering, zero-field NMR, solid-state materials-imaging spatially selective NMR with surface coils, superconducting quantum interference device (SQUID) detectors in high-sensitivity two-dimensional NMR of dipolar couplings, high-temperature NMR, multiple-pulse and iterative schemes, optical polarization of gases, and selective polarization of surfaces. The second direction is the application of usual NMR methods and instrumentation to some materials research problems in collaboration with other programs at LBL as well as with outside industries. Some of the materials and problems currently under investigation in this direction are the structure of doped semiconductors, organic and organometallic solids, ordering and phase transitions in liquid crystals, dynamics of oriented and constrained molecules, structure and motion in silicate glasses, and clustering in zeolite cavities and solid-gas interfaces. This program addresses a national need for a model effort to implement the rapid development and transfer of NMR technology to laboratories in industry and other organizations.

*This work was supported by the Director, Office of Energy Research, Office of Basic Energy Sciences, Materials Sciences Division of the U.S. Department of Energy under Contract No. DE-AC03-76SF00098.

1. Clustering of Atoms in Solids (Publications 5, 9, 12, 25, and 45)

J. Baum,[†] A.N. Garroway,[‡] K. Gleason,[§] J. Reimer,[§] and A. Pines

"Counting" atoms in clusters has been the domain of molecular beams and mass spectrometry. By use of time-resolved multiple-quantum NMR spectroscopy, it is now possible to count spins in condensed-phase clusters by observing the number of radiofrequency quanta absorbed as a function of excitation time (see Figure 1-1). Applications include molecules in zeolites, molecular and liquid crystals, chemisorbed species on surfaces, and hydrogen in amorphous silicon hydride.

[†]Present address: Inorganic Chemistry Department, Oxford University, Oxford, England.

[‡]Permanent address: Polymer Division, Naval Research Laboratory, Washington, D.C.

[§]Permanent address: Chemical Engineering Department, U.C. Berkeley, and Center for Advanced Materials, LBL.

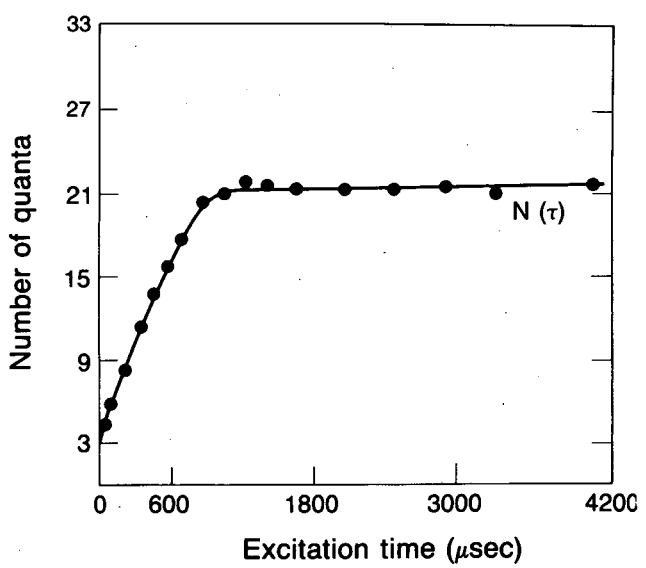

Figure 1-1. Number of quanta as a function of excitation time in liquid-crystal p-hexylcyanobiphenyl, demonstrating that the molecules behave like isolated clusters of 21 hydrogens. (XBL 8702-6165)

2. Multiple-Quantum Dynamics (Publications 11, 34, and 36)

S.-B. Liu, M. Mehring,† M. Munowitz,‡ D. Suter, and A. Pines

In a large system of strongly coupled spins, any coherence, such as a nonequilibrium magnetization, disappears rapidly due to spin diffusion just as density gradients decay when a gaseous system approaches equilibrium (see Figure 2-1). The decay of order is related to the development of many-spin correlations that can be measured by multiple-quantum spectroscopy and modeled as a random walk in Liouville space.

†Permanent address: Solid State Physics Institute, University of Stuttgart, Federal Republic of Germany.

‡Present address: Analytical Division, Amoco Research, Chicago, IL.

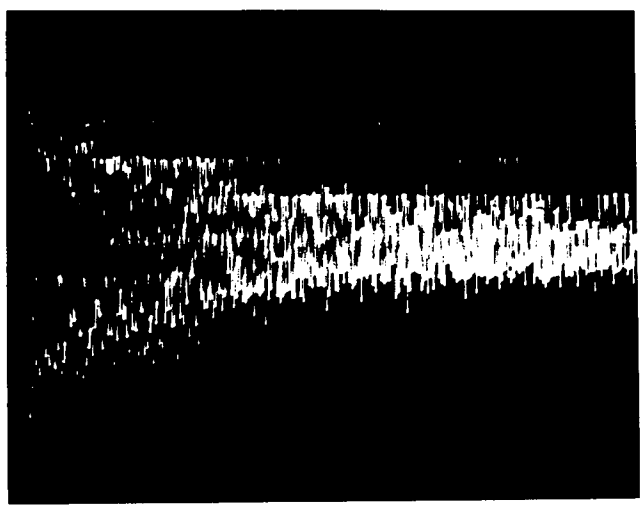

Figure 2-1. Chaotic decay of a spin system to equilibrium. The order disappears into modes of multiple-spin correlation that can be measured by multiple-quantum spectroscopy. (XBB 840-8533)

3. Iterative Schemes for Nonlinear Excitation (Publications 14, 23, 27, 39, and 48)

H. Cho,† J. Guckenheimer,‡ C. Lee, A.J. Shaka, R. Tycko,§ and A. Pines

Iterative maps on SO(3) have been developed to model the nonlinear excitation of two-level systems (see Figure 3-1). The maps F are defined as

Figure 3-1. Basin image in the x-z plane of SO(3) for the iterative map [0,0,180,135,135,150,330,0], for which $\pi/2$ (center of the light region) is a stable fixed set of points. (CBB 860-10865)

$$FU_n = U_{n+1},$$

where U_n are SO(3) propagators with fixed points $\bar{U}$:

$$F\bar{U} = \bar{U}.$$

Stable fixed points give rise to broadband behavior, unstable points to narrowband behavior, and multiple fixed points to unstable behavior. The sequences derived from these maps have been tested in experiments and are useful for broadband spin decoupling, spatially selective NMR, and information storage.

†Present address: Department of Physical Chemistry, E.T.H., Zurich, Switzerland.

‡Permanent address: Department of Mathematics, Cornell University, Ithaca, NY.

§Permanent address: AT&T Bell Laboratories, Murray Hill, NJ.

4. Spin Decoupling in Solids and Liquids (Publications 28 and 29)

C. Lee, K. Schenker,† A.J. Shaka, D. Suter, and A. Pines

In high-field magnets the NMR lines of both solids and liquids cover a wide range of frequencies,

making normal continuous-wave decoupling inefficient. New schemes based on magic-angle rotations and phase shifts have been analyzed theoretically and incorporated into decoupling experiments. These schemes are useful in high-resolution two-dimensional NMR spectroscopy (see Figure 4-1).

*Permanent address: Department of Chemistry, University of rich, Switzerland.

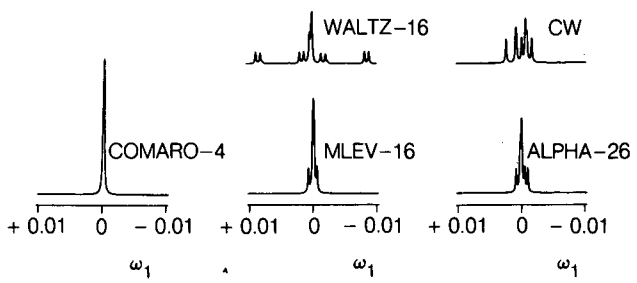

Figure 4-1. Demonstration of efficiency of new scheme, COMARO-4, for spin decoupling in dipolar coupled hydrogen-deuterium pairs. (XBL 869-9633)

5. Zero-Field NMR (Publications 1, 3, 7, 10, 13, 21, 37, and 46)

A. Bielecki,† T. Jarvie, A. Thayer,‡ and A. Pines

Two-dimensional zero-field NMR allows the identification of sites and connectivities in polycrystalline or otherwise disordered materials (see Figure 5-1). This procedure accomplishes structure determinations in such materials where x-ray and neutron-diffraction techniques are limited.

†Present address: Francis Bitter National Magnet Laboratory, M.I.T., Cambridge, MA.

‡Present address: AT&T Bell Laboratories, Murray Hill, NJ.

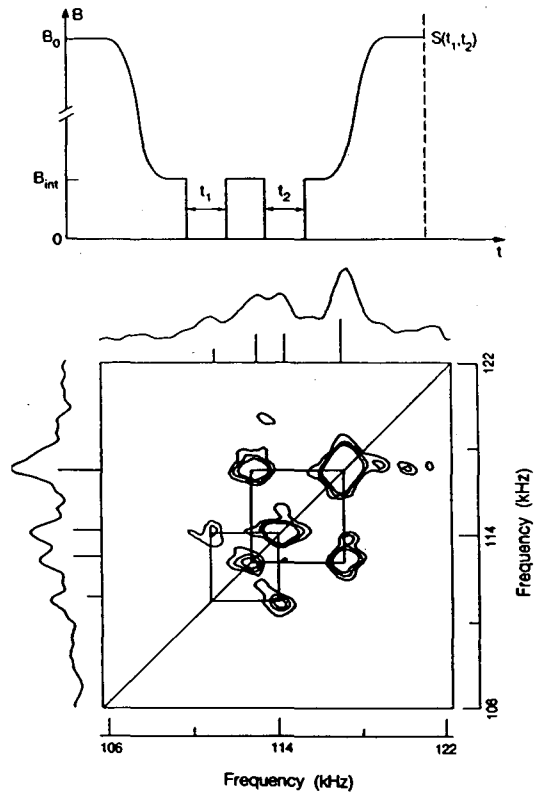

Figure 5-1. Scheme for two-dimensional zero-field NMR, with result on polycrystalline diethylterphthalate-d_4, showing connectivities in the methylene positions. (XBL 863-11043A)

6. Chemical Exchange in Zero Field (Publications 4, 19, and 40)

P. Jonsen,† G. Kothe,‡ P. Meier,‡ M. Trecoske, and A. Pines

The effects of chemical exchange can sometimes not be seen in high-field NMR, whereas the effects are clear in the new form of zero-field spectroscopy (see Figure 6-1). This new procedure can be used to

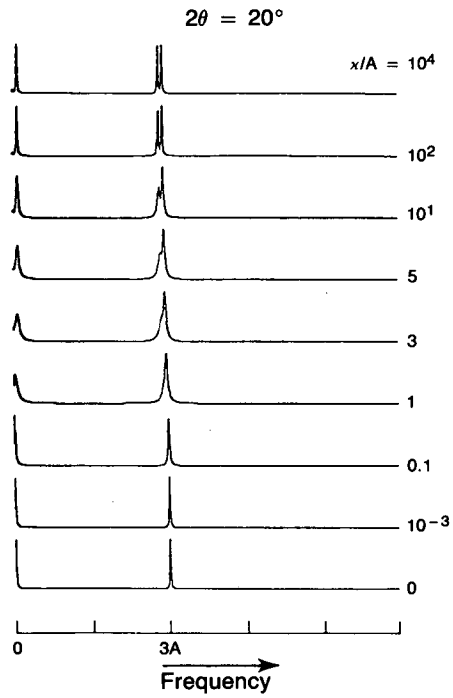

Figure 6-1. Effect of molecular rotational jumps on zero-field NMR spectrum of a proton pair. As the motion sets in, the effective symmetry of the environment is lowered, resulting in line splittings. (XBL 8702-6166)

characterize small-amplitude motions in polymers, molecular crystals, zeolites, and other materials.

†Present address: B.P. Research Centre, ASRD Spectroscopy Branch, Sunbury-on-Thames, Middlesex, England.

‡Permanent address: Institute for Physical Chemistry, University of Stuttgart, Federal Republic of Germany.

7. Correlated Proton Motion in Hydrogen Bonds (Publications 32, 33, and 44)

T. Jarvie, J. Millar,† A. Thayer,‡ and A. Pines

An important question in hydrogen-bonded materials such as ice ferroelectrics and carboxylic acid dimers is whether the proton dynamics are correlated. The correlations of motion have been measured in recent NMR experiments by measuring the asymmetry parameter in dipole-dipole couplings (see Figure 7-1).

†Present address: Department of Chemistry, Yale University, New Haven, CT.

‡Present address: AT&T Bell Laboratories, Murray Hill, NJ.

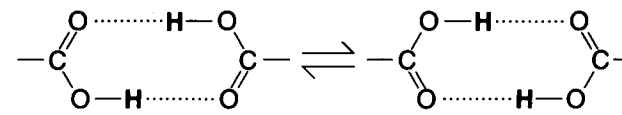

Figure 7-1. Correlated proton motion in a hydrogen-bonded dimer of solid toluic acid. (XBL 8702-6167)

8. Pake Patterns from Zero to High Field (Publication 51)

A. Bielecki† and A. Pines

By new field-cycling techniques in our laboratory, it is possible to follow the NMR spectra from zero to high field. As an example the famous Pake pattern can be followed from the zero-field three-line spectrum to the high-field powder form (see Figure 8-1). Such experiments will be useful in studying materials with wide spectra, such as dispersed metals of the type studied by Slichter, Sinfelt, and coworkers.

†Present address: Francis Bitter National Magnet Laboratory, M.I.T., Cambridge, MA.

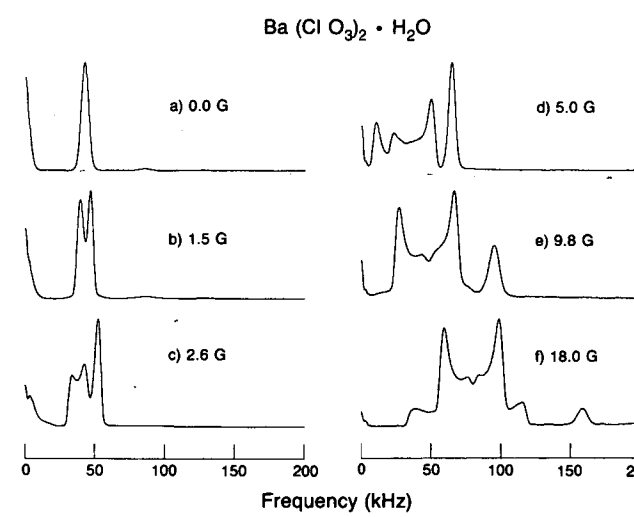

Figure 8-1. Evolution of the NMR spectrum of a polycrystalline hydrate as the field is raised from zero to high values. The emergence of the Pake pattern is clear at high fields. (XBL 8702-6195)

9. Biaxiality in Smectic Liquid Crystals (Publications 30, 35, and 38)

M. Luzar,[†] A. Thayer,[‡] and A. Pines

Smectic liquid crystals are layered or quasi-two-dimensional liquids. An important question concerns the two-dimensional ordering of the molecules in the layers of different smectic phases. By new NMR techniques the symmetries, ordering, and dynamics in these materials can now be studied (see Figure 9-1). The local symmetry can be readily ascertained even if there is no long-range order.

[†]Permanent address: Department of Physics, University of Ljubljana, 61000 Ljubljana, Yugoslavia.
[‡]Present address: AT&T Bell Laboratories, Murray Hill, NJ.

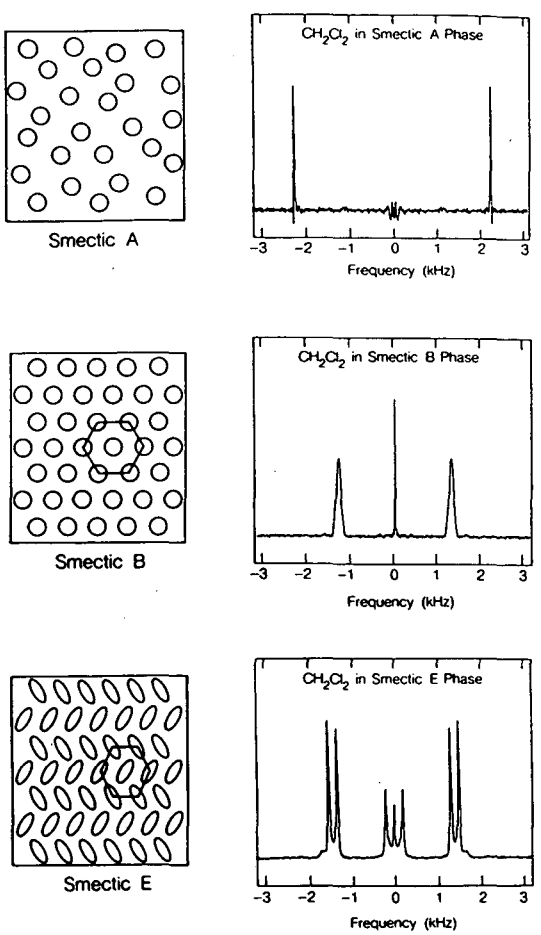

Figure 9-1. Effect of symmetry in smectic (two-dimensional) liquid crystals on zero-field NMR spectra. The herringbone structure of the smectic-E gives rise to a biaxial environment that is clearly visible in the spectra. (XBL 866-11152A)

10. Conformational Probabilities of Hydrocarbon Chains (Publications 17, 22, 31, 42, and 47)

M. Gochin, P. Neidig,[†] H. Zimmermann,[†] and A. Pines

The dynamics of molecular chains are important in many areas, including polymers and molecular biology. By measuring the pair correlations of hydrogens by two-dimensional spectroscopy in hydrocarbon chains, it is possible to establish constraints from which the conformational probabilities can be estimated (see Figure 10-1). These probabilities will be used to study the molecular dynamics of such molecules.

[†]Present address: Max-Planck-Institute, Heidelberg, Federal Republic of Germany.

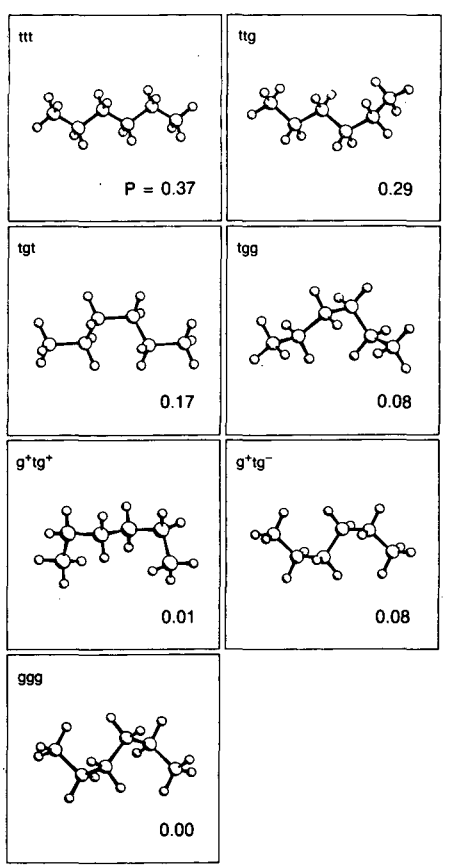

Figure 10-1. Conformational probabilities of hexane partially oriented in a nematic liquid-crystal matrix, as determined by two-dimensional NMR spectroscopy. (XBL 871-9525)

11. Spatially Reduced High-Resolution NMR (Publications 2, 45, and 47)

M. Gochin, D.P. Weitekamp,† and A. Pines

A technique that we term SHARP makes it possible to obtain high-resolution NMR spectra in spatially resolved regions of a sample (see Figure 11-1). This technique will allow the noninvasive determination of composition of a sample even in the presence of broadening by magnetic-field (or magnetic-susceptibility) inhomogeneity. A collaboration with The University of California at San Francisco is under way for medical applications of this technique.

†Present address: Department of Chemistry, California Institute of Technology, Pasadena, CA.

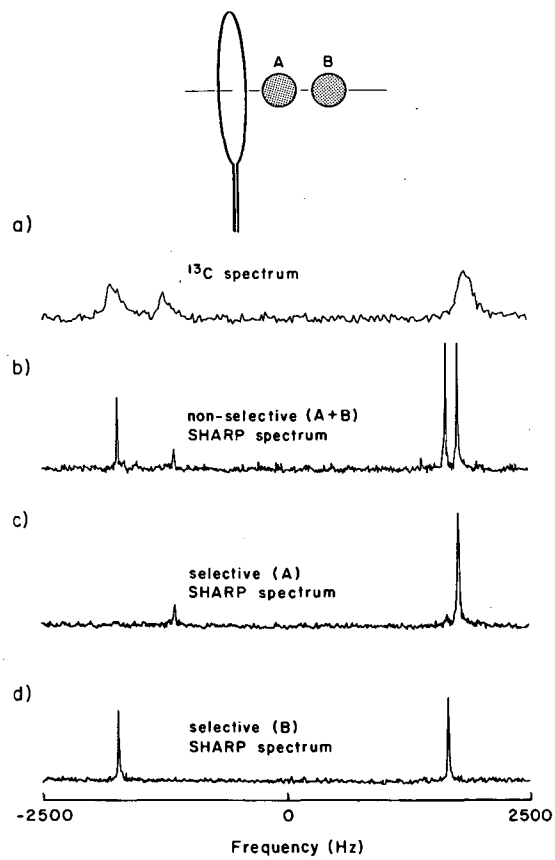

Figure 11-1. Model SHARP experiments demonstrating the spatial localization of NMR signals with high resolution from two tubes in an inhomogeneous field. (XBL 873-715)

12. Xenon NMR in Zeolites and on Surfaces (Publication 49)

L.C. de Menorval, S.B. Liu, D. Raftery, R. Ryoo, D. Shykind, and A. Pines

Xenon is being used as a probe in the study of surfaces by NMR. As an example, there is a difference in the xenon NMR for an occupied zeolite cavity versus one that is not occupied by a substrate. By optical polarization, we plan to use the sensitivity of the xenon NMR to environment in a study of surfaces and distributions of molecules in zeolites (see Figure 12-1). Clusters of molecules and of xenon in cavities have been observed.

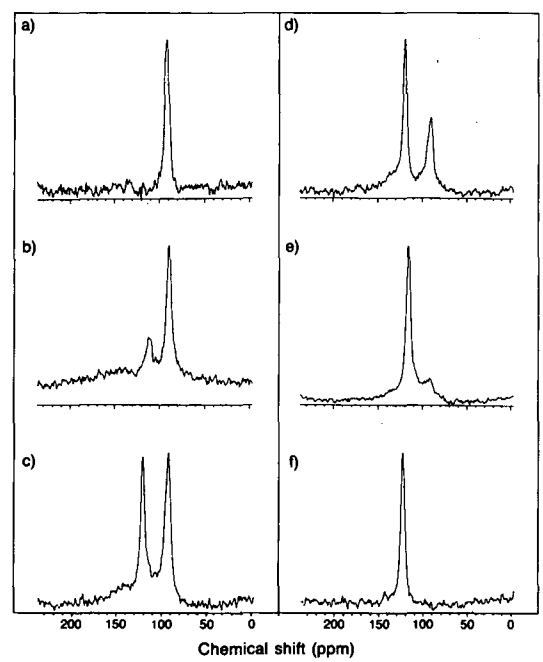

Figure 12-1. Xenon NMR spectra in a zeolite-Y sample exposed to increasing quantities of hexymethylbenzene (HMB). The xenon NMR shows two peaks, one for cavities with HMB and one for empty cavities. This shows that the HMB distribution is uniform at one per cavity at full coverage. (XBL 8702-6196)

13. High-Temperature and Magic-Angle NMR of Silicates (Publications 6, 8, 24, and 26)

S.-B. Liu, J.F. Stebbins,† and A. Pines

A new high-temperature NMR probe has been used to study chemical shifts, lineshapes, and relaxa-

tion times for ^{23}Na and ^{29}Si in alkali silicates and albite ($NaAlSi_3O$) at temperatures up to 1400 K. Spin-lattice relaxation-time data confirm the general picture of the relatively high mobility of the network-modifying alkali cation that has been drawn from studies of bulk transport properties (see Figure 13-1). Anomalies of relaxation times suggest that local-scale atomic motion of both Si and Na are closely related to the macroscopic transition. These observations, together with room-temperature magic-angle spinning NMR studies of silicate and aluminosilicate glasses, provide a first step towards understanding how local motion changes at the glass transition.

†Permanent address: Department of Geology, Stanford University, Stanford, CA.

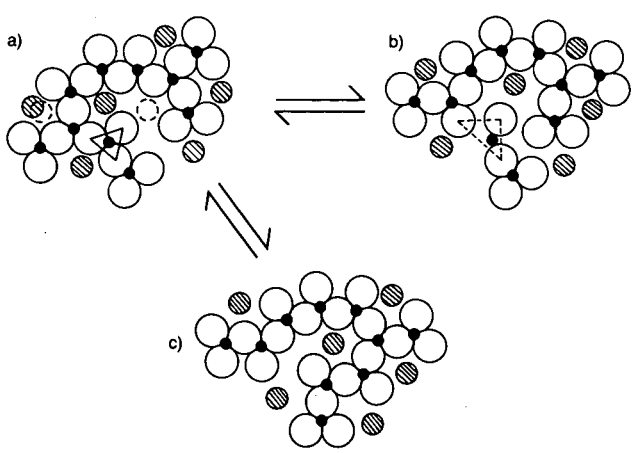

Figure 13-1. Schematic drawing of structure of silicate liquids. (a) Diffusion of the alkali ions (shaded circles). The triangle indicates a basic network forming SiO_4 or AlO_4 unit (black circles: Si or Al; open circles: O). (b) Formation of structurally distorted sites. (c) A breaking of the Si-O bond results in a change in the Si environment (e.g., from a three-coordinate (Q^3) site in (a) to a four-coordinate (Q^4) site). (XBL 8702-6198)

14. Low-Frequency NQR with a SQUID (Publication 50)

A. Bielecki,† N. Fan,‡ J. Clarke, J. Chang, G. Chingas, C. Connor, H. Huber,§ and A. Pines

In a collaborative project, a SQUID detector has been developed for the direct observation of zero-field NMR and NQR (see Figure 14-1). The SQUID should raise the sensitivity to a level that makes field cycling unnecessary. The electronics have been completed, and the SQUID has been tested. NMR experiments are currently under way.

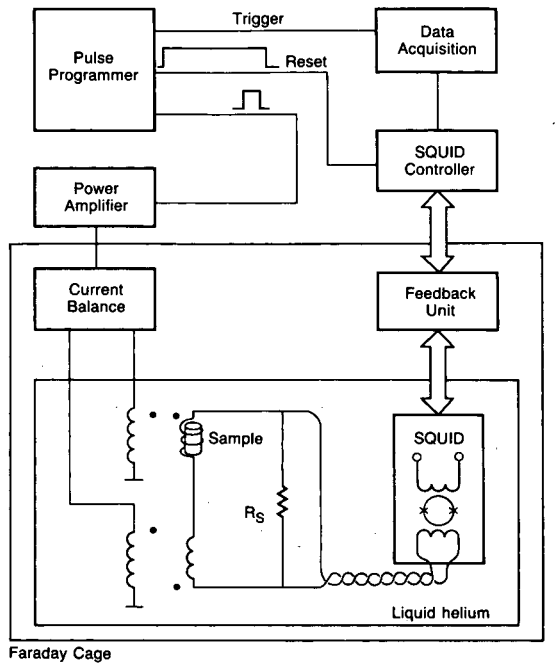

Figure 14-1. Schematic diagram of SQUID spectrometer developed for direct observation of zero-field NMR and NQR. (XBL 8702-6168)

†Present address: Francis Bitter National Magnet Laboratory, M.I.T., Cambridge, MA.

‡Permanent address: Department of Physics, University of California Berkeley, and Center for Advanced Materials, LBL.

§Present address: Institute for Crystallography and Mineralogy. Johann-Wolfgang-Goethe University, Frankfurt, Federal Republic of Germany.

15. Berry's Phase in Magnetic Resonance (Publications 15, 41, and 43)

G. Chingas, R. Harris, D. Suter, and A. Pines

According to Berry, quantum states of a Hamiltonian that varies adiabatically through a circuit C in parameter space may acquire geometrical phase factors $\exp[i\gamma(C)]$ in addition to the normal dynamical phase factors $\exp[(-i/\hbar)\int E_m(t)dt]$. This result is important since it is responsible for the appearance of fractional quantum numbers. We have carried out NMR experiments in the rotating frame that bear out these predictions for simple conical circuits, and point out that they are related to familiar behavior based on classical Bloch equations and on

Haeberlen-Waugh coherent averaging theory (see Figure 15-1). Extensions to coupled spins and electric quadrupolar effects have been made.

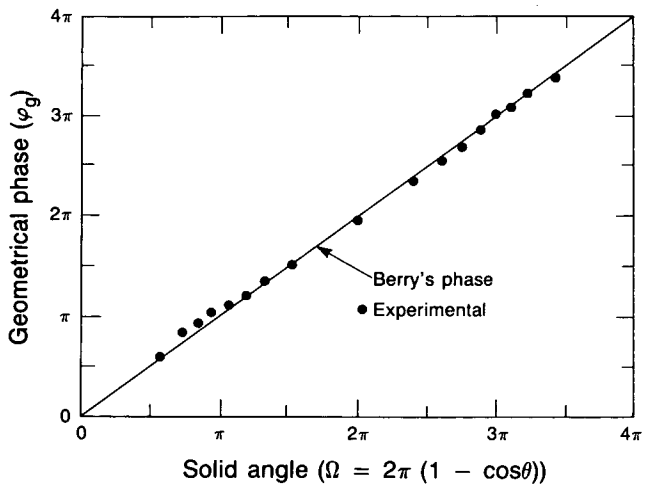

Figure 15-1. Experimental measurement of geometrical phase and comparison to Berry's prediction. (XBL 8702-6141)

1986 PUBLICATIONS AND REPORTS

Refereed Journals

1. D.B. Zax, A. Bielecki, M.A. Kulzick, E.L. Muetterties, and A. Pines, "Zero Field NMR of Solid Bis(μ-Hydrido)-decacarbonyltriosmium," J. Phys. Chem. **90**, 1065 (1986); LBL-18762.
2. J. Baum, R. Tycko, and A. Pines, "Spatially Selective NMR with Broadband RF Pulses," Chem. Phys. **105**, 7 (1986); LBL-20921.
3. A.M. Thayer, J.M. Millar, M. Luzar, T.P. Jarvie, and A. Pines, "Zero Field NMR of a Nematic Liquid Crystal," J. Phys. Chem. **90**, 1577 (1986); LBL-20414.
4. J. Millar, A. Thayer, D.B. Zax, and A. Pines, "Zero Field NMR of Small Amplitude Motions in a Polycrystalline Solid," J. Am. Chem. Soc. **108**, 5113 (1986); LBL-20484.
5. J. Baum, K.K. Gleason, A. Pines, A.N. Garroway, and J. Reimer, "Multiple Quantum NMR Studies of Clustering in Hydrogenated Amorphous Silicon," Phys. Rev. Lett. **56**, 1377 (1986); LBL-20924.
6. J.F. Stebbins, J.B. Murdoch, E. Schneider, I.S.E. Carmichael, and A. Pines, "Defects and Short-range Order in Nepheline Group Minerals: A Silicon-29 Nuclear Magnetic Resonance Study," Phys. Chem. Minerals **13**, 371 (1986); LBL-22684.
7. A. Bielecki, D.B. Zax, K.W. Zilm, and A. Pines, "Zero Field NMR and NQR Spectrometer," Rev. Sci. Instrum. **57**, 393 (1986); LBL-18842.
8. J.F. Stebbins, E. Schneider, J.B. Murdoch, A. Pines, and I.S.E. Carmichael, "A New Probe for High-Temperature Nuclear Magnetic Resonance Spectroscopy with PPM Resolution," Rev. Sci. Instrum. **57**, 39 (1986); LBL-20440.
9. J. Baum and A. Pines, "NMR Studies of Clustering in Solids," J. Am. Chem. Soc. **108**, 7447 (1986); LBL-20922.
10. J.M. Millar, A.M. Thayer, H. Zimmermann, and A. Pines, "High Resolution Studies of Deuterium by Time Domain Zero Field NQR," J. Magn. Reson. **69**, 243 (1986); LBL-20931.
11. M. Munowitz and A. Pines, "Principles and Applications of Multiple-Quantum NMR," Adv. Chem. Phys. **66**, 1 (1986); LBL-21656.
12. M. Munowitz and A. Pines, "Multiple Quantum NMR Spectroscopy," Science **233**, 525 (1986); LBL-21655.
13. A.M. Thayer, J.M. Millar, and A. Pines, "Two-Dimensional Zero Field NMR," Chem. Phys. Lett. **129**, 55 (1986); LBL-20932.
14. H.M. Cho, R. Tycko, A. Pines, and J. Guckenheimer, "Iterative Maps for Bistable Excitation Sequences of Two Level Systems," Phys. Rev. Lett. **56**, 1905 (1986); LBL-20935.
15. D. Suter, A. Pines, and M. Mehring, "Indirect Phase Detection of NMR Spinor Transitions," Phys. Rev. Lett. **56**, 242 (1986); LBL-21396.
16. G. Drobny, D.P. Weitekamp, and A. Pines, "Multiple Quantum Spectrum of Oriented Hexane," Chem. Phys. **108**, 179 (1986); LBL-17168.
17. M. Gochin, K.V. Schenker, H. Zimmermann, and A. Pines, "Determination of Dipole-Dipole Couplings in Oriented n-Hexane by Two Dimensional NMR," J. Am. Chem. Soc. **108**, 6813 (1986); LBL-21654.
18. A. Pines, book review of *Solid State NMR* by Colin F. Fyfe, J. Am. Chem. Soc. **108**, 5373 (1986); LBL-22679.
19. P. Jonsen, M. Luzar, A. Pines, and M. Mehring, "Theory of Chemical Exchange in Zero Field NMR: Two-Site Flips," J. Chem. Phys. **85**, 4873 (1986); LBL-21717.
20. A. Thayer and A. Pines, "Composite Pulses in Zero Field NMR," J. Magn. Reson. **70**, 518 (1986); LBL-22032.

LBL Reports

21. A. Thayer and A. Pines, "Zero-Field NMR," Acct. Chem. Res. (in press); LBL-21458.
22. M. Gochin, D. Hugi-Cleary, H. Zimmermann, and A. Pines, "Two-Dimensional Multiple-Quantum NMR of Isotopic Mixtures in Liquid Crystals," Mol. Phys. (in press); LBL-21815.
23. A.J. Shaka and A. Pines, "Symmetric Phase Alternating Composite Pulses," J. Magn. Reson. (in press); LBL-22031.
24. J.B. Murdoch, J.F. Stebbins, I.S.E. Carmichael, and A. Pines, "A Silicon-29 Nuclear Magnetic Resonance Study of Silicon-Aluminum Ordering in Leucite and Analcite," Phys. Chem. Minerals (in press); LBL-22552.

25. A. Pines, "Lectures on Pulsed NMR," in *Proc. Fermi School on Physics of NMR in Biology and Medicine*, B. Maraviglia, Ed. (in press); LBL-22316.
26. E. Schneider, J.F. Stebbins, and A. Pines, "Speciation and Local Structure in Alkali and Alkaline Earth Silicate Glasses: Constraints from Si-29 NMR Spectroscopy," J. Noncryst. Solids (in press); LBL-22391.
27. H. Cho, J. Baum, and A. Pines, "Iterative Maps with Multiple Fixed Points for Excitation of Two Level Systems," J. Chem. Phys. (in press); LBL-22390.
28. D. Suter, K.V. Schenker, and A. Pines, "Theory of Broadband Heteronuclear Decoupling in Solids," J. Magn. Reson. (in press); LBL-22439.
29. K.V. Schenker, D. Suter, and A. Pines, "Heteronuclear Broadband Spin Decoupling in the Presence of Homonuclear Interactions," J. Magn. Reson. (in press); LBL-22440.
30. A.M. Thayer, M. Luzar, and A. Pines, "Zero Field NMR of Nematic Liquid Crystals with Positive and Negative Magnetic Susceptibility Anisotropies," J. Phys. Chem. (in press); LBL-22436.
31. M. Gochin, H. Zimmermann, and A. Pines, "Assignment of the Dipolar Couplings and Estimation of Conformational Probabilities in Partially Oriented Hexane," submitted to Chem. Phys. Lett.; LBL-22434.
32. M. Luzar, A.M. Thayer, and A. Pines, "Quenching of Residual Fields by Asymmetric Dipolar Coupling in Zero Field NMR," J. Magn. Reson. (in press); LBL-22435.
33. T. Jarvie, A.M. Thayer, J. Millar, and A. Pines, "Effect of Correlated Proton Jumps on the Zero Field NMR Spectrum of Solid p-Toluic Acid," submitted to J. Phys. Chem.; LBL-22437.
34. D. Suter, S.B. Liu, and A. Pines, "Multiple Quantum Excitation in Solids with a One Quantum Hamiltonian," J. Magn. Reson. (in press); LBL-22438.
35. A.M. Thayer, M. Luzar, and A. Pines, "Zero Field NMR Study of the Biaxial Smectic E Phase," Liquid Crystals (in press); LBL-22441.
36. M. Munowitz, M. Mehring, and A. Pines, "Multiple Quantum Dynamics: A Directed Walk through Liouville Space," J. Chem. Phys. (in press); LBL-22443.
37. A. Thayer, M. Luzar, and A. Pines, "Zero Field NMR of Heteronuclear Spin Systems in Liquid Crystal Solvents," J. Magn. Reson. (in press); LBL-22671.
38. M. Luzar, A. Thayer, and A. Pines, "Zero Field NMR of Uniaxial and Biaxial Smectic Liquid Crystals," Liquid Crystals (in press); LBL-22677.
39. H. Cho and A. Pines, "Iterative Maps for Broadband Excitation of Transverse Coherence in Two-Level Systems," submitted to J. Chem. Phys.; LBL-22680.
40. P. Meier, G. Kothe, P. Jonsen, M. Trecoske, and A. Pines, "Theory of Dynamic NMR in Zero Field Lineshapes in the Presence of Molecular Motion," LBL-22994.
41. D. Suter, G. Chingas, R.A. Harris, and A. Pines, "Berry's Phase in Magnetic Resonance," LBL-22995.
42. M. Gochin, H. Zimmermann, and A. Pines, "Assignment of Dipolar Couplings and Estimation of Conformational Probabilities in Partially Oriented Hexane," submitted to Chem. Phys. Lett.; LBL-22434.
43. C. Lee, D. Suter, and A. Pines, "Theory of Multiple Pulse NMR in Low and Zero Fields," submitted to J. Magn. Reson.; LBL-22442.
44. J.M. Millar (Ph.D. Thesis), "Proton and Deuterium NMR Experiments in Zero Field," LBL-21260.
45. J.S. Baum (Ph.D. Thesis), "NMR Studies of Selective Population Inversion and Spin Clustering," LBL-21259.
46. A. Thayer (Ph.D. Thesis), "Pulsed Zero Field NMR of Solids and Liquid Crystals," LBL-22991.
47. M. Gochin (Ph.D. Thesis), "Two-Dimensional NMR in Liquids and Oriented Molecules," LBL-22992.
48. H. Cho (Ph.D. Thesis), "Iterative Maps on SO(3)," LBL-22993.
49. L.C. de Menorval, S.-B. Liu, D. Raftery, R. Ryoo, D. Shykind, and A. Pines, "Xenon NMR in Zeolites and on Surfaces," LBL-23084.
50. A. Bielecki, N. Fan, J. Clarke, J. Chang, G. Chingas, C. Connor, H. Huber, and A. Pines, "Low Frequency NQR with a SQUID," LBL-23085.
51. A. Bielecki and A. Pines, "Pake Patterns from Zero to High Field," LBL-23091.

Invited Talks

52. A. Pines, "NMR at Zero Magnetic Field," Mobil Research and Development Corp., Princeton, NJ, Jan. 10, 1986.
53. A. Pines, "NMR with Lots of Quanta and No Magnetic Field," University of Chicago, Jan. 13, 1986.
54. A. Pines, "Iterative Maps on SO(3)," Non-Linear Dynamics Group, Department of Mathematics, University of California Berkeley, March 6, 1986.
55. A. Pines, "Developments in Zero Field NMR," APS March Meeting, Las Vegas, NV, April 1, 1986.
56. A. Pines, "Pulsed NMR at Zero Field," Royal Society Meeting, University of Oxford, England, April 9–11, 1986.
57. A. Pines, "Applications of NQR by Pulsed Field Cycling," Imperial Chemical Industries, New Science Group, Runcorn, United Kingdom, April 8, 1986.
58. A. Pines, "Some Recent Pulsed NMR Experiments in Fields High and Low," 27th Nuclear Magnetic Resonance Spectroscopy Conference, Baltimore, MD, April 12–17, 1986.
59. A. Pines, "Disorder-Order Transitions in Modern Research and Freshman Chemistry," Conference of the California Association of Chemistry Teachers, University of the Pacific, Stockton, CA, April 19, 1986.
60. A. Pines, "NMR on Surfaces," Delaware 7th NMR Symposium, Brown Laboratories, University of Delaware, June 3, 1986.
61. A. Pines, "Studies of Clustering by Solid State Multiple Quantum NMR," 8th European Experimental NMR Conference SPA, Belgium, June 3–6, 1986.

62. M. Gochin, "Determination of Molecular Structure in a Liquid Crystal by Two-Dimensional NMR," 11th International Liquid Crystal Conference, Berkeley, CA, July 4, 1986.
63. M. Luzar, "Zero Field NMR of Liquid Crystals," 11th International Liquid Crystal Conference, Berkeley, CA, July 4, 1986.
64. A. Pines, "Some Developments in NMR of Oriented Molecules," 9th ISMAR Meeting, Rio de Janeiro, Brazil, June 29–July 5, 1986.
65. A. Pines, "Lectures on Pulsed NMR," Fermi School on Physics, Varenna, Italy, July 8–18, 1986.
66. A. Pines, "Recent Developments in Solid State NMR," Gordon Research Conference on High Temperature Chemistry, Brewster Academy, Wolfeboro, NH, July 24, 1986.
67. K. Schenker, "Multiple Quantum NMR of Liquid Crystals and Solids," 28th Rocky Mountain Conference, Denver, CO, Aug. 3–7, 1986.
68. P. Jonsen, "Chemical Exchange in Zero Field NMR," 28th Rocky Mountain Conference, Denver, CO, Aug. 3–7, 1986.
69. D. Suter, "Detection of NMR Transitions," 28th Rocky Mountain Conference, Denver, CO, Aug. 3–7, 1986.
70. A. Pines, "Developments in High and Zero Field NMR of Possible Revelance to Biology," Gordon Conference on Magnetic Resonance in Biology and Medicine, Aug. 7, 1986.
71. A. Pines, "Fact and Fiction in Chemistry," Department Seminar, Mills College, Oakland, CA, Aug. 12, 1986.
72. A. Pines, "NMR with Lots of Photons and No Magnetic Field," XXIII Congress Ampere, Rome, Italy, Sept. 15–19, 1986.
73. A. Pines, "Developments in Zero Field NMR," British Radiofrequency Spectroscopy Meeting, New Methods in Magnetic Resonance Meeting, York, England, Sept. 8–10, 1986.
74. A. Pines, "Some Developments in High and Zero Field NMR of Possible Interest in Biology," XII International Conference on Magnetic Resonance in Biological Systems, Todtmoos, Federal Republic of Germany, Sept. 8–12, 1986.
75. A. Pines, "Some Recent Pulsed NMR Experiments," Department of Chemistry, University of Iowa, Ames, Oct. 3, 1986.
76. A. Pines, "Irreversibility?" Department of Physics and Astronomy, Sonoma State University, Rohnert Park, CA, Oct. 20, 1986.
77. A. Pines, "Some Magnetic Moments," Chemistry Department, California Institute of Technology, Pasadena, Nov. 6, 1986.
78. A. Pines, Colloquium, Departments of Chemistry and Physics, Kyoto University, Japan, Nov. 10, 1986.
79. A. Pines, "Two-Dimensional and Zero Field NMR of Oriented Molecules," 25th Annual NMR Symposium, Tokyo, Japan, Nov. 12–14, 1986.
80. A. Pines, "Recent Pulse Experiments at Berkeley," Advanced FT-NMR Meeting, JEOL, Tokyo, Japan, Nov. 15, 1986.

Synthesis of Novel Solids*

Angelica M. Stacy, Investigator

INTRODUCTION

The goal of this research is to synthesize advanced materials with novel properties. Initial work is focused on transition-metal and rare-earth sulfides and phosphides. These materials have a variety of interesting properties and have uses as batteries, fuel cells, superconductors, optical detectors, catalysts, and in solar-energy conversion. Synthetic procedures involving reactions both at ambient conditions in solution and at elevated temperatures in fluxes are being investigated. Such synthetic studies will lead to numerous new classes of materials with novel optical, magnetic, electronic, and surface properties.

1. Transition-Metal Dithiophosphates (Publication 1)

M.A. Dixon and A.M. Stacy

The crystal structure, optical, and magnetic properties of di(n-butyl)dithiophosphinate cobalt II have been determined. In contrast to the phosphinate analogues, which are polymeric, this dithiophosphinate is dimeric in the solid state, with four dimers per unit cell with the formula $\{Co[S_2P(C_4H_9)_2]_2\}_2$. Two of the di(n-butyl)dithiophosphinate ligands are chelating, one on each Co^{+2} in the dimer, and two bridge between the Co^{+2} ions. The coordination about each Co^{+2} ion is a distorted trigonal prism of five sulfur atoms, with four sulfur atoms at a distance of ~2.3 Å and one at a distance of 3.0 Å.

The magnetic properties of the dimer were measured over the 5–300 K temperature range and in fields up to 40 kG. Analysis of the data above 30 K gave a Curie constant of 2.43 per mole with a calculated moment of 4.4 Bohr magnetons (BM) and a Weiss constant of −9.1 K. This corresponds well to Co^{+2} in a distorted tetrahedral environment. At low temperatures, in a field of 5 kG, a cusp is observed at 15 K with a rapid decrease in the susceptibility as the temperature is lowered below 15 K; the spins on the cobalt ions pair due to weak superexchange interactions through the S-P-S bridging ligands. It is interesting that the magnetism is affected by the field at low temperatures; at 40 kG, the cusp in the susceptibility occurs at 11 K.

2. Rare-Earth Transition-Metal Phosphides (Publication 2)

J.V. Badding and A.M. Stacy

The structure and magnetic properties of the europium nickel phosphide phase, $EuNi_5P_3$, were studied. This new phosphide crystallizes in the orthorhombic space group Cmcm into highly reflective, long, thin needles. The refinement of the crystal structure from single-crystal x-ray data shows that this phosphide is isostructural with $LaCo_5P_3$; there are four formula units per unit cell, and all the europium atoms are in equivalent positions. An interesting feature of this compound is that the Eu-Eu distance in the a direction, which is the needle axis, is 3.60 Å, while in all other directions the Eu-Eu distance is >6 Å; the magnetic behavior of $EuNi_5P_3$ with the magnetic field applied along the europium chains is quite unusual.

The magnetic properties of single crystals of $EuNi_5P_3$, measured along various crystallographic axes, were investigated in order to determine the nature of the interactions between the europium ions. A fit of the inverse susceptibility vs. temperature between 160 K and 280 K gives a moment of 8.02 BM, which is very close to the free-ion value for Eu^{+2}. In fields below 5 kG, the temperature dependence of the magnetization with the field oriented along the a, b, and c axes is characteristic of an antiferromagnet with its easy axis parallel to the a axis. The Neel temperature is near 7.5 K. Below 7.5 K, when fields larger than 5 kG are applied along the a direction, there are a series of complex steps in the magnetization with increasing field. Since hysteresis is associated with these steps, it is likely that the transitions are first order. For fields near the first transition, a magnetic aftereffect is observed with a logarithmic time dependence. Such intriguing magnetic behavior is rare and warrants further investigation.

*This work was supported by the Director, Office of Energy Research, Office of Basic Energy Sciences, Materials Sciences Division of the U.S. Department of Energy under Contract No. DE-AC03-76SF00098.

3. Work in Progress

Studies of the rare-earth thiophosphates and phosphides will continue. New synthetic routes will be designed, at both ambient temperatures and using fluxes at elevated temperatures. The solid-state properties of the RPS_4 phases and $EuNi_5P_3$ will be investigated further.

1986 PUBLICATIONS AND REPORTS

Other Publications

1. M.A. Dixon and A.M. Stacy, "Field-Dependent Antiferromagnetic Ordering in Dimeric Di(n-butyl)dithiophosphate Cobalt II," submitted to Inorg. Chem.
2. J.V. Badding and A.M. Stacy, "Magnetic Phase Transitions in $EuNi_5P_3$: Unusual Steps in the Magnetization with Field," submitted to Phys. Rev. B.

Raman Studies of Surface Processes*

Gerd M. Rosenblatt, Investigator

INTRODUCTION

This project is designed to obtain Raman frequency shifts and intensities from submonolayer adsorbates, either physically or chemically adsorbed, on well-defined metal single-crystal surfaces under ultrahigh-vacuum (UHV) conditions. For physically adsorbed molecular species, vibrational and, for the first time, rotational frequency shifts will be measured without resonant or surface enhancement. The project's long-range goals are (a) to gain new information about how molecules rotate, vibrate, move, and react on well-defined surfaces and (b) to use the fundamental understanding gained under UHV conditions to extend the technique to a range of chemically important pressures, temperatures, and interfaces. In addition, research on gas-phase Raman spectroscopy of the isotopes of molecular hydrogen, begun at Los Alamos National Laboratory, is being completed at Berkeley.

1. Raman Line Positions in Molecular Hydrogen: H_2, HD, HT, DT, and T_2 (Publication 2)†

D.K. Veirs and G.M. Rosenblatt

Spontaneous Raman spectroscopy is used to determine line positions of the six isotopomers of molecular hydrogen: H_2, HD, HT, D_2, DT, and T_2. State populations as low as 1.3×10^8 are detected with the present experimental apparatus. This sensitivity makes possible measurement of the first overtone Q-branch line positions for H_2 and D_2 and of higher rotational transitions than previous investigations. The line positions for D_2, DT, and T_2 indicated that literature values for molecular parameters do not predict accurately line positions of transitions at J values above the observed transitions from which they were determined. The results for the six molecular isotopomers show that *ab initio* energy levels restricted to the adiabatic approximation do not yield line positions within the experimental uncertainty whereas recent nonadiabatic calculations reproduce the present observations. Reexamination of literature results at high energies indicates discrepancies between the theoretical calculations and experimental vibrational-band origins for all vibrational levels in HT, DT, and T_2. No experimental measurements are currently available that test the accuracy of nonadiabatic *ab initio* rotational levels at high energies.

*This work was supported by the Director's Program Development Funds of the Lawrence Berkeley Laboratory under Contract No. DE-AC03-76SF00098.

†The experimental portion of this work was carried out at Los Alamos National Laboratory, operated by the University of California for the United States Department of Energy under Contract No. W-7405-ENG-36 through Contract No. DE-AC03-76SF00098.

2. Structure and Properties of Sputtered Carbon Overlayers on Rigid Magnetic Media Disks (Publication 3)†

H-c. Tsai,‡ D.B. Bogy,‡ D.K. Veirs, M. Hilton, and S. Mayer

In the present study, various techniques are employed to probe the microstructure and chemical bonding in sputtered carbon overlayers on rigid disks. These include routine structure characterization (Knoop microhardness and x-ray diffraction) as well as surface techniques: Auger spectroscopy, ellipsometry, and Raman spectroscopy. The routine structure-characterization techniques were unable to provide any useful information. Auger spectroscopy revealed that the carbon overlayers are amorphous, but did not indicate any differences between samples. Ellipsometry determined the thickness of the overlayers to be 180 Å. Raman spectroscopy indicated amorphous carbon with a mixture of threefold- and fourfold-coordinated carbon atoms. Peak-position shifts and changes in relative intensity in the Raman spectrum indicate that graphitization proceeds upon annealing. Raman spectra of samples from two manufactures (Figures 2-1 and 2-2) show substantial differences in chemical bonding within the overlayers between manufactures.

†The Raman spectroscopy portion of this work was supported by the Director's Program Development Funds of the Lawrence Berkeley Laboratory under Contract No. DE-AC03-76SF00098.

‡Present address: University of California, Berkeley, CA 94120.

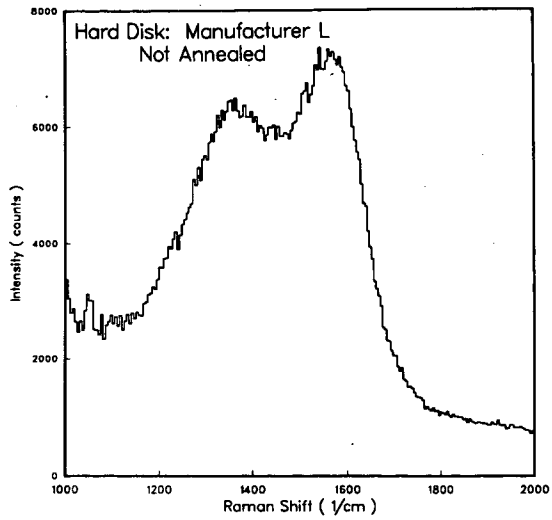

Figure 2-1. Raman spectra of carbon overcoats on rigid magnetic media (hard disks), 1000–2000 cm^{-1} region. The peaks at 1350 cm^{-1} and 1565 cm^{-1} are broad and shifted from graphite, indicative of an amorphous carbon film. (XBL 8612-4874)

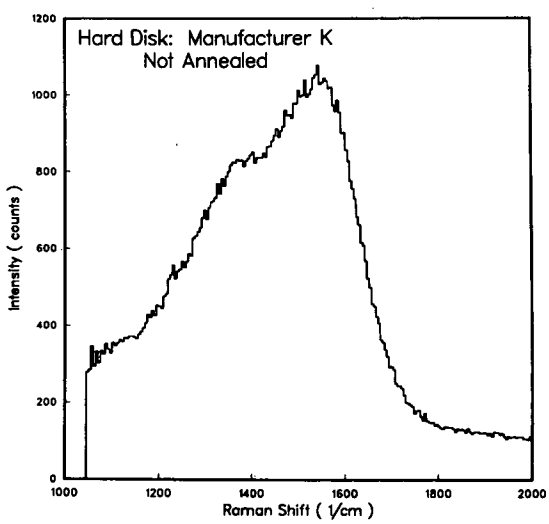

Figure 2-2. Raman spectra of carbon overcoats on rigid magnetic media (hard disks), 1000–2000 cm^{-1} region. The broadening of the 1350 cm^{-1} and 1565 cm^{-1} peaks to a single broad peak indicates a "diamond-like" carbon film with improved properties, i.e., increased hardness and electrical resistivity. (XBL 8612-4870)

3. Work in Progress

Raman spectroscopy has benefited from recent advances in the technology of lasers, optics, thin-film interference filters, and multichannel detectors. A new generation of imaging detectors based on microchannel plates with position-sensitive anodes provides true single-photon counting capability that is expected to increase the sensitivity of Raman spectroscopy. An increase in sensitivity will be particularly useful for Raman spectroscopy of interfaces without resonance surface enhancement. A Raman spectroscopy system incorporating one of these new imaging photomultiplier tubes has been constructed. The position-sensitive detector has a resolution of 70 μm in both the x and y axis on a 1-inch diameter photocathode with a dark count of 30 counts per second (cps). Characterization of this system's capabilities is in progress. Initial results indicate significant increases in sensitivity and signal:noise ratio compared to conventional scanning systems or those using standard intensified photodiode array detectors.

H_2 physically adsorbed on Ag will be investigated by integrating the Raman apparatus with a dedicated UHV system that has LEED, Auger, argon-ion sputtering, and sample-cooling capabilities. Published HREELS studies have shown that H_2 physically adsorbed on the (111) face of Ag is a 3-dimensional free rotor that may have a slightly contracted internuclear distance relative to gaseous H_2. Acquisition of heretofore unavailable pure-rotational, high-resolution Raman spectra will allow the effect of adsorption on the intramolecular potential and internuclear distance of H_2 to be studied. The molecule-surface potential will be investigated from the molecule-surface vibrational-frequency shifts that are expected to be imprinted upon the larger rotational Raman shifts. Experimental measurements of this potential are needed by theorists examining molecule-surface interactions.

1986 PUBLICATIONS AND REPORTS

Other Publications

1. D.K. Veirs and G.M. Rosenblatt, "Vibrational Spacings in Molecular Hydrogen," in *Proc. Tenth Int. Conf. Raman Spectroscopy,* W.L. Peticolas and B. Hudson, eds. 1986, p. 15; LBL-22511.

LBL Reports

2. D.K. Veirs and G.M. Rosenblatt, "Raman Line Positions in Molecular Hydrogen: H_2, HD, HT, D_2, DT, and T_2," J. Mol. Spec. (in press); LBL-20845.
3. H-c. Tsai, D.B. Bogy, D.K. Veirs, M. Hilton, and S. Mayer, "Structure and Properties of Sputtered Carbon Overlayers on Rigid Magnetic Media Disks," LBL-22762.

Invited Talks

4. D.K. Veirs and G.M. Rosenblatt, "Raman Studies of Molecular Hydrogen," Conference on Quantitative Spectroscopy and Laser Diagnostics, San Diego, CA, July 1986.

Chemical Sciences

FUNDAMENTAL INTERACTIONS

PHOTOCHEMICAL AND RADIATION SCIENCES

Photon-Assisted Surface Reactions, Materials, and Mechanisms*

Gabor A. Somorjai, Investigator

INTRODUCTION

This project explores the surface science of photocatalyzed chemical reactions that take place at the solid-vapor and solid-liquid interfaces. We focus on processes that thermodynamically could not occur without the presence of light as the energy source. The photodissociation of water to produce hydrogen and oxygen, of nitrogen to form ammonia, and of carbon dioxide to produce formic acid are investigated. The catalysts are semiconductor surfaces that absorb and convert light to separated, excited electron-electron vacancy pairs that initiate the reduction and oxidation of adsorbed species. The materials that are being used include iron oxides, silicates, and oxides of titanium, tungsten, and molybdenum. The purpose of these studies is to explore the elementary steps of the photon-assisted surface reaction by a combination of modern surface-science techniques and then to establish the optimum conditions (of surface structure, composition, temperature, and reactant mixture) to maximize the rate of production of desired chemicals.

1. Solid-State and Electrochemical Properties of Fe_2O_3 Catalysts (Publications 1–3)

C. Sanchez, M. Hendewerk, K.D. Sieber, H. Nakanishi, M. Salmeron, and G.A. Somorjai

Two types of Fe_2O_3 samples have been studied that differ in either the reduction-oxidation pretreatment or in their doping with niobium and other elements.

The reduction-oxidation pretreatment consists of a sequential reduction in a mixture of H_2 (70%) and H_2O vapor (30%) and subsequent oxidation in O_2 or air at 450°C for 10 min. This treatment produces several changes in the samples, as revealed by x-ray diffraction, chemical titration, and Mössbauer spectroscopy. They include the formation of small amounts of γ-Fe_2O_3 and Fe_3O_4 (<10%), and an even smaller amount of paramagnetic Fe(II). With the use of the surface-sensitive conversion-electric Mössbauer spectroscopy (CEMS), we hope to obtain information on the transformation of the surface region of Fe_2O_3 that appears so successful in activating the catalysts for H_2 and N_2 photodissociation reactions.

We have performed a series of studies using photoelectrochemical techniques to determine the solid-state electronic properties of iron oxides that might control their solid-liquid interfacial chemistry. Photocurrent measurements indicated the excellent behavior of our samples. At +0.5 V bias with respect to SCE (pH = 13), the photocurrents were 120 $\mu A/cm^2$ for the reduced-oxidized samples and 250 $\mu A/cm^2$ for the 0.1% Nb-doped samples, using a 150-W Xe lamp that produced 20 mW/cm^2 at the sample.

Another important parameter that controls the solid-state/liquid-phase interfacial chemistry is the flat-band potential. For any reaction that involves electron transfer to the solution to be thermodynamically feasible, the flat-band potential must be negative (cathodic) with respect to the H^+/H_2 redox potential. We have thus extensively studied the position of the flat-band potential in our samples using the Mott-Schottky technique. In both types of samples the values obtained varied between −0.9 and −1.2 V with respect to SCE at pH = 13. The variation is due probably to modifications of the surface of Fe_2O_3 in the course of the experiment whenever the bias voltage approaches the H^+/H_2 potential (−1.01 V). For that reason, the experiments are never carried beyond −0.8 V. The values obtained for the flat-band potential indicate thermodynamic feasibility if not much driving force for the H_2O reaction. The measurement of the photocurrent as a function of light wavelength indicates the existence of a threshold at 2.1 to 2.3 eV photon energy with

*This work was supported by the Director, Office of Energy Research, Office of Basic Energy Sciences, Chemical Sciences Division of the U.S. Department of Energy under Contract No. DE-AC03-76SF00098.

the sample biased at +0.5 V (SCE, pH = 13). The photocurrents varied linearly with light intensity between 0 and 30 mW/cm^2.

2. Photochemical Production of H_2, O_2, and NH_3 (Publications 5 and 6)

M. Khader, N. Lichtin, G. Vurens, M. Salmeron, I-K. Kim, and G.A Somorjai

We have performed many experiments with a new closed-loop microreactor that allowed us to measure the catalytic production of H_2 from H_2O-photosplitting reactions. The reaction has now been observed for both powders and pellets of the reduced-oxidized samples. NH_3 production from N_2 photodissociation in H_2O has also been studied. We have measured in both cases the dependence of the reaction rate on wavelength and light intensity. As in the case of photocurrent measurements, the threshold for the photoreaction is found at photon energies above 2.2 eV. In these experiments the sample is immersed in the solution without any external electrical connection.

In the case of H_2O-photosplitting reactions, we have measured the oxidation products as well. To avoid ambiguities due to possible air leaks into the reaction loop, we used $H_2^{18}O$ labeled water. The amount of O_2 detected ($^{34}O_2$, $^{36}O_2$) corresponds to 40 $\pm$ 15% of the amount of H_2 detected in the same experiment.

3. Surface-Science Studies (Publication 4)

M. Hendewerk, M. Salmeron, and G.A. Somorjai

Our major effort in this area has been the development of the new surface-sensitive CEMS, mentioned above, that will allow us to study the surface structure of Fe_2O_3 in a much better way than with x-ray photoelectron spectroscopy that we used in the past. In our first successful experiments with the gas-phase proportional counter, the surface sensitivity could be clearly demonstrated by the enhancement of the second and fifth peak intensities of the hyperfine structure peaks of α-Fe with respect to those in the corresponding bulk spectrum. These studies will next be performed in UHV using the channeltron electron multiplier detector.

We have also performed thermal-decomposition experiments to detect the evolution of O_2 from the Fe_2O_3 lattice. The purpose is to study the possible exchange between ^{18}O from the $H_2^{18}O$ solution and lattice oxygen during the photoassisted H_2O decomposition. Our first qualitative experiments indicate that $^{34}O_2$ is indeed observed after the sample is removed from the $H_2^{18}O$ solution. We are presently investigating the dependence of the intensity of the $^{34}O_2$ peak on the reaction conditions (light intensity, wavelength). We have also initiated a series of experiments aimed at characterizing the metal-oxide interface contact, as well as to provide a model system for the study of the surface properties of extremely thin films of Fe_2O_3. Using a Pt(111) substrate we have deposited Fe (and subsequently oxidized it) in a controlled way.

We have monitored the growth of the iron oxide films with Auger spectroscopy and with CO thermal desorption to titrate the amount of uncovered platinum. We have determined the monolayer coverage by this last technique and concluded that up to one monolayer the film grows two-dimensionally. After annealing to approximately 600°C an ordered oxide monolayer of iron oxide is obtained, as determined by low-energy electron diffraction. The structure formed is a coincidence lattice with a long repeating distance (several times the Pt-Pt periodicity). We are presently continuing these experiments to determine the geometric structure of this interesting oxide-metal interface. We are also performing photoemission experiments (UPS, HeI) to characterize the electronic structure. These studies will be followed by chemisorption of simple molecules (H_2, H_2O, etc.) and by CEMS to obtain information on the oxidation state and coordination structure of Fe as the film grows on the Pt(111) substrate.

4. Work in Progress

With respect to preparation and characterization of catalysts, we continue the study of the electrochemical and solid-state properties of the new Nb-doped Fe_2O_3 samples, as they show great promise in terms of enhanced photocurrents. We are also exploring a new dopant, Cu, that has been shown in preliminary experiments to produce even higher photocurrents. As in the past we are making use of x-ray diffraction techniques, scanning electron microscopy to study surface micromorphology, and electrochemical techniques (cyclic voltammetry, Mott-Schottky measurements) to characterize the solid-state properties of our samples. Mössbauer spectroscopy to characterize the bulk structure of the oxides is also used extensively.

1986 PUBLICATIONS AND REPORTS

Refereed Journals

1. C. Sanchez, M. Hendewerk, K.D. Sieber, and G.A. Somorjai, "Synthesis, Bulk and Surface Characterization of Niobium Doped Fe_2O_3 Single Crystals," J. Solid State Chem. **61**, 47 (1986); LBL-19022.
2. H. Nakanishi, C. Sanchez, M. Hendewerk, and G.A. Somorjai, "Photochemical Hydrogen Production from a Water-Methanol Mixture with Iron Oxide Suspensions," J. Phys. Chem., Mat. Res. Bull **21**, 137 (1986); LBL-19274.

Other Publications

3. M. Salmeron and G.A. Somorjai, "Surface Properties of Catalysts. Iron and its Oxides, Surface Chemistry, Photochemistry and Catalysis," NATO Advanced Research Workshop on Homogeneous and Heterogeneous Photocatalysis, Maratea, Italy, in *Homogeneous and Heterogeneous Photocatalysis*, E. Pelizzetti and N. Serpone, eds. D. Reidel Publishing Co., 1986, p. 445; LBL-20358.

LBL Reports

4. M. Hendewerk, M. Salmeron, and G.A. Somorjai, "Water Adsorption on the (001) Plane of Fe_2O_3: An XPS, UPS, Auger, and TPD Study," Surf. Sci., **172**, 544 (1986); LBL-20663.
5. M. Khader, N. Lichtin, G. Vurens, M. Salmeron, and G.A. Somorjai, "Photoassisted Catalytic Dissociation of H_2O and Reduction of N_2 to NH_3 on Partially Reduced α-Fe_2O_3," submitted to Langmuir; LBL-21759.
6. M.M. Khader, G.H. Vurens, I-K. Kim, M. Salmeron, and G.A. Somorjai, "Photoassisted Catalytic Dissociation of H_2O To Produce Hydrogen on Partially Reduced α-Fe_2O_3," submitted to J. Am. Chem. Soc.; LBL-22380.

Invited Talks

7. G.A. Somorjai, Stony Brook Chemistry Lectures, Stony Brook, NY, Mar. 4–6, 1986.
8. G.A. Somorjai, "The Surface Science of Energy Conversion through Metal Catalysis," Musher Lecture, Hebrew University, Jerusalem, Israel, April 9, 1986.
9. G.A. Somorjai, "The Surface Science of Chemical Energy Conversion," Weizman Institute, Israel, April 10, 1986.
10. G.A. Somorjai, "The Photocatalyzed Production of Hydrogen and Ammonia from H_2O and N_2 over Iron Oxide," Tenth DOE Solar Photochemistry Research Conference, Niagara-on-the-Lake, Ontario, June 10, 1986.
11. G.A. Somorjai, "Photocatalysis," The Sixth International Conference on Photochemical Conversion and Storage of Solar Energy, Paris, France, July 20–24, 1986.

Photochemistry of Materials in the Stratosphere*

Harold S. Johnston, Investigator

INTRODUCTION

This research is concerned with fundamental gas-phase photochemistry, with application to molecules and radicals that occur in the stratosphere. One goal is to measure the nonequilibrium distribution of internal energy in the fragments produced after a molecule is broken apart by an energetic pulse of light and to follow the evolution of the energy distribution as a function of molecular collisions. Another goal is to obtain optical and kinetic data in the laboratory that are needed by modelers of the atmosphere. The experimental methods include laser flash photolysis, laser resonance absorption, resonance fluorescence, dispersed chemiluminescence from photolysis products, and infrared diode lasers. This research has applications to molecular dynamics, to problems of atmospheric ozone, and to the role of trace gases other than carbon dioxide on the "greenhouse effect."

1. Nitrogen Dioxide Fluorescence from N_2O_5 Photolysis (Publication 3)

D. Oh, W. Sisk, A. Young, and H.S. Johnston

A method of photolysis-induced fluorescence introduced in last year's annual report has been improved in sensitivity by a factor of about 400, so that it is a collision-free "bulb experiment." Ultraviolet photolysis of the molecules, N_2O_5, NO_2Cl, HNO_3, and $ClNO_3$, at low pressure and at short times produces electronically excited nitrogen dioxide, which emits visible radiation. This light is dispersed, represented as a linear combination of monochromatically excited NO_2 fluorescence spectra, and interpreted as the nascent internal-energy distribution of the product molecule. The novelty of these studies is the method of interpreting the data to give molecular internal-energy distributions. The collision-free internal-energy distribution of NO_2 has been observed after photolysis of NO_2Cl at several different wavelengths, and these internal-energy distributions are strongly dependent on the photolysis energy. An example of the results obtained by this method is given by Figure 1-1, which involves the photolysis of N_2O_5 with radiation at 266 nm. The vertical scale gives the electronic energies of the product molecules, NO_2 and NO_3, and the figure includes the products, NO + O. The energy distribution of the electronically excited product, NO_2, under conditions of about one collision is shown.

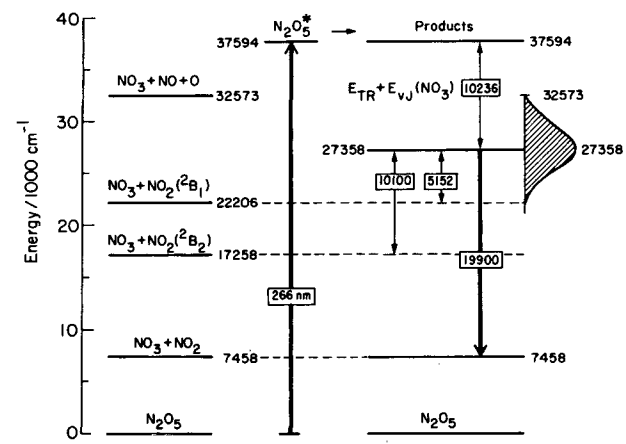

Figure 1-1. Energy-level diagram for N_2O_5 and its photolysis products, when photolysis occurs at 266 nm. As described in the text, the hatched figure gives the inferred internal-energy distribution in the (almost) nascent nitrogen dioxide. Notable features of this distribution are that it appears to be cut off at high energies by the energy threshold to produce NO_3 + NO + O and that it appears to terminate at the low-energy side near the origin of the electronic state $^2B_1$. (XBL 871-107)

2. High-Frequency Modulation Spectroscopy with Lead-Salt Diode Lasers (Publications 1 and 4)

A. Young and H.S. Johnston

As reported in last year's annual report, high-frequency (57 MHz) modulation spectroscopy in the mid-infrared region (1259.1946 cm^{-1}) with a tunable lead-salt diode laser has been demonstrated here for the first time. This technique should considerably improve detection sensitivity of diode lasers. Dr. Alex Quintanilha of the Applied Sciences Division of LBL has expressed a need for an extremely sensitive method for measuring the concentration of hydrogen peroxide in the gas phase. Calculations indicate that radio-frequency-modulated diode lasers should be able to make the needed measurements, so long as

*This work was supported by the Director, Office of Energy Research, Office of Basic Energy Sciences, Chemical Sciences Division of the U.S. Department of Energy under Contract No. DE-AC03-76SF00098.

they are carried out at low (about 10 Torr) total pressure in order to realize high resolution. At very high resolution hydrogen peroxide gas should be measurable at sub parts per billion, even in the presence of large amounts of water vapor, carbon dioxide, and trace atmospheric species.

3. Work in Progress

Energy-Transfer Studies with Highly Vibrationally Excited Photolysis Products

When the experiments described in abstract 1 are repeated with longer delay times before taking the spectrum or with higher pressures of reactants or with both, the initial collision-free energy distribution is modified. The interestingly irregular initial internal-energy distributions evolve with collision into broad more-or-less Gaussian functions. With photolysis at 248 nm, for example, the initial half-Gaussian distribution (truncated by formation of NO + O) is converted into a broad Gaussian distribution after about 10 collisions, and an interesting progression of distributions is observed for various numbers of collisions between the two limits. Because of the Douglas effect (strong interactions between the excited electronic states of NO_2 and the highly vibrationally excited levels of the ground electronic state), these energy-transfer studies primarily have the physical property of collisional deactivation of highly excited vibrational states, and as such the results are interesting in terms of RRKM theory in particular and are of more general interest as the evolution of a nonequilibrium energy distribution with number of collisions.

Quantum-Mechanical Energy and Structural Calculations on the Nitrate Free Radical[†]

On the basis of D_{3h} as the shape of the NO_3 radical, calculations have been made of the vertical energies of the first four quantum states. These calculations were made with successively higher and higher quality wave functions. Limited calculations of the structure and potential-energy functions will be made.

[†]Collaboration with Professor H.F. Schaefer.

1986 PUBLICATIONS AND REPORTS

Refereed Journals

1. M. Gehrtz,[†] W. Lenth,[†] A.T. Young, and H.S. Johnston, "High Frequency Modulation Spectroscopy with Lead Salt Diode Lasers," Opt. Lett. **11**, 132 (1986); LBL-20809.
2. H.S. Johnston, C.A. Cantrell,[‡§] and J.G. Calvert,[‡§] "Unimolecular Decomposition of NO_3 to Form NO and O_2," J. Geophys. Res. **91**, 5159 (1986); LBL-18984.
3. D. Oh, W. Sisk, A. Young, and H.S. Johnston, "Nitrogen Dioxide Fluorescence from N_2O_5 Photolysis," J. Chem. Phys. **85**, 7146 (1986); LBL-21614.

Other Publications

4. A. Young and H.S. Johnston, "High Frequency Modulation Spectroscopy With Tunable Lead Salt Diode Lasers," Laser Analyt. Lett. **7**, 5 (1986).

Invited Talks

5. H.S. Johnston, "Photolysis Induced Fluorescence," XVII Informal Conference on Photochemistry, Boulder, CO, June 22–26, 1986.

[†]Present address: IBM Research Laboratory, San Jose, CA 95193.

[‡]Present address: National Center for Atmospheric Research (NCAR), Boulder, CO.

[§]C.A. Cantrell and J.G. Calvert at NCAR were supported by the National Science Foundation.

Radiation Chemistry of Aqueous Systems*

Michael E. Jayko

Hydroxal Radical Yields in Aqueous Solutions Irradiated with High-Energy Heavy Ions (Publication 1)

M. Jayko, A Appleby,† and E. Christman†

The yields of H_2O_2 produced in dilute solutions of sodium bromide and sodium formate, irradiated with energetic ions from the Berkeley Bevalac, have been measured as a function of penetration depths of these ions into the solutions. Ions used were carbon, neon, and argon, with incident energies of 400, 370, and 450 MeV/amu, respectively. The effects of solute concentration and pH were studied.

From these data the radiation chemical yields of hydroxyl radicals have been deduced. The general behavior of G_{OH} is as expected from the theory of the structure of heavy-ion tracks, in that (a) G_{OH} decreases as the incident ions penetrate the solution, losing energy; (b) G_{OH} decreases with increasing atomic number of the primary ion; and (c) G_{OH} is higher at higher concentrations of OH scavenger. These results support earlier studies on yields from ferrous sulfate solutions,[1] bromide and formate solutions,[2] and nitrate-ethanol solutions.[3]

†Permanent address: Rutgers, The State University, New Brunswick, NJ 08903.

1. E.A. Christman, A. Appleby, and M. Jayko, "Radiation Chemistry of High-Energy Carbon, Neon, and Argon Ions: Integral Yields from Ferrous Sulfate Solutions," Radiat. Res. **85**, 443 (1981).

2. A. Appleby, E.A. Christman, and M. Jayko, "Radiation Chemistry of High-Energy Carbon, Neon, and Argon Ions: Hydroxy Radical Yields," Radiat. Res. **104**, 263 (1985).

3. A. Appleby, E.A. Christman, and M. Jayko, "Radiation Chemistry of High-Energy Carbon, Neon, and Argon Ions: Hydrated Electron Yields," Radiat. Res. (in press).

*This work was supported by the Director, Office of Energy Research, Office of Basic Energy Sciences, Chemical Sciences Division of the U.S. Department of Energy under Contract No. DE-AC03-76SF00098.

2. Radiolytic Oxidation of Aqueous Proteins (Publication 2)

W.M. Garrison and M.E. Jayko

The radiolytic degradation of proteins in oxygenated solution is initiated by the attack of OH radicals at a multiplicity of main-chain and side-chain loci to give a wide variety of oxidized protein sites.[1] A major factor of these oxidation reactions leads to the introduction of reactive carbonyl groups into the protein covalent structure.[2] With γ rays, the total carbonyl yields are found to be in the range $G(>CO)_t \cong 0.1-1.0$ for a number of different proteins, including pepsin, α-chymotrypsin, and β-lactoglobulin. A sensitive chemical-spectrophotometric procedure for quantitatively monitoring $G(>CO)_t$ over the dose range of interest in radiation biology (1–50 Krad) has been developed.[3] The procedure is now being applied in a study of the radiolytic oxidation of the histone group of chromosomal proteins, which are known to play key roles in determining the confirmation and genetic activity of the chromatin DNA-protein complex.

1. W.M. Garrison, "Reaction Mechanisms in the Radiolysis of Peptides, Polypeptides and Proteins," Chem. Rev. (in press).

2. W.M. Garrison, M.E. Jayko, and W. Bennett, "Radiation-Induced Oxidation of Proteins in Aqueous Solution," Radiat. Res. **16**, 483 (1962).

3. M.E. Jayko and W.M. Garrison, "A Sensitive Chemical Procedure for Monitoring the Radiolytic Oxidation of Proteins at γ-ray Dosages Down to 1 Krad," Radiat. Eff. Lett. **87**, 299 (1986).

1986 PUBLICATIONS AND REPORTS

LBL Reports

1. A. Appleby, E.A. Christman, and M. Jayko, "Radiation Chemistry of High-Energy Carbon, Neon, and Argon Ions: Hydrated Electron Yields," LBL-21478.
2. M.E. Jayko, and W.M. Garrison, "A Sensitive Chemical Procedure for Monitoring the Radiolytic Oxidation of Proteins at γ-Ray Dosages Down to 1 Krad," LBL-20335.

CHEMICAL PHYSICS

Energy Transfer and Structural Studies of Molecules on Surfaces*

Charles B. Harris, Investigator

INTRODUCTION

The goal of this research is to study the mechanisms that are responsible for the transfer of energy from the excited states of molecules to metal surfaces and to develop new laser techniques for probing molecule-surface interactions. The research program is both theoretical and experimental in character, and it includes nonlinear optical and picosecond laser techniques in addition to a variety of standard surface-science tools for characterizing molecule-surface interactions. The results of this program have a direct bearing on high-speed technological devices and materials, and on problems of general interest such as surface-enhanced photochemistry, the dynamics of surface photoemission, and the optical properties of thin films.

1. Work in Progress

Photoelectron Emission from Metal Surfaces and Electron Trapping in Thin-Film Overlayers

The changes in the total photoemission yield of a surface with respect to deposition of physisorbed molecular layers have been studied with optical excitation using both dynamic and static techniques. The coverage dependence of the deposition of p-methoxybenzaldehyde on Ag(111) can be understood as the sum of two separate mechanisms: a work-function shift in the first monolayer, and attenuation of the photoelectrons by succeeding layers. A change in the work function upon adsorption of molecules is well documented. Typically (as is the case here), a decrease in the work function is observed, corresponding to an increase in the photoyield. The effect is explained as a change in the surface dipole layer due to the presence of molecular dipole moments—either permanent, or induced by the surface field or by charge transfer to the substrate. The work-function shift has been reported to be almost entirely contained to the initial monolayer. Further adsorption on the Ag crystal is accompanied by a decrease in the photoyield intensity, which is caused by trapping and attenuation of the electrons emitted from the surface by the organic overlayer. The decrease in transmitted intensity can be theoretically shown to have an exponential dependence on film thickness under the assumption that only unscattered electrons are collected. The experimental data are fit well by an exponential, which is characterized by a mean free path (1/e value) of approximately 25 Å. A large range of mean-free-path values has been reported in the literature, probably in part due to the energy dependence of this parameter. Many mechanisms have been suggested as responsible for electron trapping in condensed phases. A likely possibility is trapping via the structure of the film itself, such as alignment of molecular dipoles around the electron to create a stable site. Further evidence of the existence of such traps comes from the time-resolved photoyield data obtained by gating out the much larger population of electrons occurring coincident with the laser pulse. This decay is seen to grow in monotonically with coverage after the first couple of monolayers, indicating it is a phenomenon associated with multilayer formation.

Picosecond Techniques for Surface Studies

In order to study the dynamics of molecular electronically excited states at or near (<50 Å) a metal surface, we are in the final stages of developing time-correlated single-photon counting as a means of studying surface dynamics. This apparatus relies on a synchronously pumped dye-laser system as a source of light pulses of 1–10 psec duration. A portion of the ultrashort light pulse is used to start an electronic clock, while the rest of the pulse excites a molecular adsorbate to an electronically excited state. The adsorbate then emits a photon in a manner determined by its excited-state decay law. This

*This work was supported by the Director, Office of Energy Research, Office of Basic Energy Sciences, Chemical Sciences Division of the U.S. Department of Energy under Contract No. DE-AC03-76SF00098.

fluorescent photon stops the electronic clock, and the time is represented as a voltage that is stored in a computer. In this manner a histogram of the excited-state decay dynamics is created. This apparatus possesses a dynamic range of 10^5–10^6 and is very sensitive to low-quantum-yield fluorescent species. The time resolution of this system is <50 psec and has an upper limit of a few hundred μsec. These unique capabilities will allow us to sensitively probe the excited-state dynamics of species physisorbed or chemisorbed to the metal surface, with the time resolution necessary to elucidate the excited-state dynamics. As an example of the sensitivity of the time-correlated single-photon counting apparatus, we have been able to make the first measurements of electronically excited molecules directly on surfaces. In particular, the fluorescence spectrum of tetracene on Si(111) has been obtained. Since the energy transfer to the surface severely dampens the molecular emission, all previous investigations have been restricted to the case where the damping is reduced by placing an inert spacer layer between the molecule and the surface. This work also serves as a first step towards a test of the molecule-surface distance dependence predicted by several theories for energy transfer. There have, as yet, not been any experimental studies of the small-distance regime of energy transfer.

The fluorescence spectroscopy of adsorbed tetracene has also been studied for films from monolayer to multilayer coverage and clearly shows the changes in the fluorescence for the first few monolayers. In addition to the sharply increasing intensity with respect to coverage (indicative of the energy-transfer mechanism), dramatic changes are seen in the shape and position of the spectra. These shifts are most likely associated with perturbations caused by an increasing number of tetracene neighbors with further film growth, and also by association of the individual molecules. Literature accounts of thick films and molecular crystals of tetracene suggest that such shifts are due to formation of molecular aggregates (both dimers and large units). Other work in this laboratory has verified for tetracene adsorbed on sapphire and NaCl surfaces that the shifts observed are quite sensitive to the properties of the surface. In these experiments the formation of two species (most probably lone tetracene and its dimer) with increasing coverage is indicated. Preliminary results for tetracene deposited on a spacer layer of condensed Xe on top of Si(111) show the existence of vibrational structure in the fluorescence spectrum. Although common for dilute solution and molecular crystal phases, none of the other adsorption systems discussed above (bare Si, sapphire, or NaCl) have exhibited this effect.

The fact that this structure was not observed for the monolayer directly on the Si surface could be explained several ways. Lifetime broadening of the molecular excited state caused by energy transfer to the surface can probably be eliminated based on calculations using the classical theory. The energy-transfer rate to the surface would have to be a factor of 100 higher to explain the blurring out of the vibrational structure. Another possibility is that the broadening is caused from interactions between the tetracene molecules. This also seems to contradict experimental data since the vibrational structure remains for coverages greater than one monolayer on Xe films, and no structure was observed on the sapphire and NaCl surfaces. Inhomogeneous broadening caused by the substrate itself seems the most likely answer. This suggests that Xe films deposited at low temperatures (30 K) provide a very smooth and relatively low interaction surface for molecular adsorption.

1986 PUBLICATIONS AND REPORTS

Refereed Journals

1. A.L. Harris, M. Berg, and C.B. Harris, "Studies of Chemical Reactivity in the Condensed Phase. I. The Dynamics of Iodine Photodissociation on a Picosecond Timescale and Comparison to Theories for Chemical Reactions in Solution," J. Chem. Phys. **84**, 788 (1986).
2. M.E. Paige, D.J. Russell, and C.B. Harris, "Studies of Chemical Reactivity in the Condensed Phase. II. Vibrational Relaxation of Geminately Recombined Iodine Atoms in Liquid Xenon," J. Chem. Phys. Commun. **85**, 3699 (1986).

Other Publications

3. D. Ben-Amotz and C.B. Harris, "Picosecond Studies of Barrierless Torsional Diffusion," in *Ultrafast Phenomena V*, G.R. Fleming and A.E. Siegman, eds., Springer Series in Chemical Physics, Vol. 46, p. 350, Springer Verlag, 1986.
4. D. Ben-Amotz and C.B. Harris, "Picosecond Studies of Barrierless Isomerization in Liquids," in *Proc. Int. Conf. Quantum Electronics* (IQEC'86), Optical Society of America, 1986.
5. C.B. Harris, "Ultrafast Studies Designed to Test the Fundamental Statistical Assumptions Underlying Chemical Reactivity in Liquids," in *Ultrafast Phenomena V*, G.R. Fleming and A.E. Siegman, eds., Springer Series in Chemical Physics, Vol. 46, p. 326, Springer Verlag, 1986.

LBL Reports

6. A.P. Alivisatos, M.F. Arndt, S. Efrima, D.H. Waldeck, and C.B. Harris, "Electronic Energy Transfer at Semiconductor Interfaces: I. Energy Transfer from Two Dimensional Molecular Films to Si(111)," J. Chem. Phys. (in press); LBL-22672.
7. D. Ben-Amotz and C.B. Harris, "Torsional Dynamics of Molecules on Barrierless Potentials in Liquids: I. Temperature and Wavelength Dependent Picosecond Studies of Triphenyl-Methane Dyes," J. Chem. Phys. (in press); LBL-22673.
8. D. Ben-Amotz and C.B. Harris, "Torsional Dynamics of Molecules on Barrierless Potentials in Liquids II. Test of Theoretical Models," J. Chem. Phys. (in press); LBL-22674.
9. D. Ben-Amotz, R. Jeanloz, and C.B. Harris, "Torsional Dynamics of Molecules on Barrierless Potentials in Liquids III. Pressure Dependent Picosecond Studies of Triphenyl-Methane Dye Solution in a Diamond Anvil Cell," J. Chem. Phys. (in press); LBL-22675.
10. P. Alivisatos (Ph.D. Thesis), "The Photophysical Properties of Molecules near Metal and Semiconductor Surfaces," LBL-22225.

Invited Talks

11. C.B. Harris, "Picosecond Studies of Molecular Dynamics and Chemical Reactivity in Solutions," Pennsylvania State University, State College, Oct. 17, 1985.
12. C.B. Harris, "Picosecond Studies of Molecular Dynamics and Chemical Reactivity in Solutions," University of British Columbia, Vancouver, B.C., Oct. 21, 1985.
13. C.B. Harris, "Are Stochastic Theories for Chemical Reactions in Liquids Valid on a Picosecond Timescale?" SPIE meeting on "Spectroscopy and Molecular Dynamics," Los Angeles, CA, Jan. 19–24, 1986.
14. C.B. Harris, "Fundamental Studies on the Picosecond Timescale of Chemical Reactivity in Liquids," SPIE meeting on "Laser Applications in Science and Engineering," Los Angeles, CA, Jan. 19–24, 1986.
15. C.B. Harris, "Fundamental Studies of Chemical Reactivity in Liquids on Ultrafast Timescale," National Research Council, Ottawa, Ont., Feb. 6, 1986.
16. C.B. Harris, "Are Stochastic Theories Valid in Condensed Matter Physics on Ultrafast Timescales," IBM, Yorktown Heights, NY, Feb. 11, 1986.
17. C.B. Harris, "Are Stochastic Theories for Chemical Reactions Valid? Picosecond Studies Designed to Test the Basic Assumptions Underlying Chemical Reactivity in Liquids," University of Chicago, Feb. 24, 1986; California Institute of Technology, Pasadena, CA, March 11, 1986; University of California, Santa Barbara, May 30, 1986.
18. C.B. Harris, "Fundamental Studies of Simple Chemical Reactions in Solution on Ultrafast Timescale," University of Nevada, Reno, Feb. 28, 1986; Rice University, Houston, TX, April 2, 1986; University of Texas at Austin, April 3, 1986; General Electric, Schenectady, NY, May 2, 1986.
19. C.B. Harris, "Energy Transfer and Chemical Reactions Above Metal and Semiconductor Surfaces," Rensselaer Polytechnic, Institute, Troy, NY, May 1, 1986.
20. C.B. Harris, "Ultrafast Studies Designed to Test the Fundamental Statistical Assumptions Underlying Chemical Reactivity in Liquids," topical meeting on ultrafast phenomena, Aspen, CO, June 16–20, 1986.
21. C.B. Harris, "Picosecond Studies of Barrierless Isomerization in Liquids," International Conference on Quantum Electronics '86, San Francisco, CA, June 9–13, 1986.
22. C.B. Harris, "Picosecond Studies of Vibrational Energy Relaxation and Redistribution in Condensed Phase Chemical Reactions," Gordon Research Conference on Vibrational Spectroscopy, Brewster Academy, NH, Aug. 11–15, 1986.
23. C.B. Harris, "The Nature of Chemical Reactions in Liquids on the Femtosecond Timescale," Department of Chemistry colloquium, University of Michigan, Ann Arbor, Sept. 23, 1986.

Selective Photochemistry*

C. Bradley Moore, Investigator

INTRODUCTION

The fundamental goals of this program are to understand the photophysics and photochemistry that occur following selective excitation of molecules. Of particular interest are the chemical reactions of specifically excited states and the dynamics of energy transfer, both within a molecule and to surrounding molecules. For low levels of vibrational excitation in small molecules, individual quantum states may be excited, enabling the measurement of reaction and energy-transfer rate constants for each quantum state. For larger or more highly excited molecules, it is usually not possible to excite single eigenstates. Instead, a number of eigenstates are excited simultaneously, and a redistribution of the initial vibrational excitation occurs. This process, known as intramolecular vibrational-energy redistribution (IVR), is extremely rapid and severely limits the realization of truly mode-specific unimolecular reactions.

Advances in mode-specific chemistry will come from a more complete understanding of the IVR process and the parameters that control its efficiency. By being able to predict the rates of IVR and the path of vibrational-energy flow through a molecule, experiments can be designed utilizing molecular systems that maximize the possibilities for mode-specific effects. Studies designed to elucidate the coupling mechanisms and dominant pathways for IVR are currently under way on a number of model systems.

The rates and mechanisms of free-radical reactions, such as are important in combustion, are often best studied by flash kinetic spectroscopy using lasers for thermal heating, for photolyzing, and for spectroscopic probing. Reactions can be studied as a function of individual quantum states. A fundamental understanding of these reactions is sought to serve as a basis for modeling combustion processes.

*This work was supported by the Director, Office of Energy Research, Office of Basic Energy Sciences, Chemical Sciences Division of the U.S. Department of Energy under Contract No. DE-AC03-76SF00098.

1. Coupling of CH Stretching and Bending Vibrations in Trihalomethanes (Publication 2)

J.S. Wong, W.H. Green, C.-K. Cheng, and C.B. Moore

The vibrational spectra of $HCCl_3$, HCF_3, $HCCl_2F$, and $HCClF_2$ have been measured in the vapor from the CH stretching fundamental through to the fifth overtone (i.e., $v_{CH} = 6$), using FTIR and photoacoustic spectrometers. Instead of a single strong CH overtone progression, additional strong bands attributable to Fermi-resonant combination tones are prominent in the spectra (see Figure 1-1). The CH stretch is found to be most strongly coupled to the CH bending mode and much less strongly to the heavy-atom motions. The spectroscopic structure implies a large separation of timescales between the extremely fast energy redistribution among the CH vibrational modes and the slower energy flow from the CH vibrations to the heavy-atom vibrations. These single-CH molecules are expected to be useful model systems for understanding vibrational energy flow in larger hydrocarbons, where the experimental spectra are not as well-resolved.

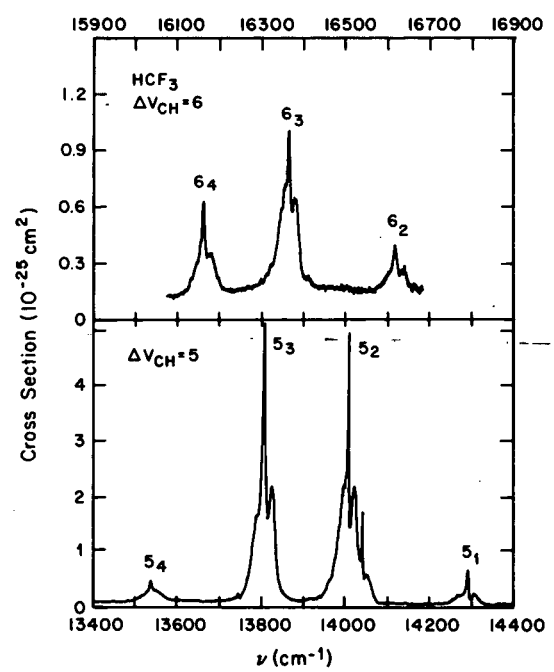

Figure 1-1. The photoacoustic absorption spectrum of HCF_3 in the $\Delta v_{CH} = 5$ (128 Torr) and $\Delta v_{CH} = 6$ (125 Torr) regions. (XBL 873-1117)

2. Kinetic Anharmonic Coupling in the Trihalomethanes: a Mechanism for Rapid Intramolecular Redistribution of CH Stretch Vibrational Energy (Publication 3)

W.H. Green, W.D. Lawrance, and C.B. Moore

The coupling of CH stretching and CH bending vibrations in trisubstituted methanes is analyzed. Improved spectroscopic constants, especially the cubic anharmonic stretch-bend coupling constants, are extracted from Fermi resonances in the overtone spectra of HCF_3 and $HCCl_3$. One of the cubic anharmonic constants of the potential-energy surface is extracted for comparison with *ab initio* calculations. That part of the coupling that arises from the kinetic energy as expressed in curvilinear coordinates is calculated and compared to the coupling calculated using the more conventional rectilinear treatment. Use of curvilinear coordinates is found to provide significant advantages. In these coordinates, the kinetic energy provides most of the experimentally observed coupling. Because the kinetic-energy coupling is relatively substituent-independent, the curvilinear model of the CH stretch-bend interaction tested for these isolated CH chromophores is expected to be useful in understanding CH bonds and vibrational-energy flow in larger hydrocarbons.

3. Work in Progress

Energy-transfer and chemical-reaction rates are being studied for CH_2 and HCO radicals. Infrared spectra of HCO have been recorded in the CH stretching region and are being analyzed. A diode laser infrared flash kinetic spectrometer is being constructed to extend this work beyond the 2–4 μm range available with our current difference-frequency spectrometer. Bending spectra of triplet CH_2 will be recorded first. Spectroscopy of radical-radical and radical-molecule reaction complexes are planned.

Unimolecular reaction dynamics are being studied by photofragment spectroscopy. A molecular-beam system has been constructed to use with the new VUV laser system being developed together with Y.T. Lee and A.H. Kung. CO and H_2 fragments from simple molecules will be studied.

Infrared spectra of intermediates in organometallic photochemistry in gas and liquid phase are being studied jointly with R.G. Bergman. Emphasis is on CH activation chemistry.

1986 PUBLICATIONS AND REPORTS

Refereed Journals

1. H. Bitto, I.-C. Chen, and C.B. Moore, "Rotational State Distribution of CO Photofragments from Triplet Ketene," J. Chem. Phys. **85**, 5101 (1986); LBL-20826.

LBL Reports

2. J.S. Wong, W.H. Green, Jr., C.-K. Cheng, and C.B. Moore, "Coupling of CH Stretching and Bending Vibrations in Trihalomethanes," submitted to J. Chem. Phys.; LBL-20825.
3. W.H. Green, Jr., W.D. Lawrance, and C.B. Moore, "Kinetic Anharmonic Coupling in the Trihalomethanes: a Mechanism for Rapid Intramolecular Redistribution of CH Stretch Vibration Energy," submitted to J. Chem. Phys.; LBL-22694.

Invited Talks

4. C.B. Moore, "Energy Levels and Energy Transfers in Unimolecular Reaction Dynamics," Department of Chemistry and Biochemistry, University of Colorado, Boulder, Feb. 21, 1986.
5. C.B. Moore, "A Spectroscopic Approach to Intramolecular Energy Transfer and Bondbreaking," Department of Chemistry, University of Washington, Seattle, May 7, 1986.
6. C.B. Moore, "Photochemistry and Unimolecular Reactions," Workshop on "Stochasticity and Intramolecular Redistribution of Energy," Orsay, France, June 24, 1986.
7. C.B. Moore, "Unimolecular Reaction Dynamics—Quantum State by Quantum State," University of Bordeaux, France, June 30, 1986.
8. C.B. Moore, "Unimolecular Reaction Dynamics—Quantum State by Quantum State," Tata Institute, Bombay, India, July 30, 1986; Department of Theoretical Chemistry, University of Syndney, Australia, Aug. 2, 1986; School of Science, Griffith University, Nathan, Brisbane, Australia, Aug. 3, 1986; School of Chemistry, University of New South Wales, Kensington, Australia, Aug. 12, 1986.
9. C.-K. Cheng, W.H. Breen, D.R. Guyer, W.D. Lawrence, W.F. Polik, and C.B. Moore, "Intramolecular Energy Transfer in Highly Vibrationally Excited Molecules," American Chemistry Society 192nd National Meeting, Anaheim, CA, Sept. 7–12, 1986.
10. C.B. Moore, "Unimolecular Reaction Dynamics—Quantum State by Quantum State," National Bureau of Standards, Gaithersburg, MD, Oct. 28, 1986.

Physical Chemistry with Emphasis on Thermodynamic Properties*

Kenneth S. Pitzer, Investigator

INTRODUCTION

The purpose of this program is the discovery and development of methods of calculation of thermodynamic and related properties of important chemical systems by the use of quantum and statistical mechanics together with experimental measurements for key systems. Current emphasis is on novel ionic systems. Systems comprising fused salts mixed in any proportion with water or other polar solvents are being studied experimentally and with theory. Current studies also include dilute ionic solutions very close to the critical point of the solvent where anomalous properties are observed. Recent theoretical advances include treatments of the dielectric constant of H_2O, the thermodynamics of ionic solutions in H_2O above its critical temperature, and the critical properties of pure ionic fluids such as NaCl. Earlier advances yielded improved equations for electrolyte solutions. These various equations are now being applied to a wide variety of systems of industrial or geological interest, including geothermal brines.

Another area of recent research is that of relativistic quantum-mechanical methods for the calculation of energies, bond distances, and other properties of the ground and excited states of molecules or molecular ions containing very heavy atoms. Such results are important in evaluating possible laser systems and for models of catalytic entities. A review of the accomplishments in this area was published (see Publication 8).

1. Large-Scale Fluctuations and the Critical Behavior of Dilute NaCl in H_2O (Publication 1)

K.S. Pitzer

It is shown that the effect on thermodynamic properties of large-scale fluctuations, an effect that is substantial near the critical point for pure water, is rapidly suppressed by the addition of very small amounts of NaCl. A classical equation of state for pure water (i.e., with the fluctuation effect removed) is related satisfactorily to the properties of dilute solutions of NaCl in H_2O on or near the critical line. This relatively simple relationship on a fully classical basis contrasts with very peculiar T-x and P-x critical lines found when the real, nonclassical properties of water have been used in an otherwise classical equation for the mixture. It is suggested that this procedure in which the effect of fluctuations is subtracted and the classical properties represented over a range of composition may be generally useful.

2. The Dipositive Dimeric Ion Hg_2^{+2}: a Theoretical Study (Publications 9 and 10)

R.P. Neisler and K.S. Pitzer

Various properties of $Hg_2^{+2}(g)$ are calculated from relativistic quantum mechanics. For comparison, calculations are also made on a nonrelativistic basis. The relativistic values of R_e and ω_e agree well with observed values in those crystals or solutions where the effects of surroundings are expected to be small. The relativistic effect reduces R_e by 0.28 Å, raises ω_e by 67 cm^{-1}, and increases D_e by 24 $kcal \cdot mol^{-1}$. A modified Born-type calculation, which recognizes the quadrupole moment and the nonspherical shape, is carried out for the hydration energy. Good agreement is obtained with experimental thermodynamic data for aqueous Hg_2^{+2}.

3. Critical Behavior of Dilute NaCl in H_2O (Publication 11)

K.S. Pitzer, J.L. Bischoff,† and R.J. Rosenbauer†

The compositions of the saturated vapor and liquid phases are measured for the system NaCl-H_2O at 380°C, which is close to the critical point of pure water. The shape of the phase-equilibrium curve is classical, which confirms a conclusion reached earlier on the basis of less accurate data (Publication 1). This implies that the long-range forces introduced by the NaCl suppress the nonclassical effects present in pure H_2O. An empirical equation of a classical type fits these data, as shown in Figure 3-1.

*This work was supported by the Director, Office of Energy Research, Office of Basic Energy Sciences, Chemical Sciences Division of the U.S. Department of Energy under Contract No. DE-AC03-76SF00098.

†U.S. Geological Survey, Menlo Park, CA 94025.

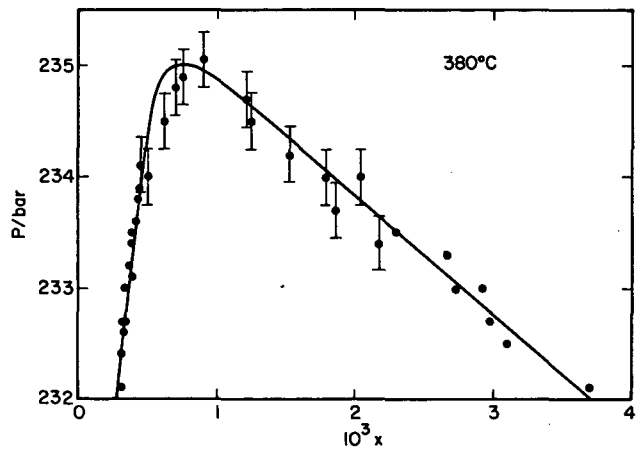

Figure 3-1. Vapor and liquid compositions for $NaCl-H_2O$ at 380.0°C as a function of pressure. An estimated uncertainty is indicated for some of the measured values. The curve is calculated. (XBL 873-1118)

4. The Restricted Primitive Model for Ionic Fluids: Properties of the Vapor and the Critical Region (Publication 12)

K.S. Pitzer and D.R. Schreiber

The vapor of an ionic fluid at low temperature is known to be dominated by ion pairs and larger neutral clusters with smaller populations of individual ions and charged clusters. Previous cluster treatments of the restricted primitive model are improved to include clusters through the hexamer and to consider interactions between clusters according to the mean spherical approximation. With these refinements it is possible to obtain good results for reciprocal reduced temperatures β^* from 6.8 to 20 that include the critical temperature ($\beta^* = z^2e^2/kTa$, where ze is the charge and a the particle diameter). The distribution among clusters (Figure 4-1) and various thermodynamic properties are calculated. The concentration of charged clusters is reported for comparison with measurements of electrical conductance. Since the approximations of this approach become serious at reduced concentrations ($c^* = Na^3/V$) above 0.02, interpolations are made with an empirical equation of Larsen[1] based in turn on various Monte Carlo simulations. These interpolations yield estimates of the saturated liquid and vapor densities and a critical β^* of 14.7. The speculative nature of the estimates of critical properties is emphasized.

1. B. Larsen, J. Chem. Phys. **65**, 3431 (1976).

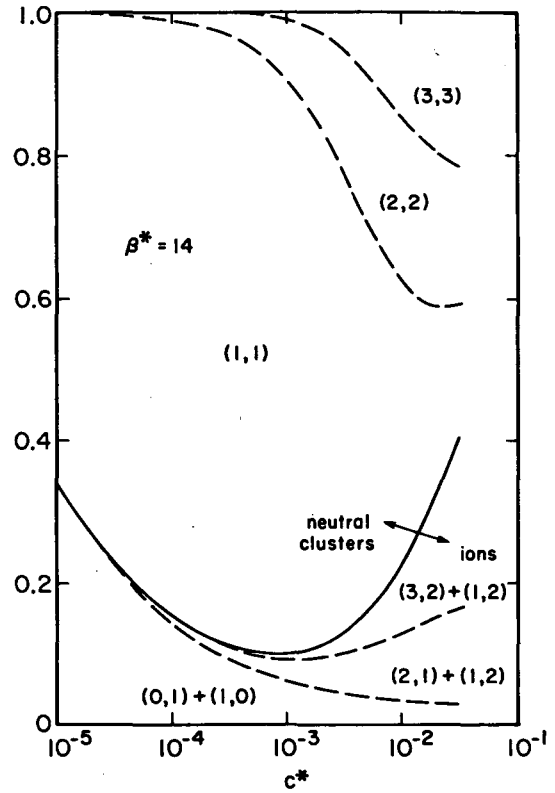

Figure 4-1. The distribution of particles among clusters at reciprocal reduced temperature $\beta^* = 14$ as a function of reduced concentration c^*. The clusters are defined by (i,j) with i and j the numbers of positive and negative particles, respectively. Note the rapid increase in three- and five-particle charged clusters at high concentration. (XBL 873-1119)

5. Work in Progress

The recently completed measurements of conductivity, density, and viscosity on the model ionic critical system (tetra-n-butylammonium picrate: 1-chloroheptane) are being extended to measurements of the vapor pressure and, possibly, the surface tension. Studies continue of $NaCl-H_2O$ above the critical temperature of pure H_2O.

1986 PUBLICATIONS AND REPORTS

Refereed Journals

1. K.S. Pitzer, "Large-Scale Fluctuations and the Critical Behavior of Dilute NaCl in H_2O," J. Phys. Chem. **90**, 1502 (1986); LBL-21016.
2. J.L. Bischoff, R.J. Rosenbauer, and K.S. Pitzer, "The System $NaCl-H_2O$: Relations of Vapor-Liquid Near the Critical Temperature of Water and of Vapor-Liquid-Halite from 300 to 500°C," Geochim. et Cosmochim. Acta **50**, 1437 (1986); LBL-20783.

3. R.C. Phutela and K.S. Pitzer, "Heat Capacity and Other Thermodynamic Properties of Aqueous Magnesium Sulfate to 473 K," J. Phys. Chem. **90**, 895 (1986); LBL-20041.†
4. K.S. Pitzer and J.M. Simonson, "Thermodynamics of Multicomponent, Miscible, Ionic Systems: Theory and Equations," J. Phys. Chem. **90**, 3005 (1986); LBL-21756.†
5. J.M. Simonson and K.S. Pitzer, "Thermodynamics of Multicomponent, Miscible, Ionic Systems: The System $LiNO_3$-KNO_3-H_2O," J. Phys. Chem. **90**, 3009 (1986); LBL-20207.†
6. K.S. Pitzer and R.T. Pabalan, "Thermodynamics of NaCl in Steam," Geochim. et Cosmochim. Acta **50**, 1445 (1986); LBL-20779.†
7. R.C. Phutela and K.S. Pitzer, "Thermodynamics of Electrolyte Mixtures. Enthalpy and the Effect of Temperature on the Activity Coefficient," J. Sol. Chem. **15**, 649 (1986); LBL-21140.†

LBL Reports

8. K. Balasubramanian and K.S. Pitzer, "Relativistic Quantum Chemistry," in *Electronic Structure Calculations*, Kenneth Lawley, Ed., John Wiley & Sons, Ltd.; LBL-20991.
9. R.P. Neisler (Ph.D. Thesis), "The Mercurous Di-Ion (Hg_2^{+2}), A Theoretical Study," LBL-21734.
10. R.P. Neisler and K.S. Pitzer, "The Dipositive Dimeric Ion Hg_2^{+2}: A Theoretical Study," submitted to J. Phys. Chem.; LBL-22064.
11. K.S. Pitzer, J.L. Bischoff, and R.J. Rosenbauer, "Critical Behavior of Dilute NaCl in H_2O," submitted to Chem. Phys. Lett.; LBL-22309.
12. K.S. Pitzer and D.R. Schreiber, "The Restricted Primitive Model for Ionic Fluids: Properties of the Vapor and the Critical Region," submitted to Molecular Phys.; LBL-22171.
13. D.R. Schreiber, M.C.P. de Lima, and K.S. Pitzer, "The Electrical Conductivity, Viscosity, and Density of a Two-Component Ionic System at its Critical Point," submitted to J. Phys. Chem.; LBL-22500.

Invited Talks

14. K.S. Pitzer, Mack Award Lectures at Ohio State University: (1) "Ionic Fluids of Chemical, Geological, or Industrial Interest" and (2) "Relativistic Effects in Chemistry," Columbus, OH, May 1–2, 1986.
15. K.S. Pitzer, "Recent Advances in the Thermodynamic Properties of Ionic Systems," National Meeting, Canadian Institute of Chemistry, Saskatoon, Sask., June 2–5, 1986.
16. K.S. Pitzer, "Thermodynamic Properties of Ionic Fluids over Wide Range of Temperature," IUPAC – Chemical Thermodynamics Conference, Lisbon, Portugal, July 14–18, 1986; LBL-21799.
17. K.S. Pitzer, "Theoretical Considerations of Solubility with Emphasis on Mixed Aqueous Electrolytes," IUPAC 2nd International Symposium on Solubility Phenomena, New Jersey Institute of Technology, Newark, NJ, Aug. 1986; LBL-21961.

†This work was supported by the Director, Office of Energy Research, Office of Basic Energy Sciences, Division of Engineering and Geosciences of the U.S. Department of Energy under Contract No. DE-AC03-76SF00098.

Molecular Interactions*

William A. Lester, Jr., Investigator

INTRODUCTION

This research program is directed at extending fundamental knowledge of atoms and molecules including their electronic structure, mutual interaction, collision dynamics, and interaction with radiation. The approach combines the use of *ab initio* methods—multiconfiguration Hartree-Fock (MCHF), configuration, interaction (CI), and the recently developed quantum Monte Carlo (QMC)—to describe electronic structure, intermolecular interactions, and other properties, with various methods for characterizing inelastic and reactive collision processes, and photodissociation dynamics. Current efforts are focused on (1) the development of efficient methods for generating optimum importance functions in QMC, (2) the introduction and application of effective-core-type methods in QMC, and (3) an adiabatic treatment of single-photon indirect polyatomic photodissociation with emphasis on product rovibrational photofragment distributions.

1. Molecular Physics and Chemistry Applications of Quantum Monte Carlo (Publication 1)

P.J. Reynolds, R.N. Barnett, B.L. Hammond, and W.A. Lester, Jr.

We discuss recent work with the diffusion QMC method and its application to molecular systems. The formal correspondence of the imaginary-time Schrödinger equation to a diffusion equation allows one to calculate quantum-mechanical expectation values as Monte Carlo averages over an ensemble of random walks. We report studies of atomic and molecular total energies, as well as properties including electron affinities, binding energies, reaction barriers, and moments of the electronic charge distribution. A brief discussion is given on how standard QMC must be modified for computing properties. Calculated energies and properties are presented for a number of molecular systems, including He, F, F^-, H_2, N, and N_2. Recent progress in extending the basic QMC approach to the calculation of "analytic" (as opposed to finite-difference) derivatives of the energy is presented, together with an H_2 potential-energy curve obtained using analytic derivatives.

*This work was supported by the Director, Office Of Energy Research, Office of Basic Energy Sciences, Chemical Sciences Division of the U.S. Department of Energy under Contract No. DE-AC03-76SF00098.

2. Is There a Zeroth-Order Time-Step Error in Diffusion Quantum Monte Carlo? (Publication 13)

P.J. Reynolds, R.K. Owen, and W.A. Lester, Jr.

During the past decade QMC methods have been increasingly applied to the determination of the electronic structure of atoms and molecules. These Monte Carlo methods are variants of the Green's function Monte Carlo approach of Kalos.[1] Recently, Moskowitz and Schmidt[2] claim to have proven that the "diffusion" Monte Carlo variant, with a particular choice of short-time Green's function, has a bias that does not vanish as the time step τ approaches zero. In other words, they claim that the short-time Green's function used by a number of workers in the past is, in fact, not a correct short-time approximation. Their proof is in error, and the correct expression for the bias to order τ has been obtained.

1. M.H. Kalos, Phys. Rev. **128**, 1791 (1962); J. Comp. Phys. **1**, 257 (1967); M.H. Kalos, D. Levesque, and L. Verlet, Phys. Rev. A **9**, 2178 (1974).
2. J.W. Moskowitz and K.E. Schmidt, J. Chem. Phys. **85**, 2868 (1986).

3. Monte Carlo Study of Electron Correlation Functions for Small Molecules (Publication 8)

Z. Sun, P.J. Reynolds, and W.A. Lester, Jr.

A study has been made of a number of electron-electron correlation functions for use in trial wave functions of small molecules. New forms have been proposed that have variational parameters whose physical meanings are easily discerned. Calculations performed on H_2, LiH, and Li_2 using these correlation functions have been compared with results from the Jastrow-Pade form often used in Monte Carlo studies. The new forms prove more efficient in use and are easier to optimize. In addition, the possibility is addressed that the correlation depends not only on the separation of a pair of electrons but also on the location in space of this pair. Results indicate that such a many-body correlation effect is observable.

4. Valence Quantum Monte Carlo: Use of *ab initio* Effective Core Potentials (Publication 14)

B.L. Hammond, P.J. Reynolds, and W.A. Lester, Jr.

In the electronic structure of molecular systems, one often can make a fairly natural division into core and valence electrons. The valence electrons largely determine chemical properties such as bond strengths, polarizabilities, electron affinities, and ionization potentials, as well as molecular geometry. Because of its success in conventional *ab initio* approaches, the effective core potential (ECP) method is a natural starting point in the investigation of valence-only techniques for use in molecular QMC.

In QMC, the need for a valence-only approach is perhaps even greater than in familiar *ab initio* methods, because the innermost electrons are responsible for a sharp increase in the computation time required for heavy-atom systems. Another difficulty arising at large Z in all-electron calculations stems from the fixed-node approximation. Although the fixed-node error is typically a very small percentage of the total energy (0.02% for CH_2), when the total energy is large, the fixed-node error could be a significant fraction of the bond energy. This was found for N_2.[1] The placement of the inner nodes can dominate the accuracy of the calculation. Treating only the valence electrons both decreases the calculated energy and eliminates the core nodes. This should reduce the fixed-node error to well below the bond energy. An approach for implementing ECPs in QMC has been derived. Preliminary results for some atomic and molecular systems are presented.

Table 4-1 summaries ECP-QMC results for the electron affinities of Li and Na, as well as the ionization potential of Mg. For comparison, Hartree-Fock (HF) and CI results are given as well as experimental values. ECP-QMC results are comparable in quality to CI determinations, and they also lie within their error bars of the experimental result ($\approx$ 0.02 eV) in all cases. Thus, the approximation made in replacing the core electrons by a pseudopotential appears to be accurate within the given error bars for these data.

Table 4-2 gives a comparison of binding energies for Na_2. This molecule is a good example of a system presently out of range of an all-electron QMC calculation. With a total energy of about −320 hartrees, and an experimental binding energy of only 0.0254 hartree, a statistical uncertainty of less than 5 parts per million would be required in a QMC run with 22 electrons. Here the valence energy is only 0.3925 hartree, which means that the present statistical uncertainty of 0.2% is sufficient to resolve the binding energy. This makes such calculations readily accessible. The ECP-QMC result in again comparable with available all-electron CI results, and agrees with the experimental results to within statistical uncertainty.

Finally, the potential-energy curve for Na_2 is given in Figure 4-1, along with the all-electron multiconfiguration–self-consistent-field (MCSCF) point of Stevens *et al*[2] and two experimental curves. Even though the energy at the MCSCF minimum is within the statistical uncertainty of the ECP-QMC energy, the MCSCF well is displaced toward longer

Table 4-1
Electron affinities and ionization potentials of one- and two-valence electron atoms. All energies are in eV.

Atom/Ion	HF	CI	QMC-ECP	Experiment
Li/Li^-	−0.122	0.615	0.611(20)	0.620(7)
Na/Na^-	−0.116	0.539	0.555(21)	0.546(5)
Mg/Mg^+	6.613	7.524	7.637(26)	7.646

Table 4-2
Binding Energy of Na_2.

	Method	D_e (eV)
All electron	HF[a]	−0.022
	CI[b]	0.732
	MBPT[c]	0.650
Valence electron	LDFT[d]	0.69
	CI[e]	0.73
	CVCI[f]	0.747
	ECP-QMC[g]	0.746(20)
Experiment	45 vib. spect.[h]	0.7424(25)
	56 vib. spect.[i]	0.7469(7)

a. Near Hartree-Fock limit.
b. Multiconfiguration SCF.
c. Quasidegenerate many-body perturbation theory.
d. Local spin-density functional.
e. CI.
f. CI with a perturbation-theory estimate of the core-valence interaction.
g. Effective core potentials in QMC, this work.
h. RKR potential from vibrational spectroscopy using levels up to 45.
i. Same as h except using levels up to 56.

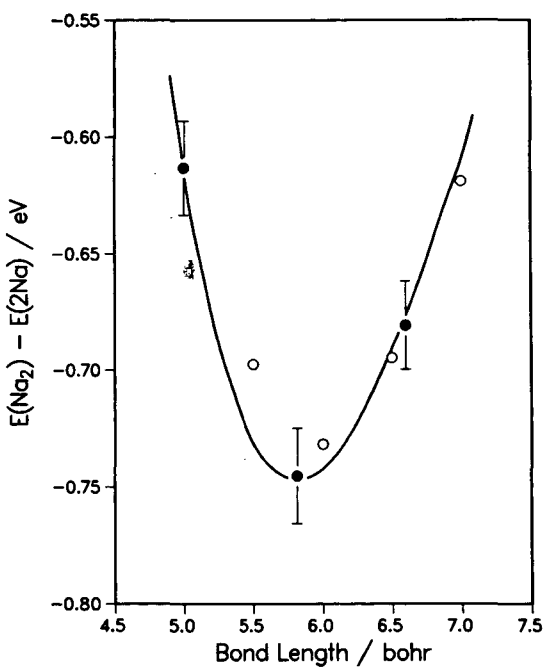

Figure 4-1. Potential-energy curves for Na_2. Solid circles: this work; open circles: all-electron MCSCF; solid line: spline fit to experimental points. (XBL 874-1813)

bond lengths, while the ECP-QMC points are consistent with the experimental curves in all cases.

1. P.J. Reynolds, R.N. Barnett, B.L. Hammond, and W.A. Lester, Jr., J. Stat. Phys. **43**, 1017 (1986).
2. W.J. Stevens, M.M. Hessel, P.J. Bertoncini, and A.C. Wahl, J. Chem. Phys. **66**, 1477 (1977).

5. Photodissociation As a Quantum Transition: Photofragment Vibrational Distributions of C_2N_2 ($\tilde{C}\ ^1\Pi_u$) Predissociation (Publications 5 and 10)

C.E. Dateo, V.Z. Kresin, M. Dupuis, and W.A. Lester, Jr.

Polyatomic indirect photodissociation is treated as a quantum transition between quasidiscrete and dissociative (photofragment) states. The adiabatic method developed in this laboratory is followed to describe the nuclear dynamics of the dissociative state. *Ab initio* MCHF excited electronic potential-energy surfaces are constructed and used to determine heavy-particle dynamics. The theory is applied to single-photon predissociation of $C_2N_2(\tilde{C}\ ^1\Pi_u)$ at 164, 158.7, and 153.6 nm to form CN ($X\ ^2\Sigma^+$) + (CN ($A\ ^2\Pi$). Theoretical predictions are found to be in good agreement with present experimental product vibrational-energy distributions.

6. On the Mechanism of Singlet-Triplet Transitions (Publication 12)

V.Z. Kresin and W.A. Lester, Jr.

A new channel for singlet-triplet relaxation has been introduced that has its origin in a nonadiabatic term of the total Hamiltonian. This term, together with the spin-orbit interaction and the radiation interaction, plays an important role in the dynamics of phosphorescence. The theory has been applied to the molecular spectroscopy of the triplet states of substituted benzenes, and it enables one to describe the experimental data obtained by Breiland and Harris.[1] The contribution of the nonadiabatic channel is directly related to the energy spectrum of triplet states. It would be interesting to have experimental studies carried out to test the effect of nonadiabaticity on the dynamics of singlet-triplet transitions in large aromatic molecules.

1. W. Breiland and C. Harris, Chem. Phys. Lett. **18**, 309 (1973).

1986 PUBLICATIONS AND REPORTS

Refereed Journals

1. P.J. Reynolds, R.N. Barnett, B.L. Hammond, and W.A. Lester, Jr., "Molecular Physics and Chemistry Applications of Quantum Monte Carlo," J. Stat. Phys. **43**, 1017 (1986); LBL-20488.
2. M. Dupuis, G. Fitzgerald, B.L Hammond, W.A. Lester, Jr., and H.F. Schaefer III, "Theoretical Study of the $H + O_3 \leftrightarrow OH + O_2 \leftrightarrow O + HO_2$ System," J. Chem. Phys. **84**, 2691 (1986); LBL-19216.
3. R.M. Grimes, W.A. Lester, Jr., and M. Dupuis, "Coupled-Channel Study of Rotational Excitation of an Electronically Excited Diatomic Molecule by Atom Impact: $He(^1S) + H_2(B\ ^1\Sigma_u^+)$," J. Chem. Phys. **84**, 5437 (1986); LBL-20534.
4. R.N. Barnett, P.J. Reynolds, and W.A. Lester, Jr., "Electron Affinity of Fluorine: A Quantum Monte Carlo Study," J. Chem. Phys. **84**, 4992 (1986); LBL-20709.

Other Publications

5. C.E. Dateo, V.Z. Kresin, M. Dupuis, and W.A. Lester, Jr., "Polyatomic Photodissociation As a Quantum Transition: Photofragment Vibrational Distribution of $C_2N_2(\tilde{C}\ ^1\Pi_u)$ Predissociation," Bull. Am. Phys. Soc. **31**, 970 (1986); LBL-21677.
6. V.Z. Kresin and W.A. Lester, Jr., "The Adiabatic Approximation and the Problem of Higher Terms: Application to Raman Scattering and Phosphorescence of Aromatic Molecules," Bull. Am. Phys. Soc. **31**, 949 (1986); LBL-22746.
7. R.M. Grimes, W.A. Lester, Jr., and M. Dupuis, "Theoretical Study of Intermolecular Energy Transfer of an Electronically Excited Diatomic Molecule by Atom Impact: $He(^1S) + H_2(B\ ^1\Sigma_u^+)$," in *Proc. Nat. Black Chemists and Chemical Engineers, Twelfth Annual Meeting*, W.A. Guillory, Ed., 1985, p. 40; LBL-19331.
8. Z. Sun, P.J. Reynolds, and W.A. Lester, Jr., "Monte Carlo Study of Electron Correlation Functions for Small Molecules," submitted to J. Chem. Phys.

LBL Publications

9. M. Dupuis and W.A. Lester, Jr., "One-Electron Property from MCHF Wavefunction: The Dipole Moment of Ozone," accepted by Theoretica Chimica Acta; LBL-21708.
10. C.E. Dateo, V.Z. Kresin, M. Dupuis, and W.A. Lester, Jr., "Photodissociation As a Quantum Transition: Photofragment Vibrational Distributions of $C_2N_2(C\ ^1\Pi_u)$ Predissociation," accepted by J. Chem. Phys.; LBL-22247.
11. R.N. Barnett, P.J. Reynolds, and W.A. Lester, Jr., "Is Quantum Monte Carlo Competitive? Lithium Hydride Test Case," accepted by J. Phys. Chem.; LBL-22503.
12. V.Z. Kresin and W.A. Lester, Jr., "On the Mechanism of Singlet-Triplet Transitions," submitted to Chem. Phys. Lett.; LBL-22524.
13. P.J. Reynolds, R.K. Owen, and W.A. Lester, Jr., "Is There a Zeroth Order Time-Step Error in Diffusion Quantum Monte Carlo?" submitted to J. Chem. Phys.; LBL-22681.
14. B.L. Hammond, P.J. Reynolds, and W.A. Lester, Jr., "Valence Quantum Monte Carlo with *ab initio* Effective Core Potential," accepted by J. Chem. Phys.; LBL-22745.

Invited Talks

15. W.A. Lester, Jr., "Quantum Chemistry by Quantum Monte Carlo," Institute for Defense Analyses, Alexandria, VA, Mar. 23, 1986.
16. W.A. Lester, Jr., "Quantum Monte Carlo for Molecules: Energies and Other Properties," Sanibel Conference and NSF Workshop, Snowbird, UT, April 21, 1986.
17. W.A. Lester, Jr., "Photodissociation and Chemical Reaction as a Quantum Transition: Theory and Applications," University of Saskatchewan, 69th Canadian Chemical Conference, Saskatoon, Saskatchewan, June 1–4, 1986.
18. P.J. Reynolds, "Quantum Monte Carlo: Achievements, Directions and Obstacles," University of Saskatchewan, 69th Canadian Chemical Conference, Saskatoon, Saskatchewan, June 1–4, 1986.
19. W.A. Lester, Jr., "Diffusion Monte Carlo for Molecules," Symposium on Computational Chemistry on CRAY Supercomputers, Minneapolis, MN, June 12, 1986.
20. P.J. Reynolds, "Quantum Monte Carlo for Atomic and Molecular Calculations," NEC Fundmental Research Laboratory, Kawasaki, Japan, July 22, 1986.
21. W.A. Lester, Jr., "Quantum Monte Carlo for Electronic Structure," Molecular Spectroscopy Division Seminar, National Bureau of Standards, Gaithersburg, MD, Aug. 15, 1986.
22. P.J. Reynolds, "Diffusion Quantum Monte Carlo: Electronic Structure as a Game of Chance," Theoretical Chemistry Seminary, University of California, Berkeley, Oct. 13, 1986.
23. P.J. Reynolds, "Parallelism in Molecular Quantum Monte Carlo: Stochastic Calculations of Electronic Structure on Supercomputers," IBM/NSF Workshop on Supercomputing, Kingston, NY, Oct. 15, 1986.
24. W.A. Lester, Jr., "Electronic Structure by Quantum Monte Carlo, "Department of Chemistry, University of California, Irvine, Oct. 28, 1986; IBM Almaden Research Center, San Jose, CA, Dec. 5, 1986.

Spectroscopy and Structures of Reactive Intermediates*

Richard J. Saykally, Investigator

INTRODUCTION

The objective of this research is to develop new techniques for the detection of unstable forms of molecules, and to use these techniques to carry out detailed measurements of the structures, properties, and dynamics of these species with the goal of improving our large-scale understanding of chemical reactions and energy transfer.

Reactive molecules, including neutral-free radicals and molecular ions, play extremely important roles as reaction intermediates in combustion processes, reactive plasmas, in the terrestrial atmosphere, and in interstellar space. The transient nature of these reactive species has made their detection and characterization a very difficult task, and comparatively few of these important reactive molecules have been studied in detail.

"Van der Waals complexes"—molecules held together at low temperatures only by very weak dispersion or induction forces or by hydrogen bonds—constitute excellent prototypes of these same weak interactions that dominate the condensed phases. One of the chemical physicist's great dreams has been to bridge the gap from the gas phase, where detailed measurements of isolated species are possible, to the condensed phases, where this is clearly impossible, through the investigation of successively more complex van der Waals aggregates in the gas phase. This dream is still a long way from being realized, as these species, like the reaction intermediates, are extremely difficult to detect and characterize. Nevertheless, a new level of understanding of van der Waals forces is emerging from studies of the vibrational motions of the weak bonds.

The primary goal of this research is to carry out detailed investigations of those reaction intermediates that are critical species in the combustion of important fuels. Exactly the same experimental and theoretical techniques employed to study reaction intermediates can be applied to van der Waals molecules; hence, studies of these two crucially important classes of molecules will be undertaken as well, with the long-range objective of correlating the measured properties of these species as a means of understanding condensed phases in more detail.

*This work was supported by the Director, Office of Energy Research, Office of Basic Energy Sciences, Materials Sciences Division of the U.S. Department of Energy under Contract No. DE-AC03-76SF00098.

1. Evidence for a Secondary Minimum in the ArHCl Potential Surface from Far-Infrared (FIR) Laser Spectroscopy of the Lowest Σ Bending Vibration (Publication 6)

R.L. Robinson, D.-H. Gwo, D. Ray,† and R.J. Saykally

Binary rare gas–hydrogen halide complexes serve as prototypes for constructing detailed models of van der Waals forces and vibrational predissociation dynamics. ArHCl is the most thoroughly investigated of these complexes, having been studied by several modern techniques, as well as by more classical methods. Nevertheless, it remains unclear whether the intermolecular potential surface exhibits minima at one or both linear configurations.[1] High-resolution spectroscopy of the low-frequency vibrations is a direct way to probe such features. We have described[2] the employment of a FIR laser-absorption technique for measurement of the lowest (34 cm^{-1}) π bend. Although precise spectroscopic information was obtained, the data could not resolve the question of a possible double-minimum potential. We report the measurement of the lowest (24 cm^{-1}) excited Σ bending vibration (the "undertone"). Analysis of these spectra in conjunction with Hutson's close-coupling results[3] provides convincing evidence for a secondary minimum in the ArHCl potential surface.

Previous descriptions of the spectrometer have been given,[2] including the incorporation of FIR-microwave double-resonance capabilities.[4] Briefly, complexes are produced in a supersonic free jet expanded into the cavity of a FIR laser. Vibration-rotation transitions in the complex are tuned into resonance with the laser by the Stark effect. Absorption spectra are detected by monitoring the intracavity laser power; spectra are displayed as the first derivative of the FIR laser gain vs. electric field for single resonance or vs. microwave frequency for double-resonance transitions. Transitions to the lowest excited Σ bending state have been measured for various Stark components of the R(0), R(1), and R(2) transitions in both single and double resonance. Figure 1-1a shows the R(0) $M_J = 1 \leftarrow 0$ single-resonance transition. The corresponding double-resonance transition is displayed in Figure 1-1b, where the $J,M_J = 1,0 \leftarrow 0,0$ ground-state rotational

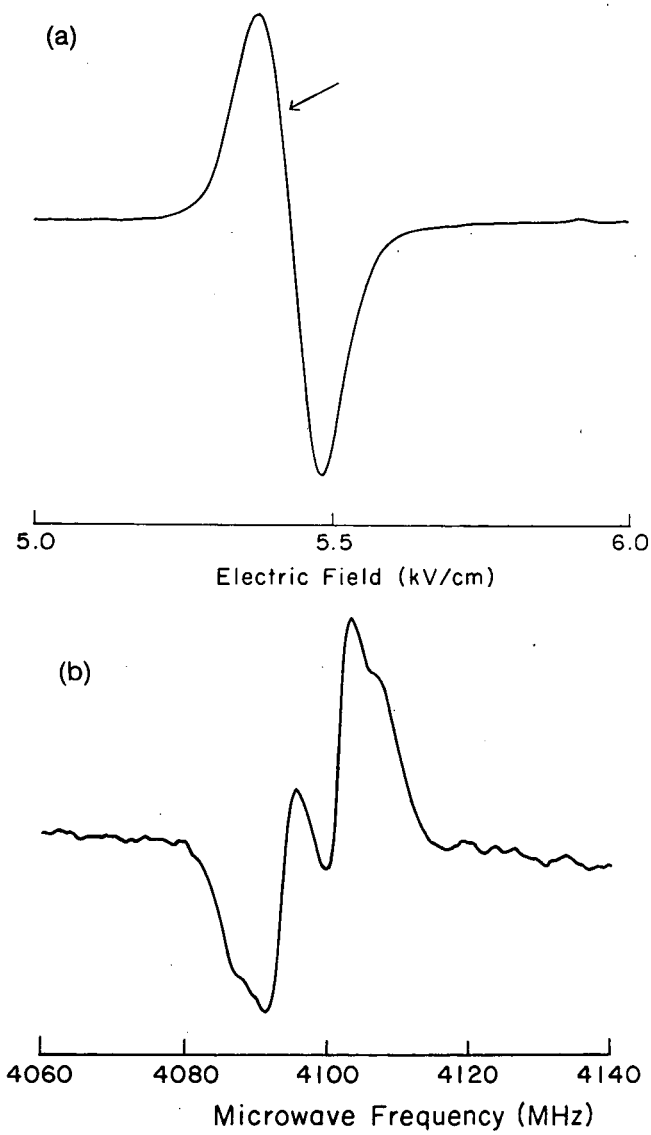

Figure 1-1. The R(0) $M_J = 1 \leftarrow 0$ transition of the lowest Σ bend in ArHCl; (a) FIR single-resonance spectrum; (b) double-resonance spectrum with microwave transition in the ground vibrational state: $J,M_J = 1,0 \leftarrow 0,0$. The electric field was fixed at 5.41 kV/cm, as indicated by the arrow in (a); the FIR laser frequency is 713.1276 GHz. [XBL 874-1715 (a), XBL 874-1716 (b)]

transition was excited and the electric field was set to the point indicated by the arrow. The 180° phase shift between the spectra demonstrates that the microwave radiation depletes the population of the lower state of the FIR transition. Because the apparatus has been temporarily configured for optimum double-resonance sensitivity by using small Stark electrodes, all spectral lines observed are inhomogeneously broadened and the quadrupole hyperfine structure is incompletely resolved.

Results from analysis of these spectra are given in Table 1-1. Ground-state constants were fixed to the precise values of Novick *et al.*[5] It was necessary to fit the frequency of one FIR laser line of CH_3OD in order to include three of the transitions. The excited-state constants are compared to the results of close-coupling calculations[3] with the M3 and M5 potentials of Hutson and Howard,[1] both of which yielded results for the Π bend in excellent agreement with experiment.[2,6] These potentials were determined from a least-squares fit to all existing experimental data for ArHCl. Although both potentials model the results equally well, the M3 potential contains a single minimum (180 cm^{-1}) at the linear ArHCl configuration, while the M5 also contains a second minimum (145 cm^{-1}) at the linear ArClH geometry. As the results show, the Σ bending frequency is extremely sensitive to the degree of double-minimum character in the potential. Although this state correlates to v = 2 of the bend in the high-anisotropy rigid-bender limit, its energy is below the v = 1 (Π bend) state even in the M3 potential because of the extreme flatness of the surface near the ArClH geometry. Nevertheless, the M5 potential predicts the Σ bend to be much lower in frequency than does the M3 surface, and our measurements yield a still lower result. In addition, the M5 dipole moment agrees very well with our value, whereas the M3 result is clearly incompatible with experiment; similarly, the M5 rotational constant is in much better accord. Although these results cannot completely exclude the possibility that ArHCl could be described in terms of a potential surface that is qualitatively different from both the M3 and M5 surfaces, the extremely good agreement of our measurement of the Σ bending "undertone" with calculations from the M5 surface strongly supports the existence of a secondary minimum at the ArClH geometry, and demonstrates the possibility of using FIR laser spectroscopy to obtain accurate anisotropic intermolecular potential functions.

Table 1-1
Results for the Σ bending state of ArHCl compared with calculations[3] from the M3 and M5 potentials.

	This Work[a,b]	M3	M5
ν_0 (cm^{-1})	23.6568(7)	28.367	24.905
B (MHz)	1763.0(1)	1694.9	1752.7
μ (D)	0.514(6)	0.085	0.499

a. Standard deviation of the fit for 8-laser Stark transitions is 9 MHz. Uncertainties are 1σ.
b. Fit of CH_3OD FIR laser-line frequency: 716957(7) MHz.

†Present address: Joint Institute for Laboratory Astrophysics and Department of Chemistry, University of Colorado, Boulder, CO 80309.

1. J.M. Hutson and B.J. Howard, Mol. Phys. **45**, 769 (1982).

2. D. Ray, R.L. Robinson, D.-H. Gwo, and R.J. Saykally, J. Chem. Phys. **84**, 1171 (1986).

3. J.M. Hutson, J. Chem. Soc., Faraday Trans. 2 **82**, 1163 (1986).

4. R.L. Robinson, D. Ray, D.-H. Gwo, and R.J. Saykally, in *Proc. Structure and Dynamics of Weakly Bound Molecular Complexes*, NATO-ARW Conference, Maratea, Italy, Reidel, 1986.

5. S.E. Novick, P. Davies, S.J. Harris, and W. Klemperer, J. Chem. Phys. **59**, 2273 (1973); S.E. Novick, K.C. Janda, S.L. Holmgren, M. Waldman, and W. Klemperer, J. Chem. Phys. **65**, 1114 (1976).

6. M. Marshall, A. Charo, H.O. Leung, and W. Klemperer, J. Chem. Phys. **83**, 4924 (1985).

2. Work in Progress

We are now developing tunable FIR laser techniques for studying reactive molecules generated by excimer laser photolysis and van der Waals complexes. Ultimately these lasers will possess extremely high sensitivity and resolution such that subtle effects on hydrogen tunneling migration effects can be explored in fluxional radicals like vinylidene and vinyl radical.

1986 PUBLICATIONS AND REPORTS

Refereed Journals

1. D. Ray, R. Robinson, D.-H. Gwo, and R.J. Saykally, "Intracavity Far Infrared Laser Spectroscopy of Supersonic Jets: Direct Measurement of the Vibrational Motions in van der Waals Bonds," J. Chem. Phys. **84**, 1171 (1986); LBL-20409.
2. M.H.W. Gruebele, R.P. Müller, and R.J. Saykally, "Measurement of the Rotational Spectra of OH^+ and OD^+ by Laser Magnetic Resonance," J. Chem. Phys. **84**, 2489 (1986); LBL-20411.
3. S.E. Strahan, R.P. Müller, and R.J. Saykally, "Measurement of the Rotational Spectrum of the Water Cation (H_2O^+) by Laser Magnetic Resonance Spectroscopy," J. Chem. Phys. **85**, 1252 (1986); LBL-21108.
4. J.M. Brown, J.E. Schubert, R.J. Saykally, and K.M. Evenson, "The Far-Infrared Laser Magnetic Resonance Spectrum of the CF Radical and Determination of Ground State Parameters," J. Mol. Spectrosc. **120**, 421 (1986).

Other Publications

5. R.L. Robinson, D. Ray, D.-H. Gwo, and R.J. Saykally, "Vibration-Rotation Spectroscopy of ArHCl by Far-Infrared Laser and Microwave/Far-Infrared Laser Double Resonance Spectroscopy," NATO-ARW Proc., Maratea, Italy, 1986; LBL-22803.

LBL Reports

6. R.L. Robinson, D.-H. Gwo, D. Ray, and R.J. Saykally, "Evidence for a Secondary Minimum in the ArHCl Potential Surface from Far Infrared Laser Spectroscopy of the Lowest Σ Bending Vibration," submitted to J. Chem. Phys.; LBL-22804.

Invited Talks

7. R.J. Saykally, "Infrared Laser Spectroscopy of Molecular Ions and van der Waals Bonds," National Bureau of Standards, Gaithersburg, MD, May 27, 1986.
8. R.J. Saykally, "Infrared Laser Spectroscopy of Simple Cations and Anions," Regional ACS Meeting, Denver, CO, June 17, 1986.
9. R.J. Saykally, "Infrared Laser Spectroscopy of Cations and Anions," IQEC Conference, San Francisco, CA, June 11, 1986.
10. R.J. Saykally, "Infrared Laser Spectroscopy of Simple Anions and Cations," Gordon Conference, Wolfsboro, NH, Aug. 15, 1986.
11. R.J. Saykally, "Infrared Laser Spectroscopy of Simple Anions and Cations," Laboratoire de Spectroscopie Hertzienne associe. au C.N.R.S., Lille, France, Sept. 19, 1986.
12. R.J. Saykally, "Vibration-Rotation Spectroscopy of ArHCl by Far-Infrared Laser and Microwave/Far-Infrared Laser Double Resonance Spectroscopy," NATO Conference, Maratea, Italy, Sept. 22, 1986.
13. R.J. Saykally, "Infrared Laser Spectroscopy of Simple Anions and Cations," University of Washington, Seattle, Oct. 20, 1986.
14. R.J. Saykally, "Infrared Laser Spectroscopy of Simple Anions and Cations," Optical Society Meeting, Seattle, WA, Oct. 21, 1986.
15. R.J. Saykally, "Intracavity Far Infrared Laser Spectroscopy with Stark and Zeeman Techniques," International Laser Science Conference, Seattle, WA, Oct. 22, 1986.
16. R.J. Saykally, "Infrared Laser Spectroscopy of Simple Anions and Cations," University of California San Diego, La Jolla, CA, Oct. 27, 1986.
17. R.J. Saykally, "Infrared Laser Spectroscopy of Simple Anions and Cations," Argonne National Laboratories, Argonne, IL, Nov. 24, 1986.

Theory of Atomic and Molecular Collision Processes*

William H. Miller, Investigator

INTRODUCTION

This research is primarily involved with the development and application of theoretical methods and models for describing atomic and molecular collision processes. Specific topics of interest include the theory of inelastic and reactive scattering, collision processes involving electronically excited atoms or molecules, collisional ionization phenomena, statistical theories of chemical reactions, scattering of atoms and molecules from surfaces, and the interactions of molecular systems with high-power laser radiation.

Much of this research is involved with the development and application of a general semiclassical mechanics that allows one to combine classical mechanics and quantum mechanics in a correct and useful manner. This approach has been extremely successful in providing an understanding of the various effects that are seen in molecular phenomena, and it also often provides simpler computational methods for carrying out quantitative calculations. Certain research topics are more amenable to a completely quantum mechanical approach, and these sorts of theoretical techniques are also used.

The ability to understand—and thus model and predict—chemical kinetic phenomena in the gas phase has widespread practical importance in a number of different areas. Among these are atmospheric chemistry and physics, the interactions of molecules with strong laser fields, and energy-transfer and chemical reactions in flames and combustion.

1. Reaction Surface Description of Intramolecular Hydrogen Atom Transfer in Malonaldehyde (Publication 1)†

T. Carrington, Jr.‡ and W.H. Miller

Intramolecular H-atom transfer in malonaldehyde is described using a reaction-surface Hamiltonian (Figure 1-1). This model utilizes two large-amplitude, reaction-coordinate-like degrees of freedom—i.e., a surface in the 3N-6 dimensional configuration space of an N-atom system—with the remaining 3N-8 degrees of freedom being local harmonic motion away from this 2D surface. The two reaction-surface degrees of freedom are chosen to be the two OH bond lengths, i.e., the bond being broken and the bond being formed. The present methodology is developed using 3N-6 internal coordinates, in contrast to our earlier reaction-surface model[1] that utilized the 3N cartesian coordinates. From our calculations we conclude that the bare barrier (i.e., with no zero-point vibrational corrections) for the H-atom transfer is between 6 and 7 kcal/mole.

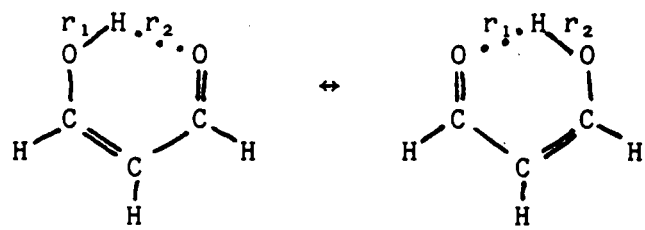

Figure 1-1. Intramolecular H-atom transfer in malonaldehyde described by a reaction-surface Hamiltonian. (XBL 871-106)

Figure 1-2 is a contour plot of the potential energy on this 2D reaction surface, and Figure 1-3 shows the OH bend frequency as a function of (r_1,r_2). This is the mode that shows the largest frequency variation over the (r_1,r_2) surface, but even there one sees that this variation is not great. This means that

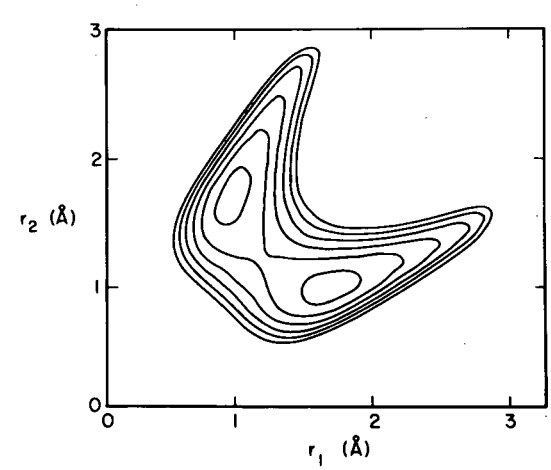

Figure 1-2. Contour plot of the potential $V_0(r_1,r_2)$ on the reaction surface. The case shown is for a classical barrier height of 4.3 kcal/mole. (XBL 858-3695)

*This work was supported by the Director, Office of Energy Research, Office of Basic Energy Sciences, Chemical Sciences Division of the U.S. Department of Energy under Contract No. DE-AC03-76SF00098.

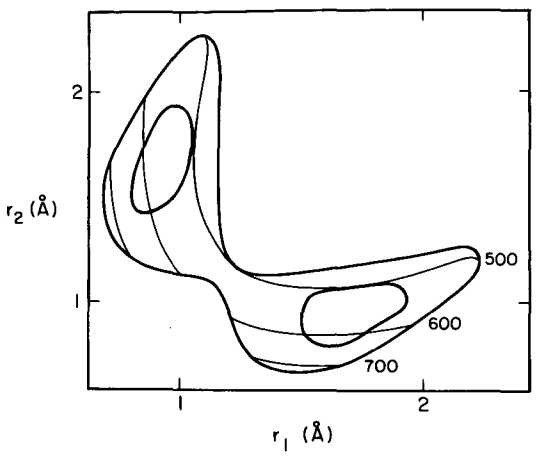

Figure 1-3. Contour plot of the OH bend frequency $\omega_k(r_1,r_2)$. (Two contours of the potential $V_0(r_1,r_2)$ are also shown.) The numbers label the frequency contours in cm^{-1}. (XBL 858-3696)

an adiabatic treatment of all the degrees of freedom other than (r_1,r_2) is quite accurate.

†Calculations were carried out on an IBM 4381 minicomputer supported by the National Science Foundation Grant No. CHE-8416345.

‡Present address: Laboratorium für Physikalische Chemie, Eidgenossische Technische Hochschule ETH-Zentrum, CH-8092 Zurich, Switzerland.

1. J. Chem. Phys. **81**, 3942 (1984).

2. Spin-Orbit and Diagonal Born-Oppenheimer Corrections for the Reaction F + H_2 → HF + H (Publication 2)†

N.C. Handy,‡ T.J. Lee, and W.H. Miller

An examination of the effect of the spin-orbit correction and the diagonal Born-Oppenheimer correction for the F + H_2 → HF + H reaction is reported, using *ab initio* self-consistent field (SCF) and configuration-interaction (CI) potential curves. At the transition state the spin-orbit correction increases the barrier height by 0.36 kcal, and the diagonal correction increases it by 0.04 kcal. Earlier in the reaction pathway, the diagonal correction has a singularity, which means that in this region it is not possible to consider the reaction taking place on a single adiabatic surface.

†Calculations were carried out on an IBM 4381 minicomputer supported by the National Science Foundation, Grant CHE-8416345.

‡Permanent address: University Chemical Laboratory, Cambridge CB2 1EW, England.

3. Quantum Mechanical Reactive Scattering Via Exchange Kernels: Comparison of Grid Versus Basis-Set Expansion of the Exchange Interaction (Publication 7)†

M.R. Hermann‡ and W.H. Miller

In the approach to quantum mechanical reactive scattering that we have been pursuing,[1] the reactive coupling is described by a nonlocal exchange interaction in a coupled-channel Schrödinger equation. This paper reports the results of systematic studies undertaken to identify the most efficient way to include the exchange interaction to infinite order, i.e., exactly. We find that the grid method used previously by Dardi *et al.*[2] can be made much more efficient by using Gaussian quadrature grids, but that still more efficient is an expansion of the exchange operator in a set of smooth basis functions via the "inner projection" approach of Adams and Miller.[3] Test problems studied are the collinear H + D_2, D + H_2, and F + H_2 reactions.

Figures 3-1 and 3-2 show typical results for two isotopic variants of the H + H_2 reaction, and Figures 3-3, 3-4, and 3-5 show typical results for F + H_2, both compared to results of earlier calculations by other workers. This work thus establishes the Schwinger-type basis-set expansion—within the multichannel distorted-wave representation—as a

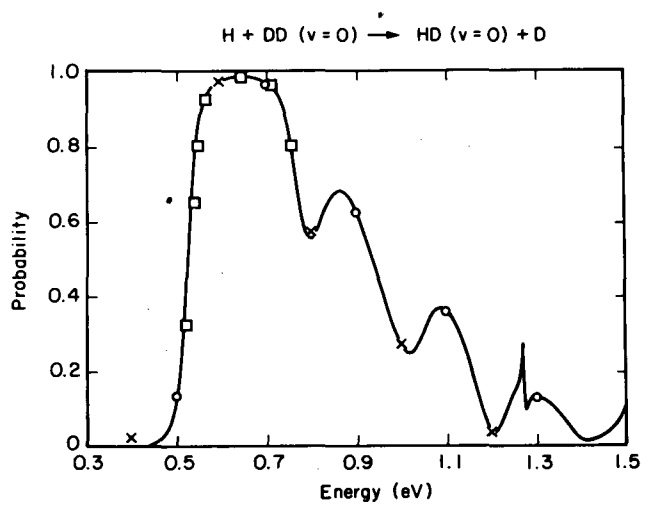

Figure 3-1. Reaction probabilities for the H + D_2(v = 0) → HD(v = 0) + D reaction as a function of total energy. The data plotted are obtained from converged-basis-set "inner projection" method (solid curve), evenly-spaced-grid method (*), Gaussian quadrature grid method (o), and previous calculations (squares). (XBL 863-1038)

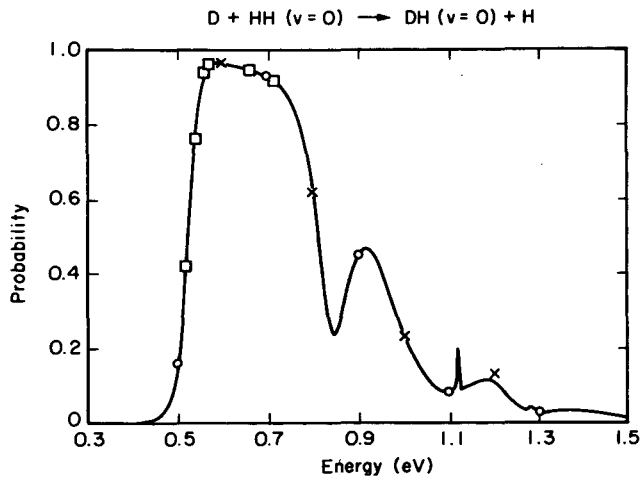

Figure 3-2. As in Figure 3-1 for the D + H_2(v = 0) → DH(v = 0) + H reaction. (XBL 863-1042)

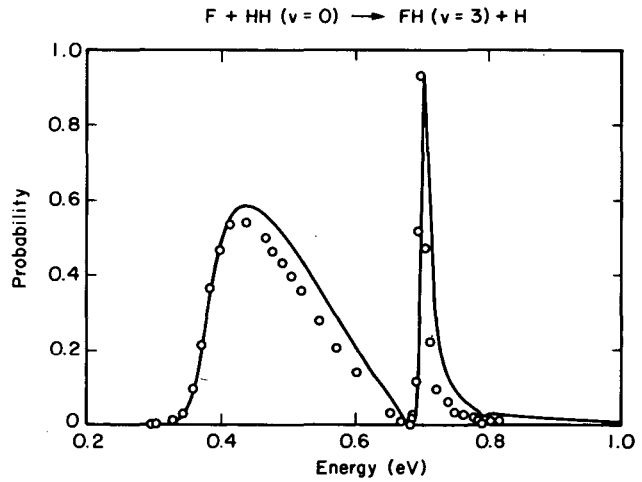

Figure 3-4. As in Figure 3-3 for the F + H_2 (v = 0) → FH (v = 3) + H reaction. (XBL 863-1040)

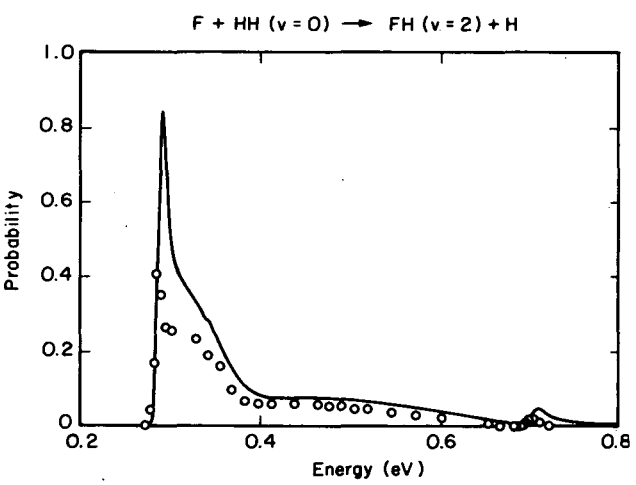

Figure 3-3. Reaction probabilities for the F + H_2(v = 0) → FH(v = 2) + H reaction as a function of total energy. The smooth curve represents the converged-basis-set "inner projection" results, while the circles are previous calculations. (XBL 863-1044)

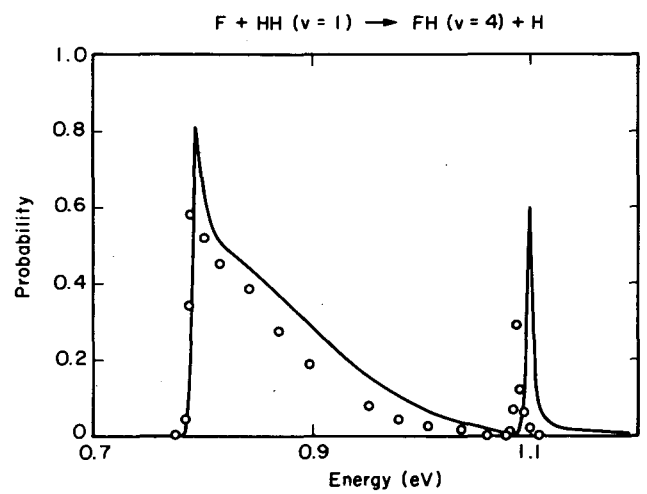

Figure 3-5. As in Figure 3-3 for the F + H_2 (v = 1) → FH(v = 4) + H reaction. (XBL 863-1039)

straightforward and liable methodology for quantum reactive scattering. It can be readily extended to 3D systems.

4. Work in Progress

A new approach for describing reaction dynamics in polyatomic molecular systems is being devised, one that is based on a totally Cartesian representation of the Hamiltonian. This avoids some of the problems encountered by our earlier approaches (reaction-path models) and is significantly easier to apply than the reaction-surface model that we have recently developed.

A number of new ideas are also being pursued for evaluating Feynman path-integral expressions for reactive-flux correlation functions. These will be used in conjunction with the above Cartesian reaction Hamiltonian to treat various dynamics processes in complex systems.

---

†Calculations were carried out on IBM 4381 and Cray 1 computers supported by the National Science Foundation, Grant CHE-8416345.

‡Present address: Lawrence Livermore National Laboratories, Livermore, CA 94550.

1. W.H. Miller, J. Chem. Phys. **50**, 407 (1969).
2. P.S. Dardi, S.-h. Shi, and W.H. Miller, J. Chem. Phys. **83**, 575 (1985).
3. Adams and W.H. Miller, J. Phys. Chem. **83**, 1505 (1979).

1986 PUBLICATIONS AND REPORTS

Refereed Journals

1. T. Carrington, Jr., and W.H. Miller, "Reaction Surface Description of Intramolecular Hydrogen Atom Transfer in Malonaldehyde," J. Chem. Phys. **84**, 4364 (1986); LBL-20616.
2. W.H. Miller and K.A. White, "Classical Models for Electronic Degrees of Freedom: The Second-Quantized Man-Electron Hamiltonian," J. Chem. Phys. **84**, 5059 (1986).
3. N.C. Handy, T.J. Lee, and W.H. Miller, "Spin-Orbit and Diagonal Born-Oppenheimer Corrections for the Reaction $F + H_2 \rightarrow HF + H$," Chem. Phys. Lett. **125**, 12 (1986); LBL-20773.
4. W.H. Miller, "Semiclassical Methods in Chemical Physics," Science **233**, 171 (1986); LBL-20774.
5. J.W. Tromp and W.H. Miller, "New Approach to Quantum Mechanical Transition State Theory," J. Phys. Chem. **90**, 3482 (1986).
6. W.H. Miller, "Comment on 'Probability Oscillations in Single Pass Curve Crossings: Semiclassical Predictions of Non-Monotonic Dependence on Crossing Velocity,' " J. Chem. Phys. **85**, 3703 (1986).
7. M.R. Hermann and W.H. Miller, "Quantum Mechanical Reactive Scattering via Exchange Kernels: Comparison of Grid versus Basis Set Expansion of the Exchange Kernel," Chem. Phys. **109**, 163 (1986); LBL-21202.

Other Publications

8. W.H. Miller, "Some Recent Initiatives in Quantum Mechanical Reactive Scattering," in *Molecular Reaction Dynamics*, R. Vetter and J. Vigue, eds., Editions du Centre National de la Recherche Scientifique, Paris, 1986, p. 147.
9. W.H. Miller, "Reaction Path Models for Polyatomic Reaction Dynamics—from Transition State Theory to Path Integrals," in *The Theory of Chemical Reaction Dynamics,* D.C. Clary, Ed., D. Reidel, Boston, 1986, p. 27; LBL-19874.
10. W.H. Miller, "Reaction Paths and Surfaces for Hydrogen Atom Transfer Reactions in Polyatomic Molecules," in *Tunneling*, J. Jortner and B. Pullman, eds., D. Reidel, Boston, 1986, p. 91; LBL-21662.

LBL Reports

11. W.H. Miller, "Tunneling and State-Specificity in Unimolecular Reactions," Chem. Rev. (in press); LBL-21203.
12. N. Makri and W.H. Miller, "Basis Set Methods for Describing the Quantum Mechanics of a 'System' Interacting with a Harmonic 'Bath,' " J. Chem. Phys. (in press); LBL-22366.

Invited Talks

13. W.H. Miller, "Classical Models for Electronic Degrees of Freedom," Nobel Laureate Signature Award Symposium, National ACS Meeting, New York, April 13–18, 1986.
14. W.H. Miller, "Reaction Paths and Reaction Surfaces for Hydrogen Atom Transfer Reactions," Jerusalem Symposium on Tunneling, Jerusalem, Israel, May 5–8, 1986.
15. W.H. Miller, "Reaction Paths and Surfaces, and their Application to Reaction Dynamics in Polyatomic Systems," Canadian Chemical Conference, Saskatoon, Saskachewan, June 1–4, 1986.
16. W.H. Miller, "A New Strategy for Polyatomic Reaction Dynamics," NATO Advanced Research Workshop on Stochasticity and Intramolecular Redistribution Energy, Paris, June 23–July 4, 1986.
17. W.H. Miller, "State Specific Reaction Dynamics in Polyatomic Molecules," Symposium on State-to-State Chemistry, National ACS Meeting, Anaheim, CA, Sept. 7–12, 1986.
18. W.H. Miller, "Some New Approaches to Polyatomic Reaction Dynamics," International Symposium "Chaos and Related NonLinear Phenomena—Where Do We Go From Here?" Jerusalem, Israel, Dec. 13–19, 1986.

Photoelectron Spectroscopy*

David A. Shirley, Investigator

INTRODUCTION

This program addresses both experimental and theoretical aspects of electron spectroscopy for the investigation of electronic structure of matter in the gaseous and condensed phases. Research is conducted using both laboratory sources at LBL and synchrotron radiation in the 5–5000 eV energy range available at the Stanford Synchrotron Radiation Laboratory, where there is participation in developing the spectroscopy of this newly accessible range of the electromagnetic spectrum. Time-of-flight measurements with synchrotron radiation are used to measure angular distributions of photoelectrons and resonant photoemission phenomena in the gas phase. Ultrahigh-resolution photoelectron spectroscopy based on molecular beams is yielding new information about small molecules and about the transition from single metal atoms to behavior characteristic of a three-dimensional solid. Employing angle-resolved, variable-energy photoemission and electron-energy-loss spectroscopy, this program examines the electronic structure of solids. The program also studies the geometric and electronic structure of surface-adsorbate systems using photoelectron diffraction, angle-resolved photoemission extended fine structure (ARPEFS), and surface extended x-ray absorption fine structure (SEXAFS).

1. Shape-Resonant and Many-Electron Effects in the S 2p Photoionization of SF_6 (Publication 20)

T.A. Ferrett,[†] D.W. Lindle,[‡] P.A. Heimann,[§] M.N. Piancastelli,[‖] P.H. Kobrin,[**] H.G. Kerkhoff,[††] U. Becker,[††] W.D. Brewer,[‡‡] and D.A. Shirley

The core-level photoexcitation and photoionization of SF_6 has been studied in the vicinity of the resonances below and above the S 2p threshold. Qualitative results for the decay channels of the S 2p → $6a_{1g}$ discrete excitation were obtained, with dominant decay to valence satellites. The S 2p continuum results on the e_g shape resonance indicate strong multielectron properties for this state, because a resonant S 2p shakeup satellite is observed, as shown in Figure 1-1. We propose a model that includes configuration interaction in the quasibound state and in the ionic and continuum state manifolds to explain this unusual behavior. Finally, the S(LVV) Auger electron asymmetry parameter shows no significant deviation from zero near the t_{2g} and e_g shape resonances.

*This work was supported by the Director, Office of Energy Research, Office of Basic Energy Sciences, Chemical Sciences Division of the U.S. Department of Energy under Contract No. DE-AC03-76SF00098. It was performed at the Stanford Synchrotron Radiation Laboratory, which is supported by the Department of Energy's Office of Basic Energy Sciences.

[†]Present address: National Bureau of Standards, Physics A251, Gaithersburg, MD 20899.

[‡]Present address: National Bureau of Standards, Quantum Metrology Group, Physics A141, Gaithersburg, MD 20899.

[§]Present address: Technische Universität München, D-8046 Garching b, München, Federal Republic of Germany.

[‖]Permanent address: Department of Chemistry, University of Rome "La Sapienza," 00100 Rome, Italy.

[**]Present address: Rockwell International, 1049 Camino dos Rios, Thousand Oaks, CA 91360.

[††]Permanent address: Technische Universität Berlin, Institut für Strahlungs- und Kernphysik, D-1000 Berlin 12, Federal Republic of Germany.

[‡‡]Permanent address: Institut für Atom- und Festkorperphysik, Freie Universität Berlin, 1000 Berlin 33, Federal Republic of Germany.

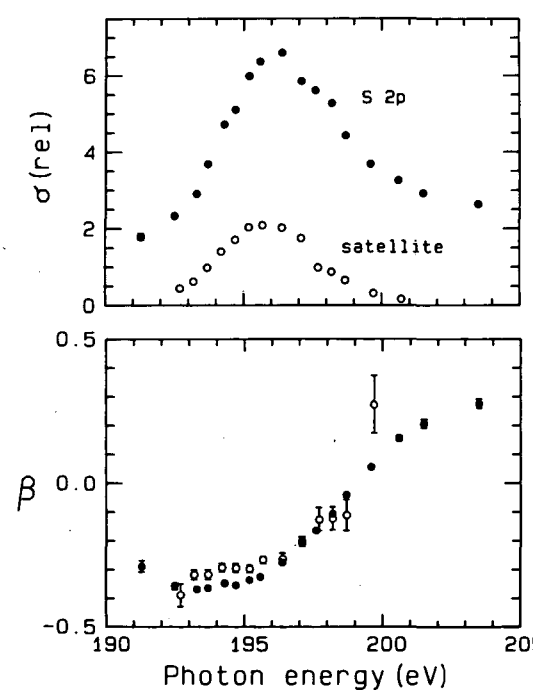

Figure 1-1. Relative cross section and asymmetry parameter for the S 2p main line (solid circles) and satellite (open circles) in an expanded energy range near the "e_g" resonance (196.5 eV). (XBL 8611-4293)

2. Helium and Neon Photoelectron Satellites at Threshold (Publication 15)

P.A. Heimann,[†] U. Becker,[‡] H.G. Kerkhoff,[‡] B. Langer,[‡] D. Szostak,[‡] R. Wehlitz,[‡] D.W. Lindle,[§] T.A. Ferrett,[‖] and D.A. Shirley

Photoionization of helium and neon to excited satellite states, He^+ nl and Ne^+ $1s^22s^22p^4nl$, was studied with synchrotron radiation and threshold electron analysis. Photoelectron satellites have been directly measured at threshold for the first time. The relative satellite cross sections were determined over the kinetic energy range from 0 to 1 eV. The angular distributions were also evaluated close to threshold. Strong correlation effects were observed in two cases. For He near threshold, the angular-distribution asymmetry parameter β is near zero for the n = 2 satellite and is increasingly negative for the higher n satellites, in agreement with the theoretical prediction of Greene.[1] In the threshold photoelectron spectrum of Ne (shown in Figure 2-1), many final states are present, some with quartet spin multiplicity and others with high L values.

[†]Present address: Technische Universität München, D-8046 Garching b, München, Federal Republic of Germany.

[‡]Permanent address: Technische Universität Berlin, Institut für Strahlungs- und Kernphysik, D-1000 Berlin 12, Federal Republic of Germany.

[§]Present address: National Bureau of Standards, Quantum Metrology Group, Physics A141, Gaithersburg, MD 20899.

[‖]Present address: National Bureau of Standards, Physics A251, Gaithersburg, MD 20899.

1. C. Greene, Phys. Rev. Lett. **44**, 869 (1980).

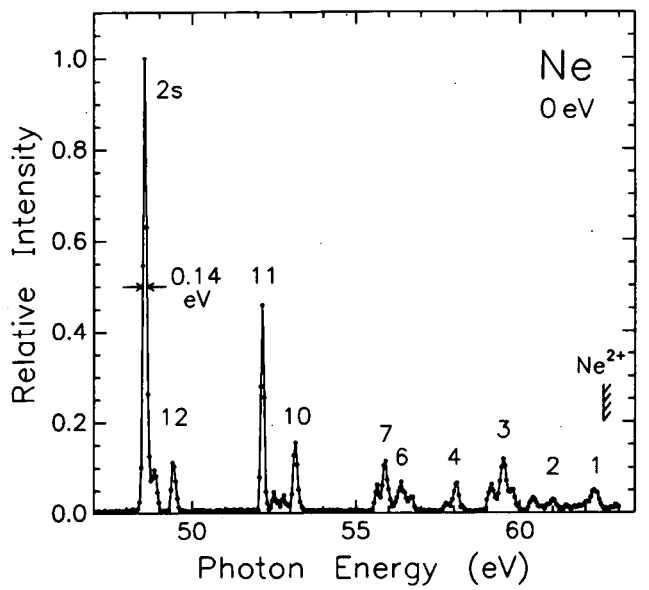

Figure 2-1. Threshold photoelectron scan of the Ne 2s main line and valence satellites. The line connects the points. (XBL 866-2141)

3. Shake-Off on Inner-Shell Resonances of Ar, Kr, and Xe (Publication 35)

P.A. Heimann,[†] D.W. Lindle,[‡] T.A. Ferrett,[§] S.H. Liu, L.J. Medhurst, M.N. Piancastelli,[‖] D.A. Shirley, U. Becker,[**] H.G. Kerkhoff,[**] B. Langer,[**] D. Szostak,[**] and R. Wehlitz[**]

Synchrotron radiation was used to excite an inner-shell electron into a Rydberg orbital at the Ar 2p → ns, nd, Kr 3d → np, and Xe 4d → np resonances. The resonant decay into shake-off channels was studied by three different electron measurements. First, threshold electron scans were obtained over the resonances and thresholds shown for Kr in Figure 3-1. On one resonance for each atom, photoelectron spectra were collected. The intensity distribution of low-kinetic-energy electrons was also determined for a few resonances. Finally, a shake calculation was carried out to compare with the

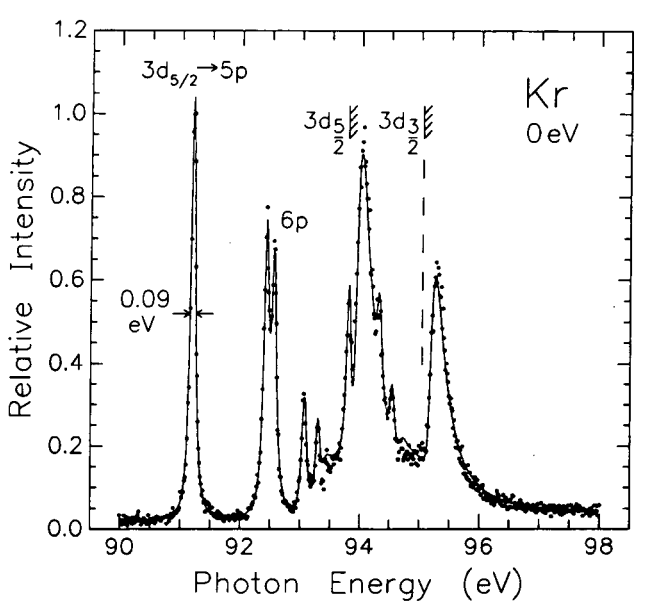

Figure 3-1. A threshold scan over the Kr $3d^{-1}$ np resonances and 3d thresholds. The curve reproduces a fit. (XBL 8611-4320)

experimental shake-off probabilities. Shake-off is observed to be a strong decay channel for these resonances.

†Present address: Technische Universität München, D-8046 Garching b, München, Federal Republic of Germany.

‡Present address: National Bureau of Standards, Quantum Metrology Group, Physics A141, Gaithersburg, MD 20899.

§Present address: National Bureau of Standards, Physics A251, Gaithersburg, MD 20899.

¶Permanent address: II University of Rome, 00173 Rome, Italy.

**Permanent address: Technische Universität Berlin, Institut für Strahlungs- und Kernphysik, Berlin, Federal Republic of Germany.

4. Helium Photoelectron Satellites: Low-Energy Behavior of the n = 3–5 Lines (Publication 23)

D.W. Lindle,† P.A. Heimann,‡ T.A. Ferrett,§ and D.A. Shirley

Photoelectron satellite branching ratios and asymmetry parameters have been measured for photoionization of atomic He to $He^+(n)$, where n = 3–5, at a few photon energies near the satellite thresholds. The photoelectron spectrum in Figure 4-1 illustrates

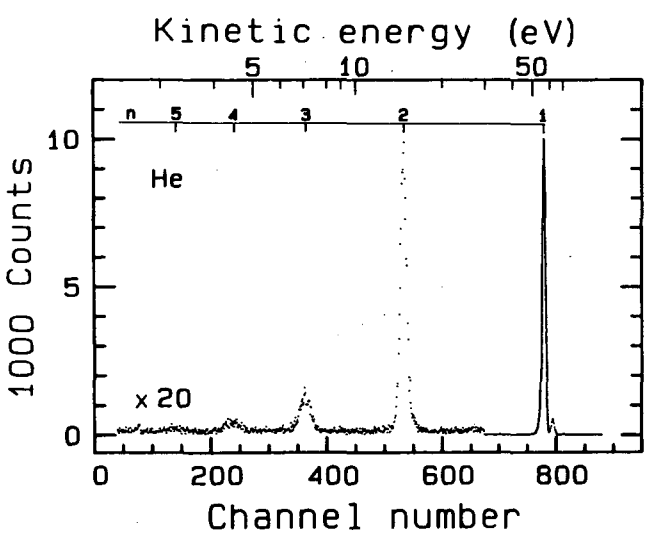

Figure 4-1. Time-of-flight photoelectron spectrum of He at 80-eV photon energy and with θ = 54.7°. The peak label n refers to the principal quantum number of the remaining electron in the He^+ final state. The small peak to the right of the n = 1 main line is a result of ringing in the timing circuit, displacing a small fraction of the true counts by a few channels. (XBL 852-1070)

the different satellite final states of He (n) at a photon energy of 80 eV. The n = 3 and n = 4 satellite branching ratios relative to the n = 1 main-line cross section exhibit behavior similar to that previously observed for the $He^+(n = 2)$ satellite. The asymmetry parameter β shows progressively more negative values as n increases, supporting a prediction by Greene[1] for the threshold behavior of the He satellites.

†Present address: National Bureau of Standards, Quantum Metrology Group, Physics A141, Gaithersburg, MD 20899.

‡Present address: Technische Universität München, D-8046 Garching b, München, Federal Republic of Germany.

§Present address: National Bureau of Standards, Physics A251, Gaithersburg, MD 20899.

1. C. Greene, Phys. Rev. Lett. **44**, 869 (1980).

5. Molecular Beam Photoelectron Spectroscopy and Femtosecond Intramolecular Dynamics of H_2O^+ and D_2O^+ (Publication 16)

J.E. Reutt,† L.S. Wang, Y.T. Lee, and D.A. Shirley

The 584-Å photoelectron spectra of supersonic molecular beams of H_2O and D_2O have been obtained with improved resolution. The spectroscopic constants of the $\tilde{X}\ ^2B_1$ and $\tilde{A}\ ^2A_1$ state ions, including ω_1^0, χ_{11}^0, ω_2^0, χ_{22}^0, and χ_{12}^0, are reported. For the first two electronic states of the ion, precise line splittings were evaluated with a least-squares fitting procedure, employing sums of empirical instrument response functions and a linear background. A simulation of the vibrational manifolds of the $\tilde{B}\ ^2B_2$ state ions with combination progressions in the symmetry-allowed modes ν_1 and ν_2 failed to reproduce the diffuse photoelectron bands observed for both H_2O and D_2O. Autocorrelation functions were calculated from the photoelectron bands of all three electronic states. The $\tilde{B}\ ^2B_2$ state correlation functions exhibit ultrafast decay, occurring on a 10^{-14} sec timescale. The ν_2 motion appears to define the decay in the correlation function. This behavior supports a previously proposed $\tilde{B}\ ^2B_2$–$\tilde{A}\ ^2A_1$ curve-crossing model for the nonradiative relaxation of the $\tilde{B}\ ^2B_2$ state ions (Figure 5-1).

†Present address: AT&T Bell Laboratories, Murray Hill, NJ 07974.

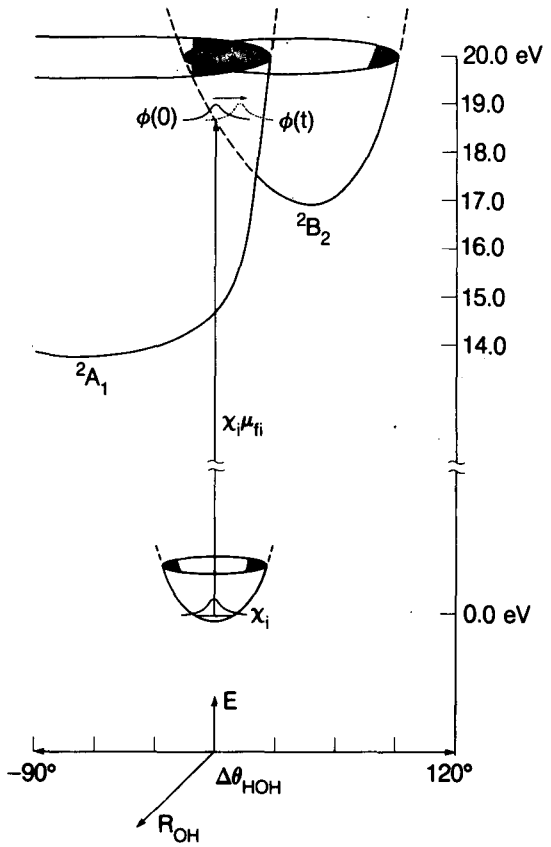

Figure 5-1. The $\tilde{B}\ ^2B_2$–$\tilde{A}\ ^2A_1$ curve-crossing model for the nonradiative decay of the $\tilde{B}\ ^2B_2$ state is depicted schematically. The diabatic $\tilde{B}\ ^2B_2$ and $\tilde{A}\ ^2A_1$ surfaces cross near the $\tilde{B}\ ^2B_2$ minimum. The wave packet $\theta(0)$ is prepared on the $\tilde{B}\ ^2B_2$ surface by photoionization. As the wave packet travels along the Δ_{HOH} (or ν_2) coordinate, it passes through the seam of intersection and can hop over to the $\tilde{A}\ ^2A_1$ surface. (XBL 856-9852)

6. Molecular Beam Photoelectron Spectroscopy: The $C_2D_4^+$ ($\tilde{X}\ ^2B_3$) Ground State (Publication 25)

L. Wang, J.E. Pollard,† Y.T. Lee, and D.A. Shirley

The HeI (584 Å) photoelectron spectrum of $C_2D_4^+$ in its ground electronic state has been measured, using a supersonic molecular beam (as shown in Figure 6-1). The combination of rotational cooling and improved resolution permits new vibrational fine structure to be observed and assigned. In particular, the ν_3 value is accurately determined. A systematic increase in the ν_4 torsional frequency with increasing excitation of the ν_2 C=C stretching vibration is observed, indicating significant coupling between these modes.

†Present address: The Aerospace Corporation, Los Angeles, CA 90009.

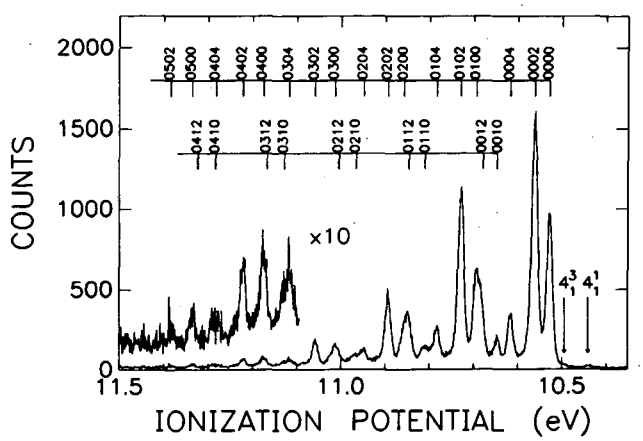

Figure 6-1. The HeI (584 Å) photoelectron spectrum of $C_2D_4^+$ ($\tilde{X}\ ^2B_3$) ground state. The vibrational levels are labeled with the ν_1, ν_2, ν_3, and ν_4 vibrational quantum numbers. The symmetry of the state is assumed to be D_2. (XBL 867-2791)

7. Molecular Beam Photoelectron Spectroscopy of SO_2: Geometry, Spectroscopy, and Dynamics of SO_2^+ (Publication 26)

Laisheng Wang, Y.T. Lee, and D.A. Shirley

We have reinvestigated the HeI (584 Å) photoelectron spectroscopy of SO_2 using a supersonic molecular beam. Improved resolution and rotational cooling allow us to observe new features and to resolve explicitly the vibrational structure in the first six electronic states, in the first three photoelectron bands (see Figure 7-1). The adiabatic ionization potentials (IPs) were accurately determined for all six states. The $\tilde{X}\ ^2A_1$ ground state is assigned to the ν_2 mode exclusively. Irregularity of the vibrational progression on the high IP side was observed for the first time. A potential barrier (to linearity) is proposed to interpret the irregular vibrational spacings in the ν_2 vibration. The barrier height is estimated to be 0.42 eV (3400 cm^{-1}). The complex second band contains two states. Abnormal vibrational structure in the $\tilde{A}\ ^2A_2$ state is explained by the principal excitation of the ν_3 mode. A potential barrier is present in the ν_3 potential surface so that the ion has an asymmetric equilibrium geometry in this state. The barrier height is estimated to be less than 220 cm^{-1}. A new progression is resolved in the $\tilde{B}\ ^2B_2$

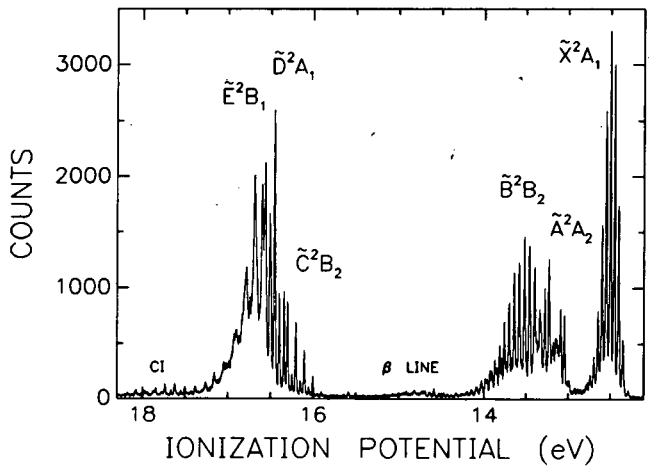

Figure 7-1. The complete HeI (584 Å) photoelectron spectrum of SO_2^+ measured with a resolution of 13 meV and a supersonic molecular beam of SO_2. (XBL 8611-4768)

state, which is assigned to be a combination of ν_2 with $2\nu_3$. The ν_2 vibration is observed to be strongly coupled with ν_3. The true adiabatic IP for the $\tilde{C}\ ^2B_2$ state is determined for the first time, as 15.902 ± 0.003 eV. The dynamics of the ion dissociation in this state is discussed and slow predissociations through the lower lying states are suggested. The $\tilde{D}\ ^2A_1$ and $\tilde{E}\ ^2B_1$ states are substantially broadened above the first few vibrational levels. Fast predissociations through the $\tilde{C}\ ^2B_2$ state are proposed to account for the spectral diffuseness. A weak band at about 14.6 eV, which had been assigned as a configuration interaction (CI) satellite band, is found to be a HeI β line (537 Å) spectrum of the third band, due to the resolved vibrational structure. A true CI band at about 17.5 eV with resolved vibrational structure is observed. It consists of two ν_1 vibrational progressions, which look like two spin-orbit split components.

8. Chemisorption Geometry of c(2×2)S/Mo(001) Determined with Angle-Resolved Photoemission Extended Fine Structure (Publication 29)

C.C. Bahr,[†] S.W. Robey,[‡] Z. Hussain,[§] L.J. Terminello, K.T. Leung, J.-R. Lou,[‖] A.E. Schach von Wittenau, and D.A. Shirley

We report the chemisorption geometry for c(2×2)S/Mo(001), as determined using ARPEFS. Sulfur is bonded as expected to the fourfold hollow sites, with a S-Mo bond distance of 2.41(2) Å. The Mo first-to-second layer spacing is within 0.03 Å of the bulk spacing, and the second Mo layer is planar within 0.03 Å. We determined the adsorption geometry of sulfur by fitting ARPEFS curves with a multiple-scattering spherical-wave theory, which provided good agreement with the data (Figure 8-1).

[†]Present address: AT&T Laboratories, Princeton, NJ 08540.
[‡]Present address: IBM T.J. Watson Research Center, Yorktown Heights, NY 10598.
[§]Permanent address: Department of Physics, University of Petroleum and Minerals, Dhahran, Saudi Arabia.
[‖]Permanent address: Department of Chemistry, University of British Columbia, Vancouver, B.C. V6T 1Y6.

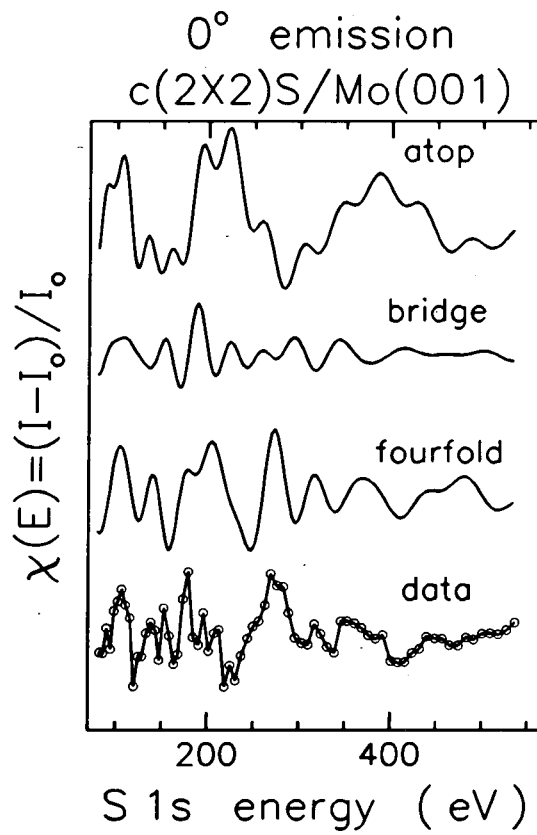

Figure 8-1. Three multiple-scattering spherical-wave calculations are shown for ideal (nonoptimized) fourfold hollow, atop, and bridge bonding sites for c(2×2)S/Mo(001), assuming a S-Mo bond distance of 2.40 Å and an unrelaxed Mo surface. The curves are calculated for the 0° experimental geometry. Further optimization provided the sulfur-to-molybdenum bond distance and interplanar spacings. (XBL 863-1029)

9. The Surface Structure of (2×2) S/Ge(111) Determined Using ARPEFS (Publication 32)

S.W. Robey,[†] C.C. Bahr,[‡] Z. Hussain,[§] K.T. Leung, J.R. Lou,[‖] A.E. Schach von Wittenau, and D.A. Shirley

Measurements of the extended fine structure in the photoemission intensity from the S(1s) core level were performed for a (2×2) overlayer of S on Ge(111). The X(k) results are given in Figures 9-1 and 9-2. This is the first application of ARPEFS to study an adsorbate on a semiconductor substrate.

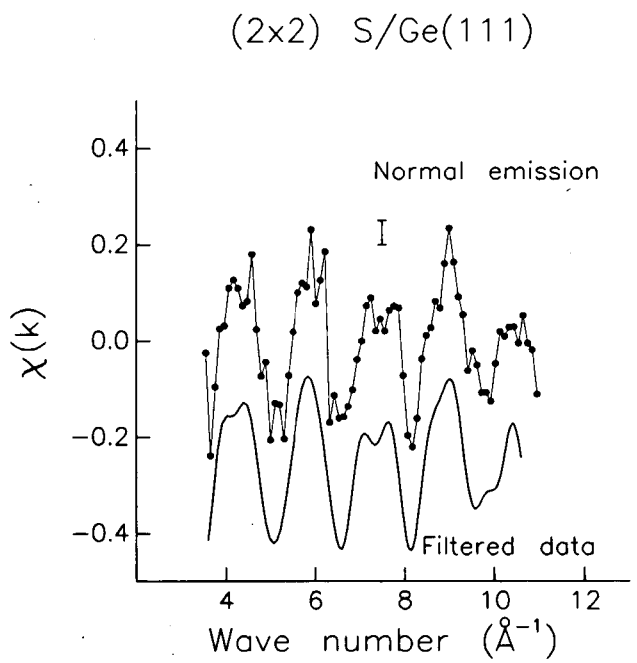

Figure 9-1. Normal emission X(k) data. The upper curve gives the raw data, and the lower solid curve represents the same data after Fourier filtering to remove "frequencies" above 10 Å. The error bar at the top displays the level of statistical uncertainty in the data. These data represent the average of two normal emission ARPEFS measurements. (XBL 864-1552)

The adsorption site and local geometry were determined from the ARPEFS using comparisons to multiple-scattering calculations. The results of this analysis indicate adsorption in a twofold bridge site 1.03 ± 0.05 Å above the Ge surface. The separation between the first and second Ge layers is contracted by 9 ± 6%, and some Ge-Ge bond lengths between the Ge bilayers are expanded by 8 ± 3%. This adsorption site is different from that determined for another chalcogenide, Te, on the Ge(111) surface on

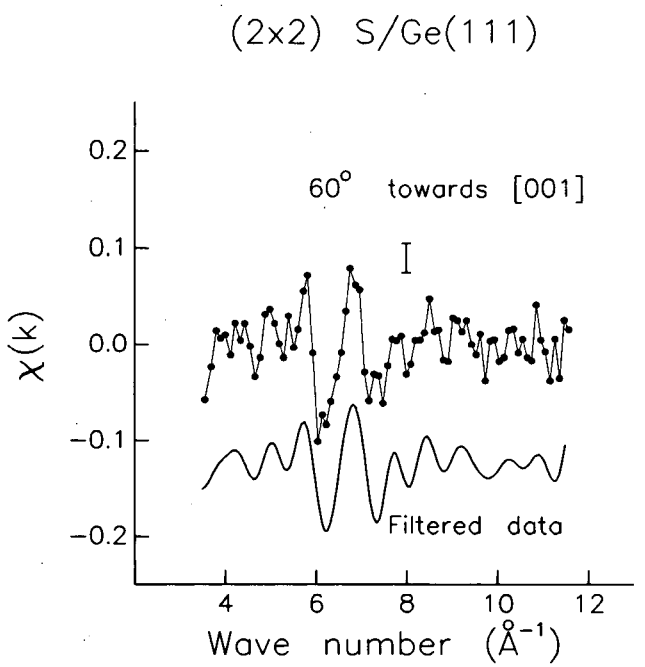

Figure 9-2. Same as Figure 9-1 for the off-normal data, except that only one measurement was performed for this geometry. (XBL 864-1550)

the basis of SEXAFS measurements, but it is the same as those found for Te/Si(111) and Se/Si(111).

[†]Present address: IBM T.J. Watson Research Center, Yorktown Heights, NY 10598.

[‡]Present address: AT&T Laboratories, Princeton, NJ 08540.

[§]Permanent address: Department of Physics, University of Petroleum and Minerals, Dhahran, Saudi Arabia.

[‖]Permanent address: Department of Chemistry, University of British Columbia, Vancouver, B.C. V6T 1Y6.

1986 PUBLICATIONS AND REPORTS

Refereed Journals

1. D.W. Lindle, P.A. Heimann, T.A. Ferrett, P.H. Kobrin, C.M. Truesdale, U. Becker, H.G. Kerkhoff, and D.A. Shirley, "Photoemission from the 3d and 3p Subshells of Kr," Phys. Rev. A **33**, 319 (1986); LBL-16941.
2. J.G. Tobin, S.W. Robey, and D.A. Shirley, "Two-Dimensional Valence-Electronic Structure of a Monolayer of Ag on Cu(001)," Phys. Rev. B **33**, 2270 (1986); LBL-15133.
3. L.E. Klebanoff, S.W. Robey, G. Liu, and D.A. Shirley, "Photoelectron Spectroscopy Studies of Cr(001) Near-Surface and Surface Magnetism," J. Magn. Magn. Mater. **54–57**, 728 (1986); LBL-21427.

4. L.E. Klebanoff and D.A. Shirley, "Surface Dependence of the Cr(001) 3s Photoemission Line Shape," Phys. Rev. B **33**, 5301 (1986); LBL-19055.
5. J.E. Reutt, L.S. Wang, J.E. Pollard, D.J. Trevor, Y.T. Lee, and D.A. Shirley, "Photoelectron Spectroscopy and Inferred Femtosecond Intramolecular Dynamics of $C_2H_2^+$ and $C_2D_4^+$," J. Chem. Phys. **84**, 3022 (1986); LBL-20558.
6. J.E. Reutt, L.S. Wang, Y.T. Lee, and D.A. Shirley, "Molecular Beam Photoelectron Spectroscopy of $Ni(CO)_4$," Chem. Phys. Lett. **126**, 399 (1986); LBL-20566.
7. A.G. Baca, L.E. Klebanoff, M.A. Schulz, E. Paparazzo, and D.A. Shirley, "The Initial Oxidation of Cr(100)," Surf. Sci. **171**, 255 (1986); LBL-19054.
8. J.J. Barton, S.W. Robey, and D.A. Shirley, "Theory of Angle-Resolved Photoemission Extended Fine Structure," Phys. Rev. B **34**, 778 (1986); LBL-19324.
9. C.E. Brion, D.W. Lindle, P.A. Heimann, T.A. Ferrett, M.N. Piancastelli, and D.A. Shirley, "Photoelectron Branching Ratios and Partial Photoionization Cross Sections for Production of the $(2a_1)^{-1}$ State of H_2O Up to 200 eV," Chem. Phys. Lett. **128**, 118 (1986); LBL-20530.
10. D.W. Lindle, T.A. Ferrett, P.A. Heimann, and D.A. Shirley, "Increasing Quantum Yield of Sodium Salicylate Above 80 eV Photon Energy: Implications for Photoemission Cross Sections," Phys. Rev. A **34**, 1131 (1986); LBL-20162.
11. A.G. Baca, L.E. Klebanoff, M.A. Schulz, E. Paparazzo, and D.A. Shirley, "Dissociative Adsorption of CO and O_2 on Cr(100), Cr(110), and Cr(111) in the Temperature Range 300–1175 K," Surf. Sci. **173**, 215 (1986); LBL-18671.
12. T.A. Ferrett, D.W. Lindle, P.A. Heimann, H.G. Kerkhoff, U.E. Becker, and D.A. Shirley, "Sulfur 1s Core-Level Photoionization of SF_6," Phys. Rev. A **34**, 1916 (1986); LBL-18825.
13. J.J. Barton, C.C. Bahr, S.W. Robey, Z. Hussain, E. Umbach, and D.A. Shirley, "Adsorbate-Geometry Determination by Measurement and Analysis of Angle-Resolved-Photoemission Extended-Fine-Structure Data: Application to c(2×2)S/Ni(001)," Phys. Rev. B **34**, 3807 (1986); LBL-20535.
14. U. Becker, H.G. Kerkhoff, D.W. Lindle, P.H. Kobrin, T.A. Ferrett, P.A. Heimann, C.M. Truesdale, and D.A. Shirley, "Orbital-Collapse Effects in Photoemission from Atomic Eu," Phys. Rev. A. **34**, 2858 (1986); LBL-16066.
15. P.A. Heimann, U. Becker, H.G. Kerkhoff, B. Langer, D. Szostak, R. Wehlitz, D.W. Lindle, T.A. Ferrett, and D.A. Shirley, "Helium and Neon Photoelectron Satellites at Threshold," Phys. Rev. A **34**, 3782 (1986); LBL-21696.
16. J.E. Reutt, L.S. Wang, Y.T. Lee, and D.A. Shirley, "Molecular Beam Photoelectron Spectroscopy and Femtosecond Intramolecular Dynamics of H_2O^+ and D_2O^+," J. Chem. Phys. **85**, 6928, (1986); LBL-21357.

LBL Reports

17. T.A. Ferrett, P.A. Heimann, H.G. Kerkhoff, U. Becker, D.W. Lindle, and D.A. Shirley, "Photoelectron Asymmetry Parameter for the S 2p Level of SO_2," LBL-22400.
18. T.A. Ferrett, D.W. Lindle, P.A. Heimann, W.D. Brewer, U. Becker, H.G. Kerkhoff, and D.A. Shirley, "Lithium 1s Main-line and Satellite Photoemission: Resonant and Nonresonant Behavior," LBL-22068.
19. T.A. Ferrett, M.N. Piancastelli, D.W. Lindle, P.A. Heimann, and D.A. Shirley, "Si 2p and 2s Resonant Excitation and Photoionization in SiF_4," LBL-20742.
20. T.A. Ferrett, D.W. Lindle, P.A. Heimann, M.N. Piancastelli, P.H. Kobrin, H.G. Kerkhoff, U. Becker, W.D. Brewer, and D.A. Shirley, "Shape-Resonant and Many-Electron Effects in the S 2p Photoionization of SF_6," LBL-18829.
21. D.W. Lindle, T.A. Ferrett, P.A. Heimann, and D.A. Shirley, "Photoemission From Xe in the Vicinity of the 4d Cooper Minimum," LBL-22028.
22. D.W. Lindle, P.A. Heimann, T.A. Ferrett, M.N. Piancastelli, and D.A. Shirley, "A Photoemission Study of Kr 3d → np Autoionization Resonances," LBL-22065.
23. D.W. Lindle, P.A. Heimann, T.A. Ferrett, and D.A. Shirley, "Helium Photoelectron Satellites: Low-Energy Behavior of the n = 3–5 Lines," to appear in Phys. Rev. A; LBL-21651.
24. D.W. Lindle, T.A. Ferrett, P.A. Heimann, and D.A. Shirley, "A Complete Photoemission Study of the He 1s → T 3s3p Autoionizing Resonance," LBL-21995.
25. Laisheng Wang, J.E. Pollard, Y.T. Lee, and D.A. Shirley, "Molecular Beam Photoelectron Spectroscopy: the $C_2D_4^+$ ($\tilde{X}$ ^2B_3B) Ground State," to appear in J. Chem. Phys.; LBL-21997.
26. Laisheng Wang, Y.T. Lee, and D.A. Shirley, "Molecular Beam Photoelectron Spectroscopy of SO_2: Geometry, Spectroscopy, and Dynamics of SO_2^+," LBL-22413.
27. S.W. Robey (Ph.D. Thesis), "Local Surface Structures of c(2×2) S/Ni(011) and (2×2) S/Ge(111) Determined Using ARPEFS," LBL-21468.
28. A.L. Johnson (Ph.D. Thesis), "Platinum Surface Chemistry Studied by Thermal Desorption Spectrometry and Near Edge X-ray Absorption Fine Structure: Adsorbate Effects," LBL-20964.
29. C.C. Bahr, S.W. Robey, Z. Hussain, L.J. Terminello, K.T. Leung, J.-R. Lou, A.E. Schach von Wittenau, and D.A. Shirley, "Chemisorption Geometry of c(2×2) S/Mo(001) Determined with Angle-Resolved Photoemission Extended Fine Structure," submitted to Phys. Rev. B; LBL-21221.
30. J.E. Reutt (Ph.D. Thesis), "Molecular Beam Photoemission and Femtosecond Intramolecular Dynamics," LBL-21322.
31. C.C. Bahr, Jr. (Ph.D. Thesis), "Chemisorption Geometries of Sulfur on Copper and Molybdenum

Surfaces: A Photoelectron Diffraction Study," LBL-21359.

32. S.W. Robey, C.C. Bahr, Z. Hussain, K.T. Leung, J.-R. Lou, A.E. Schach von Wittenau, and D.A. Shirley, "The Surface Structure of (2×2) S/Ge(111) Determined Using ARPEFS," submitted to Phys. Rev. B; LBL-20572.
33. T.A. Ferrett (Ph.D. Thesis), "Photoionization of Atoms and Small Molecules using Synchrotron Radiation," LBL-22418.
34. P.A. Heimann (Ph.D. Thesis), "Near Threshold Studies of Photoelectron Satellites," LBL-22419.
35. P.A. Heimann, D.W. Lindle, T.A. Ferrett, S.H. Liu, L.J. Medhurst, M.N. Piancastelli, D.A. Shirley, U. Becker, H.G. Kerkhoff, B. Langer, D. Szostak, and R. Wehlitz, "Shake-Off on Inner-Shell Resonances of Ar, Kr, and Xe," submitted to J. Phys. B; LBL-22412.

Invited Talks

36. D.A. Shirley, "Surface Structures from Photoemission Extended Fine Structure," 1985–86 Charles A. McDowell Lecture in Chemical Physics, Department of Chemistry, University of British Columbia, Vancouver, January 14, 1986.
37. D.A. Shirley, "Near Threshold Behavior in Photoelectron Satellites," Department of Chemistry, University of British Columbia, Vancouver, January 15, 1986.
38. D.A. Shirley, "How Can Synchrotron Radiation Benefit Chemistry?" EUCHEM Conference, The Use of Synchrotron Radiation in Chemistry, Schloss Elmau, Mittenwald, Federal Republic of Germany, April 14, 1986.
39. D.A. Shirley, "Recent Advances in Chemical Physics in the United States," Spring Meeting, American Physical Society, Washington, D.C., April 30, 1986.
40. D.A. Shirley, "Surface Structures from Photoelectron Diffraction (ARPEFS)," Physical Chemistry Colloquium, Carnegie-Mellon/University of Pittsburgh, PA, May 1, 1986.
41. D.A. Shirley, "Time-Of-Flight Spectroscopy of Atoms and Molecules," 13th Annual SSRL Users Group Meeting, Menlo Park, CA, October 23–24, 1986.
42. D.W. Lindle, "Resonant Photoelectron Spectroscopy of Atoms and Molecules Using Synchrotron Radiation," L Division, Lawrence Livermore National Laboratory, Livermore, CA, January 28, 1986.
43. D.W. Lindle, "Resonant Photoelectron Spectroscopy of Atoms Using Synchrotron Radiation," National Measurement Laboratory, National Bureau of Standards, Gaithersburg, MD, July 21, 1986.
44. S.W. Robey, "Surface Structures Determined Using Photoelectron Diffraction," Xerox Palo Alto Research Center, Palo Alto, CA, May 2, 1986.
45. J.J. Barton, "Progress and Prospects for Determining Ordered Surface Structures with ARPEFS," 191st American Chemical Society National Meeting, New York City, April 13, 1986.
46. J.J. Barton, "Progress on Methods for Determining Surface Structure with Medium Energy Electron Scattering Spectroscopies," Surface Science and Chemical Physics Division, Sandia National Laboratories, Livermore, CA, March 12, 1986.
47. T.A. Ferrett, "Photoelectron Spectroscopy of Gaseous Atoms and Molecules," Departments of Chemistry and Physics, Grinnell College, Grinnell, IA, March 7, 1986.

Crossed Molecular Beams*

Yuan T. Lee, Investigator

INTRODUCTION

The major thrust of this research project is to elucidate detailed dynamics of simple elementary reactions that are theoretically important and to unravel the mechanism of complex chemical reactions or photochemical processes that play important roles in many macroscopic processes. Molecular beams of reactants are used to study individual reactive encounters between molecules or to monitor photodissociation events in a collision-free environment. Most of the information is derived from measurement of the product fragment energy and angular distributions. Recent activities are centered on the direct probing of transition states through the experimental observation of quantum-mechanical resonance phenomena, the mechanisms of elementary chemical reactions involving oxygen atoms with unsaturated hydrocarbons, the dependence of the chemical reactivity of electronically excited atoms on the alignment of excited orbitals, the primary photochemical processes of polyatomic molecules, intramolecular energy transfer of chemically activated and locally excited molecules, the energetics of free radicals that are important to combustion processes, the infrared-absorption spectra of ionic clusters of hydrogen, and the bond-selective photodissociation through electron excitation.

1. The Lifetimes for Spontaneous Emission from the $X^3\Sigma^-(v = 1)$ and $a^1\Delta$ States of CH^- (Publication 6)

M. Okumura, L.I. Yeh,† D. Normand,‡ and Y.T. Lee

The radiative decay of excited CH^- trapped in a radio-frequency ion trap was measured, and the total excited-state population was probed by observing the depletion of trapped CH^- caused by photodetachment at 1.16 eV, below the expected electron affinity for the ground $^3\Sigma^-$ state. The signal decayed biexponentially with time. We assigned the long-lived state (lifetime 5.9 + 0.8, −0.6 sec) as the metastable $a^1\Delta$ state previously identified in the photoelectron spectrum. The fast decay, with a lifetime of 1.75 ± 0.15 msec, was attributed to the first excited vibrational level of the ground $^3\Sigma^-$ state, in good agreement with a theoretical result by Manz, Zilch, Rosmus, and Werner. These results support the electron affinity of 1.238 eV for CH^- obtained by Kasdan, Herbst, and Lineberger from photoelectron spectroscopy, and contradict the value of 0.74 eV determined by Feldmann from photodetachment spectroscopy.

*This work was supported by the Director, Office of Energy Research, Office of Basic Energy Sciences, Chemical Sciences Division of the U.S. Department of Energy under Contract No. DE-AC03-76SF00098.

†NSF Pre-Doctoral Fellow.

‡Present address: C.E.N./Saclay, DPh.G/S.P.A.S., 91191 Gif-sur-Yvette, France.

2. Molecular-Beam Photoelectron Spectroscopy and Femtosecond Intramolecular Dynamics of H_2O^+ and D_2O^+ (Publication 8)

J.E. Reutt, L.S. Wang, Y.T. Lee, and D.A. Shirley

The 584-Å photoelectron spectra of supersonic molecular beams of H_2O and D_2O have been obtained with improved resolution. The spectroscopic constants of the $\tilde{X}^2B_1$ and $\tilde{A}^2A_1$ state ions, including ω_1°, χ_{11}°, ω_2°, χ_{22}°, and χ_{12}°, are reported. For the first two electronic states of the ion, precise line splittings were evaluated with a least-squares fitting procedure, employing sums of empirical instrument response functions and a linear background. A simulation of the vibrational manifolds of the $\tilde{B}^2B_2$ state ions with combination progressions in the symmetry-allowed modes ν_1 and ν_2 failed to reproduce the diffuse photoelectron bands observed for both H_2O and D_2O. Autocorrelation functions were calculated from the photoelectron bands of all three electronic states. The $\tilde{B}^2B_2$ state correlation functions exhibit ultrafast decay, occurring on a 10^{-14} second timescale. The ν_2 motion appears to define the decay in the correlation function. This behavior supports a previously proposed $\tilde{B}^2B_2$–$\tilde{A}^2A_1$ curve-crossing model for the nonradiative relaxation of the $\tilde{B}^2B_2$ state ions.

3. Molecular-Beam Studies of Laser-Induced Multiphoton Dissociation (Publication 9)

A.S. Sudbo, P.A. Schulz, Y.R. Shen, and Y.T. Lee

The evidence from molecular-beam experiments is reviewed to establish that laser-induced multipho-

ton dissociation is a collisionless unimolecular process. We interpret the experimental results using a model in which stepwise incoherent multiphoton absorption excites the molecule through the quasicontinuum and above the dissociation threshold, and in which dissociation is described by RRKM theory. We find good agreement between the the measured and calculated translational-energy distributions.

4. The Electronic State-Selective Photodissociation of CH_2BrI at 248, 210, and 193 nm (Publication 13)

L.J. Butler,† E.J. Hintsa, S.F. Shane, and Y.T. Lee

The primary photodissociation channels of CH_2BrI following excitation at 193.3, 210, and 248.5 nm have been studied with the crossed-laser/molecular-beam technique. Product translational-energy distributions and polarization dependences were derived for the primary dissociation processes observed. The data demonstrate bond-selective photochemistry as well as some selective formation of electronically excited photofragments in bond fission and concerted dissociation. Excitation at 248.5 nm, which is assigned to excitation of primarily a n(I) $\rightarrow$ σ^*(C-I) transition with some contribution from an overlapping n(Br) $\rightarrow$ σ^*(C-Br) transition, results in both C-I and C-Br bond fission. C-I bond fission is the dominant channel, producing I atoms in both the $^2P_{3/2}$ and spin-orbit excited $^2P_{1/2}$ states in a ratio of 1.0:0.75. Excitation at 193.3 nm, assigned to a transition to primarily predissociated Rydberg levels on the I atom, leads to C-Br bond fission, some C-I bond fission, and significant concerted elimination of IBr. Analysis of the product translational-energy distributions for the dissociation products indicates that the IBr is formed electronically excited and that the halogen-atom products are spin-orbit excited. Excitation at 210 nm, of the transition assigned as n(Br) $\rightarrow$ σ^*(C-Br) based on comparison with CH_3Br, results in selective breaking of the stronger C-X bond in the molecule, the C-Br bond, and no fission of the C-I bond. Some concerted elimination of IBr also occurs; the IBr velocity distribution indicates it is probably formed electronically excited as in photolysis at 193.3 nm. The selective breaking of the C-Br bond over the weaker C-I bond is discussed in contrast to previous photolysis studies of polyhalomethanes.

---

†Present address: James Franck Institute, University of Chicago, Chicago, IL 60637.

5. On the High-Resolution HeI Photoelectron Spectrum of the $C_2D_4^+$ ($\tilde{X}^2B_3$) Ground State (Publication 14)

L. Wang, J.E. Pollard, Y.T. Lee, and D.A. Shirley

The HeI (584 Å) photoelectron spectrum of $C_2D_4^+$ in its ground electronic state has been measured with a supersonic molecular beam. The improved resolution permits new vibrational fine structure to be observed and assigned. The disputed interpretation of ν_2 and ν_3 vibrations in $C_2H_4^+$ ground state and the abnormal isotopic shift from $C_2H_4^+$ to $C_2D_4^+$ are explained by comparing the experimental results with a Franck-Condon factor calculation and a recent *ab initio* calculation. The torsional vibration (ν_4) is observed to be coupled significantly with the C=C stretching vibration (ν_2).

6. Spin-Forbidden Radiative Decay of the $a^4\Pi_u$ State of O_2^+ (Publication 15)

S.W. Bustamente, M. Okumura, D. Gerlich, H.S. Kwok, L.R. Carlson, and Y.T. Lee

The spin-forbidden radiative decay of $a^4\Pi_u$ O_2^+ has been measured in a radio-frequency octopole ion trap. Photodissociation is used to probe the $a^4\Pi_u$ population as a function of trapping time. We have found that the $a^4\Pi_u$ state exhibits a multiple exponential decay, ranging from a few milliseconds to hundreds of milliseconds. The state dependence of the decay is seen in the photodissociation spectrum ($b^4\Sigma_g^- \leftarrow a^4\Pi_u$), which changes dramatically from 0.1 msec to 100 msec. The major changes in the spectrum are simulated by assuming that the F_2 and F_3 spin components of the $a^4\Pi_u$ state decay faster than the F_1 and F_4 components. We can account for this dependence on spin sublevel by assuming that the primary mechanism for radiative decay

arises from spin-orbit coupling of the $a^4\Pi_u$ and $A^2\Pi_u$ states. Our results suggest that the $a^4\Pi_u$ radiative lifetime of 0.22 sec measured by O'Keefe and McDonald reflects the decay of only the longest-living $a^4\Pi_u$ sublevels.

7. Photodissociation of CF_2BrCH_2I at 248, 266, and 308 nm (Publication 16)

T.K. Minton, G.M. Nathanson, and Y.T. Lee

The technique of photofragmentation translational spectroscopy has been used to study the photodissociation of CF_2BrCH_2I at excitation wavelengths of 248, 266, and 308 nm. The primary photofragments are CF_2BrCH_2 and either $I(^2P_{1/2})$ or $I(^2P_{3/2})$, although some C-Br bond fission does occur at 248 and 266 nm. A large fraction of the CF_2BrCH_2 radical product contains enough internal excitation after the primary process to undergo secondary dissociation into CF_2CH_2 and Br. Secondary dissociation is also observed to take place at 248 and 266 nm via absorption of a photon by the CF_2BrCH_2 photofragment. By observing the threshold for the spontaneous secondary dissociation process, the reaction enthalpy for $CF_2BrCH_2I \rightarrow CF_2CH_2 + Br + I$ was determined to be 67.5 ± 2 kcal/mol, which leads to $\Delta H^\circ_{f0}(CF_2BrCH_2I) = -92.6 \pm 2$ kcal/mol. The center-of-mass translational-energy distributions were derived for both the $I(^2P_{1/2})$ and $I(^2P_{3/2})$ dissociation channels resulting from primary C-I bond breakage. The $I(^2P_{1/2})/I(^2P_{3/2})$ branching ratio are 3.3, 9.0, and 0.5 for excitation wavelengths of 248, 266, and 308 nm, respectively. The translational-energy distributions also reveal that a major fraction of the CF_2BrCH_2 product radicals are formed with high internal energies, averaging around 50% of the excess energy. The angular distributions of dissociation products with respect to the laser polarization indicate that the primary photodissociation process for the ground- and excited-state channels at both wavelengths proceeds via a parallel transition—i.e., the transition moment must be nearly parallel to the C-I bond.

8. Photodissociation of CH_2ClCH_2I at 308 nm (Publication 17)

T.K. Minton, G.M. Nathanson, and Y.T. Lee

The technique of photofragmentation translational spectroscopy has been used to study the photodissociation of CH_2ClCH_2I at an excitation wavelength of 308 nm. The exclusive dissociation pathway is C-I bond breakage with formation of CH_2ClCH_2 and $I(^2P_{3/2})$. The center-of-mass translational-energy distribution of the photofragments reveals that an average of about 50% of the excess energy appears in translation. The angular distribution of dissociation products with respect to the laser polarization indicates that the photodissociation process proceeds via a parallel transition—i.e., the transition moment must be nearly parallel to the C-I bond. Exclusive production of ground-state $I(^2P_{3/2})$ with a parallel polarization dependence is unexpected based on the prevailing picture for alkyl iodide photodissociation.

9. Determination of the C-H Bond Dissociation Energies of Ethylene and Acetylene by Observation of the Threshold Energies of H^+ Formation by Synchrotron Radiation (Publication 10)

H. Shiromaru, Y. Achiba, K. Kimura, and Y.T. Lee

To determine the C-H bond dissociation energies of ethylene and acetylene (R-H), we have measured the threshold energies of H^+ formation using synchrotron radiation in the wavelength region 58–70 nm. Subtracting the ionization potential of hydrogen atom (13.598 eV) from the observed threshold energies, we have deduced values of 5.06 ± 0.5 eV and 5.75 ± 0.05 eV for the C-H bond dissociation energies D_0(R-H) of ethylene and acetylene, respectively.

10. Molecular-Beam Photoelectron Spectroscopy of SO_2: Geometry, Spectroscopy, and Dynamics of SO_2^+ (Publication 20)

L. Wang, Y.T. Lee, and D.A. Shirley

We have reinvestigated the HeI (584 Å) photoelectron spectroscopy of SO_2 using a supersonic molecular beam. Improved resolution and rotational cooling allow us to observe several new features and to resolve explicitly the vibrational structure in the first six electronic states, in the first three photoelectron bands. The adiabatic ionization potentials were accurately determined for all six states. The $\tilde{X}\ ^2A_1$ state is assigned to the ν_2 mode exclusively. Irregularity of the vibrational progression on the high IP side was observed for the first time. A potential bar-

rier (to linearity) is proposed to interpret the irregular vibrational spacings in the ν_2 vibration. The barrier height is estimated to be 0.42 eV (3400 cm^{-1}). The complex second band contains two states. Abnormal vibrational structure in the $\tilde{A}\ ^2A_2$ state is explained by the principal excitation of the ν_3 mode. A potential barrier is present in the ν_3 potential surface, so that the ion has an asymmetric equilibrium geometry in this state. The barrier height is estimated to be less than 220 cm^{-1}. A new progression is resolved in the $\tilde{B}\ ^2B_2$ state, which is assigned to be a combination of ν_2 with $2\nu_3$. The ν_2 vibration is observed to be strongly coupled with the ν_3 mode. The true adiabatic IP for the $\tilde{C}\ ^2B_2$ state is determined for the first time, as 15.902 ± 0.003 eV. The dynamics of the ion dissociation in this state is discussed, and slow predissociations through the lower lying states are suggested. The $\tilde{D}\ ^2A_1$ and $\tilde{E}\ ^2B_1$ states are subtantially broadened above the first few vibrational levels. Fast predissociations through the $\tilde{C}\ ^2B_2$ state are proposed to account for the spectral diffuseness. A weak band at about 14.6 eV, which had been assigned as a configuration-interaction (CI) satellite band, is found to be a HeI β line (537 Å) spectrum of the third band, due to the resolved vibrational structure. A true CI band at about 17.5 eV with resolved vibrational structure is observed. It consists of two ν_1 vibrational progressions, which look like two spin-orbit split components.

11. Radiative-Decay Lifetimes of CH_2^- (Publication 21)

M. Okumura, L.I. Yeh, D. Normand, J.J.H. van den Biesen, S.W. Bustamente, Y.T. Lee, T.J. Lee, N.C. Handy, and H.F. Schaefer III

Recently the presence and radiative decay of vibrationally excited CH_2^-, generated in a hot-cathode discharge of methane, was established by measuring the time-dependent photodetachment from excited states of CH_2^- as it radiatively relaxed in a high-vacuum ion trap. The time dependence of the photodetachment was found to be consistent with an electron affinity of 5250 cm^{-1} (0.65 eV) for ground-state $\tilde{X}\ ^3B_1$ methylene. The radiative-decay lifetimes of the first three excited bending vibrations of CH_2^- were also tentatively assigned. Here, we report a more refined analysis of the experimental data along with theoretical *ab initio* determinations of the radiative-decay lifetimes of the first four excited bending vibrational levels of CH_2^-. There is some discrepancy between the *ab initio* values (431, 207, 118, and 68 msec for the v_2 = 1, 2, 3, and 4 levels, respectively) and the experimental values (525, 70, and 14 msec for v_2 = 1, 2, and 3, respectively) for v_2 = 2 and 3. Possible reasons for this discrepancy are discussed, but none of the alternatives are entirely satisfactory.

12. Work in Progress

Reaction of O^{18} with Unsaturated Hydrocarbons

Since the molecular-beam studies of reactions of oxygen atoms with unsaturated hydrocarbons were initiated, many surprising results have been found. It has been clearly demonstrated that the substitution reactions where O replaces H, CH_3, or halogen atoms are the major channels, and the 1,2 H-atom migration followed by C-C bond rupture is not as important, although 1,2 migration of Cl atoms was seen.

These major findings are now well accepted among combustion chemists, but there are still some questions remaining about the relative importance of 1,2 H migration in the two reactions O + C_2H_2 and O + C_2H_4 and their energy dependence. Much of the difficulty in carrying out definitive studies of some of the minor reaction channels is due to the high background of CO in the ultrahigh-vacuum mass-spectrometric detector and the difficulty in distinguishing $C^{13}H_3$ from O^{16}.

The use of O^{18} isotopes, in spite of the high cost, should alleviate all these difficulties and provide a more complete picture of these important combustion reactions. A closed-cycle O^{18} atom using fluorocarbon pump oil will be set up, and it is hoped that 85–90% of O^{18} can be recovered on each run. The initial experiment will be carried out on O + C_2H_4 and O + C_2H_2, to determine the relative importance of H migration channels forming CH_3 + HCO and CH_2 + CO, compared to the substitution channels C_2H_3O + H and C_2HO + H at various collision energies.

Dynamics of Endothermic Substitution Reactions

The promotion of endothermic reactions, by various forms of reagent excitation for atom-diatomic systems, depends critically on the nature of the potential-energy surface. For systems with an early barrier, such as $CH_3Br + I \rightarrow CH_3 + IBr$ and $CF_3Br + I \rightarrow CF_3 + IBr$, translational energy has been shown to be more effective than vibrational excitation in promoting chemical reactions.

For an endothermic substitution reaction, such as $Br + C_2H_2Cl_2 \rightarrow C_2H_2BrCl + Cl$ or $Br + C_2H_2Cl_2$

$\rightarrow C_2HBrCl_2 + H$, the intermediate $[C_2H_2Cl_2Br]^+$ is a stable radical species, and extensive vibrational-energy randomization is expected to take place. If the intramolecular relaxation is faster than the chemical reaction, a statistical theory can be used to predict the decay of the collision complex formed. One would immediately conclude that the decay back to the reactant Br + $C_2H_2Cl_2$ is most exothermic and it should be the major channel, and the substitution reaction will not be important near the threshold, unless the dynamic aspects are more important than the statistical aspects. In other words, the endothermic substitution reactions will be extremely good systems to use to understand the intramolecular dynamics of chemically activated species, especially if nonstatistical behavior is observed. We will concentrate our efforts on reactions of Br atoms with 1,1 dichloroethylene and 1,2 dichloroethylene. These two molecules will provide a good comparison of the relative importance between the kinematic aspect of collisions and chemical effects.

Vibrational Spectroscopy of Hydrogen-Bonded Cluster Ions

In spite of the recent progress made in the high-resolution infrared (IR) spectroscopy of simple, stable molecular ions, there is essentially no information available on the vibrational spectroscopy of molecular cluster ions. Recently, there was a breakthrough in the laboratory in obtaining the spectra of $H_3O(H_2O)_n^+$ using two different methods. The first method uses H_2 as a messenger and attaches a H_2 first to $H_3O(H_2O)_n^+$ and observes the absorption of IR photons by $H_3O(H_2O)_n$ through a vibrational predissociation process, $H_3O(H_2O)_n^+ \cdot H_2 \xrightarrow{h\nu} H_3O(H_2O)_n^+$. The second method uses a high-power CO_2 laser to detect the absorption of a tunable photon by cluster ions by carrying out IR multiphoton dissociation of the excited cluster ions.

These methods will be further developed and will be used for the investigation of vibrational spectroscopy of various hydrated ions and amoniated ions, $NH_4(NH_3)_3^+$ (n = 1, 2, 3, 4), as well as carbonium ions, such as $C_2H_5^+$ and $C_2H_7^+$.

The structure of these types of carbonium ions has been the source of considerable controversy. The classical structure has the odd hydrogen localized on a carbon. In the early 1950s, a symmetrical bridging structure was proposed. This structure soon gained widespread acceptance only to be challenged more recently. Vibrational and rotational spectra of these compounds will unambiguously resolve their structures.

1986 PUBLICATIONS AND REPORTS

Refereed Journals

1. A.H. Kung, R.H. Page, R.J. Larkin, Y.R. Shen, and Y.T. Lee, "Rydberg Spectroscopy of H_2 Via Stepwise Resonant Two-Photon Ion-Pair (H^++H^-) Production," Phys. Rev. Lett. **56**, 328 (1986); LBL-20378.
2. J.E. Reutt, L.S. Wang, J.E. Pollard, D.J. Trevor, Y.T. Lee, and D.A. Shirley, "Photoelectron Spectroscopy and Inferred Femtosecond Intramolecular Dynamics of $C_2H_2^+$ and $C_2D_2^+$," J. Chem. Phys. **84**, 3022 (1986); LBL-20558.
3. L.J. Butler, E.J. Hintsa, and Y.T. Lee, "Bond Selective Photochemistry in CH_2BrI Through Electronic Excitation at 210 nm," J. Chem. Phys. **84**, 4104 (1986); LBL-20770.
4. J.E. Reutt, L.S. Wang, Y.T. Lee, and D.A. Shirley, "Molecular Beam Photoelectron Spectroscopy of $Ni(CO)_4$," Chem. Phys. Lett. **126**, 399 (1986); LBL-20566.
5. M.F. Vernon, H. Schmidt, P.S. Weiss, M.H. Covinsky, and Y.T. Lee, "Reactive Scattering of $Na(3^2P_{3/2})$ + HCl," J. Chem. Phys. **84**, 5580 (1986); LBL-17396.
6. M. Okumura, L.I. Yeh, D. Normand, and Y.T. Lee, "The Lifetimes for Spontaneous Emission from the $X^3\Sigma^-(v=1)$ and $a^1\Delta$ States of CH^-," J. Chem. Phys. **85**, 1971 (1986); LBL-21408.
7. M. Okumura, L.I. Yeh, J.D. Myers, and Y.T. Lee, "Infrared Spectra of the Cluster Ions $H_7O_3^+ \cdot H_2$ and $H_9O_4^+ \cdot H_2$," J. Chem. Phys. **85**, 2328 (1986); LBL-21484.
8. J.E. Reutt, L.S. Wang, Y.T. Lee, and D.A. Shirley, "Molecular Beam Photoelectron Spectroscopy and Femtosecond Intramolecular Dynamics of H_2O^+ and D_2O^+," J. Chem. Phys. **85**, 6928 (1986); LBL-21357.

Other Publications

9. A.S. Sudbo, P.A. Schulz, Y.R. Shen, and Y.T. Lee, "Molecular Beam Studies of Laser Induced Multiphoton Dissociation," in Topics in Current Physics Volume on *Multiple-Photon Excitation and Dissociation of Polyatomic Molecules*, C.D. Cantrell, Ed., Springer-Verlag, New York, 1986, Vol. 35, p. 95.
10. H. Shiromaru, Y. Achiba, K. Kimura, and Y.T. Lee, "Determination of the C-H Bond Dissociation Energies of Ethylene and Acetylene by Observation of the Threshold Energies of H^+ Formation by Synchrotron Radiation," J. Phys. Chem. (in press).

LBL Reports

11. Y.T. Lee, "Reactive Scattering: Non-Optical Methods," in *Atomic and Molecular Beams Method*, G. Scoles and U. Buck, eds., Oxford University Press (in press); LBL-20767.
12. P.S. Weiss (Ph.D. thesis), "The Reaction Dynamics of Electronically Excited Alkali Atoms with Simple Molecules," LBL-21205.
13. L.J. Butler, E.J. Hintsa, S.F. Shane, and Y.T. Lee, "The Electronic State-Selective Photodissociation of CH_2BrI at 248, 210, and 193 nm," J. Chem. Phys. (in press); LBL-21896.
14. L. Wang, J.E. Pollard, Y.T. Lee, and D.A. Shirley, "Molecular Beam Photoelectron Spectroscopy: The $C_2D_4^+$ ($\tilde{X}\ ^2B_3$) Ground State," J. Chem. Phys. (in press); LBL-21997.
15. S.W. Bustamente, M. Okumura, D. Gehrlich, H.S. Kwok, L.R. Carlson, and Y.T. Lee, "Spin-Forbidden Radiative Decay of the $a^4\Pi_u$ State of O_2," J. Chem. Phys. (in press); LBL-22097.
16. T.K. Minton, G.N. Nathanson, and Y.T. Lee, "Photodissociation of CF_2BrCH_2I at 248, 266, and 308 nm," J. Chem. Phys. (in press); LBL-22098.
17. T.K. Minton, G.N. Nathanson, and Y.T. Lee, "Photodissociation of CH_2ClCH_2I at 308 nm," Laser Chem. (in press); LBL-22099.
18. T.K. Minton (Ph.D. thesis), "Photofragmentation of CH_2ClCH_2I at 308 nm," LBL-22100.
19. A.M. Wodtke and Y.T. Lee, "High-Resolution Photofragmentation-Translational Spectroscopy," submitted to *Advances in Gas Phase Photochemistry and Kinetics*; LBL-22264.
20. L. Wang, Y.T. Lee, and D.A. Shirley, "Molecular Beam Photoelectron Spectroscopy of SO_2: Geometry, Spectroscopy, and Dynamics of SO_2^+," submitted to J. Chem. Phys.; LBL-22413.
21. M. Okumura, L.I. Yeh, D. Normand, J.J.H. van den Biesen, S.W. Bustamente, Y.T. Lee, T.J. Lee, N.C. Handy, and H.F. Schaefer III, "Radiative Decay Lifetimes of CH_2^-," submitted to J. Chem. Phys.; LBL-22428.
22. A.M. Wodtke (Ph.D. thesis), "Very High Resolution Photofragmentation-Translational Spectroscopy," LBL-22619.
23. M. Okumura (Ph.D. thesis), "Infrared Spectroscopy and Radiative Lifetimes of Molecular Ions," LBL-22620.
24. Y.T. Lee, "Molecular Beam Studies of Elementary Chemical Processes," in *Chemica Scripta*, 1987; LBL-22621.

Invited Talks

25. Y.T. Lee, "Recent Investigation on Reaction Dynamics, Photochemistry and Spectroscopy by the Molecular Beam Method," Institute for Molecular Science, Okazaki, Japan, Mar. 20, 1986.
26. Y.T. Lee, "Energetics and Dynamics of Concerted Unimolecular Decomposition of Organic Molecules," Institute for Molecular Science, Okazaki, Japan, April 9, 1986.
27. Y.T. Lee, "Reaction Dynamics of Electronically Excited Alkali Atoms with Simple Molecules," Award Lecture, Debye and Langmuir Award Symposium, 191st ACS Meeting, New York, April 14, 1986.
28. Y.T. Lee, "Current Status and Future Prospect of Chemical Kinetics," 1st National Meeting on Chemical Kinetics, Donxi, China, May 15, 1986.
29. Y.T. Lee, "Experimental Probings of Critical Regions of Potential Energy Surfaces," Symposium on Recent Progress in Chemical Reaction Dynamics Research," Institute for Molecular Science, Okazaki, Japan, May 23, 1986.
30. Y.T. Lee, "Investigation of Reaction Dynamics from Product Angular Distributions," Symposium on "Recent Progress in Chemical Reaction Dynamics Research," Institute for Molecular Science, Okazaki, Japan, May 24, 1986.
31. Y.T. Lee, "Crossed Molecular Beam Studies of Reaction Dynamics," Department of Chemistry, Tohoku University, Sendai, Japan, May 26, 1986.
32. Y.T. Lee, "IR Multiphoton Decomposition of Nitrocompounds," Tokyo University, Japan, May 28, 1986.
33. Y.T. Lee, "Molecular Beam Studies of Electronically Excited Atoms," Tokyo University, Japan, May 29, 1986.
34. Y.T. Lee, "Recent Investigations on Reaction Dynamics, Spectroscopy and Photochemistry by the Molecular Beam Method," Department of Chemistry, Keio University, Yokohama, Japan, May 30, 1986.
35. Y.T. Lee, "Understanding Chemical Reactions through Molecular Collisions," Keio University, Yokohama, Japan, May 31, 1986.
36. Y.T. Lee, "Reaction Dynamics of Electronically Excited Sodium Atoms with Oxygen and Hydrogen Halides," Kyushia University, Fukuoka, Japan, June 2, 1986.
37. Y.T. Lee, "Molecular Beam Studies of Primary Photochemical Processes," Department of Chemistry, Kyoto University, Japan, June 10, 1986.
38. Y.T. Lee, "Infrared Absorption Spectroscopy of Ionic Clusters using the Ion Trapping Technique," Department of Molecular Engineering, Kyoto University, Japan, June 11, 1986.
39. Y.T. Lee, "Dynamics and Energetics of Primary Photochemical Processes," Plenary Lecture, XIII Informal Photochemistry Conference, Boulder, CO, June 23, 1986.
40. Y.T. Lee, "A New Experimental Method for IR Absorption Spectroscopy on Ionic Clusters," Atomic and Molecular Science Institute, Academia Sinica, Taipei, Taiwan, July 25, 1986.
41. Y.T. Lee, "Molecular Beam Studies on C-H Overtone Excitation in Benzene," American Chemical Society Annual Meeting, Anaheim, CA, Sept. 8, 1986.

42. Y.T. Lee, "Recent Advances in Molecular Beam Studies on Reaction Dynamics and Spectroscopy," Chemical Physics Retreat, University of Oregon, Eugene, OR, Sept. 27, 1986.
43. Y.T. Lee, "Spectroscopy and Dynamics of Laser and Molecular Beams," Regional Meeting on Chemical Physics, University of Waterloo, Ontario, Oct. 25, 1986.
44. Y.T. Lee, "Primary Decomposition Processes of RDX," Workshop on Energetic Materials Initiation Fundamentals, Los Alamos, NM, Oct. 14, 1986.
45. Y.T. Lee, "Molecular Beam Chemical Kinetics," Department of Chemistry, University of California, Riverside, Nov. 10, 1986.
46. Y.T. Lee, "Molecular Beam Studies of Elementary Chemical Processes," Nobel Lecture, Royal Swedish Academy, Stockholm, Dec. 8, 1986.
47. Y.T. Lee, "Infrared Absorption Spectroscopy on Hydrated Hydronium Ions by the Ion Trapping Technique," Department of Chemistry, University of Stockholm, Sweden, Dec. 9, 1986.
48. Y.T. Lee, "Mode Selective and Bond Selective Photochemical Processes," Chemical Society of Uppsala, Sweden, Dec. 12, 1986.
49. Y.T. Lee, "Concerted Unimolecular Decomposition of Organic Compounds," University of Gothenburg, Sweden, Dec. 15, 1986.
50. Y.T. Lee, "Crossed Molecular Beam Investigation of Chemical Reaction Dynamics," National Taiwan University, Taipei, Dec. 18, 1986.
51. Y.T. Lee, "Homogeneous Linewidth of C-H Overtone Excitation in Benzene Molecules," Annual Meeting, Chinese Chemical Society, Tsinghua University, Hsinchu, Taiwan, Dec. 19, 1986.

Potential-Energy Surfaces for Chemical Reactions*

Henry F. Schaefer III, Investigator

INTRODUCTION

This research program has two goals, related yet distinct. The first goal is the development of new theoretical and/or computational methods for the description of "what electrons are doing in molecules," to use the words of Robert S. Mulliken. Specifically, the single outstanding problem in the field is the correlation problem, that of formulating models for going beyond the single-particle or Hartree-Fock approximation. The second goal of our research is to apply these theoretical methods to significant problems of broad chemical interest. Currently two areas are of special concern: (1) model theoretical studies of chemisorption, metal clusters, and organometallic species, and (2) potential-energy surfaces that govern gas-phase chemical reactions. Research in the former area is ultimately aimed at a truly molecular understanding of catalysis, a subject pertinent to future energy requirements. In the second area research sometimes tends toward molecules that are potentially important in interstellar space, atmospheric chemistry, and the development of high-power laser systems. It is to be emphasized that in recent years theoretical chemistry has become a significant source not only of broad generalities, but also of specific predictions concerning molecular systems that may be very important but inaccessible to experiment.

1. All-Silicon Counterparts of Benzene and Tetrahedrane (Publications 5 and 11)†

D.A. Clabo and H.F. Schaefer III

Ab initio theoretical studies on hexasilabenzene (Si_6H_6), the silicon analogue of benzene, show that, despite the existence of a local D_{6h} minimum energy structure, hexasilabenzene contains little aromatic stabilization, on the basis of simple bond-strength arguments. In addition, the presence of a very low frequency (10 cm^{-1}) normal-mode vibration indicates for hexasilabenzene the preference shown by other silicon-containing compounds for pyramidalization at tricoordinate silicon. Other recent results have confirmed that there are lower-lying Si_6H_6 isomers that contain fewer trivalent (i.e., multiple bonded) silicon atoms. On the basis of these recent results, as well as earlier studies of other unsaturated silicon-containing molecules, it is not unreasonable to postulate that, of Si_4H_4 isomers, tetrasilatetrahedrane [tricyclo(1.1.0.$0^{2,4}$)tetrasilane] might be one of the most energetically preferred.

The use of a double-ξ-plus-polarization (DZP) basis set in conjunction with self-consistent-field (SCF) theory allows prediction of the structure of tetrasilatetrahedrane: r_e(Si-Si) = 2.395 Å, r_e(Si-H) = 1.472 Å (DZ SCF); r_e(Si-Si) = 2.308 Å, r_e(Si-H) = 1.464 Å (DZP SCF), as seen in Figure 1-1. Harmonic vibrational frequencies are also predicted and show that tetrasilatetrahedrane is a true minimum, a genuine isomer of Si_4H_4 and, thus, may be experimentally observed. However, the tetrahedral structure does not appear to be the absolute minimum on the Si_4H_4 potential-energy hypersurface. That position is held by a distorted tetrasilacyclobutadiene structure.

*This work was supported by the Director, Office of Energy Research, Office of Basic Energy Sciences, Chemical Sciences Division of the U.S. Department of Energy under Contract No. DE-AC03-76SF00098.

†The Berkeley theoretical chemistry minicomputer is supported by the U.S. National Science Foundation, Grant CHE-8218785.

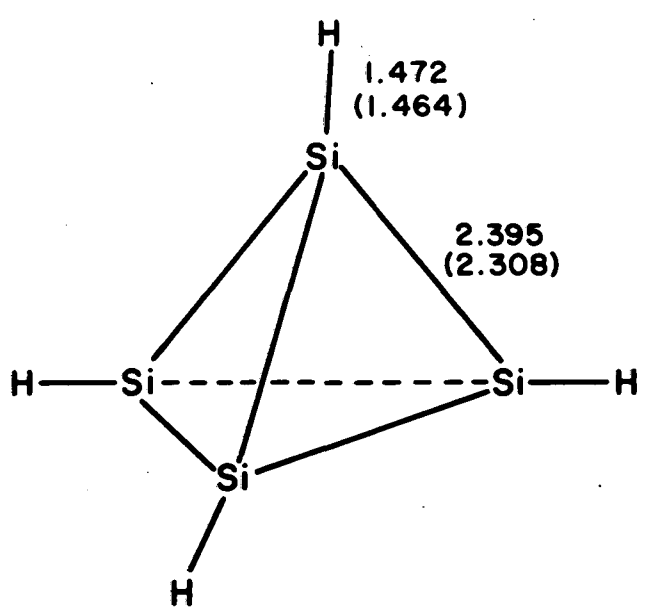

Figure 1-1. Equilibrium molecular structure of tetrasilatetrahedrane (Si_4H_4). Bond lengths with the DZ(DZP) basis sets are given in Å. DZP is an abbreviation for double zeta plus polarization. (XBL 874-1781)

2. Radiative Decay Lifetimes for CH_2^- (Publication 23)

M. Okumura, L.I. Yeh, D. Normand,[†] *J.J.H. van den Biesen,*[‡] *S.W. Bustamente,*[§] *Y.T. Lee, T.J. Lee, N.C. Handy,*[‖] *and H.F. Schaefer III*

Progress has been made on this problem by combining MMRD experimental and theoretical capabilities. Recently the presence and radiative decay of vibrationally excited CH_2^-, generated in a hot cathode discharge of methane, was established by measuring the time-dependent photodetachment from excited states of CH_2^- as it radiatively relaxed in a high-vacuum ion trap. The time dependence of the photodetachment was found to be consistent with an electron affinity of 5250 cm^{-1} (0.65 ev) for ground-state $\tilde{X}\ ^3B_1$ methylene. The radiative-decay lifetimes of the first three excited bending vibrations of CH_2^- were also tentatively assigned. Here, we report a more refined analysis of the experimental data along with theoretical *ab initio* determinations of the radiative-decay lifetimes for the first four excited bending vibrational levels of CH_2^-. There is some discrepancy between the *ab initio* values (431, 207, 118, and 68 milliseconds for the v_2 = 1, 2, 3, and 4 levels, respectively) and the experimental values (525, 70, and 14 milliseconds for v_2 = 1, 2, and 3, respectively). Possible reasons for this discrepancy were discussed, but none of the alternatives is entirely satisfactory.

[†]Permanent address: C.E.N./Saclay, Gif-sur-Yvette, France.

[‡]Permanent address: Philips Research Laboratories, 5600 J.A. Eindhoven, The Netherlands.

[§]Permanent address: Hughes Aircraft Corp., Torrence, CA 90509.

[‖]Permanent address: University Chemical Laboratory, Cambridge CB2 1EW, England.

3. Characterization of the Low-Lying Electronic States of Ketene (Publication 6)[†]

W.D. Allen and H.F. Schaefer III

Features of the potential-energy surfaces of the $\tilde{X}^1A_1$, $^3A_2(^3A')$, $^1A_2(^1A'')$, $^3A_1(^3A')$, $^1B_1$, and 2^1A_1 low-lying electronic states of ketene have been investigated using SCF and configuration-interaction singles and doubles (CISD) methods with DZP and DZP + Rydberg (DZP+R) basis sets. The DZP+R CISD vertical excitation energies are in excellent agreement with observed transition energies and suggest assignments for the $\tilde{X}^1A_1 \rightarrow {}^1B_1$ and $\tilde{X}^1A_1 \rightarrow 2^1A_1$ transitions in the electronic spectrum of ketene. Stationary points have been located at the DZP SCF level of theory for the first four states listed above, and SCF quadratic force constants and harmonic vibrational frequencies have been evaluated analytically at these stationary points. The $\tilde{X}^1A_1$ geometry and vibrational frequencies compare favorably with experimental values, the agreement being typical of DZP SCF results. Due to curve crossings and conical intersections (illustrated in Figure 3-1) of potential surfaces, the four lowest theoretical excited-state surfaces have only two valid (double) minima, corresponding to $^3A''$ and $^1A'$ states. At the DZP SCF geometries, Davidson-corrected CISD adiabatic excitation energies of 16,700 and 19,000 cm^{-1} have been obtained for the $^3A''$ and $^1A''$ states, supporting the previous experimental T_0 upper bounds of Laufer and Keller. Finally, the $\tilde{X}^1A_1$ state is predicted to lie only 5500–7000 cm^{-1} below the $^1A''$ state at the $^1A''$ optimum geometry and appears to have a significant effect on the $^1A''$ out-of-plane frequencies.

[†]The Berkeley theoretical chemistry minicomputer is supported by the U.S. National Science Foundation, Grant CHE-8218785.

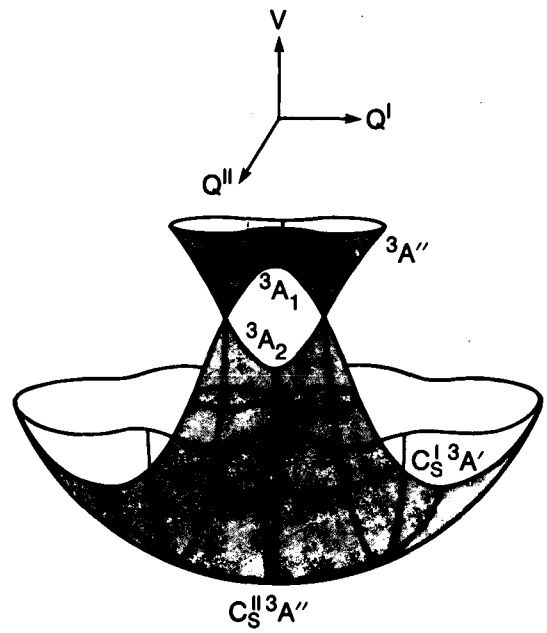

Figure 3-1. A qualitative sketch of the potential-energy hypersurfaces for the two lowest triplet states of the ketene molecule, $CH_2{=}C{=}O$. (XBL 857-8409)

1986 PUBLICATIONS AND REPORTS

Refereed Journals

1. G. Fitzgerald, T.J. Lee, H.F. Schaefer, and R.J. Bartlett, "The Open Chain or Chemically Bonded Structure of H_2O_4, the Hydroperoxyl Radical Dimer," J. Chem. Phys. **83**, 6275 (1985); LBL-19556.
2. H.F. Schaefer, "The F + H_2 Potential Energy Surface: The Ecstasy and the Agony," J. Phys. Chem. Feature Article **89**, 5336 (1985); LBL-19877.
3. H.F. Schaefer, "Methylene: A Paradigm for Computational Quantum Chemistry," Science **231**, 1100 (1986); LBL-19876.
4. Y. Yamaguchi, M.J. Frisch, J.F. Gaw, H.F. Schaefer, and J.S. Binkley, "Analytic Evaluation and Basis Set Dependence of Intensities of Infrared Spectra," J. Chem. Phys. **84**, 2262 (1986); LBL-20474.
5. D.A. Clabo and H.F. Schaefer, "The Silicon Analogue of Benzene—Hexasilabenzene (Si_6H_6)," J. Chem. Phys. **84**, 1664 (1986) LBL-20498.
6. W.D. Allen and H.F. Schaefer, "*Ab Initio* Studies of the Low-Lying Electronic States of Ketene," J. Chem. Phys. **84**, 2212 (1986); LBL-20434.
7. W.D. Allen, J.E. Bertie, M.V. Falk, B.A. Hess, G.B. Mast, D.A. Othen, L.J. Schaad, and H.F. Schaefer, "The Experimental Vibrational Spectra, Vibrational Assignment and Normal Coordinate Analysis of Thiirane-h_4 and -d_4 and *cis*- and *trans*-1,2-Dideuteriothiirane; and *Ab Initio* Theoretical IR Spectra of Thiirane, Thiirene and Isotopically Substituted Derivatives," J. Chem. Phys. **84**, 4211 (1986); LBL-20435.
8. M. Dupuis, G. Fitzgerald, B. Hammond, W.A. Lester, and H.F. Schaefer, "Theoretical Study of the H + $O_3 \leftrightarrow$ OH + $O_2 \leftrightarrow$ O + HO_2 System," J. Chem. Phys. **84**, 2691 (1986); LBL-19216.
9. J.S. Binkley, M.J. Frisch, and H.F. Schaefer, "Vibrational Frequencies and Infrared Intensities for Malonaldehyde: A Post-Hartree-Fock Theoretical Study," Chem. Phys. Lett. **126**, 1 (1986); LBL-20838.
10. G.E. Scuseria, M. Duran, R.G.A.R. Maclagan, and H.F. Schaefer, "The Halocarbenes CHF, CHCl, and CHBr: Geometries, Singlet-Triplet Separations, and Vibrational Frequencies," J. Am. Chem. Soc. **108**, 3248 (1986); LBL-20612.
11. D.A. Clabo and H.F. Schaefer, "Tetrasilatetrahedrane," J. Am. Chem. Soc. **108**, 4344 (1986); LBL-21132.
12. G.E. Scuseria and H.F. Schaefer, "Vibrational Frequencies and Geometries for the Open HF Trimer," Chem. Phys. **107**, 33 (1986); LBL-21131.
13. W.D. Allen and H.F. Schaefer, "Geometrical Structures, Force Constants, and Vibrational Spectra of SiH, SiH_2, SiH_3, and SiH_4," Chem. Phys. **108**, 243 (1986): LBL-21474.
14. R.S. Grev and H.F. Schaefer, "The Ultraviolet Spectrum of Dimethylsilylene," J. Am. Chem. Soc. **108**, 5804 (1986); LBL-21129.
15. T.J. Lee and H.F. Schaefer, "The Classical and Nonclassical Forms of Protonated Acetylene, $C_2H_3^+$. Structures, Vibrational Frequencies, and Infrared Intensities from Explicitly Correlated Wave Functions," J. Chem. Phys. **85**, 3437 (1986); LBL-21130.
16. M.E. Colvin, J. Kobayashi, J. Bicerano, and H.F. Schaefer, "The Infrared Spectrum of Silaethylene," J. Chem. Phys. **85**, 4563 (1986); LBL-21661.
17. J.E. Rice, T.J. Lee, and H.F. Schaefer, "Molecular Structure and Infrared Spectrum of Protonated Nitrous Oxide," Chem. Phys. Lett. **130**, 333 (1986); LBL-21932.

Other Publications

18. R. Murphy and H.F. Schaefer, "Vibrational Frequencies of Small Metal Clusters. The Beryllium Tetramer," in *Applied Quantum Chemistry*, V.H. Smith, H.F. Schaefer, and K. Morokuma, eds., D. Reidel, Dordrecht, Holland, 1986, p. 431; LBL-19875.

LBL Reports

19. T.L. Allen, A.C. Scheiner, Y. Yamaguchi, and H.F. Schaefer, "Theoretical Studies of Diphosphene and Diphosphinylidene in Their Closed Shell States, Low-Lying Open-Shell Singlet and Triplet States, and Transition States. Search for a Stable Bridged Structure," submitted to J. Am. Chem. Soc.; LBL-22505.
20. C.L. Janssen, W.D. Allen, H.F. Schaefer, and J.M. Bowman, "The Infrared Spectrum of the Hydrogen Bifluoride Anion: Unprecedented Variation with Level of Theory," submitted to Chem. Phys. Lett.; LBL-22199.
21. R.S. Grev and H.F. Schaefer, "Cyclopolysilanes: Structure, Strain, and Radical-Anion Aromaticity," submitted to J. Am. Chem Soc.; LBL-22429.
22. T.J. Lee, J.E. Rice, and H.F. Schaefer, "The Infrared Spectrum of the Acetylene Radical Cation $C_2H_2^+$. A Theoretical Study Using SCF, MCSCF, and CI Methods," submitted to J. Chem. Phys.; LBL-22430.
23. M. Okumura, L.I. Yeh, D. Normand, J.J.H. van den Biesen, S.W. Bustamente, Y.T. Lee, T.J. Lee, N.C. Handy, and H.F. Schaefer, "Radiative Decay Lifetimes of CH_2^-," submitted to J. Chem. Phys.; LBL-22428.

Invited Talks

24. H.F. Schaefer, "Symposium on Structure, Spectroscopy, and Dynamics of Atomic, Molecular, and Ionic Clusters," American Chemical Society, New York, April 13–18, 1986.
25. H.F. Schaefer, "Eighth Combustion Research Contractors' Meeting," U.S. Department of Chemistry, Airlie, VA, May 28–30, 1986.
26. H.F. Schaefer, Department of Chemistry, University of Canterbury, Christchurch, New Zealand, March 1986.
27. H.F. Schaefer, Department of Chemistry, University of Kansas, Lawrence, April 1986.
28. H.F. Schaefer, Department of Chemistry, University of Arizona, Tucson, April 1986.
29. H.F. Schaefer, Department of Chemistry, University of Miami, Coral Gables, FL, May 1986.
30. H.F. Schaefer, Department of Chemistry, University of Georgia, Athens, May 1986.
31. H.F. Schaefer, "Electronic Structure of Transition States," American Chemical Society, Anaheim, CA, Sept. 8–10, 1986.
32. H.F. Schaefer, "Symposium on the History of Computers in Chemistry," Divisions of History of Chemistry and Computers in Chemistry, American Chemical Society, Anaheim, CA, Sept. 8–10, 1986.

ATOMIC PHYSICS

High-Energy Atomic Physics*

Harvey Gould, Investigator

INTRODUCTION

The goal of this program is to test quantum electrodynamics (QED) in very high atomic-number (Z) ions and to understand atomic collisions of relativistic very high-Z ions. These are new areas of research that involve physics that is not accessible at lower energies or with lower-Z ions. This research is conducted at the Lawrence Berkeley Laboratory's Bevalac, the world's only relativistic heavy-ion accelerator. Recent results include the first measurement of the Lamb shift in a very high-Z atom (uranium, Z=92). This is the most sensitive test ever achieved of quantum electrodynamics in a strong (static) Coulomb field. Present activities include measurements of multiple-ionization of relativistic uranium. These measurements test for the first time the independent electron approximation in a region where multiple-ionization cross sections can be unambiguously calculated. These and earlier measurements in this program have led to an understanding of relativistic heavy-ion–atom collisions. In most cases, this understanding is now more complete than for nonrelativistic collisions. In future experiments we will channel relativistic uranium ions in silicon to make the first measurement of an electron-impact ionization cross section for a highly ionized heavy ion. A precision (0.1%) measurement of the Lamb shift in uranium will also be attempted.

*This work was supported in part by the Director, Office of Energy Research, Office of Basic Energy Sciences, Chemical Sciences Division, and in part by the Office of High Energy and Nuclear Physics, Nuclear Science Division, of the U.S. Department of Energy under Contract No. DE-AC03-76SF00098.

1. Lamb Shift in Heliumlike Uranium (U^{92+}) (Publication 1)

C.T. Munger† and H. Gould

A possible failure of QED to predict accurate radiative corrections to bound states at Z=92 is not ruled out by its success at low Z. The largest contribution to the Lamb shift at Z=92 comes from terms in the electron self-energy,[1] which are high powers of $Z\alpha$ and which are invisible in experiments at low Z.

We report a value of 70.4 (8.3) eV for the one-electron Lamb shift in uranium. It is in agreement with the theoretical value[2,3] of 75.3 (0.4) eV based on a calculation of the self-energy by Mohr.[2] We extract our Lamb shift from our beam-foil time-of-flight measurement of 54.4 (3.4) ps for the lifetime of the $1s2p_{1/2}\ ^3P_0$ state of heliumlike uranium. In heliumlike uranium the $1s2p_{1/2}\ ^3P_0$ state (Figure 1-1) decays 70% of the time to the $1s2s\ ^3S_1$ state by an electric-dipole (E1) transition. This makes the $1s2p_{1/2}\ ^3P_0$ lifetime sensitive to the $1s2p_{1/2}\ ^3P_0 - 1s2s\ ^3S_1$ energy difference of 260.0 (7.9) eV (experimental value) and hence to the Lamb shift.

In our beam-foil time-of-flight measurement, about 0.5% of a beam of 218 MeV/amu hydrogenlike uranium is converted to the $1s2p_{1/2}\ ^3P_0$ state of heliumlike uranium by electron capture in a 0.9 mg/cm^2 Pd foil. Hydrogenlike uranium is obtained from the LBL Bevalac. The decay curve spans 2.7 decay lengths with a 1/e decay length of 1.182 (0.069) cm. Its 5.8% statistical error dominates our final error in the $1s2p_{1/2}\ ^3P_0$ lifetime. Other contributions to our 6.3% total lifetime error are: 1.2% in the determination of the beam velocity and time dilation using the transverse Doppler shift of the $1s2s\ ^3S_1 \rightarrow 1s^2\ ^1S_0$ transition, and 2.3% from the experimental upper limit to contamination of our signal by cascade feeding. In addition to experimental uncertainty there is a theoretical uncertainty from the effect of small terms omitted from the calculations. These combine to give a separate theoretical error of 2.4 eV in our extracted value of the Lamb shift.

Heliumlike Uranium

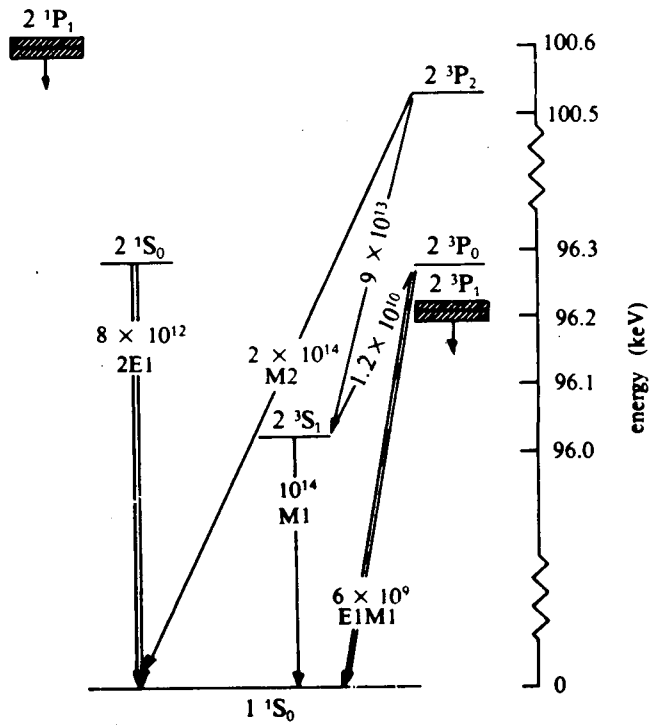

Figure 1-1. Energy-level diagram of the n = 1 and n = 2 states of heliumlike uranium. M1 and M2 decays are magnetic-dipole and magnetic-quadrupole decays, respectively, and decays without labels are electric-dipole decays. An approximate radiative width is indicated for the $^1P_1$ and $^3P_1$ states. (XBL 868-2977)

†Present address: SLAC, Stanford, CA 94305.

1. G.W. Erickson, Phys. Rev. Lett. **27**, 780 (1971); P.J. Mohr, Ann. Phys. New York **88**, 26 (1974); P.J. Mohr, private communication.

2. P.J. Mohr, Phys. Rev. Lett. **34**, 1050 (1975); P.J. Mohr, Phys. Rev. A**26**, 2338 (1982).

3. W.R. Johnson and G. Soff, Atomic Data and Nucl. Data Tables **33**, 405 (1985).

2. Work in Progress

Experiments to channel relativistic iron and uranium through single crystals of silicon and iron are in progress. For these relativistic ions, charge-changing collisions due to the interaction with the target nuclei (stripping and nonradiative electron capture) will be suppressed or eliminated in the channel. As only the electrons in the channel remain to collide with the ions, this will allow electron-impact ionization to be measured for high-Z highly charged ions for the first time.

1986 PUBLICATIONS AND REPORTS

Refereed Journals

1. C.T. Munger and H. Gould, "Lamb Shift in Heliumlike Uranium (U^{90+})," Phys. Rev. Lett. **57**, 2927 (1986); LBL-21996.

Other Publications

2. H. Gould, "New Experiments on Few-Electron Very Heavy Atoms," in *AIP Conf. Proc. No. 136: Atomic Theory Workshop on Relativistic and QED Effects in Heavy Atoms,* H.P. Kelly and Y.K. Kim, eds., AIP, New York, 1985, p. 66; LBL-19884.
3. R. Anholt and H. Gould, "Relativistic Heavy-Ion-Atom Collisions," in *Advances in Atomic and Molecular Physics,* D. Bates and B. Bederson, eds., Academic, Orlando, 1986, p. 315; LBL-20661.
4. H. Gould and C. Munger, "High Energy Atomic Physics," presented at the DOE Chemical Sciences Contractors Meeting, Boulder, CO, April 14–15, 1986; LBL-21136abs.
5. H. Gould and C. Munger, "Lamb Shift in Uranium (Z=92)," abstract, 23rd Int. Conf. on High-Energy Physics, Berkeley, CA, July, 16–23 1986; LBL-21401abs.
6. C. Munger, "The Lamb Shift in Heliumlike Uranium: A Test of QED at Z=92," invited paper, Joint Meeting of the Division of Atomic, Molecular and Optical Physics and the Division of Chemical Physics, American Physical Society, Eugene, OR, June, 18–20, 1986; Bull. Am. Phys. Soc. **31**, 952 (1986); LBL-21135abs.
7. H. Gould and C. Munger, "Lamb Shift in Heliumlike Uranium (Z=92)," abstract, Tenth Int. Conf. on Atomic Physics and Few-Body Systems, Tokyo, Japan, Aug., 24–30, 1986; LBL-21645abs.
8. H. Gould and C. Munger, "Lamb Shift in Heliumlike Uranium (Z=92)," contributed paper, 23rd Int. Conf. on High-Energy Physics, Berkeley, CA, July 16–23, 1986; LBL-21646.
9. H. Gould and C. Munger, "Experiments on Few-Electron Very High-Z Ions," invited paper at the NATO Advanced Study Institute Course on The Physics of Strong Fields, Maratea, Italy, June, 1–14, 1986; LBL-21855.
10. H. Gould and C. Munger, "Tests of Quantum Electrodynamics in Few-Electron Very High-Z Ions," invited paper at Symposium on Relativistic Many-Body Problems, International Centre for Theoretical Physics, Trieste, Italy, June 30–July 4, 1986; LBL-21856.
11. H. Gould and C. Munger, "Measurement of the Lamb Shift in Heliumlike Uranium (Z=92)," invited paper, Tenth Int. Conf. on Atomic Physics and Few-Body Systems, Tokyo, Japan, Aug. 24–30, 1986; LBL-22096.

Invited Talks

12. C. Munger, "Lamb Shift in Heliumlike Uranium," Oxford University, Oxford, England, Sept. 3, 1986; Stanford Linear Accelerator, Sept. 25, 1986; University of California, Berkeley, Atomic Physics Seminar, Oct. 10, 1986; Lawrence Berkeley Laboratory, Physics Research Progress Meeting, Dec. 11, 1986.
13. H. Gould, "Lamb Shift in Heliumlike Uranium," Lawrence Berkeley Laboratory, Nuclear Science Division Colloquium, Sept. 29, 1986; Physics Department, University of Washington, Seattle, Nov. 3, 1986.

Atomic Physics*

Michael H. Prior, Investigator

INTRODUCTION

This program utilizes the intense multiply charged ion beams available from the LBL ECR (Electron Cyclotron Resonance) ion source for studies of atomic structure, collision dynamics, and radiative processes. Emphasis is placed on topics that have relevance to applied areas such as CTR plasma diagnostics and advanced laser concepts and/or that strongly challenge the current state of atomic theory, and require the unique capabilities of the ECR source.

Presently, efforts are under way that yield metastable energy-level structure of highly charged ions, will reveal transient molecular structure via x-ray emission during ion-atom collisions, and will determine cross sections for excitation of multiply charged ion states by electron impact. The latter two studies are collaborative efforts with groups from other laboratories.

1. Forbidden Lines from Highly Charged, Metastable Ion Beams (Publication 2)

M.H. Prior

Observations of forbidden emission lines can provide important diagnostic information on astrophysical and fusion plasmas (e.g., in the solar corona, flares, and tokamak devices). This information results from the sensitivity of the forbidden lines to electron density and temperature and from the fact that these lines often lie in the visible or near-ultraviolet spectrum where efficient transmitting and reflecting optics can be used. Measurement of forbidden-line wavelengths also has high intrinsic value in establishing structure in the lowest lying electron configurations. For most highly ionized systems, this structure is known only from observations of allowed transitions that, because of their large wavenumbers, provide low precision when the differences are taken to derive the spacing of the low-lying metastable levels. Thus a direct measurement of a forbidden line with moderate precision can exceed in accuracy a value determined from allowed lines that were measured with much higher precision. Conversly, direct determination of forbidden-line wavelengths can establish, with high precision, energy intervals (or scale) in the xuv or x-ray region where the allowed lines, which connect to the metastable levels, fall.

Earthbound sources of forbidden emissions from highly charged ions have been largely limited to the fusion plasmas and foil-excited beams of fast heavy ions. This work reports observations of several forbidden lines from a new source of such emissions, namely low-velocity multiply charged ion beams from the LBL ECR ion source. Wavelength measurements have improved on previous determinations for most of the transitions observed. This improvement has been accomplished by viewing a portion of the ion beam about 5 m from the ion source. Radiation emitted from the beam is analyzed with a small spectrometer equipped with a position-sensitive photomultiplier mounted at the exit plane. For calibration purposes, a hollow cathode lamp can be mounted opposite the spectrometer entrance slit. The position-sensitive photomultiplier, and associated electronics, provide two output pulses for each photo event. The pulse amplitudes are a measure of the x and y position from which the photoelectron originated at the photocathode. The detector is oriented with the y axis parallel to the spectrometer dispersion; and the y pulses are histogrammed with a multichannel pulse-height analyzer. The flight time to the spectrometer from the source is such that only excited states with lifetimes greater than 5–10 μsec are present in the beam. Thus all states that decay by allowed electric-dipole (E1) emission (lifetimes $\approx 10^{-8}$ sec or less) have decayed before reaching the spectrometer. The beam is thus "dark" except for the forbidden emission from the metastable components.

Figure 1-1 shows an example of some of the data obtained by this technique. Similar observations have been made of 14 lines from 12 different ions, and measured values of most of these have been reported (publication 2). Many of these observations are "firsts," and nearly all have not been seen in the laboratory. Because of the efficiency of position-sensitive photon counting, the technique outlined here has a potentially large future.

*This work was supported by the Director, Office of Energy Research, Office of Basic Energy Sciences, Chemical Sciences Division of the U.S. Department of Energy under Contract No. DE-AC03-76SF00098.

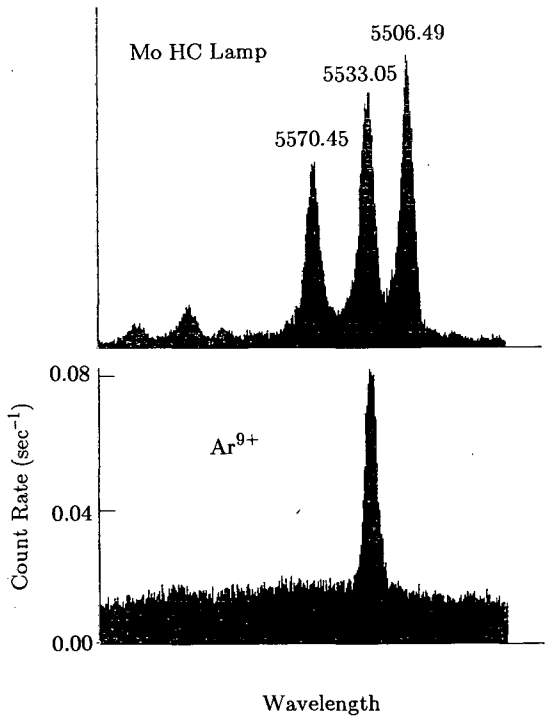

Figure 1-1. The magnetic dipole fine-structure transition $2p^5\ {}^2P_{3/2-1/2}$ from Ar^{9+} (lower) and calibration lines (upper) from a Mo hollow cathode lamp. The wavelengths are air values in Angstrom units. The Ar^{9+} data were accumulated in about 30 min from a beam of about 45 μamp (electrical). A mechanically scanned instrument with an ordinary photomultiplier would have required about 50 hours to accumulate the same data. (XBL 867-2653)

2. Work in Progress

A low-energy ion-beam facility has been designed and nearly completed at the LBL ECR ion source. This facility provides for the the deflection, steering, and focusing of ion beams from the source to any of three experimental stations or lines. This project is a collaborative effort between LBL and the Atomic Physics group from V Division of Lawrence Livermore National Laboratory (LLNL) (P. Egan, R. Fortner), which has provided most of the construction funds.† Beams from the ECR source are available for atomic-physics research approximately 40 hours per week while the 88-inch cyclotron is shut down or using alternate ion sources. The new facility will be used to provide beams for two experiments in 1987.

The first of these is a study of electron excitation of highly charged ion targets. This experiment has been designed by the LLNL group to determine cross sections for dipole allowed and forbidden excitation with special emphasis on targets relevant to recent observations of x-ray lasing at LLNL.

A second experiment to utilize the new beam facility will carry out quasimolecular x-ray interference spectroscopy on ion-atom collisions. This project is a collaborative effort with H. Schmidt-Bocking‡ of the University of Frankfurt and C.L. Cocke‡ of Kansas State University. The experiment will utilize H-like ions (such as Ne^{9+}, Mg^{11+}, and S^{15+}) in collision with atoms of Ne or Ar to study the energy-level structure of the transient quasimolecule that forms during the ion-atom collision.

†LLNL Institutional Research and Development Grant.

‡Support has been received from Kansas State University and from the Office of Basic Energy Sciences, Chemical Sciences Division of the U.S. Department of Energy under Contract No. DE-AC03-76SF00098.

1986 PUBLICATIONS AND REPORTS

Refereed Journals

1. P. Indelicato,† O. Gorceix,† M. Tavernier,† J.P. Briand,† J.P. Desclaux,† R. Marrus, and M. Prior, "Experimental and Theoretical Study of QED Corrections in the Ground State of Helium-like Iron," Zeitschrift für Physik D 2, 149 (1986).

LBL Reports

2 M.H. Prior, "Forbidden Lines from Highly Charged, Metastable Ion Beams," J. Opt. Soc. Am. B (in press); LBL-21922.

Invited Talks

3. M.H. Prior, "Atomic Physics at the LBL ECR Ion Source," Atomic Physics (DOE-BES) Contractors Workshop, University of Colorado, Boulder, April 14–15, 1986.

†Supported by a NSF-CNRS grant and NATO Grant #RG252.80.

PROCESSES AND TECHNIQUES

CHEMICAL ENERGY

Formation of Oxyacids of Sulfur from SO_2*

Robert E. Connick, Investigator

INTRODUCTION

This research is primarily concerned with the fundamental chemistry of sulfur species formed from sulfur dioxide in aqueous solution and the reactions of these species. This chemistry is of importance in the problems associated with atmospheric pollution by sulfur dioxide and the resulting formation of acid rain. Past work has dealt with the identification of species (e.g., two isomeric forms of bisulfite ion), equilibrium measurements, and the study of the dynamics of oxygen exchange with water. Present work is focused on the mechanism of oxidation of bisulfite ion by oxygen—a chain reaction. Additional oxidation-reduction reactions should be investigated, particularly reactions involving two or more oxidation states of sulfur. A secondary and not closely related goal is to determine the factors controlling rates of substitution reactions in the first coordination sphere of metal ions in solution. This research is being pursued both through measurement of such rates with NMR and by computer modeling of such processes.

1. Work in Progress

Mechanism of the Oxidation of Bisulfite Ion by Oxygen.

In previous work an intermediate formed in the reaction was detected and its formula deduced as $HOOSO_2^-$, peroxysulfite ion. Recent results from Dr. Chang's group appear to be inconsistent with this finding. The contradiction has not yet been resolved.

Earlier a system was proposed for separating the rate law into its three components: initiation, propagation, and termination. As yet clean-cut results have not been obtained, possibly because of irreproducibility in the measurements. A more careful set of measurements will be made, and modifications of the method will be tried.

Displacement Reactions of Solvent in the First Coordination Sphere of Metal Ions (in cooperation with Dr. Berni Alder of Lawrence Livermore National Laboratory).

The program for computer simulation of this reaction has now been extended from two to three dimensions. Using a radius ratio corresponding to perfect 6-fold coordination, runs are being made to determine the structure of the activated complex.

*This work was supported by the Director, Office of Energy Research, Office of Basic Energy Sciences, Chemical Sciences Division of the U.S. Department of Energy under Contract No. DE-AC03-76SF00098.

Catalytic Hydrogenation of CO*

Gabor A. Somorjai and Alexis T. Bell, Investigators

INTRODUCTION

The purpose of this program is to develop an understanding of the fundamental processes involved in catalytic conversion of carbon monoxide and hydrogen to gaseous and liquid fuels. Attention is focused on defining the factors that limit catalyst activity, selectivity, and resistance to poisoning, and the relationship between catalyst composition/structure and performance. To meet these objectives, a variety of surface diagnostic techniques are used to characterize supported and unsupported catalysts before, during, and after reaction. These techniques include low-energy electron diffraction (LEED), Auger electron spectroscopy (AES), x-ray photoelectron spectroscopy (XPS), electron-energy-loss spectroscopy (EELS), infrared spectroscopy (IRS), and temperature-programmed desorption (TPD). The information thus obtained is combined with detailed studies of reaction kinetics to elucidate reaction mechanisms and the influence of modifications in catalyst composition and/or structure on the elementary reactions involved in carbon monoxide hydrogenation.

1. The Hydrogenation of Carbon Monoxide on Mo(100) Single Crystals and Polycrystalline Foils (Publication 1)

M. Logan, A. Gellman, and G.A. Somorjai

The hydrogenation of carbon monoxide over (100) oriented single crystals and polycrystalline molybdenum catalysts produces primarily methane, ethene, and propene. The rates of formation of all products were found to be the same for both the (100) single crystals and polycrystalline foils, suggesting that the reaction is structure insensitive. The dependence of the rate of formation of methane on reactant pressure was found to be $r_{CH_4} = KP_{CO}^{0.32} P_{H_2}^{1.0}$. The unusual positive CO pressure dependence points to a mechanism of methanation that is different from that of other transition-metal methanation catalysts (Fe, Ru, Ni), although the activation energy for the reaction is similar, 24 kcal/mol. Addition of K to the surface, at coverages of less than 0.3 monolayer (ML), increased the overall rate of reaction and enhanced the olefin-to-paraffin ratio. The addition of S to the surface decreased the rate of hydrogenation but, for coverages up to ~0.25 ML, increased the ratio of ethene to methane by as much as a factor of 5.

2. The Effects of Titania and Alumina Overlayers on the Hydrogenation of CO Over Rhodium (Publication 13)

M. Levin, M. Salmeron, A.T. Bell, and G.A. Somorjai

Submonolayer quantities of TiO_x and AlO_x were deposited on a polycrystalline Rh foil. The samples were characterized by AES and then enclosed in an atmospheric-pressure chamber to evaluate their activity for CO hydrogenation. AlO_x deposition suppresses the rate of CO hydrogenation in direct proportion to the AlO_x coverage, but the product distribution and kinetics are unaffected. These observations indicate that the only effect of AlO_x is to block Rh sites. TiO_x deposition has a more complex effect. With increasing TiO_x coverage, the methanation rate passes through a maximum at a TiO_x coverage of 0.15 ML. The maximum rate is three times as large as the rate for clean Rh. The deposited TiO_x also affects the catalyst selectivity, as well as the kinetics of methane formation. The selectivity for methane reaches a minimum for a TiO_x coverage of about 0.20 ML; and in the same range, the activation energy for methanation reaches a minimum and the H_2 and CO partial pressure dependences reach a maximum. The unusual behavior of TiO_x-promoted Rh is attributed to the occurrence of highly active catalytic sites near the perimeter of the TiO_x islands making up the overlayer.

3. A Novel Method for Analyzing Transient Response Data Obtained in Isotopic Tracer Studies of CO Hydrogenation (Publication 14)

M. DePontes, G.M. Yokomizo, and A.T. Bell

A method has been developed for analyzing transient-response data obtained in isotopic tracer studies of CO hydrogenation. Methane is assumed

*This work was supported by the Director, Office of Energy Research, Office of Basic Energy Sciences, Chemical Sciences Division of the U.S. Department of Energy under Contract No DE-AC03-76SF00098.

to be produced by the independent hydrogenation of various pools of carbon present on the catalyst surface, but no assumptions are made about the number of such pools nor the homogeneity of their reactivity. The interpretation of transient-response data is handled in a mathematically rigorous fashion. Application of the method to data for Ru and Ni catalysts reveals bimodal spectra of first-order rate coefficients. The peaks in these spectra are assigned to specific forms of adsorbed carbon. It is also shown that the ability to resolve different carbon forms and the heterogeneity in the reactivity of these forms is closely linked to the noise in the experimentally observed transients.

4. The Influence of Preparation Chemistry on the Phase Distribution of Silica-Supported Titania (Publications 15, 16, 17, and 18)

M.G. Reichmann, F.G. Hollander, and A.T. Bell

Titania dispersed on high-surface-area supports such as silica or alumina exhibits properties similar to those of bulk titania. The ability of such composite materials to maintain high surface area at elevated temperatures makes them attractive as catalyst supports. An investigation has been conducted of the chemistry by which small crystallites of titania are produced on a silica support. Silica-supported TiO_2 was prepared by incipient wetness impregnation of silica with a solution containing $TiCl_4/HCl$ or $Ti(OCH_3)_4/HNO_3$. The solid was then dried and calcined. Laser Raman spectroscopy was used to characterize the impregnation solutions and the solid phases following various stages of preparation. The calcined TiO_2/SiO_2 was also examined by x-ray diffraction and transmission electron microscopy.

With increasing $TiCl_4$ and HCl concentrations in the impregnating solution, the titanium proceeds from monomeric species to dimers and finally oligomers, one of which is the cubic complex $[Ti_8O_{12}(H_2O)_{24}]Cl_8 \cdot HCl \cdot 7H_2O$. Evaporation of the impregnating solution converts all of the titanium to the octomeric complex. Calcination of the SiO_2-supported complex leads to the formation of $TiO_2(B)$ and anatase. X-ray diffraction and electron microscopy show the $TiO_2(B)$ phase to be highly dispersed. Lower titania weight loadings favor the formation of the $TiO_2(B)$ complex, whereas higher loadings favor anatase. The formation of $TiO_2(B)$ and anatase is shown to proceed in a logical fashion from the $[Ti_8O_{12}(H_2O)_{24}]Cl_8 \cdot HCl \cdot 7H_2O$ complex.

When the impregnating solution contains $Ti(OCH_3)_4/HNO_3$, Raman spectra again show the presence of titanyl ions and dimer ions. For acid concentrations below 10.0M, the impregnation solution contains monomeric titanyl ions and dimeric ions containing Ti-O-Ti bonds. For acid concentrations above 12.0M, bridging titanium nitrate species and bidentate and bridging nitrite species are observed. Impregnation of silica or alumina with a $Ti(OCH_3)_4$-HNO_3 solution and subsequent drying causes a release of NO_2 and the formation of rutile at temperatures as low as 298 K. The low-temperature formation of rutile is attributed to the decomposition of titanium nitrite ribbons dispersed on the surface of the support.

5. The Influence of Ethylene on the Hydrogenation of CO Over Ruthenium (Publication 12)

D.S. Jordan and A.T. Bell

The interactions of C_2H_4 with H_2 and CO were investigated over a SiO_2-supported Ru catalyst. To differentiate carbon sources, ^{13}C-labeled CO and unlabeled C_2H_4 were used. Product analysis was carried out by isotope-ratio gas chromatography/mass spectrometry. In the absence of CO, C_2H_4 undergoes extensive hydrogenation. Small amounts of CH_4 and C_{3+} olefins and paraffins are also observed, indicative of C_2H_4 hydrogenolysis and homologation. The presence of CO strongly suppresses C_2H_4 hydrogenolysis, but enhances C_2H_4 homologation. The hydrogenation of CO to hydrocarbons is strongly influenced by the presence of C_2H_4. With increasing C_2H_4 partial pressure, the hydrogenation of CO to hydrocarbons is progressively suppressed, but the hydroformylation of C_2H_4 to form propanal (and some 1-propanol) is enhanced. The product distributions observed for the reactions of C_2H_4 and H_2, and C_2H_4, CO, and H_2, can be described in terms of a chain-growth mechanism involving C_2 and C_2 monomer units.

6. The Influence of Dispersion on the Activity and Selectivity of Silica- and Lanthana-Supported Rhodium (Publication 19)

R.P. Underwood and A.T. Bell

The influence of Rh particle size on the activity and selectivity of Rh/SiO_2 and Rh/La_2O_3 catalysts for CO hydrogenation has been studied. Investigation of Rh/SiO_2 and Rh/La_2O_3 catalysts of a range of Rh loading included catalyst characterization by H_2 chemisorption and *in situ* infrared spectroscopy of chemisorbed CO, in addition to reaction-rate measurements obtained in a flow microreactor. The higher activity and higher product selectivity to oxygenates observed for Rh/La_2O_3 compared to Rh/SiO_2 is attributed to the existence of a metal-support interaction between Rh and La_2O_3. The catalyst characterization and kinetic results indicate that, in agreement with recent interpretations of the nature of metal-support interactions, the surface of the Rh crystallites in Rh/La_2O_3 is modified by the deposition of LaO_x moieties derived from the support. It was found that the extent of coverage of the Rh crystallites by LaO_x increases with Rh loading. The activity and product selectivity at a fixed set of reaction conditions for both Rh/SiO_2 and Rh/La_2O_3 were found to be strong functions of Rh particle size. For Rh/SiO_2, maximum selectivity to CH_3OH and C_2-oxygenates was observed for the highest-dispersion catalysts, while the lowest-dispersion catalysts were the most selective to hydrocarbons. The influence of Rh loading on the product distribution for Rh/La_2O_3 is determined by a combination of the effects of Rh particle size and the influence of the varying coverage of the surface Rh by LaO_x.

1986 PUBLICATIONS AND REPORTS

Refereed Journals

1. M. Logan, A. Gellman, and G.A. Somorjai, "Hydrogenation of Carbon Monoxide on Mo(100) Single Crystals and Polycrystalline Foils," J. Catal. **94**, 60 (1985); LBL-17952.
2. E.L. Garfunkel, J. Parmeter, B.M. Naasz, and G.A. Somorjai, "The Hydrogenation of Carbon Monoxide over Model Rhenium Catalysts: Additive Effects and a Comparison with Iron," Langmuir **2**, 105 (1986); LBL-17965.
3. K.J. Zhen, M.M. Khan, C.H. Mak, K.B. Lewis, and G.A. Somorjai, "Partial Oxidation of Methane with Nitrous Oxide over V_2O_5-SiO_2 Catalysts," J. Catal. **94**, 501 (1985); LBL-18493.
4. J. Maj, C.A. Colmenares, and G.A. Somorjai, "Methanol Production from Carbon Monoxide and Hydrogen on Thorium Dioxide," J. Catal. **95**, 385 (1985).
5. G.A. Somorjai, "Surface Science and Catalysis," Royal Soc. Disc. **318**, 81 (1986).
6. R.P. Underwood and A.T. Bell, "CO Hydrogenation over Rhodium Supported on SiO_2, La_2O_3, Nd_2O_3, and Sm_2O_3," Appl. Catal. **21**, 157 (1986); LBL-19793.
7. J S. Rieck and A.T. Bell, "Studies of the Interactions of H_2 and CO with Silica- and Lanthana-Supported Palladium," J. Catal. **96**, 88 (1985); LBL-18689.
8. J.S. Rieck and A.T. Bell, "Studies of the Interactions of H_2 and CO with Pd/TiO_2 and TiO_2-Promoted Pd/SiO_2," J. Catal. **99**, 262 (1986); LBL-19701.
9. J.S. Rieck and A.T. Bell, "Studies of the Interactions of H_2 and CO with Pd/SiO_2 Promoted with La_2O_3, CeO_2, Pr_6O_{11}, Nd_2O_3, and Sm_2O_3," J. Catal. **99**, 278 (1986); LBL-20032.
10. J.S. Rieck and A.T. Bell, "Studies of the Interactions of H_2 and CO with Pd/SiO_2 Promoted with Li, Na, K, Rb, and Cs," J. Catal. **100**, 305 (1986); LBL-20198.
11. M. Levin, M. Salmeron, A.T. Bell, and G.A. Somorjai, "The Influence of TiO_x Deposits on a Polycrystalline Rh Foil on CO Adsorption and Desorption" Surf. Sci. **169**, 123 (1986); LBL-19901.
12. D.S. Jordan and A.T. Bell, "Influence of Ethylene on the Hydrogenation of CO over Ruthenium," J. Phys. Chem. **90**, 4797 (1986); LBL-21236.

LBL Reports

13. M.E. Levin, M. Salmeron, A.T. Bell, and G.A. Somorjai, "The Effects of Titania and Alumina Overlayers on the Hydrogenation of CO over Rhodium," Faraday Trans. (in press); LBL-21607.
14. M. DePontes, G.H. Yokomizo, and A.T. Bell, "A Novel Method for Analyzing Transient Response Data Obtained in Isotopic Tracer Studies of CO Hydrogenation," J. Catal. (in press); LBL-21853.
15. M.G. Reichmann and A.T. Bell, "A Raman Study of the Preparation of SiO_2-Supported TiO_2 from $TiCl_4$ and HCl," Langmuir (in press); LBL-21902.
16. M.G. Reichmann, F.J. Hollander, and A.T. Bell, "Structure of $[Ti_8O_{12}(H_2O)_{24}]Cl_8 \cdot HCl \cdot 7H_2O$," submitted to Acta Crystallogr., Sec. C; LBL-22344.
17. M. Reichmann and A.T. Bell, "A Raman Study of the Preparation of SiO_2- and Al_2O_3-Supported TiO_2 from $Ti(OCH_3)_4$ and HNO_3," submitted to Langmuir; LBL-22345.
18. M.G. Reichmann and A.T. Bell, "The Influence of Preparation Chemistry on the Phase Distribution of Silica-Supported Titania," submitted to Appl. Catal.; LBL-22515.
19. R.P. Underwood and A.T. Bell, "The Influence of Dispersion on the Activity and Selectivity of Silica- and Lanthana-Supported Rhodium," submitted to J. Catal.; LBL-22742.

Invited Talks

20. G.A. Somorjai, "CO Hydrogenation on Metal Surfaces," Department of Chemistry, State University of New York, Stony Brook, NY, March 1986.
21. G.A. Somorjai, "The Surface Science of Chemical Energy Conversion," Weizman Institute, Rehovat, Israel, April 1986.
22. A.T. Bell, "Studies of Fischer-Tropsch Synthesis over Ruthenium Catalysts," Exxon Research & Development Laboratory, Baton Rouge, LA, Jan. 1986.
23. A.T. Bell, "Effect of Metal Oxide Promoters on the Hydrogenation of CO," Amoco Research Center, Naperville, IL, Feb. 1986.
24. A.T. Bell, "Effects of Metal–Metal Oxide Interactions on Catalyst Performance," GE Research & Development Center, Schenectady, NY, March 1986.
25. A.T. Bell, "Studies of Secondary Processes Involving Low Molecular Weight Olefins Occurring During Fischer-Tropsch Synthesis," California Catalysis Society Meeting, Richmond, CA, March 1986.
26. A.T. Bell, "The Enhancement of CO Hydrogenation Activity on Rhodium by Titania Overlayers," California Catalysis Society Meeting, Richmond, CA, March 1986.
27. A.T. Bell, "Influence of Lanthana Promotion on the Hydrogenation of CO over Supported Rhodium Catalysts," California Catalysis Society Meeting, Richmond, CA, March 1986.
28. A.T. Bell, "Determination of Rate Coefficients for Carbon Hydrogenation Occurring during Fischer-Tropsch Synthesis," Meeting on the Mechanism of Heterogeneous Catalysis, Institut de Recherches sur la Catalyse, Villeurbanne, France, April 1986.
29. A.T. Bell, "Studies of Carbon Deposition and Consumption on Ru/TiO_2 during Fischer-Tropsch Synthesis," ACS Meeting, New York, NY, April 1986.
30. A.T. Bell, "The Influence of TiO_x Promoters on the Chemisorption and Hydrogenation of CO on Polycrystalline Rh," ACS Meeting, New York, NY, April 1986.
31. A.T. Bell, "Application of NMR Spectroscopy to Studies of the Synthesis of Zeolites," Signal Research Center, Des Plaines, IL, April 1986.
32. A.T. Bell, "The Influence of Metal Dispersion and Metal–Metal Oxide Interactions on the Hydrogenation of CO over Group VIII Metals," Chicago Catalysis Club, Chicago, IL, April 1986.
33. A.T. Bell, "Application of NMR Spectroscopy to the Elucidation of Molecular Structures Present During Zeolite Synthesis," 60th Colloid and Surface Science Symposium, Atlanta, GA, June 1986.
34. A.T. Bell, "Metal Oxide Decoration of Metals. A Model for Interpreting Metal-Support Interactions," 60th Colloid and Surface Science Symposium, Atlanta, GA, June 1986.
35. A.T. Bell, "The Structure and Chemistry of Carbonaceous Deposits Formed During Fischer-Tropsch Synthesis," Division of Material Science, CSIRO Laboratory, Clayton, Australia, July 1986.
36. A.T. Bell, "The Influence of Metal Oxide Promoters on the Hydrogenation of CO over Group VIII Metals," Division of Material Science, CSIRO Laboratory, Clayton, Australia, July 1986.
37. A.T. Bell, "The Genesis of Supported Metal Oxide Catalysts TiO_2/SiO_2 and TiO_2/Al_2O_3," Division of Material Science, CSIRO Laboratory, Clayton, Australia, July 1986.
38. A.T. Bell, "The Genesis of Supported Metal Oxide Catalysts TiO_2/SiO_2 and TiO_2/Al_2O_3," Department of Chemical Engineering, University of New South Wales, Sydney, Australia, Aug. 1986.
39. A.T. Bell, "The Influence of Metal Oxide Promoters on the Hydrogenation of CO over Group VIII Metals," CSIRO Laboratory, Lucas Heights, Australia, Aug. 1986.
40. A.T. Bell, "Application of Transient Response Techniques to the Study of Catalyzed Reactions," Department of Chemical Engineering, University of Melbourne, Australia, Aug. 1986.
41. A.T. Bell, "The Structure and Chemistry of Carbonaceous Deposits Formed During Fischer-Tropsch Synthesis," Department of Chemistry, University of Tokyo, Japan, Aug. 1986.
42. A.T. Bell, "Secondary Reactions of Low–Molecular Weight Olefins During Fischer-Tropsch Synthesis," American Chemical Society Meeting, Anaheim, CA, Sept. 1986.
43. A.T. Bell, "The Effects of Titania and Alumina Overlayers on the Hydrogenation of CO over Rhodium," Royal Society of Chemistry Autumn Meeting, Faraday Division Symposium on Promotion in Heterogeneous Catalysis, University of Bath, England, Sept. 1986.
44. A.T. Bell, "Progress Towards the Rational Design of Supported Metal Catalysts," The Eighth Annual Chemical Engineering Symposium, Department of Chemical Engineering, Carnegie Mellon University, Pittsburgh, PA, Oct. 1986.
45. A.T. Bell, "Studies of Secondary Processes Involving Low–Molecular Weight Olefins Occurring During Fischer-Tropsch Synthesis," American Institute of Chemical Engineers Meeting, Miami, FL, Nov. 1986.
46. A.T. Bell, "Fischer-Tropsch Synthesis over Ruthenium. Determination of Rate Coefficients for Carbon Hydrogenation," American Institute of Chemical Engineers Meeting, Miami, FL, Nov. 1986.
47. A.T. Bell, "The Genesis of Mixed Metal Oxide Catalysts Supports, TiO_2/SiO_2 and TiO_2/Al_2O_3," American Institute of Chemical Engineers Meeting, Miami, FL. Nov. 1986.
48. A.T. Bell, "The Genesis of Mixed Metal Oxide Catalysts Supports, TiO_2/SiO_2 and TiO_2/Al_2O_3," E.I. du Pont de Nemours & Co., Wilmington, DE, December 1986.
49. A.T. Bell, "Fischer-Tropsch Synthesis over Ruthenium. Determination of Rate Coefficients for Carbon Hydrogenation," E.I. du Pont de Nemours & Co., Wilmington, DE, Dec. 1986.

Organometallic Chemistry of Coal Conversion*

K. Peter C. Vollhardt, Investigator

INTRODUCTION

The purpose of this program is to combine synthetic organic and organometallic methodology in the construction of novel organometallic materials with potential in catalysis and materials science. In particular, iterative approaches to the synthesis of organic ligands with multiple binding sites are being studied. Subsequent attachment for a variety of metal centers with control of their binding sequence should give rise to linear and angular polymetallic arrays in which the metals are held in an unnatural configuration. Such materials hold promise in potential applications as catalysts in a variety of processes of current fundamental and industrial interest, such as coal depolymerization and conversion to liquid fuels, small-molecule activation, new reaction chemistry, photocatalysis and photochemical energy storage, water splitting, and others. Moreover, the methods to be developed are anticipated to provide access to structures containing alternating organic and metallic layers with potential conducting behavior. Thus, in the long run, successful execution of the proposed work should furnish unique catalytic and potentially conducting materials.

1. The Chemistry of (Fulvalene)dimolybdenum Hexacarbonyl: A Rigidly Held Dinuclear Transition-Metal Complex (Publication 1)

J.S. Drage and K.P.C. Vollhardt

The x-ray structure of (fulvalene)dimolybdenum hexacarbonyl [$FvMo_2(CO)_6$] has been determined. Thermal, photolytic, and chemical treatment fails to yield the metal-metal triply bonded complex $FvMo_2(CO)_4$, either because it is not formed or because of its instability; this result may have been caused by excessive bond strain in the fulvalene ligand. Photolysis of $FvMo_2(CO)_6$ in the presence of alkynes affords mono- and bis(alkyne) complexes $FvMo_2(CO)_4(RC{\equiv}CR)$ and $FvMo_2(CO)_3(RC{\equiv}CR)_2$. Spectroscopic evidence indicates that the former incorporates as a ligand a μ-η^2-alkyne and that this ligand partially moves about the Mo-Mo bond in a rapid fluxional process: $\Delta G^{\ddagger} = 15 \pm 0.5$ kcal mol^{-1}. The bis(alkyne) systems contain uncoupled alkynes as determined by an x-ray diffraction study of one complex. This result is unusual in light of the frequent occurrence of alkyne coupling at a dinuclear center.

Reduction of $FvMo_2(CO)_6$ with Na-Hg or $LiBEt_3H$ furnishes the dianion $FvMo_2(CO)_6^{2-}$. The latter reacts with protic acids and haloalkanes to give the respective dihydride $FvMo_2(CO)_6H_2$ and dialkyl complexes $FvMo_2(CO)_6R_2$ (R = CH_3, CH_2Ph, or CH_2OCH_3). At 20°C the dihydride eliminates H_2 with formation of $FvMo_2(CO)_6$. Treatment of $FvMo_2(CO)_6(CH_2OCH_3)_2$ with $HBF_4.(Et_2O)$ at −20°C (CD_2Cl_2) produces $FvMo_2(CO)_6(CH_2OCH_3)(=CH_2)^+$, as determined by ^1H NMR spectroscopy. Warming to 0°C gives the carbene-coupling product $FvMo_2(CO)_6(C_2H_4)^{2+}$. The bis(carbene) $FvMo_2(CO)_6(=CH_2)_2^{2+}$ is not detected. The dianion $FvMo_2(CO)_6^{2-}$ reacts with $I(CH_2)_3I$ to give a metal-metal bonded 1-oxacyclopent-2-ylidene complex. An x-ray diffraction analysis shows that the Fischer-type carbene ligand is terminally bound. This complex exhibits fluxional behavior that may involve a bridging carbene species ($\Delta G^{\ddagger} = 18 \pm 0.5$ kcal mol^{-1}). Thermolysis (100°C) leads to efficient generation of propene and $FvMo_2(CO)_6$ by a novel pathway.

2. Carbonyl Substitution and Ring Slippage upon Reaction of Trialkylphosphines with (Fulvalene)diruthenium Tetracarbonyl. X-ray Structural Analysis of (η^0:η^4-$C_{10}H_8$)$Ru(PMe_3)_2CO$ and Fluxional Behavior of (η^5:η^5-$C_{10}H_8$)$Ru_2(CO)_3L$ (L = Phosphine) (Publication 2)†

R. Boese, W.B. Tolman,‡ and K.P.C. Vollhardt

Treatment of (η^5:η^5-fulvalene)diruthenium tetracarbonyl [$FvRu_2(CO)_4$] with a large excess (8–10 equiv.) of PMe_3 at 120°C provides *trans*-$Ru(CO)_3(PMe_3)_2$ and $FvRu(PMe_3)_2(CO)$, in which only one Cp ring is bonded to Ru, as characterized by x-ray crystallography. Reaction of $FvRu_2(CO)_4$ with 2–3 equiv. of PMe_3 or excess (5 equiv.) PEt_3 gives $FvRu_2(CO)_3L$. Both substitution products are fluxional on the NMR time scale by a mechanism

*This work was supported by the Director, Office of Energy Research, Office of Basic Energy Sciences, Chemical Sciences Division of the U.S. Department of Energy under Contract No. DE-AC03-76SF00098.

involving reversible terminal to bridged carbonyl exchange. Activation parameters for the process were determined from a line-shape analysis of variable-temperature ^{13}C NMR spectra of ^{13}CO-labeled derivatives.

---

†Work carried out in collaboration with Dr. R. Boese, Institut für Anorganische Chemie, Universität Essen — GHS, West Germany.
‡W.B. Tolman was a W.R. Grace Fellow, 1984–1985.

3. Designed Syntheses of Heterobimetallic Fulvalene Complexes (Publication 5)

M.A. Huffman, D.A. Newman, M. Tilset,† W.B. Tolman,‡ and K.P.C. Vollhardt

Two synthetic strategies to the construction of heterobimetallic fulvalene (η^5:η^5-$C_{10}H_8$) complexes have been implemented. The first is based on the previously described monometallic ring-slippage products of (η^5:η^5-$C_{10}H_8$)$Mo_2(CO)_6$ and (η^5:η^5-$C_{10}H_8$)$Ru_2(CO)_4$ that undergo recomplexation with a variety of metal carbonyls. The second uses a potentially iterative synthetic organic strategy in which cyclopentadienyl anion is subjected to an alkanoylation-ring closure sequence that assembles a new attached cyclopentadiene unit.

---

†M. Tilset was the recipient of a Fellowship from the Royal Norwegian Council for Scientific and Industrial Research (1983–1985).
‡W.B. Tolman was a W.R. Grace Fellow (1984–1985).

1986 PUBLICATIONS AND REPORTS

Refereed Journals

1. J.S. Drage and K.P.C. Vollhardt, "The Chemistry of (Fulvalene)dimolybdenum Hexacarbonyl: A Rigidly Held Dinuclear Transition Metal Complex," Organometallics **5**, 280 (1986); LBL-19539.
2. R. Boese, W.B. Tolman, and K.P.C. Vollhardt, "Carbonyl Substitution and Ring Slippage Upon Reaction of Trialkylphosphines With (Fulvalene)diruthe-.br nium Tetracarbonyl. X-ray Structural Analysis of (η^0:η^4-$C_{10}H_8$)$Ru(PMe_3)_2CO$ and Fluxional Behavior of (η^5:η^5-$C_{10}H_8$)$Ru_2(CO)_3L$ (L=Phosphine)," Organometallics **5**, 582 (1986); LBL-20720.
3. R. Moulton, T.W. Weidman, K.P.C. Vollhardt, and A.J. Bard, "The Electrochemistry of Carbonyl(fulvalene)dimetal Complexes (M_2 = Cr_2, Mo_2, W_2, Ru_2, Mo-Ru) in Aprotic Media," Inorg. Chem. **25**, 1846 (1986); LBL-20721.
4. D.J. Meyerhoff, R. Nunlist, M. Tilset, and K.P.C. Vollhardt, "Dinuclear Tungsten and Molybdenum Complexes With Fulvalene Ligands: Assignment of their ^1H and ^{13}C NMR Spectra by One-Dimensional Heteronuclear NOE Difference Spectroscopy," Magn. Reson. Chem. **24**, 709 (1986); LBL-22544.
5. M.A. Huffman, D.A. Newman, M. Tilset, W.B. Tolman, and K.P.C. Vollhardt, "Designed Syntheses of Heterobimetallic Fulvalene Complexes," Organometallics **5**, 1926 (1986); LBL-22545.

LBL Reports

6. T.W. Weidman (Ph.D. Thesis), "Synthesis, Reactivity, and Photochemistry of Fulvalene Diruthenium Tetracarbonyl," LBL-22547.

Invited Talks

7. K.P.C. Vollhardt, "From Cyclopentadienylmetals to Polyorganometallics: Remarkable Metallic Materials," Exxon Research and Engineering Co., Annandale, NJ, Feb. 3, 1986; Columbia University, New York, NY, April 3, 1986; University of Hamburg, Federal Republic of Germany, July 8, 1986.
8. K.P.C. Vollhardt, "Remarkable Rearrangements in the Coordination Sphere of Trinuclear Cobalt Biscarbyne Clusters," Max Planck Institute for Coal Research, Mülheim, Federal Republic of Germany, July 22, 1986; General Electric Company, Schenectady, NY, Nov. 6, 1986.

Synthetic and Physical Chemistry*

William L. Jolly, Investigator

INTRODUCTION

The purpose of this project is to use photoelectron spectroscopy to determine the nature of the bonding in significant inorganic and organometallic compounds. By measuring core-electron binding energies of appropriate transition-metal compounds, it is possible to study the interaction of metal d electrons with various ligands and to identify various modes of ligand-metal bonding that have analogues in the intermediates of catalyzed organic reactions. Core binding energies can also be used in conjunction with valence-shell ionization potentials to quantify the bonding or antibonding character of molecular orbitals.

1. π-Donor Character of the Dimethylamido Ligand (Publication 1)

R.A. Andersen, D.B. Beach, and W.L. Jolly

The core-electron binding energies of dimethylamides of early transition metals, when qualitatively interpreted in terms of atomic charges, are consistent with nitrogen-metal $p\pi \rightarrow d\pi$ bonding. Further support for such π bonding is obtained by the "localized orbital ionization potential" (LOIP) method, in which one compares the nitrogen lone-pair ionization potentials with the ionization potentials that the nitrogen 2p orbitals would have if they were strictly nonbonding.

2. Absolute Stabilization Energies for Molybdenum 4d Electrons Based on the Reference Compound Tetrakis(dimethylamido)-molybdenum(IV) (Publication 2)

D.B. Beach and W.L. Jolly

Until now, the only molecules with strictly nonbonding valence electrons for which core binding energies and lone-pair ionization potentials were known were the hydrogen halides, H_2O, H_2S, and H_2Se, planar NH_3, and planar PH_3. Thus it has been possible to apply the LOIP method on an absolute basis only in the case of compounds of F, Cl, Br, O, S, Se, N, and P. It has not been possible to determine the absolute stabilization or destabilization of a metal d orbital in a compound relative to a strictly nonbonding metal d orbital because the required data for a compound containing a strictly nonbonding d orbital have not been available. However, we now have the required data for one compound, $Mo[N(CH_3)_2]_4$, which possesses an essentially nonbonding d electron pair.

In this study, we determined the Mo $3d_{5/2}$, N 1s, and C 1s binding energies of $Mo[N(CH_3)_2]_4$ in the vapor phase. The Mo $3d_{5/2}$ binding energy can be used in conjunction with the ionization potential of other molybdenum compounds to quantify the bonding characters of molecular orbitals derived from the molybdenum 4d orbitals in these compounds. Consider, for example, molybdenum hexacarbonyl. Here the ionization potential of the t_{2g} electrons (8.50 eV) is 2.78 eV higher than the LOIP (the value that the ionization potential would have if the t_{2g} electrons were strictly nonbonding, i.e., 5.72 eV). Thus for the first time we have an experimental value for the stabilization of the t_{2g} orbitals in $Mo(CO)_6$ caused by back-bonding to the carbonyl groups.

As another example, consider the dimolybdenum tetracarboxylates $Mo_2(O_2CH)_4$, $Mo_2(O_2CCH_3)_4$, and $Mo_2(mhp)_4$, and the Mo 4d ionization potentials for these molecules corresponding to the Mo-Mo δ-bonding orbitals. The stabilization energies, as measured by the IP – LOIP values, are all around 1 eV, indicating that the δ contributions to these Mo-Mo quadruple bonds are quite substantial.

3. An X-Ray Photoelectron Spectroscopic Study of Uranium Compounds (Publication 3)

D.B. Beach, K.D. Bomben, N.M. Edelstein, D.C. Eisenberg, W.L. Jolly, R. Shinomoto, and A. Streitwieser, Jr.

The gas-phase x-ray photoelectron spectra of UF_6, $U(BH_4)_4$, $U(BH_3CH_3)_4$, and $U(C_8H_8)_2$ have been obtained. The core binding energy data show that the bonding in UF_6 is extraordinarily ionic and that the bonding in the other compounds, especially $U(C_8H_8)_2$, is considerably more covalent. The binding energies and shake-up spectra show that the covalencies of $U(BH_4)_4$ and $U(BH_3CH_3)_4$ are com-

*This work was supported by the Director, Office of Energy Research, Office of Basic Energy Sciences, Chemical Sciences Division of the U.S. Department of Energy under Contract No. DE-AC03-76SF00098.

parable to that of UBr_4, with $U(BH_3CH_3)_4$ being more covalent than $U(BH_4)_4$. By consideration of both core binding energies and literature valence ionization potentials, it is shown that the HOMO of UF_6 is the t_{1g} fluorine lone-pair orbital. A similar analysis of data for $U(BH_4)_4$, $U(BH_3CH_3)_4$, and $U(C_8H_8)_2$ is consistent with spectral features that suggest the uranium 5f electrons in these compounds are essentially nonbonding.

1986 PUBLICATIONS AND REPORTS

Refereed Journals

1. R.A. Andersen, D.B. Beach, and W.L Jolly, "Pi-Donor Character of the Dimethylamido Ligand," Inorg. Chem. **24**, 4741 (1985); LBL-20028.
2. D.B. Beach and W.L. Jolly, "Absolute Stabilization Energies for Molybdenum 4d Electrons Based on the Reference Compound Tetrakis(dimethylamido)molybdenum(IV)," Inorg. Chem. **25**, 875 (1986); LBL-19765.
3. D.B. Beach, K.D. Bomben, N.M. Edelstein, D.C. Eisenberg, W.L. Jolly, R. Shinomoto, and A. Streitwieser, Jr., "An X-Ray Photoelectron Spectroscopic Study of Some Uranium Compounds," Inorg. Chem. **25**, 1735 (1986); LBL-20164.

LBL Reports

4. D.H. Horne and W.L. Jolly, "Reference to Ultraviolet Photoelectron Spectra of Gaseous Molecules," LBL-22578.

High-Energy Oxidizers and Delocalized-Electron Solids*

Neil Bartlett, Investigator

INTRODUCTION

The main aim of this program is the synthesis and characterization of new materials that may have value in electrochemical applications or in the efficient conversion of light to electrical energy. The synthetic work tests models and theories that correlate physical properties (such as electrical conductivity) with chemical composition and structure. Major aims in the synthetic strategies are (1) to tailor make the band gap in semiconductor materials and (2) to achieve high carrier concentration and mobility in the conductive materials. The present emphasis is on two-dimensional networks, such as those related to graphite. Electron oxidation of such materials (with accompanying intercalation to form salts) generates durable and conductive materials (some conducting better than aluminum). The layered materials can often be oxidized (and intercalated) electrochemically in reversible processes, and some (e.g., $C_xF_{1-\delta}\cdot\delta HF$) may find use in high-energy electrodes. Physical and chemical studies are being applied to such materials to determine the structure and bonding changes that accompany oxidation and reduction. Salts that are either proton conductors or fluoride-ion conductors, and that are resistant to oxidation but are not metallic, are being sought as solid electrolytes for use with the metallic layer-material salts.

1. Novel Metallic and Semiconductive Graphites (Publication 8)

N. Bartlett, J. Kouvetakis, R.B. Kaner, and K.M. Krishnan[†]

The range of novel graphite-like materials has been extended and those prepared earlier have been more fully characterized.

Chlorination of pyridine at 800°C yields a highly conducting deposit of metallic luster, chemical analysis of which indicates a composition $\sim C_5N$: $C_5H_5N + 5/2\ Cl_2 \rightarrow C_5N + 5HCl$. Heat treatment to 1200°C leads to gross loss of nitrogen [perhaps as $(CN)_2$ and N_2], but the resulting solid of composition $\sim C_{50}N$ gives graphite-like electron and x-ray diffraction patterns that indicate a somewhat larger interlayer spacing ($\sim$3.42 Å) than in graphite itself (3.35 Å). More crystalline samples of the previously reported metallic graphite, approximating BC_3 in composition, have been made by introducing low partial pressures of the benzene/boron trichloride mixture to an inductively heated reaction zone where their deposition is localized.

In accord with the anticipated semiconductive behavior of approximately 1:1:1 B/C/N graphite, the logarithm of its conductivity has been shown to depend linearly on the reciprocal of the Kelvin temperature. The indicated thermal band gap is $\sim$0.2 eV. Electron-energy-loss spectra (EELS), both in the plasmon and the K-edge regions (illustrated for the B/C graphite in Figure 1-1) for each of the novel graphite-structure materials, indicate that the boron, nitrogen, and carbon atoms are each in sp^2 hybridization. Energy-loss peak values and assignments are given in Table 1-1. Spectra also provide for the elemental analysis of the new B/C, C/N, and B/C/N materials. Moreover, Auger spectroscopy, with accompanying argon erosion, has demonstrated that the only elements present in the B/C material are B and C and that the samples have the same composition throughout.

*This work was supported by the Director, Office of Energy Research, Office of Basic Energy Sciences, Chemical Sciences Division of the U.S. Department of Energy under Contract No. DE-AC03-76SF00098.

[†]Present address: National Center for Electron Microscopy, Lawrence Berkeley Laboratory, Berkeley, CA 94720.

2. Graphite Fluorides Made by the Electrochemical Fluorination of Graphite in Aqueous Hydrogen Fluoride (Publication 6)

M. Lerner and N. Bartlett

Recent work in these laboratories on the electrochemical synthesis of graphite fluorides in anhydrous HF has raised the possibility that highly charged fluoro-intercalation compounds might also be preparable in aqueous systems. Previous work by others[1] had indicated that the electrochemical intercalation of graphite in aqueous HF is a quasireversible process and that oxidation as far C_{48}^+ was possible. Investigations in these laboratories have now shown that graphite charging to $C_{<12}^+$ can in fact be attained, and that a material of charge $C_{\sim 14}^+$ is stable in the aqueous electrolyte.

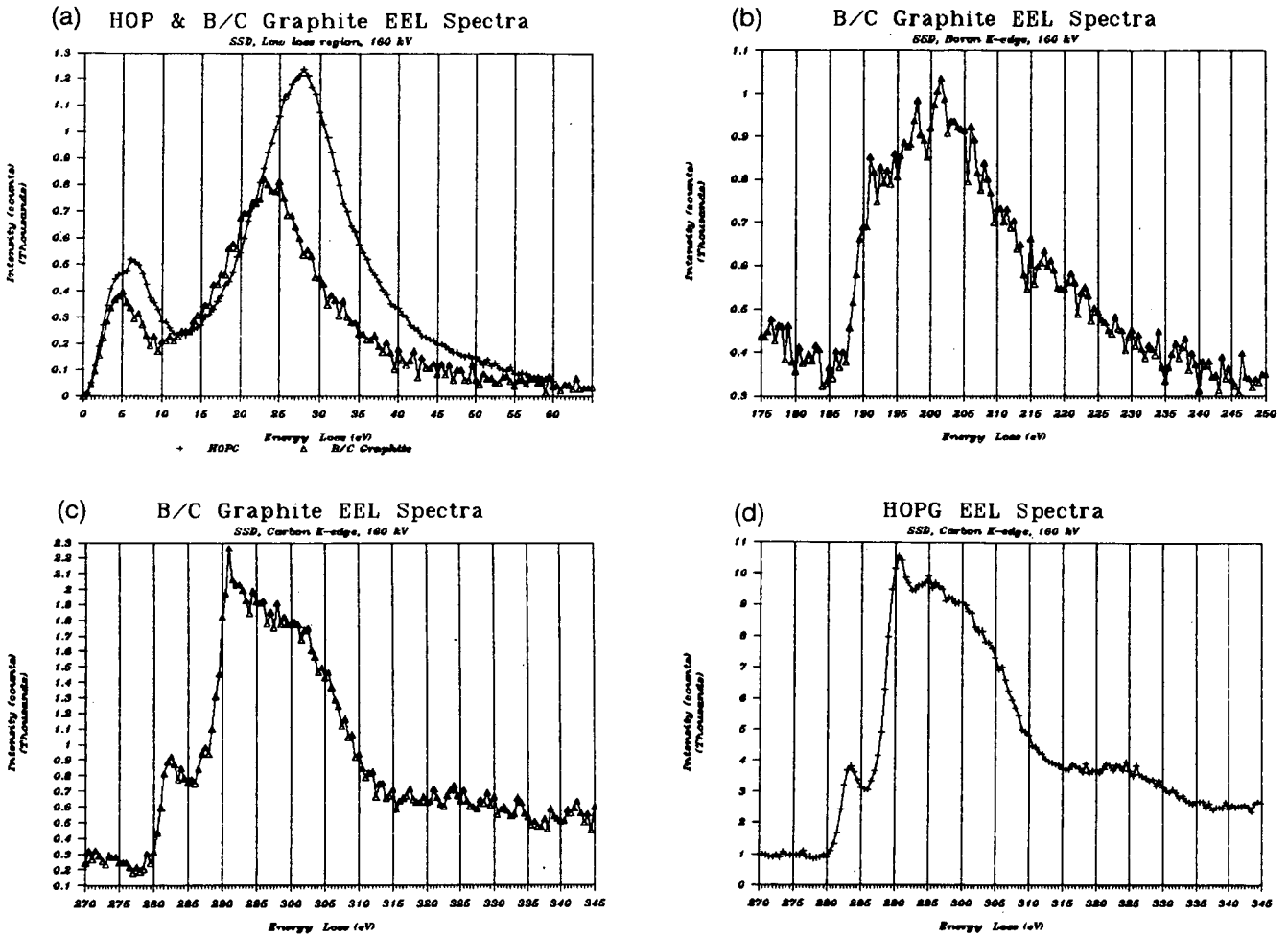

Figure 1-1. Electron-energy-loss spectra (EELS) for B/C graphite and graphite. (a) Plasmon EELS peaks for graphite (HOPG) and B/C graphite are compared. (XBL 874-1642) (b) Boron K-edge in the EELS spectrum of B/C graphite. (XBL 874-1643) (c) Carbon K-edge in the EELS spectrum of B/C graphite. (XBL 874-1644) (d) Carbon K-edge in the EELS spectrum of highly oriented pyrolytic graphite (HOPG). (XBL 874-1645)

Table 1-1
Electron-energy-loss data[a] for BC_3, graphite, $B_xC_yN_x$, and boron nitride.

			π^* edges (K-edge regions)		
Compound	$\pi\ \pi$ plasmon (eV)	$\pi + \sigma$ plasmon (eV)	Boron (eV)	Carbon (eV)	Nitrogen (eV)
BC_3	6.4	24.8	185.2	283.1	–
Graphite	6.9	27.1	–	284	–
$B_xC_yN_x$	7.5	24.5	188.5	282.2	397.0
BN	8.0	27.1	190	–	400

a. Obtained at 160 KeV at a reduction of $\leq$ 0.2 eV.

Galvanostatic charge curves for the aqueous system resemble those in anhydrous HF at low levels of charging, but the charge curves and materials produced are significantly different at higher charge levels (see Figure 2-1). At the oxidation limit, a first-stage or mixed first-second stage material of charge $C_{<12}^{+}$ is produced in the aqueous system. This coulometry is indicated by discharge in anhydrous HF. The $C_{<12}^{+}$ material is unstable in the aqueous electrolyte and is reduced chemically back to $C_{\sim 14}^{+}$. Stable materials of charge $C_{\sim 68}^{+}$, $C_{\sim 48}^{+}$, $C_{\sim 27}^{+}$, and $C_{\sim 24}^{+}$ have been prepared and characterized by x-ray diffraction, gravimetry, elemental analysis, and their electrochemical potentials. Discharge curves for these materials show that electrochemical oxidation as far as $C_{\sim 14}^{+}$ can be reversed electrochemically. The $C_{\sim 14}^{+}$ material produced in the aqueous electrolyte has a c-axis repeat of 9.5 Å *in situ* and 9.1 Å after several hours of dynamic evacuation. The material is air stable and gives a four-probe conductivity of 30 $\Omega^{-1}cm^{-1}$ at 25°C, indicating that semi-ionic fluorine is present within the galleries. Elemental analysis for oxygen by reaction with PF_5 (to produce POF_3) demonstrates that little oxygen is present in the material after evacuation. Gravimetry yields a composition near $C_{14}F(HF)_{0.7}$. These data suggest that $C_{\sim 14}^{+}$ is a second-stage analogue of the known first-stage graphite fluoride $C_xF{\cdot}\delta HF$ and is a novel material, stabilizing an unusually high charge level in a second-stage compound. Electrochemical reduction (de-intercalation) of this second-stage material has been shown to be more facile than that in the chemically or electrochemically produced first stage.

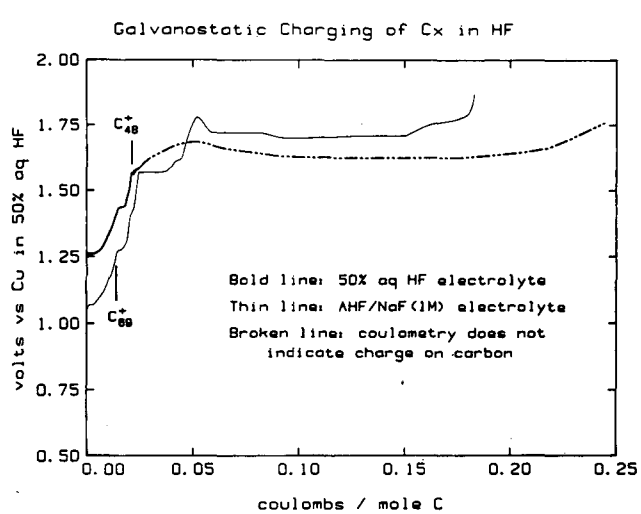

Figure 2-1. Galvanostatic charge curves for a graphite anode in 50% aqueous HF (bold line) and anhydrous HF/1M NaF (thin line). (The charge density for each was 100 $\mu A/cm^2$. Coulometry is not accurate in the aqueous system above +1.6 V because of oxidation of the electrolyte.) (XBL 874-1646)

1. F. Beck and H. Krohn, Syn. Met. 7, 193 (1983).

3. Boron Nitride Salts: Preparation, Electrical Conductivity, and Stability (Publication 7)

S. Mayorga, R. Biagioni, and N. Bartlett

The most fully characterized boron nitride salt is boron nitride fluorosulfate, $(BN)_3SO_3F$. It is prepared by exposing powdered BN to either gaseous or liquid $S_2O_6F_2$. The reaction proceeds very rapidly at room temperature, with complete intercalation occurring in less than one hour. The salt is invariably first stage. Attempts to synthesize higher-stage salts by either limited exposure of BN to $S_2O_6F_2$ or by subjecting the first-stage salt to vacuum have been unsuccessful, yielding a mixture of first-stage $(BN)_3SO_3F$ and boron nitride. The established composition of the pure first-stage material, $(BN)_3SO_3F$, is that which is anticipated for a two-dimensional closed-packed arrangement of tetrahedral fluorosulfate ions between enclosing boron nitride layers. The *c*-axis repeat distance of $(BN)_3SO_3F$ is 8.06(2) Å, which indicates an unnestled arrangement of the guests between the BN layers. This differs (see Figure 3-1) from the situation that prevails in the analogous graphite salt, $C_{\sim 7}SO_3F$, where the intercarbon layer spacing is ~7.6 Å, this latter separation being consistent with a nestled arrangement of the anions in the host. The room-temperature specific conduc-

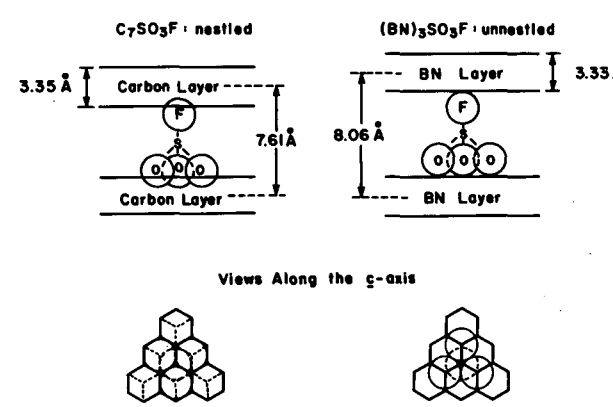

Figure 3-1. Proposed guest arrangement for graphite fluorosulfate (nestled) and boron nitride fluorosulfate (unnestled). (XBL 874-1647)

tivity of the $(BN)_3SO_3F$ is 1–2 $ohm^{-1}cm^{-1}$ (four probe) when freshly prepared. The conductivity shows a slight temperature dependence, increasing by 20% as the temperature is dropped to 77 K. The salt is not thermally or vacuum stable and loses $S_2O_5F_2$, probably in concert with NO^+ salt formation. Some decomposition to $NO^+SO_3F^-$, BN, and possibly B_2O_3 probably accounts for the conductivity being lower than that expected for a true metal in the freshly prepared sample.

A boron nitride, arsenic hexafluoride salt, $(BN)_yAsF_6$, has been prepared by displacement of the fluorosulfate anions of $(BN)_3SO_3F$. This blue salt is prepared by repeated treatment of $(BN)_3SO_3F$ with a 2:1 gaseous mixture of AsF_5/F_2. The bulk of the fluorosulfate is displaced by three such cycles, but complete displacement is not readily achieved. X-ray powder diffraction indicates a *c*-spacing of 8.19(2) Å and also reveals the presence of the salt $NO^+AsF_6^-$. The room-temperature conductivity of this impure material is 0.06–0.08 $ohm^{-1}cm^{-1}$ (four probe) and is invariant with temperature. A boron nitride salt has also been prepared by the direct reaction of SbF_5 and F_2 with BN. The blue first-stage material has a *c*-spacing of 7.9 Å, but the polymeric nature of SbF_5 and its anions, together with the difficulty of accurate assessment of the F_2 uptake, leaves formulation of the salt very uncertain.

4. Work in Progress

Synthetic strategies are being followed that promise to give more ordered and more precisely defined stoichiometries in the B|C|N graphite system, where semiconductive behavior is anticipated. Interaction of BCl_3 with CH_3CN has already given promising BC_2N material that appears to be graphitic. The material is not as crystalline as that generated in the $C_2H_2|NH_3|BCl_3$ interaction, however.

1986 PUBLICATIONS AND REPORTS

Refereed Journals

1. T.J. Richardson, F.L. Tanzella, and N. Bartlett, "The Preparation and Characterization of Radical Cation Salts Derived from Perfluorobenzene, Perfluorotoluene, and Perfluoronaphthalene," J. Am. Chem. Soc. **108**, 4937 (1986); LBL-21810.
2. S.M. Yeh and N. Bartlett, "On the Preparation and Stabilization of ReF_6^+ Salts: Evidence for Mixed Ion-Molecule Salts of Formula $ReF_6^+ReF_7MF_6^-MF_5$ (M = Sb, Au)," Revue de Chim. Minerale, **23**, 676 (1986); LBL-21750.
3. J. Kouvetakis, R.B. Kaner, M.L. Sattler, and N. Bartlett, "A Novel Graphite-Like Material of Composition BC_3 and Nitrogen-Carbon Graphites," J. Chem. Soc., Chem. Comm., 1758 (1986); LBL-20854.

LBL Reports

4. R.B. Kaner, J. Kouvetakis, C.E. Warble, M.L. Sattler, and N. Bartlett, "Boron-Carbon-Nitrogen Materials of Graphite-Like Structure," Mat. Res. Bull. (in press); LBL-20855.
5. T.J. Richardson, F. Tanzella, and N. Bartlett, "Comparison of Perfluoro- and Perhydro-Polynuclear Aromatic Hydrocarbon Cation Salts," submitted to Adv. in Chem. Series, ACS; LBL-22089.
6. M. Lerner and N. Bartlett, "Graphite Fluorides made by the Electrochemical Fluorination of Graphite in Aqueous Hydrogen Fluoride," submitted to J. Chem. Soc., Chem. Comm.; LBL-22541.
7. S. Mayorga, R. Biagioni, and N. Bartlett, "The Preparation and Characterization of Boron Nitride Salts Containing SO_3F^- and AsF_6 and Their Comparison with Graphite Relatives," submitted to Inorg. Chem.; LBL-22542.
8. N. Bartlett, J. Kouvetakis, R. Kaner, and K.M. Krishnan, "Novel Metallic and Semiconductive Graphites," submitted to Science; LBL-22543.

Invited Talks

9. N. Bartlett, "From Metal to Insulator in the Graphite Fluoride C_xF ($2 < x < 5.5$): A Novel C-F Bond and its Impact on Graphite Structure and Properties," Physics Department, U.C. Berkeley, March 19, 1986.
10. N. Bartlett, "Graphite and Boron Nitride Intercalation and The Interplay of Structural, Physical, and Chemical Studies," Tutorial Session, ACS Symposium on "Synthesis and Reactivity of Layered Compounds," New York, NY, April 13, 1986.
11. N. Bartlett, "A Thermodynamic Barrier for Intercalation of Graphite by Electro-Oxidizing Fluorospecies," ACS Symposium on Synthesis and Reactivity of Layered Compounds, New York, NY, April 14, 1986.
12. N. Bartlett, "A Novel C-F Bond and the Reversible Electrochemical Fluorination of Graphite in Hydrogen Fluoride," ACS Symposium on Synthesis and Reactivity of Layered Compounds, New York, NY, April 14, 1986.
13. N. Bartlett, "Discovery of O_2 Salts and the Chemistry of Xenon: Aspects of the Remarkable Oxidizing Properties of Some Fluorine Compounds," ACS Symposium on Fluorine Chemistry: One Hundred Years and Beyond, New York, NY, April 15, 1986.

14. N. Bartlett, "Noble-Gas Chemistry — Its Discovery and Significance," West Texas State University, Canyon, TX, April 16, 1986.
15. N. Bartlett, "Graphite Fluorides and New Graphites," ACS Presidential Young Investigator Workshop, San Diego, CA, May 3, 1986.
16. N. Bartlett, "Professor Nobuatsu Watanabe and International Fluorine Chemistry," Kyoto University, Japan, May 24, 1986.
17. N. Bartlett, "The Reversible Electrochemical Fluorination of Graphite and The Properties of The Graphite Fluorides," Nobuatsu Watanabe Retirement Symposium, Kyoto, Japan, May 26, 1986.
18. N. Bartlett, "Salts of Graphite and Boron Nitride and Related Materials," International Conference on Science and Technology of Synthetic Metals, Kyoto, Japan, June 3, 1986.
19. N. Bartlett, "Fluorine: Oxidizer Par Excellence," Centenary of The Discovery of Fluorine, International Symposium, Paris, France, Aug. 26, 1986.

Transition Metal–Catalyzed Conversion of CO, NO, H_2, and Organic Molecules to Fuels and Petrochemicals*

Robert G. Bergman, Investigator

INTRODUCTION

The goal of this program is the development of new chemical reactions in which transition metals interact with organic materials, and the understanding of how these reactions work. A recent discovery on this project was the finding that certain hydridoiridium and -rhodium complexes undergo oxidative addition into the carbon-hydrogen bonds of completely saturated hydrocarbons (M + R-H → R-M-H). Since this finding was the first example of this long-sought "alkane C-H activation" reaction, research is now being directed at examining the scope, selectivity, and mechanism of the process. During the current year, the chemistry of the first rhenium-based alkane activation system was fully explored, and the first dinuclear reversible C-H oxidative addition/reductive elimination system was developed. In related investigations, nuclear magnetic resonance (NMR) studies of iridium-based systems led to the first direct observation of resolved coupling between the proton (^1H) and lithium (^7Li) nuclei, and theoretical studies carried out in collaboration with Hoffman's group at Cornell University provided insight into the mechanism of alkene C-H activation reactions.

1. NMR Spectra of $[C_5(CH_3)_5]IrH_2SiMe_3Li$(PMDETA) and $[C_5(CH_3)_5]IrH_3Li$(PMDETA): The First Direct Observation of Resolved ^7Li-^1H Coupling (Publication 1)

T.M. Gilbert and R.G. Bergman

Observation of scalar spin-spin coupling between ^7Li and ^{13}C in NMR spectra has been critical in determining degrees of oligomerization for organolithium species in solution. It would be equally useful to obtain ^7Li-^1H coupling data. Surprisingly, however, before the present work was carried out coupling between ^7Li and ^1H nuclei had not been resolved in simple alkyl- and aryllithium complexes. This coupling has now been seen and measured quantitatively. The complexes utilized for this study are the reactive lithium species formed by removal of an iridium-bound proton from pentamethylcyclopentadienyl(hydrido)iridium derivatives. In one example, treatment of $(\eta^5\text{-}C_5Me_5)IrH_3SiMe_3$ with tBuLi in n-hexane at −40°C in the presence of pentamethyldiethylenetriamine (PMDETA) gives the salt $(\eta^5\text{-}C_5Me_5)IrH_2SiMe_3Li$(MDETA). The NMR resonance due to the chemically equivalent metal-bound hydride ligands at −20.15 ppm appears as a 1:1:1:1 quartet due to ^7Li-^1H coupling, with the coupling constant J = 8.4 Hz (Figure 1-1). This coupling was confirmed by ^7Li NMR spectroscopy, as well as by decoupling experiments in both the ^1H and ^7Li NMR spectra. It was also found that the observation of coupling is quite temperature dependent, the coupled spectra collapsing to broad lines at both higher (60°C) and lower (−40°C) temperatures. This tem-

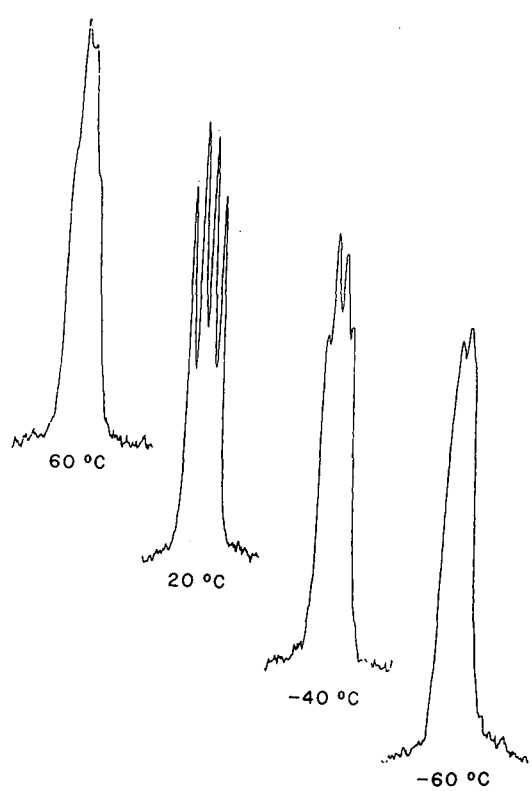

Figure 1-1. Experimental ^1H NMR spectra (300 MHz) of the hydride resonance of $(\eta^5\text{-}C_5Me_5)IrH_2SiMe_3Li$(PMDETA) at various temperatures. (XBL 873-1490)

*This work was carried out under the auspices of a collaborative Lawrence Berkeley Laboratory/industrial research project supported jointly by the Chevron Research Company, Richmond, CA, and the Director, Office of Energy Research, Office of Basic Energy Sciences, Chemical Sciences Division of the U.S. Department of Energy under Contract No. DE-AC03-76SF00098.

perature dependence may be part of the reason that ^7Li-^1H coupling had not been observed previously.

2. Inter- and Intramolecular Insertion of Rhenium into Carbon-Hydrogen Bonds (Publication 3)

T.T. Wenzel and R.G. Bergman

The C-H activation chemistry of the cyclopentadienylrhenium system, reported in preliminary form last year, has now been worked out in full detail. $CpRe(PMe_3)_3$, (**1**) in Figure 2-1, was synthesized in 38% yield by Na/Hg reduction of $ReCl_3(PMe_3)_3$ with cyclopentadiene. Irradiation of **1** in a wide range of organic solvents that contain C-H bonds, including benzene, cyclopropane, n-hexane, and cyclopentane, gave rise to C-H oxidative addition products **2** (Figure 2-1). Most of these complexes were isolable (in some cases by chromatography at −90°C); the material formed from n-hexane was identifiable only by NMR spectrometry. In contrast to results

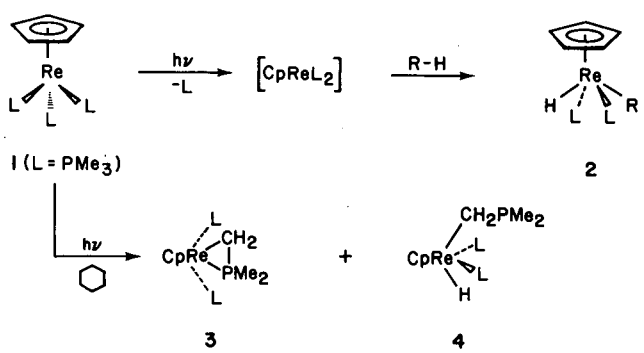

Figure 2-1. C-H insertion reactions in the cyclopentadienylrhenium system. (XBL 874-1491)

obtained earlier in the iridium and rhodium systems, stable C-H insertion products were not observed in cyclohexane solvent. Thus, for the first time, a common solvent inert to C-H activation was available, and it was used to carry out the thermal C-H activation of methane, leading to a 43% isolated yield of the hydrido(methyl) complex **2** (R = CH_3). In the absence of methane, irradiation of **1** in cyclohexane afforded cyclometalated product **3** and the unusual intermolecular PMe_3 C-H insertion product **4**. Complex **4** undergoes dimerization to a complex whose structure was determined by x-ray diffraction (Figure 2-2). Irradiation of **1** with ethylene in cyclohexane gave the ethylene C-H insertion product **2** (R = $CH{=}CH_2$), which isomerized quantitatively to the corresponding π-complex $Cp(CO)_2Re(H_2C{=}CH_2)$ at 20°C in benzene. Thus, as in the iridium system, the π-complex cannot be an intermediate in vinyl C-H activation; independent pathways leading to the π-complex and the C-H insertion product must exist.

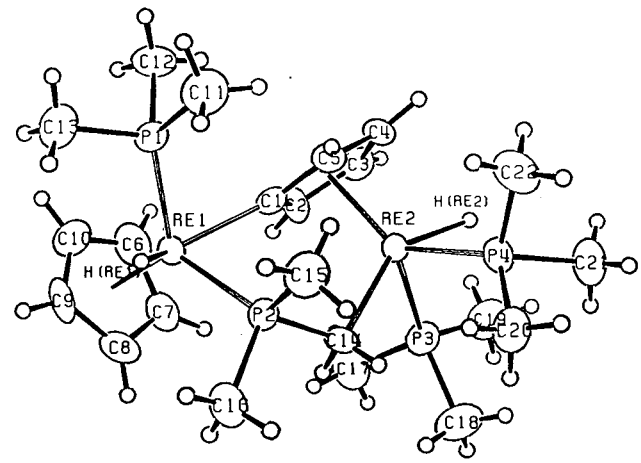

Figure 2-2. ORTEP drawing of the structure of the rhenium dimer formed from PMe_3 C-H activation product **4** in Figure 2-1. (XBL 874-1492)

3. Mild, Reversible C-H Oxidative Addition/ Reductive Elimination in a Dinuclear Iridium Complex (Publication 5)

W.D. McGhee and R.G. Bergman

Heating Cp*(η^3-allyl)(hydrido)iridium [Cp* = (η^5-C_5Me_5)] in benzene gives the new dinuclear benzene C-H activation product **1** (Figure 3-1). The structure of this material was determined by x-ray diffraction. Upon heating with dative ligands in benzene at 45°C, **1** undergoes reductive elimination of benzene and incorporation of PMe_3, CO, C_2H_4, and $P(OMe)_3$ to give substituted dinuclear complexes **2a** – **2d**. The starting dinuclear complex also reacts with benzene-d_6, acetonitrile, and H_2, leading to C-H and H-H insertion products **1**-d_6, **4**, and **5**. Crossover isotope labeling studies using mixtures of **1** and **1**-d_{10} demonstrate that the reductive elimination reaction is intramolecular. Rate studies show that the reaction exhibits good first-order kinetics. The measured rate constants are nearly identical using

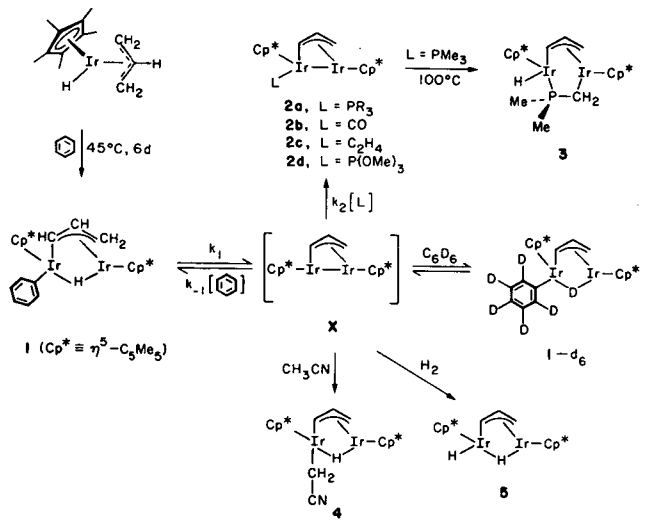

Figure 3-1. Chemistry observed in the (η^5-C_5Me_5)(π-allyl)(hydrido)iridium dinuclear C-H activation system. (XBL 874-1493)

PMe_3, $P(OMe)_3$, or benzene-d_6 as the entering group, and they do not depend on the concentration of attacking ligand. These results are consistent with a mechanism involving rate-determining elimination of benzene from **1** to give a reactive intermediate (presumably **X** in Figure 3-1), followed by trapping of this material in a rapid subsequent step. Complex **1** undergoes these reactions at temperatures at least 150°C lower than those required to induce the analogous elimination of benzene from the mononuclear complex (η^5-C_5Me_5)(PMe_3)Ir(Ph)(H), suggesting that replacing a PMe_3 ligand with a second metal produces a profound effect on the energetics of the reductive-elimination process.

4. Some Problems in the Oxidative Addition and Binding of Ethylene to a Transition Metal Center (Publication 6)

J. Silvestre, M.J. Calhorda, R. Hoffmann,[†]
P.O. Stoutland, and R.G. Bergman

The C-H activating intermediate Cp*(L)Ir (Cp* = η^5-C_5Me_5; L = PMe_3) reacts with alkenes, such as ethylene, in an unusual way: it gives both the η^2-olefin complex Cp*(L)Ir($H_2C{=}CH_2$) (**1**, formed by direct coordination of the iridium center to the ethylene π-bond) and the vinyl hydride complex Cp*(L)Ir(H)($HC{=}CH_2$) (**2**), formed by insertion of the metal into the vinyl C-H bond. Earlier studies demonstrated that the η^2-olefin complex **1** is not an intermediate in the formation of **2**, and so there must be a direct pathway that leads smoothly from Cp*(L)Ir plus ethylene to **2**. Furthermore, **2** is converted to **1** at higher temperatures, via a transition state different from either of those involved in the Cp*(L)Ir/C_2H_4 reaction.

In order to investigate the nature of this pathway, semiempirical molecular-orbital calculations have been carried out on the potential-energy surface of the system CpIrL(C_2H_4) (L = phosphine). The geometrical and electronic characteristics of the η^2-olefin and vinyl hydride complexes are examined in some detail. The olefin complex **1** is found to have a slightly lower energy than the vinyl hydride **2**, in agreement with experiment. Different routes are studied which lead to **2** from the 16-electron fragment and an ethylene. It is found that an M...H-C linear approach is favored, coupled with a very specific orientation of the ethylenic π system; this results from both electronic and steric requirements. "Snapshots" of several computed configurations along the reaction path are shown in Figure 4-1. A

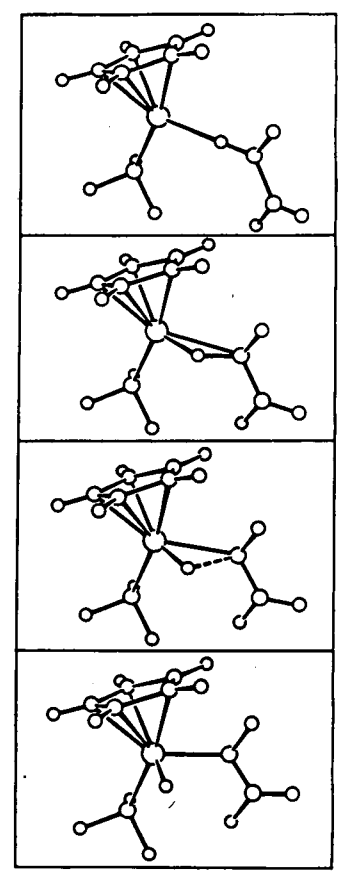

Figure 4-1. "Snapshots" calculated for points along the Cp*(L)Ir + ethylene reaction coordinate leading from the initial C-H interaction complex (top) to the vinyl hydride product **2** discussed in the text. (XBL 874-1494)

relatively small barrier is computed for the process, and the experimentally observed competition between vinyl hydride formation and direct ethylene addition is discussed. Calculations have been performed to ascertain the existence of a separate transition state taking the η^2-bound olefin into the vinyl hydride. The computations suggest the existence of two distinct transition states. The influence of substituents and steric effects is analyzed. It is shown how an increase in the size of the ligand affects the shape of the surface and more specifically narrows the energy channels governing conformational changes as well as product formation.

---

†Permanent address: Department of Chemistry, Cornell University, Ithaca, NY.

5. Work in Progress

Projects currently under way are aimed at: (a) understanding the mechanism of the rhodium-based C-H insertion system and relating it to the analogous iridium reaction; (b) devising methods for converting the C-H insertion products R-M-H into functionalized organic molecules R-X; (c) expanding the development of dinuclear C-H activation systems, to determine how the C-H insertion propensity of a metal will be influenced by the proximity of a second metal center; (d) carrying out calorimetric studies of hydrido(alkyl)iridium complexes, to learn more about the thermodynamic driving force for the C-H insertion process; (e) generating the reactive intermediates responsible for C-H insertion [e.g., (η^5-C_5Me_5)Ir(PMe_3) and (η^5-C_5Me_5)Re(PMe_3)] under conditions where they may be studied spectroscopically and the rates of the insertion reactions measured directly.

1986 PUBLICATIONS AND REPORTS

Refereed Journals

1. T.M. Gilbert and R.G. Bergman, "NMR Spectra of $[C_5(CH_3)_5]IrH_2SiMe_3Li(PMDETA)$ and $[C_5(CH_3)_5]IrH_3Li(PMDETA)$: The First Direct Observation of Resolved ^7Li-^1H Coupling," J. Am. Chem. Soc. **107**, 6391 (1985); LBL-19662.
2. J.M. Buchanan, J.M. Stryker, and R.G. Bergman, "A Structural, Kinetic and Thermodynamic Study of the Reversible Thermal C-H Activation/Reductive Elimination of Alkanes at Iridium," J. Am. Chem. Soc. **108**, 1537 (1986); LBL-19931.
3. R.G. Bergman and T.T. Wenzel, "Inter- and Intramolecular Insertion of Rhenium into Carbon-Hydrogen Bonds," J. Am. Chem. Soc. **108**, 4856 (1986); LBL-20966.
4. M.J. Krause and R.G. Bergman, "Synthesis of Dinuclear Anionic Complexes $[Cp^*Rh(CO)]_2^-$ and $[Cp^*Rh(CO)]_2^{2-}$ by Dissolving Metal Reduction and $R[Cp^*Rh(CO)]_2^-$ by Addition of Alkyllithium Reagents Across the Metal-metal Double Bond of $[Cp^*Rh(CO)]_2$. Stereoselective Synthesis of Symmetrical and Mixed Dinuclear Dialkyls $[Cp^*_2Rh_2(CO)_2(R_1)(R_2)]$, and a Study of their Ligand-induced Fragmentation Reactions," Organometallics **5**, 2097 (1986).†
5. W.D. McGhee and R.G. Bergman, "Mild, Reversible C-H Oxidative Addition/Reductive Elimination in a Dinuclear Iridium Complex," J. Am. Chem. Soc. **108**, 5621 (1986); LBL-21569.
6. J. Silvestre, M.J. Calhorda, R. Hoffmann, P.O. Stoutland, and R.G. Bergman, "Some Problems in the Oxidative Addition and Binding of an Ethylene to a Transition Metal Center," Organometallics **5**, 1841 (1986); LBL-22495.

LBL Reports

7. R.A. Periana (Ph.D. Thesis), "Mechanism of Oxidative Addition of Cyclopentadienyl-Rhodium Complexes to Carbon-Hydrogen and Carbon-Carbon Bonds," LBL-22533.
8. J.M. Buchanan (Ph.D. Thesis), "A Kinetic and Thermodynamic Study of the Reversible C-H Insertion/Elimination of Alkanes at Iridium," LBL-22534.
9. T.M. Gilbert (Ph.D. Thesis), "Synthesis and Characterization of (Pentamethylcyclopentadienyl)iridium Polyhydride and Polyphosphine Complexes," LBL-22535.
10. R.M. Gilbert and R.G. Bergman, "Tetrahydrido(η^5-Pentamethylcyclopentadienyl)Iridium," LBL-20967.
11. R.A. Periana and R.G. Bergman, "Isomerization of the Hydrido(alkyl)rhodium Complexes Formed on Oxidative Addition of Rhodium to Alkane C-H Bonds. Evidence for the Intermediacy of η^2-Alkane Complexes," LBL-21317.
12. R.A. Periana and R.G. Bergman, "C-C Activation of Organic Small Ring Compounds by Rearrangement of Cycloalkyl(hydrido)rhodium Complexes to Rhodacycloalkanes. Synthesis of Metallacyclobutanes, Including One with a Tertiary-M-C Bond, by Nucleophilic Addition to π-Allyl Complexes," LBL-21316.

Invited Talks

13. R.G. Bergman, "Formation and Cleavage of Bonds in Organic Compounds Mediated by Organotransition Metal Complexes," Department of Chemistry, UC Irvine, Jan. 16, 1986.
14. R.B. Bergman, "Formation and Cleavage of Bonds in Organic Compounds Mediated by Organotransition Metal Complexes," Department of Chemistry,

University of South Carolina, Columbia, SC, Feb. 14, 1986.

15. R.G. Bergman, "Evidence for σ-Complexes in C-H Activation Reactions," Department of Chemistry, Harvard University, Cambridge, MA, Feb. 18, 1986.
16. R.G. Bergman, "Carbon-Carbon Bond Forming Reactions of Organotransition Metal Enolates," Hoffman-La Roche Inc., Nutley, NJ, April 11, 1986.
17. R.G. Bergman, "Formation and Cleavage of Bonds in Organic Compounds Mediated by Organotransition Metal Complexes," ACS Award Address in Organometallic Chemistry, New York, NY, April 15, 1986.
18. R.B. Bergman, "Evidence for σ-Complexes in C-H Activation Reactions," Rohm & Haas Co., Philadelphia, PA, April 17, 1986.
19. R.G. Bergman, "Formation of Carbon-Carbon Bonds Using Transition Metal Enolates," Monsanto Co., St. Louis, MO, May 14, 1986.
20. R.G. Bergman, "Synthesis and Interconversion of Heterodinuclear Oxaalkyl and Bridging Oxo Complexes," 1986 NSF Organometallic Chemistry Workshop, Austin, TX, June 13, 1986.
21. R.G. Bergman, "Formation of Carbon-Carbon Bonds Using Organotransition Metal Enolate Complexes," Fifth International Symposium on Homogeneous Catalysis, Kobe, Japan, Sept. 22, 1986.
22. R.G. Bergman, "Finding and Understanding New Organometallic Reactions," NIH Workshop on Biomimetic and Organometallic Catalysis, Rockville, MD, Oct. 9, 1986.
23. R.G. Bergman, "Metal Enolates," Department of Chemistry, Tulane University, New Orleans, LA, Nov. 19, 1986.
24. R.G. Bergman, "Transformation of Organic Compounds Induced by Organotransition Metal Complexes," Department of Chemistry, Iowa State University, Ames, Nov. 20, 1986.

---

†Supported by the National Science Foundation (Grant No. CHE-8420979).

CHEMICAL ENGINEERING SCIENCES

High-Pressure Phase Equilibria in Hydrocarbon-Water (Brine) Systems*

John M. Prausnitz, Investigator

INTRODUCTION

Phase equilibria are required for efficient design of large-scale separation processes (e.g., distillation and extraction) in the chemical and related industries. In this context, "efficient" refers to optimum use of raw materials and to conservation of energy.

Since the variety of technologically important fluid mixtures is extremely large, it is not possible to obtain all desired equilibria from experiment. Therefore, the objective of this research is the development of molecular thermodynamics for the interpretation and correlation of selected phase-equilibrium data toward reliable prediction of phase equilibria for computer-aided engineering design. The correlations are expressed through semitheoretical physicochemical models. In this research, particular attention is given to those systems that are of primary interest in energy-related industries, especially those concerned with fossil fuels, aqueous mixtures containing electrolytes, fossil-fuel/water mixtures, agricultural products, and mixtures encountered in biotechnology.

Development of molecular thermodynamics calls for a combination of theoretical, computational, and experimental work. Further, it demands simultaneous awareness, first, of progress in molecular science, and second, of realistic requirements for engineering design.

*This work was supported by the Director, Office of Energy Research, Office of Basic Energy Sciences, Chemical Sciences Division of the U.S. Department of Energy under Contract No. DE-AC03-76F00098.

1. Mutual Solubilities and Vapor Pressures for Binary and Ternary Aqueous Systems Containing Benzene, Toluene, m-Xylene, Thiophene, and Pyridine in the Region 100–200°C (Publication 14)

F.E. Anderson† and J.M. Prausnitz

An apparatus has been constructed for measuring mutual solubilities and vapor pressures for aqueous-organic liquid-liquid systems in the region ambient to 200°C. Both liquid phases are sampled and analyzed using gas chromatography. Special care must be taken to assure reliable sampling because mutual solubilities are very small; it is especially important to avoid entrainment, phase change (due to temperature gradients or pressure drop), and adsorption when removing samples for chemical analysis.

Experimental results are reported for the temperature range 100 to 200°C for binary aqueous mixtures containing benzene, toluene, m-xylene, and thiophene, and for ternary aqueous mixtures containing benzene and pyridine. The binary results are in good agreement with diverse data reported in the literature.

†Present address: Cabot Corporation, Billerica, MA.

2. Characterization of Heavy Fossil Fuels: Molecular-Weight Distributions and Liquid Heat Capacities (Publications 16 and 17)

P.A. Rodgers,† A.L. Creagh, M.M. Prange, and J.M. Prausnitz

A correlation is presented for calculating molecular-weight distributions for high-boiling hydrocarbon mixtures from measurements using gel-permeation chromatography (GPC). The correlation uses GPC elution volume, hydrogen-to-carbon ratio from elemental analysis, and hydrogen distribution from proton-NMR spectroscopy. Results for 45

pure hydrocarbons give an average deviation of less than 4%. For application to fractions, the procedure is illustrated with results for an Alaskan North Slope residue. Characterization data are reported for 13 heavy fossil-fuel fractions, including coal-liquefaction products and crude oils.

Heat capacities for liquid fossil-fuel fractions are correlated as a function of characterization data. The correlation uses molecular weight from freezing-point-depression or GPC measurements, hydrogen-to-carbon ratio from elemental analysis, hydrogen distribution from proton-NMR data, and, if available, number of methyl, hydroxyl, primary amine, and secondary amine groups per molecule from IR spectroscopy. The correlation is established for temperatures below 500 K using characterization data for 118 pure hydrocarbons; the average deviation from experiment is 2.3%. When the correlation is used to predict the heat capacities of nine petroleum fractions, the average deviation is 2.6%. Average deviations for 14 coal-derived liquids are about 6.5%, but the average deviation is somewhat lower for those liquids containing more than about 3 wt% oxygen. For high-oxygen-containing fractions, the correlation presented here is significantly better than existing methods.

---

†Present address: Department of Chemical Engineering, University of Texas, Austin.

3. Vapor Pressures, Liquid Densities, and Gas Solubilities for Heavy Fossil-Fuel Fractions (Publications 18 and 19)

B.J. Schwarz, J.A. Wilhelm,† and J.M. Prausnitz

Measurements are reported for vapor pressures and saturated liquid densities of characterized fossil-fuel fractions. Vapor pressures were measured for 12 fractions and densities for 30 fractions. The fractions originated from crude oils, coal liquid, and tar sands. Initial atmospheric boiling points of the fractions range from 492 to 700 K. Vapor pressures to 575 K were measured using an ebulliometer; between one and seven percent of the sample was vaporized during these measurements. Saturated liquid densities were measured between 292 and 578 K using sealed glass cells heated in an air bath. For most samples, the measured properties showed only small observable effects of cracking. Measurements are also reported for the solubilities of methane, ethane, and carbon dioxide in six of these characterized fractions. These fractions have initial boiling points between 589 and 700 K. Solubilities were measured in a semibatch equilibrium cell at pressures between 5.8 and 21 bar and temperatures from 374 to 575 K. An equation of state was used to determine Henry's constants from the solubility data. The vapor-pressure, density, and solubility data may be useful for testing correlations used in process-design calculations.

---

†Present address: Lurgi GmbH, Frankfurt, Federal Republic of Germany.

4. Correlation of Vapor-Liquid Equilibria for the System Ammonia–Carbon Dioxide–Water (Publication 20)

K. Kawazuishi† and J.M. Prausnitz

Aqueous waste streams from petroleum or petrochemical plants often contain volatile weak electrolytes such as ammonia, carbon dioxide, sulfur dioxide, hydrogen sulfide, and hydrogen cyanide. To prevent environmental pollution, these solutes must be removed, usually by distillation. For design of a separation operation, vapor-liquid equilibria are required. A correlation for calculating such equilibria is currently given in a computer program called TIDES.

This work reports updated values for some dissociation equilibrium constants and Henry's constants used by the program. Particular attention is given to the ternary system ammonia–carbon dioxide–water; equilibria for that system are calculated at 100 to 205°C and total liquid-phase concentrations to 10 molal. Calculated results show good agreement with recent experimental data.

---

†Present address: Chiyoda Chemical Engineering and Construction Co., Ltd., Yokohama, Japan.

5. Computational Aspects of a Noncubic Equation of State For Phase-Equilibrium Calculations. Effect of Density-Dependent Mixing Rules (Publication 21)

R.J. Topliss,† D. Dimitrelis, and J.M. Prausnitz

An efficient procedure is presented for solving a noncubic equation of state for density. In phase-equilibrium calculations, the costly computing step is not the density calculation but the calculation of the

equation-of-state constants for the mixture. Illustrative calculations are given for high-pressure phase equilibria for hydrogen/ethane and methane/water. These calculations show the superiority of noncubic equations with density-dependent mixing rules.

†Present address: Amoco Chemical Co., Naperville, IL.

6. Dielectric Constants of Fluid Mixtures over a Wide Range of Temperature and Density (Publication 22)

A.H. Harvey and J.M. Prausnitz

A new expression is derived for estimating the dielectric constant of a fluid mixture as a function of temperature, density, and composition. The estimated dielectric constants (and their derivatives) are required for phase-equilibrium calculations, based on an equation of state, for systems containing electrolytes and nonelectrolytes. The new expression holds for the entire range of fluid densities, from zero to liquid-like densities. Mixing of components is performed on a volume-fraction basis at constant temperature and constant reduced density. For polar components where data are not available at the temperature and/or reduced density of interest, the well-characterized behavior of water is used to extrapolate the available pure-component data. The importance of using the correct density of the mixture is shown, and a further improvement is suggested using one adjustable parameter for each nonideal binary subsystem.

7. Equation of State for Solutions of Electrolytes in Mixed Solvents (Publication 24)

W. Raatschen,† A.H. Harvey, and J.M. Prausnitz

Based on molecular theory, an equation of state is derived for a mixture containing two solvents and a salt. The equation of state follows from an expression for the Helmholtz energy; parameters are fitted to vapor pressure, density, and osmotic-coefficient data between −10 and 120°C from infinite dilution to 15 mole% salt. For the binary systems (methanol-water, methanol–lithium bromide, water–lithium bromide), deviations in vapor pressure are about 2–4%. When applied to the ternary system, using only binary parameters, the equation of state predicts vapor pressures with a mean deviation of 6% and vapor compositions with a mean deviation of less than 1.5 mole%.

†Present address: Institut für Technische Thermodynamik, Rheinisch-Westfälische Technische Hochschule, 5100 Aachen, Federal Republic of Germany.

8. Work in Progress

Efforts are directed at experimental and molecular-thermodynamic studies of (a) high-pressure vapor-liquid equilibria in multicomponent aqueous systems containing salts and common gases; (b) liquid-liquid equilibria in aqueous systems containing heavy hydrocarbons and some of their common derivatives; (c) solubilities of agricultural products in compressed carbon dioxide; (d) phase equilibria in aqueous mixtures containing water-soluble polymers and biomolecules; (e) enzyme-catalyzed oxidation of steroids and enzyme-catalyzed transesterification in compressed carbon dioxide; and (f) phase equilibria in the critical region.

1986 PUBLICATIONS AND REPORTS

Refereed Journals

1. F.E. Anderson and J.M. Prausnitz, "Inhibition of Gas Hydrates by Methanol," AIChE J. **32**, 1321 (1986); LBL-19205.
2. D. Dimitrelis and J.M. Prausnitz, "Comparison of Two Hard-Sphere Reference Systems for Perturbation Theories for Mixtures," Fluid Phase Equilib. **31**, 1 (1986); LBL-20672.
3. R.L. Cotterman, B.J. Schwarz, and J.M. Prausnitz, "Molecular Thermodynamics for Fluids at Low and High Densities. Part 1: Pure Fluids Containing Small or Large Molecules," AIChE J. **32**, 1787 (1986); LBL-20731.
4. R.L. Cotterman and J.M. Prausnitz, "Molecular Thermodynamics for Fluids at Low and High Densities. Part 2: Phase Equilibria for Mixtures Containing Components with Large Differences in Molecular Size of Potential Energy," AIChE J. **32**, 1799 (1986); LBL-20732.
5. J.M. Prausnitz, "Abstraction and Reality. The Two Sources of Chemical Thermodynamics," J. Non-Equilibrium Thermo. **11**, 49 (1986).
6. R.L. Cotterman, G.F. Chou, and J.M. Prausnitz, "Comments on 'Flash Calculations for Continuous or Semicontinuous Mixtures Using an Equation of State,' " Ind. Eng. Chem. Proc. Des. Dev. **25**, 840 (1986).
7. D.H. Krevor and J.M. Prausnitz, "Vapor-Liquid Equilibria for Model Mixtures of Coal-Derived

Liquids. 1. Binary Systems with 2-Methylfuran," J. Chem. Eng. Data **31**, 349 (1986).

8. D.H. Krevor, F.W. Lam, and J.M. Prausnitz, "Vapor-Liquid Equilibria for Model Mixtures of Coal-Derived Liquids. 2. Binary Systems with Bicyclic and High-Boiling Fluids," J. Chem. Eng. Data **31**, 353 (1986).
9. D.H. Krevor and J.M. Prausnitz, "Vapor-Liquid Equilibria for Model Mixtures of Coal-Derived Liquids. 3. Ternary Systems with Benzene, Cyclohexane, and a Heterocycle," J. Chem. Eng. Data **31**, 357 (1986).
10. G.F. Chou and J.M. Prausnitz, "Adiabatic Flash Calculations for Continuous or Semicontinuous Mixtures Using an Equation of State," Fluid Phase Equilib. **30**, 75 (1986).
11. P.M. Mathias, T.W. Copeman, and J.M. Prausnitz, "Phase Equilibria for Supercritical Extraction of Lemon Flavors and Palm Oils with Carbon Dioxide," Fluid Phase Equilib. **29**, 545 (1986).

Other Publications

12. J.M. Prausnitz, "The Raw Materials of Creativity," Chemtech **16**, 466 (1986).
13. J.M. Prausnitz, "Thermodynamics of Complex Fluid Mixtures," Wissenschaftskolleg Jahrbuch 1984/85, Siedler Verlag, Berlin, 1986.

LBL Reports

14. F.E. Anderson and J.M. Prausnitz, "Mutual Solubilities and Vapor Pressures for Binary and Ternary Aqueous Systems Containing Benzene, Toluene, m-Xylene, Thiophene, and Pyridine in the Region 100–200°C," accepted by AIChE J.; LBL-20851.
15. M. Radosz, R.L. Cotterman, and J.M. Prausnitz, "Phase Equilibria in Supercritical Propane Systems for Separation of Continuous Oil Mixtures," accepted by Ind. Eng. Chem. Proc. Des. Dev.; LBL-20868.
16. P.A. Rodgers, A.L. Creagh, M.M. Prange, and J.M. Prausnitz, "Molecular-Weight Distributions for Heavy Fossil Fuels from Gel-Permeation Chromatography and Characterization Data," submitted to Ind. Eng. Chem.; LBL-22000.
17. P.A. Rodgers, A.L. Creagh, and J.M. Prausnitz, "Correlation of Liquid Heat Capacities for Fossil Fuels using Characterization Data," submitted to Fuel; LBL-22001.
18. B.J. Schwarz, J.A. Wilhelm, and J.M. Prausnitz, "Vapor Pressures and Saturated-Liquid Densities of Heavy Fossil-Fuel Fractions," submitted to J. Chem. Eng. Data; LBL-22250.
19. B.J. Schwarz and J.M. Prausnitz, "Solubilities of Methane, Ethane and Carbon Dioxide in Heavy Fossil-Fuel Fractions," submitted to J. Chem. Eng. Data; LBL-22383.
20. K. Kawazuishi and J.M. Prausnitz, "Correlation of Vapor-Liquid Equilibria for the System Ammonia–Carbon Dioxide–Water," submitted to Ind. Eng. Chem.; LBL-22402.
21. R.J. Topliss, D. Dimitrelis, and J.M. Prausnitz, "Computational Aspects of a Non-Cubic Equation of State for Phase Equilibrium Calculations. Effect of Density-Dependent Mixing Rules," submitted to Comp. Chem. Eng.; LBL-22470.
22. A.H. Harvey and J.M. Prausnitz, "Dielectric Constants of Fluid Mixtures over a Wide Range of Temperature and Density," submitted to J. Soln. Chem.; LBL-22520.
23. S.F. Sciamanna and J.M. Prausnitz, "Thermodynamics of Dilute Solutions and the Quest for Ultrapurity," accepted by AIChE J.; LBL-22521.
24. W. Raatschen, A.H. Harvey, and J.M. Prausnitz, "Equation of State for Solutions of Electrolytes in Mixed Solvents," submitted to Fluid Phase Equilib.; LBL-22646.
25. M. Tietz, D. Dimitrelis, and J.M. Prausnitz, "The Effect of an Aqueous Entrainer on Phase Equilibria for Supercritical Extraction of Heavy Fossil Fuels with Propane," LBL-22471.

Invited Talks

26. J.M. Prausnitz, "Molecular Thermodynamics for Chemical Process Design," Oklahoma State University, Stillwater, April 1986.
27. J.M. Prausnitz, "Versatility and the Integration of Experience," Phillips Petroleum Lecture, Stillwater, OK, April 1986.
28. J.M. Prausnitz, "Continuous Thermodynamics for Adiabatic Flash Calculations," 4th Conference on Phase Equilibria and Physical Properties, Helsingor, Denmark, May 1986.
29. J.M. Prausnitz, "Recent Progress in Equation-of-State Research," Exxon Research and Engineering Co., Florham Park, NJ, Oct. 1986.

Nuclear Sciences

LOW-ENERGY NUCLEAR SCIENCES

HEAVY-ELEMENT CHEMISTRY

Actinide Chemistry*

Norman M. Edelstein, Richard A. Andersen, Neil Bartlett, John G. Conway, Kenneth N. Raymond, Glenn T. Seaborg, Andrew Streitwieser, Jr., David H. Templeton, and Allan Zalkin, Investigators

INTRODUCTION

The purpose of this project is to study actinide materials in order to provide the basic knowledge necessary for their safe and economic utilization in present and future technology. The program includes the preparation of new gaseous, liquid, and solid phases and studies of their physical and chemical properties. Techniques for characterization include x-ray diffraction, optical and vibrational spectroscopy, magnetic resonance, and magnetic susceptibility. Equilibrium and kinetic data for complex formation are measured. From these complementary studies, new insights into the structural and chemical principles of actinide compounds are obtained with which to design new synthetic schemes to produce new materials. A major aspect of the program is the design and synthesis of sequestering agents for actinide ions. These compounds are intended for use in the treatment of actinide poisoning and for possible application in the treatment of spent reactor fuels. Preparative, structural, and physical studies of new types of organoactinide, related organolanthanide, and new actinide inorganic complexes are continuing. Studies on optical spectra of free ions and actinide ions in crystals are being pursued in order to understand their electronic structure.

*This work was supported by the Director, Office of Energy Research, Office of Basic Energy Sciences, Chemical Sciences Division of the U.S. Department of Energy under Contract No. DE-AC03-76SF00098.

ACTINIDE-SPECIFIC SEQUESTERING AGENTS†

1. Promotion by Tetrameric Catechoylamide Ligands and CaNa-DTPA of the Dissociation *in vitro* of the Pu-Transferrin (Pu-Tf) Complex Formed after Intravenous Injection of Pu-tr-N-Butylphosphate (Publication 1)

H. Metivier, R. Masse, P. Durbin, and K.N. Raymond

Extraction of Pu from a nitric acid solution with tri-N-butylphosphate (TBP) in a kerosene solvent is an important step in the separation and recovery of Pu in the Purex process. At dosages recommended for therapeutic use in man (12 μmole kg^{-1} by inhalation, 30 μmole kg^{-1} by injection) the monocalcium salt of diethylenetriaminepentaacetate (Ca-DTPA) promoted little excretion of Pu from rats that had inhaled 8×10^5 Bq kg^{-1} of ^{239}Pu-tri-N-butylphosphate (Pu-TBP) even when Ca-DTPA was administered before the Pu-TBP exposure. Subsequently, Ca-DTPA therapy was shown to promote excretion of a larger fraction of the Pu when the mole ratio of ligand to Pu-TBP was increased: however, Ca-DTPA therapy was significantly less effective than it is when similar amounts of other transportable forms of Pu are inhaled. These results demonstrate the need for new complexing agents to treat people contaminated with Pu-TBP.

Since the synthesis of DTPA and its ubiquitous and generally satisfactory use in treating cases of actinide contamination, few new chelating agents have been developed for the actinides. [One, produced by English workers, is DTPA-bis(11-carboxy-1-undecylamide) penta-sodium salt (Puchel), in which two partially lipophilic side chains are coupled to DTPA.] This sequestering agent was designed to enhance cell penetration by the ligand. However,

†This work is supported in part by the National Institute of Environmental Health Sciences, ESO2698-04, and by the Office of Basic Energy Sciences, Office of Energy Research, U.S. Department of Energy, under Contract No. DE-AC03-76SF00098.

Puchel was found to be no more effective than native Ca-DTPA for removal of Pu from animals that had inhaled Pu-TBP.

Many biokinetic properties of Pu(IV) are the result of its chemical similarity to Fe(III), e.g., its entrainment in the Fe transport and storage systems. A new class of actinide sequestering agents, the poly(catechoylamide) ligands (CAM), was synthesized to take advantage of the great stability of catechol complexes with Fe(III) and Pu(IV) at physiological pH. Two tetrameric CAM ligands—N^1, N^5, N^{10}, N^{14}-tetrakis(2,3-dihydroxy-5-sulfobenzoyl)-tetraazatetradecane, tetrasodium salt [LICAM(S)], and N^1, N^5, N^{10}, N^{14}-tetrakis(2,3-dihydroxy-4-carboxybenzoyl)-tetraazatetradecane, tetrasodium salt [LICAM(C)]—are highly effective for removing intravenously injected Pu(IV) from mice and dogs. LICAM(C) appears to be of low toxicity in both species.

The purpose of the most recent studies was to determine whether the CAM ligands promote enough dissociation of the complex that Pu forms with Tf after exposure to Pu-TBP to warrant expenditure of synthetic chemical, animal, and other laboratory resources required for *in vivo* testing.

The study (performed in collaboration with Drs. H. Metivier and R. Mosse, Comissariat a l'Energie Atomique, Buijere-le-Chatel, France, and Dr. P. Durbin, LBL) were performed using baboons as test animals. Both LICAM(S) and LICAM(C) were significantly more efficient than Ca-DTPA for promoting dissociation of Pu from its complex(es) in the presence of TBP, and both CAM ligands were effective at concentrations that have been shown to promote excretion of >50% of Pu administered as Pu(IV) citrate to mice and dogs (3–30 μmole kg^{-5} molar concentration *in vitro*).

From these results and the low toxicity of effective dosages of LICAM(C) *in vivo*, it is concluded that decorporation of a significant fraction of Pu can be achieved with this ligand in cases of contamination with Pu-TBP.

2. Decorporation of Pu and Am from Beagles with Delayed Daily Injections of 3,4,3-LICAM(C) or Zn-DTPA (Publication 2)†

C.W. Mays, R.D. Lloyd, C.W. Jones, F.W. Bruenger, G.N. Taylor, P.W. Durbin, D. White, and K.N.. Raymond

The tetrameric catechoylamide ligand LICAM(C) = N^1, N^5, N^{10}, N^{14}-tetrakis(2,3-dihydroxy-r-carboxybenzoyl)-tetraazatetradecane, tetrasodium salt, was designed specifically to chelate Pu(IV). It was more effective than $CaNa_3$-DTPA (calcium trisodium diethylenetriaminepentaacetate) for a single prompt administration following Pu contamination in mice and dogs. In some circumstances, however, delayed therapy is needed. Therefore, a study was initiated to determine the relative efficacy of LICAM(C) and DTPA when repeated therapy is started after the radioactivity has become firmly deposited in tissue. The zinc salt of DTPA, Zn-DTPA, was used in this experiment so the animals could be injected repeatedly without the toxic side effects that occur with the frequent and prolonged administration of Ca-DTPA.

Four young adult beagles were each given a single intravenous injection of a citrate solution containing ^{241}Am, ^{239}Pu, and the photon emitter, ^{237}Pu. Two weeks later, daily subcutaneous injections of the ligands were administered. The Zn-DTPA treatments, begun at 14 days after injection, decreased both the total-body Pu content and especially the total-body Am content to a greater extent during 20 weeks of chelation therapy than did the LICAM(C) treatments. For the removal of radioactivity from nonliver tissue, LICAM(C) was somewhat superior for Pu, while Zn-DTPA was superior for Am. LICAM(C) had little effect on the liver content of either Pu or Am, but Zn-DTPA was a substantially superior treatment in liver for both elements, reducing the ^{241}Am liver content in the two treated dogs to undetectable levels (<0.1%) by 16 weeks of therapy.

Because LICAM(C) has high stability constants for both Fe and Pu, there was some concern on whether repeated LICAM(C) therapy might adversely deplete Fe from the dogs. During the period of daily injections with 30 μmole LICAM(C)/kg, the Fe concentration in blood serum was about 2 standard deviations below the control value of 190 μg of Fe per 100 ml serum for untreated beagles in our colony. However, after the daily dosage was reduced tenfold to 3 μg LICAM(C)/kg, the Fe concentration in plasma fluctuated above and below control values. The blood chemistry values of both dogs given LICAM(C) remained within normal limits during the initial observation period of about 1 year.

Depending on future results, optimum therapy to remove Pu from the body might possibly involve the prompt administration of LICAM(C) and Ca-DTPA (to remove Pu and associated transplutonium elements from the blood), followed, if necessary, by repeated administration of Zn-DTPA, because of its effectiveness and proven safety.

†Supported by National Cancer Institute Grant 2 RO1 CA28314-05 and U.S. Department of Energy Contract DE-AC02-76EV-00119 (Utah); and by National Institute of Environmental Health and Safety Grant ESO298-03 and U.S. DOE Contract DE-AC03-76SF00098 (California).

3. Selective Recognition and Activation of Small Molecules and Metal Ions in Bioinorganic Chemistry (Publication 20)†

K.N. Raymond and J. Reedijk

Metal ions are involved in the most fundamental chemical transformations of life. The activation of small molecules by metal-containing enzymes and the specific binding of metal ions, either necessary for, or a hazard to, living organisms are the subjects of this workshop report. The chemical transformations observed in living systems often elicit envy from the synthetic chemist trying to achieve such specificity, or frustration from the medical researchers trying to understand a pathological process. In either example the key to progress is research to elucidate the fundamental chemistry. The purpose of this workshop was then twofold: (1) to evaluate the status of the research field and present its contributions to biology, medicine, environmental chemistry, chemical industry, and biotechnology; and (2) to point the way to promising research opportunities and (technological) applications of the field.

The report broke down the research areas into related chemical subjects. Highlights of the most promising areas of research and anticipated biotechnological applications were presented.

The area of relevance to this project is selective sequestering of metal ions. The selective recognition and binding of metal ions is achieved routinely in biological processes but is often a difficult synthetic goal. Applications include development of new anticancer drugs; new medical imaging agents; removal of toxic or radioactive materials from the environment or contaminated individuals; and the accumulation of economically important metals from low-abundance sources.

†A report from the NATO workshop held at Noordwijkerhout, The Netherlands, July 15–19, 1985.

SYNTHETIC AND STRUCTURAL STUDIES OF ACTINIDES AND OTHER COMPOUNDS

4. Preparation of $MCl_4(Me_2ECH_2CH_2EMe_2)_2$ and $MCl_4[(1,2\text{-}Me_2As)_2C_6H_4]_2$, where M is Thorium or Uranium and E is Nitrogen or Phosphorus. Crystal Structure of $UCl_4[(1,2\text{-}Me_2As)_2C_6H_4]_2$ (Publication 26)

P.G. Edwards, R.A. Andersen, and R.W. Gellert

The compounds $MCl_4(Me_2ECH_2CH_2EMe_2)_2$, where M is Th or U and E is N or P, have been prepared. Variable-temperature NMR spectra show that the geometry of the eight-coordinate complexes are based on that of a D_{2d}-dodecahedron with the chloride ligands on the B-sites and the nitrogen or phosphorus atoms on the A-sites. The nitrogen complexes, $MCl_4(tmed)_2$, are fluxional on the ^1H NMR time scale, and the fluxional process is suggested to be the $\Lambda = \Delta$ motion of the ethylene-backbone in the five-membered ring of $MN(Me)_2CH_2CH_2NMe_2$ that is fast at high temperature and slow at low temperature. The complexes $MCl_4(dmpe)_2$ are fluxional at all temperatures. The arsenic complexes $MCl_4[(1,2\text{-}Me_2As)_2C_6H_4]_2$ have also been prepared for M = Th or U. Crystals of $UCl_4(diars)_2$ are tetragonal, I42m, with a = 9.407(1) Å, b = 17.318(2) Å, z = 2, V = 1532.5 A^3, d (calc) = 2.063 g cm^{-3}, and d (obsd) = 2.07 g cm^{-3}. The structure was refined by full-matrix least squares to a conventional R-factor of 0.020 using 556 data with $F_o^2 > 2\sigma(F_o^2)$. The geometry is almost a perfect D_{2d}-dodecahedron with the chloride ligands on the B-sites and the arsenic atoms on the A-sites. The U-As distance is 3.049(1) Å, and the U-Cl distance is 2.618(3) Å. Qualitative equilibrium-constant studies in toluene show that for UCl_4 the ligand displacement series is dmpe > tmed > diars and for $ThCl_4$ the series is dmpe ⩾ tmed > diars.

5. Structure of Tetrachlorobis[1,2-bis(dimethylamino)ethane]uranium(IV) (Publication 18)

A. Zalkin, P.G. Edwards, D. Zhang, and R.A. Andersen

The tetravalent uranium complex, $UCl_4 \cdot [(CH_3)_2NCH_2CH_2N(CH_3)_2]_2$, was prepared so that the

solid-state geometry and solution-state stereochemistry of the eight-coordinate complex could be compared. The complex was prepared from UCl_4 and excess $(CH_3)_2NCH_2CH_2N(CH_3)_2$ in toluene, and large green prisms were obtained by cooling the mother liquor (−20°C). The crystals are orthorhombic, $P2_12_12_1$, with cell dimensions a = 13.094(4) Å, b = 13.265(4) Å, and c = 12.633(4) Å. For Z = 4, D_x= 1.849 g cm^{-3}. The structure was refined to an R factor of 0.041 for 2617 unique reflections with $F^2 > 2\sigma(F^2)$. The uranium atom is bonded to a distorted square of four chlorine atoms and to four nitrogen atoms (see Figure 5-1) from the 1,2-bis(dimethylamino)ethane ligands, with average U-Cl and U-N distances of 2.609(9) Å and 2.786(19) Å, respectively. Eight-coordinate molecules generally fall into three idealized geometries: the D_{2d}-dodecahedron, C_{2v}-bicapped trigonal prism, and D_{4h}-square antiprism. $UCl_4{\cdot}[(CH_3)_2NCH_2CH_2N(CH_3)_2]_2$ is best described as a dodecahedron with the nitrogen atoms on the A-sites and the chloride ligands on the B-sites.

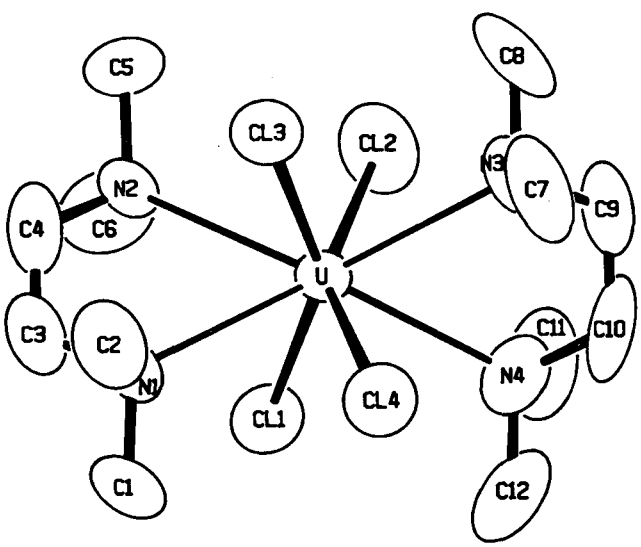

Figure 5-1. ORTEP drawing of $UCl_4{\cdot}(Me_2NCH_2CH_2NMe_2)_2$. (XBL 8612-5007)

6. Structure of Bis[tris(cyclopentadienyl)uranium(IV)][1,2-bis(dimethyldiphosphino)ethane] (Publication 38)

A. Zalkin, J.G. Brennan, and R.A. Andersen

The title complex, $[(C_5H_5)_3U]_2{\cdot}(CH_3)_2PCH_2CH_2P(CH_3)_2$, was prepared during studies of the coordination chemistry of tetra- and trivalent uranium complexes with bidentate amine, phosphine, and arsine ligands. The crystal structures of the tetravalent complexes, $UCl_4[(CH_3)_2NCH_2CH_2N(CH_3)_2]_2$, $U(OC_6H_5)_4[(CH_3)_2PCH_2CH_2P(CH_3)_2]_2$, $UCl_4[1,2\text{-}(CH_3)_2AsC_6H_4]_2$, and $U(CH_3)(CH_2C_6H_5)_3{\cdot}(CH_3)_2PCH_2CH_2P(CH_3)_2$, are known, and are all bidentate chelating ligands toward the uranium atom. In the title compound the $(CH_3)_2PCH_2CH_2P(CH_3)_2$ ligand acts not as a bidentate ligand but as a bridging monodentate ligand. The compound was prepared from $(C_5H_5)_3U{\cdot}OC_4H_8$ and $(CH_3)_2PCH_2CH_2P(CH_3)_2$. The crystals are triclinic, $P\bar{1}$, with cell dimensions a = 14.467(8) Å, b = 14.819(6) Å, c = 8.378(3) Å, α = 102.72(3)°, β = 90.03(3)°, and γ = 96.69(3)°; for Z = 2, D_x = 1.941 g cm^{-3}. The structure was refined by least-squares to an R factor of 0.035 for 1987 unique reflections with $F^2 > 2\sigma(F^2)$. The structure consists of a $(C_5H_5)_3U$ fragment coordinated to the phosphorus atoms at each end of a $(CH_3)_2PCH_2CH_2P(CH_3)_2$ ligand (see Figure 6-1). There are two crystallographically independent, though chemically equivalent, molecules in the unit cell across the inversion centers at (0,0,1/2) and (1/2,1/2,0). The phosphorus atom at each end of the bis(dimethylphosphino)ethane ligand is coordinated to a trivalent uranium; a center of inversion is located at the midpoint of the CH_2CH_2 bridge of the $(CH_3)_2PCH_2CH_2P(CH_3)_2$ ligand. Average distances (in Å) are U-C(Cp): 2.77(3); U-P: 3.022(2); and U-Cp(ring): 2.518(11).

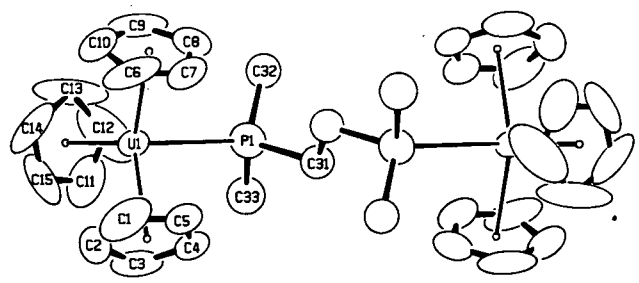

Figure 6-1. ORTEP drawing of $(Cp_3U)_2{\cdot}Me_2PCH_2CH_2PMe_2$. (XBL 8612-5015)

7. Structures of Bis(cyclopentadienyl)dimethylthorium(IV)-[bis(dimethylphosphino)ethane] and Bis(cyclopentadienyl)dichloro-thorium(IV)[bis(dimethylphosphino)ethane] (Publication 37)

A. Zalkin, J.G. Brennan, and R.A. Andersen

Compounds of the type $(C_5H_5)_2M(X)_2(L)$, where M is thorium or uranium, X is an anionic ligand such as halide or alkyl, and L is a neutral, bidentate phosphine ligand, were prepared in order to examine the details of inter- and intramolecular ligand exchange in solution.

The dimethyl complex $(C_5H_5)_2(CH_3)_2Th{\cdot}(CH_3)_2PCH_2CH_2P(CH_3)_2$ (**1**) (Figure 7-1) was made by the reaction of $(C_5H_5)_2Cl_2Th{\cdot}(CH_3)_2PCH_2CH_2P(CH_3)_2$ (**2**) (Figure 7-2) with methyllithium at −45°C. The dichloro complex (**2**) was synthesized from the reaction of sodium cyclopentadienide with $ThCl_4{\cdot}(CH_3)_2PCH_2CH_2P(CH_3)_2$ in a tetrahydrofuran solution at −70°C and crystallized from toluene. The crystals of (**1**) are monoclinic, $P2_1/n$, with cell dimensions a = 18.485(4) Å, b = 14.118(4) Å, c = 8.258(2) Å, and β = 91.05(2)°; for Z = 4, D_x = 1.672 g cm^{-3}. The structure was refined by least squares to an R factor of 0.026 for 2521 unique reflections with $F^2 > 2\sigma(F^2)$. Distances (in Å) are: Th-C(Cp): 2.84(3); Th-C(methyl): 2.562(8), 2.583(7); Th-Cp: 2.59, 2.57; and Th-P: 3.147(1) (average).

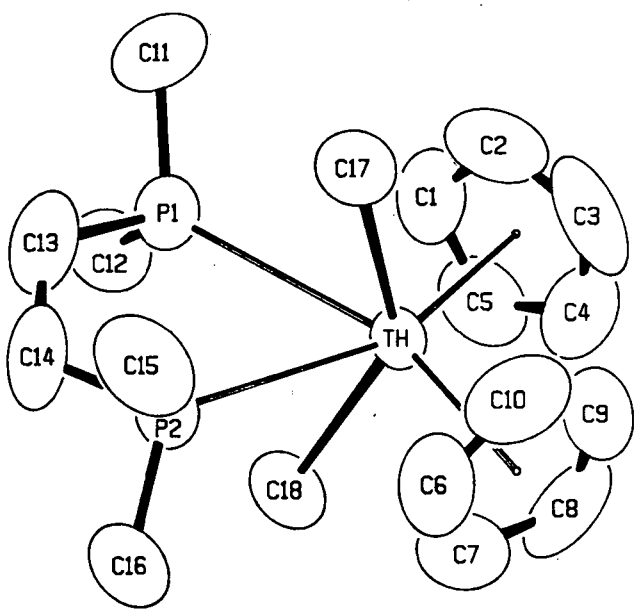

Figure 7-1. ORTEP drawing of $(C_5H_5)_2(CH_3)_2Th{\cdot}(CH_3)_2PCH_2CH_2P(CH_3)_2$ (**1**). (XBL 8612-5013)

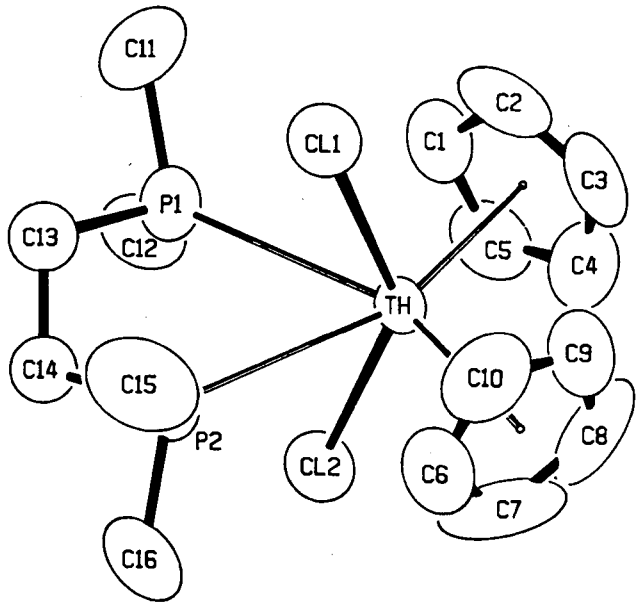

Figure 7-2. ORTEP drawing of $(C_5H_5)_2Cl_2Th{\cdot}(CH_3)_2PCH_2CH_2P(CH_3)_2$ (**2**). (XBL 8612-5014)

Crystals of (**2**) are monoclinic, $P2_1/n$, with cell dimensions a = 18.268(2) Å, b = 14.237(6) Å, c = 7.996(3) Å, and β = 92.27(4)°; for Z = 4, D_x = 1.864 g cm^{-3}. The structure was refined to an R factor of 0.020 for 2361 unique reflections with $I > \sigma(I)$. Distances (in Å) are: Th-C(Cp): 2.80(2); Th-Cl: 2.707(2), 2.708(2); Th-Cp: 2.56, 2.54; and Th-P: 3.121(1) (average).

The structures of (**1**) and (**2**) are crystallographically isomorphous. The cyclopentadienyl rings are *trans* to the bidentate ligand.

8. Structure of Bis(cyclopentadienyl)dibenzylthorium(IV)[bis-(dimethylphosphino)ethane] (Publication 36)

A. Zalkin, J.G. Brennan, and R.A. Andersen

The structure of the title compound, $(C_5H_5)_2(CH_2C_6H_5)_2Th{\cdot}(CH_3)_2PCH_2CH_2P(CH_3)_2$, is of interest because benzylic groups often behave as η^3- or η^4-benzylic ligands toward actinide centers. The complex was made by the reaction of $(C_5H_5)_2Cl_2Th{\cdot}(CH_3)_2PCH_2CH_2P(CH_3)_2$ with benzyllithium at −45°C. The crystals are triclinic, $P\bar{1}$, with cell dimensions a = 13.104(4) Å, b = 11.124(4) Å, c = 10.518(4) Å, α = 89.90(3)°, β = 92.99(3)°, and γ = 110.16(3)°; for Z = 2, D_x = 1.605 g cm^{-3}. The structure was refined by least squares to an R factor of

0.028 for 4021 unique reflections with $F^2 > \sigma(F^2)$. Distances (in Å) are: Th-C(Cp): 2.83 ± 0.05 (average); Th-C(benzyl): 2.648(6), 2.666(7); Th-P: 3.142(2), 3.237(2); Th-Cp(ring): 2.56, 2.59. The cyclopentadienyl rings are *trans* to the bidentate ligand, which is in agreement with Keppert's rules for six-coordinate complexes (see Figure 8-1). There are no interactions between the Th atom and the aryl ring. The stereochemistry of this complex is similar to that of the methyl and chloro analogues, as is expected on the bases of Keppert's rules. The averaged Th-C(benzyl) distance is longer than the equivalent Th-C(CH_3) distance in $(C_5H_5)_2(CH_3)_2Th{\cdot}PCH_2CH_2P(CH_3)_2$ of 2.573(6) Å and is consistent with previous structural results, which show that the uranium or thorium benzyl bond length is ~0.1 Å longer than the equivalent metal-carbon (sp^3-hybridized) distance.

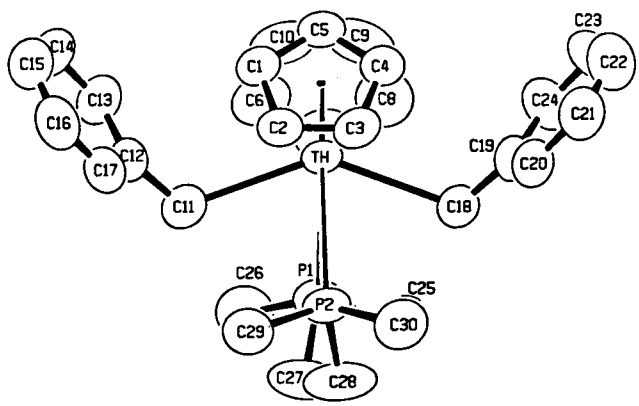

Figure 8-1. ORTEP drawing of $Cp_2(CH_2C_5H_5)_2Th{\cdot}Me_2PCH_2CH_2PMe_2$. (XBL 8612-5012)

9. Structure of Tris(trimethylsilylcyclopentadienyl)uranium(III), $[(CH_3)_3SiC_5H_4]_3U$ (Publication 32)

J.G. Brennan, R.A. Andersen, and A. Zalkin

The title compound is one of several triscyclopentadienyl complexes of uranium(III) prepared for a study of their synthetic chemistry, structures, and relative basicities. UCl_4 reacts with $K(Me_3SiC_5H_4)$ in tetrahydrofuran to give the red compound $(Me_3SiC_5H_4)_3UCl$, which when dissolved in hexane and stirred over Na/Hg or Na/K yields the green compound $(Me_3SiC_5H_4)_3U(III)$. The crystals are orthorhombic, Pbca, with a = 22.630(8) Å, b = 29.177(10) Å, and c = 8.428(3) Å at 23°C. For Z = 8 the calculated density is 1.551 g/cm^3. The structure was refined by least squares to a conventional R factor of 0.041 [2251 data, $F^2 > 2\sigma(F^2)$]. The uranium atom is in the plane of the centroids of the three cyclopentadienyl rings, to which it is bonded in a pentahapto fashion (see Figure 9-1). The U-to-ring distances are 2.54, 2.47, and 2.51 Å, and the average U-C distance is 2.78 ± 0.04 Å.

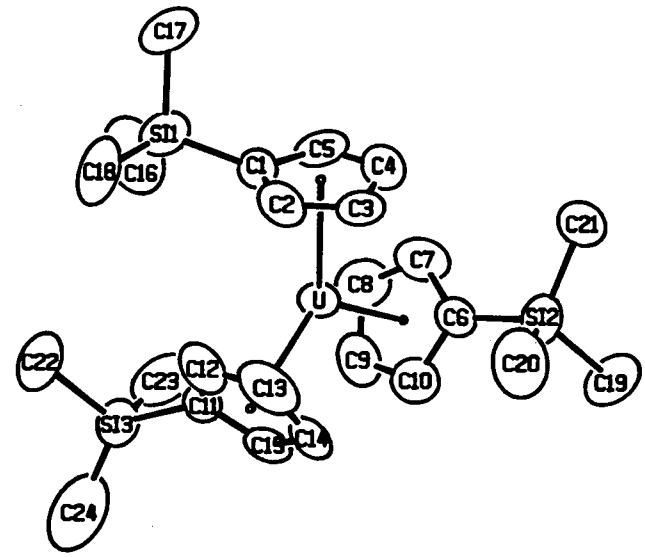

Figure 9-1. ORTEP drawing of $(Me_3SiC_5H_4)_3U$. (XBL 8612-5008)

10. The Phenyl Rotational Barrier in 1,1′-Diphenyluranocene (Publication 15)

R.M. Moore, Jr., A. Streitwieser, Jr., and H.-K. Wang

Paramagnetic organometallic U(IV)($5f^2$) compounds have served as useful probes in the observation of a variety of nuclear magnetic resonance (NMR) properties and processes.[1] The large isotropic shifts can result in greater amplification of chemical-shift differences and increase the time resolution of the pmr experiment, according to the approximate solutions of the modified Bloch equations:[2]

$$1/\tau = (\pi\Delta\nu)^2/4[1/T_2^{exch} - 1/T_2^{\circ}] , \qquad (1)$$

$$1/\tau = \pi\Delta\nu/2^{0.5} . \qquad (2)$$

As part of our study of substituted bis-π-[8]annuleneuranium(IV) (uranocene) complexes, we have used this probe to determine the rotational barrier of the phenyl ring about the C-C bond to the [8]annulene ring in 1,1′-diphenyluranocene, **1**.

At 30°C, the *ortho*- and *meta*-phenyl proton chemical shifts are average shift positions for the *endo* and *exo* proton environments (see Figure 10-1),

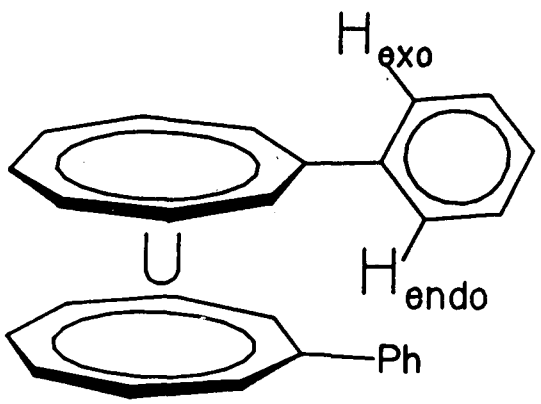

Figure 10-1. 1,1′-diphenyluranocene, showing definition of *exo* and *endo*. (XBL 874-1810)

since the phenyl ring is not coplanar with the [8]annulene ring but rotates rapidly about the C-C bond at 30°C. As the sample is cooled to −40°C, the *ortho* proton resonance begins to broaden until it collapses into the baseline at −100°C. This phenomenon is undoubtedly a dynamic NMR effect of the slowing of the phenyl rotation rate to the NMR time scale. The required $\Delta\delta$ values for the two separate states (*endo* and *exo ortho*-protons) could not be obtained directly but could be estimated from ^{1}H NMR data of 1,1′-di-*o*-tolyluranocene, **2**, which is essentially frozen in a single type of conformation, that in which the methyl group is *exo* to the uranium.

All of the protons exhibit approximate Curie-Weiss behavior throughout the temperature range studied. Simulation of the broadened fast exchange peak of the *ortho* protons in **1** (see Figure 10-2) provides the mean nuclei lifetimes τ given in Table 10-1 for the temperature range −45 to −80°C.

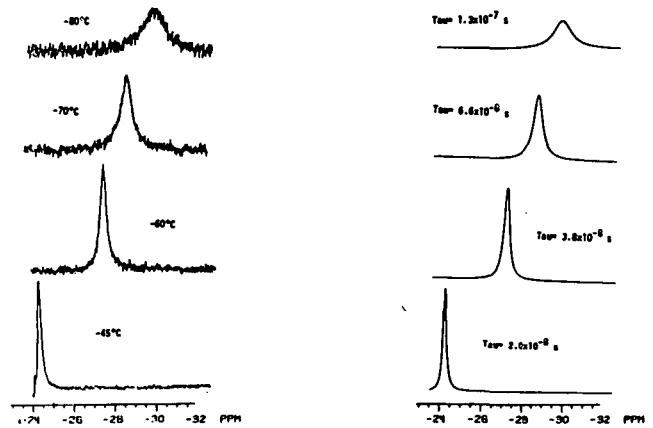

Figure 10-2. Line-shape analysis for *ortho*-proton coalescence in 1,1′-diphenyluranocene. (XBL 874-1811)

Table 10-1
Results of computer simulation to determine the mean lifetime for rapidly exchanging nuclei in 1,1′-diphenyluranocene.

T(°C)	τ(× 10^8 sec)	k(× 10^{-5} sec^{-1})
−45	2.0	250
−50	2.4	210
−55	2.8	180
−60	3.8	130
−65	5.1	98
−70	6.6	76
−75	9.6	52
−80	13	38

An Eyring plot of the rate constants results in the following activation parameters for this temperature range:

$$\Delta H^{\ddagger} = 4.4 \pm 0.3 \text{ kcal mol}^{-1},$$

$$\Delta S^{\ddagger} = 4.7 \pm 1.3 \text{ e.u.},$$

$$Ea = 4.8 \pm 0.3 \text{ kcal mol}^{-1},$$

$$A = (1.1 \pm 0.7) \times 10^{11} \text{ s}^{-1}.$$

Measuring a dynamic process with such a small barrier by ^{1}H NMR spectroscopy as in the present example is unusual but is made possible by the unique structure and paramagnetism of uranocene that results in widely different magnetic environments for the *endo* and *exo* protons ($\Delta\nu$ = 20,000–35,000 Hz at 200 MHz). The barrier is substantially larger than the analogous rotation of a phenyl group in unsubstituted biphenyl. Both semiempirical calculations[3] and experimental results[4] have shown the barrier to rotation in biphenyl to be of the order of 2–3 kcal mol^{-1}. Undoubtedly, the higher barrier in diphenyluranocene results from the wider C-C-C bond angle in the [8]annulene ring compared to benzene.

1. W. Luke and A. Streitwieser, Jr., in *Lanthanide and Actinide Chemistry and Spectroscopy*, ACS Symp. Ser. No. 131, N.M. Edelstein, Ed., 1980, p. 93.
2. H.S. Gutowsky, J. Jonas, A. Allerhand, and R.A. Meinzer, J. Am. Chem. Soc. **88**, 3185 (1966).
3. J.C. Rayez and J.J. Dannenberg, Chem. Phys. Lett. **41**, 492 (1976).
4. P.P. Poshkus and A.J. Grumadas, J. Chrom. **191**, 169 (1980).

11. Structure of $(\eta^5\text{-}C_5(CH_3)_5)_2LuCl(C_4H_8O)$ and Exchange of Coordinated Solvent (Publication 35)

L. Gong, A. Streitwieser, Jr., and A. Zalkin

The halide derivatives of organolanthanides are important starting materials for further synthetic transformations. Several such bis(pentamethylcyclopentadienyl)lanthanide(III) halide compounds have been crystallographically characterized as alkali halide complexes of the general form, $(C_5Me_5)_2LnX_2MS_2$ (X = Cl, I; M = Li, Na; S = coordinated solvent molecules).[1–3] However, no crystal studies of the simple parent solvated bis(pentamethylcyclopentadienyl)lanthanide halide complexes, $(C_5Me_5)_2LnCl(S)$ [S = tetrahydrofuran (THF), etc.], have previously been reported.

The structure is shown in Figure 11-1. The molecule with the atom numbering scheme in Figure 11-1 shows the lutetium atom in the center of a distorted tetrahedral array of two pentamethylcyclopentadienyl (Cp*) rings, a chloride atom, and an oxygen atom of tetrahydrofuran. The structure has the equal mean lutetium-carbon distance of 2.634 Å; the distance of the lutetium atom to the least-squares plane of the cyclopentadienyl (Cp) ring is 2.34 Å. The angles of C_5Me_5-Lu-C_5Me_5, C_5Me_5-Lu-Cl, and

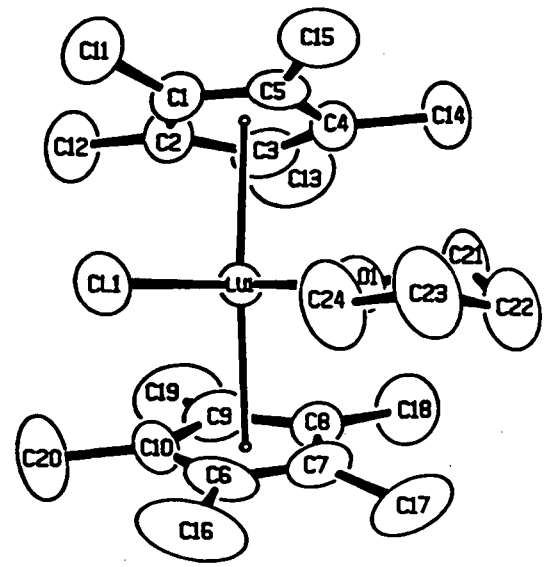

Figure 11-1. Molecular structure and atom numbering scheme for $(C_5Me_5)_2LuCl(THF)$. (XBL 874-1812)

C_5Me_5-Lu-THF are 137°, 105°, 105°, respectively. The pendant methyl groups of the C_5Me_5 rings are significantly bent from the C_5 ring planes, lying on the opposite sides of C_5 ring from Lu. They are displaced by 0.15–0.36 Å (4.5–13°) from the planes of C_5 rings, with the largest deviation in each ring being 0.36 Å (13°) for C_{13} and 0.33 Å (12.7 Å) for C_{19}. Such off-plane displacements have been explained previously for the related system $[(C_5Me_5)_2Yb(THF)]$ in terms of mutual repulsions of the methyl groups in the two coordinated Cp* rings from intramolecular contacts for the methyl groups;[1] in other respects the Cp* groups have normal geometries.

In $Cp^*_2LuCl(THF)$, the distance between the metal and C_5 ring planes is 2.63 Å. The closest distances between two methyl groups on each C_5 ring are 3.42 Å (C_{13}-C_{18}) and 3.50 Å (C_{13}-C_{19}). In addition, the distances of the chloride and oxygen atoms with the nearest methyl groups on each C_5 ring are 3.23 Å (C_{11}-Cl), 2.95 Å (C_{15}-O), and 2.73 Å (C_{17}-O). These distances are close to or within the sum of the van der Waals radii. Consequently, the corresponding methyl groups are bent away significantly because of obvious steric repulsions. However, similar comparison shows that some methyl groups are in positions where no obvious steric hindrance effects exist. For these methyls such bending puts more negative charge on the face of the ring toward the lutetium cation.

The ^{1}H NMR spectrum at room temperature of a toluene-d_8 solutions shows chemical shifts of the

coordinated THF that are different from those of free THF in toluene-d_8. A variable-temperature ^1H NMR study of a solution in toluene-d_8 0.008M in $Cp^*LuCl(THF)$ and 0.023M in free THF showed single NMR peaks for the rapidly exchanging α- and β-protons but separate peaks at $-30°C$; α-protons: δ_{free} = 719.5 Hz, δ_{coord} = 680.0 Hz, coalescence temperature = $-5.1°C$; β-protons: δ_{free} = 285.0 Hz, δ_{coord} = 220.0 Hz, coalescence temperature = 9.8°C. From the averaged rate constants, calculated from $k = 2^{-0.5}\pi\Delta\nu$, $\Delta G^{\ddagger}$ = 54 kJ mol^{-1} at 0°C for the exchange process

$$Cp^*LuCl(THF') + THF'' = Cp^*LuCl(THF'') + THF'.$$

This result provides the first determination of the bond strength of coordinating solvent in such lanthanide complexes.

1. T.D. Tilley and R.A. Andersen, Inorg. Chem. **19**, 2999 (1980).

12. The Molecular Structures of Bis(pentamethylcyclopentadienyl)calcium and -Ytterbium in the Gas Phase: Two Bent Metallocenes (Publication 5)

R.A. Andersen, R. Blom, J.M. Boncella, C.J. Burns, A. Haaland, and H.V. Volden

Gas electron-diffraction studies show that while the ligand rings in $(\eta^5\text{-}C_5Me_5)_2Mg$, Me = CH_3, are essentially parallel, the thermal average structures of $(\eta^5\text{-}C_5Me_5)_2Ca$ and $(\eta^5\text{-}C_5Me_5)_2Yb$ are bent, the intersection angle between the ligand ring planes being 20(3)° in both.

13. Bis(pentamethylcyclopentadienyl)ytterbium (II) as a Lewis Acid and an Electron-Transfer Ligand; Preparation and Crystal Structure of $[Yb(C_5Me_5)_2(\mu\text{-}OC)_2Fe(C_5H_4Me)]_2$ (Publication 27)

J.M. Boncella and R.A. Andersen

The divalent ytterbium metallocene, $Yb(C_5Me_5)_2(OEt_2)$, reacts with $M_2(C_5H_4R)_2(CO)_4$ to give dimers of composition $M_2(C_5H_4R)_2(CO)_4Yb_2(C_5Me_5)_4$, where M is Fe and R = H, Me, and Me_3Si or M is Ru and R = Me_3Si. X-ray crystallographic studies with M = Fe and R = Me show that the molecule is a centrosymmetric dimer of the structure $[(Me_5C_5)_2Yb(\mu\text{-}OC)_2(FeC_5H_4Me)]_2$, shown in Figure 13-1. The space group is $P2_1/n$, with a = 10.6069(15) Å, b = 23.4930(31) Å, c = 10.8730(20) Å, β = 92.041(13)°, V = 2707.7(13) $Å^3$, and Z = 2.

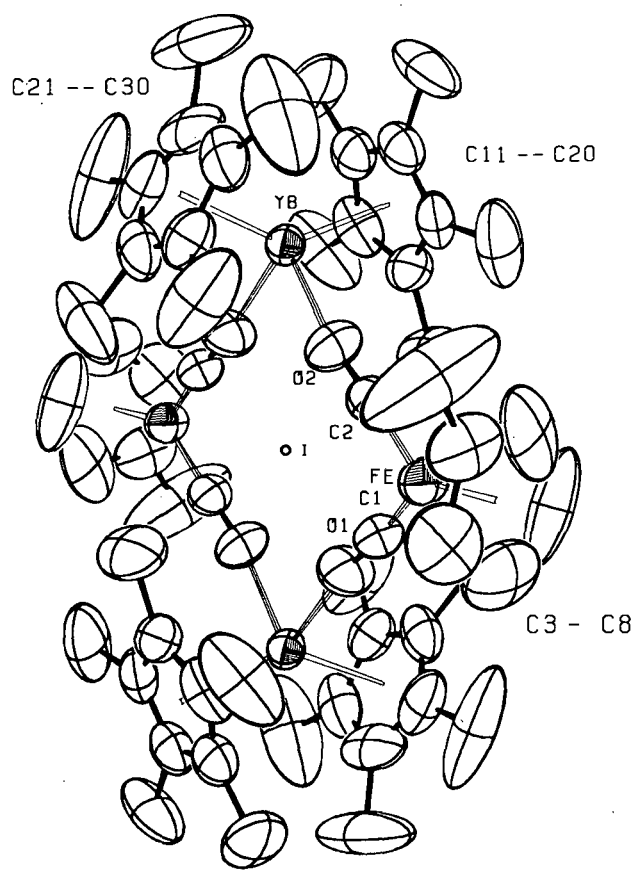

Figure 13-1. The structure of $[(Me_5C_5)_2Yb(\mu\text{-}OC)_2(FeC_5H_4Me)]_2$. (XBL 826-10528)

14. Bis(pentamethylcyclopentadienyl)ytterbium (II) as a Lewis Acid and an Electron-Transfer Ligand; Preparation, Crystal Structure, and Solution Dynamics of $[Yb(C_5Me_5)_2(\mu\text{-}OC)_2Mo(CO)(C_5H_4R)]_2$ (Publication 28)

J.M. Boncella and R.A. Andersen

The divalent ytterbium metallocene, $Yb(C_5Me_5)_2(OEt_2)$, reacts with the metal-metal bonded compound $(RC_5H_4)_2Mo_2(CO)_6$, to give dimers of composition $Mo_2(C_5H_4R)_2(CO)_6Yb_2(C_5Me_5)_4$, where R is H or Me_3Si. X-ray crystallographic studies on the Me_3Si complex show that the molecule is a centrosymmetric dimer with the $C_5H_4SiMe_3$ groups on the

molybdenum atoms *trans*-disposed, as shown in Figure 14-1. The space group is $P2_1/n$, with a = 13.771(1) Å, b = 15.294(2) Å, c = 15.607(1) Å, β = 93.434(8)°, V = 3294 Å^3, and Z = 2. Variable-temperature ^{1}H NMR spectroscopic studies show that in toluene solution the compound exists in an equilibrium between *trans* and *cis* isomers, and the activation energy for interconversion is ~20 kcal mol^{-1}. The mechanism for the interconversion is shown by crossover studies to be intermolecular. Related intermolecular exchange processes have been discovered in the $M_2(C_5H_4R)_2(\mu\text{-}CO)_4Yb_2(C_5Me_5)_4$ dimers, where M is Fe or Ru and R is Me or $SiMe_3$.

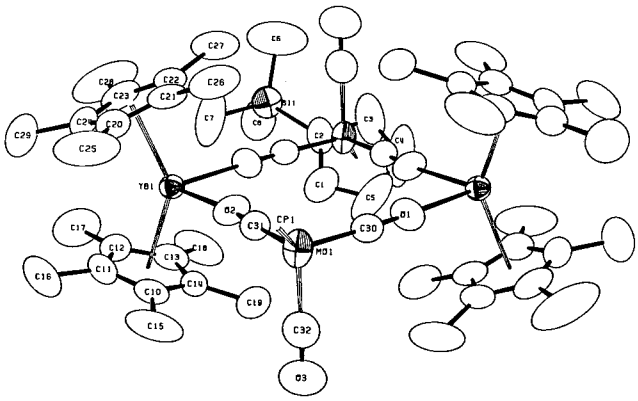

Figure 14-1. The $C_5H_4SiMe_3$ groups on the molybdenum atoms *trans*-disposed. (XBL 8310-11913)

15. Preparation and Crystal Structure of the Mixed-Valence [Yb(III,II)] Tetranuclear Complex, $(Me_5C_5)_6Yb_4(\mu\text{-}F)_4$ (Publication 29)

C.J. Burns, D.J. Berg, and R.A. Andersen

Silver fluoride and $(Me_5C_5)_2Yb$ in toluene give the novel, tetranuclear, mixed-valence complex $(Me_5C_5)_6Yb_4(\mu\text{-}F)_4$, as shown by single-crystal x-ray crystallography (see Figure 15-1).

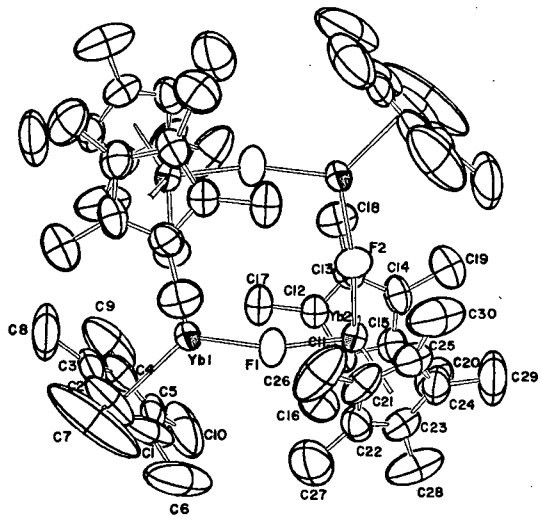

Figure 15-1. The structure of $(Me_5C_5)_6Yb_4(\mu\text{-}F)_4$, as shown by single-crystal x-ray crystallography. (XBL 868-2844)

16. Preparation of the First η^2-Olefin Complex of a 4f-Transition Metal, $(Me_5C_5)_2Yb(\mu\text{-}C_2H_4)Pt(PPh_3)_2$ (Publication 31)

C.J. Burns and R.A. Andersen

Reaction of $(Me_5C_5)_2Yb$ with the platinum olefin complex $(Ph_3P)_2Pt(C_2H_4)$ gives the first olefin complex of a lanthanide metal, $(Me_5C_5)_2Yb(\mu\text{-}C_2H_4)Pt(PPh_3)_2$, as shown by x-ray crystallography (see Figure 16-1).

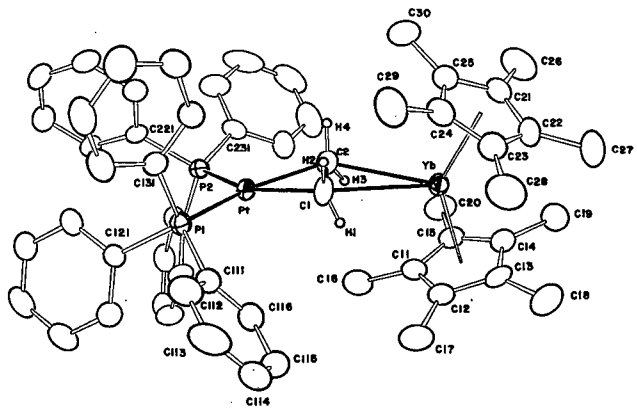

Figure 16-1. The structure of $(Me_5C_5)_2Yb(\mu\text{-}C_2H_4)Pt(PPh_3)_2$, as shown by x-ray crystallography. (XBL 868-2846)

17. Preparation of the First Molecular η^2-Acetylene Complex of a 4f-Transition Metal, $(Me_5C_5)_2Yb(\eta^2\text{-MeC}\equiv\text{CMe})$ (Publication 30)

C.J. Burns and R.A. Andersen

This communication describes the synthesis and crystal structure of the first η^2-acetylene complex of an f-transition metal, $(Me_5C_5)_2Yb(\eta^2\text{-MeC}\equiv\text{CMe})$. The geometry of the acetylene is not greatly perturbed by coordination to the ytterbium(II) center, and the complex can be viewed as a Lewis acid-base complex with little or no π-backbonding to the acetylene. An ORTEP diagram is shown in Figure 17-1.

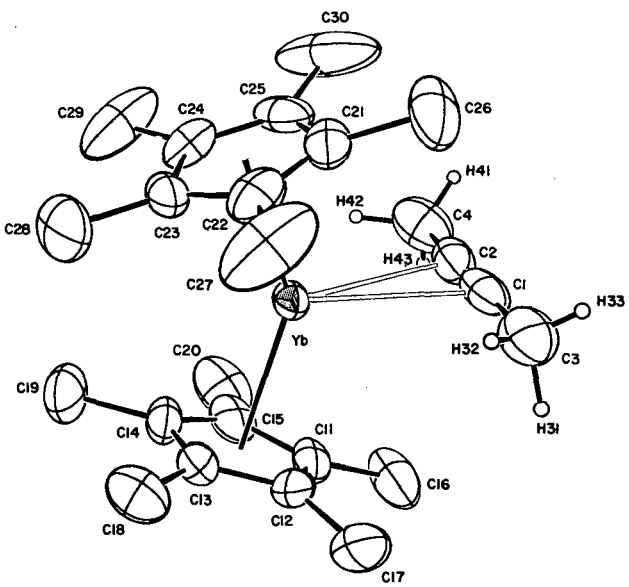

Figure 17-1. ORTEP diagram of $(Me_5C_5)_2Yb(\eta^2\text{-MeC}\equiv\text{CMe})$. (XBL 868-2898)

18. Structure of Bis(pentamethylcyclopentadienyl)ytterbium(III)-(phenylsulfide)(ammonia) (Publication 34)

A. Zalkin, T.J. Henly, and R.A. Andersen

The title compound, $[(CH_3)_5C_5]_2Yb(SC_6H_3)\cdot NH_3$, was prepared as part of an extensive study of the electron-transfer and bond-cleaving properties of the divalent ytterbium metallocene, $[(CH_3)_5C_5]_2Yb$, towards transition-metal carbonyls with metal-to-metal bonds and with organic compounds with nonmetal-to-nonmetal bonds. The trivalent $[(CH_3)_5C_5]_2Yb(SC_6H_5)\cdot(NH_3)$ was isolated in the reaction of $[(CH_3)_5C_5]_2Yb(NH_3)_2$ and diphenyldisulfide. The crystals are triclinic, P1, with cell dimensions a = 14.091(6) Å, b = 18.294(8) Å, c = 10.430(6) Å, α = 104.52(6)°, β = 96.66(5)°, and γ = 93.77(5)°. For Z = 4, D_x = 1.471 g cm^{-3}. The structure was refined by full-matrix least squares to an R factor of R = 0.038 for 6052 unique reflections with $F^2 > 2\sigma(F^2)$. Two independent but chemically similar molecules are found in the asymmetric unit. The Yb is at the center of a distorted tetrahedron consisting of an S atom, an N atom, and the centers of 2 pentamethylcyclopentadienyl rings (see Figure 18-1). Distances (in Å) are Yb-N: 2.423(8) and 2.432(8); Yb-S: 2.670(3) and 2.679(3); Yb-C: 2.64(2) (average); and Yb-Cp: 2.347(7) (average).

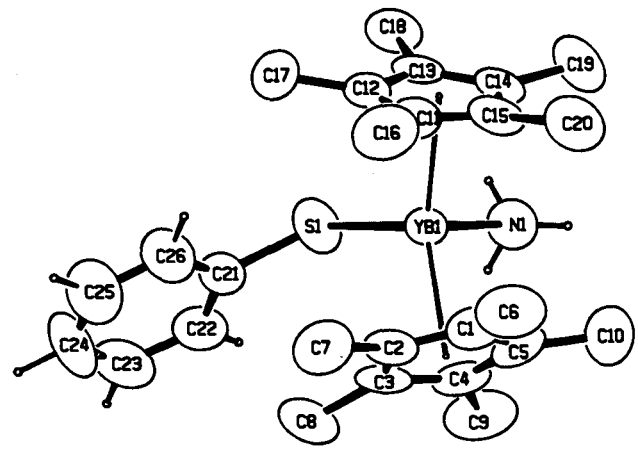

Figure 18-1. RTEP drawing of $(Me_5C_5)_2Yb(SC_6H_5)\cdot NH_3$. (XBL 8612-5009)

19. Structure of Tris(methylcyclopentadienyl)cerium(III)-trimethylphosphine (Publication 33)

S. Stults and A. Zalkin

The structure of $(CH_3C_5H_4)_3U\cdot P(CH_3)_3$ was determined as part of a study of the relative affinity of Lewis bases toward $(CH_3C_5H_4)_3U$. A parallel experiment using $(CH_3C_5H_4)_3Ce\cdot P(CH_3)_3$ was done to study the effect of a different metal atom. Interligand contacts influence the ability of a ligand to coordinate to a metal ion and must be considered when comparing ligand basicities. As part of this study the x-ray structure of $(CH_3C_5H_4)_3Ce\cdot P(CH_3)_3$, which is isomorphous with the uranium complex, was determined. Yellow air-sensitive needles of the

phosphine complex were prepared by reacting $(CH_3C_5H_4)_3Ce{\cdot}OC_4H_8$, isolated from the reaction of $CeCl_3$ with 3 equivalents of $NaCH_3C_5H_8$ in tetrahydrofuran, with $P(CH_3)_3$ in diethylether and crystallizing from diethyl ether at 253 K. The crystals are monoclinic, Cc, with cell dimensions a = 14.017(4) Å, b = 9.351(3) Å, c = 16.348(6) Å, and β = 103.92(3)°; for Z = 4, D_x = 1.448(3) g cm^{-3}. The structure was refined by full-matrix least squares to an R factor of 0.024 for 1232 reflections $[F^2 > \sigma(F^2)]$. The structure consists of cerium-centered monomolecular units in which the cerium atom is coordinated in a pentahapto fashion to three cyclopentadiene rings and to the phosphorus atom of the trimethyl phosphine molecule (see Figure 19-1). The average Ce-C distance is 2.82(4) Å, and the Ce-P distance is 3.072(4) Å.

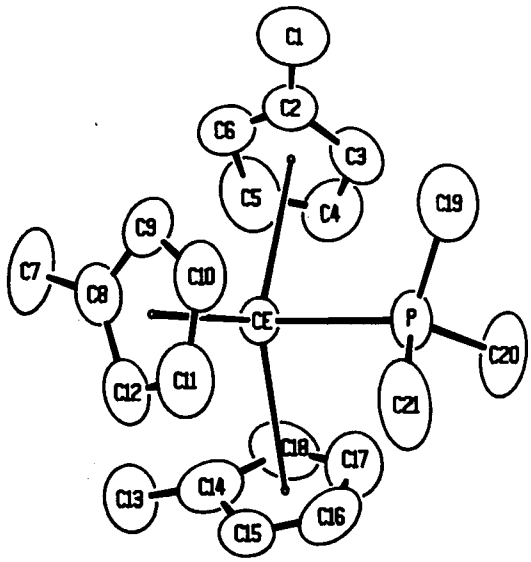

Figure 19-1. ORTEP drawing of $(CH_3C_5H_4)_3Ce{\cdot}P(CH_3)_3$. (XBL 8612-5010)

20. Structure and Characterization of $(C_5H_5)_2Zr(H)BH_3CH_3$ (Publication 40)

W.K. Kot, N.M. Edelstein, and A. Zalkin

The monomeric hydride, $(\eta^5\text{-}C_5H_5)Zr(H)BH_3CH_3$, has been prepared by reacting $(\eta^5\text{-}C_5H_5)_2ZrCl_2$ with $LiBH_3CH_3$, and its molecular structure has been determined by single-crystal x-ray diffraction. Mass spectroscopy, infrared spectroscopy, and nuclear magnetic resonance data are presented. The orthorhombic crystal belongs to the space group $Cmc2_1$ with unit cell parameters a = 13.775(3) Å, b = 9.520(3) Å, c = 8.816(2) Å, and R = 0.018. The methyltrihydroborato group acts as a bidentate ligand. The Zr–terminal H distance is 1.79 ± 0.04 Å, and the Zr-B distance is 2.558 ± 0.004 Å. The structure is shown in Figure 20-1. For a similar reaction with Cp_2UCl_2, only $Cp_3U(BH_3CH_3)_2$ is isolated with no evidence for the formation of the hydride.

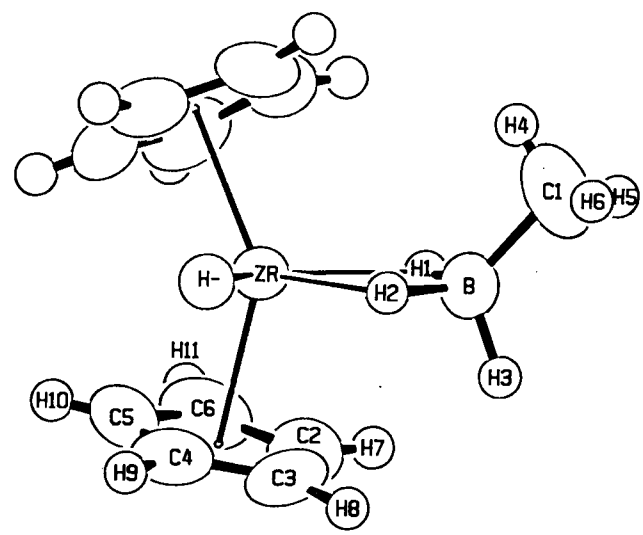

Figure 20-1. ORTEP drawing of $(C_5H_5)_2Zr(H)BH_3CH_3$. Only one conformation of the disordered methyltrihydroborate is shown. (XBL 8612-4956)

21. Structure of Trithallium(I) Phosphate (Publication 44)

A. Zalkin, D.H. Templeton, D. Eimerl, and S.P. Velsko

In a survey of optical second-harmonic generating materials, Tl_3PO_4 powder was found to produce a large second-harmonic intensity relative to quartz. This observation, and the large birefringence observed for this material, suggested that it might be a useful crystal for frequency conversion of laser light. To aid in understanding the properties of Tl_3PO_4, and to probe the relationship of its structure to those of $LiIO_3$ and $KLiSO_4$, which are well-known second-harmonic generators in the same space group, an accurate structure refinement was desirable. A thin needle-shaped crystal of the title compound was grown from an aqueous solution of Tl_2CO_3 and $(NH_4)_2HPO_4$. The crystals are hexagonal, $P6_3$, with cell dimensions a = 8.369(8) Å and c = 5.111(5) Å; for Z = 2, D_x = 7.59 g cm^{-3}. The structure was

refined by least squares to an R factor of 0.017 for 241 reflections. The structure consists of thallous and phosphate ions connected by a three-dimensional network of Tl-O coordinations (see Figure 21-1). One of the P-O bonds of the tetrahedral phosphate ion lies on the threefold axis. The thallium atom is coordinated to three oxygen atoms at distances 2.529(7), 2.553(5), and 2.555(8) Å, each from a different phosphate group. Alternating planar triads of thallium atoms at z = 0 and 1/2 form a column parallel to the c axis. The very large positive birefringence in Tl_3PO_4 is opposite in sign from that in $LiIO_3$ and much larger than that of $KLiSO_4$.

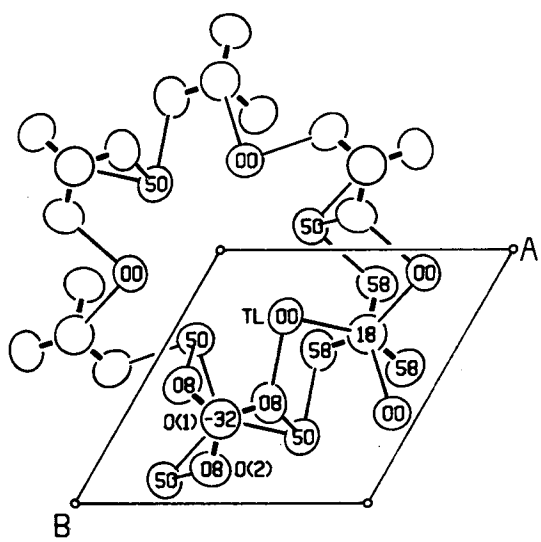

Figure 21-1. ORTEP drawing showing the contents of a unit cell and the disposition of the Tl ions about the c-axis. Numbers inside the atom boundaries are z-coordinate × 100. The P atom is hidden under the O(1) atom. (XBL 8612-5011)

PHYSICAL AND SPECTROSCOPIC PROPERTIES

22. Enthalpy of Formation and Magnetic Susceptibility of Californium Sesquioxide, Cf_2O_3 (Publication 45)

L.R. Morss,† J. Fuger,‡ J. Goffart,‡ N. Edelstein, and G.V. Shalimoff

Californium is the heaviest element that is available for scientific study in milligram amounts. Its most suitable isotope is ^{249}Cf, which can be separated as a daughter of the β^- decay of ^{249}Bk. Its half-life (351 years) and the intense accompanying γ rays (principally 388 keV) limit studies to ≈5 mg without remote-handling facilities.

The enthalpy of formation of Cf_2O_3 is an important benchmark for actinide sesquioxides, for californium(III) compounds, and for thermochemical systematics of heavy actinide compounds in general. Since the enthalpy of formation of Cf^{3+} (aq) was recently determined, measurement of the enthalpy of solution of Cf_2O_3 leads directly to its enthalpy of formation.

Cf^{3+} is at present (since Bk^{2+} and Es^{4+} compounds are as yet uncharacterized) the only accessible ion for magnetic-susceptibility study of the $5f^9$ configuration with the nominal ground-state term $^6H_{15/2}$. The only magnetic-susceptibility measurement of a sample containing this ion was as a 1-μg Cf^{3+}-loaded ion-exchange bead, yielding Curie-Weiss behavior with μ_{eff} = 9.14 ± 0.66 μ_B and θ = 5.6 ± 3.2 K. The absence of magnetic-susceptibility measurements on californium compounds, as well as the discrepancy of the above datum from the expected free-ion value of 10.18 μ_B (using the free-ion calculated g_J value of 1.279 and L-S coupling), led us to determine the susceptibility of the sesquioxide.

The enthalpy of formation of cubic (bcc, a_o = 1.0839 ± 0.0004 nm) Cf_2O_3, $\Delta_f H°(298\ K)$, has been determined to be −1652.6 ± 10.3 kJ mol^{-1} by solution microcalorimetry. The magnetic susceptibilities of two samples have been measured between 1.5 and 300 K. Cf_2O_3 obeys the Curie-Weiss law between 90 and 300 K with μ_{eff} = 9.7 ± 0.1 μ_B and θ = −80 + 10 K.

---

†Permanent address: Chemistry Division, Argonne National Laboratory, Argonne, IL.

‡Permanent address: Laboratory of Analytical Chemistry and Radiochemistry, University of Liege, Sart Tilman, B-4000 Liege, Belgium.

23. Multinuclear NMR Spectroscopy of the Tetrahedral U(IV) Complex: $U(BH_3CH_3)_4$ (Publication 41)

E. Gamp,† R. Shinomoto,‡ N.M. Edelstein, and B.R. McGarvey§

Paramagnetic shifts in the NMR spectrum of the coordinated ligands can be a powerful tool to examine interactions between the metal f electrons and the ligands. A high molecular symmetry is important in that pseudocontact (dipolar) shifts that are sometimes hard to separate from the spin-

delocalization shifts are zero in molecules of T_d symmetry such as $U(BH_3CH_3)_4$.

The temperature dependence of the ^1H, ^{11}B, and ^{13}C-NMR spectra of T_d $U(BH_3CH_3)_4$ in solution is reported. The paramagnetic shifts are interpreted as originating from purely spin-delocalization mechanisms with no contribution from the metal-orbital dipolar interaction. It is shown that the temperature dependence of both ^1H shifts (bridging and terminal protons) is identical with that calculated from a polarization theory that assumes the shift is proportional to the average value of electron spin in the inner 5f orbitals. The proportionality constant is -5.64 MHz for the bridging protons and -0.59 MHz for the terminal protons. The temperature dependences of ^{11}B and ^{13}C shifts are found to depart significantly from that predicted by the polarization theory, with the largest deviations shown by the ^{11}B shifts. These deviations can be accounted for by postulating a second spin delocalization through direct covalency involving molecular orbitals formed from the uranium 5f orbitals and ligand s and p orbitals. Figure 23-1 shows the experimental and calculated shifts.

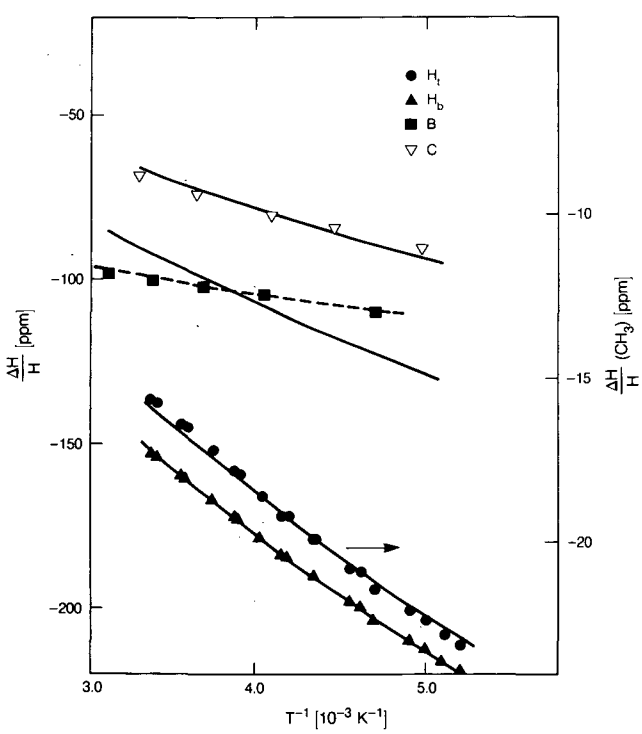

Figure 23-1. T^{-1} dependence of the paramagnetic shifts in $U(BH_3CH_3)_4$ referred to $Th(BH_3CH_3)_4$. All shifts are to lower field and given in ppm. The solid lines are calculated from the spin-polarization mechanism. The dashed line for B is a combined polarization plus covalent-shift theoretical curve. (XBL 868-10964)

†Present address: EMPA, CH-8600 Dubendorf, Switzerland.

‡Present address: Department of Chemistry, University of Southern California, Los Angeles, CA 90089.

§Permanent address: Department of Chemistry and Biochemistry, University of Windsor, Ontario N9B 3P4.

24. Optical and Magnetic Properties of Tetravalent Actinide Ions and Compounds (Publication 42)

N.M. Edelstein

Optical spectra of the $4f^n$ and $5f^n$ ions (where n is equal to the number of equivalent electrons) are characterized by relatively sharp lines due to transitions between energy levels within the f^n configuration. The f^n electrons are inner-shell electrons that are shielded from their surroundings by outer-shell electrons ($5s^25p^6$ for the $4f^n$ ions, $6s^26p^6$ for the $5f^n$ ions). Thus, even in compounds, the f^n shell retains atomic-like properties. The comparison of the spectra of the free ion with that of the ion in the solid state provides information about the effects of its surroundings on the f^n ion.

A survey is given of the optical and magnetic data available for tetravalent actinide ions in a variety of single crystals and as pure compounds. Conclusions are drawn from the values of the "free ion" parameters in crystals when compared with the values for the free ions in the gaseous phase. Problems with the theoretical model are discussed.

25. An X-Ray Photoelectron Spectroscopic (XPS) Study of Some Uranium Compounds (Publication 12)

D.B. Beach, K.D. Bomben, N.M. Edelstein, D.C. Eisenberg, W.L. Jolly, R. Shinomoto, and A. Streitwieser, Jr.

XPS spectra have been determined and interpreted for several uranium compounds.

At least part of the lower binding energy of uranium(IV) methylborohydride results from the increased polarizability of methyl compared to hydrogen. This effect has been seen in many gas-phase thermodynamic data, such as proton affinities and ionization potentials. In the present case the substitution occurs approximately one atom removed from the uranium. Appropriate analogies in core binding energies are in the effects of ethyl vs.

methyl substitution. For example, in each replacement of methyl groups by ethyl in methylamines, dimethyl ether and dimethylzinc lowers the core binding energy of nitrogen, oxygen, and zinc, respectively, by 0.1–0.2 eV.

Uranium borohydride and uranocene, bis-[8]annuleneuranium(IV), are both formally compounds of uranium(IV), but the uranium core binding energy in uranocene is more than 4 eV less than that of the borohydride. The compounds are sufficiently different that part of the decrease could result from a difference in relaxation energies. It seems more likely, however, that most, if not all, of the difference stems from the much greater ring-metal covalency in uranocene. For comparison, the metal core binding energies in ferrocene and nickelocene are unusually low relative to other compounds of these central metals.

26. The Electronic Structure of Organometallic Complexes of the f Elements—XVIII. Parameterization of the Crystal Field Splitting Patterns of Quasi Trigonal Bi-pyramidal Anionic Complexes Involving the Tris(η^5-cyclopentadienyl)uranium(IV) Moiety (Publication 39)

H.-D. Amberger,[†] H. Reddmann,[†] G. Shalimoff, and N.M. Edelstein

Complexes of the type Cp_3Ln and their adducts $Cp_3Ln{\cdot}L$ (Cp = C_5H_5; L = THF = C_4H_4O, or MeThF or CNC_6H_{11}) have been studied extensively by optical spectroscopy for over 15 years. However, the analyses of these spectra have been hampered by the lack of single crystals with which to obtain polarized spectra. Amberger and his coworkers have used the technique of magnetic circular dichroism (MCD) to obtain further data on these complexes. Our earlier work resulted in the analysis of the spectra of the above compounds for Ln = Pr and Nd. The crystal-field parameters have now been obtained for the anions $[Cp_3U(NCS)_2]^-$ and $[Cp_3U(NCBH_3)_2]^-$ by analysis of the MCD and optical data. Surprisingly, the parameters agree qualitatively with those derived from extended Hueckel calculations that have been reported by Tatsumi.

[†]Permanent address: Institut für Anorganische und Angewandte Chemie der Universität Hamburg, D-2000 Hamburg 13, Federal Republic of Germany.

27. Electronic Structure of Bis(cyclopentadienyl) Lanthanide Compounds: Photoelectron Spectra and Molecular Orbital Calculations (Publication 4)

R.A. Andersen, J.M. Boncella, C.J. Burns, J.C. Green, D. Hohl, and N. Rosch

Gas-phase He I and He II photoelectron spectra have been obtained for $Ln(\eta^5\text{-}C_5Me_5)_2$, where Ln = Sm, Eu, or Yb. Bands associated with ionization of f-electrons are identified for the Sm and Yb compounds. Ionization energies calculated from quasirelativistic xα-SW calculations are in good agreement with the experimental values. These calculations show the compounds to be highly ionic in nature, and provide no orbital reason for the established nonparallel geometry of the rings.

1986 PUBLICATIONS AND REPORTS

Refereed Journals

1. H. Metivier, R. Masse, P.W. Durbin, and K.N. Raymond, "Promotion by Tetrameric Catechoylamide Ligands and $CaNa_3$-DTPA of the Dissociation *in vitro* of the Pu-Transferrin Complex Formed after Intravenous Injection of Pu-tri-N-Butylphosphate," Health Phys. **49**, 1302 (1985); LBL-22527.
2. C.W. Mays, R.D. Lloyd, C.W. Jones, F.W. Bruenger, G.N. Taylor, P.W. Durbin, D. White, and K.N. Raymond, "Decorporation of Pu and Am from Beagles with Delayed Daily Injections of 3,4,3-LICAM(C) or Zn-DTPA," Health Phys. **50**, 530 (1986); LBL-22529.
3. J.G. Brennan, R.A. Andersen, and J.L. Robbins, "Preparation of the First Carbon Monoxide Complex of Uranium, $(Me_3SiC_5H_4)_3UCO$," J. Am. Chem. Soc. **108**, 335 (1986); LBL-20315.
4. R.A. Andersen, J.M. Boncella, C.J. Burns, J.C. Green, D. Hohl, and N. Rosch, "Electronic Structure of Bis(cyclopentadienyl) Lanthanide Compounds: Photoelectron Spectra and Molecular Orbital Calculations," J. Chem. Soc. Chem. Comm. 405 (1986); LBL-20875.
5. R.A. Andersen, R. Blom, J.M. Boncella, C.J. Burns, A. Haaland, and H.V. Volden, "The Molecular Structures of Bis(Pentamethylcyclopentadienyl)Calcium and -Ytterbium in the Gas Phase: Two Bent Metallocenes," J. Organometall. Chem. **312**, C49 (1986); LBL-21118.
6. S.A. Kinsley, A. Streitwieser, Jr., and A. Zalkin, "Diglyme Adduct of Dipotassium Bis(*tert*-butyl[8]annulene)ytterbate(II)," Acta Crystallogr. **C42**, 1092 (1986); LBL-20478.

7. J.G. Brennan, R.A. Andersen, and A. Zalkin, "The Chemistry of Trivalent Metallocenes: Electron Transfer Reactions; Synthesis and Characterization of $[(MeC_5H_4)_3U]_2E$, E = S, Se, Te and the Crystal Structure of $[(MeC_5H_4)_3U]_2S$ and $(MeC_5H_4)_3U$-$OPPh_3$," Inorg. Chem. **25**, 1761 (1986); LBL-20321.
8. J.G. Brennan, R.A. Andersen, and A. Zalkin, "The Chemistry of Trivalent Metallocenes: Electron Transfer Reaction with Carbon Disulfide; Formation of $[(RC_5H_4)_3U]_2[\mu\text{-}\eta^1,\eta_2\text{-}CS_2]$," Inorg. Chem. **25**, 1756 (1986); LBL-20322.
9. L. Soderholm, N. Edelstein, L.R. Morss, and G.V. Shalimoff, "The Magnetic Behavior of Trivalent Americium Compounds," J. Magn. Magn. Mater. **54–57**, 597 (1986); LBL-20764.
10. H.-D. Amberger, K. Yunlu, and N.M. Edelstein, "The Electronic Structure of Organometallic Complexes of the f Elements—XIV. Quantitative Interpretation of the Luminescence and Magnetochemical Properties of $Cp_3Pr{\cdot}CNC_6H_{11}$," Spectrochim. Acta **42A**, 27 (1986); LBL-21624.
11. P.C. Becker, G.M. Williams, R.E. Russo, N. Edelstein, J.A. Koningstein, L.A. Boatner, and M.M. Abraham, "Resonance Electronic Raman Scattering in Erbium Phosphate Crystals," Opt. Lett. **11**, 282 (1986); LBL-20518.
12. D.B. Beach, K.D. Bomben, N.M. Edelstein, D.C. Eisenberg, W.L. Jolly, R. Shinomoto, and A. Streitwieser, Jr., "An X-Ray Photoelectron Spectroscopic Study of Uranium Compounds," Inorg. Chem. **25**, 1735 (1986); LBL-20164.
13. H.-D. Amberger, H. Schultze, and N.M. Edelstein, "The Electronic Structure of Organometallic Complexes of the f Elements—XVI. Absorption Spectrum and Parameterization of the Crystal Field Splitting Pattern of the Cyclohexylisocyanide Adduct Derived from Tris(η^5-cyclopentadienyl)-Neodymium(III)," Spectrochim. Acta **42A**, 657 (1986); LBL-20168.
14. J.C. Green, R. Shinomoto, and N. Edelstein, "Photoelectron Spectra of Metal Tetrakis(methyltrihydroborates) and Thorium Tetrakis(tetrahydroborate)," Inorg. Chem. **25**, 2718 (1986); LBL-20649.
15. R.A. Moore, Jr., A. Streitwieser, Jr., and H.-K. Wang, "The Phenyl Rotational Barrier in 1,1′-Diphenyluranocene," Organometallics **5**, 1418 (1986); LBL-21586.
16. E.F. Worden, J.G. Conway, and J. Blaise, "Energy Levels of the Second Spectrum of Curium, Cm II," J. Opt. Soc. Am. **B3**, 1092 (1986); LBL-20691.
17. D.H. Templeton and L.K. Templeton, "X-ray Birefringence and Forbidden Reflections in Sodium Bromate," Acta Crystallogr. **A42**, 478 (1986).†
18. A. Zalkin, P.G. Edwards, D. Zhang, and R.A. Andersen, "Bis[1,2-bis(dimethylamino)ethane]tetrachlorouranium(IV)," Acta Crystallogr. **C42**, 1480 (1986); LBL-21301.

Other Publications

19. T.J. Marks and A. Streitwieser, Jr., "Organoactinide Chemistry. Properties of Compounds Having Metal-Carbon Bonds Only to π-Bonded Ligands," in *Chemistry of the Actinide Elements*, J.J. Katz, G. Seaborg, and L.R. Morss, eds., Chapman and Hall, London, 1986, p. 1547; LBL-18919.
20. K.N. Raymond and J. Reedijk, eds. "Selective Recognition and Activation of Small Molecules and Metal Ions in Bioinorganic Chemistry," report from the NATO Workshop held at Noordwijkerhout, The Netherlands, July 15–19, 1985, NATO, Brussels; LBL-22528.‡
21. N.M. Edelstein and J. Goffart, "Magnetic Properties," in *Chemistry of the Actinide Elements*, J.J. Katz, G.T. Seaborg, and L.R. Morss, eds., Chapman and Hall, London, 1986, p. 1361; LBL-14195.
22. J.J. Katz, G.T. Seaborg, and L.R. Morss, eds., *The Chemistry of the Actinide Elements, Second Edition*, Vol. I and II, Chapman and Hall, London, 1986.

LBL Reports

23. T.J. McMurry and K.N. Raymond, "Chelation (Medical Uses of Chelators)," in *1987 McGraw-Hill Yearbook of Science and Technology* (in press); LBL-22526.‡
24. S.F. Haddad and K.N. Raymond, "The Structure and Properties of Tetrakis(tironato)cerate(IV), $Na_{12}[Ce(C_6H_2O_2(SO_3)_2)_4]{\cdot}9H_2O{\cdot}6C_3H_7NO$," Inorg. Chim. Acta (in press); LBL-22456.
25. D.L. White, P.W. Durbin, N. Jeung, and K.N. Raymond, "Specific Sequestering Agents for the Actinides. 13. Initial Biological Testing and Synthesis of Polydentate Hydroxypyridinonate Ligands[1]," submitted to J. Med. Chem.; LBL-21714.
26. P.G. Edwards, R.A. Andersen, and R.W. Gellert, "Preparation of $MCl_4(Me_2ECH_2CH_2EMe_2)_2$ and $MCl_4[(1,2\text{-}Me_2As)_2C_6H_4]_2$ where M is Thorium or Uranium and E is Nitrogen or Phosphorus. Crystal Structure of $UCl_4[(1,2\text{-}Me_2As)_2C_6H_4]_2$," LBL-21473.
27. J.M. Boncella and R.A. Andersen, "Bis(pentamethylcyclopentadienyl)ytterbium (II) as a Lewis Acid and an Electron-Transfer Ligand; Preparation and Crystal Structure of $[Yb(C_5Me_5)_2(\mu\text{-}OC)_2Fe(C_5H_4Me)]_2$," LBL-21982.
28. J.M. Boncella and R.A. Andersen, "Bis(pentamethylcyclopentadienyl)ytterbium (II) as a Lewis Acid and an Electron-Transfer Ligand; Preparation, Crystal Structure, and Solution Dynamics of $[Yb(C_5Me_5)_2(\mu\text{-}OC)_2Mo\text{-}(CO)(C_5H_4R)]_2$," LBL-21983.
29. C.J. Burns, D.J. Berg, and R.A. Andersen, "Preparation and Crystal Structure of the Mixed-Valence [Yb(III,II)] Tetranuclear Complex, $(Me_5C_5)_6Yb_4(\mu\text{-}F)_4$," LBL-22007.

30. C.J. Burns and R.A. Andersen, "Preparation of the First Molecular η^2-Acetylene Complex of a 4f-Transition Metal, $(Me_5C_5)_2Yb(\eta^2\text{-}MeC{\equiv}CMe)$," LBL-22127.
31. C.J. Burns and R.A. Andersen, "Preparation of the First η^2-Olefin Complex of a 4f-Transition Metal, $(Me_5C_5)_2Yb(\mu\text{-}C_2H_4)Pt(PPh_3)_2$," LBL-22245.
32. J.G. Brennan, R.A. Andersen, and A. Zalkin, "Structure of Tris(trimethylsilylcyclopentadienyl)uranium(III), $[(CH_3)_3SiC_5H_4]_3U$," LBL-21180.
33. S. Stults and A. Zalkin, "Structure of Tris(methylcyclopentadienyl)cerium(III)trimethylphosphine, $(CH_3C_5H_4)_3Ce{\cdot}P(CH_3)_3$," Acta Crystallogr. (in press); LBL-21333.
34. A. Zalkin, T.J. Henley, and R.A. Andersen, "Bis(pentamethylcyclopentadienyl)ytterbium(III)-(phenylsulfide)(ammonia), $[(CH_3)_5C_5]_2Yb(SC_6H_5){\cdot}NH_3$," Acta Crystallogr. (in press); LBL-21445.
35. L. Gong, A. Streitwieser, Jr., and A. Zalkin, "Structure of $(\eta^5\text{-}C_5(CH_3)_5)_2LuCl(C_4H_8O)$ and Exchange of Coordinated Solvent," Chem. Comm. (in press); LBL-22427.
36. A. Zalkin, J.G. Brennan, and R.A. Andersen, "Bis(cyclopentadienyl)dibenzylthorium(IV)-[bis(dimethylphosphino)ethane], $(C_5H_5)_2(CH_2C_6H_5)_2Th{\cdot}(CH_3)_2PCH_2CH_2P(CH_3)_2$," Acta Crystallogr. (in press); LBL-22312.
37. A. Zalkin, J.G. Brennan, and R.A. Andersen, "Bis(cyclopentadienyl)dimethylthorium(IV)-[bis(dimethylphosphino)ethane] and Bis(cyclopentadienyl)dichlorothorium(IV)-[bis(dimethylphosphino)ethane], $(C_5H_5)_2(CH_3)_2Th(CH_3)_2PCH_2CH_2P(CH_3)_2$, $(C_5H_5)_2Cl_2Th{\cdot}(CH_3)_2PCH_2CH_2P(CH_3)_2$," Acta. Crystallogr. (in press); LBL-22313.
38. A. Zalkin, J.G. Brennan, and R.A. Andersen, "Bis[tris(cyclopentadienyl)uranium(IV)][1,2-bis(dimethyldiphosphino)ethane], $[(C_5H_5)_3U]_2{\cdot}(CH_3)_2PCH_2CH_2P(CH_3)_2$," submitted to Acta Crystallogr.; LBL-22499.
39. H.-D. Amberger, H. Reddmann, G. Shalimoff, and N. Edelstein, "The Electronic Structure of Organometallic Complexes of the f Elements—XVIII. Parameterization of the Crystal Field Splitting Patterns of Quasi Trigonal Bi-pyramidal Anionic Complexes Involving the Tris(η^5-cyclopentadienyl)uranium(IV) Moiety," LBL-22073.
40. W. Kot, N.M. Edelstein, and A. Zalkin, "Structure and Characterization of $(C_5H_5)_2Zr(H)BH_3CH_3$," Inorg. Chem. (in press); LBL-22223.
41. E. Gamp, R. Shinomoto, N. Edelstein, and B.R. McGarvey, "Multinuclear NMR Spectroscopy of Tetrahedral U(IV) Complex: $U(BH_3CH_3)_4$," submitted to J. Am. Chem. Soc.; LBL-22310.
42. N. Edelstein, "Optical and Magnetic Properties of Tetravalent Actinide Ions and Compounds," in *Proc. 192nd National Meeting ACS*, Anaheim, CA, Sept. 10–11, 1986; to be published in J. Less-Common Metals; LBL-22319.
43. G.T. Seaborg and W. Loveland, "Superheavy Elements," LBL-21812.
44. A. Zalkin, D.H. Templeton, D. Eimerl, and S.P. Velsko, "Trithallium(I) Phosphate, a Second Harmonic Oscillator," Acta Crystallogr. (in press); LBL-21314.[§]
45. L.R. Morss, J. Fuger, J. Goffart, N. Edelstein, and G.V. Shalimoff, "Enthalpy of Formation and Magnetic Susceptibility of Californium Sesquioxide, Cf_2O_3," J. Less-Common Metals (in press); LBL-22710.
46. P.C. Becker (Ph.D. Thesis), "Electronic Raman Scattering in Rare Earth Phosphate Crystals," LBL-22634.

Invited Talks

47. D.H. Templeton, "Anomalous Dispersion Effects," Lyle Jensen Symposium, Department of Biological Structure, University of Washington, Seattle, June 2, 1986.
48. N. Edelstein, "Optical and Magnetic Properties of Tetravalent Actinide Ions and Compounds," Symposium on Solid State Actinide Chemistry and Physics, 192nd National Meeting of the American Chemical Society, Anaheim, CA, Sept. 9–12, 1986.
49. K.N. Raymond, "Template Syntheses of Exchange-Inert Lanthanide Complexes," Rare Earth Research Conference, Hamilton, Ontario, June 8–12, 1986.
50. K.N. Raymond, "Specific Sequestering Agents," Oregon State University, Corvallis, March 3, 1986.
51. R.A. Andersen, "Studies on f-Element Organometallic Compounds," University of California, San Diego, Feb. 28, 1986; University of Minnesota, Minneapolis, April 17, 1986; 3M Company, St. Paul, MN, April 18, 1986; 17th Rare Earth Research Conference, Hamilton, Ontario, June 9–12, 1986; XXIV International Conference on Coordination Chemistry, Athens, Greece, Aug. 24–29, 1986.
52. A. Streitwieser, Jr., "The Discovery of Uranocene and Related Chemistry: Sandwiches, Half-Sandwiches and f-Orbitals," The W.M. Spicer Memorial Lecture in Chemistry, Georgia Institute of Technology, Atlanta, Oct. 9, 1986.

[†]Work supported by the National Science Foundation using facilities provided by the Department of Energy.

[‡]Review articles that also acknowledge partial support for related projects from NIH.

[§]Work supported in part by Lawrence Livermore National Laboratory.

Fossil Energy

Electrode Surface Chemistry*

P.N. Ross, Investigator

INTRODUCTION

The anode material in high-temperature fuel cells is a transition metal (e.g., nickel) stabilized with a ceramic oxide (e.g., chromia). Recently obtained thermodynamic data on intermetallic compounds suggests that at the operating temperature of the solid oxide fuel cell, solid-state reactions should occur between the metal and the ceramic oxide, leading to partial oxide reduction and intermetallic phase formation. The progress of these interfacial reactions is being followed by the use of surface analytical tools like Auger electron spectroscopy and x-ray photoelectron spectroscopy. Preliminary results have shown that the interfacial chemistry occurring during these solid-state reactions is quite complex, with unexpected surface diffusion of reduced oxide moeities over the metal surface far (>100 nm) away from the interface. The influence of the suboxide on the surface of the transition metal on the kinetics of fuel gas (hydrogen and carbon monoxide) electrooxidation is under study.

Our approach to the study of the metal/ceramic interfacial chemistry, and its influence on electrooxidation activity, is to use thin-film geometries as model systems for the real fuel-cell anode. Thin films of ceramic are deposited on metal single crystals and annealed in a hydrogen atmosphere at fuel-cell operating temperatures. Likewise, thin metal films are deposited on single-crystal ceramic materials and annealed in hydrogen. The use of single crystals makes the identification of new phase formation possible by electron-diffraction methods. The metal-on-ceramic systems are studied to determine the reactions occurring and phases forming when the ceramic is in excess, with the opposite being the case for ceramic-on-metal films. These extremes of stoichiometry will simulate the heterogeneous environment of the metal in the ceramic anode of the fuel cell. The interfacial reactions and chemisorption behavior of the surface are studied using an environmental cell coupled to a UHV surface analytical chamber.

*This work was supported by the Assistant Secretary for Fossil Energy, Office of Coal Fuel Cells, Advanced Concepts Division of the U.S. Department of Energy under Contract No. DE-AC03-76SF00098, through the Fuel Cell Project Office, NASA Lewis Research Center, Cleveland, OH 44135.

1. Modifications of the Surface Properties of Metals by Oxide Overlayers: I. Oxidized Zirconium Deposited on the Pt(100) Single-Crystal Surface (Publication 8)

U. Bardi and P.N. Ross

Metallic zirconium was deposited on a Pt(100) single-crystal surface by thermal evaporation under UHV conditions. The deposit was oxidized by exposure to oxygen immediately after deposition. The thickness of oxidized zirconium was varied from submonolayer to multilayer amounts. Annealing the oxide overlayer in UHV at temperatures above 773 K resulted in the dissolution of zirconium into the platinum substrate to form a new oxide phase of indeterminant valency ("ZrO_x"). The coverage of the surface by ZrO_x moieties could be controlled by variation of the annealing temperature and time. The adsorption of carbon monoxide on the surface was studied as a function of the ZrO_x coverage. The results showed that ZrO_x formed inert (towards CO) islands that blocked the underlying platinum from CO chemisorption, but the free platinum surface was unaffected by the presence of the nearby ZrO_x moieties. It was also possible to form a compact ZrO_x layer that completely blocked the platinum surface for the chemisorption of CO.

2. Modifications of the Surface Properties of Metals by Oxide Overlayers: II. Pt Deposited on a Preoxidized Zr(0001) Surface (Publication 9)

U. Bardi and P.N. Ross

Platinum was deposited by thermal evaporation under UHV conditions onto a Zr(0001) single crystal that had been preoxidized by dosing with oxygen at ambient temperature. The variation of the Pt/Zr Auger electron emission as a function of deposition time indicated that the platinum growth mechanism was the Volmer-Weber type (3D clusters). Upon thermal annealing in UHV at temperatures above 773 K, we observed by Auger spectroscopy a reduction in the oxygen content of the surface and the concomitant interdiffusion of platinum and zirconium. The chemical shifts in the $Zr(3p_{3/2})$ photoemission line and the angular dependence of the $Pt(4d_{5/2})$-to-$Zr(3p_{3/2})$ ratio indicated that the interdiffusion resulted in the formation of a surface-alloy

phase. The carbon monoxide thermal-desorption spectra were significantly different from those for a pure platinum surface, which is also indicative of alloy formation.

3. Work in Progress

While platinum electrodes are used with yittria-stabilized zirconia in oxygen sensors, the preferred electrode material for the solid oxide fuel cell is nickel. Although it is not necessarily the case that Ni/ZrO_2 will exhibit similar interfacial chemistry to Pt/ZrO_2, the thermochemistry of the two systems are comparable, particularly in their relatively high exothermic heat of formation of intermetallic phases. Thin films of nickel on zirconia, and vice versa, are being studied in the same manner as done previously with the Pt/ZrO_2 system. In addition, we will be studying changes in surface chemistry of nickel electrodes from prototype solid oxide fuel-cell anodes and using the data from our model thin-film systems to interpret the results.

1986 PUBLICATIONS AND REPORTS

Refereed Journals

1. U. Bardi, D. Dahlgren, and P.N. Ross, "Structure and Chemisorptive Properties of the Pt_3Ti Surface," J. Catal. **100**, 196 (1986); LBL-20004.
2. S. Mehendru, A. Anderson, and P.N. Ross, "CO Adsorption on (111) and (100) Surfaces of the Pt_3Ti Alloy: Evidence for Parallel Binding and Strong Activation of CO," J. Catal. **100**, 210 (1986); LBL-20034.
3. B. Beard and P.N. Ross, "Characterization of a Titanium Promoted Supported Pt Electrocatalyst," J. Electrochem. Soc. **133**, 1839 (1986); LBL-19970.
4. B. Beard and P.N. Ross, "Pt-Ti Alloy Formation from High Temperature Reduction of a Titania Impregnated Pt Catalyst: Implications for SMSI," J. Phys. Chem. **90**, 6811 (1986); LBL-20367.
5. M. Sattler and P.N. Ross, "The Surface Structure of Pt Crystallites Supported on Carbon Black," Ultramicrosc. **20**, 21 (1986); LBL-20873.

Other Publications

6. P.N. Ross, "Improvements in the Utilization of Platinum in Fuel Cells and Batteries," in *Precious Metals 1986*, U.V. Rao, Ed. International Precious Metals Institute, Allentown, PA, 1986, p. 365; LBL-21058.

LBL Reports

7. B. Beard and P.N. Ross, "The Structure and Activity of Pt-Co Alloys as Oxygen Reduction Electrocatalysts," LBL-21184.
8. U. Bardi and P.N. Ross, "Modifications of the Surface Properties of Metals by Oxide Overlayers: I. Oxidized Zirconium Deposited on the Pt(100) Single Crystal Surface," LBL-21772.
9. U. Bardi and P.N. Ross, "Modifications of the Surface Properties of Metals by Oxide Overlayers: II. Pt Deposited on a Preoxidized Zr(0001) Surface," LBL-21773.
10. U. Bardi, B. Beard, and P.N. Ross, "Initial Stages of Oxidation of the $CoPt_4$(111) and (100) Single Crystal Surfaces," LBL-17869.
11. U. Bardi, B. Beard, and P. N. Ross, "Structure and Chemisorptive Properties of the Pt_4Co Alloy Surface," LBL-20004.

Studies of Materials Erosion in Coal Conversion and Utilization Systems*

Alan V. Levy, Investigator

INTRODUCTION

The erosion and erosion-corrosion behaviors of commercial and experimental materials were investigated over a wide range of test conditions that simulated portions of the operating environments in coal gasifiers and fluidized bed combustors. The effects on erosion of systematic variations in the composition and morphology of composites containing hard particles in a softer, more ductile matrix were determined. Experimental materials, including an intermetallic compound structural alloy and a fiber-vapor deposited matrix composite, were tested to determine their erosion behavior. Elevated temperature combined erosion-corrosion tests using a wide range of test variables and target alloy steels were conducted to determine the interrelationships between the materials' corrosion behavior and the test conditions. The erosion-corrosion products and metal loss rates of alloy steels exposed for 9000–10,000 hours in a fluidized bed combustor were determined, as was the erosivity of particles of bed material.

1. The Erosion of Carbide-Metal Composites (Publication 15)

A.J. Ninham and A.V. Levy

A number of materials composed of carbide particles in a ductile metal binder have been eroded to determine the role of carbides in the erosion mechanism. The alloys covered two ranges of carbide volume fraction: less than 30 vol% (spheroidized plain-carbon steels and cast high carbon alloys), and greater than 60 vol% (cermets). All specimens were eroded by quartz abrasive at a range of impact angles and at 60 ms^{-1} in a nozzle type tester. In addition to mass loss data and examination of eroded surfaces to characterize the erosion behavior, specimens were taper sectioned and then examined by scanning electron microscopy. This technique allows simultaneous observation of an eroded surface and the underlying microstructure, facilitating the determination of erosion mechanisms.

For the low carbide content alloys the presence of the carbides increased the rate of erosion. The carbides disrupted plastic flow around the impact site causing void formation and carbide fracture, which, in turn, caused extreme localization of plastic flow with subsequent easy material removal. At carbide fractions of about 70 vol% some cermets eroded at rates comparable to those of plain carbon steels.

Only the highest carbide content cermets exhibited decreased erosion rates as the carbide volume fraction was increased. For these alloys the carbide content is so high that the carbides are in contact and support each other, with a diminishing reliance on the softer matrix for support. Carbide fractions of about 90 vol% were needed in most cases to effect a significant improvement in erosion resistance.

2. Effect of Test Variables on the Erosion-Corrosion of Chromium Steel (Publication 17)

A.V. Levy and Y.-F. Man

There are several different, potentially erosive particles in the operating environments of coal conversion and utilization equipment. They include coal, char, ash, various minerals, and the corrosion scales that form and spall off the surfaces of the equipment. Each type of particle has a different erosivity at different conditions. The purpose of this study was to determine the effect of particle variables on the elevated temperature erosion-corrosion of 9Cr-1Mo steel. It was determined that angular-shaped particles remove oxide scale as it forms and directly erodes the base metal at fast rates. The erosion rate caused by angular particles increases with their size. Rounded particles permit a continuous, somewhat protective oxide scale to form on the metal surface, which is eroded at much slower rates.

3. The Erosion-Corrosion of Scales on Heat Exchanger Alloys (Publication 18)

A.V. Levy and N. Jee

A number of in-bed tube sections of five different steel alloys that had been exposed in the Point Tupper atmospheric fluidized bed combustor

*This work was supported by the U.S. Department of Energy under DOE/FE AA 15 10 10 0, Advanced Research and Technical Development, Fossil Energy Materials Program, Work Breakdown Structure Element LBL-3 and under Contract No. DE-AC03-76SF00098.

(AFBC) by the Canada Center for Mineral and Energy Technology (CANMET) were metallographically analyzed. The tubes had been exposed at temperatures from 450° to 850°C for time periods from 1000 to 10,000 hours. It was determined that, generally, more metal was lost from the bottom outer surfaces of the tubes than from the tops as the result of two different scale loss mechanisms. The scale loss mechanisms were related to the different impact angles and velocities of the particles that struck the top and bottom surfaces of the tubes. The presence of AFBC bed material on and in the scales modified the scale loss behavior and, in the instance of at least one of the alloys, the 9Cr-1Mo steel, appeared to provide some protection.

4. Work in Progress

Erosion-Corrosion of Scales on Alloy Steels (B. Wang)

Several commercial, special-application steels that had compositions that were different from those commonly used in combustion process heat exchanger piping were eroded-corroded. The purpose was to determine whether corrosive scales on lower-alloy steels could provide some protection to the base metal as the result of the nature of their growth and erosion characteristics.

It was determined that a steel containing 5% chromium lost sound metal at a rate one-half to one-quarter the rate of a steel containing 20% Cr, the difference becoming greater with increasing particle impact velocity. The reason for the better performance by the lower chromium content steel relates to the morphologies and resultant behavior of the scales on the two alloys. The 5% Cr steel formed a segmented scale that cracked and chipped pieces from the surface at a relatively low loss rate. The 20% Cr steel formed a continuous scale that spalled at a higher loss rate. This behavior was observed in earlier erosion-corrosion work on steels and formed the basis for the current effort. Other alloys are under investigation to determine whether steels can be selected for use in elevated-temperature erosion-corrosion environments based on the mechanisms of formation and degradation of their scales.

Erosivity of FBC Bed Material (Z.R. Shui)

The erosivity of bed material from the Point Tupper, Nova Scotia, fluidized bed combustor was determined. The bed material was in the form of angular-shaped particles of mixed oxides and sulfides plus carbon. Elevated temperature tests were carried out on several steels, and the results were compared to their erosion rates using single-composition erodents such as SiO_2, SiC, or Al_2O_3. It was determined that the bed material was twice as erosive as angular shaped SiC particles and over ten times as erosive as rounded-shape Al_2O_3 particles.

The range of compositions of the bed-material particles promoted corrosion of the target materials in addition to combined erosion-corrosion, thus enhancing the overall destructive ability of the particles. Additional work is under way to determine how the more reactive bed material particles, compared to single compound erodents, enhance material loss rates.

Erosion of Solid Solution Strengthened Alloys (A.J. Ninham)

The erosion of solid solution strengthened alloys is being investigated. The only evidence in the literature that the erosion resistance of structural alloys can be increased by increasing the strength/hardness of a ductile metal alloy is for solid solution strengthened alloys. A series of iron-aluminum alloys containing up to 20% Al were prepared and erosion tested. It was determined that there was a general decrease in erosion rate as the aluminum percentage in the solid-solution alloy increased. However, the reduction was not consistent or even progressive. More work will be carried out using Fe-Mo and Fe-Zr solid solution strengthened alloy systems.

Elevated-Temperature Erosion of Thermal and Strain Hardened Alloys (B. Wang)

The effect of strenthening alloys by cold working and by thermal precipitation hardening processes on their elevated temperature erosion resistance was determined as part of an effort to determine what improvements could be made in the erosion resistance of ductile metal alloys. As had been observed at room temperature in earlier work, the strengthened alloys had essentially the same erosion behavior at 400° and 800°C in their cold worked or precipitation hardened states as in their annealed condition. Thus, no correlation has been made between the strength/hardness of structural alloys and their erosion behavior. They all erode by a severe plastic deformation mechanism that overcomes the effects of small lattice deformation strengthening mechanisms.

Erosion of Experimental ORNL Alloys (Z.R. Shui)

The erosion of two materials developed at the Oak Ridge National Laboratory was determined at elevated temperatures and related to their tensile strength at elevated temperatures. One material was a modified 9Cr-1Mo steel and the other a Ni_3Al-HF-B. The objective of the tests was to determine whether the erosion rate began to increase rapidly at the temperature at which their tensile strength began to decrease faster with temperature, as was observed for several chromium containing steels tested earlier.

The previously observed pattern of behavior did not occur. Rather, the erosion rate increased rapidly from about 200°C to 500°C, after which it began to decrease with increasing test temperature. The tensile strength curve increased its downward slope near 400°C. The Ni_3Al material behaved in a similar manner. The erosion rate at 800°C was less than the room-temperature rate. Thus, additional evidence was obtained that the erosion process cannot be related to normal strain rate mechanical properties. The surface morphology of the eroded Ni_3Al at three test temperatures indicated that there was no obvious difference in the nature of the eroding surface. All three surfaces had the appearance of a ductile material that was forming and losing platelets of material. This is further proof of the ductile nature of the Ni_3Al material.

1986 PUBLICATIONS AND REPORTS

Refereed Journals

1. A.V. Levy, "The Platelet Mechanism of Erosion of Ductile Metals," Wear **108**, 1 (1986); LBL-15240.
2. A.V. Levy, M. Aghazadeh, and G. Hickey, "The Effect of Test Variables on the Platelet Mechanism of Erosion," Wear **108**, 23 (1986); LBL-17835.
3. A.V. Levy, J. Yan, and J. Patterson, "Elevated Temperature Erosion of Steels," Wear **108**, 43 (1986); LBL-18256.
4. A.V. Levy and G. Hickey, "Erosion of Corrosion-Resistant Surface Treatments on Alloy Steels," Wear **108**, 61 (1986); LBL-18255.
5. A.G. Davis, D.H. Boone, and A.V. Levy, "Erosion of Ceramic Thermal Barrier Coatings," Wear **110**, 101 (1986); LBL-15667.
6. A.V. Levy, E. Slamovich, and N. Jee, "Elevated Temperature Combined Erosion-Corrosion of Steels," Wear **110**, 117 (1986); LBL-19156.
7. A.V. Levy and Y.-F. Man, "Elevated Temperature Erosion-Corrosion of 9Cr-1Mo Steel," Wear **111**, 135 (1986); LBL-17991.
8. A.V. Levy and Y.-F. Man, "The Effect of Temperature on the Erosion-Corrosion of 9Cr-1Mo Steel," Wear **111**, 161 (1986); LBL-18641.
9. A.V. Levy and Y.-F. Man, "Surface Degradation of Ductile Metals in Elevated Temperature Gas-Particle Streams," Wear **111**, 173 (1986); LBL-18686.

Other Publications

10. I. Hutchings and A.V. Levy, "The Mechanism of Erosion of Ductile Metals," in *Proc. NACE Conf. Erosion-Corrosion-Wear of Materials at Elevated Temperatures*, Berkeley, CA, Jan. 1986, A. Levy, Ed., NACE, Houston, TX, 1986.
11. A. Levy and Y.-F. Man, "Erosion-Corrosion of Chromium Steels," in *Proc. NACE Conf. Erosion-Corrosion-Wear of Materials at Elevated Temperatures*, Berkeley, CA, Jan. 1986, A. Levy, Ed., NACE, Houston, TX, 1986.
12. A.V. Levy, "The Effect of Material Properties on Erosion Behavior," in *Proc. Earl R. Parker Symp. Structure-Property Relations*, AIME Annual Meeting, New Orleans, LA, March 1986, S. Antolovitch, R. Ritchie, and W. Gerberich, eds., TMS, Waverdale, PA, 1986.
13. A.V. Levy and Y.-F. Man, "Erosion-Corrosion Mechanisms in Fe-Cr Steels," Reprint, in *Proc. NACE Conf. Erosion-Corrosion-Wear of Materials at Elevated Temperatures*, Berkeley, CA, Jan. 1986, A. Levy, Ed., NACE, Houston, TX, 1986.
14. A.V. Levy and D. Gurney, "Materials Considerations in Coal Burning Diesel Engines," in *Proc. ASM Symp. on Coal Burning Engines*, ASM Materials Week, Orlando, FL, Oct. 1986.

LBL Reports

15. A.J. Ninham and A.V. Levy, "The Erosion of Carbide-Metal Composites," LBL-22822.
16. A.J. Ninham, "The Effect of Mechanical Properties on Erosion," LBL-22823.
17. A.V. Levy and Y.-F. Man, "Effect of Test Variables on the Erosion-Corrosion of Chromium Steel," LBL-22824.
18. A.V. Levy and N. Jee, "The Erosion-Corrosion of Scales on Heat Exchanger Alloys," LBL-22825.
19. A.V. Levy, N. Jee, L. Sun, and Z.R. Shui, "Analysis of Scales Formed on AFBC Tubes," LBL-22518.

Invited Talks

20. A.V. Levy and B. Wang, "Effect of Testing Variables on the Solid Particle Erosion of Hard Coatings," General Coating Symposium, ASM Materials Week, Orlando, FL, Oct. 1986.
21. B. Wang and A.V. Levy, "The Embedment of Erodent Particles in Hard Coatings," AIME Fall Meeting, Orlando, FL, Oct. 1986.

22. A.V. Levy, "The Erosion of Metals and Ceramics," Seminar, Southern Florida University, Tampa, FL, Oct. 1986.
23. A.V. Levy, "The Erosion and Wear of Ceramic Materials," The Norton Co., Worcester, MA, Sept. 1986.
24. A.V. Levy, "Wear at Elevated Temperatures," ASM Golden Gate Chapter, Berkeley, CA, May 1986.
25. A.V. Levy, "Wear at Elevated Temperatures—Part II," ASM Golden Gate Chapter, Berkeley, CA, Sept. 1986.

Catalytic Gasification of Graphite or Carbon*

Heinz Heinemann, Investigator, with G.A. Somorjai, Investigator, and J. Carrazza

INTRODUCTION

The gasification of carbon solids with steam provides a route to hydrogen and syngas production. Thermodynamic considerations indicate that this process is feasible at temperatures as low as 300 K. In this range CH_4 and CO_2 would be the expected products, according to equation 1:

$$2C + 2\,H_2O \rightarrow CH_4 + CO_2\,, \qquad (1)$$

while at higher temperatures the production of H_2 and CO_2 and then H_2 and CO become more favorable (equations 2 and 3):

$$C + 2\,H_2O \rightarrow 2\,H_2 + CO_2\,, \qquad (2)$$

$$C + H_2O \rightarrow H_2 + CO\,. \qquad (3)$$

Since kinetic barriers are an important constraint for the process, several catalysts have been proposed in the literature to reduce the temperature necessary to run this reaction. Alkaline and alkaline-earth hydroxides, carbonates, and oxides have been, so far, the catalysts more widely studied. They are active at temperatures of about 1000 K and higher and their activity remains constant up to high carbon conversions. Use of these compounds, however, presents various problems. Large amounts of catalyst are necessary (>10% loadings); and in the case of gasification of coals and chars, they become very difficult to recover, due to their compound formation with ash components. Transition metals, in particular iron and nickel, have also been suggested as catalysts for this process, because they are active at temperatures much lower than the alkali (600 K); however, they deactivate very rapidly, due to carbon encapsulation in the case of graphite gasification and interaction with ash and sulfur compounds.

Our earlier work reported that mixtures of potassium and nickel kept most of the desirable properties of the components alone; i.e., activity at relatively low temperatures (600 K) and low deactivation rates. It was shown that a cooperative effect between the two components was responsible for these characteristics, and it was suggested that a potassium-nickel mixed oxide was the active catalyst. The present report includes more recent studies on the graphite gasification with steam using this type of catalyst and extends the work to char gasification. The results on char gasification show that the nickel-potassium mixed oxide is more active than any of the components deposited alone.

*This work was supported by the Assistant Secretary of Fossil Energy, Office of Management, Planning, and Technical Coordination, Technical Coordination Division of the U.S. Department of Energy under Contract No. DE-AC03-76SF00098, through the Morgantown Energy Technology Center, Morgantown, WV 26505.

1. Steam Gasification of Graphite (Publication 2)

J. Carrazza, G.A. Somorjai, and H. Heinemann

Figure 1-1 shows that mixtures of alkalis (Na or K) and nickel are more active for steam gasification of graphite than mixtures of alkaline earths (Ca or Mg) and nickel. The activation energy also depends on the cation, and in the case of sodium and calcium

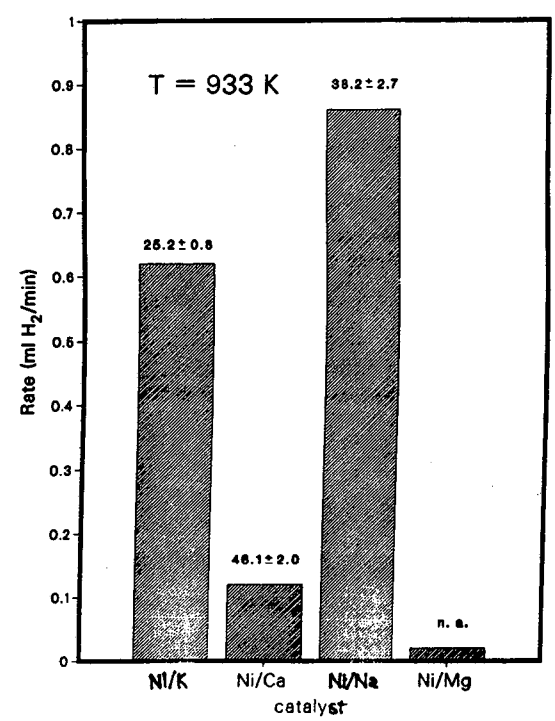

Figure 1-1. Rate of steam gasification of graphite catalyzed by four mixtures of alkali or alkaline earth oxides and nickel oxide. The numbers above each bar are the activation energies for the respective catalyst. The molar ratio of alkali or alkaline earth cation to nickel is equal to 1.0, and the molar ratio of nickel to carbon is 1×10^{-2}. (XBL 874-1616)

the values are very different from the one reported for nickel alone. In all four cases it is clear that there is an interaction between the transition metal and the group IIa or IIb cation. This conclusion is also derived from the catalytic behavior of these compounds as a function of time. While nickel deposited alone on graphite shows a very high rate of gasification that goes to zero after a few hours, a mixture of potassium and nickel maintains its initial activity for a period of six hours, even though its value is lower than the initial one for nickel alone.

For the nickel-potassium catalyst the rate is proportional to the catalyst loading up to a catalyst-to-carbon molar ratio of 2×10^{-2}; at higher loadings the rate goes down by 20%. When the ratio of nickel to potassium was changed at a constant nickel loading, a maximum in activity was observed at a molar ratio of Ni/K equal to 2.0 (nickel molar ratio X_{Ni} = 0.67). At higher Ni/K molar ratios a constant rate of gasification with time was generally observed. In contrast to the case of nickel deposited alone, the catalyst in those experiments did not deactivate completely, and after a few hours it kept an activity level similar to that of experiments where the ratio of nickel to potassium was the same but the initial burst did not occur. This initial burst was never seen when the Ni/K ratio was less or equal than 1.0, and it always occurred at higher ratios. Sample preparation was the same in all cases.

2. Steam Gasification of Chars (Publication 2)

J. Carrazza, G.A. Somorjai, and H. Heinemann

The steam gasification of four chars has been studied using nickel and potassium oxides as catalysts deposited together or by themselves. In all the experiments the potassium loading in the sample was 2.7 wt% and the nickel loading was 4.1 wt%.

Figure 2-1 shows that the activity of the nickel-potassium catalyst for steam gasification of Illinois #6 char (curve A) is much higher than the mathematical sum of the rates of the components deposited alone (sum of curves B and C), indicating again the existence of a cooperative effect between the two oxides.

Figure 2-1 also shows a different behavior for the nickel and the nickel-potassium catalysts on the gasification of Illinois #6 char and graphite. For the nickel-potassium catalyst, the initial rate of gasification of this char is 200 times higher than that of graphite, and even though the catalyst deactivates, after 6 hours the rate is still 10 times higher. In contrast

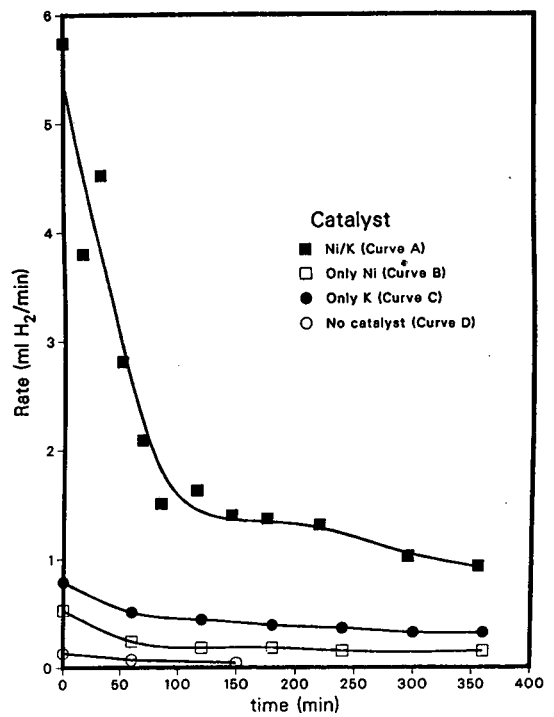

Figure 2-1. Rate of steam gasification of Illinois #6 char as a function of time for three different catalysts and for the uncatalyzed reaction. (XBL 874-1617)

with the nickel-potassium catalyst, nickel deposited alone is almost inactive for the gasification of this char, while its initial rate of gasification of graphite is extremely high. Carbon conversions obtained from integration of curves A and B in Figure 2-1 show that after 6 hours the nickel-potassium catalyst gives 34% conversion while nickel alone only gasified 3% of the carbon.

The carbon conversions obtained for four different chars and graphite using a potassium nickel catalyst are summarized in Figure 2-2. As was already mentioned for the case of Illinois #6, the carbon conversions for all four chars after 6 hours are at least 20 times higher than that of graphite. In the Illinois #6 and Montana chars, the carbon conversions measured by hydrogen production or by weight loss agree very well, indicating that the carbon is indeed gasified by reaction with water. In the case of Western Kentucky and North Dakota chars, the conversions determined by hydrogen production are higher than those measured by weight loss. This suggests that in addition to the reaction between carbon and water, the nickel-potassium mixture also probably catalyzes hydrogen production by breaking hydrogen-carbon bonds already present in the char.

The results presented clearly show that mixtures of nickel and potassium have catalytic properties for

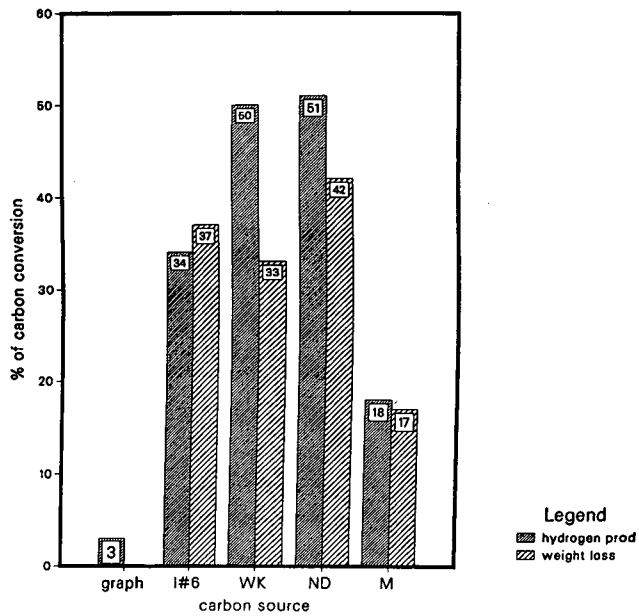

Figure 2-2. Percentage of carbon conversion after 6 hours for five different carbon sources when the reaction is catalyzed by a mixture of potassium and nickel. The carbon conversions were determined by two different methods, total hydrogen production and carbon weight loss. (XBL 874-1618)

the steam gasification of graphite or char that neither of the components alone possess. These mixtures show a higher activity than potassium hydroxide and a higher resistance to poisoning than nickel metal.

Figure 2-1 also shows that the nickel-potassium oxide activity for char gasification decreases as a function of time. An aqua regia pretreatment of the char removes the cause of the deactivation. At this point not enough results are available to further comment on the problem, but both kinetic and surface-science studies of the system will be done to obtain more information.

3. Controlled-Atmosphere Electric Macroscopy (CAEM) (Publication 2)

J. Carrazza, T.R. Baker, G.A. Somorjai, and H. Heinemann

This part of the work was performed in collaboration with Dr. R.T.K. Baker of Exxon Research & Engineering Co. The use of the Exxon instruments by LBL scientists under Dr. Baker's supervision and with his advice is appreciated.

Nickel and potassium were introduced onto single-crystal graphite transmission specimens as an atomized spray for a 0.1% aqueous solution containing a 50:50 mixture of nickel nitrate and potassium hydroxide. Conditions of spraying were selected so that upon subsequent decomposition of the precursor molecules, a mixed nickel-potassium coverage equivalent to two monolayers was obtained. Prior to reaction in a gasifying environment, the system was heated in argon at 723 K for 0.5 h in order to achieve good nucleation of nickel-potassium particles, which on average grew to 15 nm in diameter.

When the nickel-potassium/graphite was treated in a steam environment, particles located on the graphite edge regions started to undergo a transformation at temperatures between 748 K and 786 K from a nonwetting to a wetting condition and eventually disappeared due to a spreading action of material along the edge sites. On continued heating to 828 K, these regions started to erode, giving the initially uniform edges a very ragged appearance. Edge recession became more ordered as the temperature was gradually raised to 948 K, and from reference to the position of twin bands it was possible to determine that the recession was taking place in directions parallel to the <1120> crystallographic orientation of the graphite structure. The rate of edge recession continued to increase as the temperature was raised from 948 K to 1373 K. It was interesting to find that, compared to the behavior of nickel and potassium under similar conditions, the nickel-potassium catalyst did not exhibit any evidence of widespread deactivation. However, at 1228 K it was occasionally found that edge recession ceased as particles reformed and proceeded to create channels. This phenomenon may have been caused by a change in the wetting characteristics of the catalyst with graphite brought about by buildup of the hydrogen product in the gas phase.

Detailed quantitative kinetic analysis of many edge-recession sequences showed that the rates of gasification in steam were independent of the pretreatment process, and from the slope of an Arrhenius plot it has been possible to derive a value of 30.9 ± 3 kcal mole^{-1} for the apparent activation energy of the nickel-potassium/graphite steam reaction. It is interesting to find that this figure is close to those found for the influence of nickel and potassium of 33.8 ± 4 kcal mole^{-1} and 35.0 ± 4 kcal mole^{-1}, respectively. Comparison of the intrinsic activities of the three systems shows that the mixed catalyst is marginally higher than nickel, but much lower than potassium, when reacted under similar conditions. However, the activity of the mixed catalyst is maintained to higher temperatures than is possible with either of the single components. It is possible that the addition of potassium to nickel

prevents the formation of a graphite overlayer, which has been suggested as a possible reason for the deactivation of nickel in the graphite-steam reaction.

1986 PUBLICATIONS AND REPORTS

Other Publications

1. J. Carrazza, G.A. Somorjai, and H. Heinemann, in Am. Chem. Soc., Div. of Fuel Chem., Preprints **31**, 158 (1986).

LBL Reports

2. H. Heinemann, "Catalytic Gasification of Chars and Carbon," LBL-22196; LBL-22682.

Invited Talks

3. H. Heinemann, Morgantown Energy Technology Center, Morgantown, WV, June 1986.
4. H. Heinemann, American Chemical Society Meeting, Anaheim, CA, Oct. 1986.

Energy Storage Systems

ELECTROCHEMICAL ENERGY STORAGE

Lutgard C. DeJonghe, James W. Evans, Rolf H. Muller,
John Newman, Philip N. Ross, Jr., and Charles W. Tobias, Investigators

Surface Morphology of Metals in Electrodeposition*

Charles W. Tobias, Investigator

INTRODUCTION

The objective of this project is to gain understanding of the partial processes and their interactions involved in the deposition and dissolution of metals by electrolysis. Of particular interest is the influence of hydrodynamic flow on electrocrystallization, and the distribution of charge-transfer rates on advancing and receding metal profiles, as determined by the electric and concentration fields in the solution, and by the kinetics of the charge-transfer reaction. Control of the morphology of metallic deposits has been traditionally effected by addition agents that interfere with the crystallization process. In energy-storage applications, however, other means may have to be employed for the control of morphology.

- Rotating-disk electrodes and planar electrodes in channel-type electrolyzers are used for the preparation of metal deposits, over large ranges of solution properties and hydrodynamic conditions, with potentiostatic or galvanostatic control. The genesis of surface textures is studied, using *in situ* motion-picture microphotography, video recording, and *post mortem* examination by electron microscopy.
- Developing surface contours are simulated by solving the Laplace equation, using either the finite-difference, finite-element, or boundary-element method.

*This work was supported by the Assistant Secretary of Conservation and Renewable Energy, Office of Energy Storage and Distribution of the U.S. Department of Energy under Contract No. DE-AC03-76SF00098.

1. Current Distribution in Electrochemical Cells with Passivating Kinetics (Publication 5)

J.O. Dukovic and C.W. Tobias

Numerical Evaluation

A numerical model is developed for the evaluation of current distribution in electrochemical systems that exhibit passivity. The boundary-element model, based on potential theory, employs a detailed fit of the active-passive polarization curve as the anode boundary condition. The model is used to investigate the steady-state behavior of active-passive systems with nonuniform current density, in particular the condition of coexisting active and passive regions on the anode surface. Calculations are performed for a test cell of high aspect ratio using overpotential data determined on Nickel-200 in 2M H_2SO_4, 0.5M $NiSO_4$ solution. The results are compared to the predictions of simple, one-dimensional models reported in the literature. Application of the model to anodic protection is demonstrated in a series of calculations for a stainless steel sulfuric acid holding tank.

Experimental Determination

An experimental study of current distribution in passivating systems is presented with special attention to the steady-state coexistence of active and passive regions on the anode surface. Current-density profiles were measured by weight loss on a segmented rotating-cylinder anode of nickel in acid nickel sulfate electrolyte, with the cathode placed so as to produce a highly nonuniform potential field. Independent measurements of the steady-state, anodic current-overpotential characteristic were made on rotating-disk and rotating-cylinder electrodes. The measured current-density profiles were compared to predictions from a theoretical model developed for this purpose. The agreement is generally satisfactory, but the measured length of the passive zone exceeds the predicted value, implying that the model would supply a conservative estimate of throwing power in anodic protection.

2. Simulation of Leveling in Electrodeposition (Publication 5)

J.O. Dukovic and C.W. Tobias

A numerical model is developed for simulating the evolution of electrode microprofiles with deposition in the presence of a diffusion-controlled leveling agent. Current distribution is calculated by potential theory, and the electrode boundary is adjusted according to Faraday's law at each forward-Euler time step. The dependence of cathodic current density on surface overpotential and leveling-agent flux is expressed as an interpolation of electrode-kinetic data measured at several well-defined conditions of mass transfer. The agent-flux distribution is solved at each time step assuming steady-state diffusion within a concentration boundary layer. Both fields (potential and agent-concentration) are solved by quadratic boundary elements, and the boundary is advanced by a flexible algorithm. Application of the model is demonstrated (Figure 2-1) in an example with coumarin in a Watts nickel bath: published polarization data are employed, and predicted leveling performance is compared to profilometric measurements reported in the same study.

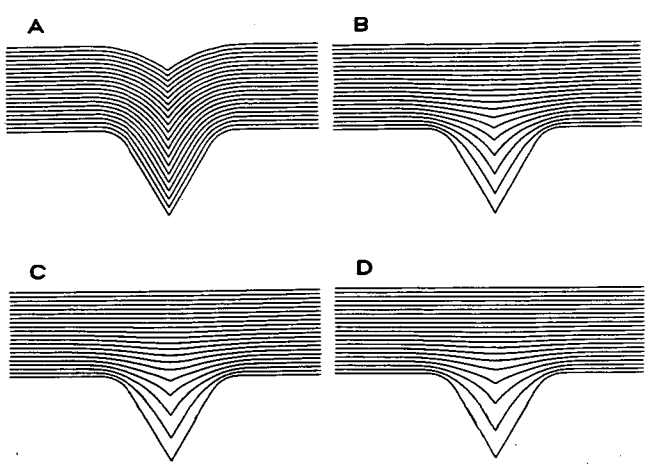

Figure 2-1. Simulated leveling of a triangular groove in a Watts-nickel bath with coumarin. Average current density: 10 mA/cm^2. A: no coumarin present. For B, C, and D, bulk concentration of coumarin: 0.86 mM. Electrode is a disk rotating at 150, 360, and 900 rpm, respectively. (XBL 873-1125)

3. The Development of a Micropatterned Electrode for Studies of Zinc Electrodeposition (Publication 11)

D.P. Sutija, R.H. Muller, and C.W. Tobias

A common feature of electrodeposited zinc is the emergence of ridges and valleys aligned in the direction of applied convective flow. These features, called striations, are the preferred loci for the initiation of dendrites, a major failure mechanism in rechargeable zinc-halide battery systems. To understand how striations result from micron-sized zinc growth centers that emerge during the nucleation process, a micropatterned electrode was designed and fabricated by processes commonly used in the manufacture of semiconductor devices. The micropatterned electrode has hemispherical protrusions, five microns in diameter, on an otherwise optically smooth surface. By controlling the orientation and separation of such protrusions, the experimenter may study the interaction of growth centers and the emergence of striations.

A series of voltammetric zinc-deposition studies was undertaken to determine the material best suited for use as a permanent electrode substrate. Gold was determined to possess the best combination of material properties: chemical inertness, low melting point, and a high work function allowing underpotential deposition of zinc, which mitigates the rate of hydrogen evolution.

Metals Couples in Non-Aqueous Electrolytes

Charles W. Tobias, Investigator

INTRODUCTION

The objective of this project is to explore practical alternatives to high-temperature molten-salt systems, for the efficient electrochemical reduction and oxidation of reactive metals. Recent developments in advanced primary cells and projected high-energy rechargeable battery systems involve the use of alkali-metal negatives. To expand the possibilities for application of reactive metals at near-ambient temperatures, new ionizing media must be sought that have high decomposition potentials and are capable of dissolving ionic compounds. The propylene carbonate (PC) family of solvents has been demonstrated in this laboratory to allow the reduction of alkali metals, at room temperature, with reasonably high efficiency. However, solvent stability in the presence of reactive metals remains a critical issue, especially so in the case of rechargeable galvanic-cell applications. Current work includes the exploration of the reduction of magnesium, the study of viable reactions for the positive electrode, and investigation of the role of co-solvents in improving stability, solubility, and conductivity. A related project, under the direction of Dr. R.H. Muller, is concerned with the chemical nature of surface films on alkali metals in propylene carbonate electrolytes.

1. Electrochemical Reduction of Potassium from Potassium Chloride in Propylene Carbonate Electrolyte with Aluminium Anodes (Publication 1)

R.T. Atanasoski, H.H. Law, and C.W. Tobias

Potassium has been cathodically deposited in a propylene carbonate electrolyte with concurrent dissolution of aluminium. Starting with an $AlCl_3$-free electrolyte, changes in the composition and conductivity of the electrolyte, as well as those of the electrode potentials, were measured as a function of charge passed. Anodic and cathodic current efficiencies were both close to 100%. The observed behavior is consistent with the overall reaction stoichiometry:

$$Al + 3KCl \rightarrow 3K + AlCl_3 .$$

This reaction and its analogues for other alkali metals may conceivably form the basis of practical processes at ambient temperatures for the recovery of alkali metals from their chlorides with concurrent production of aluminium chloride.

2. Electrochemical Analysis of Trace Amounts of Water in Propylene Carbonate Electrolytes (Publication 9)

R.T. Atanasoski, H.H. Law, R.C. McIntosh, and C.W. Tobias

Cyclic voltammetry and limiting currents to a rotating-disk electrode have been used for the determination of the water in the 0.3 to 20 ppm range in PC electrolytes. Carefully dried solutions yielded voltammetric peaks proportional to the amount of water added. In KPF_6 electrolytes, the cathodic current corresponding to the reduction of water was at 0.48 V, while in $KAlCl_4$ solutions the reduction occurred already starting at 2.8 V, both relative to a K/K^+ reference. At these potentials, the current to a rotating-disk electrode showed Levich-type dependence on rpm and was proportional to the concentration of water in the range of 0.5 to 20 ppm. The calculated diffusion coefficients of water are higher than expected: at 25°C, $D_{H_2O} = 8.5 \pm 2 \times 10^{-6}$ cm^2/s in 0.5M KPF_6, while $D_{H_2O} = 10 \pm 2 \times 10^{-6}$ cm^2/s in 0.25M $KAlCl_4$.

3. Electrochemistry of Iodide in Propylene Carbonate. I. Cyclic Voltammetry Monitored by Optical Spectroscopy. II. Theoretical Model (Publications 7 and 8)

K.J. Hanson, M.J. Matlosz, J. Newman, and C.W. Tobias

The electrochemistry of iodide in PC was investigated using cyclic voltammetry. In an anodic sweep, iodide is oxidized sequentially to triiodide and then to iodine according to

$$3I^- \rightarrow I_3^- + 2e^-, \quad (1)$$

$$2I_3^- \rightarrow 3I_2 + 2e^-, \quad (2)$$

where reaction 1 is rate-limited (Butler-Volmer kinetics) and reaction 2 is reversible (Nernst equilibrium behavior). This mechanism was conformed using UV visible spectroscopy in conjunction with cyclic-voltammetry experiments at a thin gold mesh electrode. Potential-step experiments were used to measure a diffusion coefficient of 4×10^{-6} for iodine in a $KAsF_6$/PC electrolyte.

An algorithm based on Duhamel's superposition integral is used to simulate the voltammograms. Since the nonunity stoichiometries and Butler-Volmer kinetics in the reaction sequence inhibit the use of analytical solution techniques, the superposition-integral algorithm is used as a fast and accurate method for the numerical simulation. The simulated voltammograms for the iodide system agree very well with experimental observations and support the proposed reaction sequence (Figure 3-1).

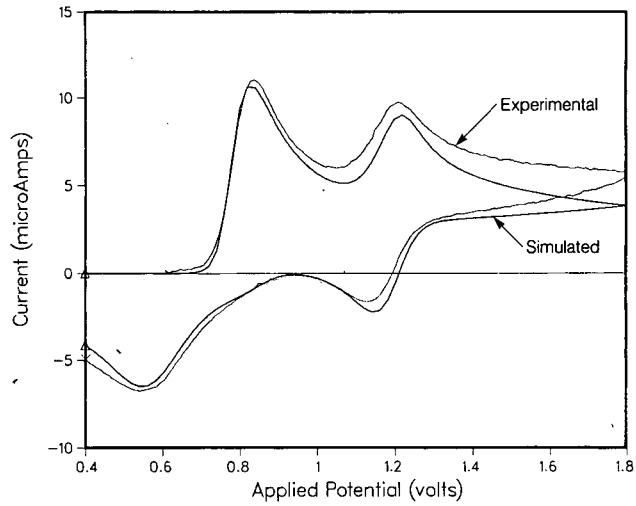

Figure 3-1. Electrochemical behavior of iodide/iodine in propylene carbonate. Comparison of model voltammograms to experimental results. Potentials are relative to saturated TlI/saturated Tl(Hg) reference electrode. (XBL 847-7739)

Engineering Analysis of Electrolytic Gas Evolution

Charles W. Tobias, Investigator

INTRODUCTION

Electrolytic gas evolution is among the most common reaction types in electrolysis and in advanced rechargeable batteries. Modern applications in energy storage and transmission (e.g., hydrogen) require much higher energy efficiency and lower capital cost than achieved in gas-generating processes in the past. This project is directed toward the quantitative description of partial processes and their interactions involved in the nucleation, coalescence, and detachment of gas bubbles. Of special interest are the effects of moving individual bubbles and of gas-electrolyte emulsions on ohmic-cell resistance and on mass transport of charged and uncharged species to and from electrode surfaces. A thorough understanding of the physical processes involved in the liberation and movement of gases at electrodes and in the electrolyte should lead to improved energy efficiency and lower capital costs in process and device technology.

1. The Limiting-Current Technique at a Sectioned Electrode for the Study of Buoyancy-Induced Convection (Publication 3)

G.M. Whitney and C.W. Tobias

The use of a micromosaic electrode with an electrochemical redox system has been demonstrated in a study of the Benard-Rayleigh problem of onset of convection in a fluid with a time-dependent density profile contained in a deep cell. The electrochemical technique offers several advantages over thermal techniques, the most important one being the precise control of the surface condition. The well-controlled experiment lends itself to a thorough analysis of the time-dependent base state, the case of diffusion and migration into a semi-infinite column of electrolyte. In addition, the electrode serves as the monitoring device, allowing a precise detection of the onset of convection, the criterion for which is a percentage deviation of the Sherwood number (current) from base-state behavior.

The critical Rayleigh number Ra_1 for the problem of onset of convection at a rigid, conducting boundary, due to a step change in the surface condition, was found to be approximately 1350, based on the equivalent, linear-segment concentration profile and using a deviation criterion of 5% of the Sherwood number. For the redox system employed here, we calculate a maximum in the density profile. The relevant length for the equivalent, linear-segment density profile, based on an equivalent destabilizing buoyant force below the density maximum, is 16% lower than that for the concentration profile of the reactant. The critical Raleigh number Ra_m based on this length is approximately 800.

At sensing elements much smaller than the wavelength of the disturbance, a sharp increase (or decrease) in mass-transfer rate occurs immediately after the first deviation from convection-free behavior. Over a larger area, some averaging takes place, and a significant enhancement of the mass-transfer rate does not occur until tens of seconds after the first deviation in the mass-transfer rate is detected.

2. Mass Transfer at Gas-Evolving Surfaces: A Microscopic Study (Publication 6)

D.W. Dees and C.W. Tobias

A novel micromosaic electrode was developed to resolve the time-dependent mass-transfer distribution in the close vicinity of bubble phenomena. The electrode, prepared on a silicon wafer using integrated-circuit manufacturing technology, consists of a 10 by 10 matrix of coplanar, electrically isolated, square platinum segments on 100-μm centers, surrounded by a relatively large buffer segment. A computer-actuated data acquisition and control system was assembled and the software developed to monitor the current to each of the segments and control the potential of selected segments. The effects of both a single hydrogen bubble disengagement and coalescence of two bubbles on the free convection limiting current of the reduction of ferric to ferrous ion were measured using the micromosaic electrode in a horizontal facing-up orientation. The mass-transfer enhancement due to bubble disengagement was found to be small when compared to that due to coalescence. Increases in the mass-transfer rate of more than an order of magnitude over the free convection limiting current were observed for the coalescence phenomena.

3. The Influence of Attached Bubbles on Potential Drop and Current Distribution at Gas-Evolving Electrodes (Publication 2)

J.O. Dukovic and C.W. Tobias

A model has been developed for predicting the current distribution and the increment in cell voltage caused by the presence of bubbles attached to the electrode surface. In describing the geometric configuration of the bubble layer, great computational savings are achieved by approximating the hexagonal symmetry cell with a cylindrical one. This approximation is shown to be successful by comparison with analogue measurements of primary resistance.[1]

When supersaturation effects do not influence the problem (either because they have been omitted or because they are precluded by irreversible electrode kinetics), both the current distribution and the resistance increment associated with attached bubbles can be accurately correlated, for a given geometric configuration, by a single parameter, the Wagner number. When supersaturation does influence the problem, the solution depends on five parameters, and the model predicts a lower voltage increment than would be calculated without including concentration effects. In this case, the current distribution is strongly nonuniform, with highest current density to the electrode region nearest the bubble contact area. These effects depend strongly on electrode kinetics as well as on contact angle and on the density of the attached-bubble layer.

Calculations made at conditions typical for hydrogen evolution in the chloralkali industry reveal that (1) the ohmic penalty paid for attached bubbles is small compared to the extra voltage needed to drive charge transfer with part of the electrode surface area masked by bubbles; (2) on conventional cathodes, operating in the Tafel region of electrode kinetics, the level of gas supersaturation (which may be significantly altered by attached bubbles) has no effect on cell voltage; and (3) on cathodes of higher catalytic activity, where there is a departure from Tafel kinetics, the attached bubbles exert a supersaturation-lowering effect, which can decrease the overall voltage increment due to attached bubbles even to the extent that a net depolarization of the electrode is achieved.

1. P.J. Sides and C.W. Tobias, J. Electrochem. Soc. **129** (12) (1982).

1986 PUBLICATIONS AND REPORTS

Refereed Journals

1. R.T. Atanasoski, H.H. Law, and C.W. Tobias, "Electrochemical Reduction of Potassium from Potassium Chloride in Propylene Carbonate Electrolyte with Aluminum Anodes," Electrochim. Acta **16**, 339 (1986).

Other Publications

2. J.O. Dukovic and C.W. Tobias, "The Influence of Attached Bubbles on Potential Drop and Current Distribution at Gas Evolving Electrodes," Extended Abstract No. 120, vol. 86-2, The Electrochemical Society; full paper accepted by J. Electrochem. Soc.; LBL-18818.
3. G.M. Whitney and C.W. Tobias, "The Limiting Current Technique at a sectioned Electrode for the Study of Buoyancy Induced Convection," presented at the Symposium on Significant Questions in Buoyancy Affected Enclosure or Cavity Flows, 107th Meeting of the ASME, Los Angeles, CA, December 7–12, 1986; HTD Vol. 60, p. 105; LBL-22036.

LBL Reports

4. L. McVay (M.S. Thesis), R.H. Muller, and C.W. Tobias, "Studies of Micromorphology and Current Efficiency of Zinc Electrodeposited from Flowing Electrolytes," LBL-21492.
5. J.O. Dukovic (Ph.D. Thesis) and C.W. Tobias, "Studies on Current Distribution in Electrochemical Cells," LBL-22084.
6. D.W. Dees and C.W. Tobias, "Mass Transfer at Gas Evolving Surfaces; A Microscopy Study," submitted to J. Electrochem. Soc.; LBL-22311.
7. K.J. Hanson and C.W. Tobias, "Electrochemistry of Iodide in Propylene Carbonate; I. Cyclic Voltammetry Monitored by Optical Spectroscopy," submitted to J. Electrochem. Soc.; LBL-22008.
8. K.J. Hanson, M.J. Matlosz, J. Newman, and C.W. Tobias, "Electrochemistry of Iodide in Propylene Carbonate; II. Theoretical Treatment," submitted to J. Electrochem. Soc.; LBL-22009.
9. R.T. Atanasoski, H.H. Law, R.C. McIntosh, and C.W. Tobias, "Electrochemical Analysis of Trace Amounts of Water in Propylene Carbonate Electrolytes," accepted by Electrochim. Acta; LBL-22467.
10. D.W. Dees and C.W. Tobias, "Experimental Observations of Free Convection Mass Transfer at a Horizontal Surface with a Micromosaic Electrode," accepted by J. Electrochem. Soc.; LBL-16176.
11. D.P. Sutija (M.S. Thesis), R.H. Muller, and C.W. Tobias, "Development of a Micropatterned Electrode for Studies of Zinc Electrodeposition," LBL-22576.

Invited Talks

12. C.W. Tobias and R.C. McIntosh, "Limiting Currents in the Reduction of Water in Propylene Carbonate," International Congress on Corrosion and Electrochemical Behavior of Metals in Non-Aqueous Solutions, Capri, Italy, June 3–6, 1986.

Surface Layers on Battery Materials*

Rolf H. Muller, Investigator

INTRODUCTION

The purpose of this work is to provide direct experimental information about formation and properties of surface layers on battery-electrode materials and to find new means for controlling properties that enhance cell performance. Present studies are concerned with anodic oxide formation and the behavior of lithium in different ambient-temperature nonaqueous battery electrolytes. A more broadly based research program supported by the Office of Basic Energy Sciences, Division of Materials Sciences, DOE, is described in the sections "Electrochemical Phase Boundaries," R.H. Muller, Investigator, and "Electrochemical Processes," C.W. Tobias, Investigator.

1. Study of the Li/Li_3N Electrode in an Organic Electrolyte (Publication 2)

J. Thevenin and R.H. Muller

Lithium nitride has been studied as a possible solid-electrolyte interphase between the lithium electrode and an organic electrolyte. The Li/Li_3N electrode has been obtained by exposing lithium to a pure nitrogen atmosphere at ambient temperature. This procedure is found to lead to the formation of a porous lithium nitride film, resulting from a decrease in the molar volume during the reaction. Mercury porosimetry has shown that most of the pores are of a radius below 25 Å (see Figure 1-1). The impedance behavior of the Li/Li_3N electrode can be interpreted by a porous-film physical model deduced from a transmission-line electrical model. The slow filling of the micropores of the film and reaction of lithium with the electrolyte at the pore bases are responsible for changes of impedance and open-circuit potential with time and under cycling.

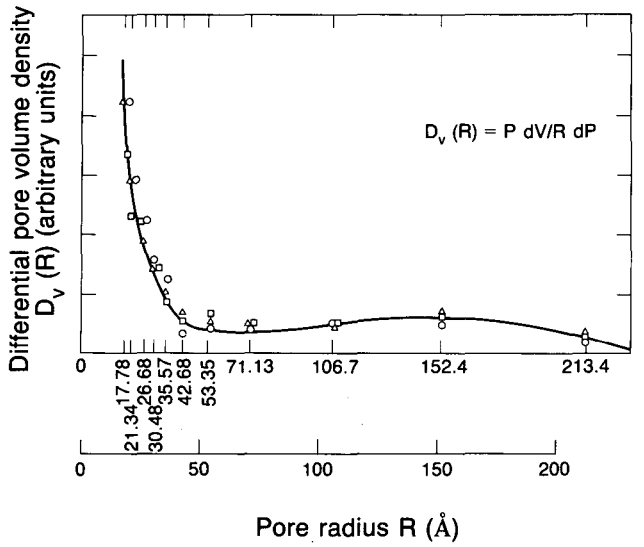

Figure 1-1. Mercury porosimetry of lithium nitride samples 0.7 cm thick and 0.3 cm in diameter. Differential pore-volume density as a function of pore radius, derived from cumulative pore-volume as a function of applied mercury pressure. (XBL 8511-11442)

2. Nucleation of Silver (I) Oxide Studied by Spectroscopic Ellipsometry (Publication 5)

S.T. Mayer and R.H. Muller

The early stages of the anodic oxidation of Ag(111) in 1M KOH during the application of potential steps, current steps, and potential sweeps have been investigated by spectroscopic ellipsometry. Film thicknesses and surface coverages have been derived from the measurements by use of a dual-layer optical model. The results are supported by SEM observations on selected specimens. Oxide crystals are found to form from a previously formed homogeneous oxide layer. The growth of larger crystals occurs at the expense of smaller crystals and results in a subsequent decrease of several orders of magnitude in the number density of crystals.

3. Data Acquisition and Reduction Software for a Self-Nulling Ellipsometer (Publication 6)

S.T. Mayer and R.H. Muller

Software and instrumental modifications have been introduced that enable a previously reported self-compensating magneto-optic spectroscopic ellipsometer, interfaced with an LSI-11 series computer,

*This work was supported by the Assistant Secretary of Conservation and Renewable Energy, Office of Energy Storage and Distribution of the U.S. Department of Energy under Contract No. DE-AC03-76SF00098.

to acquire time-dependent spectral measurements. The storage of multiple spectra has given the ellipsometer the ability to study time-dependent phenomena. Computer-controlled adjustment of the mechanical polarizer and analyzer azimuths (when the dynamic range of the Faraday-cell cores is approached) has yielded a nearly unlimited dynamic range for this instrument. Introduction of Faraday-cell cores with greater transmittance but lower Verdet coefficient, made possible by the use of computer-adjusted azimuths, has significantly increased the signal-to-noise ratio of the measurements. New FORTRAN software for the reduction of the greatly increased amount of data was developed. The programs serve both the transformation of the raw data to time-dependent optical parameters of the surface and the derivation of time-dependent physical properties of the surface by use of optical models. Software for the three-dimensional plotting of time-dependent spectra is also given.

4. Studies of Micromorphology and Current Efficiency of Zinc Electrodeposited from Flowing Chloride Electrolytes (Publication 7)

L. Mc Vay, with R.H. Muller and C.W. Tobias

Results of a study of the micromorphology and current efficiency of zinc electrodeposited from flowing, acidic chloride solutions are reported. The effects of the following variables were examined: flow rate; current density; zinc and hydrogen ion concentration; concentrations of nickel, iron, and cadmium impurity ions; and the nature of the substrate. The development of micromorphology was studied *in situ* by videomicrography and *ex situ* by scanning electron microscopy. This investigation focused on the formation of grooved deposits, which are found under a wide range of deposition conditions. The major conclusions of this study are: (1) the most important variable determining whether grooved deposits form is the interfacial concentration; (2) large protrusions orient themselves parallel to the flow direction, with the orientation starting upstream and progressing downstream; (3) large protrusions become ridges due to growth of the highest current-density portions of the electrode under mass-transport control. The current efficiency was measured using EDTA titration and weight measurements. The fraction of the current taken by zinc deposition increased with zinc concentration, ranging up to 100%, and decreased with pH. The efficiency of zinc deposition was affected by the flow rate and the substrate employed. Impurities lowered the current efficiency.

5. Development of a Micropatterned Electrode for Studies of Zinc Electrodeposition (Publication 8)

D.P. Sutija, with R.H. Muller and C.W. Tobias

Procedures have been developed for the preparation of a micropatterned electrode to be used in the study of electrocrystallization. Using microlithography, in conjunction with evaporation and pulse electrodeposition of thin films, a set of artificially roughened electrodes with hemispherical surface features 5 μm in diameter was developed. Electrodes with different orientations and separations of protrusions will be used to study the interaction of growth centers and the genesis of striations. Voltammetric studies were conducted to determine the material best suited as substrate for the micropatterned electrode. Gold, platinum, and various carbon surfaces were evaluated for zinc nucleation density and hydrogen overpotential. Surface homogeneity was examined by light and scanning electron microscopy. Gold was determined to possess the best combination of material properties: chemical inertness, low melting point, and a high work function, allowing underpotential deposition of zinc to reduce the rate of hydrogen evolution.

1986 PUBLICATIONS AND REPORTS

LBL Reports

1. J.G. Thevenin and R.H. Muller, "Impedance of Lithium Electrodes in a Propylene Carbonate Electrolyte," submitted to J. Electrochem. Soc.; LBL-21192.
2. J.G. Thevenin and R.H. Muller, "Study of the Li/Li_3N Electrode in an Organic Electrolyte," submitted to J. Electrochem. Soc.; LBL-21191.
3. J.G. Thevenin and R.H. Muller, "Study of the Impedance Behavior of the Surface Layer Formed on the Lithium Electrode in Propylene Carbonate-Based Electrolytes," LBL-20660.
4. J.G. Thevenin and R.H. Muller, "The Li/Li_3N Electrode: Study of its Electrochemical Behavior in an Organic Electrolyte by means of Electrode-Impedance Spectroscopy," LBL-20659.

5. S. Mayer and R.H. Muller, "Nucleation of Silver (I) Oxide Studied by Ellipsometry," presented at the 170th Meeting of the Electrochemical Society, Oct. 19–24, 1986, San Diego, CA, Ext. Abs. 506; LBL-21490abs.
6. S. Mayer and R.H. Muller, "Automatic Self-Nulling Spectral Scanning Ellipsometer: Data Acquisition and Data Reduction Software," LBL-20677.
7. L. Mc Vay, (M.S. thesis), with R.H. Muller and C.W. Tobias, "Studies of Micromorphology and Current Efficiency of Zinc Electrodeposited from Flowing Chloride Electrolytes," LBL-21492.
8. D.P. Sutija, (M.S. thesis), with R.H. Muller and C.W. Tobias, "Development of a Micropatterned Electrode for Studies of Zinc Electrodeposition," LBL-22576.

Invited Talks

9. J.G. Thevenin and R.H. Muller, "Impedance Studies of Li Electrodes," Technology Base Research Project Review, Office of Energy Storage and Distribution, DOE, Washington, D.C., Dec. 16–17, 1986.

Electrode Kinetics and Electrocatalysis*

P.N. Ross, Investigator

INTRODUCTION

Complex electrochemical reactions in which chemical bonds are broken and/or formed are invariably catalytic, with electrode kinetics varying by many orders of magnitude for different electrode materials. The structural conformation of the electrode material can also have a pronounced effect on electrode kinetics. The structural effects complicate the optimization of catalytic materials for technological applications, and they are not effects that are well understood. The study of structure-related effects in electrocatalysis is a central theme in our research.

Metal/metal-ion (Me/Me^{Z+}) couples form the largest class of negative-electrode types for batteries. The kinetics of Me/Me^{Z+} couples used in batteries are relatively rapid, but they are not usually controlled by only a charge-transfer step. These reactions are often quasireversible, in the sense that they proceed at high rate and small overpotential, but they do not follow "ideal" charge-transfer rate expressions. Phenomena frequently cited as contributing to the "nonideal" behavior of Me/Me^{Z+} systems are critical nucleation, intermediate or precursor formation, and impurity adsorption. The structural transformations to the metallic surface as a result of cyclic Me^{Z+} formation are not well known, particularly at the atomic scales of structure. Yet these structural transformations may control critical phenomena in Me/Me^{Z+} cyclability.

Bifunctional air electrodes, which both consume and evolve oxygen, are especially attractive positive electrodes that can be coupled with Zn negative electrodes to form high-energy-density (150–200 Wh/kg) ambient-temperature batteries. Bifunctional air electrodes require the development of catalytic materials that are both active and corrosion-resistant over a demanding range of electrode potentials. Electrode structures based on catalyzed carbon black appear attractive on the basis of cost. The corrosion resistance of carbons is under investigation.

*This work was supported by the Assistant Secretary of Conservation and Renewable Energy, Office of Energy Storage and Distribution of the U.S. Department of Energy under Contract No. DE-AC03-76SF00098.

1. A New Concept in an Electrically Rechargeable Zinc-Air Alkaline Battery: I. The Zinc Electrode (Publication 3)

P.N. Ross

A new concept for an alkaline zinc battery was explored that would overcome the cycle-life-limiting phenomena characteristic of most zinc-electrode concepts. The new concept is a flowthrough porous zinc electrode with recirculating supersaturated zincate solution. An alkaline zinc battery with recirculating zincate is not a new concept itself, but all of the prior systems used an inert (usually flat) current collector with recirculating zinc particles. The concept employed here uses an inert substrate having an open "honeycomb" type porosity onto which zinc is plated (and from which it is stripped) while electrolyte circulates through the open pores. Materials having this type of porous structure are commercially available as either "metal foams" or "carbon foams." We have studied in some detail the use of copper foam-metal, shown in Figure 1-1. The open honeycomb or reticulated structure is apparent; the nominal "cell" diameter is 0.2 cm, and the characteristic diameter of the filaments is ~0.4 mm. This

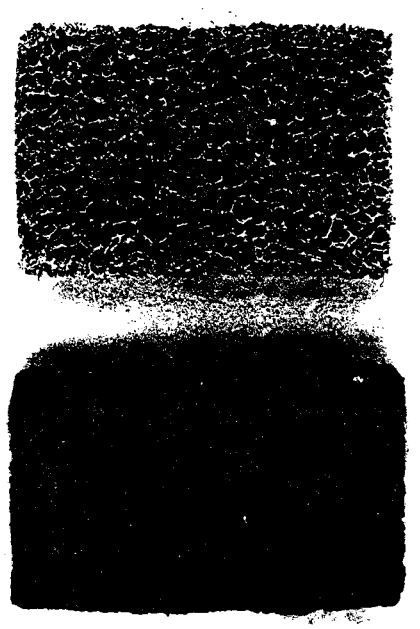

Figure 1-1. Photograph of the copper foam metal used as a substrate for zinc: (top) before zinc deposition; (bottom) after deposition of 160 mAh/cm^2 of zinc. (CBB 850-8423)

particular foam has a bulk density of 3% (97% porosity) of the bulk density of copper with a total BET surface area of $\sim 10^4$ m^2/m^3. Using a 0.3-cm thickness, the internal surface area is roughly 30 times the superficial area, so the "true" current density for zinc deposition/stripping will be more than an order of magnitude lower than the nominal current density. Low current density is known to promote uniform zinc deposition/stripping and should extend cycle life. A full parametric study of the influence of current density, electrolyte flow rate, and zincate concentration on zinc distribution was conducted. Figure 1-1 shows the appearance of the electrode after after the deposition of 160 mAh/cm^2 of zinc (at 10 mA/cm^2), which appeared to be the maximum amount of zinc that could be deposited uniformly. The zinc deposit mirrored the cellular structure of the substrate, and the distribution was found to be uniform and invariant with the number of cycles over a wide range of conditions of flow rate, zincate concentration, and current density.

2. A New Concept in an Electrically Rechargeable Zinc-Air Alkaline Battery: II. The Bifunctional Air Electrode (Publication 4)

N. Staud and P.N. Ross

The new concept employed here was to use carbon materials exclusively as the structural elements of the electrode to minimize both cost and weight. An inexpensive transition-metal oxide catalyst of proven stability was used to maintain the low cost. As a result of several man-years of effort at LBL, we have identified two types of carbon materials that can be used to form the structural elements having the required stability: (1) graphite fibers woven into a "cloth" that serves as the current collector; (2) a high-surface-area graphite powder formed by heat treatment of a carbon black. The latter was impregnated with a mixture of transition-metal oxides to form the active catalyst. The electrode was fabricated by bonding the catalyst layer to one side of the graphite cloth and a hydrophobic polytetrafluoroethylene (PTFE) film to the other. The resulting polarization curves for these electrodes are shown in Figure 2-1 at room temperature in 12 N KOH containing 200 g/l zincate. After 300 cycles, the electrode was still showing acceptable voltage in the current-density region of 10–20 mA/cm^2.

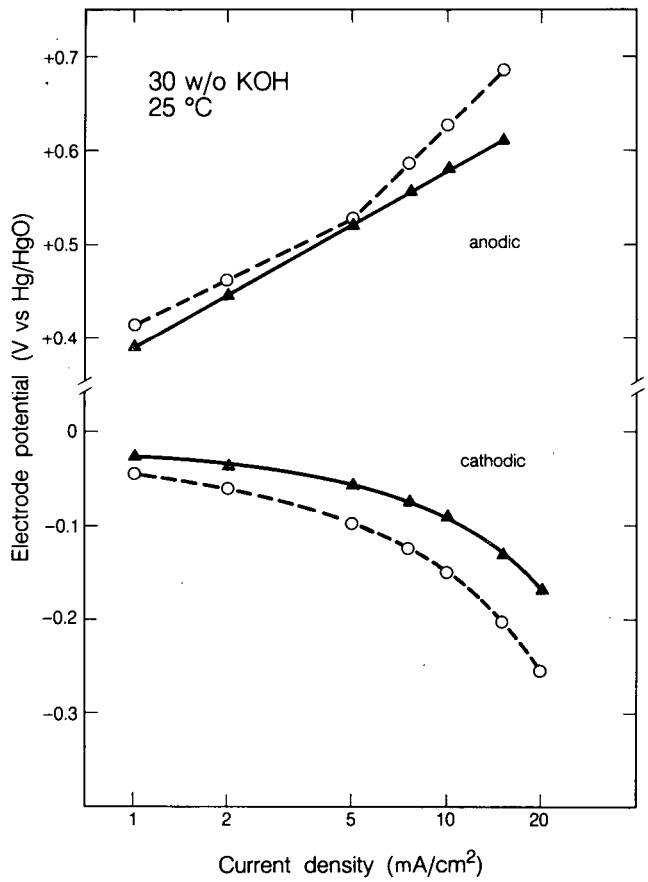

Figure 2-1. Polarization curves for bifunctional air electrodes fabricated from graphite materials with nickel oxide and nickel-cobalt spinel oxide as catalysts. (XBL 862-11022)

3. A New Concept in an Electrically Rechargeable Zinc-Air Alkaline Battery: III. Engineering Analysis (Publication 5)

P.N. Ross

Proof-of-principle experiments were conducted on a 1.5-Ah zinc-air prototype battery employing the new concepts in zinc and air electrodes described in abstracts I and II. The design of the 1.5-Ah prototype is shown in Figure 3-1. The cell was cycled at the three-hour rate, producing 1.2 V on discharge; it required 2.0 V on charge and operated satisfactorily for over 150 cycles. Based on the 1.5-Ah prototype performance characteristics, engineering design calculations were made for a 32-kWh battery. These calculations project an energy density of 110 Wh/kg,

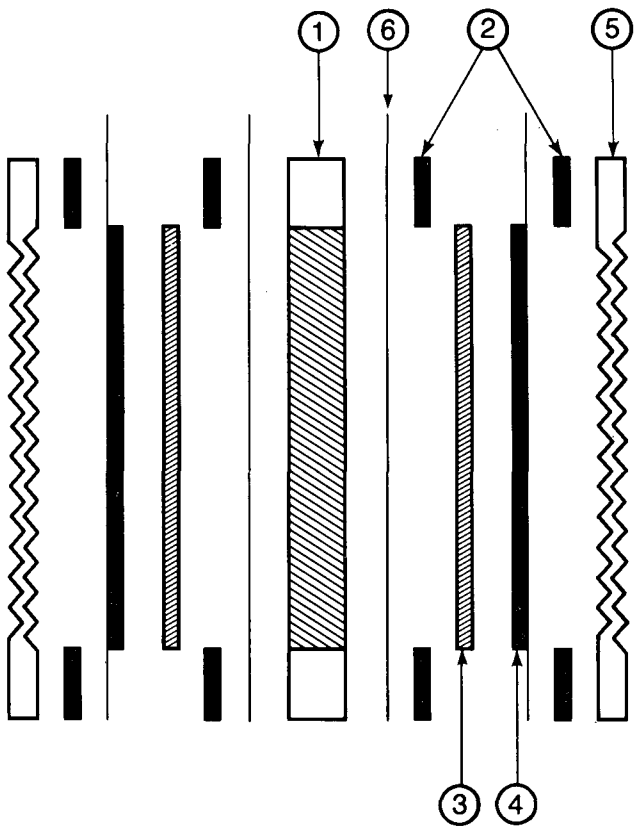

Figure 3-1. Schematic diagram of the zinc-air battery single-cell prototype used in these studies. (XBL 863-6199)

peak power density of 140 W/kg, electrical efficiency of 60%, and an attractive materials cost of <$20/kW. The prototype testing revealed a number of problem areas that would have to be addressed in further studies using multicell prototypes: shunt currents in the electrolyte manifold; the effect of air-electrode dissolution products in the electrolyte on zinc cyclability; and component reliability.

4. Work in Progress

New work is being started on catalysts for the direct oxidation of methanol in fuel cells. These studies will use modern surface-analytical methods coupled with electrochemical methods to determine the surface composition dependence of the catalytic activity for selected platinum alloys. Two of the most promising catalysts for methanol oxidation are Pt-Sn and Pt-Ru, but the surface composition of these alloys in electrolyte is not known, nor is there a consistent theory about why these alloys are more active than platinum alone. In addition, we are studying the effect of the electrolyte on methanol-oxidation kinetics, as there are new fluorosulfonic acid electrolytes available that have very different properties from the inorganic (e.g., sulfuric) acids used previously.

1986 PUBLICATIONS AND REPORTS

Refereed Journals

1. N. Staud and P.N. Ross, "The Corrosion of Carbon Black Anodes in Alkaline Electrolyte: II. Furnace Process Carbons and the Effect of Graphitizing Heat Treatment," J. Electrochem. Soc. **133**, 1079 (1986).

Other Publications

2. P.N. Ross, "Feasibility Study of a New Zinc-Air Battery Concept Using Flowing Alkaline Electrolyte," in *Proc. 21st I.E.C.E.C.*, Vol. 2, The American Chemical Society, Washington, DC, 1986, p. 1066; LBL-21437.

LBL Reports

3. P.N. Ross, "A New Concept in an Electrically Rechargeable Zinc-Air Alkaline Battery: I. The Zinc Electrode," LBL-22912.
4. N. Staud and P.N. Ross, "A New Concept in an Electrically Rechargeable Zinc-Air Alkaline Battery: II. The Bifunctional Air Electrode," LBL-22913.
5. P.N. Ross, "A New Concept in an Electrically Rechargeable Zinc-Air Alkaline Battery: III. Engineering Analysis," LBL-22914.
6. P.N. Ross, "Structure Property Relations for Processes at the Metal/Solution Interface," J. Vac. Sci. Technol. (in press); LBL-22105.
7. W. Cieslak, A. Brown, V. Dantam, B. Lichter, W. Paden, S. Pensabone, and P.N. Ross, "Corrosion in Batteries and Fuel Cell Power Sources," in *Corrosion*, Vol. 13, Metals Handbook, American Society for Metals, Metals Park, NJ (in press); LBL-22489.

Invited Talks

8. P.N. Ross, "Structure Property Relations in the Electrochemistry of Gold and Platinum," Gordon Research Conference in Electrochemistry, Santa Barbara, CA, Jan. 23, 1986.
9. P.N. Ross, "Structure Property Relations at Electrochemistry Interfaces," Gordon Research Conference in Interfacial Chemistry, Meriden, NH, July 21, 1986.
10. P.N. Ross, "Structure Property Relations for Processes at the Metal Solution Interface," 6th International Congress on Solid Surfaces (ICSS-6), Baltimore, MD, Oct. 27, 1986.

Electrical and Electrochemical Behavior of Particulate Electrodes*

J.W. Evans, Investigator

INTRODUCTION

This work is concerned with the use of particulate electrodes (especially zinc) in the storage of electrical energy. One of the major difficulties encountered in the use of monolithic (e.g., slablike) zinc electrodes in batteries is the change in the morphology of the electrode as the battery is cycled. For example, there is a tendency for zinc to form nodular or dendritic growths; this growth can have an impact on battery performance by forming shorts or by penetrating cell diaphragms. These problems might be overcome by use of a particulate electrode where the zinc is present either as particles or as a thick coating on a particle substrate; the morphology and mechanical integrity of the particle is then of less concern.

One possible particulate electrode is a fluidized-bed electrode where zinc particles are maintained in a state of agitated suspension by upward-flowing electrolyte. Fluidized-bed electrodes appear to be especially suitable for the charging of zinc particles (i.e., the electrodeposition of zinc), and zinc deposition onto such electrodes has been one subject of investigation in 1986. One characteristic of such electrodes is that the potential of both the particles and the electrolyte at any point in the electrode undergoes rapid fluctuations. The effect of potential fluctuations on zinc deposits formed from alkaline electrolytes has been another topic of investigation.

A second type of particulate electrode is the moving-bed electrode, where a bed of particles settles slowly downwards under the influence of gravity. This electrode appears attractive for discharge of zinc particles (i.e., electrodissolution of zinc), and a cell equipped with such an electrode and a commercially available air anode has been the third object of study in 1986.

*This work was supported by the Assistant Secretary of Conservation and Renewable Energy, Office of Energy Storage and Distribution of the U.S. Department of Energy under Contract No. DE-AC03-76SF00098.

1. An Investigation of Zinc Electrodes Relevant to Zinc-Air Batteries (Publication 1)

H. Choi†

The particulate electrode (fluidized-bed electrode or moving-bed electrode) has been studied to evaluate its possible application to energy storage.

The first part of this study is concerned with the effect of current fluctuation on the morphology of zinc electrodeposited on the rotating-disc electrode from alkaline zincate electrolyte. The effect of the fluctuation on the morphology was examined by scanning electron microscopy. The deposits under the condition of fluctuating current density were smoother than those formed under constant current density.

The second part is concerned with the electrodeposition of zinc from alkaline electrolyte with the cell employing a fluidized-bed electrode that simulates the recharge process of the secondary battery employing a particulate electrode. Figure 1-1 shows some representative results obtained during electrodeposition of zinc from an alkaline zincate electrolyte containing 20 g/L of zinc in a fluidized-bed electrode. The superficial current density is the current per unit cross sectional area of the cell and contrasts with much lower current densities employed in cells with planar electrodes. Results from two runs using

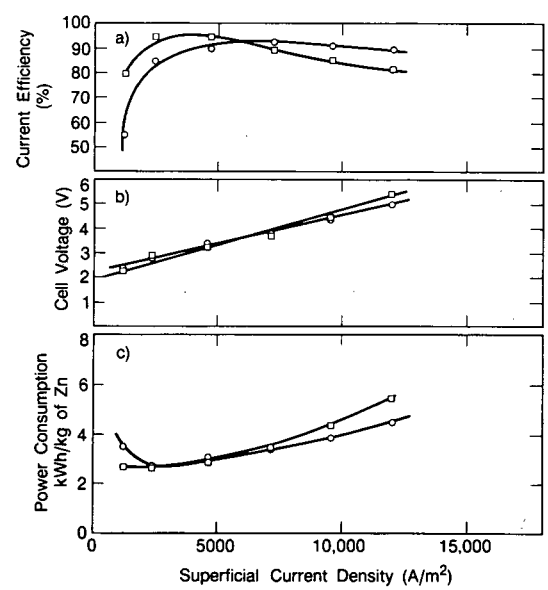

Figure 1-1. Results of experiments using a fluidized zinc cathode to deposit zinc from alkaline zincate electrolytes containing 20 g/L zinc (O = electrolyte containing 27.5 g/L of sodium silicate, □ = silicate-free electrolyte). (XBL 869-8937)

different electrolytes (one containing sodium silicate, which is known to enhance cell capacity on discharge) are shown, and the energy consumption on charging the cell is 2.5–3 kWh/kg Zn at current densities up to 5 kA/m^2. This is approximately twice the theoretical energy consumption and is less than the 3–4 kWh/kg Zn for commercial electrowinning of zinc (from acid electrolytes).

A laboratory cell with a particulate zinc electrode and an air counterelectrode was constructed, and discharge characteristics were studied to evaluate the cell.

[†]Present address: McGill University, Montreal, Québec.

2. Zinc Electrodeposit Morphology Under Conditions of Fluctuating Current Density (Publication 2)

V. Jiricny,[†] H. Choi,[‡] and J.W. Evans

Previous investigations have shown that particles within a fluidized-bed electrode undergo rapid fluctuations in overpotential. This investigation has been concerned with the effects of such fluctuations on zinc-electrodeposit morphology. Both a fluidized-bed electrode and a rotating-disc electrode were used, with the latter being driven at either constant or fluctuating current density. The effect of the fluctuations on the morphology of one-hour deposits for neutral and acidic sulfate electrolytes was determined by examination under the scanning electron microscope. Both pure electrolytes and ones containing additives (nickel, cobalt, antimony, and a commercially available glue) were employed. Wide variation in microstructure was observed, with the fluctuations having a marked effect. These results are partly explicable in terms of differing nucleation and growth rates of zinc crystallites.

[†] Present address: Institute of Chemical Process Fundamentals, Czechoslovak Academy of Science, 165 02 Praha 6, Suchdol, Czechoslovakia.

[‡]Present address: McGill University, Montreal, Québec.

3. Work in Progress

Studies continue on the discharge of a laboratory cell equipped with a moving bed of zinc-coated particles as an anode and a commercially available air cathode.

1986 PUBLICATIONS AND REPORTS

LBL Reports

1. H. Choi (M.S. Thesis), "An Investigation of Zinc Electrodes Relevant to Zinc-Air Batteries," LBL-22705.
2. V. Jiricny, H. Choi, and J.W. Evans, "Zinc Electrodeposit Morphology Under Conditions of Fluctuating Current Density," accepted by J. Appl. Electrochem.; LBL-21986.

Invited Talks

3. J.W. Evans, "Fluidized Bed Electrodes," Proc. Symp. Education, Electrochemical Society 169th National Meeting, Boston, May 1986.
4. J.W. Evans, "Electrochemical Cells with Particulate Electrodes," Chemical Engineering Department, Case Western Reserve University, Cleveland, OH, Oct. 1986; Chemical Engineering Department, Washington State University, Pullman, Sept. 1986.
5. J.W. Evans, "Electrometallurgy," Department of Metallurgy, University of British Columbia, Vancouver, March 1986; SRI International, Menlo Park, CA, April 1986.

Electrochemical Properties of Solid Electrolytes*

Lutgard C. De Jonghe, Investigator

INTRODUCTION

In the past decade great strides have been made towards the efficient storage of energy with high-energy-density batteries. Without exception these advanced secondary batteries have been based on inorganic galvanic couples operating at relatively high temperatures (300–400°C). These temperature ranges necessitate the use of solid or molten salt electrolytes and allow the use of unusual, low-equivalent-weight couples such as Li/FeS_2, Li/Cl_2, Na/S, etc. Among the advantages of such temperatures is that the rates of electrode processes are increased to such an extent that very high current/power densities are possible. However, the high operating temperatures also exact a technical price in that corrosion rates are also greatly enhanced, with concomitant problems of cell seals, safety, and thermal management.

One of the various high-energy-density batteries that has been targeted for potential commercialization is the sodium/sulfur battery. This cell has demonstrated high specific power and energy and long cycle life. Early in its development, premature cell failure was often due to catastrophic failure of the beta″-alumina solid electrolyte. Due in part to investigations carried out at LBL, the mechanisms for such failures were identified, and consequently higher-quality ceramic electrolytes that rarely give rise to such failure were fabricated. Accordingly, the limiting factor to cell reliability to date is the corrosion of the positive-electrode container by molten sodium polysulfide at the temperature of operation. This can be minimized by the use of advanced surface coatings, such as E-brite, on the steel container, but this technology is expensive and not yet completly effective.

Various research groups have attempted to lower the operating temperature of the Na/S battery by dissolving the polysulfide electrode in solvents. These cells potentially were able to operate in the 120°C temperature range but suffered severe kinetic limitations and were largely abandoned. Mamantov developed a Na/SCl_3AlCl_4 cell that gave impressive results at 200°C, but this cell also suffered from the corrosive nature of the positive electrode. The research group at LBL has gone a different route by introducing a new class of positive-electrode materials, organic sulfur compounds, for high-energy-density batteries that operate at moderate temperatures (120–150°C). The basic features of these batteries are similar to those of the Na/S cell in that they both use a molten sodium electrode separated from a molten positive electrode by a beta″-alumina solid electrolyte. The key features of these novel cells are open circuit voltages of 2.2 to 2.5 V, theoretical energy densities of 350–600 Whr/Kg, operating temperatures of 120 to 150°C, and nonaggressive behavior of the molten positive electrode towards many metals, including aluminum.

*This work was supported by the Assistant Secretary of Conservation and Renewable Energy, Office of Energy Storage and Distribution of the U.S. Department of Energy under Contract No. DE-AC03-76SF00098.

1. The Sodium/(Tetraethylthiuram disulfide) Battery

S.J. Visco, C. Mailhe, and L.C. De Jonghe

To operate a sodium electrode at temperatures approaching the melting point of sodium metal, one must reduce the problem of asymmetric polarization at the Na/beta″-alumina interface, which can be quite severe at low temperatures. This issue was studied as part of the program on degradation of beta″-alumina in the Na/S battery. It was concluded that asymmetric polarization is strongly influenced by the presence of oxygen in the sodium electrode and is most likely due to the formation of a resistive layer by adsorption of oxygen on the electrolyte surface. When electrolytically generated sodium or chemically gettered sodium was used in a sodium/sodium cell, completely symmetric behavior was observed from just above the melting point of sodium to the operating temperature of the Na/S battery (110–350°C). This work provided the necessary foundation for the sucessful operation of an intermediate-temperature high-energy-density battery, the sodium/(tetraethylthiuram disulfide) cell.

The Na/TETD battery is only one of a variety of possible candidates for energy storage based on a novel class of organosulfur positive-electrode materials. These new cells share similar features with the Na/S cell, including the sodium anode, beta″-alumina electrolyte, and an operating temperature given by the requirement of maintaining molten electrodes over the entire charge/discharge cycle. However, while for the Na/S cell the operating temperature is defined by the melting point of the polysulfide electrode (>300°C), in the Na/

organosulfur cell some of the sodium thio salts actually melt at temperatures lower than the sodium metal electrode (<100°C). Of the many organic redox couples to choose from, this program has worked mostly with the group of disulfides known as the thiuram disulfides and their corresponding sodium salts, the dithiocarbamates. The sodium dithiocarbamates are characterized by their low melting points (due to strong resonance stabilization of the thio anion) and reversible oxidation to the thiuram disulfide,

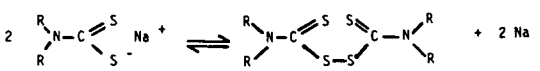

where R = an organic functional group (C_2H_5, CH_3, C_6H_5, etc.)

Depending on the electronic and/or steric influence of the R groups attached to the nitrogen atoms, the sodium salts can melt at surprisingly low temperatures (50–150°C). The oxidized form, the thiuram disulfides, $(R_2NCSS)_2$, melt at even lower temperatures (RT to 100°C) and are easily recrystallized to high purity. Fortunately, the dithiocarbamate salts are also very soluble in the corresponding disulfides, allowing an operating temperature somewhat below the melting point of the salt. There are many thiuram disulfides that may have merit as energy-storage electrodes; of these this program has focused on tetraethylthiuram disulfide (TETD).

The theoretical energy density of a Na/TETD battery is 360 Whr/Kg, and practical cells have been constructed in the laboratory with energy densities exceeding 110 Whr/Kg, and average open circuit voltages of 2.2 V (see Figure 1-1). At 120°C these cells

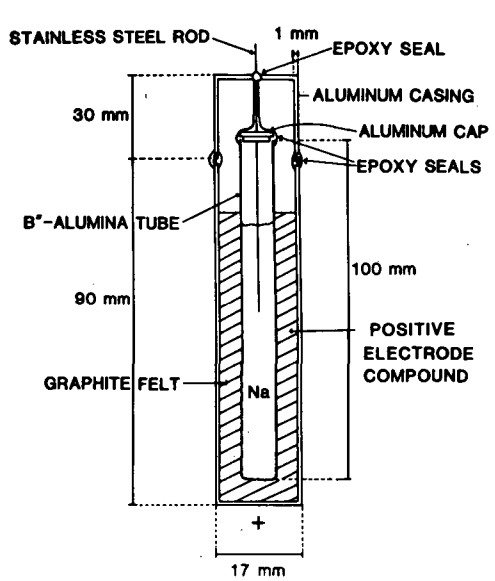

Figure 1-1. Schematic diagram of the Na/organosulfur battery. (XBL 875-2317)

have been cycled to close to theoretical capacity at current densities of greater than 5 mA/cm^2. The Na/TETD batteries have also demonstrated peak discharge rates exceeding 50 mA/cm^2 (electrolyte surface area: 20 cm^2) at 1.2 V for 3% of available capacity (see Figure 1-2) or discharge rates of 25 mA/cm^2 at 1.5 V for 9% of available capacity. Although far from being optimized, these cells have already demonstrated the remarkable nature of this new class of positive-electrode materials.

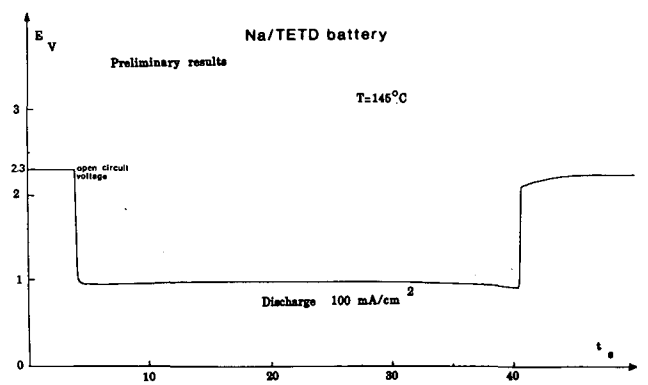

Figure 1-2. Pulse discharge of the Na/TETD battery. (XBL 876-2948)

2. The Alkoxy Alkyl Disulfide Battery

S.J. Visco, C. Mailhe, and L.C. De Jonghe

In an effort to boost further the energy density of the experimental batteries in this program, the novel class of positive electrode materials was extended to include the simple alkyl disulfides. The theoretical energy densities for the akyl disulfides range from 500 to 800 Whr/Kg, which of course rival those of the high-temperature battery systems such as the Na/S battery (780 Whr/Kg theoretical). The overall cell reaction for such a cell is

$$RSSR + 2\ Na \rightarrow 2\ NaRS\ .$$

Unfortunately, due to their very low dielectric constants, the simple alkyl disulfides are incapable of dissolving the sodium thioalkyl salts generated on cell discharge. This was verified experimentally with a sodium/(propyl disulfide) cell. In order to use these organosulfur compounds in a viable cell, a more polar R group such as an alkoxyalkyl (CH_3O, C_2H_5O, etc.) moiety is necessary. The only such compound presently commercially available is hydroxyethyl disulfide (HEDS).

A series of Na/HEDS cells was designed and tested. Preliminary tests showed negligible reduction of the terminal hydrogens on graphite felt at the discharge potential of the cell. The theoretical energy density for the Na/HEDS cell is 590 Whr/Kg. The completed batteries had capacities of 4.5 Ah and practical maximum energy densities of over 200 Whr/Kg. At an operating temperature of 120°C, the batteries displayed impressive performances. The Na/HEDS cells were discharged to over half of the available capacities at current densities of up to 20 mA/cm^2 with remarkably little evidence of time-dependant polarization, and they could be discharged for close to 5 minutes at up to 50 mA/cm^2 with similar results. One of these cells was recharged to 96% of the available capacity. Although the preliminary results were encouraging, hyroxyethyl disulfide probably has little practical value as an electrode due to its tendency towards self-condensation at elevated temperatures to yield viscous polysulfide polymers. One solution to this dilemma is to use alkoxy alkyl R groups on the disulfide. Although these compounds are not commercially available, their preparation is relatively straightforward.

3. Work In Progress

Ongoing work concerns the fundamental chemical and electrochemical properties of this novel class of positive storage electrodes, as well as continued characterization and optimization of the charge/discharge behavior of the Na/(organosulfur) batteries. The key features of the organosulfur electrodes include the ability to tailor the physical and chemical properties through choice of the functional groups attached to the disulfide linkage, the absence of electronic conductivity in the melt, and the continuous change of melt properties on discharge from that of a dilute electrolyte dissolved in an electroactive solvent to that of a molten salt at 100% discharge. Due to the low operating temperature of the cells, the density, viscosity, and ionic conductivity will be determined as a function of composition over the entire discharge range in a straightforward manner. The diffusion coefficients for both the reduced and oxidized forms can also be determined using standard electrochemical techniques. Accordingly, a thorough picture of mass transport for this system can be established that together with information gained from charge/discharge cycling of actual cells will allow for accurate modeling of the novel sodium/organosulfur batteries.

Research on the Na/TETD battery will establish the effects of current density on power and energy density as well as cycle life of the battery. Charge/discharge behavior will also be correlated with the viscosity of the system, which will determined as a function of discharge, and with the addition of various high-dielectric/low-viscosity solvents. The ionic conductivity of the system will be determined similarly. The Na/(alkoxyalkyl disulfide) batteries will be studied upon receipt of the custom synthesized chemicals. The chemical and electrochemical properties of the disulfides will be investigated as described above, providing a wide base of information on the organosulfur electrodes. These studies will provide the criteria to decide which organosulfur electrodes should be targeted for eventual application.

1986 PUBLICATIONS AND REPORTS

Refereed Journals

1. D.C. Hitchock and L.C. De Jonghe, "Time Dependent Degradation in Sodium-Beta″ Alumina Solid Electrolytes," J. Electrochem. Soc. **133**, 355 (1986); LBL-19223.
2. D.C. Hitchock and L.C. De Jonghe, "Oxygen Depletion and Slow Crack Growth in Sodium Beta″ Alumina Solid Electrolytes," J. Electrochem. Soc. **133**, 6 (1986); LBL-19358.
3. D. Olson and L.C. De Jonghe, "Zirconia Toughened Sodium Beta″ Alumina Solid Electrolyte," J. Mat. Sci. **21**, 4221 (1986).

Other Publications

4. L.C. De Jonghe, M.B. Armand, S.J. Visco, and C.C. Mailhe, "Alkali Metal Battery and Positive Electrode Therefor," LBL Patent Application IB-634.
5. S.J. Visco, C.C. Mailhe, M.B. Armand, and L.C. De Jonghe, "Sulfur-Type Positive Electrode for Alkali Metal Battery," LBL Patent Application IB-658.
6. D.C. Hitchcock, C. Mailhe, and L.C. De Jonghe, "Electrochemical Cells Utilizing Molten Alkali Metal Electrode Reactant," US Patent 4,609,596.

LBL Reports

7. M. Liu and L.C. De Jonghe, "Chemical Stability of Sodium Beta″ Alumina Electrolyte in Sulfur/Polysufide Melts," LBL-21712.
8. C. Mailhe, S. Visco, and L.C. De Jonghe, "Oxygen Activity and Asymmetric Polarization at the Sodium/Beta″ Alumina Interface," accepted by J. Electrochem. Soc; LBL-19359.

Invited Talks

9. L.C. De Jonghe, "Electrochemical Properties of Solid Electrolytes," R.M. Fulrath Award, Berkeley, Oct. 1985.
10. L.C. De Jonghe, "Solid Electrolytes: Problems and Solutions," Sendai, Japan, Jan. 1986.
11. L.C. De Jonghe, "Properties of Solid Electrolytes," Naval Defense Academy, Yokohama, Japan, Jan. 1986.

Analysis and Simulation of Electrochemical Systems*

John Newman, Investigator

INTRODUCTION

This program involves fundamental investigations of the transport and interfacial phenomena important in electrochemical systems. Results of this work are used to analyze experimental data, to identify important system parameters, and to aid in the design and scale-up of electrochemical systems. Specific projects include analysis of the thin-gap flow cell for electrochemical synthesis and energy storage, mathematical modeling of the Li-Al/FeS battery and the Li-Si/FeS_2 battery, an investigation of porous electrodes with applications to molten-salt systems, and an AC impedance analysis of both zinc and iron corrosion.

1. Mathematical Modeling of Lithium(alloy), Iron Disulfide Cells (Publication 10)

D. Bernardi and J. Newman

Results obtained from computer programs simulating the behavior of LiAl/FeS_2 and Li(Si)/FeS_2 high-temperature molten-salt cells are presented. The models predict the cell voltage, temperature, and heat-generation rate during cell operation. Position-dependent behavior, such as reaction rates and concentrations within the cell, is also calculated. The models predict operational characteristics and determine the influence of changes in design parameters on the performance of the cells. The effects of state of discharge, initial electrolyte composition, temperature, and discharge current density on cell behavior are investigated. Factors that can limit a cell during operation are identified. The cell discharge behavior is compared with available experimental data. The models clarify our understanding of these battery systems and can help guide experimental research.

*This work was supported by the Assistant Secretary of Conservation and Renewable Energy, Office of Energy Systems Research, Energy Storage Division of The U.S. Department of Energy under Contract No. DE-AC03-76SF00098.

2. Experimental Investigation of a Porous Carbon Electrode for the Removal of Mercury from Contaminated Brine (Publication 4)

M. Matlosz and J. Newman

A flow-through porous electrode, made of reticulated vitreous carbon (RVC), has been designed to remove mercury from contaminated brine solutions. Experiments with a bench-scale reactor show that the mercury concentration of contaminated brine solutions can be reduced by as much as a factor of 5000 during a single pass through the electrode. The process is mass-transfer limited, and the results of the experiments are used to develop a general correlation for the dependence of the mass-transfer coefficient on the flow rate of electrolyte through RVC. In addition, the effect of counterelectrode placement on the cell resistance is examined, and the experimental data are compared to predictions from a mathematical model of the system. The model agrees favorably with the experimental results, and the benefits of upstream counterelectrode placement, indicated by the model, are verified.

3. Corrosion of a Rotating Iron Disk in Laminar, Transition, and Fully Developed Turbulent Flow (Publication 1)

C.G. Law, Jr., and J. Newman

Electrochemical corrosion generally involves the interaction of numerous phenomena. A model is presented that accounts for the different hydrodynamic regimes across the surface, ohmic potential variations, and the simultaneous occurence of oxygen reduction and oxidation of iron. The active-passive transition for iron is presumed to occur at a specific value of the electrode potential. Results illustrate the importance of disk size, oxygen concentration, and solution conductivity on the corrosion rate distribution.

4. The Kramers-Kronig Relations and Evaluation of Impedance for a Disk Electrode (Publication 3)

M.M. Jaksic and J. Newman

It is shown that the Kramers-Kronig (K-K) relations for frequency dispersion (or variation with fre-

quency) describe the impedance properties of a disk electrode. The accuracy and interpretation of impedance by the K-K relations depend on the accuracy with which one fits the functions for the capacity and the effective resistance. It is also shown how to use the K-K relations to calculate the capacity from the effective resistance, and vice versa. The previously published theory of impedance at a disk electrode is thereby shown to be consistent with the K-K relations. The method of evaluation of the resistance and reactance for the disk electrode from the K-K relations is given and discussed.

5. Work in Progress

A mathematical model of the electrode/electrolyte interface is being developed to calculate the frequency response of a rotating disk. The working algorithm accounts for the effect of surface coverage owing to specific adsorption and charge-transfer reactions. Double-layer theory is used to calculate the potentials at the interfacial planes and the surface excesses of all the electroactive species present in the solution. Presently, the microscopic model of the interface predicts qualitatively the measured complex impedance for the zinc chloride system. This mechanistic approach allows the proposed reaction process to be changed to account for the experimental observations. Finally, the generalized model can be used to identify system limitations and to guide further experimental research. This microscopic model of the interface will be coupled with the previously developed macroscopic model accounting for convection, migration, and multicomponent diffusion in concentrated solutions, in addition to homogeneous and heterogeneous reactions.

A computer model is being developed to predict the response to alternating current signals of a redox reaction with soluble reactants and products in a flow-through porous electrode. Terms accounting for double-layer capacity have been added to the model. An experimental investigation is under way to accompany the modeling efforts.

The corrosion of iron in sulfuric acid is being studied experimentally, using rotating iron hemispherical electrodes. The anodic polarization curve, the sustained electrochemical oscillations, and the alternating current impedance for this system are being determined. The impedance data are being checked for consistency with the Kramer-Kronig relations. Finally, the experimental impedance results will be compared with the predictions of recently developed theoretical models to elucidate the fundamental processes governing the behavior of the iron–sulfuric acid system.

Double-layer adsorption is an important phenomenon in heavy-metal ion removal from waste streams and in discharge transients in high-pulse-power battery systems. An experimental and theoretical investigation of double-layer adsoption of zinc ions on high-surface-area porous carbon is under way.

The solution of Laplace's equation is important to many modeling efforts. Its solution is often expensive and difficult to obtain accurately. The feasibility of a boundary-integral technique for use in current-distribution problems is being investigated. Preliminary observations appear promising. This technique is being applied to primary and secondary current distributions and can be used for more general problems involving Laplace's equation.

Solid electrodes of varying composition exist in several important battery systems. A theoretical and experimental study is under way to determine how the conductivity varies in solid mixtures of several phases.

1986 PUBLICATIONS AND REPORTS

Refereed Journals

1. C.G. Law, Jr., and J. Newman, "Corrosion of a Rotating Iron Disk in Laminar, Transition, and Fully Developed Turbulent Flow," J. Electrochem. Soc. **133**, 37 (1986); LBL-18157.
2. P. Russell and J. Newman, "Anodic Dissolution of Iron in Acidic Sulfate Electrolytes: I. Formation and Growth of a Porous Salt Film," J. Electrochem. Soc. **133**, 59 (1986); LBL-19816.
3. M.M. Jaksic and J. Newman, "The Kramers-Kronig Relations and Evaluation of Impedance for a Disk Electrode," J. Electrochem. Soc. **133**, 1097 (1986); LBL-19201.
4. M. Matlosz and J. Newman, "Experimental Investigation of a Porous Carbon Electrode for the Removal of Mercury from Contaminated Brine," J. Electrochem. Soc. **133**, 1850 (1986); LBL-19611.
5. P. Russell and J. Newman, "Current Oscillations Observed within the Limiting Current Plateau for Iron in Sulfuric Acid," J. Electrochem. Soc. **133**, 2093 (1986); LBL-19759.

Other Publications

6. G.G. Trost, V. Edwards, and J. Newman, "Electrochemical Reaction Engineering," in *Chemical Reaction and Reactor Engineering*, J.J. Carberry and A. Varma, eds; Marcel Dekker, Inc., New York, 1987, p. 923; LBL-15984.

LBL Reports

7. D. Bernardi (Ph.D. Thesis), "Mathematical Modeling of Lithium (alloy), Iron Sulfide Cells and the Electrochemical Precipitation of Nickel Hydroxide," LBL-20858.
8. P. Russell and J. Newman, "Anodic Dissolution of Iron in Acidic Sulfate Electrolytes, Part II: Mathematical Model of Current Oscillations Observed under Potentiostatic Conditions," submitted to J. Electrochem. Soc.; LBL-19773.
9. M. Matlosz and J. Newman, "Solving One-Dimensional Boundary-Value Problems with Band-Aid: A Functional Programming Style and a Complementary Software Tool," submitted to Computers in Chem. Eng.; LBL-21589.
10. D. Bernardi and J. Newman, "Mathematical Modeling of Lithium(alloy), Iron Disulfide Cells," submitted to J. Electrochem. Soc.; LBL-21764.
11. V. Edwards (Ph.D. Thesis), "Design of Thin-Gap Channel Flow Cells," LBL-21848.
12. J. Newman, "Modeling of Porous Electrodes in Molten-Salt Systems," LBL-21867.

Invited Talks

13. J. Newman, "Modeling of Porous Electrodes in Molten Salt Systems," International Molten Salt Workshop, Argonne National Laboratory, Batavia, IL, April 16–18, 1986; LBL-21867.
14. J. Newman, chaired session on "Catalysis and Chemically Modified Electrodes," Alcoa Laboratories Centennial Technical Symposia 1986–1988, Electrochemistry Technical Agenda, Pittsburgh, PA, June 4, 1986.

Health and Environmental Sciences

Semiconductor Materials and Devices*

Eugene E. Haller, Investigator

INTRODUCTION

The recently achieved ultrahigh purity and crystalline perfection of large germanium single crystals and, to a lesser degree, silicon single crystals have led to the discovery of a large number of novel impurity and defect complexes that exhibit energy levels in the band gap of these semiconductors. Understanding the composition and electronic structure of these novel acceptors and donors through the use of sensitive far-infrared spectroscopy techniques and novel radioactive-tracer schemes represents one component of this research effort. Another closely coupled component focuses on the formation of these centers during crystal growth.

Two factors have helped greatly in identifying the composition of these novel acceptors and donors: (1) correlations between composition and electronic structure of a given center, and (2) control of the materials involved in the crystal growth and purification, such as the crucible material (typically synthetic silica or graphite) and the ambient (typically H_2, N_2, or vacuum). One of the major findings is that atomic hydrogen plays an important role in the formation and composition of many of the new impurity complexes. The information gained through this research is of immediate use to LBL's semiconductor radiation-detector program, which originated this research.

The use of ultrapure crystals as starting material for specially doped crystals is studied in connection with the development of sensitive far-infrared photoconductors for low-photon-flux applications in outer space and neutron-transmutation-doped germanium bolometers. The high ratio of intentional-dopant concentrations and residual-impurity concentrations has led to photoconductors with very high responsivity working close to the photon noise limit.

The close coupling between crystal synthesis and analysis has enabled us to effectively study and use these extremely pure and structurally perfect materials.

*This work was supported by the Director, Office of Energy Research, Office of Health and Environmental Research, U.S. Department of Energy under Contract No. DE-AC03-76SF00098.

1. Isotope-Induced Symmetry Change in Dynamic Semiconductor Defects (Publication 13)

J.M. Kahn, L.M. Falicov, and E.E. Haller

Two hydrogen nuclei and a hole bind to the triple-acceptor copper in germanium. The result is a single acceptor whose electronic states are modified by coupling to the zero-point motion of the nuclei. That motion displays a qualitative change from rotation to libration induced by an increase in hydrogen isotopic mass. The acceptor $A(CuH_2)$ has full tetrahedral symmetry and a complex ground-state manifold. All heavier isotope combinations display only a single ground-state component of symmetry lower than tetrahedral.

Figure 1-1 shows the photothermal ionization (PTI) spectra of acceptors $A(CuH_2)$ in Ge samples grown in different ambients. The PTI spectrum of a sample grown in a pure H_2 ambient (a) shows at least 11 overlapping hydrogenic line series. Comparison of spectra taken between 4.2 and 14 K shows

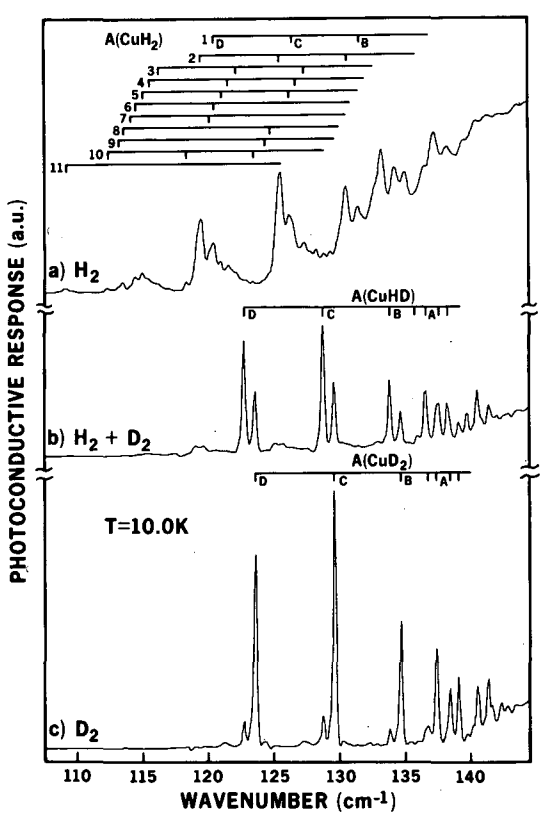

Figure 1-1. PTI spectra of sample grown in pure H_2 ambient (a), a 1:1 mixture of H_2 and D_2 (b), and nearly pure D_2 (c). (XBL 863-1157B)

that at higher temperatures, series at a lower wave number become relatively stronger, consistent with a single center that has a manifold of 1s-like states. The spectrum of the sample grown in a nearly pure D_2 atmosphere (c) is dominated by one hydrogenic series of lines that does not match any series observed in samples grown in H_2. The spectrum of sample (b), grown in a 1:1 mixture of H_2 and D_2, contains the multiple-line series of the center containing H, as well as the single-line series of the center containing D. But the spectrum is dominated by yet another hydrogenic line series, due to a center containing both H and D. We estimate the relative concentrations of the three centers by comparing integrated peak areas of the D or C transition, where we include all the series of the center containing H. We find the following relative concentrations: [containing H]:[containing H,D]:[containing D] $\simeq$ 1:2:1. It immediately follows that the centers are $A(CuH_2)$, A(CuHD), and $A(CuD_2)$, respectively. Given an equal number of H and D atoms, there are twice as many ways to make HD as either H_2 or D_2. Reexamination of (c) shows that the sample contains a small amount of A(CuHD), caused by traces of H in the D_2 gas used during crystal growth.

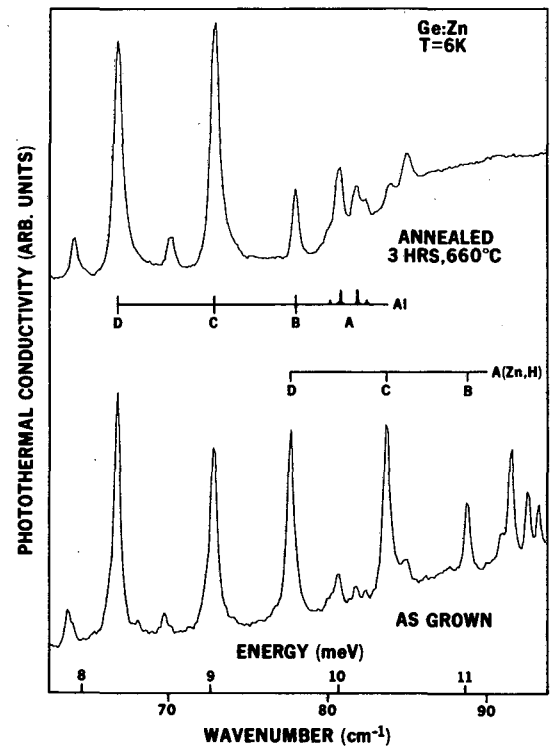

Figure 2-1. Lower: PTI spectrum at 6 K of as-grown zinc-doped Ge sample, grown in hydrogen ambient, showing A(Zn,H) and Al spectra. Upper: Spectrum of annealed sample. Note the absence of A(Zn,H) after 3 hr at 660°C. (XBL 848-3328)

2. Beryllium-Hydrogen and Zinc-Hydrogen Shallow-Acceptor Complexes in Germanium (Publication 21)

R.E. McMurray, Jr., N.M. Haegel, J.M. Kahn, and E.E. Haller

New shallow-acceptor complexes with hydrogenically spaced excited states have been discovered in intentionally doped crystals of ultrapure germanium. The doping consists of $>10^{14}$ cm^{-3} of the group II impurities beryllium or zinc, and the crystals were grown under a hydrogen atmosphere. The identification proposed in this paper is that of hydrogen-group II impurity complexes, with piezospectroscopic behavior of a <111>-oriented defect. Figure 2-1 shows the PTI spectrum of a zinc-doped Ge sample grown in an H_2 ambient.

3. Transient Response of Ge:Be and Ge:Zn Far-Infrared Photoconductors under Low-Background Photon-Flux Conditions (Publication 9)

N.M. Haegel and E.E. Haller

An experimental study of the transient behavior of Ge:Be and Ge:Zn photoconductors to changes in photon flux rates has been performed under the low-background-flux conditions ($p \simeq 10^8$ photons/sec) typical of astronomy and astrophysics applications. A characteristic transient behavior with time constants ranging from 0.1 to > 5 sec has been observed in both materials when the shallow levels are very closely compensated. The detector response consists of both a fast and a slow component. The amplitude of the slow component can be up to 10 times greater than the initial fast component. It has been established that this phenomenon cannot be explained by current models of carrier sweep-out or dielectric relaxation. The transient behavior has been characterized as a func-

tion of temperature, electric field, photoconductive gain, and material parameters.

4. Intrinsic Linewidths of 1s → np Donor Transitions in Ultrapure Germanium (Publication 23)

E.E. Haller, H. Navarro, and F. Keilmann

In an attempt to investigate the fundamental linewidths of dipole transitions of donor-bound electrons in ultrapure semiconductors, we have performed magnetoptical spectroscopy. The stress-insensitive donor complex D(O,H),[1] which can be generated in ultrapure germanium with concentrations of the order of 10^{11} cm^{-3}, was investigated. Various 1s → np (n = 2, 3, 4, 5, 6) transitions were tuned with a variable magnetic field to far-infrared laser lines with wavelengths of 115.8, 110.4, 108.7, 103.4, and 103.1 μm, and the photothermal ionization response was recorded (see Figures 4-1 and 4-2). The laser linewidths were estimated to be smaller than 10 MHz (2.4 neV). The transitions 1s → 2p− and 1s → 3p− lead to Lorentzian lines with a full

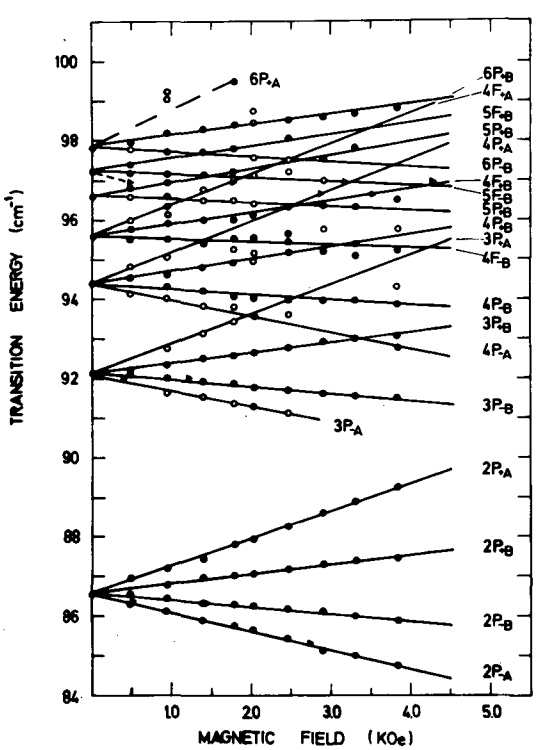

Figure 4-1. The Zeeman diagram of the D(H,O) donor transition lines, measured with a Fourier-transform interferometer. (XBL 8612-5063)

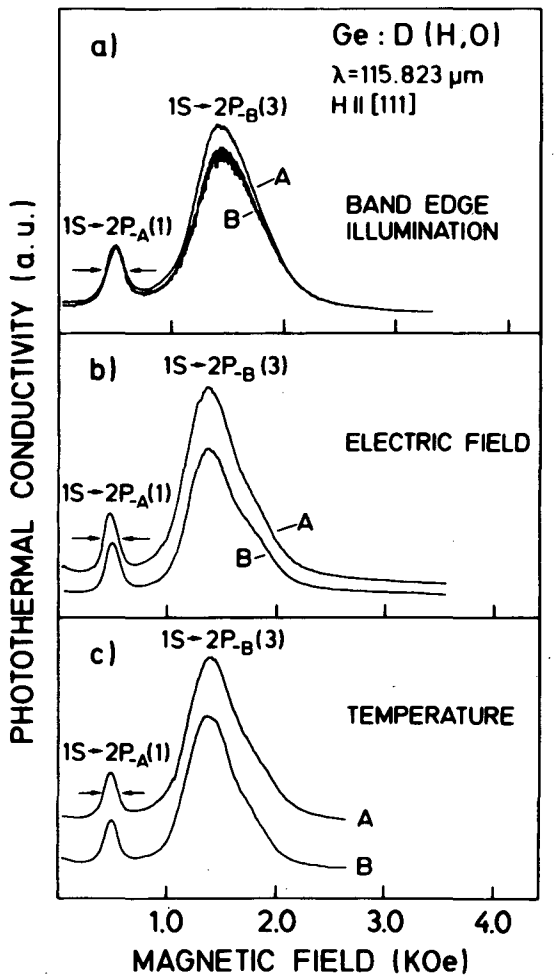

Figure 4-2. Photothermal conductivity spectra of the D(H,O) donor as a function of the magnetic field. The symbols (1) and (3) denote the number of equivalent valleys with respect to H. (XBL 8612-5064)

width at half maximum of about 8.4 μeV. Higher excited states produced lines as narrow as 3 μeV, to our knowledge the narrowest lines ever recorded in a semiconductor. A systematic investigation has shown that the observed linewidths do not depend on the sample temperature below 9 K, the applied electric field below 1.4 V cm^{-1}, and on band-edge light, which creates free electrons and holes. The latter neutralize a large fraction of the compensating acceptors, thereby reducing the random Coulomb fields. The independence of the linewidths from all the above factors, together with the special property of the selected donor D(O,H), suggest that either some neutral defects (impurities such as Si, C, H, or O), which are present at concentrations as high as 10^{14} cm^{-3}, or radiative decay dominates the linewidths. We favor the latter process because of

the decrease of linewidths with increasing quantum number n.

1. E.E. Haller, W.L. Hansen, and F.S. Goulding, Adv. in Phys. **30**, 93 (1981); see also B. Joos, E.E. Haller, and L.M. Falicov, Phys. Rev. B **22**, 832 (1980).

1986 PUBLICATIONS AND REPORTS

Refereed Journals

1. J.C. Culbertson, J.E. Furneaux, and E.E. Haller, "A Study of the Dynamics of the Electron-Hole-Liquid Free Exciton System in Ge Using No-Phonon Luminescence," in *Proc. 17th Int. Conf. Phys. of Semiconductors*, J.D. Chadi and W.A. Harrison, eds., Springer, p. 1281 (1985).
2. K.M. Yu, J.M. Jaklevic, and E.E. Haller, "Applications of Heavy-Ion Rutherford Backscattering Spectrometry (HIRBS) to the Analysis of Contact Structures on GaAs and Ge," Nucl. Instrum. Methods **B10/11**, 606 (1985); LBL-18466.
3. J.C. Culbertson, J.E. Furneaux, and E.E. Haller, "A Study of the Dynamics of the Electron-Hole-Liquid Free-Exciton System in Ge Using No-Phonon Luminescence Mediated by Shallow Impurities," Solid State Commun. **53**, 1147 (1985).
4. J.C. Culbertson, J.E. Furneaux, and E.E. Haller, "A New Probe of the Electron-Hole-Liquid Free-Exciton System in Ge: No-Phonon Luminescence," Solid State Commun. **54**, 417 (1985).
5. K.M. Yu, J.M. Jaklevic, and E.E. Haller, "Investigation of Metal/GaAs Reactions by Heavy Ion Rutherford Backscattering Spectrometry (HIRBS)," Mat. Res. Soc. Symp. D Proc. **69**, 281 (1986); LBL-20510.
6. E.E. Haller, "Semiconductor Physics in Ultra-Pure Germanium," *Festkörperprobleme/Adv. Solid State Phys.*, P. Gross, Ed., **XXVI**, 203 (1986); LBL-20624.
7. P.N. Luke and E.E. Haller, "Imaging of Radio-Carbon Clusters in High-Purity Germanium Using a Self Detection Scheme," J. Appl. Phys. **59**, 3734 (1986); LBL-20658.
8. T.A. Germer, N.M. Haegel, and E.E. Haller, "Photo Hall Effect Characterization of Closely Compensated Ge:Be," J. Appl. Phys. **60**, 1055 (1986); LBL-20428.
9. N.M. Haegel and E.E. Haller, "Transient Response of Ge:Be and Ge:Zn Far-Infrared Photoconductors Under Low Background Photon Flux Conditions," Infrared Phys. **26**, 247 (1986); LBL-21009.
10. A. Amirav, W.R. Lambert, M.J. Cardillo, P.L. Trevor, P.N. Luke, and E.E. Haller, "Electron-Hole Pair Creation at a Ge(100) Surface by Ground-State Neutral Xe Atoms," J. Appl. Phys. **59**, 2213 (1986).
11. G.H. Rieke, C. Lada, M. Lebofsky, F. Low, P. Strittmatter, E. Young, J. Arens, E. Haller, P. Richards, C. Beichman, T.N. Gautier, J. Mould, G. Neugebauer, S. Galema, and M. Werner, "MIPS: The Multiband Imaging Photometer for SIRTF," in *Instrumentation for Optical Remote Sensing from Space*, SPIE **589**, 252 (1985).
12. J.Q. Wang, P.L. Richards, J.W. Beeman, N.M. Haegel, and E.E. Haller, "Optical Efficiency of Far-Infrared Photoconductors," Appl. Opt. **25**, 4127 (1986); LBL-21958.
13. J.M. Kahn, L.M. Falicov, and E.E. Haller, "Isotope-Induced Symmetry Change in Dynamic Semiconductor Defects," Phys. Rev. Lett. **57**, 2077 (1986); LBL-21885.
14. K.M. Yu, S.K. Cheung, T. Sands, J.M. Jaklevic, N.W. Cheung, and E.E. Haller, "Schottky Barrier Degradation of the W/GaAs System After High Temperature Annealing," J. Appl. Phys. **60**, 3235 (1986); LBL-21268.
15. E.E. Haller, "Extrinsic Germanium Photoconductor Material: Crystal Growth and Characterization," 3rd International Symposium on "Optical and Optoelectronic Applied Sciences and Engineering," Innsbruck, Austria, March 15–16, 1986; SPIE Proc. **659**, 188 (1986).
16. M.L.W. Thewalt, D. Labrie, E.C. Lightowlers, and E.E. Haller, "Effects of <001> Uniaxial Stress on the Photoluminescence Spectrum of Ge-Doped with Zn," Solid State Commun. **54**, 1043 (1986).

Other Publications

17. J.C. Culbertson, R.M. Westervelt, and E.E. Haller, "Free Exciton Diffusion and Decay in Zero Stress Ge," submitted to Phys. Rev. B.
18. H. Navarro, J. Griffin, and E.E. Haller, "The Zeeman Spectra of Phosphorus and the D(H,O) Donor Complex in Ultrapure Germanium," in *Proc. 2nd Int. Conf. on Shallow Impurity Centers*, Trieste, Italy, July 28–Aug. 1, 1986.
19. H. Navarro, J. Griffin, R.E. McMurray, Jr., and E.E. Haller, "Experimental Study of Three Ground-State Components of the Hydrogen-Oxygen Donor in Germanium," submitted to Solid State Commun.
20. M.L.W. Thewalt, D. Labrie, I.J. Booth, B.P. Clayman, E.C. Lightowlers, and E.E. Haller, "Photoluminescence and Infrared Absorption Studies of Double Acceptors in Germanium," in *Proc. 2nd Int. Conf. on Shallow Impurity Centers*, Physica *B* (in press).

LBL Reports

21. R.E. McMurray, Jr., N.M. Haegel, J.M. Kahn, and E.E. Haller, "Beryllium-Hydrogen and Zinc-Hydrogen Shallow Acceptor Complexes in Germanium," Solid State Commun. (in press); LBL-20881.
22. J.M. Kahn, E.E. Haller, and L.M. Falicov, "Copper-Dihydrogen Acceptors in High-Purity Germanium," in *Proc. 18th Int. Conf. on Physics of Semiconduc-*

tors, Stockholm, Sweden, Aug. 1986, O. Engstroem, Ed. (in press); LBL-21183.

23. E.E. Haller, H. Navarro, and F. Keilmann, "Intrinsic Linewidths of 1s → np Donor Transitions in Ultra-Pure Germanium," in *Proc. 18th Int. Conf. on Physics of Semiconductors*, Stockholm, Sweden, Aug. 1986, O. Engstroem, Ed. (in press); LBL-22120.
24. D.D. Nolte, E.E. Haller, and P. Omling, "Uniaxial Stress DLTS Measurements on Iron Acceptor Pairs in Silicon," in *Proc. 14th ICDS*, H.J. von Bardeleben, Ed. (in press); LBL-21280.
25. J.M. Kahn, E.E. Haller, and L.M. Falicov, "Copper-Dihydrogen Acceptors in High-Purity Germanium," LBL-21424.
26. E.E. Haller, "Infrared Spectroscopy of Impurity Complexes in Germanium," in *Proc. 2nd Int. Conf. on Shallow Impurity Centers*, Physica *B* (in print); LBL-21955.
27. K.M. Yu, S.K. Cheung, T. Sands, J.M. Jaklevic, and E.E. Haller, "Correlation Between Solid State Reaction and Electrical Properties of the Rh/GaAs Schottky Contact," submitted to J. Appl. Phys.; LBL-21889.
28. D.D. Nolte, E.E. Haller, L.M. Falicov, and P. Omling, "The Effect of Uniaxial Stress on Iron-Boron and Iron-Aluminum Defects in Silicon," submitted to Phys. Rev. B; LBL-22110.
29. K.M. Yu, T. Sands, J.M. Jaklevic, and E.E. Haller, "Interfacial Interactions of Evaporated Iridium Thin Films with (100) GaAs," submitted to Conf. on Phys. and Chem. of Semiconductor Interfaces; LBL-22376.
30. D.D. Nolte, W. Walukiewicz, and E.E. Haller, "Deformation Potentials of Transition Metal Defects in GaAs," Bull. Am. Phys. Soc. Series II (in press); LBL-22605abs.
31. N.M. Haegel (Ph.D. Thesis), "Transient and Temperature-Dependent Phenomena in Ge:Be and Ge:Zn Far Infrared Photoconductors," LBL-20627.
32. J.M. Kahn (Ph.D. Thesis), "Hydrogen-Related Acceptor Complexes in Germanium," LBL-22652.
33. M. Tabache (M.S. Thesis), "Effect of Indium and Silicon Doping on the Deformation Behavior of GaAs Single Crystals," LBL-20947.
34. S.K. Cheung (M.S. Thesis), "High Temperature Stability of W/GaAs Schottky Contacts: Structural and Electrical Studies," LBL-22711.

Invited Talks

35. E.E. Haller, "Semiconductor Physics in Ultra-Pure Germanium," MPI für Festkörporschung, Stuttgart, Federal Republic of Germany, Feb. 2, 1986.
36. E.E. Haller, "Tunnelnde Störstellenkomplexe in Germanium," Wacker Chemitronic Burghausen, Federal Republic of Germany, Mar. 10–11, 1986.
37. E.E. Haller, Hauptvortrag: "Semiconductor Physics in Ultra-Pure Germanium" (talk given in German), Spring Meeting, German Physical Society, Freudenstadt, Federal Republic of Germany, March 7–15, 1986.
38. E.E. Haller, "Komplexe in Ultra-Reinem Germanium," University of Tuebingen, Federal Republic of Germany, April 24, 1986.
39. E.E. Haller, "Ge:XX Photoleiter: Materialsynthese und Characterisierung," Battelle Institute, Frankfurt, Federal Republic of Germany, May 6, 1986.
40. E.E. Haller, "Störstellenkomplexe in Ultra-Reinem Germanium," ETH, Zürich, Switzerland, May 12, 1986.
41. E.E. Haller, "Physics in Ultra-Pure Germanium," Instituto di Fisica, Modena, Italy, May 20, 1986.
42. E.E. Haller, "Impurity Complexes in Ultra-Pure Germanium," Scuola Normale Superiore, Pisa, Italy, May 23, 1986.
43. E.E. Haller, "Semiconductor Physics in Ultra-Pure Germanium," MPI für Festkörperforschung, Stuttgart, Federal Republic of Germany, May 26, 1986.
44. E.E. Haller, "Störstellenkomplexe in Ultra-Reinem Germanium," Physik. Techn. Bundesanstalt, Braunschweig, Federal Republic of Germany, May 28–29, 1986.
45. E.E. Haller, "Störstellenkomplexe in Ultra-Reinem Germanium," University of Göttingen/Clausthal, Federal Republic of Germany, May 30, 1986.
46. E.E. Haller, "Novel Defect Centers in Ultra-Pure Germanium: Composition and Structure," University of Gent, Belgium, June 1–3, 1986.
47. E.E. Haller, "Störstellenkomplexe in Ultra-Reinem Germanium," University of Köln, Federal Republic of Germany, June 3–4, 1986.
48. E.E. Haller, "Ultra-Pure Germanium: Crystal Synthesis and Analysis," and "Novel Centers in Ultra-Pure Germanium: Their Structure and Composition," University of Lund, Sweden, June 4–6, 1986.
49. E.E. Haller, "Störstellenkomplexe in Ultra-Reinem Germanium," University of Regensburg, Federal Republic of Germany, June 10–11, 1986.
50. E.E. Haller, "Advanced Materials Research: Ultra-Pure Germanium as an Example," University of Paderborn, Federal Republic of Germany, June 12–13, 1986.
51. E. E. Haller, "Flache Elektronenzustände im Halbleiter: Analogie zum Wasserstoffatom," University of Erlangen/Nürnberg, Federal Republic of Germany, June 16, 1986.
52. E.E. Haller, "Ge Photoleiter und Bolometer," MPI für Radiosastronomie, Bonn, Federal Republic of Germany, June 26, 1986.
53. E.E. Haller, "Novel Complexes in Ultra-Pure Germanium," MPI für Festkörperforschung, Hochfeld Magnetlabor, Grenoble, France, July 1–2, 1986.
54. E.E. Haller, "GaAs Research at the Center for Advanced Materials," HCA Laboratories, Zürich, Switzerland, July 3, 1986.

55. E.E. Haller, "Störstellenkomplexe in Ultrareinem Germanium," Siemens Forchungszentrum Perlach, München, Federal Republic of Germany, July 16, 1986.
56. E.E. Haller, "Infrared Spectroscopy of Complexes in Germanium," 2nd International Conference on Shallow Centers in Semiconductors, Trieste, Italy, July 28–Aug. 1, 1986.
57. E.E. Haller, "Copper-Dihydrogen Acceptors," 18th International Conference on the Physics of Semiconductors, Stockholm, Sweden, Aug. 11–15, 1986.
58. E.E. Haller, "Uniaxial Stress DLTS Measurements on Iron-Acceptor Pairs in Silicon," 14th International Conference on Defects in Semiconductors, Paris, France, Aug. 18–20, 1986.
59. E.E. Haller, "Defects in Pure Semiconductors: Compositions and Structure," Department Seminar, University of California, Berkeley, Oct. 23, 1986,
60. E.E. Haller, "Hydrogen Related Complexes in Ultra-Pure Germanium," University of British Columbia, Vancouver, B.C., Oct. 29, 1986; Simon Fraser University, Vancouver, B.C., Oct. 30, 1986.

Work for Others

OFFICE OF NAVAL RESEARCH

Quantum Monte Carlo for Molecular Studies*

William A. Lester, Jr., Investigator

INTRODUCTION

We are pursuing the use of the quantum Monte Carlo (QMC) method for the computation of molecular properties. This approach, borrowed from statistical mechanics, allows one to calculate essentially exact quantum-mechanical expectation values. Thus, it provides an alternative to traditional *ab initio* quantum chemical approaches. The method takes advantage of the formal similarity of the Schrödinger equation in imaginary time to a diffusion equation.

1. Quantum Monte Carlo Approach to Elecronically Excited Molecules (Publications 1 and 2)

R.M. Grimes, B.L. Hammond, P.J. Reynolds, and W.A. Lester, Jr.

QMC has demonstrated an ability to accurately compute ground-state energies for atoms and molecules. Excited states having a different symmetry than the ground state have also been studied with great precision. However, excited states having the same symmetry as the ground state are of considerable interest. Following the fixed-node approach, such excited states of H_2 have been studied recently and over 95% of the correlation energy obtained. It was necessary, however, to abandon the commonly used single-determinant form of importance function. Instead, a small multiconfiguration–self-consistent-field (MCSCF) wave function of 8 determinants was necessary.

Other approaches to obtaining excited-state energies are currently being investigated. One method involves the calculation of a matrix of energy correlation functions, from which the entire (low-lying) spectrum of excited states may be obtained. These energies are, in principle, variational like the usual QMC ground-state energies. By applying this approach to the nuclear-motion problem, the vibrational excitation frequencies may be obtained for molecules whose potential-energy surface is known.

2. Is Quantum Monte Carlo Competitive? Lithium Hydride Test Case (Publication 3)

R.N. Barnett, P.J. Reynolds, and W.A. Lester, Jr.

QMC with fixed nodes is shown to be computationally competitive with large-scale state-of-the-art quantum chemical techniques. LiH has been studied extensively in the past and has often been used as a test of new methods. Recently, very accurate LiH energies have been reported using numerical-orbital many-body-perturbation-theory coupled-cluster (CC)[1] and configuration-interaction (CI)[2] methods (see Table 2-1). QMC has been applied in the past few years to a number of molecular systems, generally yielding excellent energies. Nevertheless, the issue of the method's competitiveness with traditional approaches has often been raised. In the present study of LiH, the fixed-node QMC approach was able to obtain over 99.4% of the correlation energy (CE) for LiH at 3.015 bohr with a very small statistical uncertainty, a result obtained in less CPU time than the best CI. The QMC statistical uncertainty was 0.0004 h (0.25 kcal/mole), which is only 0.5% of the CE and 0.005% of the total energy. Finally, we note that QMC memory requirements (<20,000 words) are insignificant in comparison to those of large-scale CI calculations.

*This work was supported by the Office of Naval Research through an agreement with the U.S. Department of Energy under Contract No. DE-AC03-76SF00098.

1. L. Adamowicz and R.J. Bartlett, J. Chem. Phys. **84**, 6837 (1986).
2. N.C. Handy, R.J. Harrison, J.J. Knowles, and H.F. Schaefer III, J. Phys. Chem. **88**, 4852 (1984).
3. R.J. Harrison and N.C. Handy, Chem. Phys. Lett. **113**, 257 (1985).

Table 2-1
Computed total energies, correlation energies, and percentage of the correlation energy for LiH. The "exact" total energy of LiH is derived from the experimental energy of Li obtained from ionization potentials and corrected for relativistic and finite-mass effects, and the experimental binding energy of LiH are corrected for zero-point motion. Energies are in Hartrees. Values in parentheses represent one standard deviation from the mean in a Gaussian distribution.

Method	Energy	CE	%CE
SCF	−7.98735	0.0	0.0
CI	−8.06904	0.08169	98.2
CC	−8.06951	0.08216	98.8
GFMC[a]	−8.071(1)	0.0837(10)	100.7(12)
GFMC[b]	−8.071(2)	0.0837(20)	100.7(24)
QMC[c]	−8.0700(4)	0.0827(4)	99.4(5)
QMC[d]	−8.0701(4)	0.0828(4)	99.5(5)
Exact	-8.07050	0.08315	100.0

a. Released-node
b. Fixed-node
c. One-determinant trial function; this work.
d. Two-determinant trial function.[3]

3. Work in Progress

Energy Derivatives by QMC (B.L. Hammond, P.J. Reynolds, and W.A. Lester, Jr.)

While conventional *ab initio* approaches regularly compute the analytic derivative of the energy with respect to nuclear coordinates in order to determine equilibrium geometries, and (by finite difference or higher analytic derivatives) vibrational frequencies, thus far only a preliminary study has been attempted with QMC. To compute the energy derivative with respect to a nuclear coordinate ρ, one writes

$$\frac{d < E >}{d\rho} = \frac{d}{d\rho}\left\{\frac{\int \phi(\underline{R})\Psi_T(\underline{R})\, E_L(\underline{R})\, d\underline{R}}{\int \phi(\underline{R})\Psi_T(\underline{R})\, d\underline{R}}\right\} =$$

$$< \frac{\partial E_L}{\partial \rho} > + < \frac{1}{\phi}\frac{\partial \phi}{\partial \rho} E_L > - < \frac{1}{\phi}\frac{\partial \phi}{\partial \rho} > < E_L >$$

$$+ < \frac{1}{\Psi_T}\frac{\partial \Psi_T}{\partial \rho} E_L > - < \frac{1}{\Psi_T}\frac{\partial \Psi_T}{\partial \rho} > < E_L > .$$

The second equality is obtained from differentiation using the chain rule, followed by expression of the resulting ratios as averages over the distribution $\Psi_T\phi$. The derivative $\partial\phi/\partial\rho$ is unknown; it is, however, possible to sample it. The other terms may be evaluated straightforwardly during the QMC simulation. Rather than sampling $\partial\phi/\partial\rho$, as a first approximation one may take $\phi^{-1}\partial\phi/\partial\rho = \Psi_T^{-1}\partial\Psi_T/\partial\rho$. This turns out to be a good approximation even when Ψ_T is only of moderate accuracy (e.g., double-zeta basis set in the Hartree-Fock approximation). Using this approach, calculations on H_2 at a few nuclear separations have given excellent results.

Molecular Properties and Transition Matrix Elements (R.N. Barnett, P.J. Reynolds, and W.A. Lester, Jr.)

Since its inception, QMC has been used primarily to compute energies of atoms and molecules. Other properties, not directly related to the energy, are also of considerable interest. In particular, moments of the charge distribution as well as transition matrix elements are of prime concern.

To compute permanent moments the standard QMC algorithm must be modified. Currently, a highly vectorized code that calculates moments as well as the energy with very little overhead (6% for LiH and less for larger molecules) is in use. Permanent moments have been computed for H_2, LiH, and BH.

For H_2 the fixed-node solution is exact, and as expected the value for the quadrupole moment obtained by QMC,[1] 0.529(15), agrees well with the exact value of Kolos and Wolniewicz[2] of 0.523. For LiH, fixed-node solutions that yield over 99% of the correlation energy are readily obtainable. Thus accurate moments should also be achieved by QMC. Here QMC gives a dipole moment of 5.89(2) versus the exact value[3] of 5.83 and an extended CI value[4] of 5.86. For the quadrupole moment of LiH, QMC does as well as other recent theoretical calculations. In particular, QMC predicts −4.04(5), while other approaches have given[5,6] −4.13 and −4.29. (An experimental value is not available here.) Preliminary results on BH have also yielded a dipole moment in agreement with experiment and other theoretical calculations. This initial success has encouraged the continued exploration of the accuracy obtainable by QMC in computing permanent moments of molecules.

Accurate values of transition matrix elements—for example, transition dipole moments—are of considerable interest but have remained difficult to com-

pute. To calculate these properties using QMC requires a novel implementation of the algorithm that has recently been developed. Although a fast vectorized code is not yet operational, work on transition matrix elements of simple systems is planned.

1. Dipole moments are in Debye (10^{-18} esu-cm), and quadrupole moments are in units of 10^{-26} esu-cm^2. Numbers in parentheses represent one standard deviation in the mean.

2. W. Kolos and L. Wolniewicz, J. Chem. Phys. **41**, 3674 (1963).

3. L. Wharton, L. Gold, and W. Klemperer, J. Chem. Phys. **37**, 2149 (1962).

4. N.C. Handy, R.J. Harrison, P.J. Knowles, and H.F. Schaefer III, J. Chem. Phys. **88**, 4852 (1984).

5. B.O. Roos and A.J. Sadlej, Chem. Phys. **94**, 43 (1985).

6. C.E. Dykstra, S. Liu, and D.J. Malik, to appear in *Advances in Chemical Physics.*

1968 PUBLICATIONS AND REPORTS

Refereed Journals

1. P.J. Reynolds, R.N. Barnett, B.L. Hammond, R.M. Grimes, and W.A. Lester, Jr., "Quantum Chemistry by Quantum Monte Carlo: Beyond Ground-State Energy Calculations," Int. J. Quant. Chem. **29**, 589 (1986); LBL-20089.
2. R.N. Grimes, B.L. Hammond, P.J. Reynolds, and W.A. Lester, Jr., "Quantum Monte Carlo Approach to Electronically Excited Molecules," J. Chem. Phys. **85**, 4749 (1986); LBL-21934.

Other Publications

3. P.J. Reynolds and W.A. Lester, Jr., "Quantum Monte Carlo for Molecules," Physics in the News 1985, Phys. Today **39**, S-14, 1986.

Properties of Superconducting Thin Films; Electron-Phonon and Non-Phonon Coupling*

Vladimir Z. Kresin, Investigator

INTRODUCTION

Several interrelated problems concerned with the properties of superconductors have been studied. The superconducting state in semiconductors and semimetals can be induced by the proximity effect. As a result, one can take advantage both of the properties of semiconductors (semimetals) and of superconductivity, which is promising from the point of view of various applications (e.g., the field effect).

Another problem that has been studied is connected with the properties of superconductors with strong coupling, and an analysis of the phonon and nonphonon contributions.

1. Josephson Current in Low-Dimensional Proximity Systems and the Field Effect (Publication 1)

V.Z. Kresin

The system $S_\alpha - M_\beta - S_\gamma$ (where S_α and S_γ are superconductors, and M_β is a semiconductor, a semimetal, or a normal metal) is studied. Particular attention is paid to the case when M_β contains a two-dimensional electron gas (e.g., an inversion layer). A one-dimensional case is also considered. The Josephson current is evaluated, and the main factors determining the field effect are studied. A special diagrammatic method allowing one to calculate the thermodynamic Green's function and, consequently, the Josephson current, has been developed. The current depends strongly on the electron concentration, which leads to a noticeable field effect. The dependence of j_m on other factors, such as temperature, mobility, effect mass, etc., is also studied. The field effect appears to be stronger for low-dimensional systems. An analysis of the experimental data obtained recently for the Nb-InAs-Nb system is carried out.

*This work was supported by the U.S. Office of Naval Research under Contract No. N00014-86-F0015, through an agreement with the U.S. Department of Energy under Contract No. DE-AC03-76SF00098.

2. Critical Temperature for Any Strength of the Electron-Phonon Coupling (Publication 2)

V.Z. Kresin

The analytical expression describing T_c, the critical temperature, is obtained. The expression is valid for any strength of the electron-phonon coupling λ. The evaluation is based directly on the Eliashberg equation (EE), and the result is a generalization of the limiting expressions obtained analytically, also directly from the EE. The dependence of T_c on a shift of the phonon spectrum can be studied for any region of the value λ. A nonmonotonic dependence of T_c on the electron concentration is obtained.

3. Two-Dimensional Electron System and Josephson Tunneling (Publication 3)

V.Z. Kresin

The properties of the system superconductor–2D electron gas–superconductor have been studied. The most important case is when the 2D system is an inversion layer. This case is related to the investigation of the effect of electric field on the Josephson current. The dependence of the supercurrent on temperature and the length of weak coupling has been studied. A special diagrammatic method allowing one to study the effect at any temperature has been developed. We are interested particularly in the dependence of the Josephson current on the electron concentration. The field effect appears to be different in different temperature regions.

4. Field Effect and Josephson Junctions (Publication 4)

V.Z. Kresin

The value of the Josephson current in an S-M-S system, where M contains a low-dimensional electron gas, can be affected noticeably by an applied voltage (field effect). This effect is related directly to the possibility of building a three-terminal device. The dependence of the current on the carrier concentration is studied. The peculiar situation when the state of the lowest subband is described by the "dirty" limit, whereas the higher subband represents the "clean" limit, appears to be realistic. Intersub-

band scattering results in a nonmonotonic behavior of the current.

5. Work in Progress

The effect of radiation on the properties of semiconductor-superconductor proximity systems is being studied. A method of separating the nonphonon contribution based on analysis of tunneling and heat-capacity data is being developed.

1986 PUBLICATIONS AND REPORTS

Refereed Journals

1. V.Z. Kresin, "Josephson Current in Low Dimensional Proximity Systems and the Field Effect," Phys. Rev B **34**, 7587 (1986); LBL-21145.

Other Publications

2. V.Z. Kresin, "Critical Temperature for Any Strength of the Electron-Phonon Coupling," submitted to Bull. Am. Phys. Soc.; LBL-22760.
3. V.Z. Kresin, "Two-Dimensional Electron System and Josephson Tunneling," Bull. Am. Phys. Soc. **31**, 385 (1986); LBL-20751.

LBL Reports

4. V.Z. Kresin, "Field Effect and Josephson Junction," accepted by IEEE Proc. Magnetics; LBL-22185.

Invited Talks

5. V.Z. Kresin, "Field Effect and Its Applications," Naval Research Laboratory, Washington, DC, April 18, 1986.
6. V.Z. Kresin, "Induced Superconducting State in Semiconductors," Ames National Laboratory, Ames IA, Sept. 26, 1986.

UNITED STATES AIR FORCE

Quantum Monte Carlo Study of Tetrahydrogen*

William A. Lester, Jr., Investigator

INTRODUCTION

The purpose of this project is to investigate properties of tetrahydrogen (H_4) using the fixed-node quantum Monte Carlo (FNQMC) method. Properties of interest include formation mechanisms, potential-energy surfaces (pes's), lifetimes, and decay channels. At long range, the H_4 species of interest correlates with $H_2(^1\Sigma_g^+)$ + $H_2(B\ ^1\Sigma_u^+)$ at one asymptote and H + H_3 at the other asymptote (see Figure 1-1). Efforts are directed at confirming the existence and stability of the maximum-ionicity excited state (MIES) predicted by Nicolaides *et al.*,[1] using multireference configuration-interaction wave functions. The FNQMC approach will be used to determine decomposition pathways and, in particular, classical barriers to formation of the MIES and other excited forms. Hartree-Fock, multiconfiguration Hartree-Fock, and configuration-interaction wave functions will be used, where appropriate, as importance functions in the FNQMC study.

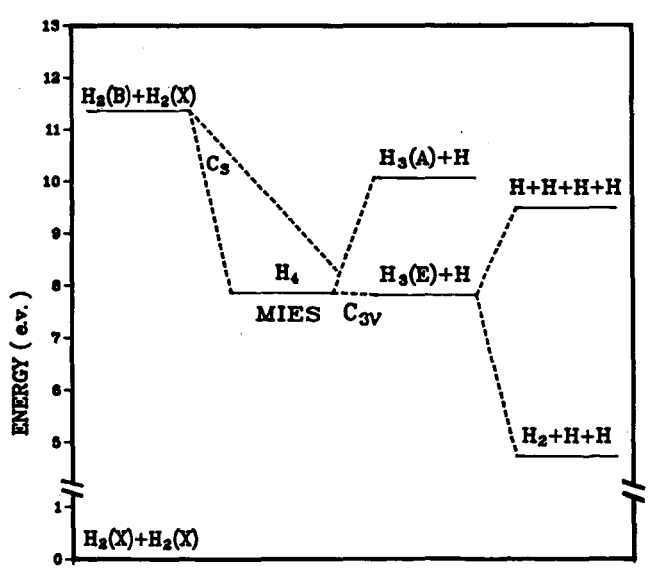

Figure 1-1. Correlation diagram for the H_4 MIES. (XBL 873-1123)

*This work was supported by the U.S. Air Force Rocket Propulsion Laboratory under Contract No. F04611-85-X-0068, through an agreement with the U.S. Department of Energy under Contract No. DE-AC03-76SF00098.

1. C.A. Nicolaides, G. Theodorakopoulos, and I.D. Petsalakis, J. Chem. Phys. **80**, 1705 (1984)

1. Work in Progress

Using a new trial-function optimization method and MCSF functions where appropriate, the E and A states of H_4 in trigonal pyramidal geometry are being computed following the FNQMC approach to reduce statistical error to satisfactory limits. The E-state pes will be computed for $3.8 < R < 6.0$ a.u., where R is the distance from H^- to the plane of H_3^+ in D_3h symmetry (see Figure 1-2). Pathways connecting the $H_2(X)$ and $H_2(B)$ asymptotes to the H_4 MIES system will be thoroughly explored, as well as the pathways connecting the H_4 MIES to ground and first-excited H_3 + H asymptotes. The emphasis in these studies will be placed on quantitative estimates of barriers along the pathways because of the question of H_4 MIES stability. The focus here is on pes characterization.

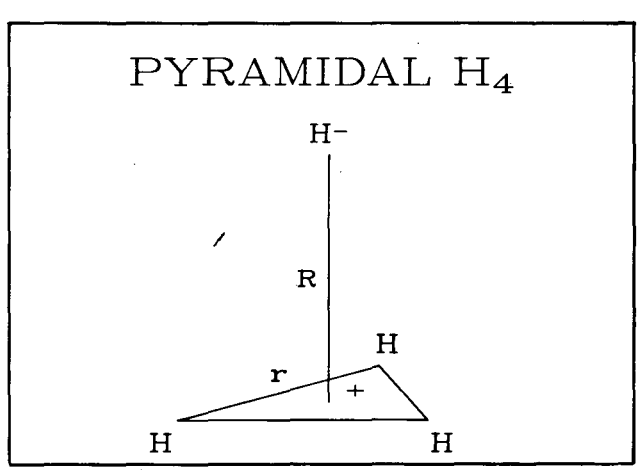

Figure 1-2. Geometry of the MIES. R is the distance from H^- to the H_3^+ plane, and r is the length of a side of the H_3^+ equilaterial triangle. (XBL 873-1124)

UNITED STATES DEPARTMENT OF TRANSPORTATION

Materials for Enhanced Heavy Fuel Capability Marine Diesels*

Alan V. Levy, Investigator

Performance of Ceramic Coatings in Diesel Engines (Publication 1)

A.V. Levy and S. MacAdam

The surface of all of the combustion-zone components—i.e., exhaust valves, piston crowns, and cylinder heads of a medium-speed marine diesel engine—were coated with 250–375 μm thick ceramic thermal barrier coatings and tested in an engine operating on a tow boat on the inland water system. The coatings were applied by two suppliers; one applied an 8%Y_2O_3-ZrO_2 ceramic coating over a NiCoCrAlY bond coat, and the other applied a 22% MgO-ZrO_2 ceramic coating over a NiCrAlY bond coat.

The engine was disassembled after 9000 hours of operation and the coatings were analyzed. All of the coatings on the larger water-cooled surfaces of the piston crowns and cylinder heads appeared to be intact, and these parts were transferred to the other engine on the towboat; the parts currently have over 15,000 hours of service. Several of the smaller, uncooled valves were destructively analyzed. It was determined that the coatings that were stabilized by magnesia had failed because the magnesia had been leached out of the ZrO_2 by the sulfur in the combustion gas, resulting in destabilization and spalling off of the coating. The valve coated with pre-alloyed yttria stabilized zirconia performed satisfactorily. Thus, the durability of ceramic coatings in diesel engines has been demonstrated.

*This work was supported by the U.S. Department of Transportation, Maritime Administration, P.O. No. 400-49002, through an agreement with the U.S. Department of Energy under Contract No. DE-AC03-76SF00098.

1986 PUBLICATIONS AND REPORTS

Other Publications

1. A.V. Levy and S. MacAdam, "Performance of Ceramic Coatings in Diesel Engines," Reprint, NACE Corrosion 86, Houston, TX, March 1986.
2. S. MacAdam and A.V. Levy, "The Behavior of CTBC's on Diesel Engine Combustion Zone Components," in *Proc. Int. Conf. Metallurgical Coatings*, San Diego, CA, April 1986.

LBL Reports

3. A.V. Levy and S. MacAdam, "Performance Analysis of Ceramic Thermal Barrier Coatings after 9000 Hours Service in a Marine Diesel Engine," LBL-22826.

Invited Talks

4. A.V. Levy and S. MacAdam, "Performance of Zirconia Coatings in 9000 Hour Test in Towboat Diesel Engine," General Coatings Symposium, ASM Materials Week, Orlando, FL, Oct. 1986.

ELECTRIC POWER RESEARCH INSTITUTE

Inhibitive Salts for Reducing High-Temperature Oxidation and Spallation*

John Stringer, Acting Investigator†

INTRODUCTION

It has been known for many years that the addition of reactive elements such as yttrium, cerium, lanthanum, or hafnium to heat-resistant alloys forming Cr_2O_3 or Al_2O_3 protective oxides could have a number of beneficial effects. Most notably, the scale adhesion is considerably improved. However, treatments that appear to be superficial can also be beneficial. These include ion implantation of the reactive elements, and the use of an aqueous solution of a water-soluble salt of the reactive element, or of a sol-gel containing the element. From the point of view of elucidating the mechanism of the "reactive-element effect," these superficial techniques are particularly interesting, since several aspects of the most successful current model imply that the reactive element is present within the alloy. No systematic study of these techniques has been made, however; they have been used only as a means of enhancing the oxidation resistance of already resistant materials.

*This work was supported by the Electric Power Research Institute under Contract No. RP 2261-1, through an agreement with the Director, Office of Energy Research, Office of Basic Energy Sciences, Materials Sciences Division of the U. S. Department of Energy under Contract No. DE-AC03-76SF00098.

†Dr. Stringer is affiliated with the Electric Power Research Institute, Palo Alto, California. He is continuing to direct the research program of the late Dr. D. P. Whittle.

1. The Effect of Surface-Applied Reactive Elements on the High-Temperature Oxidation of Chromium-Containing Alloys (Publication 3)

P.Y. Hou and J. Stringer

In order to investigate the cause of the reactive-element effects, this study is concerned with the influence of the reactive metals and/or their oxides when they are present only on the alloy surfaces prior to the oxidation at 1000°C and 1100°C in 1 atm O_2. Three binary alloys were used: Co-15wt%Cr, a non-Cr_2O_3 former that will develop the Cr_2O_3 scale with reactive metal oxide additions to the alloy; Co-25wt%Cr, a borderline Cr_2O_3 former; and Ni-25wt%Cr, a good Cr_2O_3 former. The oxides of Ca, Ce, La, Y, Hf, and Zr were applied as a thin surface coating through the application and decomposition of their aqueous nitrate salts. Y and La were also introduced in their metallic form by ion implantation.

Unlike the case where the reactive elements are present in the alloy, none of the surface-applied oxides promoted a continuous Cr_2O_3 external scale with alloys that are not already good Cr_2O_3 formers. Some—La, Y, and especially Ca oxides—could locally enhance Cr_2O_3 formation on Co-25Cr at 1000°C, but they lost their effectiveness at 1100°C. The degree of such an effect was sensitive to the amount of applied oxides, and it appears that in these cases the surface-applied oxides act only as a physical barrier to oxygen. The implanted Y or La also had no effect on the oxidation of Co-15Cr but showed a little effect on the Co-25Cr. With the latter alloy, the implanted species caused the formation of a slightly more Cr-rich scale. The degree of this chromium enrichment increased with increasing implantation dosage. Only when the dose was as high as 1×10^{18} ions/cm^2, which corresponds to a peak concentration of approximately 20 at%, could a continuous external Cr_2O_3 scale be promoted. However, this scale did not remain protective but broke down after its thickness exceeded 7–8 times that of the implantation depth.

The surface oxides appeared to be most beneficial on the established Cr_2O_3 forming alloy.

Surface-applied CeO_2, Y_2O_3, and La_2O_3 were particularly effective in reducing the growth rate of the Cr_2O_3 scale and improving the scale adhesion. The presence of these surface oxides also prevented base metal oxide formation and changed the growth direction of the scale. All of these observed effects were similar to those found when the reactive element oxides were present within the alloys. Nevertheless, the surface-applied ZrO_2 and CaO showed very little effect, and the presence of applied HfO_2 even made the oxide scales nonadherent, causing a breakaway behavior at the early stage of the oxidation process. Implantation of Y and La produced essentially the same effects as the beneficial surface-applied oxides. Results have provided a better understanding of the improved scale adherence caused by the reactive metal or oxide additions.

2. Work in Progress

Study of the effect of reactive elements will continue using the ion-implantation technique. Yttrium and hafnium ions will be used on Ni-25wt%Cr alloy. The nucleation and growth of oxides formed on the implanted vs unimplanted specimens will be characterized using transmission electron microscopy, scanning electron microscopy, Auger electron spectroscopy, and secondary-ion mass spectroscopy. The mechanism of scale adhesion promoted by the presence of these reactive elements will be the major concern of the study.

1986 PUBLICATIONS AND REPORTS

LBL Reports

1. P.Y. Hou and J. Stringer, "The Effect of Surface-Applied Reactive Metal Oxides on the High Temperature Oxidation of Alloys," accepted by Mat. Sci. Eng.; LBL-21683.
2. P.Y. Hou and J. Stringer, "Effect of Surface-Applied Reactive Element Oxides on the Oxidation of Cr-Containing Binary Alloys," submitted to J. Electrochem. Soc.; LBL-21781.
3. P.Y. Hou (Ph.D. Thesis), "The Effect of Surface-Applied Reactive Elements on the High Temperature Oxidation of Chromium-Containing Alloys," LBL-22647.

Erosion-Corrosion of Materials in Coal-Water Slurries*

Alan V. Levy, Investigator

INTRODUCTION

A project was carried out to determine the mechanism, rates, and comparative erosion behavior of several materials for service in coal-water slurry pipelines carrying coal into coal gasifiers in coal fired combined-cycle power plants. Several types of materials were selected, including ceramics, hard carbide-metal matrix composites, surface hardened steels, rubber, and mild steel for a baseline. It was determined that the materials could be divided into 3 classes of performance. The materials with the lowest erosion rates were corrosion-resistant ceramics, including alumina, silicon nitride, and fused basalt. In the middle performing class were the carbide composites, and in the highest erosion rate class of materials were the mild steel, the surface hardened steels, and the rubber. Within each class the erosion rates were essentially the same even though measured properties such as hardness differed greatly. The mechanism of erosion is being determined for each material to account for the major differences in their performance.

*This work was sponsored by EPRI under Purchase Order No. RP2048-9.

OTHER PRIVATE-SECTOR CONTRACTORS

THE NORTON COMPANY

Sliding Wear of Thermal Spray Chromia Coatings*

Alan V. Levy, Investigator

1. Sliding Wear of Chromia Base Coatings (Publication 1)

B. Wang, Z.R. Shui, and A.V. Levy

The unlubricated sliding wear behavior of thermal sprayed chromia coatings on mild steel substrates was investigated at room and elevated temperatures. The need for thermal barrier coatings to protect the cylinder-wall liners of ceramic coated diesel engines requires ceramics that have low coefficients of friction and sliding wear rates at elevated temperatures. Both flame and plasma-sprayed chromia from different starting powders and rod were tested up to 400°C. A 2.5-cm diameter, hard chromium plated washer with a 1.5 mm wide wear surface was worn against a larger diameter, ceramic-coated disk at 0.69 and 6.9 MPa contact pressure in an oscillatory, 90° reversal wear motion.

It was determined that a major reduction in both the friction coefficient and wear rates occurred in the 400°C tests compared to the behavior of the coatings at room temperature. The mechanism appeared to be a glazing of the chromia that produced a supersmooth surface. The effect was most pronounced for the flame sprayed chromia coating. The friction coefficient in the unlubricated sliding wear tests was in the 0.2 range, which is the threshold for feasibility of unlubricated wear in diesel engines.

1986 PUBLICATIONS AND REPORTS

LBL Reports

1. B. Wang, Z.R. Shui, and A.V. Levy, "Sliding Wear of Chromia Base Coatings," LBL-22819.

*This work was sponsored by a grant from the Norton Co.

CUMMINS ENGINE COMPANY

Unlubricated Sliding Wear of Ceramic Materials*

Alan V. Levy, Investigator

INTRODUCTION

The potential use of thermal insulating ceramic coatings on the cylinder walls of diesel engines at elevated temperatures requires that an understanding of the operative friction and wear mechanisms be gained. An investigation was carried out to determine the unlubricated sliding wear behavior of a number of thermal insulating oxide coatings in combination with carbide, boride, and mixed-oxide coatings and carbide-graphite fiber composites at room and elevated temperatures to 730°C. The coatings were applied up to several hundred microns thick by plasma-spray and chemical vapor deposition (CVD) processes on flat washers and discs and tested at contact pressures up to 14 MPa to steady-state wear conditions in an oscillatory, 90° reversal wear motion. Wear rates, coefficients of friction, and wear surface compositions and morphologies were determined.

It was determined that the binder metal in sprayed metal-carbide composites had a dominant influence on the wear, more so than the composition of the carbide. Different wear surface morphologies and attendant wear rates occurred at each of the test temperatures. The shape of the deposited grains in the CVD coatings had a major effect on the wear rates, rounded grains being better than angular grains of the same material. A film formed on the TiB_2–mixed oxide pairs that could have a significant effect on their wear behavior. The use of graphite fibers in a SiC matrix provided a dry film lubricant for the wear surface of the composite material that resulted in a relatively low wear rate.

1986 PUBLICATIONS AND REPORTS

Other Publications

1. A.V. Levy and N. Jee, "Elevated Temperature Sliding Wear of Ceramic and Hard Metal Coatings," Reprint, NACE Corrosion 86, Houston, TX, March 1986.
2. A.V. Levy and N. Jee, "The Elevated Temperature Sliding Wear Behavior of Carbide and Mixed Oxide Coatings," in *Proc. Int. Conf. Metallurgical Coatings*, San Diego, CA, April 1986.

Invited Talks

3. A.V. Levy, "Sliding Wear Behavior of Coatings for Cylinder Wall–Piston Ring Service," ASME-ETCE Conference, New Orleans, LA, Feb. 1986.
4. A.V. Levy and N. Jee, "Role of Microstructure in the Unlubricated, Elevated Temperature Sliding Wear of Ceramic Coatings," General Coatings Session, ASM Materials Week, Orlando, FL, Oct. 1986.

*This work was sponsored by the Cummins Engine Co., Inc., under Agreement No. 85-43.

WESTINGHOUSE ELECTRIC CORPORATION

Erosion of Hard Material Coating Systems*

Alan V. Levy, Investigator

1. Erosion of Hard Material Coating Systems (Publication 2)

A.V. Levy and B. Wang

The use of coating systems to protect structural metal surfaces from small, solid particle erosion and erosion-corrosion at elevated temperatures can extend component life and permit operation in more severe environments. The room temperature and elevated temperature erosion behavior of several hard-material coating system—i.e., carbides, borides and nitrides—was determined over a range of test conditions. Particle velocities from 70 to 150 m/s and test temperatures from 25°C to 540°C were used. Mechanisms of erosion were established and related to erosion rates in a manner that defined the requirements of composition, morphology, and defect levels of coating systems for long-term performance.

It was determined that small grain size, low porosity, and the absence of cracks were microstructural features that enhanced erosion resistance. Hardness levels and the composition and distribution of second phase hard particles had less effect on coating performance. Angular silicon carbide particles were considerably more erosive than either alumina or chromite/mixed oxide round-shaped particles, and the rankings of the coatings' performances were different for each erodent and set of test conditions.

1986 PUBLICATIONS AND REPORTS

Other Publications

1. J. Qureshi, A.V. Levy, and B. Wang, "The Erosion of Protective Coatings on Ferritic Stainless Steel," in *Proc. Int. Coating Conference on Metallurgical Coatings*, San Diego, CA, April 1986.

LBL Reports

2. A.V. Levy and B. Wang, "Erosion of Hard Material Coating Systems," LBL-22821.

Invited Talks

3. J. Qureshi, A.V. Levy, and B. Wang, "Elevated Temperature Erosion Evaluation of Selected Coating Processes for Steam Turbine Blades," Symposium on High Temperature Coatings, AIME-TMS Fall Meeting, Orlando, FL, Oct. 1986.

*This work was sponsored by a grant from Westinghouse Electric Corp.

Appendices

APPENDIX A

DIVISIONAL PERSONNEL

1986 Scientific Staff

Investigators	Postdoctoral and Other Scientists	Graduate Students		Participating Guests
Neil Bartlett		K. Kourtakis M. Lerner	S. Mayorga	T. Richardson T. Sasaki
Alexis Bell	M. Sattler	J. Brown D. Jordan K. Krishna	S. Lombardo G. Went G. Yokomizo	R. Rosin
Robert Bergman		E. Burkhardt J. Chang T. Foo D. Glueck K. Goldberg J. Hartwig D. Johnson	D. Klein W. McGhee P. Stoutland M. Trost P. Walsh E. Wasserman	
Robert Bragg	A. Lachter	M. Tidjani		
Leo Brewer	C. Meyer	J. Bularzik B. Ebbinghaus J. Kouvetakis	K. Krushwitz S. Leonard	
John Clarke		A. Cleland N. Fan M. Ferrari M. Heaney	J. Pelz J. Schmidt F. Wellstood	
Marvin Cohen	K. Chang	S. Zhang		
Eugene Commins		K. Abdullah		
Robert Connick				
Didier de Fontaine		A. Berera J. Hoyt	J. Kulik	B. Clark M. Kraitchman
Lutgard De Jonghe	M. Rahaman S. Varanasi S. Visco	Y. Boiteux M. Chu M. Lin M. Liu	C. Mailhe E. Reiner M. Weiser	S. Shinde

Investigators	Postdoctoral and Other Scientists	Graduate Students		Participating Guests
Norman Edelstein Richard Andersen Kenneth Raymond Andrew Streitwieser, Jr. David Templeton Allan Zalkin	P. Becker J. Brennan J. Bucher J. Chambron G. Feige G. Freeman H. Gehmecker T. McMurry I. Poirot G. Shalimoff A. Stuart D. White	P. Becker D. Berg T. Boussie J. Brennan D. Eisenberg M. Fabiano T. Franczyk G. Freeman W. Kot W. Mallet R. Moore	D. Piehler J. Rigsbee R. Rosen P. Sasse P. Smith J. Stewart S. Stults B. Tanas L. Uhlir G. Williams	C. Burns S. Evans S. Gokcen E. Hahn S. Kretchmar M. Silva L. Templeton D. White
James Evans		B. Li	O. Rego-Monterio	E. Luh H. Tsai
Leo Falicov		D. Chrzan	A. Reich	
Andreas Glaeser		W. Carter L. Edelson	J. Roedel	M. Shalz
Harvey Gould		C. Munger		S. Pugh
Ronald Gronsky				J. Camberos M. Kundmann H. Okamoto S. Packer J. Punglia
Eugene Haller*				
Charles Harris		M. Arndt J. Brown	C. Parsons	R. Hoff R. Jordan W. Merry M. Paige E. Peterson M. Prisant D. Russell B. Schwartz D. Smith
Heinz Heinemann				J. Munoz
Carson Jeffries		P. Bryant Y. Kim	Q. Lam	
Harold Johnston	A. Young	P. Hunter B. Kim D. Kinnison C. Miller	B. Oh K. Patten W. Sisk	
William Jolly				
Yuan Lee		B. Balko R. Brudzynski P. Chu R. Continetti M. Covinsky E. Cromwell H. Davis M. Helfand	E. Hintsa J. Meyers J. Price G. Robinson A. Schmoltner L. Yeh X. Zhao	G. Nathanson D. Neumark T. Trickl

Investigators	Postdoctoral and Other Scientists	Graduate Students		Participating Guests
William Lester, Jr.	V. Kresin P. Reynolds	R. Barnett C. Dateo B. Hammond	S. Huang R. Owen	B. Bernu
Alan Levy	S. MacAdam			Z. Shui B. Wang
Steven Louie		S. Fahy		H. Lin
William Miller	J. Chang	Y. Chang T. Gray	A. Makri B. Ruf	B. Jansen
C. Bradley Moore		T. Butenhoff I. Chen Y. Choi D. Darwin M. Foltz	J. Frisoli W. Green Y. Guo V. Venturo	M. Chuang A. Kung M. Ochsner
Rolf Muller		M. Armstrong D. Barkey R. Crocker	J. Gyory S. Mayer	
John Newman		C. Hali A. Hauser A. Mason	P. Shain G. Sisler A. West	
Donald Olander	M. Derzon	J. Abrefah K. Kim M. Moalem	A. Motta K. Park D. Sherman	R. Allred M. Ballooch H. Harrell
Joseph Pask				A. Tomsia J. Zhu
Norman Phillips	C. Marcenant	S. Lacy	J. Olsen	R. Fisher
Alexander Pines	G. Chingas D. Suter K. Takegoshi	A. Bielecki J. Chang H. Cho C. Connor M. Gochin T. Jarvie C. Lee	K. Mueller J. Pearson M. Raferty S. Rucker D. Shykind A. Thayer M. Trecoske	L. DeMenorval H. Huber S. Liu K. Neidig A. Shaka
Kenneth Pitzer	D. Schreiber J. Tanger			
John Prausnitz		R. Cotterman A. Harvey	A. Wu	
Michael Prior				H. Shugart
Paul Richards		G. Bernstein M. Fischer	A. Lange R. Phelps	
Robert Ritchie		R. Dauskardt J. Mason	T. Oh J. Shang	F. Haubensak H. Hayashigatani J. Miwa P. Spencer W. Yu
Gerd Rosenblatt	K. Viers	V. Chia		

Investigators	Postdoctoral and Other Scientists	Graduate Students		Participating Guests
Philip Ross	K. Gaugler			L. Johnson
Richard Saykally		K. Busanow R. Cohen D. Gwo D. Hovde	K. Laughlin R. Robinson D. Steyert	
Henry Schaefer III		W. Allen B. Besler C. Blahous D. Clabo	R. Grev C. Janssen A. Scheiner	J. Rice
Alan Searcy	P. Hou D. Meschi	J. Bierach		
Y. Ron Shen		W. Chen M. Feller A. Karn	C. Mullin X. Zhu	P. Guyot-Sionnest H. Hsiung L. Martinez-Miranda R. Pan
David Shirley	S. Kim	P. Heimann Z. Huang L. Medhurst B. Niu	A. Schach von Wittenau L. Terminello L. Wang L. Wang	K. Leung S. Liu X. Zhang
Gabor Somorjai	M. Van Hove	G. Blackman M. Bussell J. Carrazza D. Godbey C. Kao D. Kelly	K. Lewis P. McAnally T. Rucker G. Vurens M. Xu	J. Adams S. Fu J. Houlihan M. Khader H. Ohtani R. Pande D. Sullivan P. Xu
Angelica Stacy		J. Badding M. Dixon W. Ham	R. Hoskins J. Womack H. zur Loye	G. Holland
Gareth Thomas		L. Chan J. Chen M. Dass	H. Ho S. Miyasoto R. Ramesh	J. Ahn T. Bielicki D. Callahan T. Huynh J. Kim J. Kim V. Radmilovic L. Sidjanin K. Srikrishna
Charles Tobias	M. Verbrugge	P. Andersen S. Elliott S. Galante S. Hessami K. Jordan	L. McVay D. Sutija G. Whitney B. Wines	R. Anderson
K. Peter Vollhardt		M. Huffman P. McGovern R. Myrabo	D. Newman W. Tolman M. West	

Investigators	Postdoctoral and Other Scientists	Graduate Students		Participating Guests
Jack Washburn	C. Lampert Z. Liliental J. Mazur Y. Shih	L. Allen R. Caron J. Ding	C. Jou J. Lou D. Olson	D. Ah Tye M. Hong J. Mazur
Kenneth Westmacott	U. Dahmen R. Kilaas K. Krishnan M. O'Keefe			P. McDougall J. Posthill
Peter Yu	D. Erskine	E. Hess Y. Haung D. Kim		

*Also affiliated with the Engineering Division

Support Staff

Division Administrative Staff

C. Peterson — Assistant Division Head, Administration
K. McArthur — Division Administrator

Administration

M. Janzen
L. English
J. Leonard
R. Rodriguez

Personnel/Financial

M. Montgomery
C. Coolahan
P. Paladini

Purchasing

S. Stewart
C. Sterling
J. Leonard

Technical Editor

R. Albert

Special Projects

E. Skrydlinski

Travel

S. Quarello

Administrative/Secretarial Staff

T. Allyn
R. Arcol
M. Atkinson
C. Becker
H. Benson
M. Bishop
M. Borgrink
G. Brazil
D. Carmichael
H. Conti
N. Corwin
J. Denney
L. Dory
E. Edelson
S. Ewing
S. Gangwer
C. Gliebe
C. Gloria
R. Jones
B. Kuchinsky
E. Lemos
N. Miller
M. Momii
M. Moore
B. Moriguchi
T. Narasimhan
M. Noyd
G. Osterloh
M. Penton
P. Ray
R. Rodriguez
B. Tung
A. Weightman
A. Wingfield
K. Wong
S. Yamagishi
C. Yoder
B. Zambrano
J. Zissler

Technical Staff

D. Krieger — Technical Coordinator

D. Ackland
H. Ackler
H. Brendel
R. Cinque
N. Claytor
D. Colomb
K. Desai
C. Echer
C. Flor
G. Gager
L. Gill
A. Gronsky
J. Holthuis
J. Jacobsen
D. Jurica
E. Mah
E. Nelson
T. Prussin
P. Ruegg
L. Rumaner
J. Severns
M. Shalz
W. Smith
H. Sokol
B. Sun
L. Sun
J. Turner
W. Wong
J. Wu

APPENDIX B

DIVISION COMMITTEES

DIVISIONAL COUNCIL

A. Bell
L. De Jonghe
H. Johnston
S. Louie
K. Raymond
R. Ritchie
P. Ross
G. Thomas
K. Westmacott*

DIVISIONAL RESEARCH STAFF COMMITTEE

N. Edelstein
K. Raymond
R. Muller*
K. Westmacott

ELECTRON MICROSCOPE USERS COMMITTEE

R. Gronsky
P. Ross*
K. Westmacott

EQUIPMENT REVIEW COMMITTEE

J. Clarke
H. Johnston
R. Muller*
R. Ritchie
P. Yu

TECHNICAL STAFF AND SHARED FACILITIES COMMITTEE

L. De Jonghe*
R. Gronsky
P. Ross
G. Somorjai

ADMINISTRATIVE STAFF COMMITTEE

K. McArthur*
C. Peterson
M. Van Hove
P. Yu

MMRD SAFETY COORDINATOR

D. Meschi

SAFETY AND LABORATORY STANDARDS COMMITTEE

Buildings 62 and 72

D. Ackland
M. Cima
D. Colomb
L. English
K. Gaugler
J. Haley
J. Holthuis
J. Jacobsen
L. Johnson
D. Jurica
D. Krieger*
J. Leonard
E. (Fong) Mah
K. McArthur
D. Meschi
R. Muller
E. Perez
C. Peterson
P. Ruegg
J. Severns
G. Shalimoff
S. Stewart
W. Wong
J. Wu

Building 70

D. Lindle
T. Minton
G. Shalimoff*
A. Weightman

CERAMICS PROGRAM ADVISORY COMMITTEE

R. Gronsky
R. Ritchie
A. Searcy

BUILDING AND SPACE COMMITTEE

R. Gronsky
D. Meschi
R. Muller*
A. Zalkin

MMRD Building 62 Building Manager: D. Meschi (Alternate: C. Peterson)

MMRD Building 72 Building Manager: K. Westmacott (Alternate: D. Ackland)

*Chairman

APPENDIX C

LIST OF DIVISIONAL SEMINARS

Surface Science and Catalysis Seminars

Date	Speaker and Affiliation	Seminar Title
1-9-86	M.S. Daw, Sandia National Laboratories, Livermore, CA	Application of the Embedded Atom Method to Reconstructed Surfaces and Atomic Adsorption on Metals
1-16-86	A. Kummel, G. Sitz, and R. Zare, Stanford University	Can Gas-Surface Scattering Polarize Molecules?
1-23-86	T.E. Madey, National Bureau of Standards, Washington, DC	The Structures of Adsorbed Molecules Using Electron Stimulated Desorption
1-30-86	C. Francis, University of Southern California	From Metal Atoms to Macromolecules: Metal Complexes in Polymer Media
1-31-86	S.M. Davis, Exxon, Baytown, TX	Surface Science Studies Using Practical Petroleum Processing Catalysts
2-5-86	A. Heller, AT&T Bell Laboratories	Transparent Group VIII Metal Catalyst Films and Their Electrical Contacts with Semiconductors
2-6-86	M. Yacaman, UNAM, Mexico	Fractal Structure of Small Particles
2-13-86	J. Margrave, Rice University, Houston, TX	Reactions of Iron Atoms, Dimers, and Small Clusters with Saturated and Unsaturated Hydrocarbons and Their Derivatives
2-18-86	G.W. Keulks, University of Wisconsin, Milwaukee	A Comparison of Selective Oxidation Catalysts Using Program Temperature Desorption
2-24-86	E. Wachs, Exxon Research and Engineering Co.	Characterization and Catalysis of Surface Oxides
3-6-86	J. Ward, Union Oil Co.	Zeolite Catalysts in Hydroprocessing
3-12-86	J.B. Pendry, Imperial College, London	The Dynamics of Electrons at Surfaces
3-13-86	A.J. Nozih, Solar Energy Research Institute	Quantization Effects in Superlattice Photoelectrodes and Semiconductor Colloids
3-20-86	J.E. Houston, Sandia National Laboratories, Albuquerque, NM	Structural, Electronic, and Chemical Properties of Thin Cu Overlayers on Ru(0001)
3-27-86	M. Strongin, Brookhaven National Laboratory	How do Metals Oxidize at Low Temperatures?
4-3-86	J.-E. Sundgren, University of Illinois, Champaign-Urbana	Structure and Properties of TiN Coatings and TiN-Steel Interfaces
4-10-86	C.T.W. Chu, Mobil Research and Development Corp., Princeton, NJ	Isomorphous Substitution in Zeolite Frameworks — Chemical, Physical, and Catalytical Properties

Date	Speaker and Affiliation	Seminar Title
4-17-86	B. Gates, University of Delaware	Hydrocarbon Conversion Catalyzed by Oxide-Bound Organorhenium Complexes: A Molecular Basic for Structure Sensitivity in Catalysis
4-24-86	F. Zaera, Brookhaven National Laboratory	
5-1-86	P. Avouris, IBM, Yorktown Heights, NY	Unoccupied Levels and Excited States at Surfaces
5-8-86	L. Petrakis, Chevron, Richmond, CA	Searching Spectroscopically for Catalytic Sites: Molybdena-Based Model Hydrodesulfurization Catalysts
8-14-86	S. Ferrer, Universidad Autonoma, Madrid	Thermal-Energy Helium Scattering Study of the Early Stages of Growth of Pb Overlayers on Cu(100)
8-18-86	J. Norskov, NORDITA, Copenhagen	From Surface Science to Heterogeneous Catalysis
8-28-86	R. Prins, Eindhoven, The Netherlands	The Role of the Cobalt Promoter in Hydrodesulfurization Catalysis
9-4-86	Y. Inoue, Nagaoka, Japan	Polarization Effects of Ferroelectric Materials upon Their Adsorptive and Catalytic Properties
9-11-86	T.T. Tsong, Pennsylvania State University	Atomic Behaviors and Atomic Structures of Solid Surfaces, an Atom-Probe and FIM Study
9-16-86	E. Shustorovich, Kodak, Rochester, NY	Heats of Chemisorption, Dissociation and Recombination Barriers: Calculations Based on Bond-Order Conservation
9-18-86	J.T. Yates, University of Pittsburg	Reflection-Infrared Study of the Alkali-CO Surface Interaction
9-25-86	D. Tomanek, Department of Physics, U.C. Berkeley	*Ab Initio* Calculations for Chemisorption Systems
10-2-86	P.S. Bagus, IBM, San Jose, CA	Vibrational Frequencies of Adsorbates on Metal Surfaces: Cluster Model Theoretical Studies
10-9-96	J. Stöhr, IBM, San Jose, CA	X-Ray Absorption Studies of Chemisorbed Molecules and Molecular Chains
10-10-86	J. Paul, Exxon, Clinton, NJ	CO Chemisorption on Clean AP(100) and on AC(100) Modified by Oxide Formation or Potassium Adsorption
10-16-86	R. Stulen, Sandia National Laboratories, Livermore, CA	Low-Temperature States of Hydrogen on Palladium
10-23-86	J.C. Hemminger, University of California, Irvine	Laser-Driven Thermal Processes at Surfaces: Desorption and Other High-Activation Energy Channels
10-30-86	D.J. O'Rear, Chevron Research Corp., Richmond, CA	Improving the Selectivity of Hydrocracking by use of Shape Selective Zeolites
11-6-86	A. Melmed, National Bureau of Standards, Washington, DC	Field-Ion Microscopy and the Icosahedral Structure Problem
11-13-86	D.W. Goodman, Sandia National Laboratories, Albuquerque, NM	Adsorption and Reaction on Strained Metal Overlayers
11-20-86	P.B. Venuto, Mobil	

Date	Speaker and Affiliation	Seminar Title
12-4-86	K.A.R. Mitchell, University of British Columbia	Structures and Bond Lengths from Surface Crystallography
12-11-86	K. Lynn, Brookhaven National Laboratory	Positron Studies of Interfaces and Surfaces

Chemical Dynamics Seminars

1-15-86	Prof. Stephen R. Leone, Joint Institute for Laboratory Astrophysics, University of Colorado, Boulder	Product States and Alignment Effects in Chemical Dynamics
1-29-86	Prof. Max L. Berkowitz, Department of Chemistry, University of North Carolina, Chapel Hill	A Classical Fluid-Like Approach to the Density Functional Formalism of Many Electron Systems
2-12-86	Prof. Cleanthes Nicolaides, Theoretical and Physical Chemistry Institute, Hellenic Research Foundation, Athens, Greece	Quantum Chemistry of Excited States from a State-Specific Theory Point of View
2-26-86	Prof. Robert W. Field, Department of Chemistry, Massachusetts Institute of Technology, Cambridge	Vibrationally Hot Formaldehyde: Is There Any Connection Between Spectroscopic and Collisional Properties?
4-2-86	Prof. Richard A. Friesner, Department of Chemistry, University of Texas, Austin	A New Method of Solving the Hartree-Fock Equation for Atoms and Molecules
5-12-86	Prof. James Lisy, Department of Chemistry, University of Illinois, Urbana	Vibrational Predissociation Spectroscopy of Molecular Clusters
5-20-86	Prof. Jean Futrell, Department of Chemistry, University of Utah, Salt Lake City	Charge and Energy Transfer in Small Ion/Atom Systems
6-27-86	Dr. Hideto Kanamori, Institute for Molecular Science, Myodaiji, Okazaki, Japan	Infrared Diode Laser Kinetic Spectroscopy for Small Molecules
7-3-86	Dr. Ian W.M. Smith, Department of Chemistry, University of Birmingham, England	Vibrational Adiabaticity in Biomolecular Reactions
7-7-86	Prof. Richard N. Dixon, Department of Chemistry, University of Bristol, England	Vector Correlations in Photodissociation
8-6-86	Prof. John Hall, Atlanta University Science Research Institute, Georgia Institute of Technology, Atlanta	Some Reactions of Importance to Tropospheric and Stratospheric Chemistry
9-17-86	Dr. Jospeh Gerratt, School of Chemistry, University of Bristol, England	Modern Valence Bond Theory — Was Kekulé Right?
10-1-96	Dr. Warren Warren, Department of Chemistry, Princeton University, Princeton, NJ	Effects of Arbitrary Pulse Shapes in Laser and NMR Spectroscopy
10-20-86	Prof. J. Barrie Peel, Department of Chemistry, La Trobe University, Australia	Photoelectron Spectroscopy of Molecular Dimers and Clusters
10-29-86	Prof. Alan G. Marshall, Department of Chemistry, Ohio State University, Columbus	Fourier Transform Ion Cyclotron Resonance Mass Spectrometry
10-31-86	Prof. James Weisshaar, Department of Chemistry, University of Wisconsin, Madison	Gas Phase Transition Metal Ion Reactions with Alkanes

Date	Speaker and Affiliation	Seminar Title
11-6-86	Dr. C.N.R. Rao, Indian Institute, Bangalore	Studies of Novel Solids and Solid-State Transformations
11-7-86	Prof. K. Kaya, Keio University, Japan	Spectroscopy and Dynamics of Hg van der Waals Complexes as Revealed by Jet Spectroscopy
11-19-86	Prof. R.B. Gerber, Department of Chemistry, Northwestern University, Evanston, IL	Dynamics and Level Structure of Highly Excited Vibrational States

Electron Microscopy Seminars

1-31-86	Dr. William Tivol, N.Y. State Health Department	Side-Entry Differentially Pumped Environmental Chamber for the HVEM
5-19-86	Dr. F.H.M. Spit, University of Amsterdam	Diffusion of Donor Elements in Polycrystalline Silicon
6-6-86	Dr. Christian Colliex, University of Paris	Recent Advances in Electron Energy Loss Spectroscopy
11-11-86	A. Thorel, CNRS, Paris	Interfaces in SiAlON
11-11-86	J.L. Maurice, CNRS, Paris	Structure and Electrical Properties of Grain Boundaries in Semiconductor Polycrystals
11-25-86	Dr. J.-Y. Laval, CNRS, Paris	Atomic Structure of MBE Grown III-V Superlattice
12-9-86	Dr. Peter McDougall, University of South Wales, Australia	The Crystallography of FCC $\leftrightarrows$ BCC Diffusional Transformations Having Invariant Plane and Invariant Line Characteristics
12-18-86	Dr. M. Lancin, CNRS, Paris	Microstructural Studies of Ceramics and Composites

Other Seminars Hosted

5-23-86	Prof. M.F. Lappert, Department of Chemistry, University of Sussex, Brighton, England	The Role of Heavy Main-Group IV Element Carbene Analogues, MX_2, in Transition Metal Chemistry
8-5-86	M.N. Piancastelli, Department of Chemistry, University of Rome "La Sapienza"	Breakdown of One-Electron Approximation in the Inner Valence Shells of Hydrides
8-26-86	F. Larkins, Department of Chemistry, University of Tasmania	Photonization Calculations of Atoms and Molecules
10-27-86	Prof. J.A. Koningstein, Ottawa-Carleton Institute for Research and Graduate Studies in Chemistry, Carleton University, Ottawa, Ontario	Time-Resolved Electronic Raman Spectra of TbAl Garnet and Ruby

APPENDIX D

INDEX OF INVESTIGATORS*

Andersen, Richard A. 189, **205**

Bartlett, Neil **191, 205**
Bell, Alexis T. 22, **183**
Bergman, Robert G. **196**
Bragg, Robert H. **58**
Brewer, Leo **101**

Carrazza, J. **229**
Clarke, John **79**, 125
Cohen, Marvin L. 77, **87**, 92, 93
Connick, Robert E. **182**
Conway, John G. **205**

de Fontaine, Didier **31, 34**
De Jonghe, Lutgard C. **54, 233, 248**

Edelstein, Norman M. 189, **205**
Evans, James W. **29, 233, 246**

Falicov, Leo M. **34, 84**, 255

Glaeser, Andreas M. **61**
Gould, Harvey **177**
Gronsky, Ronald **1, 17**, 49, 50

Haller, Eugene E. 66, **255**
Harris, Charles B. **139**
Heinemann, Heinz **229**

Jayko, Michael E. **138**
Jeffries, Carson D. **74**
Johnston, Harold S. **136**
Jolly, William L. **189**, 218

Kresin, Vladimir Z. 149, **264**

Lee, Yuan T. 71, 160, 161, **166**, 174
Lester, William A., Jr. **147, 261, 266**
Levy, Alan V. **225, 267, 270, 271, 272, 273**
Louie, Steven G. 89, **92**

Miller, William H. **154**

Moore, C. Bradley **142**
Muller, Rolf H. **106, 233**, 234, **240**

Newman, John **233**, 235, **252**

Olander, Donald R. **103**

Pask, Joseph A. **43**
Phillips, Norman E. **75**
Pines, Alexander **119**
Pitzer, Kenneth S. **144**
Prausnitz, John M. **201**
Prior, Michael H. **180**

Raymond, Kenneth N. **205**
Richards, Paul L. **64**
Ritchie, Robert O. **36**
Rosenblatt, Gerd M. **131**
Ross, Philip N., Jr. 22, **223, 233, 243**

Saykally, Richard J. **151**
Schaefer, Henry F., III 169, **173**
Seaborg, Glenn T. **205**
Searcy, Alan W. 21, **45**
Shen, Yuen-Ron **69**, 109, 166
Shirley, David A. **158**, 166, 167, 168
Somorjai, Gabor A. 69, **109, 133, 183, 229**
Stacy, Angelica M. **129**
Streitwieser, Andrew, Jr. 189, **205**
Stringer, John **268**

Templeton, David H. **205**
Thomas, Gareth **5, 17**
Tobias, Charles W. **99**, 106, 107, **233, 235, 237**, 241

Vollhardt, K. Peter C. **187**

Washburn, Jack **49**
Westmacott, Kenneth H. **14, 17**

Yu, Peter Y. **77**

Zalkin, Allan **205**

*Boldface numbers indicate investigators' main programs.

GPO 788-799/79003

LAWRENCE BERKELEY LABORATORY
TECHNICAL INFORMATION DEPARTMENT
UNIVERSITY OF CALIFORNIA
BERKELEY, CALIFORNIA 94720